PROCEDIA UNDERGRADUATE MECHANICAL ENGINEERING RESEARCH

VOLUME 1
SEPTEMBER 2019

EDITOR
DR SHAHARIL MAD SAAD
DR MASTURA AB WAHID

OPTIMIZING SAFETY OF SHIP CONSTRUCTION PROCESS AT SHIPYARD

Muhammad Syafiq and Ab Saman Abd Kader
School of Mechanical Engineering, Faculty of Engineering,
Universiti Teknologi Malaysia, 81310 UTM Skudai, Johor, Malaysia

INTRODUCTION

Shipbuilding industry is a highly cost industry which can make a huge impact and tremendous positive outcomes. This industry additionally turns into appealing and viewed as a major outcomes industry for some countries in the world. In addition, the international shipping industry carries about 90% of world trade. [1] Shipbuilding and repair work at the shipyard are among the riskiest industries in the world, which implies that quite complicated tasks have to be performed in parallel. Thus, safety in shipyard is a very important thing in these industry including worker's awareness towards risk and compliance of safety precaution at the shipyard.

EXPERIMENTAL SETUP

This section presents research instrument used for this study. Five-point Likert scale was used in the questionnaire that measures the severity and frequency of occurrence. The questionnaire is consists of 3 section which are section A (Demography), section B (level of worker's awareness) and, section C (Compliance of safety precaution). The respondent is basically shipyard workers in Malaysia.

The data were analysed by using Microsoft Excel and Social Statistical Package Science (SPSS). All the data were anayzed using two tools which are descriptive analysis and relative importance index (RII)

RESULTS AND DISCUSSION

At the end of research, the literature review was done to improve general comprehension of the research to get clear data. Books, journals, articles, conference paper and others were used as reference for further understanding. The main process of shipbuilding is identified and discussed. Figure 1 shows the main processes are including designing, cutting or forming, block assembly, pre-outfitting or painting, pre-erection, erection and quay.

In order to achieve level or worker's awareness at the shipyard, the descriptive analysis is used to identify level of worker's awareness at the shipyard by calculated the percentage of occurrence and mean score. The lowest mean indicated the least aware towards safety and the highest mean indicated the most frequent aware towards safety at workplace. Based on the findings, the average mean score for both internal and external factor is 4.08 and 3.85 which are highly aware based on the mean score. It can be concluded that, the workers at the shipyard has highly aware towards safety at their workplace.

In order to achieve compliance of safety precautions at the shipyard, the relative importance index analysis is used to identify level of safety compliance at the shipyard by measured their compliance of safety precautions at each risk of workplace. The method had been proposed by determining their level of safety compliance for safer ship construction work. Based on the findings, the average of safety precautions is mostly complied at the shipyard. The relative importance index is used for easier method to rank the level of compliance of safety precaution at the shipyard.

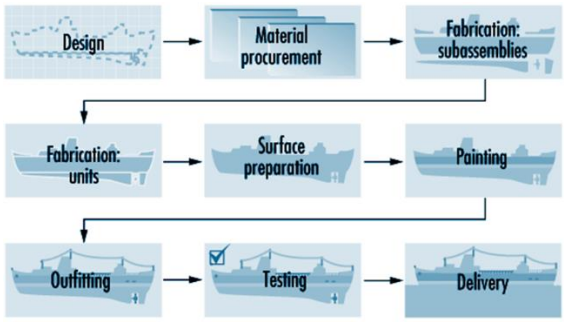

Figure 1: Flow chart of ship production process.

CONCLUSION

The problem identified and recommendations had been forward in this thesis. An optimization is proposed mainly for major concern which is safety compliance in shipyard for safer ship construction process. Based on the findings, several method had been used and proposed in determining the level of safety in the shipyard for safe ship construction process. It can be concluded that, the shipyard has a high level of safety compliance of safety precautions. In addition, major concern from the employer is needed to minimize number of risk as well in order to keep good reputation of the company.

REFERENCES

[1] Isomaki, S. (2012) 'Development of a New Service Concept in the Field of Ship Industry'.

INTEGRATED MAINTENANCE SYSTEM IN SHIP POWER PLANT SYSTEM

Muhammad Afifi Abdul Aziz and Saman Abd Kader
School of Mechanical Engineering, Faculty of Engineering,
UniversitiTeknologi Malaysia, 81310 UTM Skudai, Johor, Malaysia

INTRODUCTION

Power plant is very important in industrial activities or other activities that use electricity as a source of energy. Power plant is a facility for the generation of electric power by rotating machine that converts mechanical power into electrical power. Most power plant contains one or more generators and this also same as ship power plant. In ship power plant, the main generator on ship usually use for propulsion system where by using propulsion forces, ships are able to maneuver themselves in the water. The most commonly used marine propulsion system is diesel propulsion system by converting mechanical energy from thermal forces. Diesel propulsion systems are mainly used in almost all types of vessel along with small boats and recreational vessel. [1]

EXPERIMENTAL SETUP

First, the initial study was conducted to find out the problem that was related to research object, which is the most common failure in the power plant system is boiler. Then the literature review was conducted to find out more about what happened to the boiler operation and to determine the problem. From the potential failure mode, boiler tube is the most problem.Then, the data and other information required for the assessment are collected. At this stage the RBM method is implemented. Based on data, risk assessments are performed in the part of each section. All medium and high risk areas are investigated by PoF and CoF for each item and estimate the damage rate, PoF and CoF calculation can be done with other alternatives using the FMEA method.After the assessment done we will see the risk of failure. Then the risk matrix is used when designing a check interval. Based on the matrix risk, critical risks will be through maintenance planning to reduce the risk. Reassessment will be performed to compare risk factors and operations will be repeated if problems are detected.From the potential failure mode, boiler are chooses. 5 types of boiler tube are chooses for the analysis.

RESULTS AND DISCUSSION

Figure 3.1 shows the result of the risk analysis in matrix form with the category allocated based on API 581. The result show that the highest risk present is medium high from tube 2, 3, 4 and 5. The lowest risk is in medium category from tube 1. The risk values for each tube are 1.03 for tube 1, 13.6 for tube 2, 3 and 4 and 15 for tube 5. the probability for tube 2, 3, 4 and 5 to fail exceed the medium category is on day 20. Therefore, to reduce the probability of the risk to occur is by doing maintenance before day 20. To reduce the maintenance cost, maintenance for tube 1 will be delay because the probability of the tube to fail does not exceed the medium category within a month.

Feed water and boiler water treatment are added in maintenance plan as a preventive method. Feed water and boiler water shall be analyzed at least twice a day. Amount of chemicals to be added and amount of boiler water to be blow down shall be controlled referring to the results of the analysis so as to maintain each chemical content of the water within the prescribed limit. Operators are required to have correct understanding about the action and effect of each chemical and calculation method of required quantity of it.The recommended chemicals are as follows For adjusting pH value and PO 3-: Na HPO and Na PO.

For deoxidization and rising pH value : Hydrazine hydrate

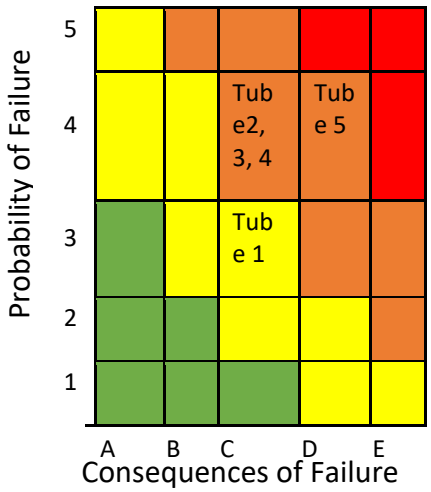

Figure 1: shows the risk matrix area based category

CONCLUSION

The potential area to develop an offshore wind turbine is at Area 6 in order to harness wind energy despite the seasonal variation wind speed. This is because there are not much of exploration contract area or production of oil and gas at the area despite the low of technical energy.

REFERENCES

[1] Sharda. (8 October, 2017). Different Types of Marine Propulsion System Used in the Shipping World. Retrieved 2 January, 2019, from Marine Insight: https://www. marineinsight. com/main-engine/different-types-of-marine-propulsion-systems-used-in-the-shipping-world/

RISK BASED INSPECTION FOR BOILER OPERATION IN MARINE POWER PLANT SYSTEM

Muhammad Rizuwan Zakaria and Ab Saman Abd Kader
School of Mechanical Engineering, Faculty of Engineering,
Universiti Teknologi Malaysia, 81310 UTM Skudai, Johor, Malaysia

INTRODUCTION

To minimize the risk of failure for boiler operation, the Risk-based inspection (RBI) is applied. RBI is an approach which seeks to optimize inspection activities based on probability and consequence of failure of components and systems to optimize the time-based inspection. Nowadays the requirement of using RBI for managing risk is really popular in marine power plants because RBI provides a methodology for determining the most cost effective inspection program. RBI is carried out to reduce costs of inspection and maintenance while still maintaining an acceptable amount of risk. By focusing on equipment which is higher risk, inspection and maintenance plans can be developed focusing on the higher risk equipment while inspection and maintenance on lower risk equipment is reduced to appropriate level. Risk is defined as the potential consequence based on a specific hazard or danger driven by its individual probability of occurrence. [1]

EXPERIMENTAL SETUP

Five types of tube had been taken into consideration in this study, they are Rear Bank Tube; Screen Tube; Front Wall Tube; Rear Wall Tube and Side & Roof Wall Tube. In each type, one tube was selected in order to conduct the RBI analysis. These tube will be called Tube 1, Tube 2, Tube 3, Tube 4 and Tube 5. Risk assessment will identify the potential failure or degradation mechanism, and their potential consequences. Analysis on the probability of failure and consequence of failure will be done and conduct in qualitative analysis. The result is the risk level of the pipes and the inspection plan and mitigation plan. In case of the inspection plan can no longer to give the confident level of risk, mitigation plan need to be done.

RESULTS AND DISCUSSION

Figure 1 shows the risk matrix for area-based analysis.

It is clear that the Tube that has the highest risk is Tube 5 because it is the only one in medium-high area, this also show that the risk faced by Tube 5 is COF driven compared to other Tubes. Tube 2,3 and 4 located in medium region which is typical, whereas Tube 1 has the lowest area-based risk compared to others.

Figure 2 Risk Matrix for Financial-based Analysis

Tube 1 has the lowest financial-based risk and the other Tubes; Tube 2,3,4 and 5 has medium risk for financial. This may be resulted from the cost of repair and production lost are low, but the result just for a sample tube taken from different location surrounding the boilers.

The inspection planning is focus on Area-based risk analysis, since all risk in Financial-based fall within range. The reassessment of mitigation and inspection plan are necessary to achieve maximum effectiveness of a mechanism. Tube 5 need to have shorter time inspection interval and Tube 1 can have longer time interval based on area analysis. For Financial, only Tube 1 need rearrangement of inspection planning since the normal procedure waste cost on unnecessary inspection.

CONCLUSION

In conclusion, the main objective which is to conduct Risk Based Inspection for boiler operation in marine power plant has been fulfilled. This analysis produced a qualitative risk assessment and comes out with risk ranking for tubes in high risk or lower risk region. An inspection plan is suggested.

REFERENCES

[1] API RP581. (2016). Risk-Based Inspection Methodology. Document. *API Publication 581* . Washington: API Publication.

REDUCTION OF DISC BRAKE SQUEAL NOISE BY BRAKE PAD MODIFICATION

Ahmad Sulaiman Ahmad Tajuddin and Abd Rahim Abu Bakar
School of Mechanical Engineering, Faculty of Engineering,
Universiti Teknologi Malaysia, 81310 UTM Skudai, Johor, Malaysia

INTRODUCTION

One of the common noise issues in automotive industry is disc brake squeal. This annoying noise cause discomfort to people and warranty issue. The disc brake squeal noise was generated in the frequency range between 1 kHz and 15 kHz with the sound pressure level above 70 dBA [1]. Brake squeal can be generated by several conditions such as temperature, humidity, pressure on the pads, and speed [2]. Previous research has been made where the brake pad's geometry is modified either cutting chamfers or slot to reduce the high frequency noise [3]. Due to variety of brake designs, one type of pad modification may or may be not effective in eliminating squeal.

EXPERIMENTAL SETUP

The experimental test was carried out by using a prepared brake squeal test rig in the automotive laboratory of the Universiti Teknologi Malaysia (UTM). The original brake pads of the Malaysian national car were utilized in this study experiment by adopting the test procedures implied by the SAE J2521 drag test procedures. Multiple tests were conducted using the original brake pads by varying the brake squeal main parameters which are the hydraulic applied pressure and the disc rotor rotational speed.

RESULTS AND DISCUSSION

The brake pads utilized in this project were modified in 4 different ways. The first one is machined a straight slot at the centre of each pad. The second set was machined with a straight slot at the centre of pad with chamfer at each pad edge for each pad. The third set was machined with a trigonal slot at the centre of the pad. The fourth set was machined with a trigonal slot at the centre of the pad with chamfer at each pad edge for each pad. The brake squeal testing on the first brake pads modification resulted in a reduction in the brake squeal by 6 % with a maximum sound pressure squeal intensity of 93 dBA. The testing on the second brake pads modification resulted in a squeal reduction of 12 % with an SPL maximum value of 87 dBA. The testing on the third brake pads modification resulted in a squeal reduction of 19 % with an SPL maximum value of 80 dBA. The testing on the fourth brake pads modification resulted in a squeal reduction of 22 % with an SPL maximum value of 77 dBA.

The fourth brake pads modification show the greatest reduction of brake squeal noise of 22% compared to other modifications with an SPL maximum value of 77 dBA. It is noticed that the maximum sound pressure level is detected at Test 1 with SPL of 77 dBA by referring Table 1. Figure 1 show the frequency distribution for the fourth brake pads modification with a uniform distribution.

Table 1: Squeal data for the fourth brake pads modification.

	Pressure (kg/cm2)	Speed (rpm)	SPL (dBA)	Squeal Frequency (Hz)
Test 1	1	26	77	4189, 8408
Test 2	1	31	74	4199, 8408
Test 3	1	36	72	4189, 8369
Test 4	1	41	74	4218, 8437
Test 5	1	45	72	4208, 8417
Test 6	1	50	74	4189, 8388

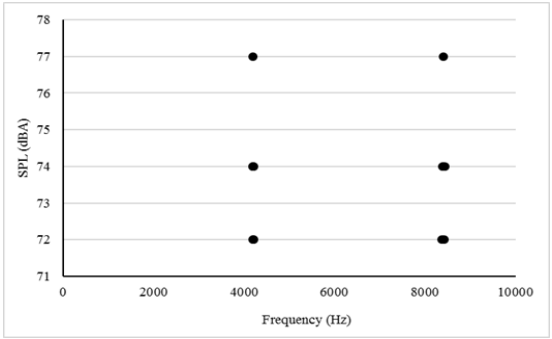

Figure 1: SPL for the fourth brake pads modification with different frequencies.

CONCLUSION

All the proposed modification can reduce the disc brake squeal noise. It is proved that the modification with a trigonal slot and chamfer has the greatest reduction of squeal compared than other modifications.

REFERENCES

[1] Kim, C., & Zhou, K. (2016). Analysis of Automotive Disc Brake Squeal Considering Damping and Design Modifications for Pads and Disc. International Journal of Automotive Technology, 17(2), 213-223.

[2] Hetzler, H., & Willner, K. (2012). On the influence of contact tribology on brake squeal. Tribology International, 237-246.

[3] Kumar, V. (2014). Automotive Brake Disc Design to Suppress High Frequency Brake Squeal Noise. International Journal of Engineering Research & Technology (IJERT), 165-169.

Study of Solar Chimney Performance to Improve Ventilation of an L-shaped Shipping Container in Tropical Environment

Boo Wen Hao and Abu Hasan Abdullah
School of Mechanical Engineering, Faculty of Engineering,
Universiti Teknologi Malaysia, 81310 UTM Skudai, Johor, Malaysia

INTRODUCTION

In 21st century, researches had been done in investigating the passive cooling techniques to improve the energy consumption. Solar chimney had been recognize as one of the technique to improve the ventilation. Application of solar chimney could cause a decrease in room temperature for 1.0-3.5 °C lower than ambient air [1]. The aim of the project is to explore enhancement methods to boost natural convection heat transfer to ventilate an L-shaped shipping container home using solar chimney.

METHODOLOGY

An L-shaped shipping container home is modeled as well as meshing using Salome. Then, the simulation is running using Code_Saturne after mesh file is imported. Different case studies on the chimney is done. In this case, Boussinesq approximation is used without solving full Navier-Stokes equation due to density variation:
$\rho_c (1-\beta(T-T_c)$ where $\beta=1/T_c$

This equation represents the density law. Assumption of only natural convection as heat transfer method is applied to this case. The boundary condition of each wall, inlet and outlet are set up. Then the results are post-processed using ParaView to obtain the temperature contour distribution of shipping container home. Also, EAHE is introduced to enhance the ventilation within the container.

RESULTS AND DISCUSSION

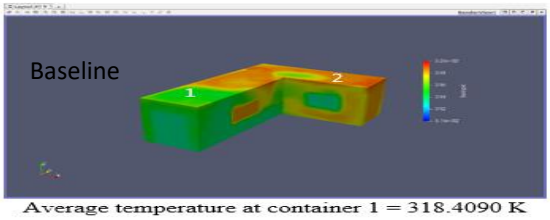

Average temperature at container 1 = 318.4090 K
Average temperature at container 2 = 318.5981 K

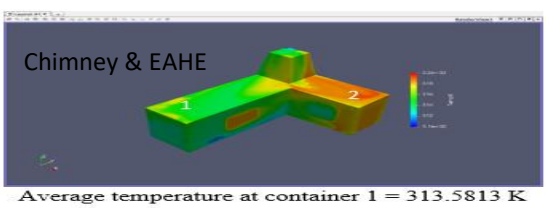

Average temperature at container 1 = 313.5813 K
Average temperature at container 2 = 313.9742 K

Figure 1: Comparison between baseline and chimney with EAHE

Application of chimney and EAHE result 5°C lower in temperature, 2.97% heat reduction and tolerably comfortable environment (PMV≈1) The numerical simulation result is consistent with experimental results from [1].

REFERENCES

[1] Chungloo, S. and Limmeechokchai, B. (2007) 'Application of passive cooling systems in the hot and humid climate: The case study of solar chimney and wetted roof in Thailand', Building and Environment, 42(9), pp.3341-3351.

VERTICAL VANE CURRENT GENERATOR PROTOTYPE PERFORMANCE

Izral Roslan and Adi Maimun Abd Malik
School of Mechanical Engineering, Faculty of Engineering,
Universiti Teknologi Malaysia, 81310 UTM Skudai, Johor, Malaysia

INTRODUCTION

Over the years, the world excessively reliant on diminished non-renewable energy source such as petroleum, natural gas, coal and fossil fuel. Non-renewable is proven very efficient and productive however it's contributed to bad effect, damaging the environment and to human health (Herzog *et al.*, 2001*)*. Optionally, renewable energies such as biomass, wind energy, solar energy, geothermal and water energy provides a good perspective to be an alternative to non-renewable energy such as fossil fuel. As is known that the form of hydropower sources, especially ocean energy, can be categorized into tidal gradients, waves, currents, thermal gradients and thermal cathars (Bedard *et al.*, 2010). Among them, the marine currents present a relatively new and almost unexploited source with a worldwide diffusion of potentially highly-productive sites.

EXPERIMENTAL SETUP

This paper presents an electrical system for a Vertical Vane Current Generator (VVCG) to estimate the power produce by vertical axis marine current turbine so that the power output can increase and generate more electricity. Besides, this paper also presents an estimation of power produce by multi-turbine system. Moreover, the estimation of power produce will compare with the collecting data and measure data from experiment.

RESULTS AND DISCUSSION

For each data and parameter that been set will be calculated to get the power output. Through the MATLAB, there have several that can be collected such as power output, power available, RPM, torque and efficiency for every configuration. So, will discuss the result of a Simulink of velocity and power produce by calculation from the formula set. Other than that, it will discuss the effect that produced from the array configuration either wake effect, blockage effect or turbine interaction effect. This is to ensure that the array configuration will fit perfectly at the selected location and all the limiting factors are fulfilled.

Figure 1 show the power produce for each water velocity. The power produce is increase when the velocity of the water is increase.

Figure 2 shows a comparison between the configuration use. The configuration 6 get the highest power available than the others configuration. The power available for configuration 3 is the lowest.

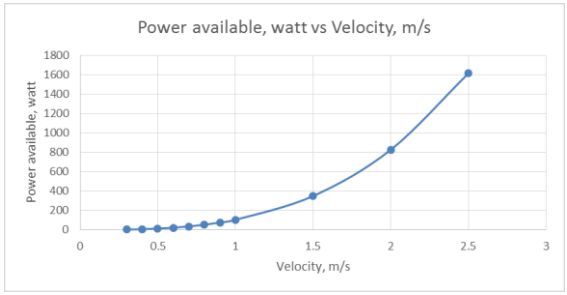

Figure 1: Power available vs velocity.

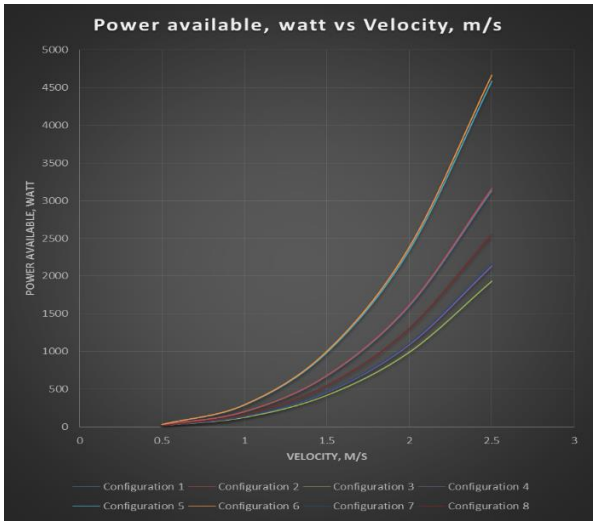

Figure 2: models between control condition

CONCLUSION

The electrical system for a Vertical Vane Current Generator in MATLAB SIMULINK was developed. Power available was calculated respect to water velocity. The electrical energy produced for a multi turbine system were estimated. For 2 Turbines, Configuration 2 and Configuration 1 have high efficiency than others configuration. For 3 Turbines, Configuration 6 get the highest efficiency.

REFERENCES

[1] Herzog, A. V., Lipman, T. E., & Kammen, D. M. (2001). Renewable energy sources. Encyclopedia of Life Support Systems (EOLSS). *Forerunner Volume-'Perspectives and Overview of Life Support Systems and Sustainable Development*.

[2] Bedard, R., Jacobson, P. T., Previsic, M., Musial, W., & Varley, R. (2010). An overview of ocean renewable energy technologies. *Oceanography*, *23*(2), 22-31.

SAILING JONG STABILITY

Ahmad Nasrul Nizam Nassiruddin and Adi Maimun Malik
School of Mechanical Engineering, Faculty of Engineering,
Universiti Teknologi Malaysia, 81310 UTM Skudai, Johor, Malaysia

INTRODUCTION

The resistance of a ship at a given speed is the force required to tow the ship at that speed in smooth water assuming no interference from the towing ship. This total resistance made up of different component, which interact with each other in an extremely complicated way. This research will focus on the evaluation of the performance of sailing Jong stability and propose for its improvements.”

EXPERIMENTAL SETUP

In order to evaluate the stability of Sailing Jong, we need to have all hydrostatic data. We can produce hydrostatic data of Sailing Jong by using software such as Maxsurf stability or using manual calculation in excel. Before we can use Maxsurf or manual calculation, we need to have all offset data of Sailing Jong. From the hydrostatic data that produce, we can calculate for GZ curve and plot in to a graph. From the GZ curve graph, we can evaluate the stability of Sailing Jong by referring to IMO criteria. So that we can determine whether the Sailing Jong is stable or not.

From the offset data that obtain by measuring at MTC, Maxsurf was used to calculate hydrostatic data by assign the offset data as the input. First click on the Maxsurf window and choose marker. After that, click on the marker and choose add marker. Copy and paste all offset data on the marker slot.

RESULTS AND DISCUSSION

GZ curve is the stage to analyse the basic intact stability of Sailing Jong in order to evaluate its stability. The easiest and handiest tool for analysing a surface ship’s stability, is by graphs or curves. By looking on this curve, the stability characteristic can be predicted. Since the stability of a ship can be directly commented on by the nature and value of its metacentric height (GM), a direct method to track the stability of a ship for a range of heel angles would be, to generate a curve that relates this parameter to the angle of heel. Since metacentric height is directly related to the righting lever (GZ) and angle of heel, the curve of static stability is a plot between the righting lever and angle of heel.

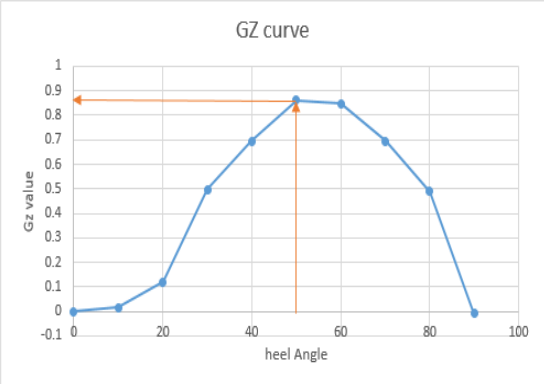

Figure 1: GZ curve of existing Sailing Jong

The above graph is plotted assuming that the ship is in static condition. Some of the important information that can be derived from any GZ curve of a ship are discussed. The maximum righting lever (GZ_{MAX}), represented at 60-degree heel angle, in the graph is proportional to the largest static heeling moment that is required to bring the ship back to its upright position. The value of maximum GZ and the angle at which it occurs, are important values. In other words, the maximum righting lever when multiplied with the displacement of the ship, gives us the value of the maximum heeling moment that the ship can sustain without capsizing. Beyond this angle, the righting lever (in other words, the stability) of the ship decreases drastically.

CONCLUSION

From the analysis, it shows that the Sailing Jong is stable enough since it has all criteria that follow International Marine Organisation, IMO. For this project is still not fully completed since analysis of sail that compute to stability of Sailing Jong is neglected.

REFERENCES

[1] Thompson, J. M. T., Rainey, R. C. T., & Soliman, M. S. (1990). Ship stability criteria based on chaotic transients from incursive fractals. Phil. Trans. R. Soc. Lond. A, 332(1624), 149-167.

[2] Soumya Chakraborty Ship Stability – Understanding Intact Stability of Ships

REDUCTION

OF CONVERSION TIME BY IMPROVING DESIGN OF EJECTION PLATE HOLDER

Seh
Ahmad Illyasya' Seh Omar and Adnan Hassan
School of Mechanical Engineering, Faculty of Engineering,
Universiti Teknologi Malaysia, 81310 UTM Skudai, Johor
, Malaysia

INTRODUCTION

Current manufacturing scenario demands performance of production output [1]. Company should focus on mitigating non-productive time as to remain competitive. The critical element is comprising by quick change. Companies essentials to reduce setup times as well as eliminate wasting time [2]. Quick change refers as changeover or conversion reduction which emphasizes on eliminating or reducing non-value added activities during setup. This helps companies to achieve a great amount of efficiency in a way to change tool from one specification to another.

PROBLEM DEFINITION

Aim to reduce setup time by mitigating repetition work during conversion for ejection station. The bending displacement of fixture need to enhance in order to lengthen life span of good shape of fixture. This allow the fixture to be performed without having repetition during conversion. The process of validating the strength of fixture clamp need to be conducted.

EXPERIMENTAL SETUP

This section presents the experimental setup for validating the fixture. In analyzing the fixture, determining the applied pressure via comparison of model simulation and experiment results. These values involve with strain and displacement where it measures with the instrument of strain gage and linear variables differential transformer (LVDT) respectively. As the pressure value which equivalent to rotation of screw had been achieved, this pressure indicates as reference level for bending displacement. Design of fixture have been improved by using concept of Design of Experiment (DOE) with the measure response of bending displacement. The optimum design is based on the least response for bending displacement.

RESULTS AND DISCUSSION

From the generated result of DOE, the most significant is thickness of clamp and followed by height. By constructing an optimal setting for a new design, the bending displacement could be reduced which shown in the Figure 1. By using the reference pressure which obtained from model simulation, overall bending displacement reduced about 51% from existing design. From the obtained pressure which specified to each level on X-axis of the graph. Both lines are considered linear despite from 0° to 90° which having an exponentially increased. Although the bending displacement is successfully improved, the gap between this clamp continue to develop as from time to time. This is due to the elastic region for clamp only occupied below than 8.79 MPa which is lower than the practical pressure used. The common pressure used by workers are in the range more than 16 MPa.

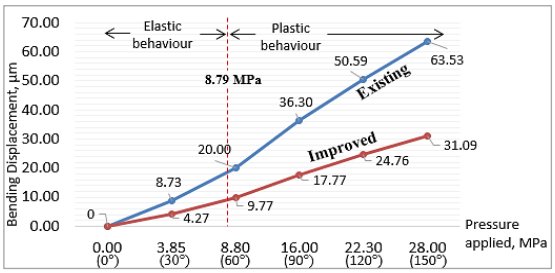

Figure 1: Improvement for bending displacement

CONCLUSION

From improved design, the rate of expanding for fixture clamp is slower compared to existing design. This means the life span with good condition for improved design is extended which results the issues for repetition works can be eliminated for certain period. This can be seen in the Figure 2 with the estimation of 2 years additional. By conducting conversion without having any repetition may reduce the conversion time to 12 minutes per setup.

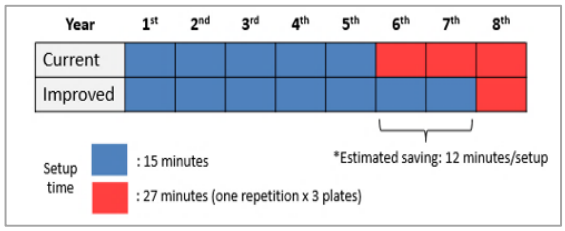

Figure 2: Estimated time saving for conversion

REFERENCES

[1] Arun Abraham, Ganapathi K.N., and Kailash Motwani. (2012). "Setup time reduction through SMED technique in a stamping production line." sasTECH.

[2] C. Rosa , F.J.G. Silva, L. Pinto Ferreira, and R. Campilho. 2017. "SMED methodology: The reduction of setup times for steel wire-rope assembly lines in the automotive industry." Manufacturing Engineering Society International Conference, MESIC. Vigo (Pontevedra): Elsevier B.V. 1034 - 1042.

IMPROVEMENT OF VEHICLE INSPECTION PIT WORKSTATION IN AUTOMOTIVE WORKSHOP

Keeshoban Rao Jagaiah and Adnan Hassan
School of Mechanical Engineering, Faculty of Engineering,
Universiti Teknologi Malaysia, 81310 UTM Skudai, Johor, Malaysia

INTRODUCTION

Inspection works inside the vehicle inspection pit could be considered as one of the most risky and hazardous work at an automotive workshop environment. Workstations in vehicle inspection pit could have many risks and hazards that can lead to unsafe situations to the workers [1, 2]. Any work areas that has holes or pits can cause serious injuries regardless its depth [3].This existence of hazards and risks could be because of poor design of the vehicle inspection pit workstation, working tools or equipment and also poor work practice. This project focuses on identifying the risk and hazards that are present at vehicle inspection pit workstation at an automotive workshop and improve the risk levels using engineering design approach.

METHODOLOGY

The methodology that were used to collect the data in this study was interviews, observation and risk assessment. For the interview, 2 workers had been chosen as respondents. For the observation, a total of 2 rounds of observation was held. The first round was to have a look on the condition of the workstation and second one was to observe the work activities that has been involved. Then risk assessment was done based on condition of workplace and based on the work activity involved. After identifying the problem, a proposal of design was developed using engineering design approach as a solution.

RESULTS AND DISCUSSION

Based on the data collection and data analysis, it was found that the access stairs of the vehicle inspection pit has the highest risk where the worker uses the access stairs to enter and exit the workstation. The results of data analysis can be seen in Figure 1 and Figure 2.

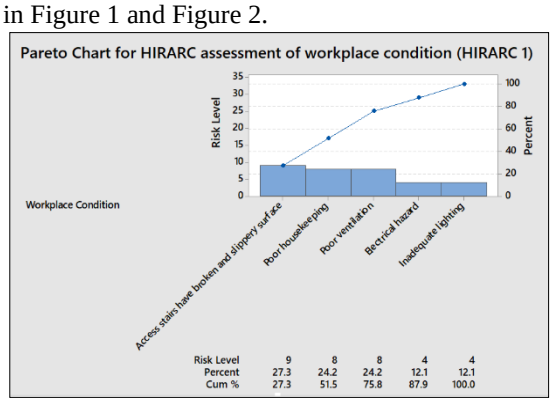

Figure 2: Paretto chart for HIRARC assessment on workplace condition

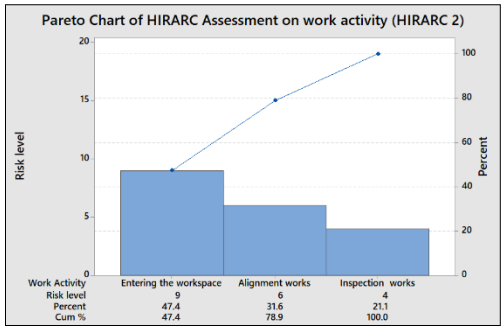

Figure 3: Paretto chart for HIRARC assessment on work activity

To improve the risk level which was identified as the major risk, an elevating platform design was developed to be proposed as an alternative method for the worker to enter and exit the space.The development of the design was done by following the arrangement of steps of engineering design process. Figure 3 shows the Solidworks design which was proposed as the solution.

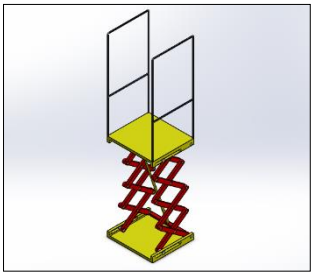

Figure 4: Proposed Design of Elevating Platform

CONCLUSION

In conclusion, the objective of this study which were to identify the risks and hazards that are present at vehicle inspection pit workstation and to propose an improvement of the risk level using engineering design was achieved.

REFERENCES

[1] Health and Safety Executive (2012). Health and safety in motor vehicle repair and associated industries.
[2] Safework SA (2012). Automotive workshop work health and safety guidelines.
[3] Department of Occupational Safety and Health (2007). Guidelines for Preventions of Falls at workplace.

QUALITY IMPROVEMENT IN MARKER MANUFACTURING COMPANY

Muhammad Hasif Mohd Hazardi and Adnan Hassan
School of Mechanical Engineering, Faculty of Engineering,
Universiti Teknologi Malaysia, 81310 UTM Skudai, Johor, Malaysia

INTRODUCTION

Over recent years, the demand of customer for marker product keep increasing. The possibility of rejected rate occur during marker manufacturing are quite high. Therefore, the company wants to have a quick solution on how to handle and reduce the number of defects occur during manufacturing of marker process and increase the quality of product at the same time. Six Sigma methodology has been using throughout this entire project to identify the problem and completing the objective of the case study.

EXPERIMENTAL SETUP

This section presents the steps taken on using DMAIC methodology. Define phase is the first phase of the Lean Six Sigma improvement process. This phase is used to defining project's scope and boundary. 2 tools are used in this project which are voice of customer (VOC) and SIPOC diagram. The second phase is measurement phase which is to evaluate the baseline status of process. This phase is highly data driven because measurement of current state is based on historical data collected. This section include data collection plan and Pareto chart for marker defective rate. Analysis phase is to identify the causes of the problem and selected the root causes with the help of data and analysis. Brainstorming has been done and all the causes and possible has been list down. In this phase, cause and effect diagram is conducted. The fourth phase is the improve phase. This phase is used to improve the current condition by proposing solution that could be a result to decrease the number of reject rate in the company. In this phase, results are obtain. The final phase is the control phase where tools are used to monitor the process to ensure it does not vary from optimized state. The tools used are Statistical Process Control (SPC) and control plan.

.

RESULTS AND DISCUSSION

At measurement phase, data is collected, and Pareto Chart is plotted. It is shown that the highest defective rate occur is at printing process which is an average of 554 unit per day. Thus, this process become the focus of this project for improving the current situation. From the chart, cause-and-effect diagram has been conducted. It is found that the root cause for marker defects in printing process are at the sorting section where the current machine does not sort the marker properly into conveyer which leave the slot empty. This will cause the ink at arm printing to be over spillage and cause defect. For improve phase, a new design is proposed using a more suitable mechanism for maker sorting. It is expected that the new design could reduce the reject rate by 75% of the current reject rate due to the minimization of critical cause in sorting. Figure 1 shows the final design proposed to the company.

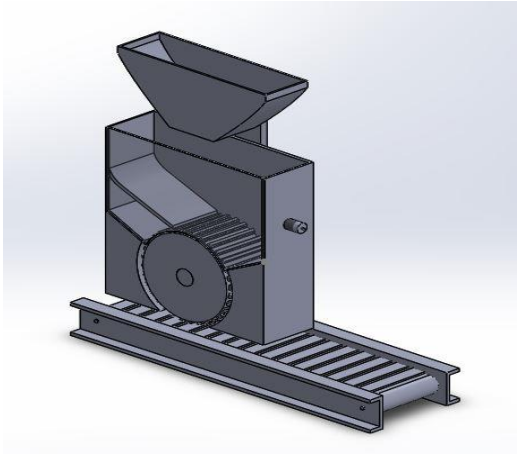

Figure 1: Final Design for marker sorting machine

However, the process control plan could not be carried out due to studies limitation which needs to implement prototype in that company.

CONCLUSION

The project has been completed by using DMAIC methodology. The new design is compared with the current design and the result were satisfied. The reject rate could be decrease and the company could improve the quality of the product and even save up more cost. As a conclusion, the objective of this project has been achieved successfully.

REFERENCES

[1] Chiu, W.-F. (2012). Achieving Quality Improvement In the Mask Manufacturing Industry by Using Six Sigma.
[2] Basavaraj, Y., Sreenivasa P.K.V, & R.N.N.V. (2011). Improvement of process capability through Six Sigma and robus design: Case study at an Indian Steel Manufacturing, International Journal of Industrial Engineering, 18(9), 482-492.
[3] Huertas-Quintero, L. a. M., Conway, P. P., Segura –Velandia D.M & West, A. A (2011). Root cause analysis support for quality improvement in electronics manufacturing. Assembling Automation 31, 38-46.

MECHANICAL TEST AND ANALYSIS OF 3D PRINTED POLYMER ENCLOSURE FOR MEDICAL APPLICATION

Norsyahirah Ali and Aini Zuhra Abd Kadir
School of Mechanical Engineering, Faculty of Engineering,
Universiti Teknologi Malaysia, 81310 UTM Skudai, Johor, Malaysia

INTRODUCTION

Rigorous testing need to be performed because there are a lot of products that need to be recalled. Same goes to the medical device. Based on IEC 60601-1 standard, all medical device need to undergo the testing. For the hand-held enclosure, it need to perform the drop test, push test and mold stress-relief test. Drop test should be performed on hardwood surface with a density >600kg/m3 (Iec and Brousseau, no date). Plastic that undergo push test, not suitable to compress up to 60% (INSTRON, no date). The purpose mold stress-relief test to find the weakness of plastic enclosure [3].

EXPERIMENTAL SETUP

This section presents the experimental setup for all the testing. For sample preparation, the ABS enclosure was designed as previous study and printed using Stratasys uPrint SE Plus 3D Printer. For drop test, it was performed on hardwood surface, Resak wood and drop on it from 1m. The results were complied with the pass-fail criteria. For push test, it was performed using INSTRON 5982 machine using speed 0.5mm/min and compressed up to 1%, 5% and 10% for three sample respectively. While, for mold stress-relief test, placed the enclosure in an oven for 7 hours at raised temperature with the minimum 70°C.

RESULTS AND DISCUSSION

11 ABS enclosure already printed for all testing. For drop test, visual inspection was performed after the testing and the results were complied with the pass-fail criteria. And overall results are failed because most of the list of results were categorized in fail criteria. For push test, the results of testing for three sample were plotted in load-displacement curve as shown in Figure 1.

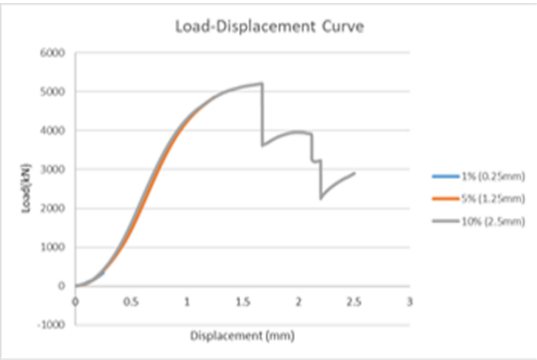

Figure 1: Load-Displacement Curve

The result of push test is passed because the maximum load for the enclosure start to fail is 5.21kN, while the load requires by standard is 250N. for mold stress-relief test, CMM used for measured the deviation on the sample at each part, top, bottom, and battery. Based on the results, it shown that the % of shrinkage and warpage, mostly the highest is sample 5 where the temperature used was 115°C. However, this was not give a huge impact to the enclosure and there is no any big damage. Based on IEC 60601-1, no damage resulting in an unacceptable risk(A and Forest, 2013). So, the result is passed.

CONCLUSION

The performance of 3D printed polymer enclosure successfully analysed using mechanical test (mold stress-relief test, push test, and drop test). The tests results indicated that the enclosure passed the mold stress-relief test with temperature of 70°C, 85°C, 100°C, 115°C and melts at certain edges when reaches 115°C. Next, the enclosure passed the push test with the results of test were more than the requirement of standard. While, the enclosure failed the drop test due to poor mounting and snap fit of design. As recommendation in the future, improvement focus on the snap fit, cover battery pattern, and change the snap fit to use screw as connection.

REFERENCES

[1] Iec, M. and Brousseau, M. (no date). Major IEC 60601-1 3rd Ed. Changes. 1(978).
[2] Compression Test. https://www.instron.us/en-us/our-company/library/test-types/compression-test (Accessed: 25 March 2019)
[3] Whitepaper, W. (2018). Understanding the Mold Stress Test.
[4] A, I. T. S. N. and Forest, L. (2013). Medical electrical equipment Part 1 : General requirements for basic safety and essential performance. pp. 1–147.

DESIGN AND ANALYSIS OF A PLASTIC PACKAGING FOR MEDICAL DEVICE OPTIMIZATION

Choo Zi Qi and Aini Zuhra Abdul Kadir
School of Mechanical Engineering, Faculty of Engineering,
Universiti Teknologi Malaysia, 81310 UTM Skudai, Johor, Malaysia

INTRODUCTION

Plastic material has been widely used in packaging application. Other than acquire unique properties, plastic are widely used in different range of temperatures, are resistant to chemical and light as well as very strong and tough[1]. The purposes of packaging are for shipment and storage of sensitive items[2]. Packaging displays the items inside[3] at the same time it ensures the authenticity by preventing the access to the device packaged. Packaging as protection to the packaged items from damage[4] and conforms to the product standard of the manufacturer(4). In medical field, packaging is important to maintain sterilization[5] to reduce the rate of infections in hospitals and other healthcare settings[6].

EXPERIMENTAL SETUP

Vacuum forming is performed by using Formech 300XQ to fabricate a designed plastic packaging for medical device. Polyvinyl chloride (PVC) and High Impact Polystyrene (HIPS) plastic sheets were used to study and make comparison on the effects of materials in manufacturability. A Computer Aided Design (CAD) SolidWorks was fully utilized in the design activity as an additive 3D machine FLASHFORGE was used to print out the mould of the illustrated. The prototypes were tested the functionality and performance by carried out packaging testing methods-visual inspection and drop test.

RESULTS AND DISCUSSION

Webbing is one of the major defects of vacuum forming due to absence of draft angles at the corners and the excessive material in the small mould, depth of mould is too depth from its surface as well as the vertical angle of the compartment from the surface. Thinning of wall of spray bottle compartment is another defect that is observed in PVC plastic plackagings due to the formation of the plastic sheet in order to conform to the shapes and depth of a mould. Both PVC and HIPS plastic packagings tend to have misalignment issue due to absence of jigs to secure the moulds. Besides, the occurrence of blunt corner is due to the vent holes are not ideally located, hence the evacuation of air during vacuum forming is affected and cause the rate of drawing the plastic sheet to be slower and inefficient. HIPS plastic packaging has shrinkage defect and size variations.

The impact of falling mostly affect the dropped packaging at the edges. The big surface areas of both top and bottom side of packaging allows even distribution of impact on the packaging when hitting on the hardwood and cause no flipping. The inspection of the condition of inner packaging and items packaged shows that PVC plastic packagings tend to deform and crush due to the impact of because the strength of the PVC plastic sheet which is not rigid and hardly to stand when holding the spray bottle and medical device because absence of reinforcement rib for strengthening. Besides, the deformation of the PVC is due to the poor structural integrity caused by thinning on the wall of the wall of the packaging. Thin material of PVC allows it to absorb the impacts and lead to the deformation of the plastic packaging results the soft impact and no rebound on the PVC plastic packaging. HIPS plastic packagings has no effect after the drop test which means the energy is penetrated by the packaging due to the hard impact.

CONCLUSION

The thin PVC plastic packaging is recommended for single-use purpose to protect the medical items during transition due to its low material cost yet capable to provide protection to the packaged items. While HIPS plastic packaging is suggested for multiple usage because of its good rigidity and strength. However, the rigid HIPS plastic packaging is poor in impact absorption and may lead the packaged items to indirectly receive the impact when dropping.

REFERENCES

[1] Andrady AL, Neal MA. Applications and societal benefits of plastics. Philosophical Transactions of the Royal Society of London B: Biological Sciences. 2009;364(1526):1977-84.
[2] Merrill KV. Reversible snap dome container package. Google Patents; 1994.
[3] Campbell J, Kaniewski J, Milburn S, Toma J. Chip clamshell packaging. Google Patents; 2003.
[4] Glenn S, Turner R. Packaging system for medical devices. Google Patents; 2007.
[5] Landis LR. Medical packaging. Google Patents; 2010.
[6] LLC U. Validating Medical Device Packaging. 2016.

RISK MANAGEMENT ASSESSMENT OF A MEDICAL DEVICE BASED ON ISO 14971 STANDARD

Siti Nurasyikin Ramlan and Aini Zuhra Abd Kadir
School of Mechanical Engineering, Faculty of Engineering,
Universiti Teknologi Malaysia, 81310 UTM Skudai, Johor, Malaysia

INTRODUCTION

The number of injury is increased year by year which leads to death, life threatening, disability and hospitalization. This shows that medical device should undergo rigorous assessment and following strict regulations and procedures. Risk assessment is a compulsory step for any product development in order to get the approval of Medical Device Authority (MDA) and Standard and Industrial Research Institute of Malaysia (SIRIM) before entering commercialization in Malaysia. For medical device, risk assessment must be compliance by ISO 14971 standard. So, this may be a big challenge for medical device manufacturer to get the approval from the MDA and SIRIM.

METHODOLOGY

The risk assessment was using Failure Mode and Effect Analysis (FMEA) technique and conducted among the expertise person in this project. Expert opinions involve in giving the rating of Severity (S) and Occurrence (O) for the potential failures that may occur for the device. So, from this rating, risks prioritization should be calculated by multiple the S and O. Then, the risks should be categorized into low, medium and high risk. Then, the improvements and control measure should be suggested and implemented to the high risks and medium risks. Hence, the Risk Management File should be developed based on the results of FMEA and DFMEA analysis.

RESULTS AND DISCUSSION

Based on the (Carlson, 2017), it states that the prioritization of risks by multiple S and O rating. This called as "criticality". So, this technique of prioritization of risks was used for this research.

Table 1 shows the summary of the results from the FMEA analysis. The green colour means low risk which is the acceptable risk that did not need any control measure. Then, for yellow means medium risk where the control measure should be provided and red is high risk in which the improvement should be suggested and implemented to reduce the risk. (Grzegorz, Mianowski, Rosołek, & Gołaszewski, 2017) said that the preventive actions taken have allowed to reduce the level of risk to the acceptable level (average and low level of risk).

The high risk that obtained from the FMEA analysis was the snap fit lock hinge of the battery cover is broken. This is because the current design that being used not suitable with the material used. We decide to change the design of the battery cover into the slide battery cover concept.

Table 1: ***Summary of FMEA Results***

Step No	Failure	Critical Number
2	Snap fit lock hinge broken	25
1b	Sharp edges	4
3a	Cable ease to elongate	12
3b	Weak cable joint with steel plate	9
4b	inappropriate knob size and shape	12
6b	Sponge easy to detach from electrode	9
7a	Poor gel absorption	9
7b	Sticky condition	9
10	Sudden current surge flow	9
13	Electrode may drop easily	12
1a	Device drop	2
4a	Overturn/under turn due to loose knob	1
4b	knob easy to detach	1
5	button switch on broken, unable to withstand repeated pressing	1
6a	sponge easy to detach from electrode	1
8	Inaccurate electrode position	1
9	Unstable current quality resulting longer setting	1

CONCLUSION

Analysis of FMEA has been conducted and the risks categorizations have been identified. The improvement and control measure have been provided and implemented for high and medium risk to ensure the risk is reduced. Lastly, the Risk Management File has been developed according to the results of FMEA.

REFERENCES

[1] Carlson, C. S. (2017). Is there a better way than RPN? Retrieved 29 April 2019, from https://www.weibull.com/hotwire/issue202/fmeacorner202.htm

[2] Grzegorz, K., Mianowski, K., Rosołek, R., & Gołaszewski, T. (2017). Risk assessment on spine corrector.pdf.

AUGMENTED REALITY TRAINING GUIDE OF A PRODUCT ASSEMBLY LINE -AN INDUSTRIAL CASE STUDY

Tan Wei Pin and Aini Zuhra Abdul Kadir
School of Mechanical Engineering, Faculty of Engineering,
Universiti Teknologi Malaysia, 81310 UTM Skudai, Johor, Malaysia

INTRODUCTION

The industry revolution 4.0 is changing the landscape of manufacturing industry. The revolution is increasing complexity of manufacturing process. The operators of modern industrial plants face additional challenges because of the increased complexity Nazir et al. [1]. Due to increasing complexity of the manufacturing process, the traditional training for the new operator is no longer effective. The skill gap between the experienced operator and new operator is an issue for most of the manufacturing industry. The case study company faces the same problems. The company is one of the leading bus body manufacturers and bus assemblers However, the skill transfer process can be improved by the contemporary technology which is AR application

EXPERIMENTAL SETUP

The methodology of this study was referred to [2]. This methodology is systematic and suitable for the selected case study. By referring to the Figure 3, the methodology is started with the concept development of AR application. The several concepts of AR application need to be designed and proposed to the process engineer. The process engineer is responsible to rate the concepts of application base on criteria, if rating of the concepts is lower than average rating, the new design of AR concept must be proposed again. The purpose of this step is to find the best concept of AR application that is most suitable to the case study. Next, the step is assembly process selection to select the assembly process that is fit on this final year project. There are many processes that can implement AR application. However, due to the constraint of time of this final year project, the process must be optimum in considering the time constraint and its effectiveness of implementation. If rating of the processes is lower than average rating, other processes must be proposed.

An evaluation is conducted by using that a common quantitative method and questionnaires [3]. The quantitative method is collecting time taken to complete the assembly and number of human errors in the assembly process with the augmented reality guide and manual work instruction guide respectively. Besides, the qualitative analysis is used which is questionnaires to assess the experience of the users. The questionnaire was developed based on the questionnaire used in and aims at assessing acceptability in the aspects of ease-of-use, satisfaction level, and approval.

RESULTS AND DISCUSSION

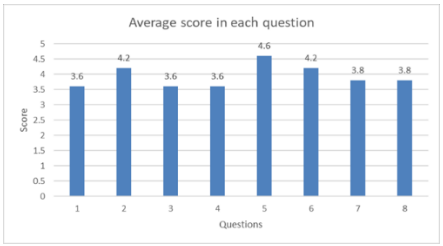

Figure 1: The average score in each question

From Figure 1, the highest average score is question 5 which its scoring is 4.6. Referring to Table 1. question 5 is used to analyze comprehensiveness of AR application. The highest scoring in question 5 indicates that the AR application has high level of understand presentation of the content to the workers. Besides, question 2 and question 6 have the same average score 4.2 achieving second highest average score. The question 2 is to analyze the helpfulness of AR application to solve the current issues in the assembly process.

Table 1: Experience survey question

No	Experience survey questions
1	The system was user friendly and ergonomic
2	AR system was helpful to solving the issues in this assembly process
3	It was easy to interact with the system.
4	It was enjoyable to use the system.
5	I found the AR system easy to understand
6	I found it easy to use the AR system to complete the assembly process.
7	I felt that I performed quickly with the AR system.
8	If I had to use an AR system like this on a regular basis, this is a technique I would appreciate having available.

Table 2: Comparison of time taken and improvement summary

Parameters	Experienced worker	New worker
Assembly cycle time with work instruction manual guide, minute	46	93
Assembly cycle time with AR guide, minute	22	43.33
Improvement in time, minute	24	49.67
Improvement in percentage, percent	52.17	53.41

By referring to Table 2, the improvement in cycle time on both experienced workers and new workers are up to 50 percent. On experienced workers, the cycle time is reduced from 46 minute to 22 minute and reduction is 24 minutes. On the new worker, the cycle time is reduced from 93 minute to 43.33 minute and the reduction is 49.67 minutes. The percentage of cycle time improvement on the experienced workers are 52.17 percent while on the new workers is 53.47 percent. The percentage of cycle time improvement on the new workers is slightly higher than experienced workers, it indicates that the AR application is more effective on the new worker, Hence, it directly indicates that the AR application can be the training kit for the new workers.

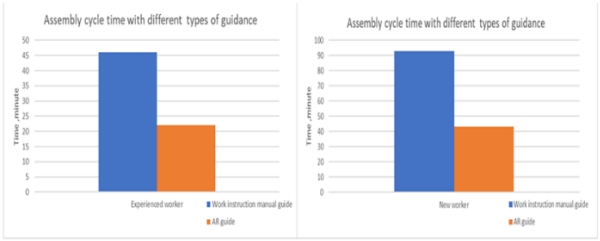

Figure 6:(a) Efficiency of experienced worker using two different types of guidance(b) Efficiency of new worker using two different types of guidance

By referring to Figure 6(a) and Figure 6(b)both figures show that the AR application can significantly reduce the assembly cycle time. In the Figure 6(b), the Figure shows that the AR application can reduce the assembly cycle time for new worker. This result indicates the AR can be the training kit to guide the new workers to work

Based on the results, the developed prototype of AR application can improve the assembly process. One of the improvements is shortening the cycle time of assembly process which similar with findings in [4]. One of the findings of the paper is that the AR application shorten the cycle time to perform the assembly processes. Another justification to valid the comparison of result is that the concept of AR in the mentioned is similar with of prototype of this case study project. Both prototypes are is applying handheld tablet or big screen of mobile phone to deploy the AR application with overlay display. Moreover, [5] support results that the AR application can speed up performance in works.

CONCLUSION

The prototype of AR-based instruction manual is successfully developed. The demonstrated functionality of the AR application has great potential to experienced workers as well as new workers to use it as training kits. Besides, it also increases the understanding level of the work procedures of an assembly process.

REFERENCES

[1] Nazir, S., & Manca, D. (2015). How a plant simulator can improve industrial safety. Process Safety Progress, 34(3), 237-243. [2] Neumann, N., & Kubler, A. (2003). Training locked-in patients: a challenge for the use of brain-computer interfaces. IEEE Transactions on Neural Systems and Rehabilitation Engineering, 11(2), 169-172.

[2] Ong, S., & Wang, Z. (2011). Augmented assembly technologies based on 3D bare-hand interaction. CIRP Annals-Manufacturing Technology, 60(1), 1-4

[3] Syberfeldt, A., Danielsson, O., Holm, M., & Wang, L. (2015). Visual assembling guidance using augmented reality. Procedia Manufacturing, 1, 98-109.

[4] Webel, S., Bockholt, U., Engelke, T., Gavish, N., Olbrich, M., & Preusche, C. (2013). An augmented reality training platform for assembly and maintenance skills. Robotics and Autonomous Systems, 61(4), 398-403.

[5] Syberfeldt, A., Danielsson, O., Holm, M., & Wang, L. (2016). Dynamic operator instructions based on augmented reality and rule-based expert systems. Procedia CIRP, 41, 346-351.

DEVELOPMENT OF AIRLINER PASSENGER SEAT (V2)

Izzuwan Mohamad Saufi and Ainullotfi Abdul Latif
School of Mechanical Engineering, Faculty of Engineering,
Universiti Teknologi Malaysia, 81310 UTM Skudai, Johor, Malaysia

INTRODUCTION

Over recent years, there has been an explosive growth of passenger to 8.2 billion in 2037 as China will monopoly the market in the next ten years [1]. The space saving concept that become a trend for airlines operator is achieved by increase the density of the number of seat in one aircraft. The increase number of seat has increase the weight of the aircraft which not only consume a lot of fuel but it also contributes to the emission of greenhouse gas [2].

METHODOLOGY

The process of designing is divided into three sections where is start with preliminary design, strengthen design and topology design. All the design process is done in SolidWorks which focus on the primary structure of the aircraft passenger seat.

For the FEA section, the simulation is done in Abaqus software with focusing into three different load condition which are 9G, 4G and 6G which based on SAE AS8049(A) requirements. The mesh convergence study as the final step to ensure that maximum stress is produced. In this paper, the deflection of the structure are also being recorded to ensure that the value of the deflection is not too high.

RESULTS AND DISCUSSION

For the 9G load condition (Figure 1), the mesh sensitivity study shows that seat rest has a good converging result. At the number of elements at 314961, the maximum stress 198.3 MPa and the safety factor is at 1.772. The deflection also of the rod shows the small value which around 3.91mm which is still not huge change that can affect the structure.

Figure 2 shows the 4G load condition as the mesh sensitivity study show that it converges nicely. At the number of elements of 775907, the maximum stress produced is 205.75 MPa and the deflection on the seat frame is 2.18mm which still does not in a big scale.

For Figure 3, the mesh density or number of elements for the seat pan is quite high compared to the seat rest. This is due to the large coverage area for the element to occupied. The number of element increases alongside the value of maximum stress. At the maximum stress, the stress that simulates is 104.3 MPa with the 3801936 of mesh density. The deflection of the seat pan also shows the minimum change of circular rod which is around 0.3765 mm.

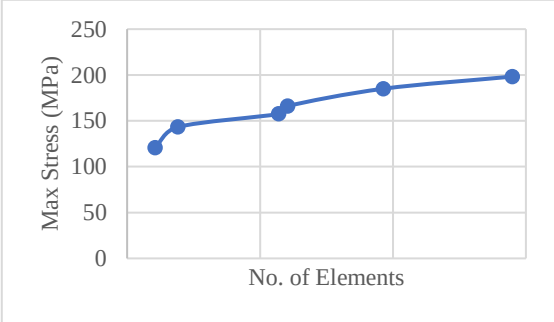

Figure 1: Mesh convergence for seat rest at 9G load condition

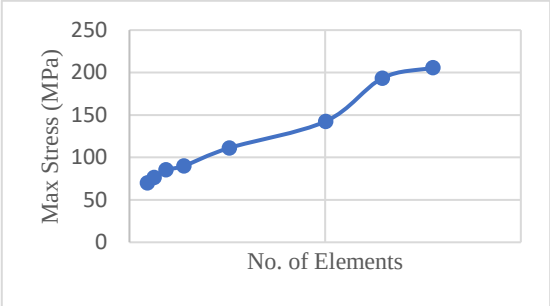

Figure 2: Mesh convergence for seat rest at 4G load condition

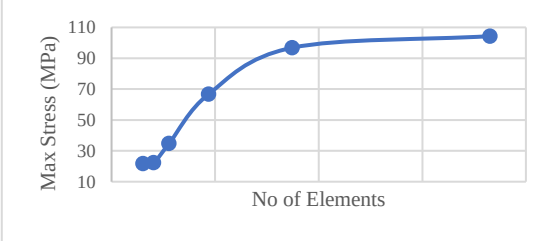

Figure 3: Mesh convergence for seat rest at 4G load condition

CONCLUSION

The minimum safety factor requirement for all load conditions are still above minimum 1.5 and the weight of the structure followed the needed of lightweight seat.

REFERENCES

[1] IATA. (2018). IATA Forecast Predicts 8.2 Billion Air Travelers in 2037. IATA - IATA Forecast Predicts 8.2 Billion Air Travelers in 2037, www.iata.org/pressroom/pr/Pages/2018-10-24-02.aspx.

[2] Lee. (2017). An MCDM approach for selecting green aviation fleet program management strategies under multi-resource limitations.

COMPARATIVE STUDY BETWEEN CONVENTIONAL AND CONTINUUM SHELL FINITE ELEMENTS FOR CARBON LAMINATES

Patrick Sujang Anak Abing and Ainullotfi Abdul Latif
School of Mechanical Engineering, Faculty of Engineering,
Universiti Teknologi Malaysia, 81310 UTM Skudai, Johor, Malaysia

INTRODUCTION

The objective of the study is to compare between behaviour in term of theoretical formulation, definition and the end results on Conventional and Continuum shell element by improving the limitation and finally applied to carbon laminates case. Continuum defies it shell by nodal geometry whereas conventional shell is on the mid plane as the reference. Both uses Kirchhoff and Reissner Midlin assumption and compute it mathematical formulation. On the conventional it reduce the effect of transverse shear while the continuum model base on the nodes and later shell thickness. Reduce integration is use to improve locking and modelling of composite on multiplies on continuum and single layer on conventional shell. Economically, conventional shell is a good investment but continuum is good accuracy.[1]

EXPERIMENTAL SETUP

Beam problem of 2 plies and 3 point bending problem on 12 plies oriented symmetrically is the cases studied. Processing of the element in term of applying defining the geometry, interaction, boundary condition, meshing of both cases. The mesh convergence study also computed and the data is plotted. 4.4822N is applied on beam problem throughout the shell element and 70 N is applied on the continuum. Load and displacement is also plotted on 3 point bending by increasing the load to 210, 300, 350 and 480 N. the gradient equation is plotted for the gap between the continuum and conventional result. The CPU for convergence study, number of element and the stress and displacement and the storage size is obtain and plotted

RESULTS AND DISCUSSION

For beam problem, the modelling using continuum shell has more accuracy than conventional shell in term of its displacement as verified by [2] in his experiment. This inaccuracy is result of the conventional shell overestimate the effect of transverse stress and the transverse shear. The continuum shell also from both problem uses more time, space and elements than conventional shell in Figure 1 a reason on this is that continuum shell uses a node geometry so the formulation is much bigger than conventional shell.

Load against displacement result is plotted, both continuum and conventional show an almost linear graph and presented a numerical ratio that can be formulated its equation. In this case, we are able to improve the accuracy of conventional shell by formulating the gradient ratio and a new gradient ratio equation. As for this most of the stress and strain and load and displacement before the failure to plasticity the elastic curve, the result of continuum can be predicted as in Figure 2.

$$y = 53.28\% (x) + x \quad (1)$$

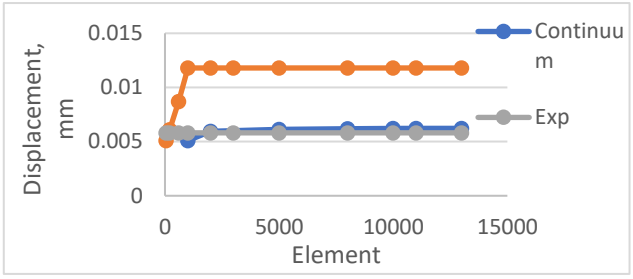

Figure 1: Beam Problem of its displacement.

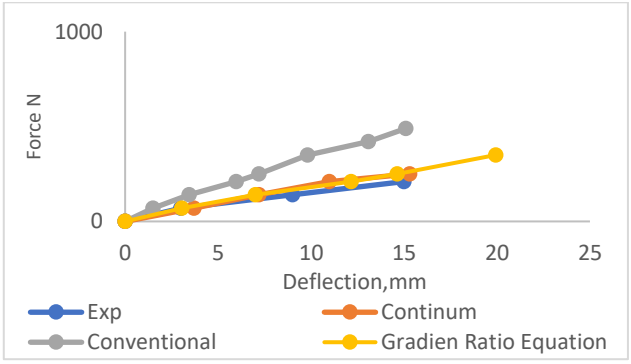

Figure 2: Elastic Curve of continuum and conventional shell

CONCLUSION

Conventional shell can be modelled and the huge gap to the continuum shell result can be formulated so that we can use shell element with any bucklessness. Conventional show is loss in accuracy but improve by the ratio of 53.28%

REFERENCES

[1] Koutromanos, I., Fundamentals of Finite Element Analysis: Linear Finite Element Analysis. 2018: John Wiley & Sons.

[2] Stemple, A.D. and S.W. Lee, Finite-element model for composite beams with arbitrary cross-sectional warping. AIAA journal, 1988. 26(12): p. 1512-1520.

COMPARATIVE STUDY BETWEEN CONVENTIONAL AND CONTINUUM SHELL FINITE ELEMENTS FOR CARBON LAMINATES

Patrick Sujang Abing and Ainullotfi Abdul Latif
School of Mechanical Engineering, Faculty of Engineering,
Universiti Teknologi Malaysia, 81310 UTM Skudai, Johor, Malaysia

INTRODUCTION

The objective of the study is to compare between behaviour in term of theoretical formulation, definition and the end results on Conventional and Continuum shell element by improving the limitation and finally applied to carbon laminates case. Continuum defies it shell by nodal geometry whereas conventional shell is on the mid plane as the reference. Both uses Kirchhoff and Reissner Midlin assumption and compute it mathematical formulation. On the conventional it reduce the effect of transverse shear while the continuum model base on the nodes and later shell thickness. Reduce integration is use to improve locking and modelling of composite on multiplies on continuum and single layer on conventional shell. Economically, conventional shell is a good investment but continuum is good accuracy.[1]

EXPERIMENTAL SETUP

Beam problem of 2 plies and 3 point bending problem on 12 plies oriented symmetrically is the cases studied. Processing of the element in term of applying defining the geometry, interaction, boundary condition, meshing of both cases. The mesh convergence study also computed and the data is plotted. 4.4822N is applied on beam problem throughout the shell element and 70 N is applied on the continuum. Load and displacement is also plotted on 3 point bending by increasing the load to 210, 300, 350 and 480 N. the gradient equation is plotted for the gap between the continuum and conventional result. The CPU for convergence study, number of element and the stress and displacement and the storage size is obtain and plotted

RESULTS AND DISCUSSION

For beam problem, the modelling using continuum shell has more accuracy than conventional shell in term of its displacement as verified by [2] in his experiment. This inaccuracy is result of the conventional shell overestimate the effect of transverse stress and the transverse shear. The continuum shell also from both problem uses more time, space and elements than conventional shell in Figure 1 a reason on this is that continuum shell uses a node geometry so the formulation is much bigger than conventional shell.

Load against displacement result is plotted, both continuum and conventional show an almost linear graph and presented a numerical ratio that can be formulated its equation. In this case, we are able to improve the accuracy of conventional shell by formulating the gradient ratio and a new gradient ratio equation. As for this most of the stress and strain and load and displacement before the failure to plasticity the elastic curve, the result of continuum can be predicted as in Figure 2.

$$y = 53.28\% (x) + x \qquad (2)$$

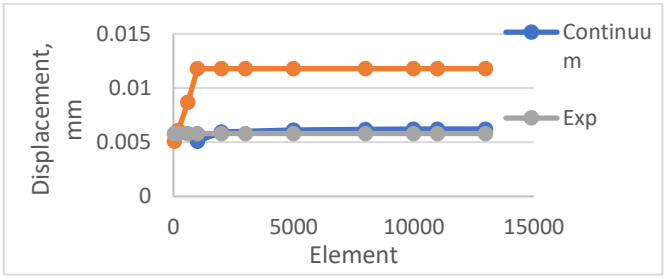

Figure 1: Beam Problem of its displacement.

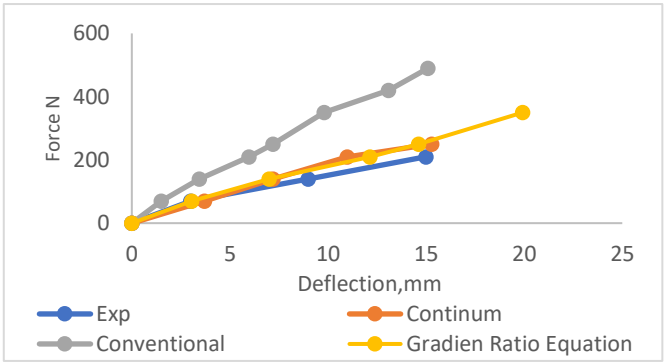

Figure 2: Elastic Curve of continuum and conventional shell

CONCLUSION

Conventional shell can be modelled and the huge gap to the continuum shell result can be formulated so that we can use shell element with any bucklessness. Conventional show is loss in accuracy but improve by the ratio of 53.28%

REFERENCES

[1] 1. Koutromanos, I., Fundamentals of Finite Element Analysis: Linear Finite Element Analysis. 2018: John Wiley & Sons.

[2] Stemple, A.D. and S.W. Lee, Finite-element model for composite beams with arbitrary cross-sectional warping. AIAA journal, 1988. **26**(12): p. 1512-1520.

MECHANICAL CHARACTERIZATION OF POROUS IRON SCAFFOLD

Mohd Faez Fadzil and Amir Putra Md Saad
School of Mechanical Engineering, Faculty of Engineering,
Universiti Teknologi Malaysia, 81310 UTM Skudai, Johor, Malaysia

INTRODUCTION

Nowadays, the bone graft has high demand and the donator less .Therefore many augment bone repair and regeneration requires a bone graft or scaffold. The engineer has create the synthetic bone graft. Among materials for bone platforms, metallic biomaterials, for example, stainless steel, cobalt-chromium alloys, and titanium alloys are the ones most utilized when a mechanical load is available. However, despite their high mechanical strength and fracture toughness [1], the hardness can make the bone broken. This disadvantage has open the new era in biodegradable metals.

The metal is iron, zinc alloys, magnesium and its alloys are the most investigated biodegradable metals for their potential application as biomedical implants this metal and its alloys possess interesting mechanical properties similar to that of human bone.

METHODOLOGY

The firs method, using Solidworks to draw 3 model bone scaffold. This 3 model has different porosity which is 20%,40% and 60%.Then using section technique for to get the section every increment 0.025mm.Using this section image in Image J. Using Image J is to calculate the BV/TV,Tb.Th and Tb.Sp. lastly, using abaqus for finite element analysis. Using this, must put the mechanical properties, displacement, and size global .Then it can simulate the model.

RESULTS AND DISCUSSION

Figure 1 shown that model A is the highest between two models. From this model
A has highest modulus. It mean that the decreasing BV/TV will affect the modulus and modulus also decreasing.
From other aspect, model C has the highest porosity than two model. From this model C has the lowest modulus. It mean the increasing porosity will affect the modulus and modulus will decreasing.

Figure 2 shows modulus has decreasing. This happen because it stiffness has decreasing. This decreasing happen because 4 model has different morphological characteristic and parameter. The highest porosity will affect the modulus, stiffness and area under the graph.

model	BV/TV	porosity	modulus
A	0.806	20%	12725.69
B	0.608	40%	12340.09
C	0.403	60%	11967.70

Figure 1: The relation BV/TV and porosity with modulus

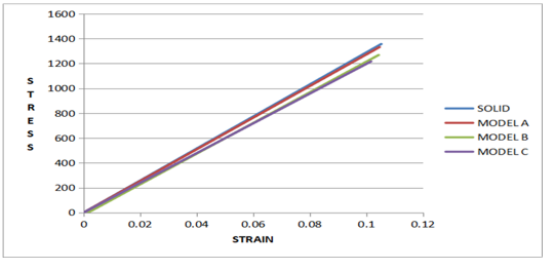

Figure 2: Stress vs Strain

CONCLUSION

We have shown the highest porosity will have the smaller value of modulus. Hence, morphological indices will affect the mechanical properties.

REFERENCES

[1] X. M. Liu, S. L. Wu, K. W. K. Yeung, Y. L. Chan, T. Hu, Z. S. Xu, X. Y. Liu, J. C. Y. Chung,

INFLUENCE OF POROUS ARCHITECTURE TOWARDS THE MECHANICAL PROPERTIES OF POROUS IRON FOR BONE REPLACEMENT

Ahmad Nabeel Hakimi Roslan and Amir Putra Md Saad
School of Mechanical Engineering, Faculty of Engineering,
Universiti Teknologi Malaysia, 81310 UTM Skudai, Johor, Malaysia

INTRODUCTION

Tissue engineering can provide solutions that can replace the currently used tissue repair solutions including transplants, surgical reconstruction and mechanical devices. In addition, the need of effective regenerative treatment is on the rise pertaining to the rapidly aging population, growing lifestyle disorders such obesity, diabetes and growing in trauma cases. Bone scaffold were created by a wide scope of the biomaterials. Rather than metallic biomaterials, others than that have been created is unsuitable for load bearing purposes [1]. By utilizing load bearing bone scaffold, patients will ready to speed up in performing out their every-day lives exercises which could likewise add to a superior mending process [2].

METHODOLOGY

For this study, a methodology of experiments were done by using only the facilities provided at Faculty of Mechanical Engineering Universiti Teknologi Malaysia. By following instructions and safety guidelines, all the experiments were done successfully and safely as no injury at all has been reported. The mechanical testing is conducted in this study to investigate the mechanical properties of iron porous scaffold of 20%, 40% and 60% porosity. The properties and the characteristics such as stress, strain, young modulus, yield strength and compressive strength value are to be investigated in this study. Compression test was performed using a universal testing machine (The FastTrack 8874, Instron, Norwood, USA). The mechanical properties of the porous Fe specimens before and after the immersion tests were evaluated under the compression test, at a strain rate of 0.005mm/s untill 30% strain. The Compressive strength, Yield strength, and Young's modulus were determined as per the ASTM D1621 and ISO 844 standards. Three repetitions were done.

RESULTS AND DISCUSSION

In Figure 1, the stress strain curve of solid and porous Iron under the compression test at different porosity is shown. All of the graph show the behavior of ductile material, the resulting strain is proportional to the magnitude of the forces. The straight-line implies that stress and strain share a linear or direct relationship throughout elastic region, the material obeys the Hooke's law. Beside, point at the end of the elastic region is called the proportional limit because beyond this point, stress and strain cease to share their linear relationship. Solid sample also compressed to set as a benchmark to another sample. The trend of the graph show the decreasing value of stress as the level of porosity increased. The average difference in Young's modulus for all sample as the level of porosity increase is observed to be big. The effect of different porosity has greatly affect the Young's modulus of Iron. From the stress strain curve the value of Yield strength also can be obtained. First, yield point for every sample has shown on the curve. Yield point is the point on a stress strain curve that indicates the limit of elastic behavior and the beginning of plastic behavior. The highest compressive strength obtained from the experiment is Solid sample that is 612.62 Mpa and the lowest value of compressive strength is Sample C, 183.40 Mpa.

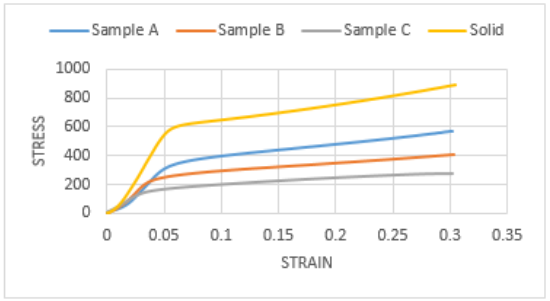

Figure 1: Stress strain curve for solid and porous sample

CONCLUSION

The different porosity level used showed significant decrease in mechanical properties of the porous Iron. We have exhibited that the level of porosity may be used as a dependent parameter to evaluate bone structure and adds to the predictive power of porosity to clarify the Young's modulus, Yield strength and Compressive strength of human cancellous bone. Besides, this method requires further approval over a more extensive range of porosities and cancellous bone tissues, its potential has been demonstrated.

REFERENCES

[1] S. Wu, X. Liu, K.W.K. Yeung, C. Liu, X. Yang, Biomimetic porous scaffolds for bone tissue engineering, Mater. Sci. Eng. R Reports. (2014) 80 :1–36

[2] M.B. Schaffler, W.Y. Cheung, R. Majeska, O.Kennedy,Osteocytes: Masterorchestrators of bone, Calcif. Tissue Int. (2014) 94 :5–24

MECHANICAL PROPERTIES OF SOLID FREE FORM SCAFFOLDS FOR CANCELLOUS BONE

Luqman Haqim Neza and Amir Putra Md Saad
School of Mechanical Engineering, Faculty of Engineering,
Universiti Teknologi Malaysia, 81310 UTM Skudai, Johor, Malaysia

INTRODUCTION

Over recent years, magnesium material has been centre of interest as the most suitable material for cancellous bone replacement. This is because it satisfies the requirement for bone remodelling which are allows new tissues growth which is from the structure porosity, have load bearing function as well as allow nutrient transport. Porous pure magnesium is a good material for bone replacement because the mechanical properties of the material can be manipulated close to mechanical properties of cancellous bone [1].

Major different on the mechanical properties of the material with the bone can only cause to failure. Very high young's modulus than the one can cause stress shielding in the bone as the stiffer material tend to handle all the load and prevent the load from reaching throughout the whole bone and making the bone become weaker and not fully develop. This is because, bone will develop in response to the load it is placed under according to Wolff's law [2].

EXPERIMENTAL SETUP

This section presents the simulation setup for the system. We used SolidWorks for CAD modelling and Abaqus for finite element analysis. The CAD model need to have high porosity (20% - 95%) in order to satisfy mimicking cancellous bone. During initialize of Abaqus, pure magnesium properties is inserted which are density of 1.74E-9, Young's Modulus is 3500MPa and poison ratio of 0.35. As for boundary condition, the bottom of the model need to be fixed (Encastre) and the top of the model will undergo displacement.

RESULTS AND DISCUSSION

At the end of compression test simulation, a graph of strain-stress curve plotted in order to determine the young's modulus of each models. The stress – strain curve shows only on the elastic region as it is the only region we interested. Figure 1 shows the young's modulus of each models. Based on the trend alone, it shows decreasing trend as the smaller size geometry tend to have higher young's modulus. For bulk, it shows similar trend toward unit cell.

To observe the different young's modulus between the models, we can explain from Hooke's Law equation ($\sigma = \varepsilon E$) [3]. The Hooke's law can be manipulated and have directly proportional to the stiffness as the smaller size geometry tend to be stiffer compare to bigger size. The compressive strength is determines using Von Mises Stress Criterion as shown in Figure 2 as smaller geometry need more energy in order for the model to deform.

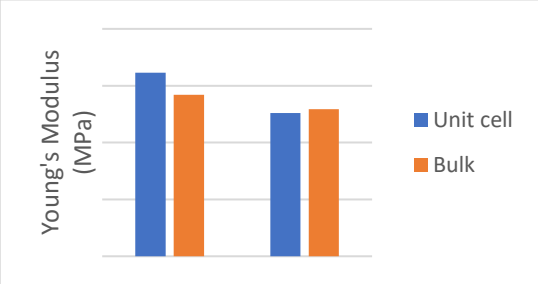

Figure 1: The young's modulus of all the models.

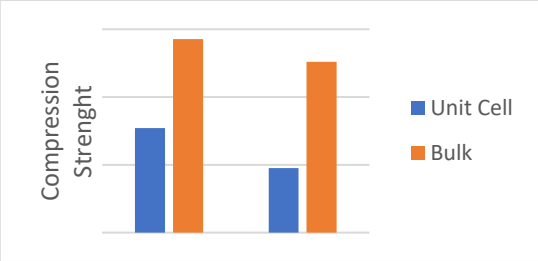

Figure 2: The compression strength of all model based on Von Mises Stress Criteria.

CONCLUSION

Based on the results, both bulk model young's modulus is near to cancellous bone which is acceptable. However, bulk of 1mm is the closest hence it is a better structure for bone replacement.

REFERENCES

[1] Saad, A. P. M., & Syahrom, A. (2018). Study of dynamic degradation behaviour of porous magnesium under physiological environment of human cancellous bone. Corrosion Science, 131, 45-56.

[2] Pearson, O. M., & Lieberman, D. E. (2004). The aging of Wolff's "law": ontogeny and responses to mechanical loading in cortical bone. American Journal Of Physical Anthropology, 125(S39), 63-99.

[3] Ali, D., & Sen, S. (2017). Finite element analysis of mechanical behavior, permeability and fluid induced wall shear stress of high porosity scaffolds with gyroid and lattice-based architectures. Journal Of The Mechanical Behavior Of Biomedical Materials, 75, 262-270.

RESISTANCE ANALYSIS OF SAILING JONG HULL

Muhammad Syazwan Bin Hamzah and Arifah Binti Ali
School of Mechanical Engineering, Faculty of Engineering,
Universiti Teknologi Malaysia, 81310 UTM Skudai, Johor, Malaysia

INTRODUCTION

Miniature Jong races were the popular events in Johor in the 1940s, 1950s and 1960s especially among those living in coastal areas. The performance of sailing boat in any competition are very important in order to be the best. The people do not practice this knowledge in the tournament. The study of performance and resistance prediction have not been done before. people have lack of naval architecture theory in design the Jong sailboat and the study of main hull parameters at the predesign state are very essential. Resistance test can be conducted to the Jong sailboat to predict the behaviour and other characteristic of the Jong running at certain speed and conditions. This is important to improve the performance of the Jong by minimize the hull resistance and increase the speed[2].

EXPERIMENTAL SETUP

There are various methods used for evaluating the model's resistance that are used commonly. In the present, modern methods to perform ship resistance evaluation are based on CFD (Computational Fluid Dynamics), an easy and less time-consuming application. The accuracy of the CFD analysis is proven accurate, and most naval architects use this method instead of towing tank experiment method which is slow and time consuming [1]. This research is a resistance determination for a planing hull using CFD approach. There are two types of planning hull been compared which is round bottom hull and v-hulls. All the process of the design of the hull is using Rhino and Maxsurf. The CFD analysis was performed using Ansys Fluent [3].

RESULTS AND DISCUSSION

In this study, the results are obtained from the simulation program are for both model's round bottom hull and v-hulls. The data obtain been analyse for prediction of resistance of the hull in steady state. The simulation program produced the results in term of total resistance of the simulations. The round bottom hull indicate Model A and the V-hull indicate Model B in the simulation.

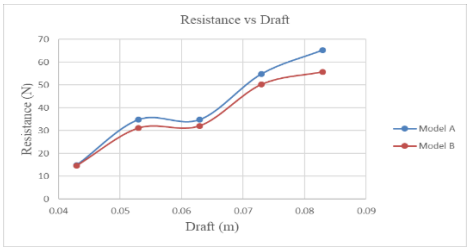

Figure 5: Graph resistance versus draft

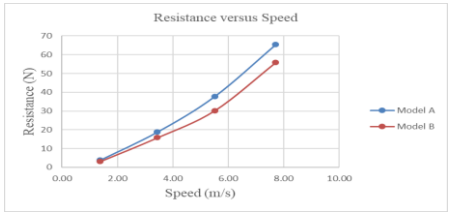

Figure 6: Graph resistance versus speed

The objective of this study resistance was successfully achieved which is to evaluate the resistance of a sailing Jong. In this study, there two type of hull of Jong sailboat has been compare round bottom hull and v hull. The graph plotted using the obtained data give a slight pattern of exponential graph. The graph of resistance against draft show an increasing pattern. The line graph for Model A show higher result compare to the Model B. This show Model A show more resistance impact than Model B. The graph of resistance against speed been plotted show steady increase pattern. Moreover, the gap value of resistance different increase as the speed increase which show that round bottom hull is not applicable at high speed compare to the v-hull shape. The analysis of V-hull shape shows reduced amount of resistance result compare to the round bottom hull.

CONCLUSION

From the study, it can be concluded that Model B show reduced amount of resistance result compare to the Model A. This indicate that as the running speed and draft of the hull increased, then the total resistance will also, be increased. Lastly, this show that by changing the hull shape and optimize the hull is one method for resistance improvements of the sailing Jong.

REFERENCES

[1] [1] Ahmed, Yasser M., O. B. Yaakob, M. F. A. Rashid, and A. H. Elbatran. 2015. "Determining Ship Resistance Using Computational Fluid Dynamics (CFD)." Journal of Transport System Engineering 2(1):20–25.

[2] Amoroso, C. L., A. Liverani, and G. Caligiana. 2018. "Numerical Investigation on Optimum Trim Envelope Curve for High Performance Sailing Yacht Hulls." Ocean Engineering 163(May):76–84.

[3] Rosemurgy, William J., Deborah O. Edmund, Kevin J. Maki, and Robert F. Beck. 2011. "A Method for Resistance Prediction in the Design Environment." FAST 2011 11th International Conference on Fast Sea Transportation (September).

HYDRODYNAMIC ANALYSIS OF SUPERCAVITATED FIN STABILIZER ON SEMI - SWATH

Arief Mazlan and Arifah Ali
School of Mechanical Engineering, Faculty of Engineering,
Universiti Teknologi Malaysia, 81310 UTM Skudai, Johor, Malaysia.

INTRODUCTION

The velocity for the underwater vehicle was low due to the viscosity friction that the vehicle undergoes as the vehicle moving. Therefore, the supercavitation resistance reduction technology, most of the body surface of the vehicle will be wrapped with the cavities that results the cut off the contact of the liquid with the surface. This advantages to supercavitating vehicle received a large amount of attention paid by researchers [1]. With the application of supercavitation, part of the fin surface is wrapped in a cavity. This may affect the normal operation of fin stabilizers [2].

EXPERIMENTAL SETUP

Environment condition setting. The size of the calculation domain is 7m in length, 4m in height, and 4m in width. The direction of the flow from the x-axis negative axis to the x-axis positive axis. Geometric condition setting. This article uses NACA0012 fins, the span is 3.11m, the chord length is 2.59m. Fin boundary conditions set to wall, wall model set to free-slip.

Material condition setting. The water density is set to 998.3 kg/m3, the operating temperature is set to 288.15 K the viscosity model is set to newtonian, the dynamic viscosity is set to 0.001 Pa/s. Simulation condition setting. Refinement algorithm is set to adaptive refinement, resolved scale is set to 0.8, target resolved scale set to 0.01m.

RESULTS AND DISCUSSION

This research focuses on the hydrodynamic analysis on the supercavitated.

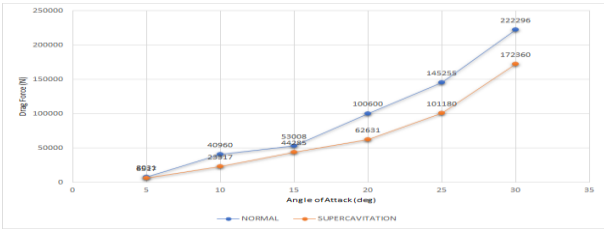

Figure 1: Drag Characteristics of Fin Stabilizer

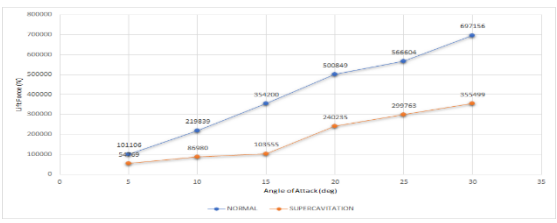

Figure 2: Lift Characteristics of Fin Stabilizer

For the lift forces and drag forces of fins wrapped with supercavity was lower than normal fins stabilizer. As the angle of attack increases, the different between two fins condition gradually increases.

It can be found by observing that the area of the downward surface of the fin stabilizer is enlarged with the supercavity when the angle of attack increases. The area of the upward surface of the fin stabilizer is smaller when the angle of attack increases.

When the angle of attack is close to 30 degrees, the lift of the fin stabilizer begins to decrease. The area of the supercavity wrapped on fin stabilizer has been more than 50%, fin stabilizer began to stall and may cause the ship to swing sharply and cause the ship to capsize. To prevent this situation, a dead zone should be set for the range of the fin stabilizer.

CONCLUSION

The drag of the fin stabilizer wrapped with supercavity is smaller than the drag of fin stabilizer in normal condition. These situations are same for lift. The area of the fin wrapped in the supercavity increases as the angle of attack increases. The parts that are not covered by the supercavity provide most of the lift. Therefore, it is necessary to set a limit switch to prevent the stall.

When the angle of attack is reach 30 degree, a larger separation zone appears on the upper fin surface. As the angle of attack reaches a critical value, the lift reaches its maximum. If the angle of attack is increased, lift will not increase but fall backward which resulting in stall. The set of limit the range of motion of the fin stabilizer was necessary.

REFERENCES

[1] Yuan, X., & Xing, T. (2016). Hydrodynamic characteristics of a supercavitating vehicle's aft body. Ocean Engineering, 114, 37-46.

[2] Zhigang, Q., Yanwen, L., & Hong, J. (2015, August). Research on the lift characteristic of morphing bionic fin stabilizer at zero/low speed. In 2015 IEEE International Conference on Mechatronics and Automation (ICMA) (pp. 1374-1378). IEEE.

NUMERICAL COMPARISION ON THE RESISTANCE CHARACTERISTICS OF CONVENTIONAL AND UNCONVENTIONAL SHIPS

Azimuddin A. Halim and Arifah Ali
School of Mechanical Engineering, Faculty of Engineering,
Universiti Teknologi Malaysia, 81310 UTM Sekudai, Johor, Malaysia

INTRODUCTION

The efficiency of the ship is very important to ensure the ship working in a good performance. The main factor that influences the efficiency of the ship is ship resistance. To know the resistance effect is very important to ship operators. This because ship operators must find a balance between voyage costs, i.e. increase in fuel costs or reduced speed, and maintenance costs [1]. Thus, low ship's resistance, which results in decreased fuel consumption, increased ship speed and decreased engine stress [2].

EXPERIMENTAL SETUP

The differences in resistance characteristics of conventional and unconventional ships is analysed. The conventional ship is representing as Catamaran and unconventional ship will be represented as Semi-SWATH. In analysing ship's resistance, the size of the model was modified by adjustment the length of the ship and the Froude number.

The resistance performance of catamaran and semi-swath is obtaining from Computational simulation using CFD (Computational Fluid Dynamics). Hence, the accuracy of simulation result will be compare with experiment result for both catamaran and semi-SWATH. The experiment result was collected at UTM Marine Technology Centre.

RESULTS AND DISCUSSION

The total resistance for both models was analyzed based on ANSYS CFD program. The differences of resistances characteristics between two type of ship has been determined. In this result, the graph comparison between conventional and unconventional was provided. In addition, the graph comparison between simulation and experiment also provided for validation purposed. The resistance component was determined by using ITTC 1957 method.

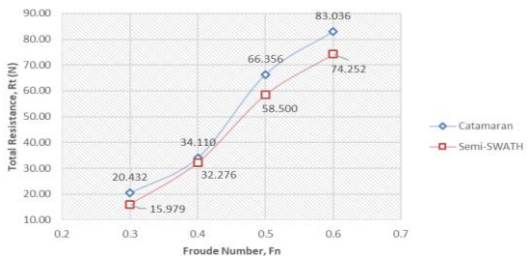

Figure 1: Resistance Comparison Between Catamaran and Semi-SWATH

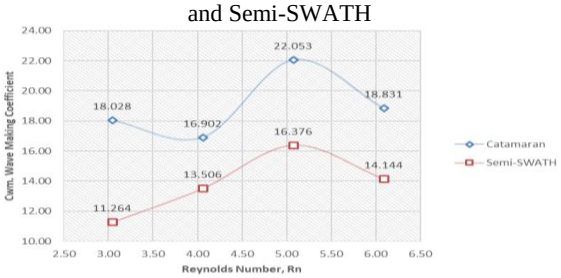

Figure 2: Wave Making Coefficient Comparison Between Catamaran and Semi-SWATH

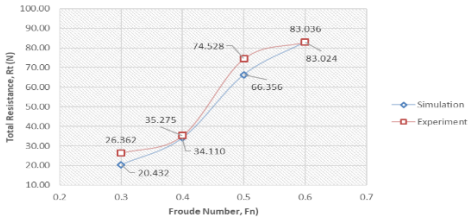

Figure 3: Resistance Comparison Between Simulation and Experiment for Catamaran

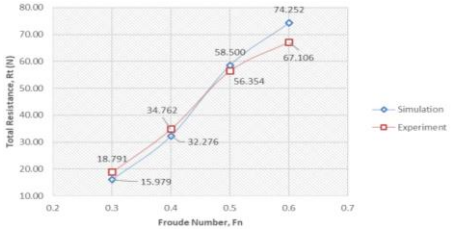

Figure 4: Resistance Comparison Between Simulation and Experiment for Semi-SWATH

CONCLUSION

The resistances behavior had been successfully analyzed and the comparison for conventional and unconventional hull form completely determines. The performance of resistance characteristics for the unconventional hull is better than the conventional hull.

REFERENCES

[1] Oliveira, D., Larsson, A. I., & Granhag, L. (2018). Effect of ship hull form on the resistance penalty from biofouling. Biofouling, 34(3), 262–272.

[2] Bixler, G. D., & Bhushan, B. (2012). Review article: Biofouling: Lessons from nature. Philosophical Transactions of the Royal Society A: Mathematical, Physical and Engineering Sciences, 370(1967), 2381–2417.1]

WORK STATION DESIGN FOR TYRE LINER SANDING DEPARTMENT: ERGONOMIC SOLUTION

Muhamad Lutfi Aziz and Azanizawati Ma'ram
School of Mechanical Engineering, Faculty of Engineering,
Universiti Teknologi Malaysia, 81310 UTM Skudai, Johor, Malaysia.

INTRODUCTION

Humans have always been curious about the powers and capabilities of their brains, and scientists have been seeking ways to control its amazing feats. A new field of research has been born that focuses on a growing technology called brain stimulation where healthcare professionals can modify the brain to treat diseases. Some recent organizations have published astonishing results that can lead to the future of medicine and completely change the approach physicians take with the treatment of diseases. Stimulating the brain with a low current that is focused on specific regions of the brain has been shown to modify brain function and treat various neurological diseases. Transcranial direct current stimulation (tDCS) has been an effective and life changing alternative treatment for a vast range of neurological conditions including depression, epilepsy, stroke rehabilitation, addiction and chronic pain but only if it is administered correctly. This study focuses on the analysis of electrode positioning for mental illness device and the design development of electrode housing. Data is collected with questionnaire and interview in order to develop a product design that fulfill the consumer requirement. Moreover, the developed design is going through design analysis and further improvement in order to produce the best final design.

PROJECT OBJECTIVES

The aim of the study is to analyse the electrode positioning for mental illness stimulation device and designing the electrode housing for the mental illness device.

METHODOLOGIES

The methodology of this study started with data collection. The data collection method used in this study are survey and interview. The data obtain from the survey and interview will be used in the conceptual design development process. the concept design will go through scoring and further improvement to come up with the final design.

RESULT AND ACHIEVEMENT

After going through design process and design analysis, the final design can be developed. The final design is the upgraded version of the conceptual design 1 that was selected with the design selection metric. The design consists of four parts. The parts assembly is divided into two, the electrode housing and the housing base. The electrode housing is the assembly that used to house the electrode for mental illness stimulation devise. It is key component of the device as its function to deliver the direct current for the treatment, the housing base on the other hand, is attach permanently on the head gear to act as base or platform for electrode housing to be attach to.

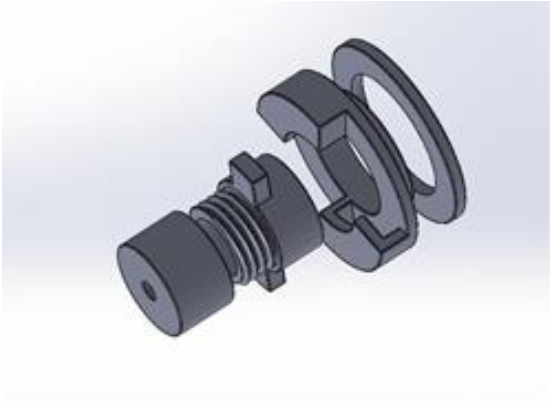

Figure 1: Final Design (disassembled)

This design is using a better Snap-On mechanism that is less complicated than the previous version. This Snap-On design eliminates the reliability problems on the previous design which using the spring type Snap-On. Spring type Snap-On have the tendency to break or loss its elasticity after long period of usage.

REFERENCES

[1] Abrams, R., Fink, M., Dornbush, R. L., Feldstein, S., Volavka, J., and Roubicek, J. (1972). Unilateral and bilateral electroconvulsive therapy: effects on depression, memory, and the electroencephalogram. *Archives of general psychiatry*, 27(1), 88-91.

[2] Squire, L. R. (1977). ECT and memory loss. *The American journal of psychiatry.*

DEVELOP OF ERGONOMICS MENTAL ILLNESS STIMULATION DEVICE WEARABLE

Mohammad Haqimi Mohammad Thaib Teoh and Azanizawati Ma'aram
School of Mechanical Engineering, Faculty of Engineering,
Universiti Teknologi Malaysia, 81310 UTM Skudai, Johor, Malaysia.

INTRODUCTION

This thesis describes the development mental illness stimulation wearable for Malaysian population. Mental illness stimulation wearable develops for patient of mental illness to use as their treatment for overcome their mental illness disease. In way to develop mental illness stimulation wearable, data collection and analysis will be done to collect the suitable size and comfortable wearable for the patient. Design process needed to satisfy user requirement for this mental illness stimulation wearable. Ergonomic can be defined as the scientific study of interaction between man-machine at workplace. Basically, ergonomic objectives are to fit man and machine together to improve the worker's performance and reduce fatigue and stress of the workers at workplace. Application of the ergonomics is very useful and significant in area where manual activities affect physical and mental health of the workers directly [1].Ergonomics also is one of the safeties and health components that if implemented will contribute to job satisfaction. [2].There has been little progress in reducing the burden of mental illness around the world, prompting calls for improved access to quality mental health care and assessment of mental disorders and for "programs to prevent mental disorders and promote mental health" [3].The distinction between mental disorder and mental health is a fundamental underlying element of this call for improvement, but this important distinction is often misunderstood.

PROJECT OBJECTIVES

Based on the problem statement, this research is conducted in order to achieve the target and objectives. The objective of this project is to classify classes of head profile for Malaysian population and to analysis main class of head profile for Malaysia Population. Design mental illness stimulation device wearable is the main objective.

METHODOLOGIES

Question been release to hospital that having mental illness patient. For this research, this questionnaire been responded by Hospital Permai and Hospital Sultanah Aminah (HAS), Johor Bahru, Johor. From the respond, I got information of existing mental illness wearable that being use and its usage are support by using slime gel, 20-30 minutes duration and unfixed positional of hole for the electrode Besides, I receive feedback from respondent on design wearable requirement of future mental illness wearable. Interview held at Department of Psychiatry, Hospital Sultanah Aminah, Johor Bahru, Johor. Dr Marina from Department of Psychiatry, Hospital Sultanah Aminah, Johor Bahru, Johor help me for some data collection in this interview. From the interview, I received statistical data for mental illness and statistical data for major group of age for mental illness patients. Besides, I get to know the effect from existing mental illness wearable are not portable, fixed sizes and not safe (burn mark to patient head).

DESIGN PROPOSED

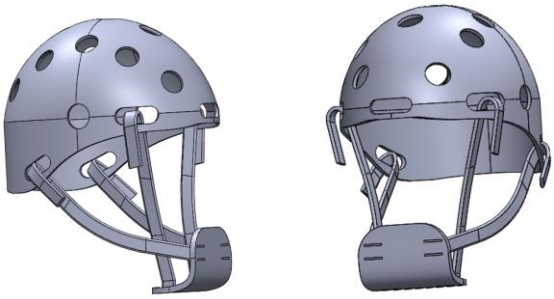

Using material of Neoprene Nylon. This design requires to flexible and elastic. From material selection matrix, Neoprene lead other material. So, this design has to suggest of material depend on part of the wearable. First suggestion, all part of wearable is from Neoprene and for the second suggestion is all part made from Neoprene except the belt support form rubber because the belt support have to used material that have high elasticity. Neoprene is available within 1 to 35 mm thickness and for this design. Three millimetre of thickness being use. (Neoprene: ASTM D 2000, SAE J-200: BC-BE). The advantages of Neoprene as the material are polychloroprene (PC- Rubber), synthetic rubber, latex, electrical insulation, high Burning Point (260 Degree/500 Fahrenheit), waterproof and, elastic.

REFERENCES

[1] K. &. C. S. and Parkes, F. E. (2005). Musculo-skeletal disorders, mental health and the work environment.
[2] S. Z. T. Z. and Dawal, I. Z. (2009). Effect of job organization on job satisfaction among shop floor employees in automotive industries in Malaysia. *International Journal of Industrial Ergonomics*.
[3] W. H. Organization, (2018). Global Burden of Disease Study 2017.

RELIABILITY CENTERED MAINTENANCE II (RCMII) FOR OLEOCHEMICAL PLANT

Aizat Salim and Azanizawati Ma'aram
School of Mechanical Engineering, Faculty of Engineering,
Universiti Teknologi Malaysia, 81310 UTM Skudai, Johor, Malaysia

INTRODUCTION

Reliability Centered Maintenance II (RCM II) is one of the most currently implemented maintenance strategies in most chemicals plant around the world. But this RCM II has not been implemented yet in Emery Oleochemical plant. So, RCM II seems to be one of the tools used to determine the right maintenance task for all pumps in EOS Plant at this company. The main objective of RCM II is to preserve the system function of the pump in each plant. RCM II also will identify and prioritize the failure modes that can affect the system function by using Equipment Critical Analysis (ECA) and Failure Mode and Effect Analysis (FMEA) method. Then, it will select the applicable and the most effective tasks in order to control the failure modes.

METHODOLOGY

This section presents the methodology of the research. Firstly, a discussion with a manager of Mechanical Department in this company to get the confirmation in order to get the research data was done. Then, the risk parameter was determined and the ECA was start to develop. From the analysis, the critical pump was identified and classified into Rank A, B and C. After that, the most critical pumps with Rank A classification were selected to be analysed on FMEA. Next, the development of FMEA was started after all the data of Rank A pumps have been collected. Finally, the recommended action was proposed on each Rank A pumps in order to overcome the maintenance problem in this company.

RESULTS AND DISCUSSION

From Table 1, the total number of the pump which have classified into Rank A, Rank B and Rank C was 3, 6 and 13 respectively. The pump number 2, 14 and 19 in the ECA tools also known as feed pump (P1201), blower pump (K1201) and thermo oil pump (TOHPO1) were classified as Rank A pumps because the pumps have risk value > 100. Hence, all these three pumps need to be considered as a first priority action plan in EOS Plant.

Besides that, from Table 2 the main part that frequently breakdown in the pumps was the bearing part, motor pumps, mechanical seal, impeller, V-belt, and gear shaft. Each of these parts have their own potential causes that lead to the potential failure mode to the pump One of the FMEA was done on TOHPO1, the oil refilling part has the higher RPN which is 576 compared to other part. This is because of the thermo oil contaminated with water that will affect the pump operation. The bearing part in the pump also frequently breakdown because of the vibration of the pump was too high during operation. So, the gear shaft will rotate unsteadily and make the bearing cannot enhance the resistance of the shaft.

After the problem has been highlight in the FMEA, the action plan will be suggested in order to overcome the problems. TOHPO1 was come out with a new design of concrete plinth and base plate that can prevent the thermo oil contaminated with water as shown in Figure 1.

Table 1: ECA Table for 22 Pumps in EOS Plant

NO	EQUIPMENT DETAILS			RISK PARAMETER EVALUATION									RISK	
	EQUIPMENT TAG NUMBER	EQUIPMENT NAME	DIVISION	Failure Frequency (FF)per Year	Score	Operational Impact (OI)	Score	Operational Flexibility (OF)	Score	Maintenance Cost (MC)	Score	Impact on Environment & Safety (IES)	Score	Risk Value	Criticality	RANK
1	R1101-P1101	Feed PP Reactor PUMP FOR R1101	MECH	2	2	Immediate plant shutdown	10	No spare for alternative operation	4	Above than MYR 5000	2	Minor accidents and incidents	2	160	SEMI CRITICAL	B
2	E1201-P1201A	COOLER Feed PUMP FOR P1201	MECH	3	3	Immediate plant shutdown	10	No spare for alternative operation	4	Above than MYR 5000	2	Minor accidents and incidents	2	432	CRITICAL	A
3	D1107-P1104	WASHING SOLUTION PUMP FOR P1104	MECH	1	1	Operational cost associated with impact	2	No spare for alternative operation	4	Above than MYR 5000	2	Minor accidents and incidents	2	8	NON CRITICAL	C
4	D1701-P1701	PCSU TERSTRY PUMP FOR P1701	MECH	1	1	Immediate production lossis or	4	No spare for alternative operation	4	MYR 2001 to MYR 4999	1.5	MINOR accidents and incidents	2	66.5	NON CRITICAL	C

Table 2: FMEA for TOHPO1

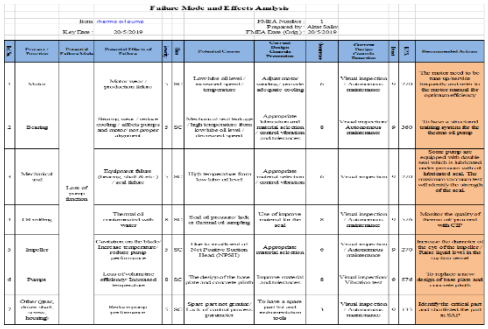

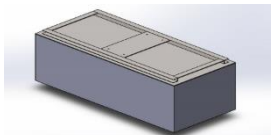

Figure 1: Concrete Plinth and Base Plate Design

CONCLUSION

By using Equipment Criticality Analysis (ECA) and it was able to classified the pump into Rank A, Rank B and Rank C. Then, by using failure mode and effect analysis (FMEA), the significant characteristic that lead to pump problems is identified and able to provide the solution. Besides that, the new design of concrete plinth and base plate for thermo oil pump also produced.

REFERENCES

[1] Alexis et. al. (2016). Critical Equipment Identification and Maintenance
[2] Prabhakar and Jagathy Raj (2013). A New Model for Reliability Centered Maintenance In Petroleum Refineries behavioural studies. Neuropsychologia, 22(1), 65-72.
[3] Moubrey, J. (2001). RCMII: Reliability-centered Maintenance.Industrial Press Inc.

FABRICATION OF FABRIC COATED WITH AEROGEL FOR THERMAL INSULATION APPLICATION

Muhammad Hazim Mohd Johari and Muhamad Azizi Mat Yajid
School of Mechanical Engineering, Faculty of Engineering,
Universiti Teknologi Malaysia, 81310 UTM Skudai, Johor, Malaysia

INTRODUCTION

Currently, firefighter's suit made of material that is high in weight per volume and need to be improve. Aerogel is a solid material that have impressive properties which are specifically in its density, thermal expansion and thermal conductivity that have in very low value. These remarkable properties make it to become one of lightest solid and have better heat insulation than current firefighter's suit material. Aramid honeycomb use as frame structure of the composite not only good in flame retardant but also an effective structure to increase strength and stiffness of structure from core. [1,2]

EXPERIMENTAL SETUP

This section presents experimental setup for this flame retardant test. Laboratory flame test are prime method of qualifying fire-resistant materials for use [3]. Thermocouples were clamp at both side of the composite surface to measure the temperature difference when heat applied from flame torch. Data logger (pico technology USB TC-08) were used for temperature measure of both side of surface. The flame torch was then directed to composite surface with distance 1cm from surface composite and flame torch source. The experiment stops until the back temperature reach 43°C as skin starts to irritate when further increase according to [4].

RESULTS AND DISCUSSION

The exact temperature of the flame measured is 660°C as illustrates in figure 1. Temperature difference is 617°C of heated surface and back surface with nearly the same thickness of 4mm composites. Figure 2 shows the different in layer of composites varies in time to reach 43°C. From the graph can be observe the full layer composite marks as the longest time to reach exact temperature which is 54 seconds. Next, composite of no aerogel which need 28 seconds to reach the temperature which the layer prepared is same as the full layer composite just no aerogel presence. The second most time to reach the temperature is 35 seconds which is without aerogel layer composite. Meanwhile, the commercial aerogel composites and RHA aerogel composites share the same time for both to reach 43°C.

Comparing the burning rate, full layer composite has it the lowest which is 0.23 which marks the longest time. Without aerogel composite also can be observe to be low which is 0.28. Moreover, as for no aerogel composite and commercial aerogel composite, both have nearly the same rate of 0.31 and 0.35 respectively. RHA aerogel have it the highest rate which value is 0.44.

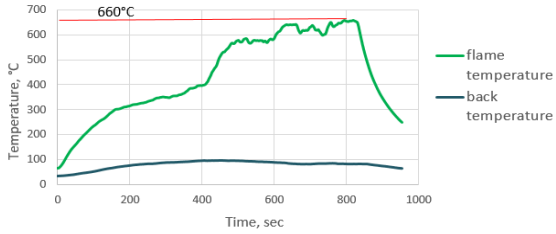

Figure 1: Maximum temperature of flame torch

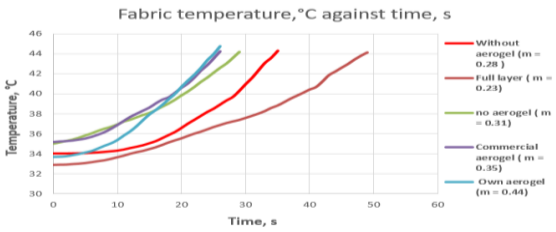

Figure 2: Time for composites to reach 43°C

CONCLUSION

In overall, aerogel addition helps to improve thermal insulation and RHA aerogel synthesize is comparable with commercial aerogel. Aerogel also acts as the most function in composite layer as it has low in thermal conductivity.

REFERENCES

[1] Jyoti L. Gurav, In-Keun Jung, Hyung Ho Park, Eul Son Kang, and Digambar Y Nadargi (2010) Silica aerogel: synthesis and application. Journal of Nanomaterials Volume 2010, article ID 409310, 11 pages.

[2] Hafeezur Rahman (2013) Effectiveness of honeycomb structure in main battle tank design. Thesis for: MSc in Military Vehicles Technology

[3] J. G. R. Hansen, B.J. Frame (2008) Flame penetration and burn testing of fire blanket materials. Fire and Materials International Journal/Volume 32, Issue 8

[4] Ronald HEUS, Emiel A. Denhartog (2017) Maximum allowable exposure to different heat radiation levels in three types of heat protective clothing. Industrial Health National Institute of Occupational Safety and Health, 55, 529-536

POLYVINYL BUTYRAL (PVB) – AEROGEL COMPOSITE PREPARED FROM RICE HUSK ASH PRECURSOR FOR FLAME RETARDENT STRUCTURAL APPLICATION

Tuan Amir Mohsin Tuan Nordisham and Muhamad Azizi Mat Yajid
School of Mechanical Engineering, Faculty of Engineering,
Universiti Teknologi Malaysia, 81310 UTM Skudai, Johor, Malaysia

INTRODUCTION

Aerogels are the lightest solid material ever known and were discovered for more than 60 years ago which were widely used in chemical industries. They have various potential in wide range of application. In this research it is intended to study on the effect of polyvinyl butyral (PVB) -aerogel mixture on the flame retardancy property of polymatrix composite (PMC). The study will be carried out through experimental method for about 3 – 4 months including the initial preparation of hydrophobic aerogels precursor from rice husk ash and synthesis of PVB-aerogel composite by mixing of hydrophobic aerogel, PVB powder and acetone solution with accurate proportion. Samples are made based on content of aerogel in percentage in PVB matrix. Characterization of microstructure analysis by using SEM-EDX and chemical analysis by using TGA-IR are made. Horizontal burning is to calculate the burning rate of each samples. The paper will include the implication of the current research and the improvement and suggestion for the next related research.

EXPERIMENTAL SETUP

Hydrophobic aerogel was synthesis initial by mixing 33.33g rice husk ash, 250ml of water and 16.67g sodium hydroxide pallet. Then, it was heated at 80°C for 24 hours to produce sodium silicate. Sodium silicate will purify to produce aquagel, then ethanol was added to produce alcogel. Surface modification on alcogel is made by using TMCS and n-hexane to produce hydrophobic aerogel. PVB-aerogel composite was synthesis by mixing hydrophobic aerogel, polyvinyl butyral powder and acetone solution with accurate proportion. Samples are made with different aerogel content in percentage.

RESULTS AND DISCUSSION

Scanning electron microscope is used to characterized the surface morphology of hydrophobic aerogel and PVB-aerogel composite. Result show that hydrophobic aerogel have a pore structure and Atomic % is major in silica and oxygen which proof it as an aerogel. Surface morphology of PVB-aerogel matrix show that the higher aerogel content in PVB matrix, the agglomeration of aerogel will decrease.

Energy Dispersive X-Ray (EDX) mapping is used to detect the dispersibility of aerogel in PVB composite matrix. Result show that the higher aerogel content in PVB matrix, the dispersibility of aerogel is better. Thermogravicmetric analysis (TGA) for PVB-aerogel composite is shown on figure 1 which describe the weight loss % of each sample (0% aerogel content, 10% aerogel content, 30% aerogel content and 50% aerogel content) from 50°C up to 600°C. result show phase 1 as weight loss of water, phase 2 is polymer and phase 3 is char/residue. The higher aerogel content, the rate of weight loss is lowest at phase 3. Efficiency of aerogel affected at phase 2 due to less curing and formation of bubble in composite. Horizontal burning test show that the higher aerogel content, the lower burning rate of composite.

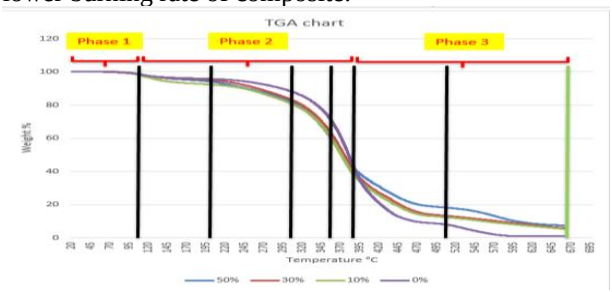

Figure 1: TGA graph

CONCLUSION

Hydrophobic aerogel is suitable to mix with PVB powder with existence of acetone solution but manage to mix with right condition which under hot pressing mechanism. Based on current result, conclusion can be made that the cured PVB-aerogel composite will decrease the burning rate.

REFERENCES

[1] Halim, A., Alif, Z., Yajid, M., Azizi, M., & Hamdan, H. (2016). Synthesis and Characterization of Rice Husk Ash Derived-Silica Aerogel Beads Prepared By Ambient Pressure Drying. In Key Engineering Materials (Vol. 694, pp. 106-110). Trans Tech Publications

[2] Kim, G. S., & Hyun, S. H. (2003). Effect of Mixing on Thermal and Mechanical Properties of Aerogel-PVB Composites. Journal of materials science, 38(9), 1961-1966

[3] Smirnova, I., & Gurikov, P. (2018). Aerogel Production: Current Status, Research Directions, and Future Opportunities. The Journal of Supercritical Fluids, 134, 228-233

CERAMIC COATING ON STEEL FOR HIGH MACHINING CUTTING TOOL

Raja Nur Izzati Raja Abd Razak and Muhamad Azizi Mat Yajid
School of Mechanical Engineering, Faculty of Engineering,
Universiti Teknologi Malaysia, 81310 UTM Skudai, Johor, Malaysia

INTRODUCTION

Al, Si, Ti and N have widely applied as the protective films in machining industry due to their hardness, good wear resistance and high thermal stability at elevated temperature [1]. The thickness for machining industry is 2-3µm on the cutting tool surface. [2] . The purpose of the study to analyse the AlTiSiN dilms by using PVD sputtering and identify the influence of various temperature and bias voltage on the microstructure and mechanical properties.

EXPERIMENT

The parameter use is for first temperature 300ºC and room temperature. Moreover, the different value of bias voltage from 0v to -120v was use for deposited the TiN/AlTiSiN on the stainless steel substrate. Taget for AlTiSi is diameter 70mm and 597 for length. For temperature, time deposition for multilayer is TiN is 1 Hour and 2 hour for AlTiSiN. Bias voltage time deposition change to TiN is 30 minutes and 1 hour for AlTiSiN. Flow rate 100 sccm for gas argon and 50 sccm on nitride gas. By using the pressure and rotation is 5mTorr and 5 rpm. Lastly, set position pressure was Ti (45%) and AlSiN (45.0%).

RESULT

By using SEM and EDX, the thickness and the microstructure result was obtained by observed on the mapping and line scan graph. Moreover, the AFM was use to do analysis for the surface roughness on the coating film. On the 300ºC, the thickness was 2.3µm and RT was 1.5µm. the higher temperature deposition on coating it will increase the thickness due to nuclei density was increase by deposition rate. Bias voltage increase will decrease the thickness because high energy come from bias voltage, forcing atom to move on voids between the grain. The coating will become more compact and dense.

Moreover, higher the bias voltage the surface roughness on the coating from rough transform to smooth. It happened because reduction in grain size due to increase in ion bombardment. It helps to anneal the imperfections in coating structure. Lastly, for the mechanical properties when the higher temperature and the bias voltage the coating film dense, higher hardness and lower surface roughness is also conducive to toughness enhancement of film.

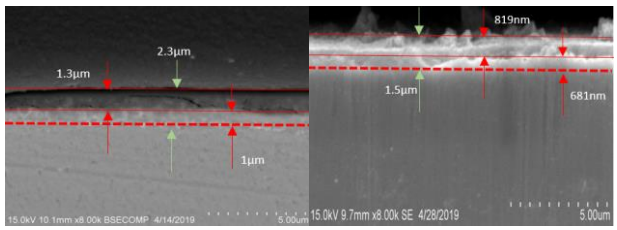

Figure 1 :The thickness of effect in temperature a) 300 ºC b) RT

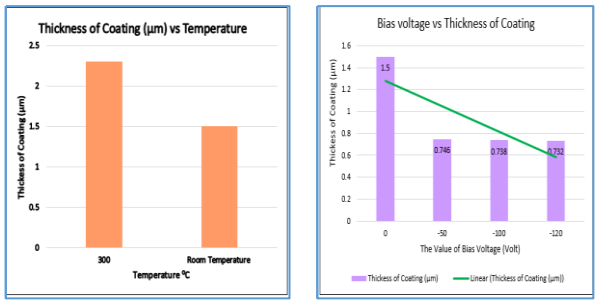

Figure 2 :The graph show different in thickness of effect in temperature a) 300 ºC b) Bias voltage

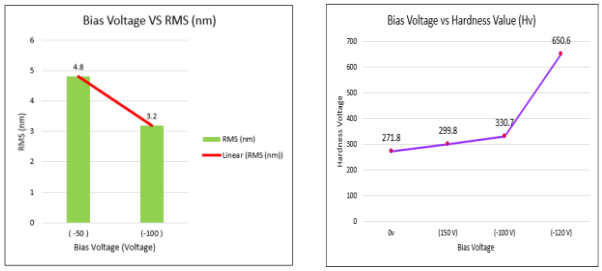

Figure 3 :The graph show for bias voltage effect a) AFM result and b) relative surface hardnesss

The temperature effect the thickness on the coating which is the higher the deposition temperature, the coating thickness also increase. The higher the value of bias voltage, the lower thickness of coating.

REFERENCES

[1] S.K. Pradhan, M.A Djoudi, (2005). Deposirion on CrN coating by PVD method for mechanical application , Surf. Coating. Technology. 142-145

[2] Eero Posti, (1988). Influence of coating thickness on the life of Ti-N coated high speed steel cutting tools.

A GENERIC VEHICLE MODEL TO PREDICT FUEL CONSUMPTION FROM PASSENGER CARS

Wai Ming Tan and Mohd Azman Abas
School of Mechanical Engineering, Faculty of Engineering,
Universiti Teknologi Malaysia, 81310 UTM Skudai, Johor, Malaysia

INTRODUCTION

The purpose of the Vehicle Emission Modelling is a work to used to reduce the emission pollution of the vehicle base and estimate the emission by the different type of factor, for example vehicle related factor is model, size, fuel type, technology level and mileage and operation factor is speed, acceleration, gear selection, road gradient, and ambient temperature. The main source of the vehicle emission is carbon monoxide (CO), volatile organic compounds (VOCs), oxides of nitrogen (NOx) and particular matter (PM). Besides that, the exhaust gas consist the carbon dioxide (CO_2) and methane (CH_4) and nitrous oxide (N_2O) will causes the greenhouse effect. Above all is effect by fuel consumption of vehicle.

EXPERIMENTAL SETUP

The based theory of the QSS Toolbox is from the vehicle population system. The idea of the QSS Toolbox is reverse the causes and the effect relationship in the vehicle dynamic system. The QSS Toolbox is using the speed of the vehicle with time to calculate the acceleration and necessary force. First set the drive cycle need to used, after this, the vehicle block will calculate the wheel torque based on the vehicle speed and acceleration. The transmission converts the wheel torque to the engine torque based on the gear ratio. The IC engine is converting the engine torque to the power produce. The tank is converting the power to the fuel consumption, liter per 100km.. [1]

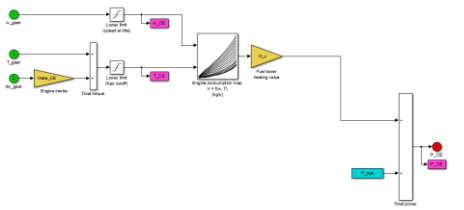

(a)

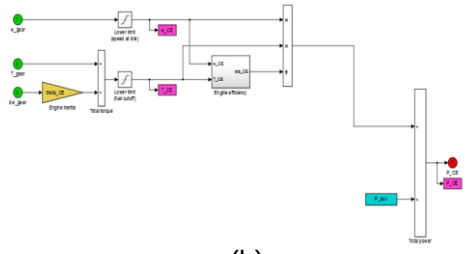

(b)

Figure1: Internal combustion engine structure

Figure 1 (a) Show the model 2 (consumption map) (b) Show the model 3 (William Approximation)

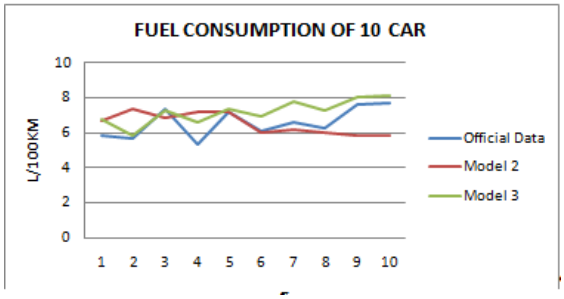

RESULTS AND DISCUSSION

Used the experiment data to tuning the model and estimate the fuel consumption of 10 cars

Figure 2: The fuel consumption of 10 cars (Official Data)

Figure2 show the comparison result of fuel consumption estimate by the model 2, model 3 and the official data. In the result, the correlation of model 3 and model 2 is 0.82 and -0.45.

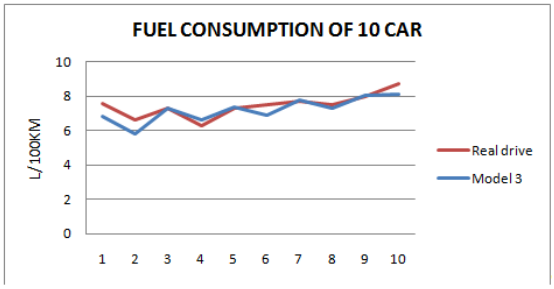

Figure 3: The Fuel consumption of 10 cars (Real Drive Data)

Figure 3 show the comparison result of fuel consumption estimate by model 3 and the real drive data. The correlation coefficient is 0.83.

CONCLUSION

The model 3 is more precision and accuracy than the model 2. The correlation coefficient in model 3 is 0.82 and 0.83

REFERENCES

[1] L. Guzzella, A. Amstutz, *The QSS Toolbox Manual*, 2005

WASTE GLASS ADDITION ON LIGHTWEIGHT AGGREGATES PREPARED FROM COAL FLY ASH

Nurhazirah Ishak and Engku Mohd Nazim Engku Abdul Bakar
School of Mechanical Engineering, Faculty of Engineering,
Universiti Teknologi Malaysia, 81310 UTM Skudai, Johor, Malaysia

INTRODUCTION

Coal fly ash are the product of coal combustion in thermal power plants that being composed of the fine particles of burned fuel driven out of coal-fired boiler together with flue gases. 68 million of fly ash were produced since 2001 [1]. Coal fired electric and steam generating plants are produced fly ash with air into the boiler combustion chamber where it immediate ignites and generating heat to produce a molten mineral residue. Particles fly ash is a fine powder that is carried on the smokestack and captured by the control of pollution and coarse material fly ash will fall to the bottom of the furnace. In other name, fly ash considered as pozzolans because it substance contain silica and alumina and has unique spherical shape and particle size distribution of fly ash to make it good mineral filter in any application that will improve of fluidity of flow able fill and grout [2]. During combustion the main impurities been found in fly ash are SiO2 and Al2O3 is merge in suspension and flew away with exhaust gases. When it cools down, the fly ash being solidifies into spherical glassy particles [3].

METHODOLOGIES

Sample preparation was prepared into two part of composition, coal fly ash and 25% of waste glass was added into the coal fly ash. The composition was mix using mixing machine for 15 minutes at low speed mixing about 100 RPM. When the mix composition was mix properly, it will change their physically composition to be forming. The green pellet was form with dimension of 15mm x 30mm per sample using pressing molding. The green pellet was compact at 45kN with 5 minutes holding time. The green pellet was sinter at temperature between 800℃, 1000℃ and 1200℃ for 10 minutes using electric high temperature with pre-heating at temperature 200ºC for 2hour to give the sample well dry. Then the specimen was naturally cool at atmosphere before their physical and characteristic were investigated.

RESULTS AND DISCUSSION

Figure 1 illustrate the peak of quartz in coal fly ash mix with 25wt.% of soda lime silica glass have a higher intensity and gradually decrease with increasing temperature. This is because sintering reaction alters the fractional quartz to the cristobalite phase due to high-temperature silica de-verification product, and it is thermodynamically more stable than silica. In figure 2 give the information of water absorption at different temperature. The 25wt% of SLSG mix fly ash was about 38% at 800ºC. when increase the temperature the mix composition slightly decreases about 20% at 1200ºC. It shows that increasing the temperature will reduce water absorption because big pore become less.

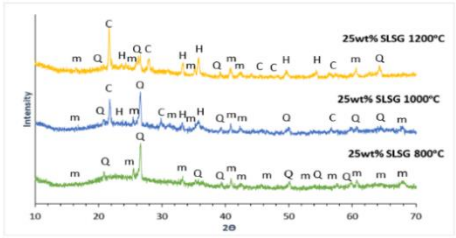

Figure 7: XRD pattern 25wt% of SLSG mix with fly ash at different sinter temperature

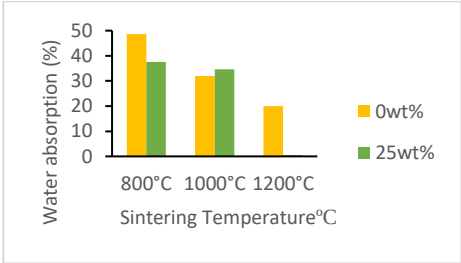

Figure 8:Water absorption at different sinter temperature

CONCLUSION

In this research objective was completely achieved by glass addition into fly ash able to lowers the firing temperature sintering. Addition, addition of glass has improved and change the physical and mechanical properties of aggregates product. The composition mixture of coal fly ash with 25wt% of glass at high sintering temperature able to reduce water absorption and increase compressive strength of the aggregate.

REFERENCES

[1] R. S. Iyer and J. A. Scott, “Power station fly ash - A review of value-added utilization outside of the construction industry,” *Resour. Conserv. Recycl.*, vol. 31, no. 3, pp. 217–228, 2001.

[2] Y. L. Wei, S. H. Cheng, and G. W. Ko, “Effect of waste glass addition on lightweight aggregates prepared from F-class coal fly ash,” *Constr. Build. Mater.*, vol. 112, pp. 773–782, Jun. 2016.

[3] P. Sultana, S. Das, B. Bagchi, A. Bhattacharya, R. Basu, and P. Nandy, “Effect of size of fly ash particle on enhancement of mullite content and glass formation,” *Bull. Mater. Sci.*, vol. 34, no. 7, pp. 1663–1670, 2011.

STRESS CORROSION CRACKING TEST OF CARBON STEEL EXPOSED IN 3.5 % SODIUM CHLORIDE SOLUTION SIMULATED SEAWATER ENVIRONMENT

Low Jia Ming and Esah Hamzah
School of Mechanical Engineering, Faculty of Engineering,
Universiti Teknologi Malaysia, 81310 UTM Skudai, Johor, Malaysia.

INTRODUCTION

Stress corrosion cracking (SCC) is the sudden brittle fracture of specific metals or alloys in specific corrosive environment which is subjected to tensile stress. The effect of SCC can be devastating and catastrophic because of its nature of sudden failure. In this case, low carbon steel had been selected as candidate material to be tested in 3. 5% NaCl simulated seawater environment. Constant load test had been conducted using modified creep machine. Machine calibration had been done using load cell and data logger. Performances of five specimens were evaluated, and they are as received, annealed, normalized, quenched and quenched & tempered specimen. Reduction in grain size is effective against SCC. There were several important parameters tested including hardness, elongation, fracture duration, grain size and initiation site of SCC. IGSCC had been observed on fracture surface of normalized specimen. The aim of this project is to calibrate and verify the parameters of the stress corrosion cracking test setup and evaluate the stress corrosion cracking behaviour of carbon steels exposed in simulated seawater.

EXPERIMENTAL SETUP

Constant load test had been conducted using modified creep machine. Machine calibration had been done using load cell and data logger. Performances of five specimens were evaluated, and they are as received, annealed, normalized, quenched and quenched & tempered specimen. The schematic diagram of SCC test experimental setup after assembly of all machine parts is shown in Figure 1.

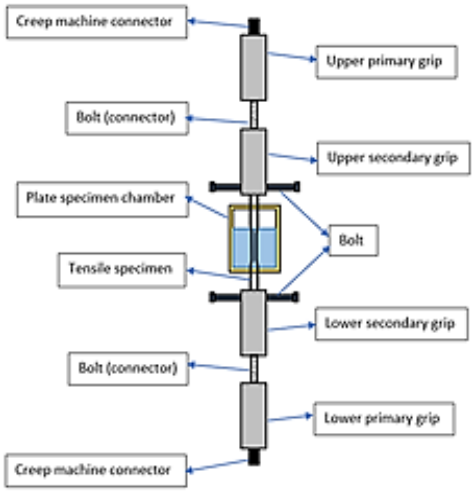

Figure 1: The schematic diagram of SCC test experimental setup after assembly of all machine parts.

RESULTS AND DISCUSSION

Improvement and further modifications on the creep machine had been successfully completed according to the ASTM E8 standard sub-size plate specimen. Constant load SCC test had been carried out with 3.5% NaCl solution and 13kg load applied. The test results obtained were in elongation, time taken to fracture / elongate, grain size, hardness, and SCC initiation site in microscopic view. Grain size reduction had been proven to be effective against SCC. This was exemplified by the quenched specimen which has the smallest average grain size, hence contributing to its highest SCC resistance among 5 specimens. IGSCC was the dominant types of SCC in low strength steel especially low carbon steel, indicating cracking occurs along grain boundaries. Transgranular SCC (TGSCC) was not found during fractography, since branching of crack was absent. There was insufficient time for further crack propagation to go through ferrite grains.

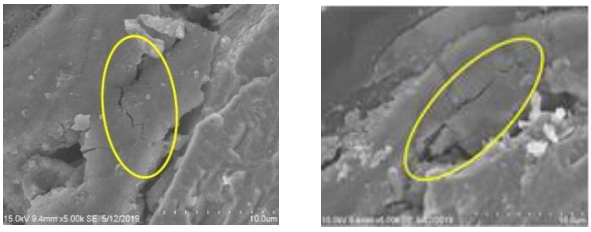

(a) (b)

Figure 2: (a) and 2(b) show the occurrence of intergranular SCC (IGSCC)

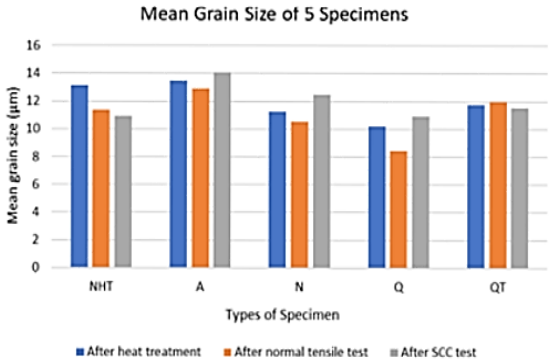

Figure 3: Mean grain size of five specimens

CONCLUSION

In this project the parameters of the stress corrosion cracking test setup has been calibrated and verified. The stress corrosion cracking behaviour of carbon steels exposed in simulated seawater has also been evaluated. Grain size reduction had been proven to be effective against SCC.

EFFECT OF POLYCAPROLACTONE (PCL) INCORPORATED WITH X-COPPER COATING ON THE CORROSION BEHAVIOUR OF MG-ZN-RE ALLOY

Wong Jie Wei and Esah Hamzah
School of Mechanical Engineering, Faculty of Engineering,
Universiti Teknologi Malaysia, 81310 UTM Skudai, Johor, Malaysia.

AIM

The aim of the project is to produce a PCL polymer incorporated with Chitosan-xZnO coating which can reduce the corrosion speed of magnesium substrate which is commonly used for biomedical implant.

OBJECTIVES

1. To synthesis polymer-based coating to be coated on Mg-Zn-RE alloy.
2. To determine effect of different proportion of polycaprolactone
(PCL) and copper addition in coating on corrosion behaviour of Mg-Zn-RE alloy.
3. To evaluate corrosion resistance of the coating when coated on Mg-Zn-RE alloy.

ABSTRACT

Magnesium (Mg) and its alloys have been used as biodegradable implant material due to unnecessity of removal after primary surgical procedure compared to conventional implant materials. Besides, its mechanical properties are similar to human bone. Apart from that, the shortcoming of Mg and its alloy is poor corrosion resistance. Hence, this study is to investigate effect of polycaprolactone (PCL) and copper (Cu) coating on corrosion behaviour of Mg-Zn-RE alloy in Kokubo SBF solution.

RESULTS

The s specimens coated with 100 % PCL has highest corrosion resistance (0.004 mm/year) than all coated and uncoated Mg-Zn-RE alloy specimens. Among the coated specimens, the corrosion rate of specimen coated with 5 % Cu and 95 % PCL is highest at 2.154 mm/year, followed by specimens with 3 % Cu and 97 %PCL and 1 % Cu AND 99 % PCL in descending order with the values of 2.089 mm/year and 1.682 mm/year respectively. In immersion test, the pH value is increased due to the formation of magnesium hydroxide indicated by pH evaluation. Needle-like morphology of hydroxyapatite (HA) crystal can be observed in corroded Mg-Zn-RE alloy specimens. Pits and cracks also can be observed in all corroded specimens.

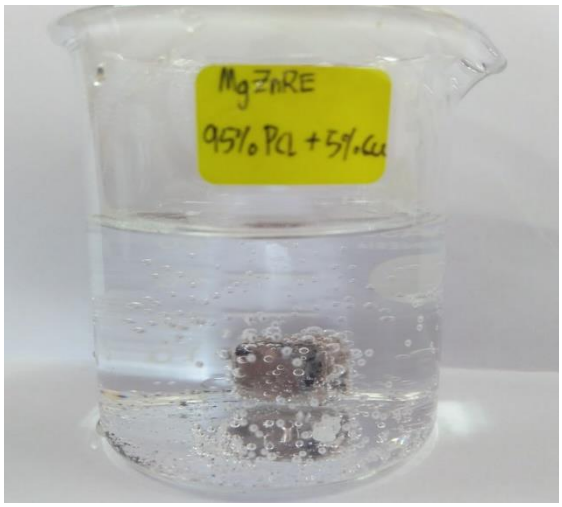

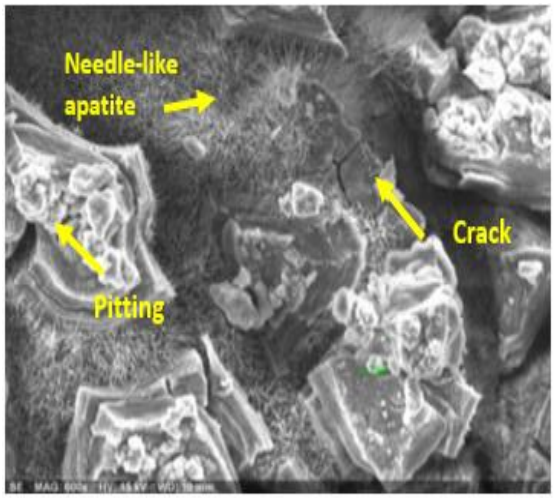

Figure 1 Biodegradable materials

CORROSION BEHAVIOR OF MAGNESIUM COATED WITH POLYCAPROLACTONE (PCL) POLYMER INCORPORATED WITH CHITOSAN-XZNO

Wong See Ying and Esah Hamzah
School of Mechanical Engineering, Faculty of Engineering,
Universiti Teknologi Malaysia, 81310 UTM Skudai, Johor, Malaysia.

AIM

The aim of the project is to produce a PCL polymer incorporated with Chitosan-xZnO coating which can reduce the corrosion speed of magnesium substrate which is commonly used for biomedical implant.

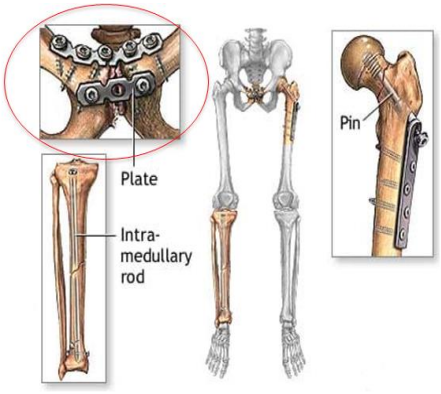

Figure 1 Biomaterials as implant

OBJECTIVES

1. To produce and determine the properties of Polycaprolactone (PCL) polymer with Chitosan-xZnO as coating material.
2. To evaluate the corrosion resistance of the coating when coated on Magnesium.

ABSTRACT

Magnesium and its alloy has been widely used in biomedical implant. However, due to its poor corrosion resistance, coating should be applied on magnesium substrate surface to enhance their corrosion resistance. Substrate has been prepared by wire cutting and dip coated with 6 types of coating slurry which made up of Polycaprolactone, Chitosan and varies concentration of Zinc Oxide that is 2, 4 and 6 wt%. The completed specimens will be Mg, Mg – PCL, Mg – PCL/CS, Mg-PCL/CS/2ZnO, Mg-PCL/CS/4ZnO, and Mg-PCL/CS/6ZnO. After coating, the specimens were sent for material characterization and corrosion testing.

RESULTS

Coating slurry were successfully produce and coated on substrate surface. Coated magnesium has higher corrosion resistance compared to uncoated magnesium. PCL/CS/2ZnO slurry has highest viscosity, produced thickest coating. As concentration of ZnO increase, granular boundary is seen on the specimen surface, coating became brittle as cracks are observed on coating and fresh metal are for further corrosion. PCL/CS/2ZnO produced best corrosion resistance with low corrosion rate, that is 0.0385mmpy and with I_{corr} = 1.707uA/cm^2.

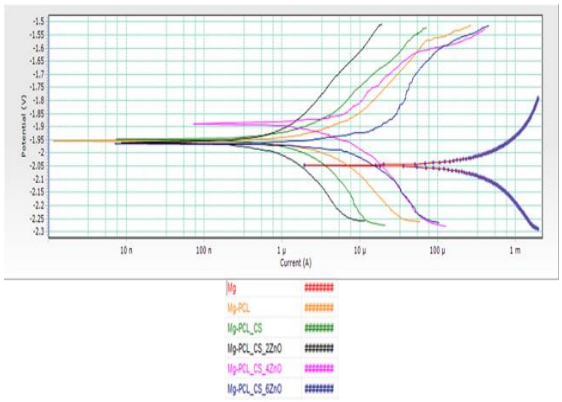

(a)

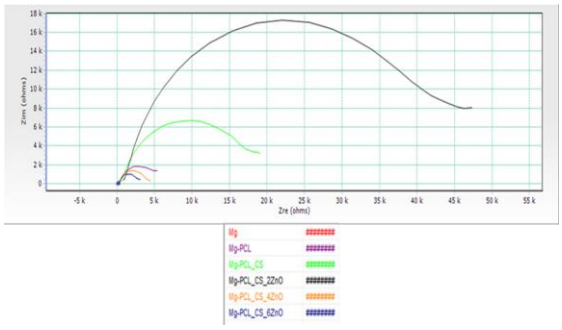

(b)

Figure 2 (a) Tafel Extrapolation plot and (b) Nyquist plot for EIS testing

SHIP-MOUNTED RENEWABLE ENERGY HARVESTING SYSTEM

Muhammad Daniel Khalilullah bin Md Suhaimi and Farah Ellyza Binti Hashim
School of Mechanical Engineering, Faculty of Engineering,
Universiti Teknologi Malaysia, 81310 UTM Skudai, Johor, Malaysia

INTRODUCTION

Renewable energy application in Malaysia is still in growing state. With the lack of professionals, there is quite a challenge to make this source being used commercially. With the rate of pollution that keep increasing with time, alternatives action must be taken in order to reduce the dependency on fossil fuel usage. Ship is one of the most contributor of pollutant for transportation class. With this alternative, hopefully the pollution that come from ship can be reduced in the future. [1]

EXPERIMENTAL SETUP

This research have been depending on the data achieved by researchers and journal about the potential of wave energy in Malaysia. With the data collected, consideration must be taken in order to apply this source of energy. With the patented design of wave energy converter, the output of the device mainly affected by input that comes from the wave energy. With low average of wave energy, the output also may be quite low to supply the demand of the ship. Basically, this source valid to supply a small ships as the big ships demand high power of electricity to operate.

Ferry is chosen to be applied with this system as this type of vessel is quite low demand in term of electricity power to operate compared to huge ships. Idle condition is chosen where loading and unloading people occur. Besides the lowest electric power demand, this is where the pollutant at the current location occur as the vessel is static at one place for a certain period in a day. This may lead to a high rate noise and air pollution. Gigantic ship basically will stop a long time at the port that included with wave breastructure that may kill the waves for the beginning. It is not practical to apply this system for huge vessels where the possibility to harvest wave energy is quite low.

With the data obtained, stability assessment can be done by applying Maxsurf Stability application. The modified device data shows depict the output of electrical power from the wave energy.

RESULTS AND DISCUSSION

From the result obtained, this system is reliable for the idle ferry as it demands the lowest amount of electrical power compared to other condition. Besides that, this system will have a low operational cost compared to conventional type of ferry that relying on auxiliary engine. With the suitable place of installation, the maintenance process may be easier compared to conventional auxiliary engine.

CONCLUSION

This system is practical in term of stability and economics based on theory and application assessment. To have a reliable result, this system need a serious attention and investment to make it happen in real life.

REFERENCES

[1] Reliability assessment of point-absorber wave energy converters (2018) (A. Kolios et al)
[2] Wave energy device and breakwater integration: a review (2017) (M.A. Mustapa et al Prospect of wave energy in malaysia (2014) (N.H. Samirat et al (Universiti Of Malaya)
[3] Satellite-based wave data and wave energy resource assessment for south china sea (O. Yaakob et al.) (Universiti Teknologi Malaysia)
[4] Review of wave energy technologies and the ecessary power-equipment (2013) (I. Lopez) (University Of The Basque Bountry Upv/Ehu, Spain)

FURTHER STUDY ON SEAKEEPING OF X-BOW HULL DESIGN FOR DISPLACEMENT HULL

Muhammad Rizal Jamaludin and Farah Ellyza Hashim
School of Mechanical Engineering, Faculty of Engineering,
Universiti Teknologi Malaysia, 81310 UTM Skudai, Johor, Malaysia

INTRODUCTION

As newly introduced to shipping industries, performance of x-bow hull still under analysis. Even though there are almost 100 unit of ships using x-bow concept but there are still study need to be conduct before this concept can be truly trusted among the shipbuilder. The knowledge gap of X bow performance on seakeeping study in irregular sea lead to conducting research on the behavior of ship with X-bow design at regular sea condition. The data will be compare with ship using normal conventional bow, which will be using bulbous bow. Thus, how will the X bow hull response if subjected on regular sea condition.

EXPERIMENTAL SETUP

In his thesis, tanker ship with identification number MTL036 was used as parent hull and MTL036B is the tanker ship performing x-bow. For this project, same ship type with different bow is needed. Unfortunately, only lines plan MTL036B can readily be used as reference as lines plan for MTL036 need to be generate back from body plan drawing to produce the hull form.

Upon completion of the seakeeping analysis, the result will determine whether the stabilization system is needed or not. The determination is based from the result of RAO and vertical acceleration. The limiting RAO will be based from the regulation from international societies and vertical acceleration will be from motion sickness incidence (MSI).

RESULTS AND DISCUSSION

Result from the Maxsurf Motion Advanced for both hull is assessed into NordForsk, 1987 limiting criteria evaluation to observed the performance of hull with regulation provided.

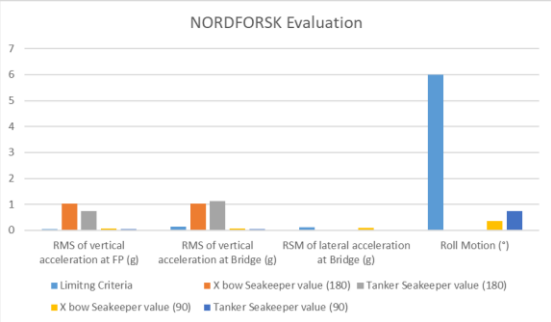

Figure 1: Overall NordForsk 1987 limiting criteria

Figure 1 summarized the NordForsk limiting criteria evaluation for both hull at head sea and beam sea condition. From the graph clearly show both hull to pass all the limiting criteria stated by NordForsk 1987, thus actually failed to have permission continuing further design process. But for this simulation, NordForsk limiting criteria was used in comparing performance to decide which one better in design.

CONCLUSION

The objectives of this research have been achieved. By conducting seakeeper simulation between X bow hull (MTL 036B) and Tanker hull (MTL 036). The seakeeping performance between the two bow has been compared. The simulation result showed that the seakeeping performance for tanker which is conventional bow is better than x-bow hull. From MSI result and NordForsk limiting criteria result, tanker hull is more preferable to sail rather than x-bow hull.

REFERENCES

[1] Azmi, A. M. (2012). X-bow Design Study For A Displacement Hull. Skudai: Universiti Teknologi Malaysia.
[2] Couser, P. (2013). Seakeeping analysis for preliminary design. Formation Design System.
[3] Naukowe, Z. (2012). The prediction of the Motion Sickness Incidence index at the initial design stage. Scientific Journals.
[4] Lloyd, A. (1989). Seakeeping: Ship Behavior in Rough Weather. Chichester, West Sussex, England: Ellis Horwood Limted.
[5] Hoyle, J. H., Cheng, B. H., Hays, B., Johnson, B., & Nehrling, B. (1986). A Bulbous Bow Design Methodology for High-Speed Ships.
[6] Yaakob, A. M. (2006). Seakeeping Analysis of A Fishing Vessel Operating in Malaysian Water. Jurnal Mekanikal.
[7] Sobri, M. A. (2007). Comparative Seakeeping Studies in Irregular Waves. Skudai: Universiti Teknologi Malaysia.
[8] Perez, T., Fossen, T. I., & Serensen, A. (2004). A discussion about seakeeping and manoeuvering models for surface vessels. Trondheim, Norway: Nowegian University of Science and Technology.
[9] Silva, M. T. (2015). Ocean Surface Wave Spectrum.

PRACTICAL MAPPING OF OFFSHORE WIND ENERGY IN MALAYSIA

Sarah Anak Johson Lapok and Farah Ellyza Hashim
School of Mechanical Engineering, Faculty of Engineering,
Universiti Teknologi Malaysia, 81310 UTM Skudai, Johor, Malaysia

INTRODUCTION

Malaysia is way behind in terms of development of renewable energy as compared to other countries. It is stated that among the major problems associated to the implementation of the wind energy system were the lack of local expertise, spare part availability, transportation and inefficient energy management. However, Malaysia has the probable into developing alternative energy. This is because wind farming is feasible that offers high theoretical potential as a renewable source of energy. Therefore, there is an essential responsibility to find the potential area at the offshore area to develop offshore wind turbine in Malaysia. [1]

EXPERIMENTAL SETUP

15 locations are chosen based on the Exclusive Economic Zone (EZZ) with each of the location is a square of $2^o \times 2^o$. 2 types of wind data which is the satellite altimeter data and buoy data is used to validate the multi-mission satellite altimeter data. The method used to validate the data is by applying the concept of correlation coefficient method and percentage difference between the buoy measurement data and satellite data to measure the strength of relationship between the two data. Thirdly, three offshore wind turbine that is available in the market is chosen. From there, an energy analysis is made on the three offshore wind turbine in order to find and select the offshore wind turbine that has the highest capacity factor. Next, other than implementing the exclusive economic zone and exclusion area. Lastly, 13 practical map development will be made with the aid of ArcMap 10.1 used.

RESULTS AND DISCUSSION

The result to determine the strength of the relationship between the buoy and multi-mission data is strong as the value of correlation coefficient is 0.806. For percentage difference, the result of the percentage difference that correlate with the buoy measurement and satellite multi-mission wind speed data. The calculation of average percentage difference throughout year 2002 until 2011 is 18.92% which is small difference. Despite the difference, the difference between the wind data if compared from the several example of data between buoy data measurement and satellite data is only 2-3 m/s. For capacity factor, the result of the capacity factor of the three offshore wind turbine. The NW 40/500 Offshore with rated power 500kW has the highest rated capacity factor with 1.332% among the others. The capacity factor of all three offshore wind turbine is considered really low as the normal capacity factor of an offshore wind turbine is 20-30%. Despite that, the NW 40/500 offshore wind turbine is chosen to proceed with the map development.

For map development, Figure 1 shows the map development of practical map development for year 2010 by using the satellite altimeter data, applying the technical power of NW 40/500 offshore wind turbine and with the consideration of exploration contract area and oil and gas field. Based on Figure 1, the map shows that the darker coloured area has higher technical power value and the lighter colour shows that the area has low technical power value in 2010.

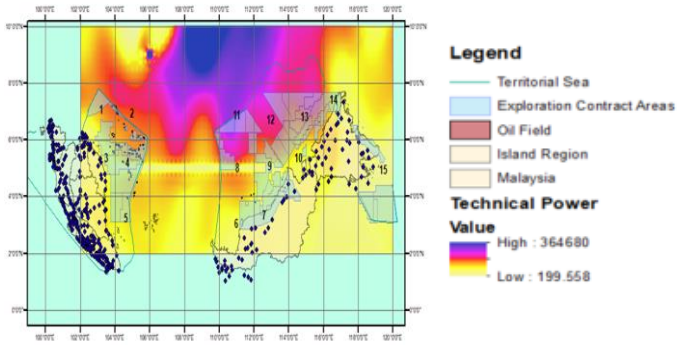

Figure 1: The map development of practical map development for year 2010

CONCLUSION

The potential area to develop an offshore wind turbine is at Area 6 in order to harness wind energy despite the seasonal variation wind speed. This is because there are not much of exploration contract area or production of oil and gas at the area despite the low of technical energy.

REFERENCES

[1] Najid, S., Zaharim, A., Razali, A., Zainol, M., Ibrahim, K., & Sopian, K. (2009). Analyzing the East Coast Malaysia Wind Speed Data. International Journal Of Energy And Environment, 3(2), 53-60.

OPTIMIZATION OF THE LACQUERING PROCESS PARAMETER ON THE PLASTIC LENS PRODUCT

Shahrul Naim Ab Halim and Mohd Faridh Ahmad Zaharuddin
School of Mechanical Engineering, Faculty of Engineering,
Universiti Teknologi Malaysia, 81310 UTM Skudai, Johor, Malaysia

INTRODUCTION

Manufacturing is one of the major scopes in the Mechanical Engineering. The biggest process in the manufacturing is the molding process because this process determines the shape of the product or part, based on the mold case shape use [1]. The next process, lacquering determines the quality of the finished product. Quality and productivity cannot be separate [2]. Good productivity is the achievement when the reject is less and the performance of quality is better. By improving the quality, the rate of reject product can be reduced. There are about only 30% of the total of the pieces' produce can pass to the customers. The reason for the high percentage of the reject parts suspected on the parameter setting of the lacquering machine.

EXPERIMENTAL SETUP

This section presents the experimental setup for the system. We used Six Sigma Tools such as Pareto Chart and Fishbone diagram for the root cause analysis and the Design of Experiment (DOE) for the optimisation of the lacquering machine.

The DOE method applied with the 2^4 have been conduct at the company with 16+1 test parameter. Each testing use 15 specimens to increase the validity of the result comparison.

RESULTS AND DISCUSSION

From the uses of Pareto Chart in figure 1, result shown that there are 3 main defect contributes to about 71% of the total number of rejected plastic lens part at lacquering process. It is Paint Dust, Contamination, and Fisheye. The Fishbone Diagram have been used to identify the root cause of the 3 major defects.

From the results of fishbone diagram, there are 3 common main causes that all 3 defects face, it is on the error method of handling, long process cycle and outdated machine parameter applied. The process improvement modification has been applied in DOE method

From the DOE method applied, it resulted that there are 3 testing parameter have shown the huge increment in the number of good product produced. The highest percentage of the good product produced is from the testing parameter 3.

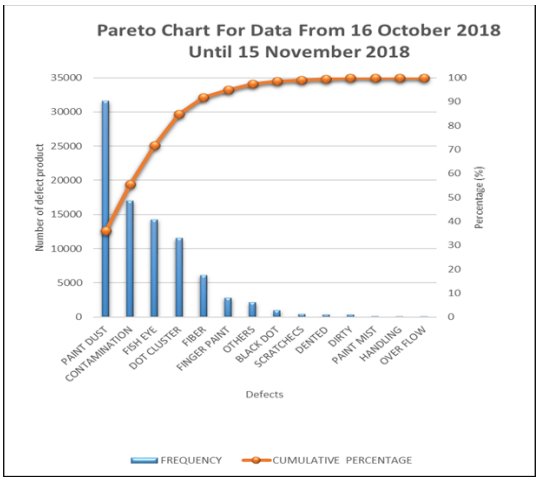

Figure 1: Pareto Chart of the Defect occur on Plastic Lens.

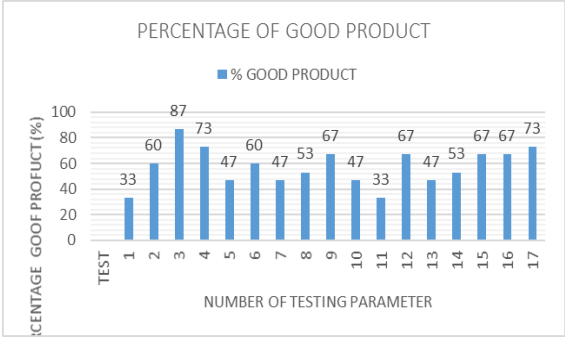

Figure 2: Percentage of Good Product

CONCLUSION

Based on the result from the Design of Experiment method, there is about 54% increment of the percentage of the good product when using the test parameter 3 compare to the OI Parameter. So, the objectives have been achieved.

REFERENCES

[1] Valles, A., Sanchez, J., Noriega, S. and Gómez Nuñez, B. (2009) 'Implementation of Six Sigma in a manufacturing process: A case study', International Journal of Industrial Engineering: Theory Applications and Practice, 16(3), pp. 171–181.

[2] Park, S. H. (2003) Six Sigma for Quality and Productivity Promotion.

OPTIMIZATION OF SPOT WELDING IN WIRE MOUNTING PROCESS

Shahfuan Shamsokahar and Mohd Faridh Zaharuddin
School of Mechanical Engineering, Faculty of Engineering,
Universiti Teknologi Malaysia, 81310 UTM Skudai, Johor, Malaysia

INTRODUCTION

Spot welding is an important joining method that joins two or more sheet metals. It had been widely used in automotive industry for many years. Many materials can be joined by using spot welding. The quality of spot welding is greatly depends on the important parameter such as welding current, welding voltage and welding time. However, many problem can occur if the parameters of spot welding are not set properly. Hence, the purpose of this study is to determine the optimum parameter setting for the application of spot welding at Hacker machine in order to reduce the wire break problem. There are two factors that only considered in this research which are welding voltage and welding time run with three replication

EXPERIMENTAL SETUP

This section presents the experimental setup for the system. The number of run order is 9 which is determined by using Design of Experiment as shown in Table 1 below, two-factor factorial experiment. All the specimens will be do the pull bond test by using the Chatillon X equipment. The data collection will be analyse by using Minitab Software and generate several result such as Analysis of Variance (ANOVA) others statically graph. There two type of analysis in this research which is first bonding analysis and second bonding analysis.

Table 1**:** The setting of the parameters in the experiments

Run order	Welding Voltage (V)	Welding Time (ms)
1	1	22
2	1.05	22
3	1.15	22
4	1	35
5	1.05	35
6	1.15	35
7	1	45
8	1.05	45
9	1.05	45

RESULTS AND DISCUSSION

The data collection for first bonding and second bonding will be analyse using Minitab software to generate several results. Figure 1 shows a main effect plot for first bonding analysis. The figure shows that the highest response output which is bonding strength for factor welding voltage is at low level (1) value while for lowest response output, the welding voltage should set at medium level (2). For welding time factor, to obtain the highest bonding strength, the factor should be set at low level (1) while to obtain the lowest response output, high level (3) setting may require. Figure 2 shows a main effect plot for second bonding analysis. The figure shows that the highest response output which is bonding strength for factor welding voltage is at low level (1) value while for lowest response output, the welding voltage should set at high level (3). For welding time factor, to obtain the highest bonding strength, the factor should be set at low level (1) while to obtain the lowest response output, medium level (2) and high level (3) setting require.

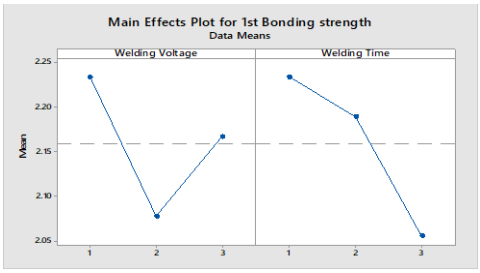

Figure 1: Main effect plot for 1st bonding

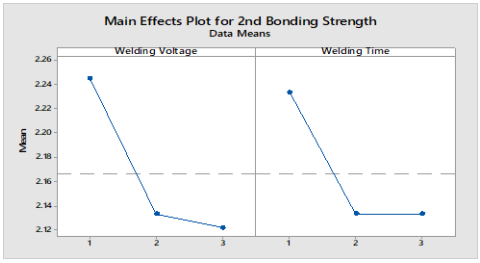

Figure 2: Main effect plot for 2nd bonding

CONCLUSION

As a result for first bonding analysis, in order to obtain highest bonding strength, the welding voltage and welding time parameter should be set at low level (1). For second bonding analysis, to achieve highest bonding strength, the welding voltage and welding time parameter is set at low level (1).

REFERENCES

[1] Sia, P. C. (2012). Spot Welding Analysis Using Stainless Steel Sheet for Automobile Application, Universiti Teknologi Malaysia.

[2] Montgomery, D. C. (2017). Design and analysis of experiments, John wiley & sons.

NUMERICAL INVESTIGATION AND OPTIMAL AERODYNAMICAL DESIGN OF LID SHROUD FOR HORIZONTAL AXIS WIND TURBINE (HAWT)

Fitri Ali Aznan Ali and Fazila Mohd Zawawi
School of Mechanical Engineering, Faculty of Engineering,
Universiti Teknologi Malaysia, 81310 UTM Skudai, Johor, Malaysia

INTRODUCTION

Wind power technology has been developed rapidly since the end of 1970. The lid shroud wind turbine able to create a low-pressure area at the downstream of the wind turbine resulting in increase of local wind speed through the turbine. Diffuser type shroud with flange can accelerate the wind by 50 % [3] and [2] stated diffuser augmented wind turbines show two times increase of coefficient of power compare to bare wind turbine.

SIMULATION SETUP

ANSYS FLUENT commercial software was used to develop an effective numerical model of shrouded wind turbine. Optimized blade was design based on Betz Theory in term of chord and twist distribution at optimum TSR of 6 while the shroud was design based on ratio to rotor diameter. There were two computational domains and the boundary conditions were assigned to the model. For meshing processes, structured hexahedral mesh for the stationary domain and unstructured tetrahedral mesh for the rotating domain. The inlet velocity was kept at 5 m/s while the rotor tip speed ratio (TSR) was varied from 4 to 8. Steady state time based and k-omega SST turbulent model was chosen to simulate the flow behaviour. k-omega turbulent model able to simulates outer region of boundary layer and flow behaviour near the wall [1].

RESULTS AND DISCUSSION

There are two type of results obtain from the ANSYS post-processing which is the qualitative and quantitative result. Figure 1 shows the vortex formation behind the flange. The formation on vortex create a pressure drop from 14.4 to -10.5 Pa and thus increase the wind speed through the turbine almost 14 % from the actual wind speed. An increase of wind speed through the turbine will increase the performance of wind turbine as the power is directly proportional to wind speed cube.

Figure 2 shows a parabolic trend for shrouded and bare wind turbine at different TSR. By analysing the trend, shrouded and bare wind turbine operates optimally at TSR= 6 which is the on-design operation. The shrouded wind turbine shows an increment of performance compared to the bare wind turbine and it capable to exceeds the Betz limit which is 59.3 %. At every TSR value, the power augmentation by shrouding it shows more than one times as compared to bare wind turbine. [3] stated that shrouded wind turbine capable to increase the power coefficient two times compare to bare wind turbine

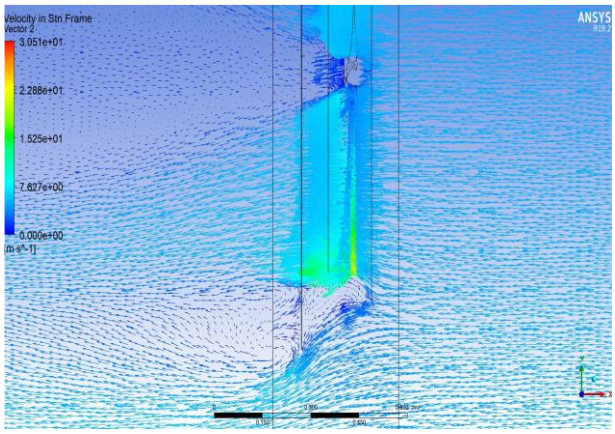

Figure 9: Vortex formation at downstream the shrouded wind turbine.

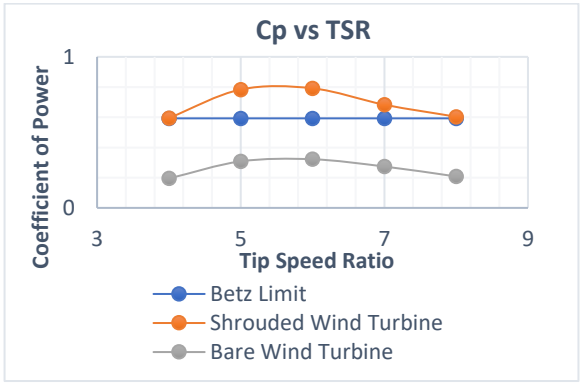

Figure 2: Coefficient of power vs. TSR.

CONCLUSION

The formation of vortex creates a low-pressure area downstream the wind turbine and increase the wind speed through the body. Thus, the performance exceeds Betz limit and has improved more than 1 times compared to the bare wind turbine.

REFERENCES

[1] Heikal, H. A., Abu-Elyazeed, O. S., Nawar, M. A., Attai, Y. A., & Mohamed, M. M. (2018). On the actual power coefficient by theoretical developing of the diffuser flange of wind-lens turbine. Renewable energy, 125, 295-305.

[2] Kosasih, B., & Hudin, H. S. (2016). Influence of inflow turbulence intensity on the performance of bare and diffuser-augmented micro wind turbine

[3] Ohya, Y., & Karasudani, T. (2010). A shrouded wind turbine generating high output power with wind-lens technology. Energies, 3(4), 634-649.

CFD INVESTIGATION ON THE JET-ENGINE INSPIRED WIND TURBINE

Nur Shamimi Amirah Md Sunhazim and Fazila Mohd Zawawi
School of Mechanical Engineering, Faculty of Engineering,
Universiti Teknologi Malaysia, 81310 UTM Skudai, Johor, Malaysia

INTRODUCTION

Renewable energy is being commercialize to use in this world as it replenished naturally and does not have limited supplies compared to non-renewable energy. There are a few common renewable energies that are commonly used which are solar, wind, water (hydro), biomass, and geothermal. Comparing all these renewable energies, wind energy is the cleanest energy, as it does not produce any CO_2 emissions [1,2]. Therefore, wind energy is having a high demand to be used and commercialized by installing and designing an efficient wind turbine, in order to capture the optimum energy from the wind.

OBJECTIVE

The aim of this project is to develop and effective numerical model for accessing the capability of the jet-engine inspired wind turbine as a power generation system by determining its performance with the influence of the curly shroud on the induced flow.

EXPERIMENTAL SETUP

Computational Fluid Dynamics (CFD) was used to simulate the jet-engine inspired wind turbine to study its performance. The jet-engine inspired wind turbine was designed by using SolidWorks before being imported to ANSYS Fluent 18.0. Two domains were created to study the flow of the fluid, which are rotating and stationary domain. The mesh grid used in this study is tetrahedral mesh along with the sizing method to refine the meshing and reduce the skewness. By varying the Tip Speed Ratio (TSR) values from 2 to 5, the simulation was done twice for each TSR values, which were jet-engine inspired wind turbine with and without shroud. The moment values and the contour of the flow were then being analysed.

RESULTS AND DISCUSSION

Moment data obtained from the ANSYS Fluent was used to calculate the mechanical power of the wind turbine. From this values of mechanical power and wind power, the power coefficient of the wind turbine can be obtained. Table 1 shows the percentage difference in power coefficient for the jet-engine inspired wind turbine with and without shroud. The highest percentage obtained is 21.9%, which is for TSR value of 5 while the lowest percentage is 5% with TSR value of 2.

Table 2: Percentage difference on the Power Coefficient between Jet-Engine Inspired Wind Turbine with and without shroud

TSR	With Shroud	Without Shroud	Percentage Difference (%)
	Power Coefficient (Cp)	Power Coefficient (Cp)	
2	0.20	0.20	5
3	0.29	0.26	11.5
4	0.34	0.32	6.25
5	0.39	0.32	21.9
6	0.38	0.35	8.6

Besides that, the influence of the curly shroud can be studied from the velocity and pressure contour obtained. Figure 1 indicates the swirl formation happened at the shroud, which contributes in pressure dropping at the back of the wind turbine. This will eventually increase the wind speed at the inlet of the wind turbine due to the suction happened by the high pressure region to the low pressure region.

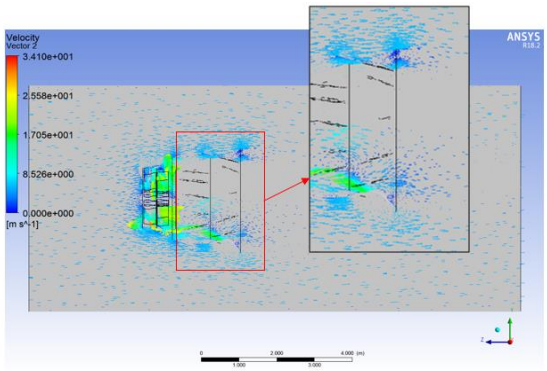

Figure 10 Swirl formation at the back of the wind turbine

CONCLUSION

The positive values of percentage indicate that the wind turbine having a shroud can help in enhancing the wind turbine performance. This shows that jet-engine inspired wind turbine is capable to be as a power generation system.

REFERENCES

[1] Hansen, M. O. L. (2015). Aerodynamics of Wind Turbines: Taylor & Francis.
[2] Chiras, D. (2010). Wind Power Basics: A Green Energy Guide: New Society Publishers.

NUMERICAL ANALYSIS OF IMPELLER FOR WHIRLPOOL VORTEX HYDRO TURBINE CASE STUDY: LEMOI, CAMERON HIGHLANDS

Alif Murtadza Muhamad and Fazila Mohd Zawawi
School of Mechanical Engineering, Faculty of Engineering,
Universiti Teknologi Malaysia, 81310 UTM Skudai, Johor, Malaysia

INTRODUCTION

Gravitational Water Vortex Power Plant (GWVPP) is another alternative to generate electricity and channel it to the rural areas. GWVPP is capable to convert low head potential energy into kinetic energy to power turbines through a gravity vortex pool. In addition, the costs for development and power generation in GWVPP are very low as simple construction can be conducted. Not only financial cost is reduced, the damage towards environment also decreased.

EXPERIMENTAL SETUP

The aim of this project is to develop a reliable numerical model of gravitational vortex hydro turbine. The model was first being developed using Solidworks and then imported to ANSYS Fluent for simulation. ANSYS Fluent was used to analyze the fluid flow through the channel and results were used to identify the optimal condition which can maximize its efficiency. The effect of parameters such as the rotational speed of output shaft and the mass flow rate of water were studied to investigate its effect on electricity power generation. Lastly, the results was validated by measuring its mechanical power generation and comparing it with the actual power generation at Lemoi, Cameron Highlands.

RESULTS AND DISCUSSION

There are two fluid domain had been created: a stationary domain which the fluid flows through and a rotating domain where the turbine model will rotates. The fluid domain is shown as figure below. Next, the modelled domain was imported to ANSYS Fluent for further simulation. For the stationary domain, a hex dominant method with free face mesh set to “All Quadrilateral” is used to get a structured mesh where majority of the cell consists of hexahedral cell and small portion of prism cell. . Mapped hex meshing also being added to obtain a better quality of mesh. Due to the complexity of rotating domain’s geometry, unstructured mesh is generated for the rotating domain which consists of tetrahedral cell

As for boundary condition, the velocity inlet for stationary domain was set to be 0.167m/s and outflow with flow rate weighing of 1 was set for outlet boundary. The wall surface was set to be stationary with no slip condition. The working fluid in the computational domain zone condition will be set to water. To study the effect of rotational speed, the domain motion in rotating domain was varied with the angular velocity ranging from 0 to 100 rpm in anticlockwise direction. While, the inlet velocity was varied from 0.1 to 1.0 m/s to study the effect of mass flow rate to the turbine performance. For all cases, the k- turbulence model has been used for numerical simulation process considering the water flow is incompressible.

Figure 1 shows the trend of mechanical power changes when the rotational speed had been increased. At 60 rpm, the resulted mechanical power from simulation is 1046.95 W which is likely close with the actual mechanical power in Lemoi. With the similar condition of 60 rpm, almost 835.81 W had been generated in Lemoi.

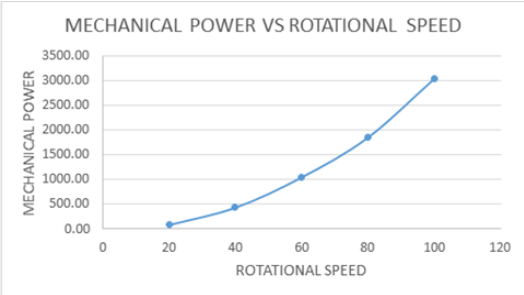

Figure 1: Graph of mechanical power versus rotational speed at output shaft

REFERENCES

[1] Dhakal, R., Bajracharya, T. R., Shakya, S. R., Kumal, B., Khanal, K., Williamson, S. J.,Ghale, D. P. (2017). Computational and experimental investigation of runner for gravitational water vortex power plant.

POWER PRODUCTION BY THE INTEGRATED BLADES ON WATER WHEEL

Azizi Shaharuddin and Fazila Mohd Zawawi
School of Mechanical Engineering, Faculty of Engineering,
Universiti Teknologi Malaysia, 81310 UTM Skudai, Johor, Malaysia

INTRODUCTION

All countries worldwide are searching for alternatives to sustain and meet the rising in energy demand and reduce carbon emission produced by fossil fuel. Water wheel is regarded as clean and reliable renewable energy to generate electricity. Generation of electricity is produced by the rotation of water wheel. However, due to low volumetric flowrates of water that goes into the buckets of water wheel, the water wheel produce less torque, which eventually produce less power output. Thus, a new concept is investigated by implementing an integrated blades on the water wheel with the objective that it could enhance the power output. These blades are attached to the wheel and harness the air surrounding as the water wheel rotates.

SIMULATION SETUP

The geometry of integrated blades is modelled in 2D by using Solidworks software. Once the geometry is imported to Ansys Fluent for simulation, the meshing process was performed by using triangle methods. The inflation layer is used around the airfoils to obtain more precise results. Meshing consist of 461608 nodes and 490291 elements.

Realizable k-epsilon model is used as turbulence model. 8 cases are investigated by varying the angle of blades and the speed of rotation (rpm).

RESULTS AND DISCUSSION

The analysis conducted by varying angle of blades with 30° and 60° (clockwise and anticlockwise) angles respectively. For these four model cases, the boundary condition is set for the airfoil to make rotation in anticlockwise direction by varying the rotational speed (20rpm and 500rpm). The velocity contour of 30° anticlockwise angle is shown in Figure 1.

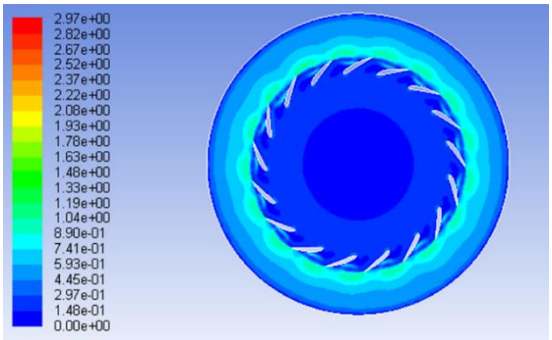

Figure 1: Velocity contour of 30° anticlockwise angle

It is observed that the velocity on top of the blades surface is higher compared to the bottom surface. Fundamentally, velocity is inversely proportional to pressure. Due to the difference in pressure between top and bottom surface of blades, an external force created a torque to the blades.

From the comparison of the results taken for four different angles of blades and 2 different rotational speed, it is found that 30° anticlockwise angle creates the highest torque, which produce about 218.86W/m. If this configuration is used with the water wheel, the power it could produce is about 2.2kW/m. Figure 2 illustrate the coefficient performance of 4 different blade angles by maintaining speed of 500rpm.

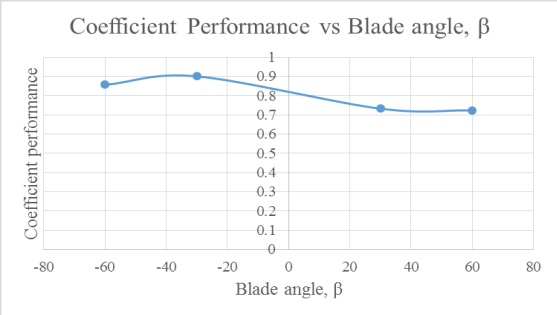

Figure 2: Coefficient performance for 500rpm speed

CONCLUSION

As the conclusion, the 30° anticlockwise angle of blades could generate the highest torque and highest power output. By implementing this concept with the optimum configuration, the efficiency could increase by 8.5% from 81.5% to 90% considering there is no power losses by the water wheel.

REFERENCES

[1] Quaranta, E., & Revelli, R. (2018). Gravity water wheels as a micro hydropower energy source: A review based on historic data, design methods, efficiencies and modern optimizations. Renewable and Sustainable Energy Reviews 97 (2018) 414-427

[2] Quaranta, E., & Revelli, R. (2015). Performance characteristics, power losses and mechanical power estimation for a breastshot water wheel. Energy 87 (2015) 315-325

[3] Muller, G., & Kauppert, K. (2010). Performance characteristics of water wheels. Journal of Hydraulic Research Vol. 42, No. 5 (2004), pp. 451-460

RENEWABLE ENERGY THROUGH LORRY MOUNTED WIND TURBINE

Sulaiman Ismai and Fazila Mohd Zawawi
School of Mechanical Engineering, Faculty of Engineering,
Universiti Teknologi Malaysia, 81310 UTM Skudai, Johor, Malaysia

INTRODUCTION

Among renewable energies, the most valuable, safe and fastest growing renewable energy is wind energy. At the end of 2016, wind energy has served approximately 957.94 GW. Furthermore, wind energy cost is low (0.12/kWh), its carbon footprints is low (<5CO2/kWh), it has minimum sound pressure level (50-60 dB from 100 feet) and it is easy to integrate with other sources of energy. However, since wind energy requires big land, high installation cost, lack of energy storage and not portable, commercial wind turbine is not suitable for small scale application. Moreover, a commercial or domestic wind turbine cannot be run in some places as its wind speed is not adequate. Thus, it is necessary to modify a wind turbine which can be efficient under this kind of circumstances. Consequently, the idea of mobile wind turbine for vehicle came along for small scale energy harvesting.

CFD SIMULATION SETUP

This section presents the CFD simulation setup for the system of lorry mounted wind turbine. At first, optimized small horizontal axis wind turbine (HAWT) design was generated using Betz Limit Theory. Then, the HAWT is modelled mounted on lorry using drawing software. The model was then simulated by using kω-SST model. Inlet velocity at 27.78 m/s. Rotational velocity of turbine at 6366 rpm. The scheme used is SIMPLEC. Moment of wind turbine is extracted from the simulation to know the power mechanical, p_{mech} generated and power coefficient produced, c_p. Besides that, wind velocity with respect to distance from wind turbine is also extracted to know the next row of turbine location. Lastly, the simulation for wind turbine with different tip speed ratio, TSR is run to investigate its p_{mech} and c_p.

RESULTS AND DISCUSSION

When simulation is done, it is found out that a spiral vortex is formed in the flow which agrees to Theory of Betz Limit. Figure 1 shows the flow. Besides that, after following the flowchart steps to know the next location of row of wind turbine, it has been decided to be put at distance 0.72m from first row wind turbine. Other than that, the graph of different TSR effect towards c_p is shown in Figure 3. From graph of c_p vs TSR, power coefficient increases as TSR increases. Supposedly, the c_p should decrease after the design TSR=6 because that is the most uniform flow. However, we can see that the gradient for the graph start to decrease. Perhaps, the line can be seen lower after TSR more than 8. This might also happen due to the mesh is not fine enough in CFD simulation. Moreover, the c_p for wind turbine 2 and 3 for TSR=8 is 1.00 and 1.02 respectively. This is not right since there is no way a wind turbine can fully capture wind power and generate 100% or 102% of it to become electrical energy. This may happen due to bad meshing in CFD simulation. Other than that, it may also happen because convergence criteria when running the simulation is not low enough. This make the torque not constant yet when the scaled residual is already converged.

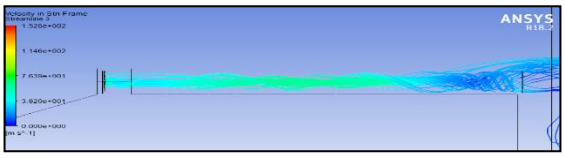

Figure 1 flow behaviour of lorry mounted wind turbine

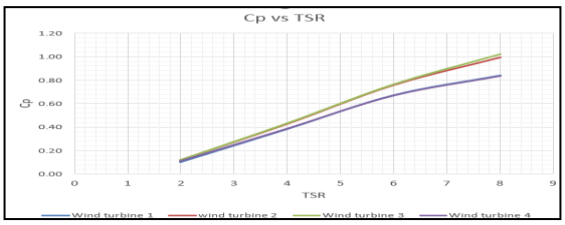

Figure 2 Graph of c_p vs TSR

CONCLUSION

The flow behaviour of lorry mounted wind turbine has been simulated. It follows Betz Limit Theory. The location for next row of wind turbine has been decided at 0.72m form first row of wind turbine. Increase TSR give increase c_p.

REFERENCES

[1] Awal, M. R., Jusoh, M., Sakib, M. N., Hossain, F. S., Beson, M. R. C., & Aljunid, S. A. (2015). Design and implementation of vehicle mounted wind turbine. *ARPN J Eng Appl Sci*, *10*, 8699-8706.

[2] Glynn, K. P. (2010). *U.S. Patent No. 7,808,121*. Washington, DC: U.S. Patent and Trademark Office.

[3] Wen-Long Yao, A. Chiu, C. (2015) Development of a Wind Power System on Trucks. National Kaohsiung First University of Science and Technology, Taiwan: Universal Journal of Mechanical Engineering 3(5) 151 - 163.

NUMERICAL INVESTIGATION OF RENEWABLE ENERGY THROUGH BANKI HYDRO TURBINE-TYPE SYSTEM

Mohamad Shahnizam Sabiran and Fazila Mohd Zawawi
School of Mechanical Engineering, Faculty of Engineering,
Universiti Teknologi Malaysia, 81310 UTM Skudai, Johor, Malaysia

INTRODUCTION

Cross flow Banki-Turbine is the solution of hydro turbine that requires the low water velocity. In this context, the Cross flow Banki-Turbine are extensively used due to the simple design [1], easy in maintenance and low cost. Although this Banki-Turbine has moderate efficiency, but it is suitable to be apply in rural area with low head. In this research, the performance of this Banki-Turbine is run in simulation using ANSYS FLUENT 18.2 in 2-D design by applying the shear stress transport k-omega turbulence model. The design of the runner blade is taken from [2] as it gives the highest power coefficient, Cp.

SIMULATION SETUP

From the Table 1, we can see that simulation is chosen as the steady where, the flow of the fluid is constant as the time changing. Then, K – omega with Shear Stress Transport (SST) is chosen for perfect calculation [3].

Table 1: General setting for the simulation

Type	Setting
Simulation	Steady
Turbulence Model	K – omega, SST
Cell Zone	Water-liquid
Dynamic Mesh	Smoothing, layering, remeshing
Scheme	SIMPLE, Second Order

RESULTS AND DISCUSSION

From the Figure 1 below, we can see that Cp for the Case 3, (0.775) is the highest followed by Case 2, (0.614) and lastly is Case 3, (0.515). For the Case 1, the value of Cp is increasing until reach the maximum at 0.515 for TSR 0.877 before decreasing. Then, the Cp value for Case 2 is gradually increasing until 0.614 as the maximum for TSR 1.202. And for the Case 3, the highest Cp which is 0.775 at TSR 1.070.

Overall we can say that, the increases of water velocity, V will increase the power output, Pout of this banki-turbine. But keep increasing RPM of runner beyond the optimum runner RPM, will reduce the power output, Pout.

From the Figure 2 below, we can see that Ct for the Case 3, (0.333) is the highest followed by Case 2, (0.331) and lastly is Case 3, (0.330). For all 3 cases, the pattern of the graph of Ct against TSR is quite similar where the graph is gradually decrease as TSR increase.

Overall we can say that, the torque coefficient, Ct also will decrease as the angular velocity of runner, ω increase.

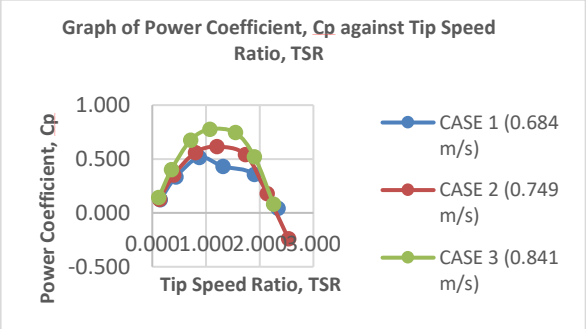

Figure 1: Graph of Cp against TSR

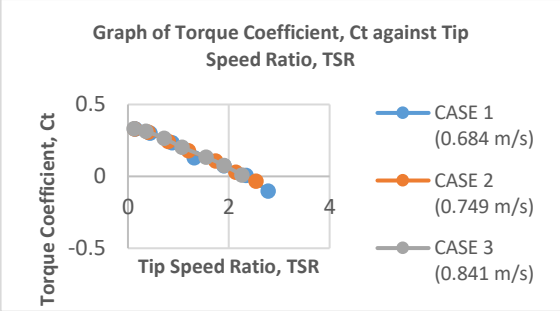

Figure 2: Graph of Ct against TSR

CONCLUSION

As conclusion, from the numerical investigation, we can study on how efficient the performance of Banki-turbine. We also can get the optimum parameters and optimum TSR for this Banki-turbine.

REFERENCES

[1] Chichkhede, S., Verma, V., Gaba, V., & Bhowmick, S. (2016). A Simulation Based Study of Flow Velocities across Cross Flow Turbine at Different Nozzle Openings. Procedia Technology, 25, 974-981.

[2] Elbatran, A., Yaakob, O., Ahmed, Y., & Shehata, A. (2018). Numerical and experimental investigations on efficient design and performance of hydrokinetic Banki cross flow turbine for rural areas. Ocean Engineering, 159, 437-456.

[3] Adhikari, R., & Wood, D. (2018). The Design of High Efficiency Crossflow Hydro Turbines: A Review and Extension. Energies, 11(2), 267.

MULTIPURPOSE CORN SEED SOWING MACHINE

Zulaikha Haibir and Hairul Anuar Abdullah
School of Mechanical Engineering, Faculty of Engineering,
Universiti Teknologi Malaysia, 81310 UTM Skudai, Johor, Malaysia

INTRODUCTION

The design process of the multipurpose corn seed sowing jig undergoes several stages before the fabrication process can start. First and foremost, literature review was done on patent that includes necessary function and mechanism, existing product and also the tractor specification. Next, several design methods or tools are used to develop the concept design. Methods or tools that was used are Functional Block Diagram, Morphological Chart and Concept Selection by using Evaluation Matrix and Pugh Matrix. These tools are used to generate three concept design and final concept design. Then, the first detailed design is created and analysed by using Design for Manufacture and Assembly (DFMA) analysis and Failure Mode and Effect Analysis (FMEA). From there, an engineering analysis was done on the final detailed drawing. Engineering drawing was also generated for the fabrication of prototype. Lastly, the prototype was tested by a car.

METHODOLOGY

1. Functional Block Diagram
2. Morphological Chart
3. Three Concept Design
4. Concept Selection
5. Final Concept Design

RESULTS AND DISCUSSION

The figure below shoes the final detailed design in the form of CAD modelling and the prototype for multipurpose corn seed sowing jig. Due to miscommunication with the farmers, I was not able to have access to their land and tractor. Hence the prototype was tested by hitching it to a car. The result is that the jig is able to drop the seed one by one and dislodge it at the correct interval. However the jig is quite inconsistent as the prototype have a low fabrication quality and incorrect testing parameter.

(a) (b)

Figure 1(a) : CAD model for multipurpose corn seed sowing jig (b) : Prototype of multipurpose corn seed sowing jig

CONCLUSION

The multipurpose corn seed sowing jig for a tractor has been designed, fabricated and tested. From the result of functionality testing, the multipurpose corn seed sowing jig can't assist farmers in reducing the plantation time if it's not fabricated properly according to the design.

REFERENCES

[1] KUBOTA Ltd. (n.d.). Operator's Manual KUBOTA TRACTOR. Japan: KUBOTA Ltd.
[2] Lester F. Larsen Tractor Museum. (1997). Test 1725: John Deere 7610 Powershift Diesel. Nebraska: University of Nebraska-Lincoln.
[3] Maury, J.-P. (1983). United States Patent No. 4,399,757.
[4] McCanse, J. E., & Dhaliwal, J. (1983). United States Patent No. 4,386,661.
[5] Okoko, P., Ajav, E. A., & Olosunde, W. A. (2018). Draft and power requirements for some tillage implements operating in clay loam soil. Agricultural Engineering International: CIGR Journal, 95-102.

THERMAL COMFORT ENHANCEMENT IN A PROTON IRIZ CAR CABIN

Mohd Syafik Sabudin, Haslinda Mohamed Kamar and Nazri Kamsah
School of Mechanical Engineering, Faculty of Engineering,
Universiti Teknologi Malaysia, 81300 UTM Skudai, Johor, Malaysia

INTRODUCTION

The ideal condition in a car cabin with equally distributed airflow velocity and temperature are desirable in any vehicle. However, in a real condition, there is uneven airflow velocity and temperature distributions in the cabin. Therefore, this study is intended to improve the airflow velocity and temperature distributions inside the car cabin. A simulation work on the airflow velocity and temperature was carried out by using the commercial CFD software. Then, parametric analysis was carried out to investigate the suitable enhancement in terms of geometry and layout that can be implemented inside the car cabin.

EXPERIMENTAL SETUP

This section presents the numerical setup for the system. The simplified model was developed using SOLIDWORKS software based on the actual dimension of the PROTON Iriz interior car cabin. The computational domain is needed for CFD software to generate a meshed domain. Mesh generation is the practice of generating a polygonal or polyhedral mesh that approximates a geometric domain.

The result obtained from the CFD simulation was compared with the experimental data provided by PROTON. From the literature review, a 20 % difference between the simulation and measured data is considered acceptable [1].

RESULTS AND DISCUSSION

To improve the airflow velocity and air temperature distributions inside the car cabin, 2 additional air vents were added to the B-pillar at rear passenger section (Case 4).

Figure 1 shows the comparison of airflow velocity contour between baseline case and Case 4. From the figure, the average airflow velocity distribution is improved a lot compared to the baseline. For the rear section, the average airflow velocity increased significantly by 155.74 %

From the figure 2, the air temperature distribution improved a lot compared to the baseline. For the rear section, the average air temperature decreased by 11.71 %.

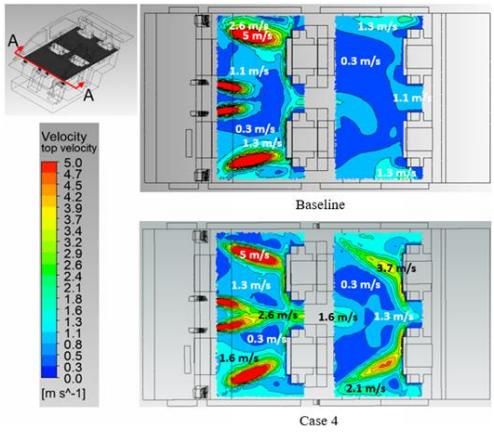

Figure 11: Comparison of airflow velocity contour between Case 4 and baseline

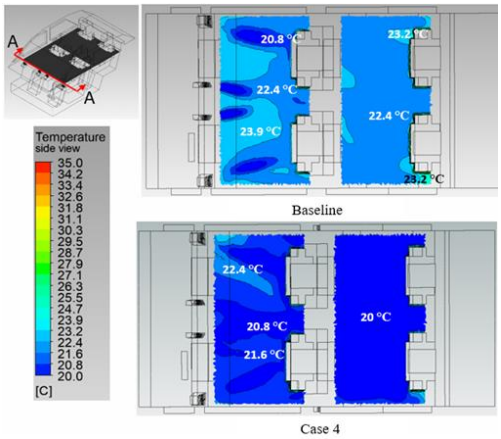

Figure 12: Comparison of air temperature contour between Case 4 and baseline

CONCLUSION

From the CFD analysis, It was found that the additional air vents at the B-pillar is capable of providing more uniform distributions of air flow velocity and air temperature for the front and rear passenger sections. Higher air flow velocity is obtained in the rear passenger section.

REFERENCES

[1] Tao H., Chen H., Xie J. and Jiang, J. (2011). Comparison on simulation and experiment of supply air through vehicle air conditioning duct. *Applied Mechanics and Materials*. 44-47: 1724-1728.

SPAWN TREATMENT AND GROWTH OF OYSTER MUSHROOM BY ATMOSPHERIC PLASMA TECHNIQUE

Muhammad Farid Aidil Mohd Ali and Hayati Ahmad
School of Mechanical Engineering, Faculty of Engineering,
Universiti Teknologi Malaysia, 81310 UTM Skudai, Johor, Malaysia

INTRODUCTION

Plasma is considered to be fourth state of matter [1] after solid, liquid and gas. It is fully ionized gas that consists of ions, electrons and uncharged particles such as atoms, molecules and radicals. Non-thermal plasma has become one of the new technologies which are rapidly developed. This happen due to ability of cold plasma to modify the surface properties of a material or product without changing the original characteristics of the material.

Oyster mushroom is the most versatile mushrooms and in Malaysia, oyster mushroom can easily obtained in market because it's generally low in saturated fats and high in fiber and protein, and may reduce harmful blood cholesterol and act as an appetite suppressant [2]. Immune system can also be enhanced using mushrooms.

EXPERIMENTAL SETUP

To treat the spawn, plasma pencil is used. Treat the spawn with different flowrate (2 SLM – 6 SLM) and duration of treatment (5s – 60s) with constant carrier gas (air) and voltage output (8 kV).

After plasma treatment, the spawn is inject into substrate. To observe effectiveness of treated spawn, mycelium growth, quantity of mushroom and characterization of mushroom are investigated

RESULTS AND DISCUSSION

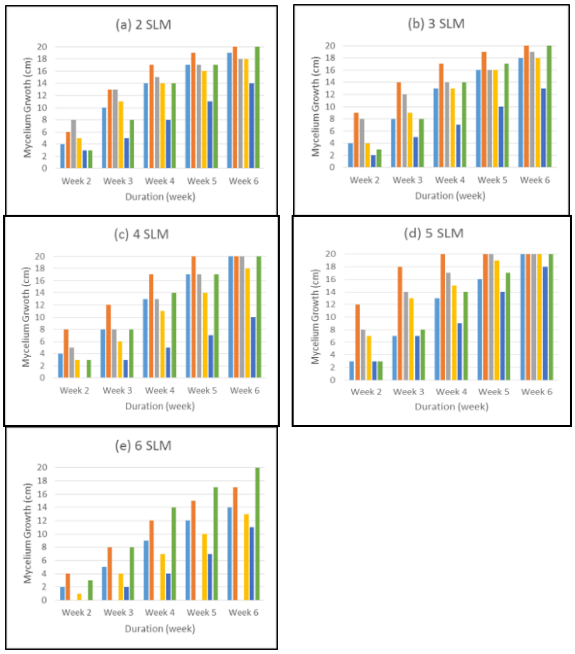

Figure 1: Duration of mycelium growth

Figure 1 shows that from overall graph, 5 SLM and 15s treated spawn fastest to complete the mycelium growth with only need 4 week compare to untreated that need 6 week.

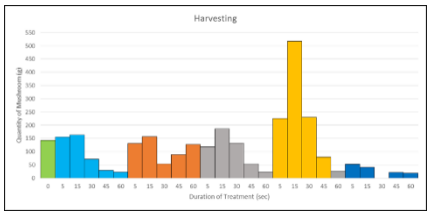

Figure 2: quantity of mushroom produce by treated and untreated spawn in the 1st cycle

Figure 2 shows quantity of mushroom produce by treated and untreated spawn in the 1st cycle where 5 SLM 15s treated spawn produce highest amount of mushroom more than 500g compare to untreated spawn only produce almost 150g. Table 1 shows diameter of cap, length and stalk thickness of mushroom where no significance different between them. The different only can be seen in quantity of mushroom where 5 LSM 15s produce 30 mushroom compare to untreated spawn only 10 mushroom at one time.

Table 1: Characterization of Mushroom

Flowrate	Duration of Treatment	Diameter of the cap (cm)	Length (cm)	Stalk Thickness	Number of Mushroom
Control	0s	6.5	6.2	1.0	10
2 SLM	15	7.5	7.2	1.32	16
3 SLM	15	7	4.16	1.48	14
4 SLM	15	6.6	3.6	1.5	17
5 SLM	15	8	6	1.7	30
6 SLM	15	7.4	4.62	1.08	7

CONCLUSION

Spawn was successful treated with cold plasma. 5 SLM and 15s duration of treatment is the best parameter. 5 SLM and 15s has the highest growth rate of mycelium and produce the most mushroom.

REFERENCES

[1] Niemira, B. A. (2014). Decontamination of Foods by Cold Plasma. *Emerging Technologies for Food Processing*,327-333.

[2] Kim, K., Choi, B., Lee, I., Lee, H., Kwon, S., Oh, K., & Kim, A. Y. (2011).Bioproduction of mushroom mycelium of Agaricus bisporus by commercialsubmerged fermentation for the production of meat analogue. *Journal of the Science of Food and Agriculture,91*(9), 1561-1568

SPAWN TREATMENT AND GROWTH OF OYSTER MUSHROOM BY ATMOSPHERIC PLASMA TECHNIQUE

Muhammad Farid Aidil Mohd Ali, Hayati Ahmad
School of Mechanical Engineering, Faculty of Engineering,
Universiti Teknologi Malaysia, 81310 UTM Skudai, Johor, Malaysia

INTRODUCTION

Plasma is considered to be fourth state of matter [1] after solid, liquid and gas. It is fully ionized gas that consists of ions, electrons and uncharged particles such as atoms, molecules and radicals. Non-thermal plasma has become one of the new technologies which are rapidly developed. This happen due to ability of cold plasma to modify the surface properties of a material or product without changing the original characteristics of the material.

Oyster mushroom is the most versatile mushrooms and in Malaysia, oyster mushroom can easily obtained in market because it's generally low in saturated fats and high in fiber and protein, and may reduce harmful blood cholesterol and act as an appetite suppressant [2]. Immune system can also be enhanced using mushrooms.

EXPERIMENTAL SETUP

To treat the spawn, plasma pencil is used. Treat the spawn with different flowrate (2 SLM – 6 SLM) and duration of treatment (5s – 60s) with constant carrier gas (air) and voltage output (8 kV).

After plasma treatment, the spawn is inject into substrate. To observe effectiveness of treated spawn, mycelium growth, quantity of mushroom and characterization of mushroom are investigated

RESULTS AND DISCUSSION

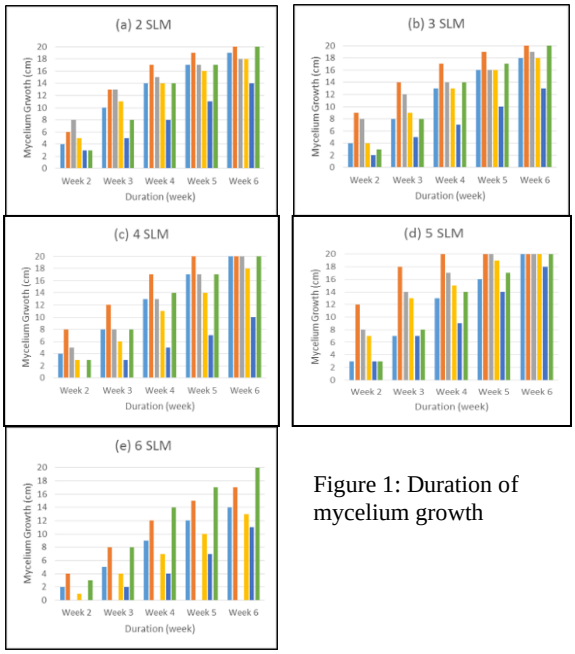

Figure 1: Duration of mycelium growth

Figure 1 shows that from overall graph, 5 SLM and 15s treated spawn fastest to complete the mycelium growth with only need 4 week compare to untreated that need 6 week. Figure 2 shows quantity of mushroom produce by treated and untreated spawn in the 1st cycle where 5 SLM 15s treated spawn produce highest amount of mushroom more than 500g compare to untreated spawn only produce almost 150g. Table 1 shows diameter of cap, length and stalk thickness of mushroom where no significance different between them. The different only can be seen in quantity of mushroom where 5 LSM 15s produce 30 mushroom compare to untreated spawn only 10 mushroom at one time.

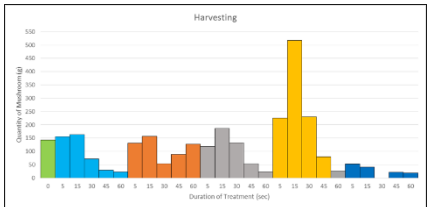

Figure 2: Quantity of harvest mushroom in 1st

Flowrate	Duration of Treatment	Diameter of the cap (cm)	Length (cm)	Stalk Thickness	Number of Mushroom
Control	0s	6.5	6.2	1.0	10
2 SLM	15	7.5	7.2	1.32	16
3 SLM	15	7	4.16	1.48	14
4 SLM	15	6.6	3.6	1.5	17

Table 1: Characterization of Mushroom

CONCLUSION

Spawn was successful treated with cold plasma. 5 SLM and 15s duration of treatment is the best parameter. 5 SLM and 15s has the highest growth rate of mycelium and produce the most mushroom.

REFERENCES

[1] Niemira, B. A. (2014). Decontamination of Foods by Cold Plasma. *Emerging Technologies for Food Processing*,327-333.

[2] Kim, K., Choi, B., Lee, I., Lee, H., Kwon, S., Oh, K., & Kim, A. Y. (2011).Bioproduction of mushroom mycelium of Agaricus bisporus by commercialsubmerged fermentation for the production of meat analogue. *Journal of the Science of Food and Agriculture,91*(9), 1561-1568

DYNAMIC BEHAVIORS OF DAMAGED STABILITY FOR SHIP STRUCTURE

Hau-Wei Choo and Hooi-Siang Kang
School of Mechanical Engineering, Faculty of Engineering,
Universiti Teknologi Malaysia, 81310 UTM Skudai, Johor, Malaysia.

INTRODUCTION

The transient dynamic behavior of ship is a result of coupling between three non-linear effects: sloshing of flood water, wave loading and ship dynamics. CFD shows great potential in simulating these transient effects. In this research, the OpenFOAM simulation was done for flooding of primitive shape barge as shown in Figure 1.

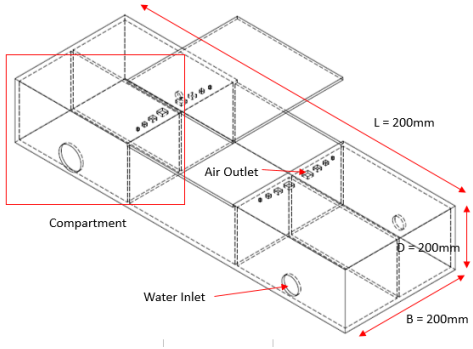

Figure 1: Dimension of Model of Primitive Shape Barge

OBJECTIVE

(a) To determine the dynamic response of ship structure under the effect of floodwater and wave in a transient stage
(b) To determine the flooding time of the transient stage of a damaged ship structure

METHODOLOGY

The research methodology is separated into two part:

(a) Simulation and experiment of damaged stability in still water condition with different size of water inlet and air outlet.
(b) Simulation of damaged stability in Stoke fifth-order beam wave and head wave of period 2.06s, wavelength 4.2m, and wave height 1m.

RESULTS AND DISCUSSION

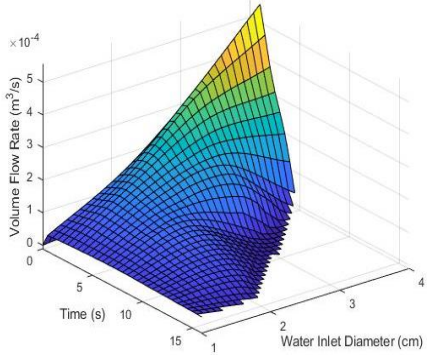

Figure 2: Surface Plot of Volume Flow Rate for Still Water Condition

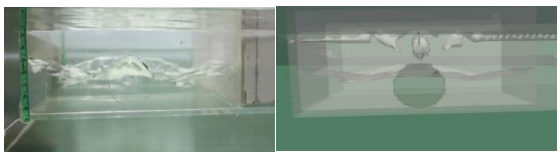

Figure 3: Flow Visualisation Comparison

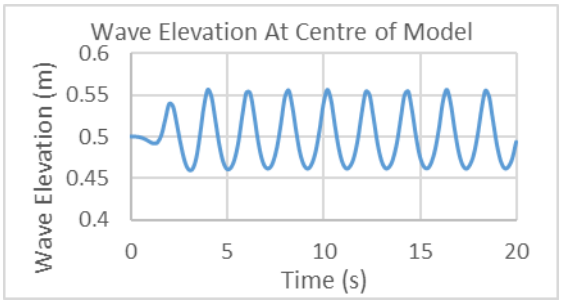

Figure 4: Wave Input

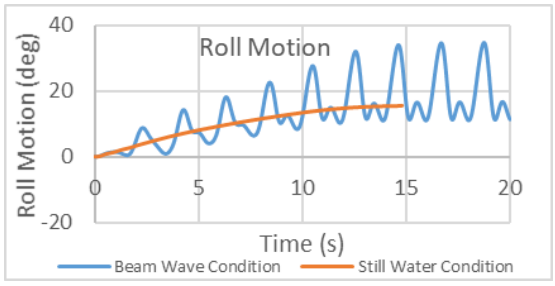

Figure 5: Roll Motion Under Beam Wave

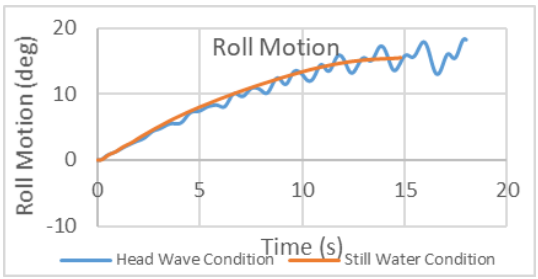

Figure 6: Roll Motion Under Head Wave

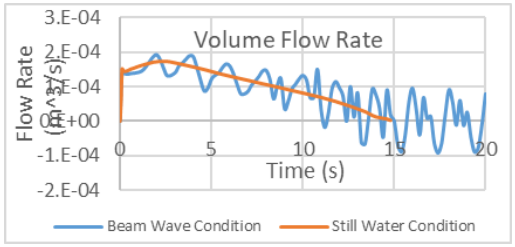

Figure 7: Volume Flow Rate Under Beam Wave

CONCLUSION

It can be concluded that the flow visualization comparison between simulation and experimental result also showed an acceptable agreement. The larger the water inlet area and air outlet area, the higher the volume flowrate. Sloshing of floodwater will cause ship structure to vibrate in the secondary vibrational motion.

DRAG MEASUREMENT ON HELICOPTER FUSELAGE

Mongkhul Bun Chea and Iskandar Shah Ishak
School of Mechanical Engineering, Faculty of Engineering,
Universiti Teknologi Malaysia, 81310 UTM Skudai, Johor, Malaysia.

INTRODUCTION

The primary sources of parasite drag for the helicopter is source by bluff body drag which is from pylon, rotor-hub, fuselage and landing gear flow separation and interference [1]. Drag of the helicopter is also caused by flow separation in the region where the pylon to the tail boom. Large drag penalties results when using pylon with large frontal area because these can promote flow separation and also the formation of wake region at the end of fuselage. A great design of pylon can reduce the drag of helicopter but other consideration must be taken to avoid the others effect such as tail shake phenomenon. Due to the lack of experimental drag data, this research aims to investigate the aerodynamic drag characteristic on the helicopter fuselage by conduct wind tunnel testing and numerical analysis.

EXPERIMENTAL

This section presents the experimental setup for the system. We used single EEG signals of 10- 20 international standard location (F8). The reference potential position was placed at the right ear lobe. An EEG paste was used to increase the electrode conductivity. The channel was directly connected into BMA-400 EEG-amplifier which provides specific gain constant for bio signal amplification.

The EEG signal was digitized using National Instruments (NI)-PCI-6229 Data Acquisition Card (DAQ) which was connected into Peripheral Component Interconnect (PCI) slot of a personal computer's (PC) motherboard.

RESULTS AND DISCUSSION

The wind tunnel testing were conducted at the Universiti Teknologi Malaysia-Low Speed Tunnel (UTM-LST). The test section size is 2m x 1.5m x 5.8m and the maximum wind speed of 80m/s [2]. Model that selected in this investigation is an ellipsoidal fuselage based on a simplified NASA standard model [3]. Main rotor-hub and pylon (or fairing) is also added were attached with the fuselage for the investigation. The wind tunnel tests were conducted for three different configuration of pylons which, 1) no pylon, 2) ellipsoidal pylon, 3) rectangular pylon. This experiment was test at 20 m/s and 30 m/s wind tunnel speed and at -5˚angle of attacks. Each configuration of pylon was run with the variation of rotor-hub speed which is 0 rpm, 1400 rpm, and 1600 rpm. In addition, numerical analysis were also conducted to validate the results.

The Figure 1 depicts the results of the comparison between these three configurations of pylon with two differences wind tunnel airspeed. The drag coefficient show the same trend for the both velocities. The results show that at 0 rpm of main rotor speed, the drag coefficient for rectangular pylon is the highest for the both wind speed. The value of drag coefficient for rectangular pylon is 0.35998 at 20 m/s and 0.35585 ant 30 m/s. Besides, the drag coefficient for the no pylon configuration is the second highest while the fuselage with ellipsoidal pylon configuration has experience the least drag. When the main rotor rpm is increasing, the trend for the drag coefficient for no pylon configurations become the lowest. It means that, the main rotor speed is also contribute and effects the helicopter aerodynamics drag. The results for 30 m/s wind speed is can acceptable when validate and proven with the previous. The results for theirs study are within 0.2 to 0.3 where in the same range with this research [4]. While the range for drag coefficient at 20 m/s wind speed is slightly high and not stable when the rotor speed is increase.

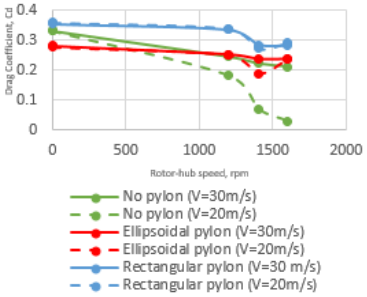

Figure 1: Comparison of drag coefficient for different type of pylons at wind speed, V=20m/s and 30 m/s and variable rotor-hub speed.

CONCLUSION

In conclusion, the objective of this study is achieved. Drag coefficient of the helicopter is dependent to the shape of pylon while it was independent to the wind speed and rotor-hub speed.

REFERENCES

[1] Prouty, R. W., "Helicopter performance, stability, and control," 1995.

[2] Noor, A. M., "Measuring aerodynamic characteristics using high performance low speed wind tunnel at Universiti Teknologi Malaysia," Journal of Applied Mechanical Engineering, 2014.

[3] Lorber, P. F. and Egolf, T. A., "An unsteady helicopter rotor: fuselage interaction analysis," 1988.

[4] Batrakov, A., Kusyumov, A., Mikhailov, S., Pakhov, V., Sungatullin, A., and Valeev, M., "Helicopter Fuselage drag-combined CFD and experimental study," 5th european conference for aeronautics

RESEARCH ON HELICOPTER TAIL CONFIGURATION

Muhammad Heyqal Sazlan Mohd Hifnie and Iskandar Shah Ishak
School of Mechanical Engineering, Faculty of Engineering,
Universiti Teknologi Malaysia, 81310 UTM Skudai, Johor, Malaysia

INTRODUCTION

This research been done to investigate the aerodynamic drag characteristics, longitudinal and directional static stability on 3 three difference helicopter tails where it is chosen by commonly used and rarely used in real world. As we all know that the helicopter tail is contributed of vertical and horizontal stabilizer [1]. All the data for drag characteristic, longitudinal and directional static stability were gained by wind tunnel test at UTM-LST and Computational Fluid Dynamics (CFD).

EXPERIMENTAL SETUP

For making the wind tunnel models, 3 processes are taken into account which are lathing and milling process, finishing process and attachment process. Next, for CFD models it all been designed by using Solidworks application using same dimensions that can be used at ANSYS application.

RESULTS AND DISCUSSION

For Figure 1 the graphs for all three models portray increase in drag coefficient with increase of angle of attack and at zero angle of attack, the least drag coefficient is produced like example research done by Ishak, Mansor, and Lazim [2] and by Batrakov et.al [3].

For Figure 2, the fuselage only pitching moment coefficient graph portrays unstable longitudinal static stability which it has positive slope graph. Meanwhile, the graph for model 1, model 2and model 3 graph respectively show negative slope graph where it is considered stable in longitudinal static stability like example research done by Ishak, Mansor and Lazim [2].

For Figure 3, as we can analyze, all helicopter models with tail show positive slope graph for yawing moment coefficient against yaw angle. This can be said that for the three of the models is directionally stable as shown research done by Ishak [4].

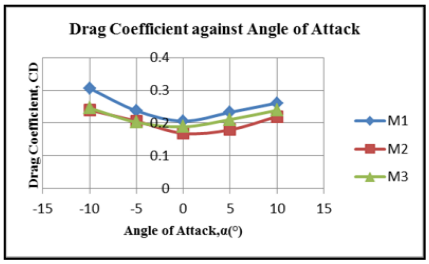

Figure 13: Comparison drag coefficient of all models for wind tunnel test in pitch

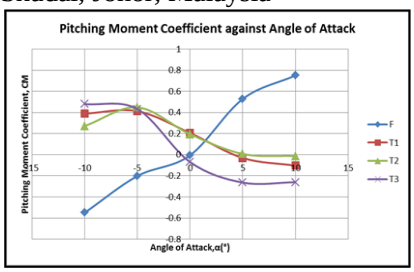

Figure 2: Comparison pitching moment coefficient of all models for wind tunnel test

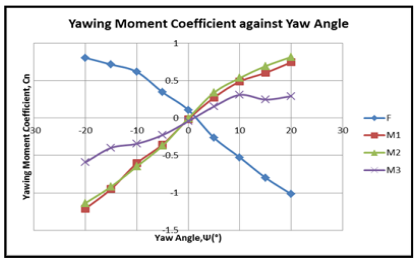

Figure 3: Comparison yawing moment coefficient of all models for wind tunnel test

CONCLUSION

Based on all the results gained from both CFD and wind tunnel testing, it finalizes that fuselage with set pair of stabilizer of model 2 is the best for aerodynamics in drag characteristics and stability performance.

REFERENCES

[1] J. John D Anderson. and Emeritus, *Introduction to Flight*, 6th. ed. New York: McGraw-Hill, 2008.

[2] I. S. Ishak, S. Mansor, and T. H. M. Lazim, "Experimental Research on Helicopter Tail Shake Phenomenon," in *Proceedings of the 2nd Regional Conference on Vehicle Engineering & Technology*, Hotel Istana, Kuala Lumpur, 2008, July.

[3] A. Batrakov *et al.*, "Helicopter Fuselage Drag: Combined Computational Fluid Dynamics and Experimental Studies," presented at the Progress in Flight Physics, Kazan, Russia, 2015.

[4] I. S. Ishak, "Unsteady Aerodynamic Wake of Helicopter Main-Rotor-Hub Assembly," Ph.D. dissertation, Universiti Teknologi Malaysia, Johor Bahru, 2012.

PRESSURE DISTRIBUTION ON HELICOPTER FUSELAGE

Anas Faiz Aris and Iskandar Shah Ishak
School of Mechanical Engineering, Faculty of Engineering,
Universiti Teknologi Malaysia, 81310 UTM Skudai, Johor, Malaysia

INTRODUCTION

In helicopter performances, tail shake phenomenon plays an important role as it can affect overall performance, occupant comfort and handling qualities of helicopter. By knowing cause of tail shake phenomenon can help rotorcraft industry to manufacture helicopter with a good design. General complexity of modern, compact helicopter design, associated with scaling difficulties, are contributing factors towards limited success in predicting Interactional Aerodynamic (I/A) related vibration problems[1].

OBJECTIVE

The objective of this undergraduate project is to conduct wind tunnel tests and numerical analysis to investigate the pressure characterization on fuselage in relation to the helicopter tail shake phenomenon.

EXPERIMENTAL SETUP

This experimental study is based a simplified NASA standard fuselage model was mated to a main-rotor-hub assembly from a remote-control helicopter[2]. The model also equipped with two different types of pylon which is ellipsoidal pylon and rectangular pylon. The width of the pylon is 66mm, 296mm of length and 35mm of height. Blade-stubs configuration is a combination of main-rotor-hub assembly with short blades. To determine the pressure distribution around the helicopter fuselage, the model was equipped with 28 pressure taps.

RESULTS AND DISCUSSION

The tail area shows that for fuselage rectangular pylon, the pressure slightly changes as the reduction of tail shake for rectangular pylon is the lowest. This shows that the rectangular pylon reduces the effect of rotation of rotor hub. The pressure changes for fuselage without pylon is decreases as rotation of rotor hub increases. This show that as the pressure increases the tail shake reduction decreases. Pressure in front of rectangular pylon is highest may cause from turbulence occur there. Meanwhile at the both sides of pylon the pressure distribution is unsymmetrical in comparison because the complex flow phenomena[3]. At tail area the rectangular pylon also has the highest pressure while most of time the fuselage without pylon has the lowest pressure. When no rotation of main rotor hub the pressure for fuselage with ellipsoidal pylon decreases but fuselage with rectangular pylon increases the pressure when compare to fuselage without pylon for right side of fuselage for both speed. This shows that when reduction of tail shake phenomenon from wake of rotor hub is decreases the pressure at the area of tail increases. Figure 1 show pressure for left fuselage with different configuration of pylon at different rotation of main rotor hub at 30 m/s.

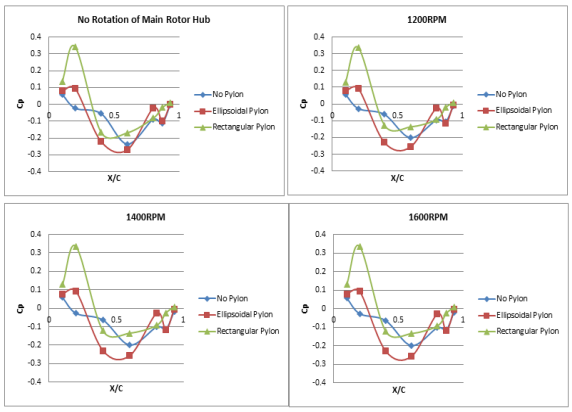

Figure 14: Graph of Cp against x/c for left fuselage with different configuration of pylon at different rotation of main rotor hub at 30 m/s.

CONCLUSION

As conclusion the rotation of main rotor hub does affect the upper part of fuselage at tail area and in front of pylon that does not change with rotation of main rotor hub. The rotation of main rotor hub will cause the wakes that make the pressure changes does contribute to tail shake phenomenon. The presence of pylon does decrease the tail shake phenomenon while increases the pressure around the pylon especially in front and rear of pylon. The side of fuselage also changes when the main rotor hub rotates according to direction of flow and the configuration of pylon.

REFERENCES

[1] Waard, P. G. d.&Trouvé, M., "Tail Shake Vibration," *National Aerospace Laboratory (NLR)*, 1999.

[2] Ishak, I. S., "Unsteady Aerodynamic Wake Of Helicopter Main-Rotor-Hub Assembly," Doctor of Philosophy (Mechanical Engineering), Faculty of Mechanical Engineering, Universiti Teknologi Malaysia, 2012.

[3] Ishak, I. S., Mansor, S., Lazim, T. M., &Rahman, M. R. A., "Computational Fluid Dynamic Studies on Helicopter Main Rotor-Hub Assembly Wake," *Regional Conference on Mechanical and Aerospace Technology*, 2012..

FLIGHT CONTROL IMPROVEMENT OF QUADROTOR WITH ULTRASONIC SENSOR

Mohd Syafiq and Istas Fahrurrazi
School of Mechanical Engineering, Faculty of Engineering,
Universiti Teknologi Malaysia, 81310 UTM Skudai, Johor, Malaysia

INTRODUCTION

Quadcopter or quadrotor aircraft is one of the UAV that is major focal points of dynamic researches as of late [2]. These days installed sensors are executed on the MAV, for example, IR sensors, Laser sensors, Stereo cameras and Ultrasonic sensor in order to evade obstacle and improve quadrotor flight control [3]. The linear control procedures dependent on PID feedback structure are habitually utilized with smaller scale copters for flight control. The quadrotor used ultrasonic as a sensor to measure distance and the data will be used to trigger the avoidance mode. During flight, the measurement experience noise which will disturb the flight mode. Therefore, a filter should be applied to reduce those noise such as median filter method according to Muhammad Fazlur Rahman [4].The obstacle avoidance algorithm or concept divides into two parts which are operation control and collision avoidance control. Then, the collision avoidance control divided into slow avoidance area and rapid avoidance area in order to make sure the pitch angle not to be changed largely. In this project, the algorithm of obstacle avoidance system is design and implemented to the quadrotor in order for the quadrotor to avoid obstacle. The result of pitch angle and roll angle will be discussed to prove that quadrotor able to avoid obstacle.

EXPERIMENTAL SETUP

The study of quadrotor with implementation of obstacle avoidance by using ultrasonic sensor is carried out. Quadrotor is fabricated with additional ultrasonic sensor to aided the obstacle avoidance system. The fabricated quadrotor undergoes flight testing and the performance and response will be analyses and discussed.

RESULTS AND DISCUSSION

Two types of flight test method are conducted in this project which is static test and flight test. Initially, static test is carried out to ensure the quadrotor calibration process and the obstacle avoidance response accordingly.

When there is an obstacle detected, at around time 07:59:56.000 the output value of roll angle increase drastically which show that the quadrotor reacts when there is an obstacle detected. There are several reasons for this behavior, the increasing in output value of roll angle tells that the quadrotor moving to the right. The more positive value of roll angle show that the quadrotor moves to the right while the more negative value of roll angle means vice versa which is to the left. For about 6 to 8 seconds the roll angle stay higher or maintain the output value around -0.7 where the motion of quadrotor is moving to the right because the obstacle is still detected. After certain amount of time the output value of roll angle decrease and return to its original level and stabilize the quadrotor again.

At the start. the pitch angle also begin with around 0.8 this is because there might be some error or miss calibration occur. However, the quadrotor is still stable in this flight mode. Let assume the pitch angle begin with 0, the result of roll angle and pitch angle is quite the same, both of them gives appropriate response when there is an obstacle introduce to the sensor. The output value of pitch angle around 07:59:56.000 decreasing or towards negative value which means that the quadrotor is moving to the front because the obstacle is at the back of quadrotor. After the obstacle is clear from the sensor detection range, the pitch value of quadrotor return to its original point to maintain back the attitude position of quadrotor.

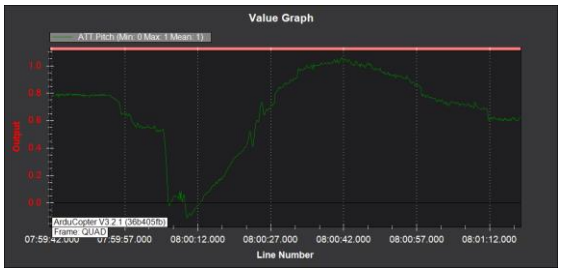

Figure 1 : Pitch angle result

CONCLUSION

The implementation of obstacle avoidance for quadcopter using ultrasonic sensor have been done. The result shows that quadcopter successfully avoiding or keep distance in obstacle avoidance flight mode when the obstacle's distance is less than defined distance parameter. This project can be further studied to development more stabilize and improve quadrotor with obstacle avoidance system by using ultrasonic sensor.

REFERENCES

[1] A. Rodic and Mester, G., "Control of a Quadrotor Flight," 2013.
[2] A. Adriansyah, Amin, S. H. M., Minarso, A., and Ihsanto, E., "IMPROVEMENT OF QUADROTOR PERFORMANCE WITH FLIGHT CONTROL SYSTEM USING PARTICLE SWARM PROPORTIONAL-INTEGRAL-DERIVATIVE (PS-PID)," *Jurnal Teknologi*, 2017.
[3] M. F. Rahman and Sasongko, R. A., "Obstacle Avoidance for Quadcopter using Ultrasonic Sensor," *Journal of Physics: Conf. Series 1005 (2018) 012037*, 2018.

STUDY OF AIRBUS A380 FLIGHT CONTROLS WITH FLIGHTGEAR

Chuah Ching Chuen and Istas Fahrurrazi
School of Mechanical Engineering, Faculty of Engineering,
Universiti Teknologi Malaysia, 81310 UTM Skudai, Johor, Malaysia

INTRODUCTION

FlightGear is used to simulate the flight of A380. FlightGear is a free, open-source flight simulator. A380 is the largest double-deck commercial aircraft flying today. It is the world's largest passenger airliner manufactured by Airbus. In this study, only one type of aircraft motion is focused – longitudinal motion. The mode for the longitudinal motion of an aircraft can be divided into two: short period and phugoid. The dynamic response of A380 is then studied and compared to the longitudinal flying qualities.

EXPERIMENTAL SETUP

This section presents the experimental setup for the system. By setting and communicate between FlightGear and Octave programs, FlightGear able to send the flight data to Octave. Then, A380 is flied the simulation software. The baca2.m is run simultaneously in Octave to record the flight data for analysis purpose.

The short period and phugoid motion of the aircraft are performed in the FlightGear simulation. The flight data is plot by using Octave and the graphs will show the motion of the aircraft. From the graphs plotted, the damping ratio and natural frequency for that particular flight condition can be obtained. The damping ratio for both motions are compared to the aircraft longitudinal flying qualities (Ref: MIL-SPEC-8785C).

RESULTS AND DISCUSSION

A380 is flied in FlightGear with different flying conditions. The flying conditions are changed with different altitude with constant speed. The flight data is recorded and the aircraft's dynamic response is plotted. From the data and graphs obtained, analysis on the damping ratio of the aircraft can be done and make a comparison.

Table 1 demonstrates that the damping ratio for A380 flying at various altitude (with and without autopilot) has fulfilled the Level – 1 of flying quality which is the damping ratio is between 0.35 and 1.3. Level – 1 of flying qualities. Besides, when autopilot is activated, the damping ratio for the aircraft is greater compared to without autopilot activated when flying at the same altitude.

In order to fulfil Level – 1 of flying quality, the phugoid damping ratio has to greater than 0.04. Table 2 shows that the phugoid flying qualities for all the flying cases (with autopilot and without autopilot) is Level 1. And similar to the short period motion, the damping ratio for phugoid motion in activated autopilot mode is greater compared to flying cases without autopilot.

Table 1: Short period results

	Altitude (ft)	Velocity (knots)	Damping ratio	Flying Quality
Without AUTOPILOT	8202.5	540.0	0.551867798	Level 1
	27560.4	545.0	0.540864641	Level 1
	41645.7	523.8	0.508345549	Level 1
	Altitude (ft)	Velocity (knots)	Damping ratio	Flying Quality
With AUTOPILOT	6562.0	550.8	0.786714635	Level 1
	27752.5	560.1	0.669171918	Level 1
	41583.4	545.3	0.580435721	Level 1

Table 2: Phugoid results

	Altitude (ft)	Velocity (knots)	Damping ratio	Flying Quality
Without AUTOPILOT	8202.5	540.0	0.360128697	Level 1
	27560.4	545.0	0.352481147	Level 1
	41645.7	523.8	0.306077806	Level 1
	Altitude (ft)	Velocity (knots)	Damping ratio	Flying Quality
With AUTOPILOT	6562.0	550.8	0.59919326	Level 1
	27752.5	560.1	0.428602967	Level 1
	41583.4	545.3	0.404368797	Level 1

CONCLUSION

From the analysis on A380's longitudinal motion, the results show that A380 has a very good and stable longitudinal flight control as the flying qualities are all in Level – 1. The damping ratio of the aircraft is significant affected by the flying altitude. For both short period and phugoid motion, the aircraft will damp less when it is flying at higher altitude.

REFERENCES

[1] Aschauer, G., Schirrer, A., & Kozek, M. (2015). Co-Simulation of Matlab and FlightGear for Identification and Control of Aircraft.

[2] Haibin, D., Daobo, W., & Xiufen, Y. (2008). Realization of nonlinear PID with feed-forward controller for 3-DOF flight simulator and hardware-in-the-loop simulation. Journal of Systems Engineering and Electronics, 19(2), 342-345. doi: 10.1016/s1004-4132(08)60089-4

[3] Vargas, F. J. T., Moreira, F. J. O., & Paglione, P. (2018). Longitudinal stability augmentation design with two degree of freedom control structure and handling qualities requirements.

TO STUDY AND IMPROVE BOEING B777 FLIGHT CONTROLS IN FLIGHTGEAR FLIGHT SIMULATION SOFTWARE

Muhammad 'Abdin Shakirin Zainol and Istas Fahrurrazi Nursyirwan
School of Mechanical Engineering, Faculty of Engineering,
Universiti Teknologi Malaysia, 81310 UTM Skudai, Johor, Malaysia

INTRODUCTION

The engineering flight simulators reduce lifecycle costs because development and testing of complex aircraft systems can be done before actual flight tests[1]The simulator provides useful data that can be used to assess performance and behaviour of the aircraft and its systems. Moreover, the response of aircraft systems can be visualized in various platforms[2]. Flying qualities of an aircraft are related to the stability and control characteristics. It can be used to describe the stability and control characteristics of an aircraft for given flight cases which allow pilot to give opinion toward the level of flying qualities[3].

EXPERIMENTAL SETUP

The aircraft will be experimented with the PID systems or the autopilot system turn off and turn on. Thus, we can see whether the autopilot system is helping the aircraft in terms of stability or not. The aircraft also will be flying at 3 different altitudes; 10,000ft, 35,000ft and 50,000ft. From these 3 altitudes, there might be a relationship between the altitudes and the stability system of the aircraft. Specifically, we will be investigating its Pitch Rate and Pitch Angle Response, obtaining the damping ratio, δ, and natural frequency, ω_n, can be calculated. These damping ratio values will be compared with the aircraft Flying Qualitites and get the level at all 3 different altitudes for short period and phugoid motions.

RESULTS AND DISCUSSION

At all 3 experimental altitudes show that the aircraft is flying with stability. We can see that for both motions; Phugoid and Short Period, when the aircraft is flying with PID systems turn off, the damping ratio is much higher as compared to when the aircraft is flying with the PID systems turn on. This can be assumed that the PID systems would allow the aircraft to fly with a better stability as the damping ratio is higher thus the aircraft can perform both motions; Phugoid and Short Period, easily and without causing a mess or disturbances on the aircraft. Table below shows data for short period motions.

CONCLUSION

In short, as the aircraft possess PID system that would definitely help with the stability augmentation of the aircraft, it is correct to assume that with the use of PID system the aircraft can produce a better flight dynamic. The use of control laws with non-conventional response characteristic, specifically a normal acceleration response characteristic, gives very desirable flying qualities for the approach and landing task with a reduced workload compared to a classical aircraft, and these control law types may be used in other tasks such as a formation flying task.

	Altitude, ft	Velocity, knots	Damping Ratio	Flying Quality
Without Autopilot	10,000	543	0.482859977	Level 1
	35,000	545	0.4054794	Level 1
	50,000	545	0.383831896	Level 1

	Altitude, ft	Velocity, knots	Damping Ratio	Flying Quality
With Autopilot	10,000	543	0.389376986	Level 1
	35,000	541	0.27281987	Level 1
	50,000	540	0.417530827	Level 1

Table 1: Aicraft Characteristic Without Autopilot
Table 2: Aircraft Characteristic with Autopilot

REFERENCES

[1] E. Sorton and S. Hammaker, "Simulated Flight Testing of an Autonomous Unmanned Aerial Vehicle Using FlightGear," in *Infotech@Aerospace*, 2005.
[2] N. Wahid and N. Hassan, "Self-tuning fuzzy PID controller design for aircraft pitch control," in *Proceedings - 3rd International Conference on Intelligent Systems Modelling and Simulation, ISMS 2012*, 2012.
[3] U.S. Department of Defense, "Flying Qualities of Piloted Aircraft," *MIL-STD-1797A*, 1997.

1. DEVELOPMENT OF SIMULTANEOUS LOCALIZATION AND MAPPING WITH COLLISION AVOIDANCE FOR UNMANNED AERIAL VEHICLE

Khoo Hung Siang and Istas Fahrurrazi Nusyirwan
School of Mechanical Engineering, Faculty of Engineering,
Universiti Teknologi Malaysia, 81310 UTM Skudai, Johor,
Malaysia

2. INTRODUCTION

In SLAM, a robot must construct a map of the environment, while simultaneously localizing itself relative to this map. The problem of SLAM is described in probabilistic form of robot state vector [1]. There exists a probability of robot in estimating its state vector while observing any landmark. This problem is more challenging than localization or mapping, since neither the map nor the robot poses are provided making this problem a 'chicken or a egg' problem. While the robot vehicle is mapping its surroundings and localizing itself at the same time, it is possible for the vehicle to collide with the obstacle either in manual or autonomous mode, especially UAV with 6 DOF motion.

3. FLIGHT TESTING SETUP

The simulated UAV is assembled with 3DR Iris quadcopter body model, multiple HC-SR04 ultrasonic sensors and Microsoft Kinect camera controller with Ardupilot as autopilot firmware. It will be tested with Software In The Loop (SITL) and Gazebo simulator on top of Robot Operating System (ROS). MAVlink will be used as the communication protocol with UAV during flight testing. The simulated indoor environment is constructed with multiple walls to form a sets of maze-liked obstacles. Each wall is differentiated with uniques images for testing of visual odometry performance.

4. RESULTS AND DISCUSSION

The UAV flight evaluation test is performed by evaluating its localization performance to hold vehicle altitude and position using visual odometry data from RTAB-Map VO node. Figure 1 and 2 shows that the x-axis and y-axis localization data from mavros indicates that EKF2 system of UAV fails to fluctuate along the two axes but keep deviating from its origin as simulation time increases. Although RTAB-Map visual odometry provides larger errors of localization data from origin in both axes, the EKF2 system of UAV only accepts localization data from

RTAB-Map with errors less than certain guess values. UAV is then manually positioned in the simulated indoor environment at guided flight mode. The results collected is the constructed 3D maps in the representation form of octomap as shown in figure 3. All the walls had been successfully mapped with their respective location but some alignment of the walls are not properly mapped. These mapping errors of structure alignment occur when UAV yaw angle is not exactly of 90 degrees in turning motion of headings.

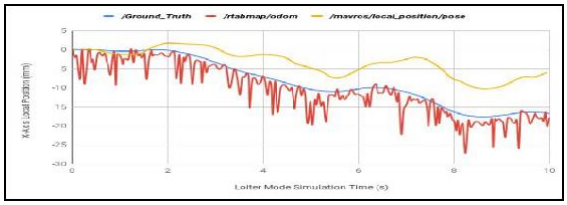

Figure 1: Graph of x-axis localization data for simulation of loiter mode

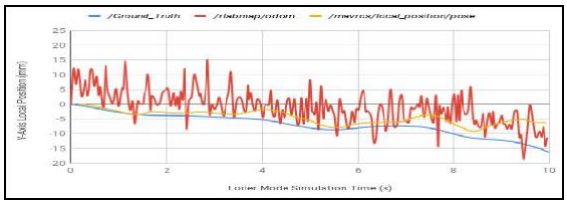

Figure 2: Graph of y-axis localization data for simulation of loiter mode

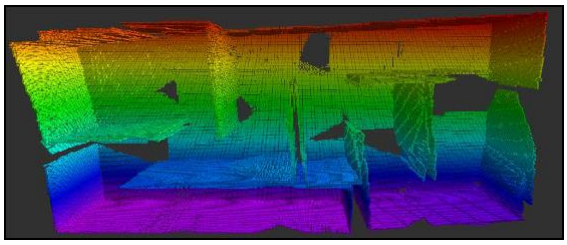

Figure 3: Plan view for constructed octomap

5. CONCLUSION

UAV flight testing had been performed through simulation with evaluation of SLAM, collision avoidance and path planning performance.

6. REFERENCES

[1] Bailey, T., & Durrant-Whyte, H. (2006). Simultaneous localization and mapping

MODELLING OF A DC MOTOR USED TO VARY RATIO IN ELECTRO-MECHANICAL DUAL ACTING PULLEY CONTINUOUSLY VARIABLE TRANSMISSION

Muhammad Darwis Abu Bakar and Izhari Izmi Mazali
School of Mechanical Engineering, Faculty of Engineering,
Universiti Teknologi Malaysia, 81310 UTM Skudai, Johor, Malaysia

INTRODUCTION

EMDAP CVT uses an Electro-Mechanical (EM) actuation that consist of DC motors, gear reducer and power screw mechanism. DC motor plays the main part for this system as it actuates the power screw mechanism to move the pulley sheaves simultaneously in order to change the CVT ratio.
A control system is needed in order to get the desired CVT ratio as it can control the final position of the pulley sheaves. In order to developed a control model, a DC motor model must be developed first to get the output that will needed for the actuation system. In this project, a DC motor model is developed and a simulation is running using Matlab-Simulink.

MODELLING OF A DC MOTOR

In EMDAP CVT, DC motor acts as the main actuator for the system. The related equation for this system will be used to get the transfer function and block diagram for DC motor.Then the parameters values are identified by using the equation and the model of a DC motor is developed by using Matlab-Simulink software. The specification of the DC motor used in this project is shown in Table 1.

Table 1: Specification of the DC motor

Voltage	Torque [Nm]		Power [W]		Speed [RPM]		Current [A]	
[V]	Rated	Max.	Rated	Max.	Rated	Max.	Rated	Max.
24	0.731	4.000	370	720	3000	3600	19.3	54

The block diagram of a DC motor is as shown in Figure 1:

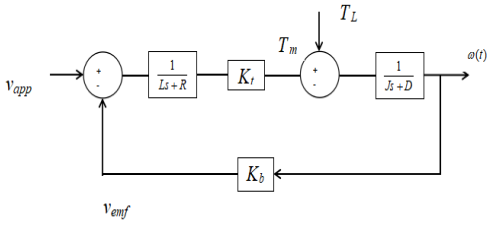

Figure 1: Block diagram of a DC motor

Table 2: DC motor parameters values

Description	Symbol	Value
Back emf constant	K_b	0.0637 Nm/A
Torque constant	K_t	0.0637 Vs/rad
Motor armature resistance	R_a	0.39 Ω
Motor armature inductance	L_a	0.001 H
Viscous friction coefficient	D	0.0021 Nm/s
Motor inertia	J	0.00007 kg m^2

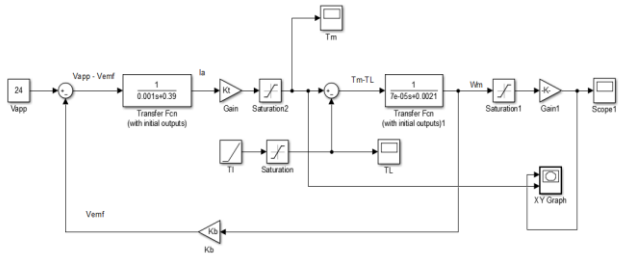

Figure 2: DC motor Simulink model

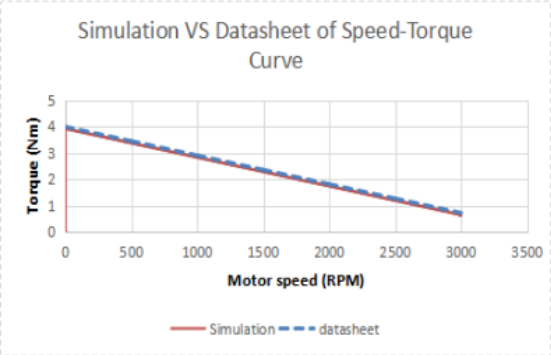

Figure 3: Speed-torque curve simulation result compared to data sheet

RESULTS AND DISCUSSION

The simulation results is plotted and compared with speed-torque curve given on data sheet. The maximum data sheet torque is 4 Nm while simulation result is 3.948 Nm. As for the rated torque, from the data sheet the value is 0.731 Nm while simulation result is 0.657 Nm. By compared the result of the simulation and the data sheet curve, the mean error percentage calculated is 1.3 %. The small percentage of error make the result reliable and conclude that this DC motor Simulink model can be used for EMDAP CVT simulation to vary the ratio.

CONCLUSION

The simulation results show that this model can be apply to vary the ratio of the EMDAP CVT. The study of the project had shown that the EMDAP CVT actuator behaviour can be ideally modeled by mathematical equations.

REFERENCES

[1] K.B.Tawi1,B.Supriyo S. Ariyono, N. A. Husain, A.R.A. Hamid, M.A.Azlan, I.I.M. and M. S.C.K. (n.d.). The design concept of Electro Mechanical Dual Acting Pulley CVT.
[2] Abdol Aziz, A. H. (2015). PID Based Controller for independent ratio actuator control of EMDAP CVT 16(July).

REVERSE FORWARD MECHANISM FOR CONTINUOUS VARIABLE TRANSMISSION

Aiman Mustaqim Muhammad and Izhari Izmi Mazali
School of Mechanical Engineering, Faculty of Engineering,
Universiti Teknologi Malaysia, 81310 UTM Skudai, Johor, Malaysia

INTRODUCTION

Pulley-based continuously variable transmission (CVT) with Metal Pushing V-belt is a variety of automotive transmission that is commonly applied by many car manufacturers worldwide. The motivation for using a continuously variable-transmission in an automobile is to achieve a continuously variable-transmission of power, which allows the internal combustion engine to operate at its most efficient operating point for a given power requirement. Since CVT is only able to transmit the power from input to the output in one direction, therefore a reverse-forward mechanism is needed for the CVT. Electro-Mechanical Dual Acting Pulley (EMDAP) CVT consists of two movable primary pulley sheaves at the input shaft, two movable secondary pulley sheaves at the output shaft and a metal pushing V-belt joining these two pulleys. In this project, to design reverse-forward mechanism for CVT. The reverse-forward mechanism must be able to adapt Electro-Mechanical Dual Acting Pulley (EMDAP) CVT UTM.

EXPERIMENTAL SETUP

The study is focusing on the basic concept for reverse-forward mechanism. Problem identified by go through the existing design of reverse-forward mechanism. Product design requirement need to be done after identify the problems. Several conceptual designs are proposed and evaluated to select final design. When the final design has been decided, each of the component will be considered based on force flow analysis. Any modification can be made if there is any problem.

RESULTS AND DISCUSSION

In neutral mode, neither synchronizer nor brake band mechanism is engaged. Power inputted to the sun gear will not transmitted to the output Assume the sun gear is rotating in clockwise direction. First planet gears are rotated by sun gear in opposite direction while second planet gears are rotated by first planet gears in clockwise direction. Ring gear is forced to rotate same direction as the second planet gears. No power transmitted to the planet carrier and the output is stationary. In forward motion, the synchronizer which is splined on the input shaft slides to engage with the planet carrier second side member. The synchronizer sleeve slides over the external protrusions of the synchronizer ring and planet carrier second side member. This locks the planet carrier side member to the input shaft. As a result, the planet carrier is forced to rotate as input shaft. All gears in the planetary gear set rotate synchronously as a single unit.

In reverse mode, the synchronizer is disengaged from the planet carrier second side member. Next, brake band mechanism is engaged to locked the rotation of ring gear. In this state, power flows from sun gear to planet gears to planet carrier. Assume sun gear is rotating in clockwise direction. It turns the first planet gears in opposite direction and second planet gears are rotated in clockwise direction by the first planet gears. Since the ring gear is locked by the brake band mechanism, the planet carrier is forced to turn in opposite direction as the input shaft. As a result, it will move in reverse motion.

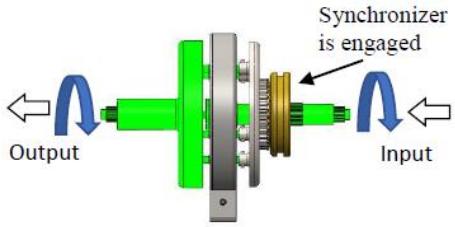

Figure 1: Power flow through the reverse forward mechanism (forward mode)

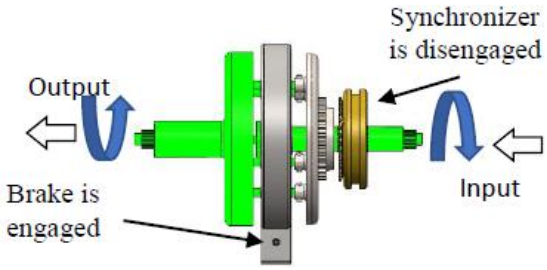

Figure 2: Power flow through the reverse forward mechanism (reverse mode)

CONCLUSION

The design consists of a planetary gear set with double planet gears, synchronizer, and brake band mechanisms. It is capable to operate in three output modes which are reverse, forward and neutral mode.

REFERENCES

[1] Masahiro Ohkubo (Kyoto,JP) and Koji Yoneyama (Osaka, JP) (2003). Forward-reverse rotation device for a continuous variable transmission. US Patent 6,645,111.

[2] William, H. Crouse. and Donald L. Anglin. (1993). Automotive Mechanics. 10th ed. Singapore: McGraw-Hill.

DEVELOPMENT OF TEST RIG FOR CLAMPING FORCE SYSTEM OF ELECTRO-MECHANICAL CVT

Aizat Farhan Azzuwan and Izhari Izmi Mazali
School of Mechanical Engineering, Faculty of Engineering,
Universiti Teknologi Malaysia, 81310 UTM Skudai, Johor, Malaysia

INTRODUCTION

In recent years, the world fuel price continue rise and give an impact on cost of living standards [1]. Therefore manufactures have focused on the production of a vehicle that can save fuel consumption. The products is on the development of an efficient automotive transmission and a pulley-based continuously variable transmission (CVT) has been selected as the best transmission to eradicate the problem [2]. However todays, there are many type of CVT transmission and some consume high power from the engine. So there is a solution which to use the Electro-Mechanical Dual Pulley (EMDAP) CVT. EMDAP CVT utilizes with two brushless DC electric motors as actuator and power screw mechanism [3]. These two brushless DC (BLDC) motor are uses to actuate axial movement of primary and secondary pulley during the changing of ratios transmission. Thus, it can save power consumption from engine.

EXPERIMENTAL SETUP

This section presents the experimental setup for the system. There include of the mechanical setup and the electrical setup. For the mechanical parts, the BLDC motor should be place at the motor holder and with the 24v battery, the BLDC motor will directly operate. For the electrical setup only focus on the connection between the force sensor LC8300 Series Donut and the Arduino Leonardo Microcontroller. This sensor is set to read the force up to 22kN and gives 5v signal voltage with the help of DMD4059 amplifier. After that, MATLAB Simulink Arduino Model is being builds so that clamping force and torque of BLDC motor required well earned.

RESULTS AND DISCUSSION

There are two outputs obtained from the experiment conducted on the EMDAP CVT. The two outputs are the clamping force from the disc spring and the torque from the BLDC motor. The results of the clamping force should be taken from both side of the V-belt because the force occurs in between the V-belt. The experiment result also has been shortened because the condition only consider the earlier process of clamping, middle clamping and the maximum limits for the clamping force. The result of the experiments is as shown in the Table 1. The simple graph as shown in Figure 1 also has been made to show the relation between these two outputs which are the torque from BLDC motor and the clamping force from disc spring. The torque from BLDC motor rises as the clamping force from the disc spring increase. The sufficient clamping force is important to the performance from CVT.

Table 1: Experiment results

Clamping Force, F (kN)	Clamping Force both side of v-belt, F (kN)	Torque Secondary Motor, T_{SM} (Nm)
0.8	1.6	0.07
4.0	8.0	0.37
5.6	11.2	0.52
8.0	16.0	0.74
12.2	24.4	1.13

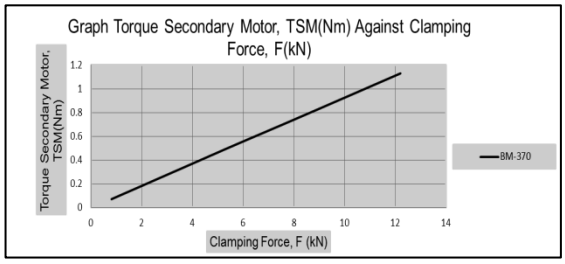

Figure 1: Torque BLDC motor against clamping force

CONCLUSION

As the conclusion, the objective of the final year project that been carried out is successful archived since the specification of the brushless DC (BLDC) motor obtain is suitable with the Electro-Mechanical Dual Acting Pulley (EMDAP) CVT test rig.

REFERENCES

[1] Ylanan, N. (2018, March 14). Retrieved from Here are the different types of Automatic Transmissions: https://www.autodeal.com.ph/articles/car-features/here-are-different-types-automatic-transmissions

[2] Gong, S. (2014). A generalized IC engine propulsion method and corresponding transmission design for improving vehicle fuel efficiency. European Transport Research Review, 6(3), 225-239. doi:10.1007/s12544-013-0124-y

[3] Izmi Mazali,I., Baharin Tawi, K., Supriyo, B., Sabri Che Kob, M., Husain, N., & Salman Che Kob, M. (2015). Application of disc spring in clamping force mechanism for electro-mechanical continuously variable transmission (Vol. 77)

DESIGN OF MANUAL TRANSMISSION TEST RIG

Ahmad Asri Abdullah and Izhari Izmi Mazali
School of Mechanical Engineering, Faculty of Engineering,
Universiti Teknologi Malaysia, 81310 UTM Skudai, Johor, Malaysia

INTRODUCTION

Transmission is mechanism that transmit the power developed from the engine to the driving wheels. For manual transmission, the driver has to manually select and engage the gear ratio. However, the visibility of the manual transmission operation is hard to be seen in real life as it works in internal housing. The objective of this study is to design a test rig that will demonstrate the operation of changing ratio in manual transmission. The design should be done until CAD (Computer-Aided Diagram) and also come along with analysis of structure.

EXPERIMENTAL SETUP

This section presents the information gathered and setup for the design process. Start with the gear selector of manual transmission. It is controlled by a shift lever that connected to 3 rods and each of them connected to a fork. The fork will engage to the gear ratio desired.

Some study on existing test rig also has been done. There are some improvement need to be done based on the existing test rig. The input shaft of the transmission should be operate to make the operation more clear. Then, it also not portable to make it easier for exhibition.

Design needs have been listed before it comes to design requirements and also PDS (Product Design Specification). Several conceptual design sketched based on the PDS. Then, the conceptual designs evaluated to be chose as the best conceptual design. .

RESULTS AND DISCUSSION

In this chapter, the final design has been selected based on the ability of the design to achieve the main objectives and also the design requirements. The design concepts also produced with some changes and improvements on the selected proposed design concepts. The improvements are needed so the final design concepts is suitable to be fabricated.

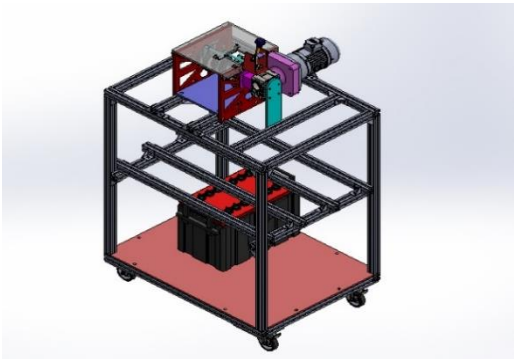

Figure 1: CAD drawing of final design

Figure 1 shows the final design concept being simulated by using Computer-Aided Diagram (CAD) software. The design of the Manual Transmission Test Rig comprises of a few primary significant parts which is rig structure, gear shifter, the wall structure and also the adapter.

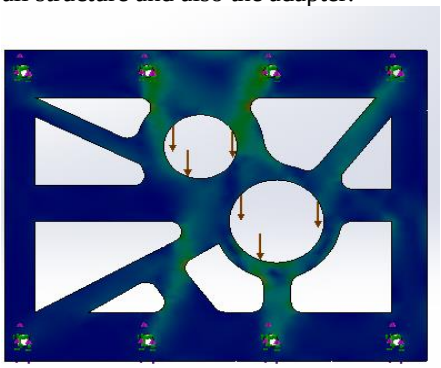

Figure 2: Stress analysis on the wall of final design

Analysis has been done in several relevant parts. Figure 2 shows o the stress analysis simulation done by using SOLIDWORKS after taking consideration of 10kg load. the stress occur at the wall is not in critical condition. The maximum stress occur on the component is around 1.795e+005N/m^2

CONCLUSION

Manual transmission test rig is designed according to the factor of safety and customer needs. The main objective for the test rig is to demonstrate the operation of changing transmission ratio in the manual transmission. For this project, test rig can help the development of transmission and study their behaviour

REFERENCES

[1] Matthias D., Andreas H., Patrick S. (2012) Gear Shifting Mechanism with a Locking Mechanism for a Gear Shift Transmission
[2] E.B. Weston Revised by R.F. Withes. (1985) Automobile Transmission System. (2nd edition)
[3] Mubeen, A. (2011). Mechanics Of Solids, 2nd Edition. India: Pearson India
[4] Brain, M. (2018). How Manual Transmission Works. Retrieved from HowStuffWorks: https://auto.howstuffworks.com/transmission4.htm

MEASURING SYSTEM FOR RATIO USING PULLEY'S POSITION SENSOR IN ELECTRO-MECHANICAL DUAL ACTING PULLEY CVT

Mohamad Fazrin Mohd Lutfi and Izhari Izmi Mazali
School of Mechanical Engineering, Faculty of Engineering,
Universiti Teknologi Malaysia, 81310 UTM Skudai, Johor, Malaysia

INTRODUCTION

This paper introduces an electro-mechanical, dual acting pulley, continuously variable transmission (EMDAP CVT) in term of measuring the ratio by simple manual calculation. The power screw mechanism introduces in EMDAP CVT, hence there is a relation between the DC motor to the CVT ratio. This system use DC motor to rotates the power screw mechanism. So, the relation from DC motor is determine to know the ratio because there is still no system that relate the DC motor to the CVT ratio. The rotation of DC motor determines how much the CVT ratio. Hence this objective is to establish the relationship between DC motor and CVT ratio and also to design and develop MATLAB Simulink to the corresponding relation. EMDAP CVT consists of sheaves that control the arrangement of the pulley whether to clamp or release according to its corresponding action [1] and also consist of two DC motor which control the movement of the primary pulley and secondary pulley which is triggered the power screw and also adjusting the clamping force [2]. As conclude, the relation from DC motor to CVT ratio is increasing linearly and positive slope.

METHODOLOGY

Depending the angle wrapped pulley which is from 0° to -12°, the value for primary and secondary radius will be identified and to be used to calculate the power screw movement. This is to ensure the problem might be happening can be reduced when conduct the project.

Before proposing a measuring system for this project, several assumptions for this system conditions are made to simplify the calculation for this EMDAP CVT. The ratio consider is underdrive ratio which is from 1.0 to 2.0 and the angle wrapped pulley is set up from 0° to -12°.

RESULTS AND DISCUSSION

At the end of control procedure, the reference value for the calculation is set up which is angle wrapped pulley (θ). Next, the equation length of belt equation is use to gain the value radius of primary and secondary pulley by simultaneously with equation radius of primary. Then, the value obtained is use to fit in to the equation form displacement to get the value. To get the relation, value of displacement calculated is applied to get the relation to the DC motor. After that, the voltage from position sensor or potentiometer is achieved followed by axial movement from the both pulley. Hence, the result is discussed and analysed.

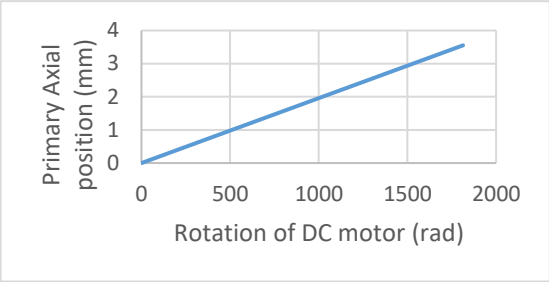

Figure 1: Power screw Vs Rotation of DC motor

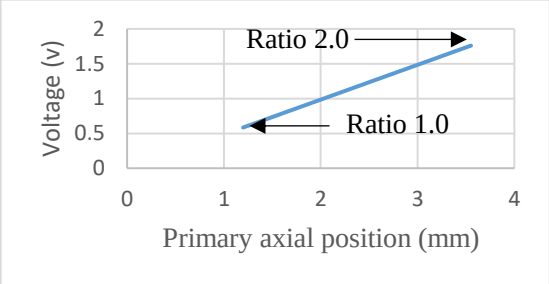

Figure 2: Voltage Vs Primary Axial Position

CONCLUSION

We have shown the relation of the DC motor to the power screw. The value can be used to calculate the CVT ratio. Also, the voltage gain is increasing linearly to the primary axial position.

REFERENCES

[1] Bambang Supriyo, Kamarul baharin Tawi, Hisyamuddin Jamaluddin, Mo. H. (2014). *Experimental Study of Electro-Mechanical Dual Acting Pulley Continuously Variable Transmission Ratio Calibration Bambang*. *2*, 121–127.

[2] Tawi, K. B., Mazali, I. I., Supriyo, B., Husain, N. A., Che Kob, M. S., & Abidin, Y. Z. (2014). Pulleys' Axial Movement Mechanism for Electro-Mechanical Continuously Variable Transmission. *Applied Mechanics and Materials*, *663*, 185–192. https://doi.org/10.4028/www.scientific.net/amm.663.185

EFFECTS OF GRAPHENE OXIDE COMPOSITE IN ZINC RICH EPOXY COATING ON CORROSION RESISTANCE OF CARBON STEEL PIPE OIL AND GAS APPLICATION

Siti Syahirah Jaafar, Sudin Izman and Mohd Zamri Mohd Yusuf
School of Mechanical Engineering, Faculty of Engineering,
Universiti Teknologi Malaysia, 81310 UTM Skudai, Johor, Malaysia

INTRODUCTION

Low carbon steel pipeline is being widely used in oil and gas industries due to its flexibility to low cost and ease of fabrication. However, the drawback of using this kind of steel is low corrosion resistance due to its low carbon content in it, only up to 0.3%, added with exposure to harsh environment, causing high tendency to increase the corrosion rate. As for that, the right choice of coating material on the pipeline may reduce the frequency of painting maintenance and the pipe life. Recently, Graphene Oxide had been studied by many researchers in alternative to enhance corrosion protection. However, its application is not well reported especially in offshore industries.The aim of this study is to compare the effectiveness of zinc rich epoxy coating with GO as a filler on corrosion resistant.

MATERIALS AND EXPERIMENT SETUP

Zinc rich epoxy was mixed with GO at 1% wt., 3% wt. and 5% wt. GO. and the thickness that were study were 80 µm, 160 µm and 240 µm. The substrate material was a low carbon steel with 0.3% Carbon content. Corrosion performances on the coated pipes were evaluated using OCP and Potentiodynamic Polarisation curve. Salt solution used in Potentiodynamic tests was 3.5% wt. NaCl.

RESULTS AND DISCUSSION

Based on OCP plot in Figure 1, the studied samples from 80 µm, 160 µm and 240 µm for different composition of GO show the same trend overall in which it observed that 5% wt. GO is thermodynamically resistant to 3.5% wt. NaCl followed by 3% wt. GO and 1% wt. GO. This trend is compatible to previous study such that the nearest OCP that shifted to positive values is the one that added GO in the coating system.

Based on Potentiodynamic Polarization curve in Figure 2, the studied samples at 160 µm for different composition of GO show the trend such that 5% wt. GO show significance value of corrosion rate that is slower compared to 1% wt. GO. The lowest corrosion rate was in the 5% wt. GO at 4.31633e-6 mmpy compared to 1% wt. GO, the corrosion rate calculated is 0.117451e-3 mmpy. The corrosion rate is decreasing in the trend of increasing composition of GO. This is understandable since the polymer in paint combined with high surface area of semi-conductive properties and oxygen functionalities introduce in GO structure [1,2] make the behaviour of coating insulated to the resistive electrolyte and thus slowing down the charge transfer from metal substrate to corrosive environment.

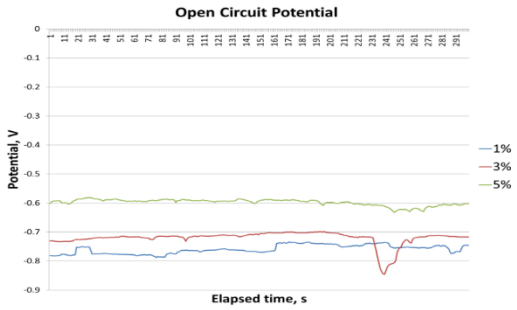

Figure 1: OCP plot

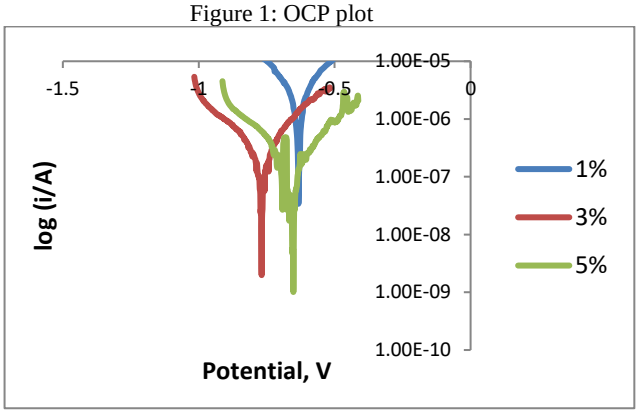

Figure 2: Potentiodynamic Polarisation curve

CONCLUSION

The OCP and Potentiodynamic Polarisation curve have proved the fact that it is possible to develop anti corrosion properties for low carbon steel pipe in offshore industries.

REFERENCES

[1] S. William, J. R. Hummers, R. E Offeman. (1958). Preparation of graphitic oxide. J. Am. Chem. Soc. 80, 1339-1339.

[2] C. Mattevi, E. Goki, A. Stefano, et al. (2009). Evolution of electrical, chemical and structural properties of structural properties of transparent and conducting chemically derived graphene thin films . Adv. Funct. Matr. 19, 2577- 2583.

7. APPLICATION OF SIX SIGMA ON RING TAG TO IMPROVE THE INNER DIAMETER PRECISIONS FOR YIELD IMPROVEMENT

8. Lionel Lau and Jafri Mohd. Rohani
School of Mechanical Engineering, Faculty of Engineering,
Universiti Teknologi Malaysia, 81310 UTM Skudai, Johor, Malaysia

INTRODUCTION

Nowadays, the urgency of the always growing markets require continuous adaptation of company offers. The development and constant improvement of the quality would be to anticipate the developments to fully satisfy the requirements and expectation of each partner (staff, customers and other stakeholders) and to maintain competitive value. Company will try to minimize the cost with the increasing of the revenue, same goes to the company that we conduct our experiment. The product ring tag need to be done in a good condition between the specification because it's used for medical purpose but with the high of reject finished product, the company suffer loss thus improvement should be made to reduce the overall defect rate of the final product as well improve overall process.

METHODOLOGY

The methodology of the project comes out as a step by step process. First is to be looking at defects data that have occurred for the past one-year, raw data will be obtained and then analyzed using quality control tools. The steps to defining the problem, to measuring the problem, to analyze the factor that affecting the problem, to improve process so that the yield loss can be reduce and to control the improved process

RESULTS AND DISCUSSION

An experiment has been conducted for the product by using full factorial experiment based on three factors with two levels for each factors, and from the result we plot the main effect and the standardize pareto chart to determine the optimum parameter and significant factor, as shown in Figure 1 and Figure 2.

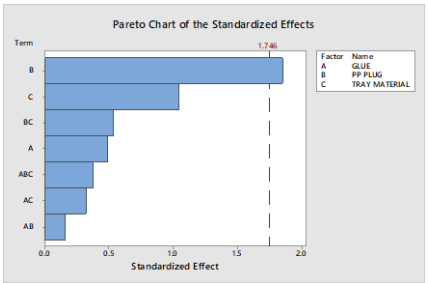

Figure 1: Pareto chart of the standardized effects

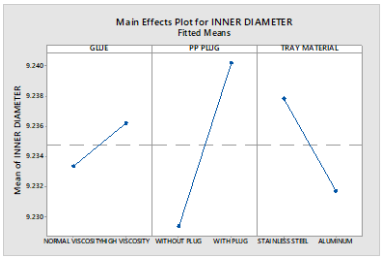

Figure 2: Main effects plot for inner diameter fitted means

CONCLUSION

It can be concluded that optimal combination of process parameters toward the response for inner diameter of the ring tag which is the normal viscosity glue, without using pp plug and aluminum tray material increase the process capability from 1.10 to 1.55 as shown in Figure 3 (a) and (b).

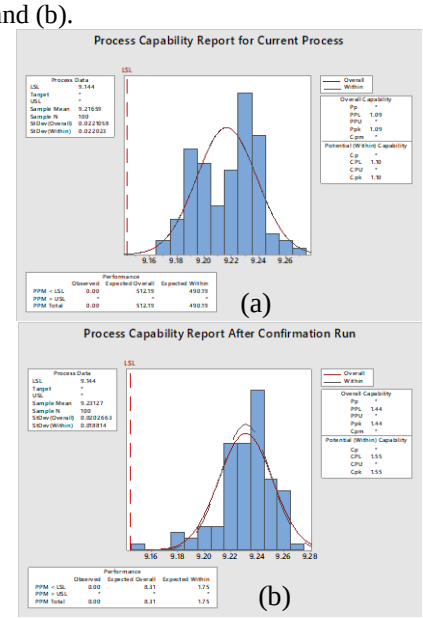

Figure 3: Optimal combination of process parameters (a) for current process (b) after confirmation run

REFERENCES

[1] Erdoğan, A., & Canatan, H. (2015). Literature search consisting of the areas of six Sigma's usage. Procedia Social and Behavioral Sciences, 95(0212), 695–704.

[2] Kwak, Y. H., & Anbari, F. T. (2006). Benefits, obstacles, and future of six sigma approach. Technovation, 26(5–6), 708–715.

[3] Mcadam, R., Joan, S. H., Mcadam, R., & Hazlett, S. (2007). A critical review of six sigma. International Journal of Organizational Analysis, 13(2), 151–174.

APPLICATION OF DESIGN OF EXPERIMENT IN ULTRASONIC FUSION WELDING OF THERMOPLASTIC PROCESS

Nur Muhammad Afiq Azizi and Jafri Mohd Rohani
School of Mechanical Engineering, Faculty of Engineering,
Universiti Teknologi Malaysia, 81310 UTM Skudai, Johor, Malaysia

INTRODUCTION

The case study is done at a brush manufacturing company. This company is located at Senai, Johor. The company actually need to produce the products according to Dyson's specification because this company is a sub-contract to Dyson. There are a lot of variety of component for vacuum parts such as motor head, brush bar, air brush and others. The main focus of this case study is for brush bar component. DOE method is use because it is a systematic method which can determine the relationship between factors affecting the manufacturing process and the output of the process.

EXPERIMENTAL SETUP

This experiment is actually to identify the most crucial factors which is in term of impact on the response variable by consider the number of factors that can be deal with feasibly. Then, the process identification for desirable levels of the selected factors need to be done [1]. By focusing on ultrasonic thermoplastic welding process, full factorial experiment design is used and there are three control factors that affecting the strength of welding that have been identified. Since the number of factors is not too many, this full factorial experiment design is suitable to use. The total number of treatments is $2k$. Thus, three factors, each at two levels, 8 treatments. The full flow of experimental procedures which indicate the ANOVA been adopted for determining the optimal conditions.

RESULTS AND DISCUSSION

The parameters and the high and low setting of each parameters is based on discussion and brainstorming among the engineers at the company which is weld time, pressure and delay. From the result of ANOVA table, we assume that the confidence interval will be (α=0.05). The results of Pareto Chart in Figure 1 exists when data have been analysed. The bars that represent factors C, ABC, AB and A cross the reference line in Pareto Chart which is at 2.12. These factors are statistically significant at the 0.05 level with the current model terms.

Model development and prediction of weld strength. Confirmation runs is done after the analysis of the experiment was completed. The value coefficient of significant factor from the AVOVA table will be included in the calculation. In order to increase the weld strength, the optimum setting will be selected from main and interaction plot which have the high mean value of strength weld. A new model and setting has been develop.

The run for confirmation run test will based on the new model as shown as in Table 1. The results obtained for average strength weld at the optimal condition is about 33.33 N which is plus/minus 10% from the predicted value, so the results is valid. Besides, the effect on the microstructure at welding surface also been explained and the experiment was conducted by Scanning Electron Microscope (SEM) machine.

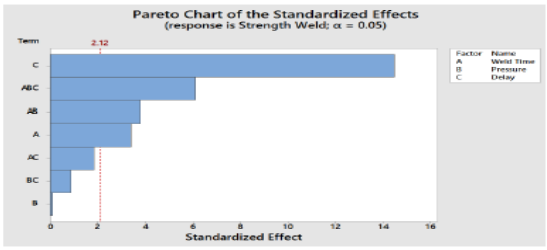

Figure 1: Pareto Chart of the Standardized Effects.

Table 1: Confirmation Run Test Results

Sample	A	B	C	Strength Weld (N)
Sample 1	-	+	+	31
Sample 2	-	+	+	35
Sample 3	-	+	+	34

CONCLUSION

The objectives of this study have been achieved which is to identify the parameters that affect the ultrasonic welding process, performing the DOE and to verify the factor that affected the strength of welding.

REFERENCES

[1] Sonam Ranga, Manish Jaimini, Sanjay Kumar Sharma, Bhupendra Singh Chauhan and Amit Kuma. (2014), A Review on Design OF Experiments (DOE), International Journal Of Pharmaceutical And Chemical Sciences , Vol. 3 (1) Jan-Mar 2014

[2] Daniel Granato and Veronica Maria de Ara ujo Calado. (2013). The use and importance of design of experiments (DOE) in process modelling in food science and technology, State University of Ponta Grossa Ponta Grossa, Brazil.

SCOUR PROPAGATION OF OTEC COLD SUBSEA PIPELINE

Mohammad Fahmi Zaimi and Jaswar Koto
School of Mechanical Engineering, Faculty of Engineering,
Universiti Teknologi Malaysia, 81310 UTM Skudai, Johor, Malaysia.

INTRODUCTION

With the increasing use of pipelines, it is necessary to assess the long–term operation of pipelines in the ocean. Over the last decades, the stability of submarine pipelines has been a subject of significant concern for engineers and researchers. They found it is often the currents and the waves that lead to scouring below the pipelines and cause pipelines to become suspended, and finally broken. They also realized that in scouring it is always the s factor that induces failure of submarine pipelines. With the force of currents and waves, the sediment under the pipeline is first eroded, and then a hole is formed, and then, the hole becomes deeper and wider, at the same time, scouring propagates along the axis of the pipeline. That is briefly the scour process.

NUMERICAL MODEL

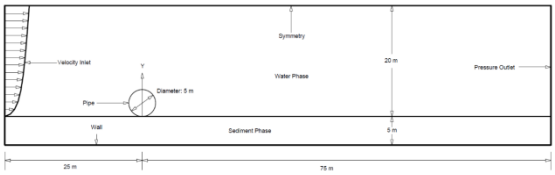

Figure1: Computational domain and phase configuration

Simulations showed that this time-step is small enough to ensure the solutions and are independent on time-steps.

The steps for our simulation can be summarized as follows:

1) Generate the grid.
2) Use the mixture turbulence model in the Flow 3D solver to calculate the fully developed velocity and turbulence for the fluid phase.
3) Use the Eulerian two-phase model in the Flow 3D solver to calculate the solid-fluid interactions as well as the velocity of solid phase, using fully developed velocity from step 2) as the input.

RESULTS AND DISCUSSION

The current scouring around the pipelines are concern in engineering safety. Meanwhile, the pipeline will also cause local hydrodynamic environment changes. The simulation results showed that for several depth of pipeline, considering only unidirectional currents caused by local scour. The location of maximum scour depth is at the downstream side of the pipe. Along with the narrowing of the initial gap between the pipeline and sand bed, scour depth increases. Around the pipeline, strong wakes and vortexes usually occur, resulting in even stronger scour around the pipeline. For the deep water, tidal flow is thought to be the main factor that induces local scour.

A faster scouring rate during the period between 500 and 1,500 minutes indicates that the bottom layer depth determines the initial scour rate. The solid line shown indicates that the scour depth no longer changes after 2,500 minutes. The effects of initial velocity, pipe diameter and sediment particle size are considered simultaneously in analysing the movement of sediment around the pipeline. The scour depth shows a general reasonableness for sediment particle size distribution. When sediment particle size is large, the bed surface sediment gradually becomes difficult to start. This can be reflected in the figure 6.9. When the sediment particle size is small, the situation is not different, which results in the size of the relevant response for scour depth. The scour depth increases with time and then tends to limit the final equilibrium state.

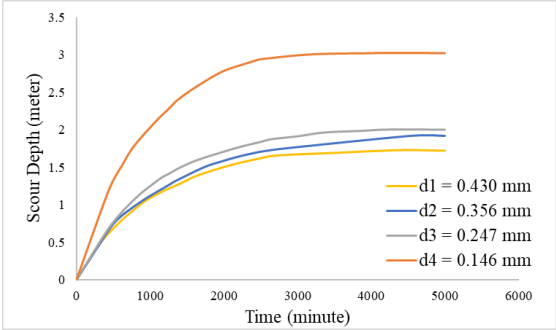

Figure 2: Comparison between 4 different grain size

CONCLUSION

Scour prediction scour depth and scour protection showed in this paper.

REFERENCES

[1] Mao, Y. (1988). Seabed scour under pipelines. In OMAE 1988 Houston. *Proc. 7th Int. Conf. on Offshore Mechanics and Arctic Engineering*, Am. Soc. Civ. Engineers, Houston, TX, 7-12.

[2] Sumer, B. M., & Fredsoe, J. (1991). Onset of scour below a pipeline exposed to waves. *The First International Offshore and Polar Engineering Conference.*

ALLOWABLE FREE SPAN LENGTH OF OTEC COLD SUBSEA PIPELINE

Hariz Azhar and Jaswar Koto
School of Mechanical Engineering, Faculty of Engineering,
Universiti Teknologi Malaysia, 81310 UTM Skudai, Johor, Malaysia

INTRODUCTION

Ocean Thermal Energy Conversion (OTEC) is a marine renewable energy technology and a process that can produce electricity by using temperature difference between the warm surface ocean water and deep cold ocean water. The OTEC power plant uses warm water at sea level with temperature around 25 degrees Celsius to vaporize a working fluid, which has a low boiling point, such as ammonia [1]. The water vaporizes ammonia will drive the turbine and generate electricity. The critical part of the entire operation for this subsystem is the cold water pipe (CWP) due to its large size of diameter and height, and the operating environment. The OTEC power plant extract large amount of cool water from the deepest layer of the ocean through a long cold-water pipe (CWP). The floating ocean thermal energy conversion (OTEC) system usually consist an up to 500m long cold-water pipe (CWP) [2]. This study mainly focuses on the design criteria and allowable free span length analysis of OTEC cold water.

METHODOLOGY

This section presents the research flow of the study. The procedure of the cold water pipe design was calculated based on the allowable code [3]. Next, the allowable free span length is then calculated by using the recommended practice allowable code [4]. The initial span length of the cold water pipe is 1000 meters.

If the span length of the cold water pipe has exceeded the allowable limit, the top mooring line is proposed to hold the pipeline structure at fixed position. Then, the deflection and the span length of the cold water pipe is analysed.

RESULTS AND DISCUSSION

The pipeline analysis is performed to verify the pipeline is within the allowable stresses. The free spanning in cold water pipe occurs due to un-uniform vertical current acting on the pipe. The deflection of pipeline in different span length is analysed.

Based on the calculation of allowable span length for the cold water pipe in dynamic analysis, 1000 meter has exceeded the limit criteria of 230m. Therefore, the top mooring line is proposed to reduce the span length of the structure. The maximum deflection of 1.448m can be reduced to 0.09m. Reducing the span length may reduce the in-flow effect on the pipe structure.

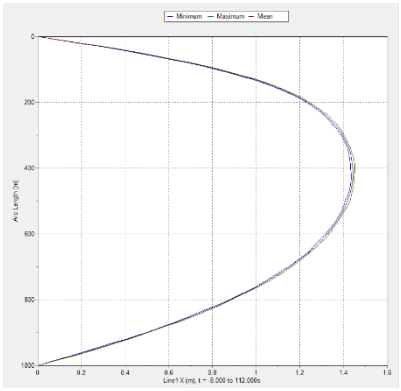

Figure 1: Deflection of pipeline without mooring

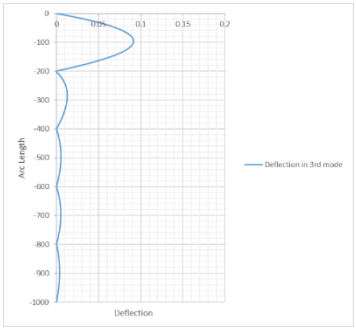

Figure 2: models between control conditions

CONCLUSION

The cold water pipe design stresses have not exceeded the stresses limit that was set by the allowable code [3]. Apart from that, both static and dynamic analysis methods were used to study the maximum allowable span length in the deep water. Improvement can be practiced in further studies by considering the RAO effect of the floating structure and the wave effect.

REFERENCES

[1] J. Koto, “Potential of Ocean Thermal Energy Conversion in Indonesia,” *Int. J. Environ. Res. Clean Energy*, vol. 4, no. 1, pp. 1–7, 2007.

[2] M. Zaki Prawira, “Vortex Induced Vibration On Cold Water Pipe of OTEC,” 2018.

[3] T. H. E. United and S. Of, “ASME B31.4 Pipeline Transportation Systems for Liquids and Slurries,” in *American Society of Mechanical Engineers*, vol. 552, 2012, p. 140.

[4] MMS, “of the Interior Minerals Management Service,” in *Project Consulting Services, INC.*, vol. 7406, no. 97058, 1997.

SIMULATION OF ANCHOR LOADS ON OCEAN THERMAL ENERGY CONVERSION COLD SUBSEA PIPELINE

Ten Ki Hong and Jaswar Koto
School of Mechanical Engineering, Faculty of Engineering,
Universiti Teknologi Malaysia, 81310 UTM Skudai, Johor, Malaysia

INTRODUCTION

Ocean Thermal Energy Conversion (OTEC) cold water pipe (CWP) is a large slender pipe extended to deep water and thus required mooring system to avoid failure in bending or buckling. Relatively, the load on CWP and mooring system will be transferred to anchor as anchor load. Thus, the anchor required sufficient capacity to resist the anchor loads. For this research, floating OTEC in Layang-Layang Island [1] is considered to use suction caisson anchor with taut mooring system. The source of anchor load considered was drag force due to current flow F_x, buoyant force F_z and tension T_p of mooring lines.

METHODOLOGY

Finite element analysis was performed for the response of CWP to current flow by using MATLAB. By that, the suitable mooring system with appropriate number of mooring lines and material were chosen.

Since the sources of anchor loads were determined, simulation of anchor loads was done. With regards to the loads determined, a preliminary design parameter of suction caisson anchor was proposed with calculated capacity with respect to the anchor loads. Then, the design was verified with regards to recommendations.

RESULTS AND DISCUSSION

The MATLAB output of OTEC CWP with mooring system response to the current flow as shown in Figure 1 indicated that the design of mooring system is suitable.

Then, the simulation of anchor loads was done by assuming anchor installation on flat seabed. The anchor loads were resolved into horizontal (H) and vertical (V) components. The resulted inclined anchor loads were ranged from 926.2 kN to 2802.3 kN. Thus, the designed anchor capacity in horizontal (H_{max})and vertical (V_{max}) directions respectively as tabulated in Table 1. The safety factor of the designed anchor was about the recommendation of 2.10 for ultimate limit state [2].

Nevertheless, the simulation was repeated according to topography of Layang-Layang Island [1]. The main modification required was the length of the mooring line as illustrated in Figure 2. Thus, this also affected the design of anchors. Due to the uncertainties of the actual topography, the design safety factor was increased to 3.10.

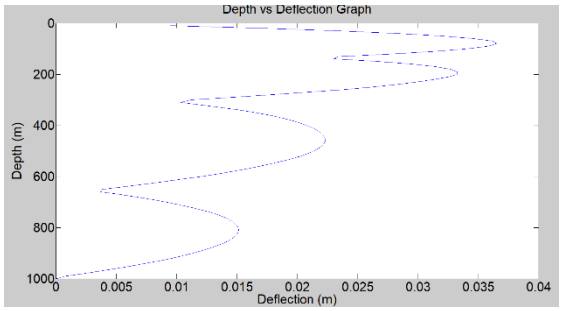

Figure 1: Graph of depth vs deflection of OTEC CWP with mooring.

Table 1: Capacity of designed anchor

Sets of Anchor	V_{max} (kN)	H_{max} (kN)
1, 2, 3, 4	4490	4675
5, 6, 7, 8	3549	3669
9, 10, 11, 12	2398	2448
13, 14, 15, 16	1348	1347

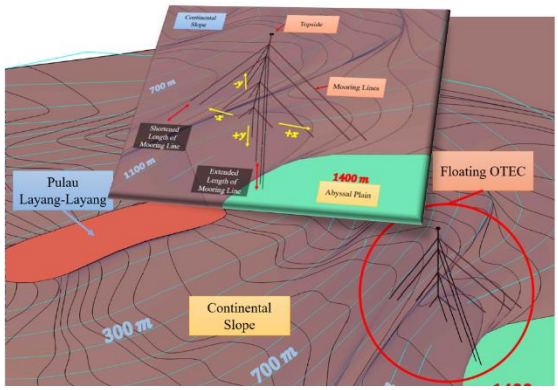

Figure 2: models between control condition

CONCLUSION

The risk of floating OTEC CWP failure was resolved by mooring system that strengthen it. The relative anchor loads of the entire system was also determined partially. It is recommended to include more consideration of environmental effect to increase the reliability of the simulation.

REFERENCES

[1] Fahmie, M., Jaswar, K., Nofrizal, Edu, A., Zulkarnain, U., 2018. Ocean Thermal Energy Conversion in Layang-Layang and Kuala Baram, Malaysia. *International Journal of Environmental Research & Clean Energy Vol.11 No.1*, 12-21.

[2] DNVGL, 2017. DNVGL-RP-E303 Geotechnical Design and Installation of Suction Anchors in Clay. Norway, DNVGL, Norway

HYDRODYNAMIC OF SINGLE MOORING FLOATING VERTICAL AXIS TURBINE FOR TIDAL CURRENT ENERGY

Mohamad Khairul Ikhmal Jaafar and Jaswar Koto
School of Mechanical Engineering, Faculty of Engineering,
Universiti Teknologi Malaysia, 81310 UTM Skudai, Johor, Malaysia

INTRODUCTION

Conventional electricity generation using fossil fuels alone is no longer sufficient and sustainable to meet the demands of the global population. Additionally, the burning of fossil fuels emits undesired greenhouse gases. Thus, developing the potential renewable energy is an urgent affair and much focus has been placed on this field. Among the plenty of renewable energy resources, the regular and predictable tidal current energy is great potential which is environmentally friendly to reduce both visual and noise pollution. In order to have better utilize the tidal current energy, plenty of researchers focus on the analysis and design of tidal current turbine. The vertical axis current turbine is the most developed type and can be used to extract a large amount of tidal current energy from tidal streams.[1]

EXPERIMENTAL SETUP

The research consist of influence of vertical blade to mooring line system experiment at Kukup and measuring current speed at 15 position around Kukup including selected location of Fish Farm. The measurement is conducted at different location around Kukup, with the same setup. Before the experiment start, the wire rope was fixed at current meter. Buoy also is attached at current meter, in order to ensure the device is safe and can be detect if any incident happen. Current meter is hanging 1 meter below the surface of water. The experiment setup began with the process of fabrication for supporting structure and load cell calibration. The whole model consist of supporting structure, vertical blade, floater and single wire mooring will be float 1m from the surface of water. The experiment will manipulate the surface area of vertical blade and fixed the dimension of wire mooring.

RESULTS AND DISCUSSION

Based on the measured current speed around Kukup, the suitable water depth to conduct experiment is at 1m from the surface of seawater. Most of position experience highest current speed at 1m from the surface of seawater. Moreover, the selected highest current speed was at position C which is located at Fish Farm. The measurement of current speed continue after selecting Fish Farm as the potential by conducting measurement around fish farm to select the suitable location to conduct mooring line experiment. After analyse the data and compare with other position, position A is selected due to several reason by considering factor such as environmental effect and the distance of location with power source generator. Based on the experiment conducted, the data analysis show constant average force of mooring line which is 7N for each of design vertical blade. The result of experiment is validated with drag force calculation. The percentage difference between experiment and calculation is small thus it made the influence of vertical blade to mooring line system is insignificant.

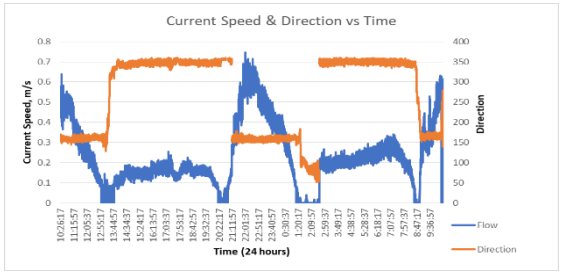

Figure 1: Kukup Current profile and direction in 24 hours at position A

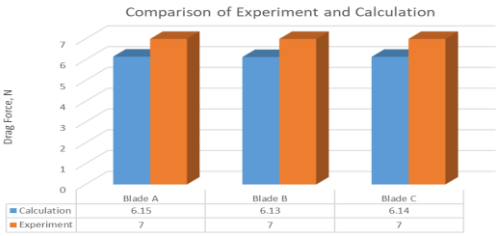

Figure 2: Comparison mooring line force data between experiment and calculation

CONCLUSION

As a conclusion, the objective of all experiment achieved successfully by conducting experiment**.** The high performance location already decided with the outcome Position A as the selected position with coordinate 1.3378°N 103.4354°E. The influence of blade design of vertical current turbine to wire mooring system is insignificant. The research regarding wire mooring related with renewable energy is conducted through this study.

REFERENCES

[1] Barbarelli, S. F. (2017). First techno-economic evaluation of array configuration of selfbalancing tidal kinetic turbines. *Renewable Energy*, 183-200.

EXPERIMENTAL STUDY OF TORQUE PERFORMANCE ON DIFFERENT BLADE DESIGNS ON VERTICAL AXIS CURRENT TURBINE

Alif Mustaqim Mohamed Rawi and Jaswar Koto
School of Mechanical Engineering, Faculty of Engineering,
Universiti Teknologi Malaysia, 81310 UTM Skudai, Johor, Malaysia

INTRODUCTION

Extraction of current energy using vertical axis current turbine, is necessary in order to counter wise the global warming, hence a solution to encounter associated with turbine configuration, enhancing the efficiency and achieve high output power using the best design of turbines that can be employed in low speed current. We chose an innovative vertical axis current turbine design for low speed current turbine as the water turbine because the tidal current changes direction periodically. The turbine has a vertical axis of rotation and therefore is perpendicular directional to tidal current.

EXPERIMENTAL SETUP

The research methodology to investigate effect of arm and self-adjusting blades on vertical axis current turbine (VACT) performance in low speed current is explained. The research methodology is divided into two areas. The areas of research are Experimental design methodology to determine and analyse data of characteristics of turbine performance such as torque calibration, design and fabrication of cage structure, blades and determination of design speed of current speed and Experimental tests on 4 different type of blade designs and fixed arm turbine. To achieve this, model tests have been carried out on Marine Technology Centre (MTC) -Universiti Teknologi Malaysia (UTM).

RESULTS AND DISCUSSION

Based on graph, TSR vs torque coefficient, RPM vs current speed, and power vs current speed, the result shows self-adjustable turbine blade #3 has the highest efficiency followed by self-adjustable turbine blade #2. This is due to the surface area of convex side is reduced. The convex side have a greater force due to self-adjusting blade and the surface area is constant while on the concave side, the drag force applied on the blade is smaller caused by self-adjustable blade that turned almost 90 degrees in angle to the outflow of the direction of current. Hence, the hydrodynamic characteristics which is the drag force reduce significantly. The power produce for self-adjustable turbine blade #3 and self-adjustable turbine blade #1 demonstrate almost the same values. This is because the surface area of concave and convex side is same. Thus, the drag force of the both blades may almost the same.

The error of the experiment may cause by the turbine cage structure itself. During the experiment, the vibration occurred because of the size or the design not too strong enough to overcome turbulent flow of produced by turbine cage structure itself when towed by towing carriage. Next, torque meter is too sensitive to the surrounding, such as vibration from generator and electric drive motor of the towing carriage.

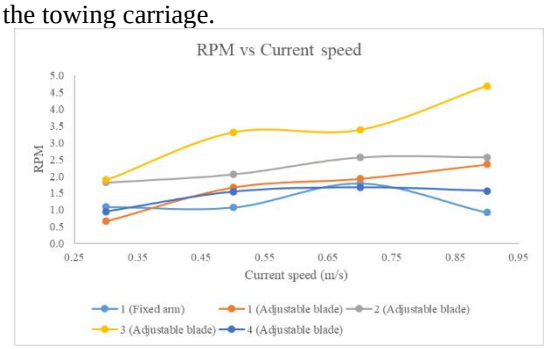

Figure 1: RPM vs current power

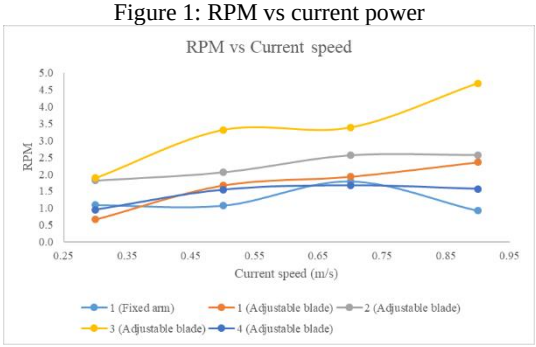

Figure 2: Power vs current speed

CONCLUSION

The results show that surface area of concave has a strong effect on the performance of turbine. The lesser surface area of concave side, the lesser drag force acted on it. Thus, increase the power output of turbine. The self-adjusting blades increased the power and RPM compared to the fixed blades turbine. This fact happens because the returning blade angle is in closed position, which decreases the hydrodynamic resistance which is the drag force acting on the blade.

REFERENCES

[1] Chong, H.-Y., & Lam, W.-H. (2013). Ocean renewable energy in Malaysia: The potential of the Straits of Malacca. Renewable and Sustainable Energy Reviews, 23, 169-178.

DEEP REINFORCEMENT LEARNING BASED TRAFFIC CONTROL SYSTEM

Bryan Chua Seck How and Kamarulafizam Ismail
School of Mechanical Engineering, Faculty of Engineering,
Universiti Teknologi Malaysia, 81310 UTM Skudai, Johor, Malaysia

.

INTRODUCTION

One of the major causes of jams in cities, are the existence of ineffective traffic lights. Existing traffic light control either deploys fixed programs without considering real-time traffic or considering the traffic to a very limited degree. In this research, we propose a deep reinforcement learning algorithm that can extract all key features useful for adaptive traffic signal control from raw real-time traffic data. A deep reinforcement learning model is a reward-based algorithm that can learn to select an optimal action selection policy using feedbacks from rewards [1].

RESEARCH OBJECTIVES

To determine if deep learning-based traffic light algorithm can perform better than conventional traffic management at Pulai Perdana intersection.

METHODOLOGIES

Deep Q Learning is used to find the optimal traffic action control policy for Pulai Perdana Intersection. The goal of the agent is to reduce the cumulative waiting time of vehicles at the intersection. The states are defined as velocity, position and traffic light states. The actions the agent can take are to control the green signal time of each of the direction at the junction. The rewards were defined as the different between cumulative waiting times of vehicles at the intersection. A Deep Convolutional Neural Network is used to approximate the Bellman's Optimality Equation.

$$Q^{\pi*}{}_{(s,a)} = E_{s'}\left[r_t + \gamma \max_{a'} Q^{\pi*}(s', a') | s, a\right]$$

RESULTS AND DISCUSSION

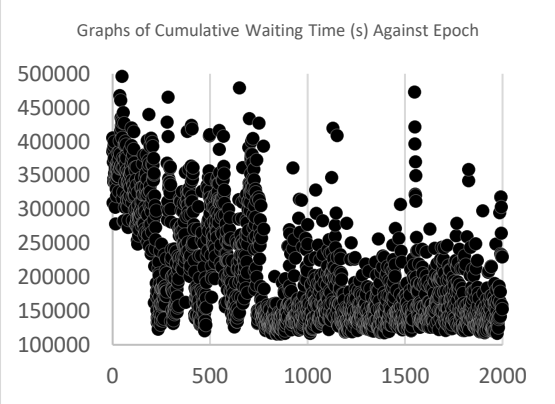

Figure 1: Cumulative waiting time of vehicles against epoch

Figure 1 shows results of the agent after 2000 epochs. We can see that the agent starts off by taking more explorative actions, it explores the environment searching for actions that leads to reduction in waiting time. After running the training for 2000 episode, the agent learnt a good action selection policy and managed to reduce the cumulative waiting time. It is proven in the experiment that a deep reinforcement learning model was able to reduce the cumulative waiting time of all the vehicles at a given traffic intersection as compared to a fixed time algorithm-based traffic management system at Pulai Perdana by 47.31%. When the traffic is scaled down to 50% and 20 %, the agent improved the waiting time by 69.56% and 68.36 % respectively.

REFERENCES

[1] Genders, W., & Razavi, S. (2016). Using a deep reinforcement learning agent for traffic signal control. arXiv preprint arXiv:1611.01142.

SUPPRESSION OF LIQUID SLOSHING IN LNG CARRIER WITH FLOATING BAFFLE CONCEPT

Ching-Yun Loo and Hooi-Siang Kang
School of Mechanical Engineering, Faculty of Engineering,
Universiti Teknologi Malaysia, 81310 UTM Skudai, Johor, Malaysia

INTRODUCTION

Sloshing motion within the Liquefied natural gas (LNG) carrier's tank can cause structural damages. Hence, the purpose of anti-sloshing device is to reduce the sloshing displacement and impact pressure toward the tanks wall. In this paper, the slosh behaviour with floating baffle in membrane tank was excited in regular unidirectional sway motion $y\ (t) = A \sin (2\pi t/Tp)$ with amplitudes, A = 3.0 cm, and period, Tp = 1.1 sec. was investigated numerically.

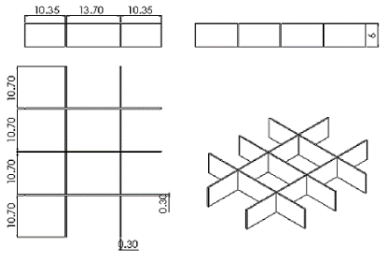

Figure 1: Principal Dimensions of the model of floating baffle (unit in centimetre)

This study was verified by comparing the previous experiment research. The objectives of this study are to numerically analyze the surface deformation and pressure of liquid with- and without floating baffle by using CFD software, OpenFOAM and to evaluate the sensitivity of different excitation period for floating baffle in suppress liquid sloshing.

METHODOLOGY

The methodology of the simulation are

i. Pre-processing(Define solver, Geometry modelling, Floating baffle Modelling, Dict Setting (amplitude and frequency identification)
ii. Run simulation (Filling ratio= 30% and 50%, various excitation period ratio= 0.5,0.8,1.0,1.2,1.5 and 2.0)
iii. Post-processing (sloshing profile and Pressure indication)

RESULTS AND DISCUSSION

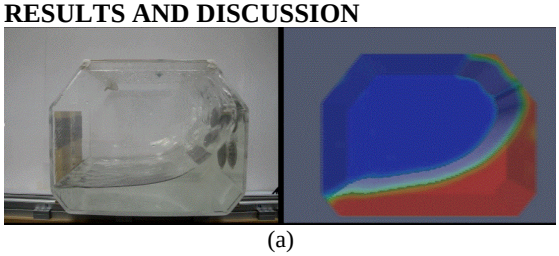

(a)

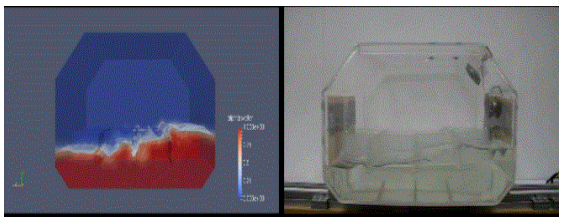

(b)

Figure 2: The comparisons between experiment and simulation with (a) and without (b) floating baffle on 30% filling ratio

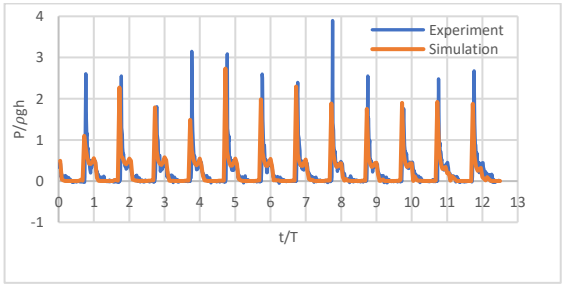

(a)

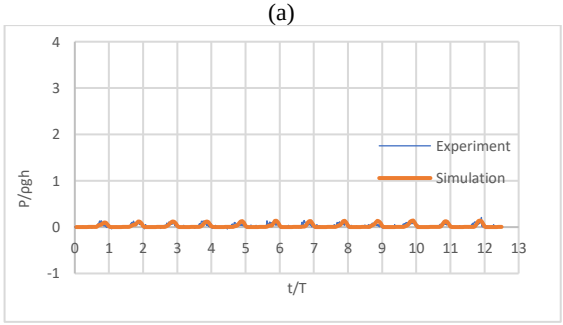

(b)

Figure 3: (a) Comparison of pressure at location sensor 1 between simulation and experiment result at 30% filling ratio, without floating baffle and (b) with floating baffle

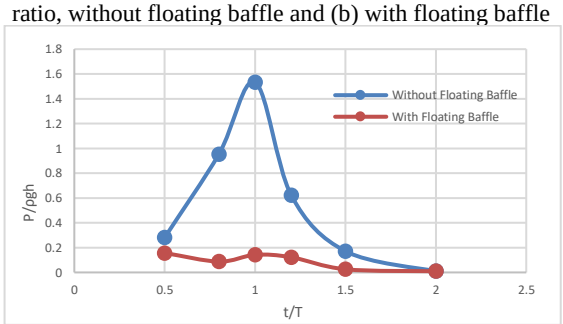

Figure 4: Comparison of maximum pressure at various period between with- and without floating baffle at 30% filling ratio

CONCLUSION

a) Flow visualization of simulation (OpenFOAM) and experimental showed an acceptable agreement.
b) The floating baffle suppresses the impact pressure effectively at various period.

REDUCTION OF EXTREME MOORING TENSIONS DUE TO SNAP LOADS BY USING MAGNETO-RHEOLOGICAL DAMPER

Hanafi, M. I. and Kang, H. S
School of Mechanical Engineering, Faculty of Engineering,
Universiti Teknologi Malaysia, 81310 UTM Skudai, Johor, Malaysia.

INTRODUCTION

Failure in the mooring/hawser system has been a major problem in offshore safety and reliability. The snap load along the hawser line is still unresolved due to its non-linear force. The snap load can lead to catastrophic failures and structural destruction which may cause fatality to personnel. A mooring system consists of a mooring line, anchor, and connectors. It is used to hold a ship or a floating platform in all depths of water. A mooring line connects an anchor with a floating structure to the seabed. Next, hawser system consists of thick rope or cable used in mooring or towing a ship. The breaking loads of these mooring ropes will depend on the quality of the synthetic material used to make them.

EXPERIMENTAL SETUP

The experiment was conducted with 2 different setups. The first experiment is run without the MR damper and the second is run with MR damper installed. The experiment was conducted by the Universal test machine (UTM) pulled the cable (rope) until reached its maximum breaking load (MBL). The force caused the line to generate a high inline tension is then measured by the load cell pre-installed in the machine. The maximum load is then recorded for further comparison with the MR damper install. The experiment was repeated for few times with the different condition of the input current.

RESULTS AND DISCUSSION

The data of the rope test is compared with and without damper installed. The main contribution to of this experiment is at the compensation region. The extension elongation made by the damper is an important part of this experiment. The comparison between of data is shown in figure 4.1.

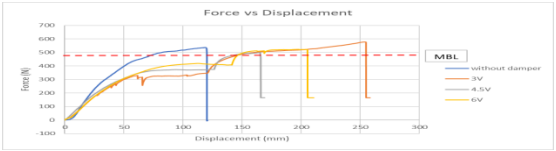

Figure 1: Graph of rope with and without damper installed.

Based on the graph plotted, the rope can extend their displacement few millimetres compared with the rope without damper. For the rope at 3V, the rope that installed with damper able to elongates up to 254mm before reaching its breaking point compares with the rope without damper that reaches up to 120mm. With this, the total extension by these 2 different cases is 134mm. Next, figure 2 shows a comparison graph on a rope with 4.5V. The total elongation for the rope until reaches breaking point is at 205mm. This shows the extra displacement up to 85mm.

Figure 2: Comparison of rope extension at 4.5V

Finally, at 6V of the input voltage. The maximum elongation of the rope is at 168mm and the maximum force is at 496N. The total extension compares without is about 48mm. The data is shown in figure 3 below.

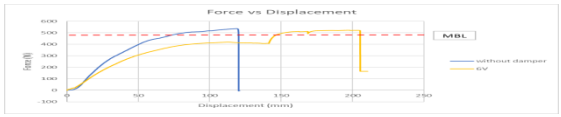

Figure 3: Comparison of rope extension at 6V

CONCLUSION

Based on the experiment, the result obtained manage to solve the problem of reducing the extreme mooring tension by using the magneto-rheological damper. With damper install, it able to give an extra extension of the rope before reaching its breaking point. With this, it can reduce the likelihood of snap loads in the hawser line to occur.

REFERENCES

[1] Hu, G., Lu, Y., Sun, S., & Li, W. (2017). Development of a self-sensing magnetorheological damper with magnets in-line coil mechanism. *Sensors and Actuators, A: Physical*, 255: 71–78.

[2] Chen, Jen San, & Hung, S. Y. 2012. Exact snapping loads of a buckled beam under a midpoint force. *Applied Mathematical Modelling*, 36(4), 1776–1782.

[3] Lee, K. H., Han, H. S., & Park, S. (2015). Failure analysis of naval vessel's mooring system and suggestion of reducing mooring line tension under ocean wave excitation. *Engineering Failure Analysis*, 57, 296–309.

[4] Giusti, A., Stabile, G., Marino, E., & Borri, C. (2017). Coupling effects on the dynamic response of moored floating platforms for offshore wind energy plants.

[5] Hsu, W. ting, Thiagarajan, K. P., & Manuel, L. (2017). Extreme mooring tensions due to snap loads on a floating offshore wind turbine system. *Marine Structures*, 55, 182–199.

COUPLE DYNAMIC OF SHALLOW WATER MOORING SYSTEM INTEGRATED WITH ARTIFICIAL SEABED

Teng Hao Yuan and Kang Hooi Siang
School of Mechanical Engineering, Faculty of Engineering,
Universiti Teknologi Malaysia, 81310 UTM Skudai, Johor, Malaysia

INTRODUCTION

The shallow water mooring system of floating offshore wind turbine (FOWT) is modified into tension-leg mooring system with artificial seabed to reduce the footprint area. However, the tension-leg mooring system is affected by the tidal effects such as tidal force and the variations of sea level that will produce excessive in-line tension to the mooring line.

Therefore, the experiments are conducted to determine the minimum breaking force (MDF) that can be supported by the mooring line. The magneto-rheological (MR) damper is incorporated with the mooring line in the experiment to determine its efficiency in increasing the MDF of mooring lines.

EXPERIMENTAL SETUP

This section presents the experimental setup for the experiment. Firstly, the nylon line is selected as the mooring line sample in the experiment. Next, the force-displacement and force-velocity characteristics of MR damper are tested by using the Instron universal testing machine. Then, based on a specific part of the FOWT, a free body diagram is drawn from the real scenario. The free body diagram can be classified into two types which are mooring line with and without MR damper.

The free body diagram is then converted into the experimental setup. The apparatus and instruments used in the experiments including 20cm, 80lb nylon line, a MR damper model LORD RD-8041-1, a MR damper holder and the universal testing machine.

RESULTS AND DISCUSSION

From the force-displacement and force-velocity characteristic testing of MR damper, the maximum damping force from MR damper increases when the voltages input increases from 1.5V to 3V and 4.5V and the velocity of stroke of MR damper increase from 20mm/min to 40mm/min and 60mm/min respectively. The distance of stroke moving from all cases are constant which is 20mm.

Figure 1 shows trends of force of nylon line against its displacement integrated with MR damper. Comparison is made between the nylon line with and without MR damper. The nylon line without MR damper extends from region 1 to region 2 until it breaks at MBF of 486N and 83mm. The nylon line integrated with MR damper extend at region 1 and the extension of nylon line is compensated by the stroke of MR damper in region 2 and finally breaks at MBF at region 3.

However, the MBF and final extension are not consistent due to non-linear properties at the breaking phase.

The average value is obtained from the experiments at different voltages input and it is showed in Figure 2.

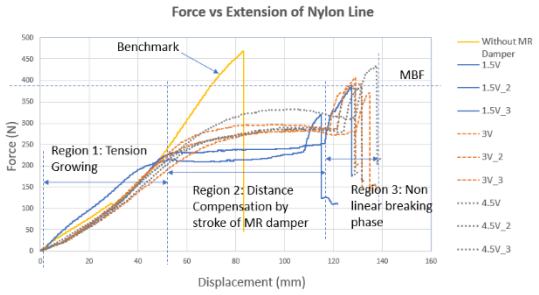

Figure 1: Graph of Minimum Breaking Force of 20cm, 80lb Nylon Line with MR Damper (Divided by Regions).

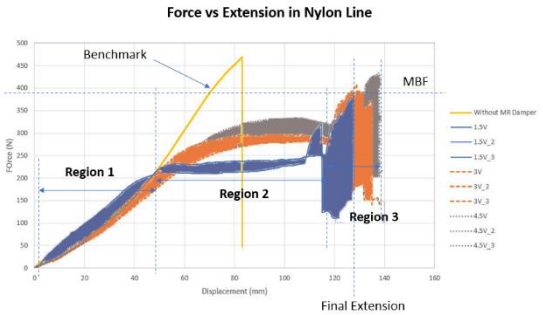

Figure 2: Range of Effective Values of Force and Displacement for Different Voltages Input

CONCLUSION

From the experiments, we conclude that the compensation on the extension of length of nylon line shifts backwards when the voltages the voltages input of MR damper increases. The MDF and final extension of nylon line should be always constant.

REFERENCES

[1] Kang, H., Mohamed, A. H., Foad, M., Hamid, A., Saman, A., Kader, A., Tamin, M. N. and Quen, L. K. (2018) 'Dynamic Responses of Tensioned-Leg Mooring with Gravity-based Foundation for Floating Offshore Wind Turbine'.

[2] Hazwan, A. (2018) 'Coupled Dynamics of Mooring System and Floating Structure in Shallow Water Condition', p. 89.

WAVE GENERATION AND PROPAGATION IN NUMERICAL WAVE TANK

Muhammad Safuan Shamshol Kang Hooi Siang
School of Mechanical Engineering, Faculty of Engineering,
Universiti Teknologi Malaysia, 81310 UTM Skudai, Johor, Malaysia

INTRODUCTION

Offshore structures have been rapidly growth in sea regions. Ships and offshore structure in the sea are exposed to effect of rogue wave thus, need to design with a very high safety factor and undergone rigorous model testing in order to make sure it is safe to be used. A common approach of model testing is by conducting the experiment in laboratory wave tanks. But this approach has significant problems such as the model test are costly and subjected to the instrumentation and physical limitations of the wave tank. By using wave simulations, it can give comprehensive time history data in terms of waveforms, flow velocity fields and energy variation to understand the evolution and impact mechanism with less costs and technical limitations [1]. However, combination of laboratory experiment and numerical are preferred because it can complete the weakness of each approach.

EXPERIMENTAL SETUP

This section presents the experimental setup for the system. We used OpenFOAM v1812 to generate 2D regular wave in numerical wave tank. OpenFOAM solves the Stokes equations for two incompressible phases. The solver used in this operating system is *interFoam*. *interFoam* is used to tracks the free surface movement by using the Volume of Fluid (VOF) method which is to describe an incompressible of two-phase flow mixture. The method to generate simulation wave by OpenFOAM is separated into three significant stages which are pre-processing, solver and post-processing.

RESULTS AND DISCUSSION

There a 4 set of data that are used to study the behaviour and the accuracy of wave elevation between experimental dan simulation result. This 4 set of data in divided into two categories which based on the wave steepness. The first category is wave steepness below 0.05 and the other one is above 0.05. Figure 1 shows the wave elevation of wave steepness of 0.025 with the wave height. Hw=0.06m and wave period, T=1.49s. The results in represent the case of wave steepness below 0.05. While, Figure 2 shows the other case which wave steepness above 0.05. Wave steepness in Figure 2 is 0.134 with a wave height, Hw=0.17m and period, T=0.9s. Table 1 shows the root means square error for all cases study. From the results, there is a limitation in OpenFOAM where on wave steepness below 0.05 can be generate properly and show a good degree of accuracy with experimental data.

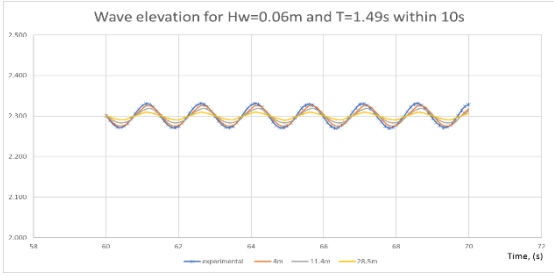

Figure 1: Wave elevation of wave steepness 0.025

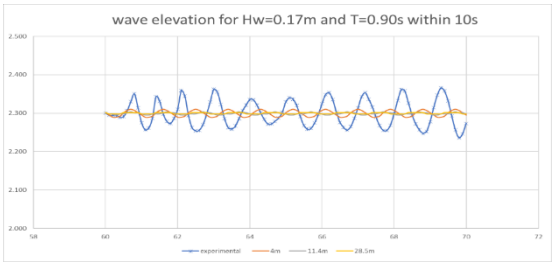

Figure 2: Wave elevation of wave steepness 0.134

Table 1: Root Mean Square Error

Table of Percentage Root Mean Square (RMSE) Error (%)									
Wave height	period, T								
	0.90s			1.20s			1.49s		
	location of wave probe								
	4m	11.4m	28.5m	4m	11.4m	28.5m	4m	11.4m	28.5m
0.06m							0.59	0.96	1.49
0.10m							1.27	1.55	2.28
0.12m							1.45	1.63	2.67
0.15m									
0.17m	3.55	3.52	3.44						

CONCLUSION

OpenFOAM can successfully model a numerical wave tank for regular wave if the condition and parameter are appropriately set. OpenFOAM can be a valuable tool for the wave energy industries especially in order to study the behaviour of the wave.

REFERENCES

[1] Li, M. et al. (2018) 'Generation of regular and focused waves by using an internal wave maker in a CIP-based model', Ocean Engineering. Elsevier Ltd, 167(August), pp. 334–347.doi:10.1016/j.oceaneng.2018.08.048.

DESIGN AND DEVELOPED AN ENERGY HARVESTING SYSTEM FROM CAR SHOCK ABSORBER

Amerudin Mohd Sabri and Khairul Anuar Hanafiah
School of Mechanical Engineering, Faculty of Engineering,
Universiti Teknologi Malaysia, 81310 UTM Skudai, Johor, Malaysia

INTRODUCTION

Over recent years, sustainability issue has always been one of the major problem in industries. Losses of energy in vehicle came in many form. Vibration is one of the contributor where 70% of the fuel combustion energy goes to the surrounding instead of producing power [1]. Previous studies have demonstrated various method to generate electricity with few modification to the internal system being made [2]. By channelling extra source of power to the vehicle battery, its surely improve the efficiency of the car energy usage and profitable to the user in long term application.

EXPERIMENTAL SETUP

We use concept of linear electromagnetic induction which consist of an insulated copper coil and two unit of permanent magnet (N35) which act as the excitation and levitation unit.

Theoretical analysis being made by applying Faraday's Law of electromagnetic induction which observed the manipulation of several important parameter. The no of turn of coil, the magnetic field strength, diameter of coil (resistance related) and the speed of excitation. Electromagnetostudy was done on the module by using EMS on SolidWorks to describe the pattern of flux density on the coil.

The test was conducted using fabrication module which consist 6 tube harvester. The test unit is clamped around the shock absorber perimeter. The clearance gap was checked to avoid interference with the car's internal component. Result was tested using multimeter to find the output power under different situation which expect various excitation input to the harvester.

RESULTS AND DISCUSSION

The testing was made to stimulate usual daily driving, consisting driving on the road, facing a bumper and taking a corner.

To observe the generation of power, we can only manipulate the coil turn, diameter and magnet's grade. Speed of excitation is dependent on the road condition. In road roughness condition, average power obtained is 0.8Watt and highest at 10.39Watts. During cornering test, the highest output reading recorded at 1.85Watts and average at 0.44Watts. In both of this testing, its been prove by the result that the speed and cornering is not significant enough to excite more power instead it need more impact and shock. Figure 1 illustrates the power output generated during bumpering which taken at initial speed of 30km/h..

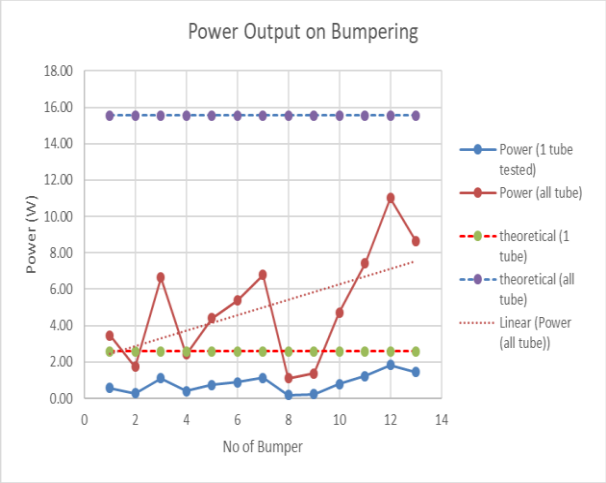

Figure 1: Power output vs no. of bumper.

Highest power emitted by the module obtained during bumper test which is expected to be. Most of the rebound from contact with the bumper exerts an impact and recoil during and after facing the bumper. Average power of 5Watts achieved and 11Watts recorded at the highest reading. Comparing with the theoretical data , the value is off by nearly 70% since the maximum excitation occur is not in continuous mode but rather on a step input.

CONCLUSION

We have shown the feasibility of the harvester to extract a small amount of electrical power from the shock absorber. Better scale of electricity can be estimated by using stronger permanent magnet, thicker coil diameter (less resistance and support higher current transmission) and higher no of turn of coil.

REFERENCES

[1] Zutao. (2016). A high-efficiency energy regenerative shock absorber using supercapacitors for renewable energy applications in range extended electric vehicle. Applied Energy, 177-188

[2] Waleed. (2018). A high-efficiency energy regenerative shock absorber using helical gears. Energy 159, 361-372

DESIGN AND DEVELOPED A PORTABLE INCINERATOR FOR DOMESTIC USER

Muhammad Yusup Amrizal and Khairul Anwar Hanafiah
School of Mechanical Engineering, Faculty of Engineering,
Universiti Teknologi Malaysia, 81310 UTM Skudai, Johor, Malaysia

INTRODUCTION

There are several ways to dispose this waste material from the houses and one of it is get rid through the burning process [1]. This process of handling waste usually had been completed without proper method where people will burn it in open area which easily for them to access. The way of handling municipal waste from domestic users are being an issued where it is a big concern of the environment, society and health. Collect, bury and covered-up the waste with a layer of soil on a patch of identified land is one of the common methods used for disposal of solid waste [2]. To reduce the harmful potential from the material waste, incineration is one of the most effective method comparing incineration to other dumping options such as land burial, and disposal at sea or in lagoons.

DESIGN METHODOLOGY

Idea concept generation generated a few ideas before proceeding to the final design scoring matrix. The highest mark for the evaluation meets the criteria of the product design specification needed. The final design was simulated using Computer Aided Engineering (CAE) and the validation proposed concept to use the high-pressure steam for filter the fly ash was confirmed by the prototype demonstration.

RESULTS AND DISCUSSION

The results for the internal flow simulation shown in figure 1. For this simulation, the flow of the flue gas from the waste combustion was simulated through the flue gas tube and the chimney. Figure 1 shows the flow of flue gas from the combustion chamber. One of the objectives of this project is to reduce the air pollution generated from the waste combustion and it is important to know the quantity of carbon dioxide and nitrogen oxide before released it to the atmosphere. Two aluminium cones were designated to obstruct this air pollution from directly flow out through the chimney while the high-pressure steam from the water tank will trap and confined the fly ash particle to fell into the water tank. This proposed idea used to reduce the air pollution by trap the fly ash. From this simulation, mass fraction of nitrogen and carbon dioxide was measured at eight different places along the flue gas tube and the chimney.

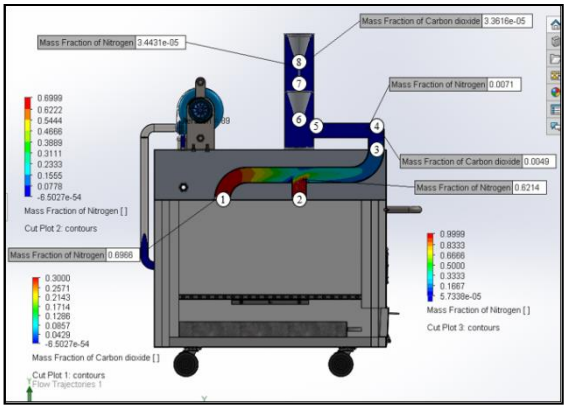

Figure15: Contour of The Mass Fraction of Nitrogen and Carbon Dioxide in The Flue Gas Tube

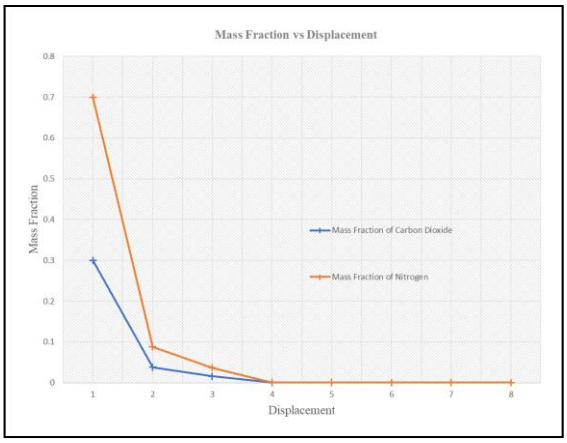

Figure 16: Mass Fraction of Carbon Dioxide and Nitrogen Against Displacements

CONCLUSION

In conclusion, the air pollution from the combustion process can be reduced by using the proposed concepts in the final design of the portable incinerator.

REFERENCES

[1] Shigeki Yamaguchi, Norio Ohiwa, Tatsuya Hasegawa, "Ignition and burning process in a divided chamber bomb," *Combustion and Flame*, vol. 59, no. 2, pp. 177-187, 1985.

[2] Hussein I.Abdel-Shafy, Mona S.M.Mansour, "Solid waste issue: Sources, composition, disposal, recycling, and valorization," *Egyptian Journal of Petroleum*, vol. 27, no. 4, pp. 1275-1290, 2018.

DESIGN AND FABRICATION OF MOTORIZE STAIRCASE CLIMBING TROLLEY

Muhammad Amir Akmal Saadun and Khairul Anwar Hanafiah
School of Mechanical Engineering, Faculty of Engineering,
Universiti Teknologi Malaysia, 81310 UTM Skudai, Johor, Malaysia

INTRODUCTION

It is seen that there is a major problem in people carrying heavy load while climbing upward and downward the staircase which is very dangerous to their safety, as it is prone to incident. It is important to reduce injuries that we can prevent before we experience it.

Also, frequent strain injuries predominantly for the lower back, shoulder and arm muscle joint restrain people to do job better. Even though there is available product that could help ease their work, they are considering that it is not worth it based on its prices and its limited functionality. As, most of it difficult to travel with more luggage, cannot move over obstacle, and hard to manoeuver on uneven ground. Additionally, some people occasionally bumped their lower leg to the wheel of the trolley, as example, the 4-wheel trolley that is commonly used at supermarket. The slipping and skidding also cause a difficulty to the user during moving load between two place. This is due to the wheel tire has worn out or disorientated wheel.

EXPERIMENTAL SETUP

A few test was conducted by using 5 different type of load and the degree of difficulty was determined. The staircase for the experiment has 8 steps with 17 cm height, so the total height is 1.36 m. A few steps of procedure need to be used to make sure the control condition was maintained throughout the testing. The procedure of the experiment are as follows:

a) Position the trolley perpendicular to the staircase.
b) Place the load at the middle of the front plate to make sure it is in balance.
c) Simultaneously, turn on the switch for motor and start climbing the staircase.
d) The climbing was at slow pace to avoid the load from staggering and sliding from the front plate.
e) The climbing end at the 8th step.
f) Step 1 to 5 was repeated for other loads.

RESULTS AND DISCUSSION

First run was tested by placing the rubbish in box onto the middle position of the front plate of trolley. The first step quiet easy to climb and effortlessly. This might due to it is lightweight compare to other load. Second run was by using a bucket with a pile of clothes. The climbing become slightly difficult due to extra load than previous test. There different is hard to distinguish between the two first run. Possibly the margin between both load is small. The third run become much harder. The climbing pace helps maintained the load positioned on the trolley efficiently. The motor seemed to help providing a small force to climb the steps better. The wheel rotates slowly due to the presence of much bigger load. Fourth run was tested with the mineral water with weight about 5 kg. The difficulty increased greatly, as a step by step climbing was harder. A portion of the load was supported by the motor. The motor maintained the climbing activity and prevent from the trolley to slip downward the staircase. The climbing much easier than without using motor. Final run was tested using the water extinguisher with a weight of 6kg. This is the hardest climbing tested with the biggest load type available. At first the trolley hardly abled to climb the stair. With an extra force applied upward and force provided by the motor, the climbing take place at slower rate than the controlled pace. The weight of 6 kg seemed to be the maximum load the trolley can handle for this experiment. It is still possible to increase the load until about 15 kg at most, with efficiently and safe to the user.

CONCLUSION

Although there are a few limitations from the design built and strength, it still considered as small step forward to improve the trolley. The testing has been conducted to prove that the trolley able to help reducing load during staircase climbing and the posture used also much lower risk than using normal hands lifting activity. The product could be widely commercialized to suit the needs of the consumer.

REFERENCES

[1]. A. Jardon, A. Gimenez, R. Correal, R. Cabas, S. Martinez, C. Balaguer. (2006). "A portable light-weight climbing robot for personal assistance applications". Industrial Robot: An International Journal. Vol. 33 Issue: 4. pp.303-307.

[2]. Bijo Sebastian, Dip Narayan Ray, S. Majumder. (2015). “Design and analysis of a tree climbing robot”. *Proceeding AIR '15 Proceedings of the 2015 Conference on Advances in Robotics Article No. 17.*

[3]. Gandhi, Mridul & Gurunathan, C. (2017). “Design and Development of Movable Furniture”.1-6.10.1109/INDICON.2017.8487873.

[4]. Gangadia, Hardik & Shukla, Hardik & Patel, Sanket & Jani, Milan & Upadhyay, Rahul & Thakar F, Ishan. (2015). *Design and Modeling of Stair Climbing Trolley*. Sarjan. 4. 62.

DESIGN AND BUILD A FLYING MACHINE WHICH USES FLAPPING WINGS FOR PROPULSION

Muhammad Asyraf Abd Wahab and Khairul Anwar Hanafiah
School of Mechanical Engineering, Faculty of Engineering,
Universiti Teknologi Malaysia, 81310 UTM Sekudai, Johor, Malaysia

INTRODUCTION

Bird and insects have evolved to fly with flapping its wings, unlike aeroplane and helicopter which are designed with fixed-wings and rotary-blades, respectively to fly up from the ground. Flapping wings flight is more complicated than light with fixed wings because of the structural movement and it results unsteady fluid dynamics. Flapping wings mechanism is also called as Ornithopter. In this project, with a full understanding in aerodynamics principle, relative flight parameters and appropriate design consideration, a motorized flapping wings machine can be designed and built.

SYSTEM DESIGN

There are four main components or parts that need to be considered in designing an ornithopter – flapping mechanism, power transmission, wings, and power supply. Firstly, flapping mechanism must perform upstroke and downstroke to produce propulsion. Flapping mechanism was designed by using reciprocating motion and done by position analysis. Secondly, power transmission was design by using spur-type gearing system to transmit motor speed and power to flapping mechanism. Gear design was analysed by geometry, nomenclature, and gear force analysis. Next, the geometry of wing is quarter elliptical shape with 140mm major and 100mm minor. Aspect ratio of the wings is 3.46 which suitable for flapping flight. Lastly, a very light and small Li-Po battery with 3.7V was used as a power supply for flapping mechanism. After obtaining these four main components, prototyping was conducted for testing purpose.

RESULTS AND DISCUSSION

Flapping mechanism was designed with dihedral wings with angle of 20°. There were four sheets of wings attached to the arms. Average flap frequency was 30 Hz (cps) by using Pennycuick's Power Law equation [1]. One of end side of connecting rod was attached to the gear and another end side attached to the wing arms. This results in reciprocating motion. Figure 1 shows the flapping mechanism.

Power transmission system consists of two gears with diameter of Ø15mm, and a pinion with diameter of Ø4mm. Both gears have the same number of teeth – 39 teeth, while the pinion has 10 teeth. Gear ratio is 4. Input speed from motor is 21,000 rpm, and the output speed is reduced to 5,348 rpm. The magnitude of output speed is established to perform flapping operation.

Geometry of wings used in this project. The geometry of wing is quarter elliptical shape with 140mm major and 100mm minor. Aspect ratio of the wings is 3.46 which suitable for flapping flight in steady airflow.

Figure 2 shows a 3D modelling as a final design. 3D model was built by using SOLIDWORKS 2018.

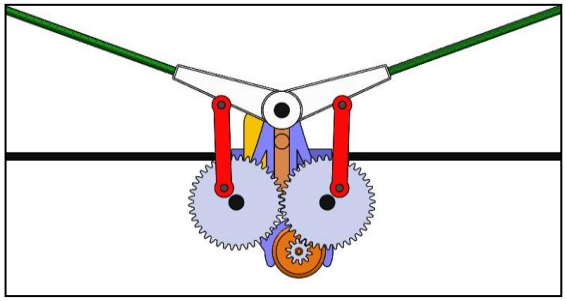

Figure 1: Flapping mechanism and gear design

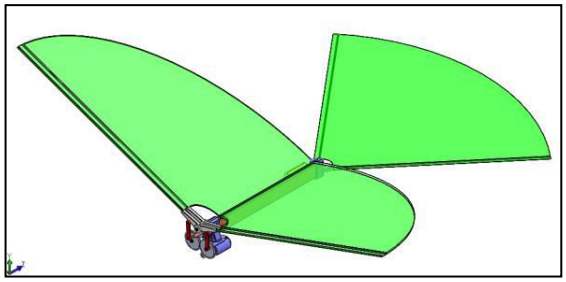

Figure 2: 3D model of final design

CONCLUSION

During the testing session, the model was successfully fly up from the ground and hovering in the air for approximately 10 minutes before land down. Objective of the project is achieved.

REFERENCES

[1] C. J. Pennycuick, "Wingbeat frequency of birds in steady cruising flight: New data and improved predictions," *Journal of Experimental Biology*, pp. 1613 1618, 1996.

[2] Snorri Gudmundsson, 2014, The Anatomy of The Wing, General Aviation Aircraft Design Applied Methods and Procedures, pp. 299-399

DESIGN & FABRICATION OF FOOTSTEP POWER GENERATOR

Tengku Mohamad Izham Syafiq Tuan Mohd Sukri and Khairul Anwar Hanafiah
School of Mechanical Engineering, Faculty of Engineering,
Universiti Teknologi Malaysia, 81310 UTM Skudai, Johor, Malaysia

INTRODUCTION

Nowadays, people always overly dependent on electricity. People use electricity for their needs in everyday life. For example, using laptop, charging smartphones.
conditioner and other electrical appliances which uses more energy from electricity. The utilization of waste energy of foot power with human motion is very important for highly populated countries. India and China have the most populated people in the world. They have millions of people move around the clock. The major problem that can be figure is people always waste their energy by walking or running. For an example, people go to the park for jogging or sightseeing. We can see that the people waste their energy and got tired. By using this design, people can fully utilize their energy. This design can convert mechanical energy into electrical energy [1]. This design also can help people who needed electricity if they are no current supply. For example, the problem that occur for traveler is charging their phone. If this design is applied to them. It will help them to generate electricity by their own by just walking. In this project, I use piezo disc. It used to produce low voltage of supply [2].

METHODOLOGY

This section presents the method that being used to develop the product. The first step is doing functional analysis. It describes the desire part we want to do and try not to limit down the design choices. Then we will identify alternatives, optimize them, and select the best ones to make up the complete system. The second step is do morphological chart. Morphological chart is a table based on the function analysis. On the left side of the chart the functions are listed, while on the right side, different mechanisms which can be used to perform the functions listed are drawn. It is a visual aid used to come up with different ideas.

RESULTS AND DISCUSSION

At the end of the fabrication. The data has been recorded to observe the voltage supply when apply on certain pressure or load. The figure 1 shows the voltage generated versus weight and energy generated per tap versus weight. When the weight is increase, the voltage will increase too. This is because to generate an electricity by using piezo, it needs to applied a force into it. When the applied force is huge, the piezo can generate more voltage. It same goes to figure 2 which is energy generated per tap versus weight. The higher the applied force, the higher the energy generated per tap.

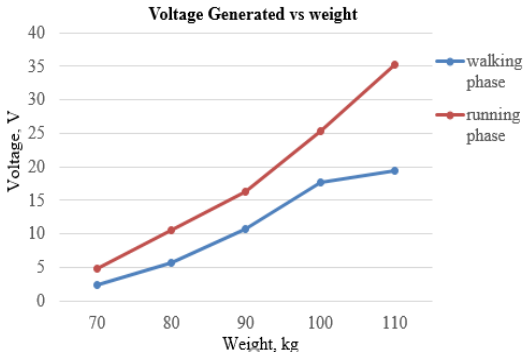

Figure 1: Graph of voltage generated versus weight

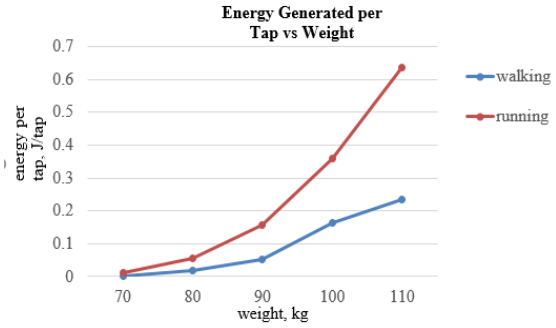

Figure 2: The graph of energy generated per tap vs weight

CONCLUSION

As conclusion, the objective of this project has been achieved which is to design and fabricate footstep power generator system that capable to generate an electricity, to reduce the cost of electricity and to reduce the waste energy develop by a person. The piezo disc can produce electrical energy when the pressure was applied on it. This project is used to supply a low voltage.

REFERENCES

[1] Marshiana. D, Elizabeth Sherine. M, Sunitha. N, Vinothkumar. C. (2016). Footstep Power production using Piezoelectric Sensor

[2] Henry A.Sodano, Daniel J.Inman, and Gyuhae Park.(2004). Estimation of Electric Charge Output for Piezo electric Energy Harvesting, pp. 49-58.

DESIGN HYDRAULIC SYSTEM FOR POWER TRANSMISSION OF BICYCLE

Muhammad Afif Abdul Rahman and Khairul Anwar Hanafiah
School of Mechanical Engineering, Faculty of Engineering,
Universiti Teknologi Malaysia, 81310 UTM Sekudai, Johor, Malaysia

INTRODUCTION

In this modern era, transportation in Malaysia was dominated by engine powered vehicle such as car, motorcycle, bus, and much more. This is because this type of vehicles are very convenient to travel. However, engine powered vehicle is one of the air pollution source. Beside that, majority of the transportation in Malaysia is on road vehicle which has high running expenses. The fuel expense is one of the expenses that need to be paid for the engine power vehicle. Hence, one of the best way to save our earth and also our pocket is reducing the dependency to this type of vehicle by riding the human power vehicle. While the existing human powered vehicle such as bicycle and trishaw required a lot of human energy to go off road. Going uphill or going through uneven terrain required a lot of driving energy to overcome the drag force. Because of that it is necessary to improve the power transmission system. One of the best way to produce high mechanical power is using hydraulic drive system. A hydraulic drive system is a hydro-static drive or transmission system that uses pressurized hydraulic fluid to power hydraulic machinery. The term hydro-static refers to the transfer of energy from pressure differences, not from the kinetic energy of the flow. The function of hydraulic drive system is to transmit a small torque into a large force.

FUNCTIONAL ANALYSIS

The product will be functioning went there is a rider who give power to the bicycle pedal that connected to the pump. The pump will operate when the pedal crank rotating and produce pressure to the fluid. The pressurized fluid will flow to the hydraulic motor and the motor will produce mechanical energy that will rotate the tire.

RESULTS AND DISCUSSION

Hydraulic bicycle is a non-motorized vehicle that used hydraulic system to transmit the cycling power. Current bicycle using chain to transfer rider's power to the driving wheel that need a lot of energy during climbing uphill terrain.The purpose of the design project is to develop a bicycle that more convenient to the cyclist and passenger during climbing uphill. Most of the bicycle parts are standard parts that can be obtain from the bicycle shop. The special parts such as the frame, pump, hydraulic motor,and reservoir have been designed specifically to fulfill the objective of the project

Figure 1 shows the final design of hydraulic bicycle. The frame for the selective design has been modified to improve the performance of the hydraulic system and also to reduce the cost of product. The brake system was not included in this 3D drawing because the braking system used is standard. This bicycle has 1.15m length, 0.5m width and 0.8m height. The bicycle has been design to used a pair of 17 inch tires.

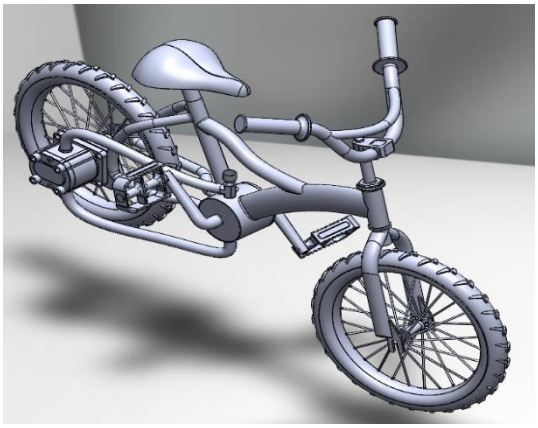

Figure 1: Hydraulic bicycle

To calculate the gain ratio of the bicycle the volumetric displacement of the pump and the motor had been analyse.

CONCLUSION

The objective of this project can be achieved with this hydraulic bicycle. The bicycle can transmit rider's cycling power to driving wheel by using hydraulic system. The reason to used hydraulic system is to produce higher torque compare to average bicycle.

REFERENCES

[1] Douglass C, Brackett. HYDRAULIC BICYCLE WITH CONJUGATE DRIVE MOTOR.
[2] Gannon, M. (2013). What are hydraulic motors?.Mobilehydraulictips.com. https://www.mobilehydraulictips.com/hydraulic-motors/.
[3] George A, Harriger. HYDRAULIC DRIVE SYSTEM FOR BICYCLES AND THE LIKE.
[4]

FURTHER IMPROVEMENT ON DUEL OVEN HEATING MACHINE: AUTO *LEMANG*

Muhammad Firdaus Zulkefli and Khidzir Zakaria
School of Mechanical Engineering, Faculty of Engineering,
Universiti Teknologi Malaysia, 81310 UTM Sekudai, Johor, Malaysia

INTRODUCTION

In 2014, a new invention has been made on process of cooking *lemang* from UTM student. The machine is made to ensure the cooking process is more environmental friendly and convenient to be used. It is using natural gas as the burning material and the rotating mechanism is using the motor to operate the gearing scheme with the electric automobile generation of elevator car battery. [1]

EXPERIMENTAL SETUP

The *lemang* machine is using natural gas as the burning material and the rotating mechanism is using the motor to operate the gear system with the electric generation of car battery.

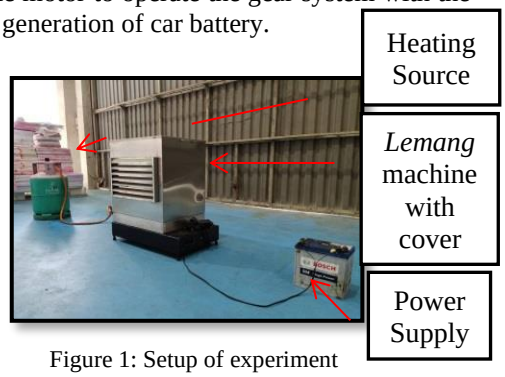

Figure 1: Setup of experiment

First experiment was conducted and two location of *lemang* were taken for the experiment as shown in Figure 2. The experiment was held for 1 hour and 30 minutes and 2 hour and 30 minutes for the second experiment with the same location of *lemang*

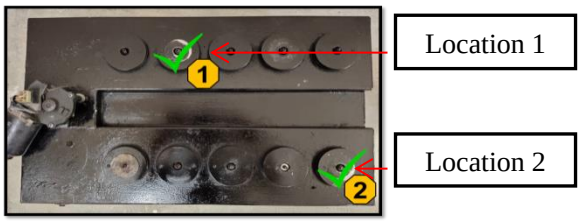

Figure 2: Location of *Lemang*

RESULTS AND DISCUSSION

At the end of experiment, the result for the quality of *lemang* was observed. Figure 3 shows that at location 1 have a good quality of *lemang* compared to location 2.

Figure 3 *Lemang* at location 1 (left) and *lemang* at location 2 (right)

A plate with dimension 5cm × 12cm × 0.5cm were cut to be added below the spring. In order to add the plate, the welding process was occurred. Arc welding is used to join the plate and the base.

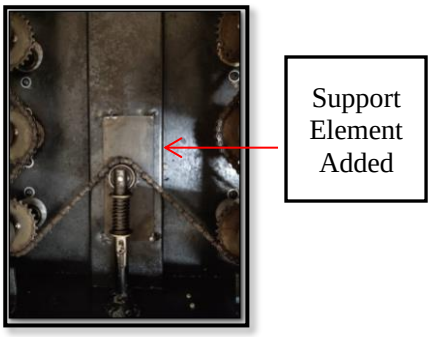

Figure 3: Plate was added as support element

CONCLUSION

The *lemang* machine after improvement consists of support element for the spring to overcome the issues of vibration that constitute the rotating mechanism is not smooth. The chain will not fall from the spring as the gap between the spring and the support element is too little. Besides that, a new fabrication of washer to make the cup stable when rotates. The diameter between the new washer and the cup is not too big.

REFERENCES

[1] B. Araminta, F. . Octavia, M. Hadipraja, S. Isnaeniah, and V. Viriani, "Lemang (Rice Bamboo) as Representative of Typical Malay Food in Indonesia," *J. Ethn. Food*, 2017.

[2] K.S. Tee, "Further Development Of Low Cost Lemang Machine For Commercialization Tee Kuang Seng," 2014.

FACILITY LAYOUT IMPROVEMENT IN A FOOD MANUFACTURING INDUSTRY

Zuhairi Meskari and Masine Md Tap
School of Mechanical Engineering, Faculty of Engineering
Universiti Teknologi Malaysia, 81300 UTM Skudai, Johor, Malaysia

INTRODUCTION

Facilities layout design refers to the arrangement of all equipment, machinery, and furnishings within a building [1]. Based on observation made during Industrial visit to Siantan Wangi Enterprise Sdn. Bhd, their existing layout planning designed in the factory is not systematic and efficient. There are few techniques in facility planning but Systematic Layout Planning (SLP) is a highly used methodology especially in small or mid-size companies, due to its accessibility [2]. Hence, the main objectives in this study are to propose improvements on facility planning and design and evaluate its performance.

METHODOLOGY

Identification of problem is done by using Industrial Engineering tools. The first IE tools used is Pareto Chart. By applying this tool, the main products can be recognized. This study proceeds by creating Process Flow Chart for each product. Process Flow Chart helps in constructing From-To Chart. Function of From-To Chart is to calculate the total distance travelled. Ishikawa Diagram is constructed to identify and analyse factors that caused the problem. Relayout process basically based on SLP method. WITNESS Simulation Software is used in evaluating the proposed solution.

RESULT AND DISCUSSION

This study will discover on quantitative and qualitative analysis. Better rating will be selected as finalized closeness rating after merge both results to each department pair. Space analysis is done by calculating required and available space. Space Relationship is designed to illustrate the relationship between the department pair's closeness rating and space required. Several alternative layouts are generated based on the activity relationship chart and the space relationship diagram. The evaluation is conducted by comparing several layout features that are total travelled material distance, number of backtracking and cross traffic, and monthly production capacity. Alternative 2 as shown in Figure 1 is selected as an optimum alternative compare to Alternative 1 due to its higher percentage of improvement.

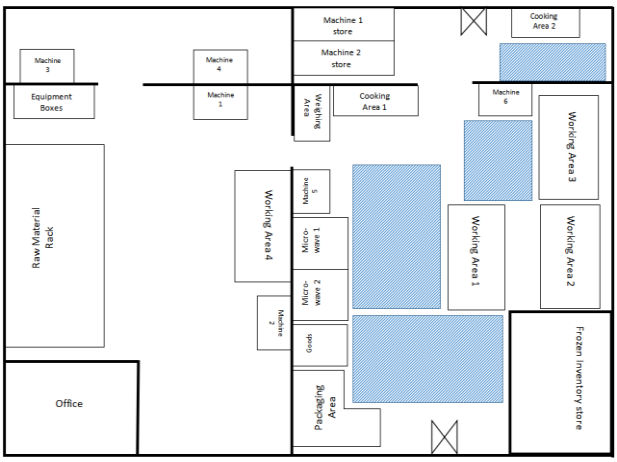

Figure 1: Alternative 2

REFERENCES

[1] Tompkins, J., White, J. A., Bozer, Y. A., and Tanchoco, J. M. A. (2010). Facilities lanning Four Edition. John Wiley & Sons, Inc., Fourth edition

[2] Gilbert, J. (2004). Construction office design with systematic layout planning.15th Annual Conference on POM, Cancun, May 15-18.

WORK IMPROVEMENT IN ELECTRONIC COMPANY

Faizzudin Mohd Yasin and Masine Md Tap
School of Mechanical Engineering, Faculty of Engineering,
Universiti Teknologi Malaysia, 81310 UTM Skudai, Johor, Malaysia

INTRODUCTION

This research was conducted at HID Global Sdn. Bhd. Every month, the number of scraps produced by the Rapidline Machine were very high and the main contribute to those problems are the chip clamp. Daily adjustment are needed to that part since the components are too small, easy to misplace, wear and tear. A solution is recommended in the form of a jig designed to standardize the spring force and positioning the screw level. The jig enable to reduce one wire bonding, chip crack and chip missing problems.

PROPOSED DESIGN

The engineering design process step is followed to make sure the designing work is done correctly. Figure 1 shows the sketching based on the product design specification and morphological chart while figure 2 shows the final CAD drawing using SolidWorks. Push and pull gauge are used in order to measure the spring force of the chip clamp which could give high impact to the chip condition. The frame are designed in order to positioning the screw level of the chip clamp.

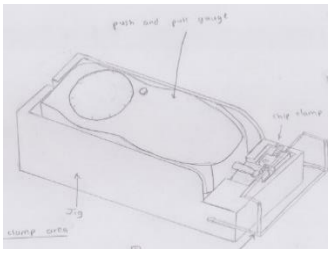

Figure 1: Sketching of the jig

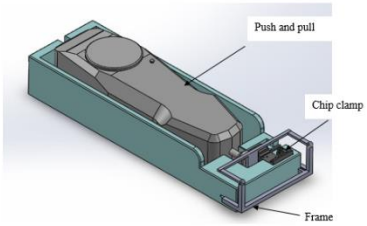

Figure 2: Final CAD drawing

ANALYSIS

Engineering analysis is executed using Solidworks simulation, force parameter is applied at the middle of the T-Joint. Largest Von misses stress occurs at the both side of T-Joint of the component with the value of 16.504 N/mm2 (MPa) whereas the yield strength of the component material is 172.369 N/mm2 (MPa). These values would yield 10.44 safety factor and it should not break in case the force is apply. For the displacement analysis, the maximum deflection is at the middle of the bottom part where the maximum value is 0.034 mm, which is insignificant to make any visible shape distortion on the components.

Next, cost analysis was carried out to calculate the cost involved for this project. By referring to table 1, the total number of rejects produce in July 2018 is 154 077 unit and the company had lost about RM120180.00. The product cost per unit is RM0.78. Based on table 6.2, the jig cost is estimated about RM102.50. By investing money to produce the jig, if the jigs can reduce the rejects by 0.086 % that is 132 unit, the jig is already economical.

Table 1: Cost Analysis

Product cost per unit	**RM 0.78**
Reject	154 077 Unit
Total Lost	RM120,180.00
Jig Price	RM102.50/unit
Saving if 100% reject is eliminate	RM120, 180.00
Saving if 50% reject is eliminate	RM60, 090.00
Saving if 0.086% reject is eliminate	RM 103.00

CONCLUSION

Both objectives have been achieved. Even though the jig is not actually tested but costing analysis showing that a reduction of 0.086% (132 unit out of 120800 is already sufficient to make the jig economical / break-even. Thus, it is confident that the use of this jig will produced more benefit.

REFERENCES

[1] Ahmed, M., & Ahmad, N. (2011). An application of Pareto analysis and cause-and-effect diagram (CED) for minimizing rejection of raw materials in lamp production process. Management Science and Engineering, 5(3), 87.

[2] Chong Y.F.(2010). Analysis and Improvement in an Assembly Line through Line Balancing and Work Design. UTM:Skudai..

[3] Leong P. W (2010), Productivity improvement using wok study and line balancing. UTM:Skudai.

UAV OBSTACLE AVOIDANCE USING PID CONTROLLER

Mohamad Fitri Asreen Mohd Asri and Mastura Ab Wahid
School of Mechanical Engineering, Faculty of Engineering,
Universiti Teknologi Malaysia, 81310 UTM Skudai, Johor, Malaysia

INTRODUCTION

Unmanned Aerial Vehicle (UAV) is an aircraft without human on-board has become popular due to rapid growth of its application in the most field exist. Many researches has been focusing on technology advancement of UAV to increase its operational experience[1]. Since there are no humans on-board so, for this research we are interested to develop the control system using PID controller. The development of the transfer function should be done first using the linearized lateral motion equations since the manoeuvring for the UAV are using the coordinate turn[2]. With helps of the PID gain in PID control system could make the UAV can follow the desired trajectory to avoid the obstacle with stable [3].

EXPERIMENTAL SETUP

First we need to do a linearization process upon the twelve non-linear, ordinary differential equation that comprise the equations of motion for an aircraft. From that, we will obtain the transfer function for rolling angle due the deflection of aileron and rudder. Next we can introduced the PID controller to the system with the reasonable PID gain for the system and we can see either the UAV can response to the trajectory desired quickly or stable or not.

RESULTS AND DISCUSSION

For both transfer function $\frac{\emptyset}{\delta a}$ and $\frac{\emptyset}{\delta r}$ are not stable when the system are in open loop (no feedback) but when give a feedback to the system the UAV become stable but still not follow the trajectory So, because of that this system are implemented the PID controller with the suitable gain and we can see that the UAV are stable following the trajectory path desired.

CONCLUSION

In short, as the aircraft possess PID system that would definitely help with the stability augmentation of the aircraft, it is correct to assume that with the use of PID system the aircraft can produce a better flight dynamic. The use of control laws with non-conventional response characteristic, specifically a normal acceleration response characteristic, gives very desirable flying qualities for the approach and landing task with a reduced workload compared to a classical aircraft, and these control law types may be used in other tasks such as a formation flying task.

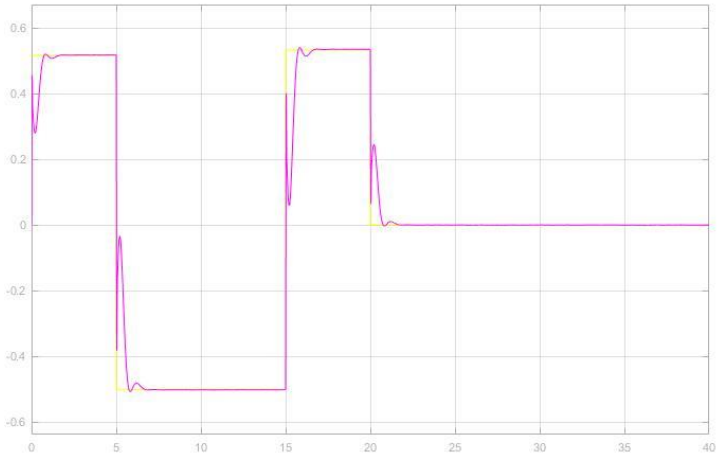

Figure 1 : $\frac{\emptyset}{\delta a}$ transfer function with PID controller

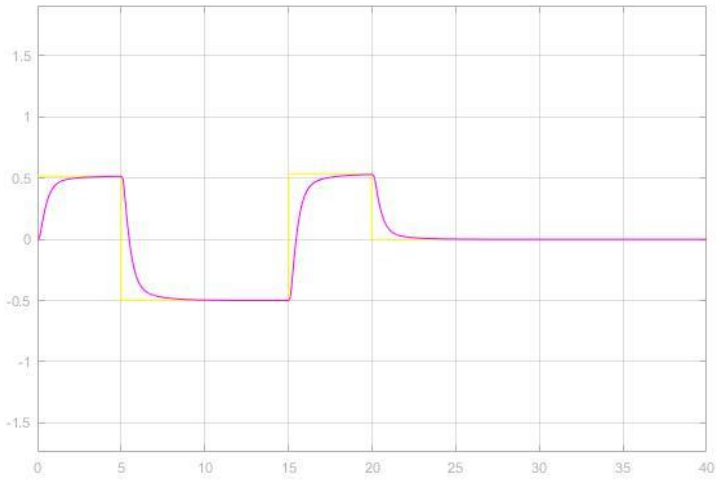

Figure 2 : $\frac{\emptyset}{\delta r}$ transfer function with PID controller

REFERENCES

[1] N. Amalina (2018) 'Transient Aerodynamics Effect on V-Tail, Aircraft in Lateral Stability', PHD thesis, pp. 54-252.
[2] Abdulrahim, M., & Sheridan, J. (2010). 'Dynamic Sensitivity to Atmospheric Turbulence of Unmanned Air Vehicles with Varying Configuration.', Jornal of Aircraft, 47(^), 1873-1883..
[3] Robert C. Nelson (1998) 'Flight Stability and Automatic Control', WCB/ McGraw-Hill pp. 100-379.

FUZZY-PID CONTROL AND MODELLING OF SEMI-ACTIVE SUSPENSION SYSTEM USING MAGNETORHEOLOGICAL DAMPER BASED ON HYPERBOLIC TANGENT MODEL

Student
Muhammad Haizar Bin Zainal Lim and Mat Hussin Bin Ab Talib
School of Mechanical Engineering, Faculty of Engineering,
Universiti Teknologi Malaysia, 81310 UTM Skudai, Johor, Malaysia

INTRODUCTION

At the recent time, automotive engineer has developed a suspension system which called semi-active where by this suspension can help to solve the conflict faced by the passive suspension system, and give better result in handling and passenger comfortability compared to passive suspension system. The semi-active term used in this suspension system is because the flexibility of the suspension to change its viscous damping coefficient of shock absorber and never add extra energy to the suspension system. Besides this suspension has lower power consumption to operate and cheaper than the fancy active suspension system. Moreover, the Magneto rheological fluid filled in the damper can produce high damping force with low power energy which means this semi-active suspension is possible operate by using car's battery

EXPERIMENTAL SETUP

This MR damper has various applications, most application is in the semi-active suspension system of vehicle, in order to change the behaviour of damper depending on the road condition, and this will be monitored by the sensor in the vehicle[1]. However, the MR damper force/displacement and hysteretic force/velocity characteristic are very complicated. Due to this matter, the vast applicable usage is prevented because the design of a proper control strategy for MR dampers is based on a tractable model of their behaviour. So, in order to tackle this issue, must to address a reliable model of an MR damper is required before can be applied to the controller that intended to design [2]. In this project, the models that will be used to allow the project can be proceeding are by using Hyperbolic Tangent model, and controlled by Fuzzy-PID.

RESULTS AND DISCUSSION

As stated in the objective, the simulation of suspension system will be tested on two different road profile which are sinusoidal (amp=0.05, 1.0 Hz) and also bump (0.01m, 0.1s) road. In quarter car model, only a single wheel will decide to go through the rough input road profile. The result obtained, sprung acceleration gives better performance when road input with sinusoidal profile is applied. The measured magnitude parameter using semi-active suspension system shows improvement when comparing with the passive suspension system.

The semi-active suspension system with Hyperbolic Tangent model has greatly improved the sprung displacement and acceleration by absorbing the disturbance half of the passive suspension system could. Meanwhile, as for the bump road input, there is slight improvement of MSE of sprung displacement in semi-active suspension systems compared to the passive suspension system but there are no sign of improvement in the sprung acceleration. However, the settling time has been improved than the one in passive suspension system. The settling time of passive suspension system is 6.5s and as for semi-active suspension system with Bouc-Wen Model, Modified Bouc Wen Model And Hyperbolic Tangent Model are 5.2 s, 3.8 s and 3.5 s respectively.

Sinusoidal Road Input | Bump Road Input

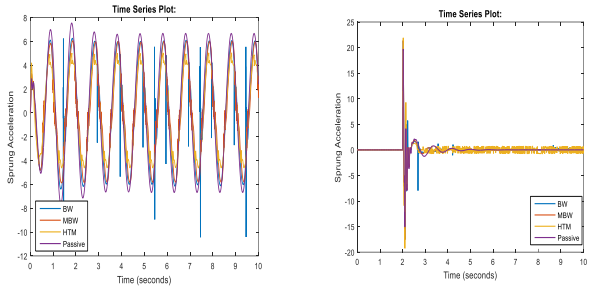

Figure 17: Spring acceleration vs time

CONCLUSION

The purpose of using the Fuzzy-PID is to provide the wide range of controllable damping force in various obstacle even there are improvement in the sprung suspension system but the acceleration show no sign of improvement which need to be look upon. Besides, the objective to prove that hyperbolic tangent model can be one of the good mathematical models to help in provides appropriate damping force to the system. Hyperbolic tangent model also has a simpler equation and lesser parameter needed to be tuned compare to the Bouc-wen model and modified Bouc-wen model.

REFERENCES

[1] H. U. Oh, "Experimental demonstration of an improved magneto-rheological fluid damper for suppression of vibration of a space flexible structure," Smart Mater. Struct., vol. 13, pp. 1238–1244, 2004.

[2] G. Z. Yao, F. F. Yap, G. Chen, W. H. Li, and S. H. Yeo, "MR damper and its application for semi-active control of vehicle suspension system," Mechatronics, vol. 12, no. 7, pp. 963–973, 2002.

DEVELOPMENT OF PORTABLE ATTENDANCE SYSTEM USING FACE RECOGNITION ALGORITHM

Zikri Arif Azmi Rais and Maziah Mohamad
School of Mechanical Engineering, Faculty of Engineering, Universiti Teknologi Malaysia, 81310 UTM Skudai, Johor, Malaysia

INTRODUCTION

Attendance system in education play important role as a determinant of success and monitoring academic performance. Over recent years, there has been an improvement in attendance system that replace conventional attendance system which is easy to manipulate by student. Moreover, it is tedious and cumbersome process to take hand-written data and then calculating percentage of attendance, sorting, transferring it onto computer for further website backup. New portable attendance system device design was developed to create better user experience and easy to use. By implementing biometric authentication such as face recognition on this device, the ability to manipulate the attendance system can be demolished because it is hard to duplicate where it is unique for every person [1, 2].

EXPERIMENTAL SETUP

This portable will be divide into two part in this section which is hardware and software. The hardware part consists of hardware selection and casing design to assemble all the component together. Software will start with process of installing library needed in the raspberry pi followed by development of image database, face recognition algorithm, attendance system and Graphical User Interface (GUI).

The performance of the portable device was determined by selecting 5 different users to be test with this system. Using lighting condition and distance between the device and the user as constant variable in this test. 3 session will be done by each person.

RESULT AND DISCUSSION

The result of this portable device divides into software and hardware. The hardware such as casing is very light as it was printed with plastic material. Good casing design and attractive color give aesthetic appearance to the device. The curve created at the casing make this hardware easy to hold.

Moreover, an application launcher was created at the main GUI of the device. GUI for the application consists of 6 buttons with different function and simple to use as shown in figure 1. Adding different color on GUI to make it more attractive. The attendance list successfully created in excel file with accurate time. The recognition process takes 5 seconds for each person. The result of the process must be confirmed by user before the attendance list can be updated. The accuracy of this device shown in Table 1.

Figure 1 GUI result

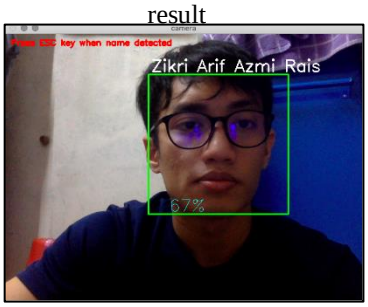

Figure 2 Face recognition process

Table 1 Accuracy of the portable device

User Name	User without		User with	
	No of succ	Accuracy Percen	No of succ	Accuracy Percen
Azirul	1	10	1	86
Afi	9	6	6	4
Shahrun	7	46	5	33
Syafiq	8	10	1	10
Zik	1	53	9	6
Total	72		64	

CONCLUSION

A portable facial recognition attendance system was successfully developed providing easy to manage attendance system with simple step to follow and able to avoid attendance manipulation by student.

REFERENCES

[1] S. Dey et al., "Speech biometric based attendance system," 2014 20th Natl. Conf. Commun. NCC 2014, 2014.

[2] I. A. Ujan and I. A. Ismaili, "Biometric attendance system," 2011 IEEE/ICME Int. Conf. Complex Med. Eng. C. 2011, pp. 499–501, 2011.

DEVELOPMENT OF FACE RECOGNITION SYSTEM

Shahrun Naim Ab. Rahim and Maziah Mohamad
School of Mechanical Engineering, Faculty of Engineering,
Universiti Teknologi Malaysia, 81310 UTM Skudai, Johor, Malaysia

INTRODUCTION

One of the fastest growing technology nowadays is biometric technology including face recognition system. Over the years, in order to get perfect performance of the face recognition system, researchers have proposed different feature descriptors, implemented different classification methods, and carried out test experiments on different datasets in realizing an automatic Face recognition system [1][2]. The experiment was intended to find the robustness of different face recognition algorithm that most performance wise. The best face recognition algorithm also can be used as facial recognition attendance system for future works.

EXPERIMENTAL SETUP

This section presents the experimental setup for the system. I used Windows and MacOS as my work platform to conduct the test. In order to study the comparison robustness of the system, I proposed 4 different techniques to be tested. The algorithms that been tested were Local Binary Pattern Histogram (LBPH), Eigenface, Fisherface, and Dlib (HOG+SVM). The conducted test was intended to find the accuracy rate and time taken for the system execute the task. The experiment was done by using own face dataset that contain 10 UTM student with various style. All the result was calculated by the system or computer itself.

RESULTS AND DISCUSSION

At the end of control procedure, a face recognition system was tested in 4 parameters which are normal expression face, happy expression face, side face and low illumination. The training set will contain 9 images and single image as testing set. However, before conducting the test, the validation process need to be done first to ensure the algorithm is working well and verified. Figure 1 shows the accuracy rate of different face recognition algorithm. All the algorithm achieved a high rate when the input image tested were either normal face or happy face expression. LBPH and Dlib algorithm achieved high accuracy when tested in normal and happy face parameters. However, both algorithm achieved low accuracy rate when being tested in side face and low illumination parameters. It can be concluded that Dlib and LBPH algorithm only work better when the input image is in controlled environment. Figure 2 shows a comparison results of time taken of the different face recognition algorithms to execute the task of recognizing person. The test shows that for the normal face, the algorithms will took longer time compare to other parameters. The results also stated that, the algorithm will take shorter time when tested in happy face expression and low illumination image. In conclusion all the algorithm still in acceptable rate in term of time taken for the system execute the task.

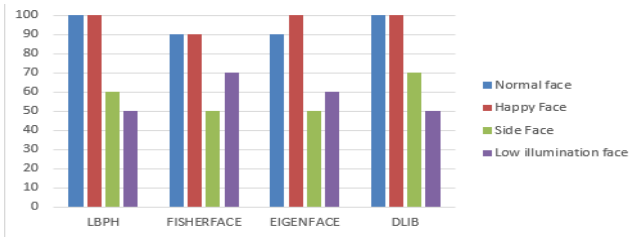

Figure 1: Overall accuracy rate

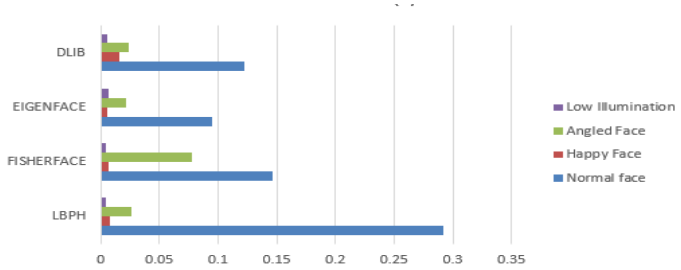

Figure 2: Time taken for system execute the task

CONCLUSION

Both figures show the results of different face recognition algorithms in term of accuracy rate and time taken. In conclusion Dlib and LBPH algorithms work better in controlled environment. The proposed attendance system can use either both algorithm but the user need to be in controlled environment such as stand straight and has enough illumination rate.

REFERENCES

[1] C. F. Liew and T. Yairi, “Facial Expression Recognition and Analysis: A Comparison Study of Feature Descriptors,” IPSJ Trans. Comput. Vis. Appl., vol. 7, no. 0, pp. 104–120, 2015.

[2] Z. Cao, Q. Yin, X. Tang, and J. Sun, “Face recognition with learning-based descriptor,” in Proceedings of the IEEE Computer Society Conference on Computer Vision and Pattern Recognition, 2010.

NUMERICAL SIMULATION OF FLAMELESS COMBUSTION SYSTEM

Akmal Hakim Asha'ari and Mazlan Abdul Wahid
School of Mechanical Engineering, Faculty of Engineering,
Universiti Teknologi Malaysia, 81310 UTM Skudai, Johor, Malaysia

INTRODUCTION

Flameless combustion was first found by Wunning [1]. Because of its main advantage over conventional combustion process, which is flameless combustion produces almost zero NOx as the product of the combustion process, it has been developed from there until today. This is due to the process itself in which complete combustion can be achieved without flame and the temperature was well below the standard NOx formation temperature of around 1200ºC. To reduce emissions and simultaneously generate high efficiency in the combustion process, this flameless combustion method is recently developed for industrial chambers.

EXPERIMENTAL SETUP

The aim of this project is to validate the experimental data from previous study. Comparing the temperature distribution across the axial distance. Investigate the influence of swirl air inlet position on the flameless combustion. Numerically determine the mass flow rate of internal exhaust gas recirculation under different operationg conditions.

RESULTS AND DISCUSSION

By following the procedure based from the previous study, we can obtain several parameters that cab be use to input in boundary conditions. The methodologies of the study are as follow:

1. Modelling the combustion chamber
2. Use appropriate meshing method
3. Define and input all the parameters
4. Simulating the model
5. Analysing the temperature distribution
6. Investigate the position of swirl air inlet
7. Numerically determined the mass flow rate of internal exhaust gas recirculation.

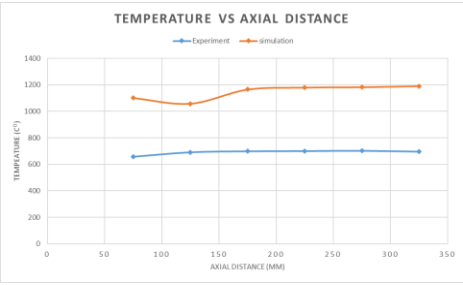

Figure 1: Temperature distrbution for middle air inlet

The temperature distribution for the middle swirl air inlet as shown in Figure 1. The trend is most likely the same but due to high residual, the error for this case is 65%. Figure 2 was obtained using data from velocity in the combustion chamber. Then, the data is input into a modified equation for mass flow rate of recirculation.

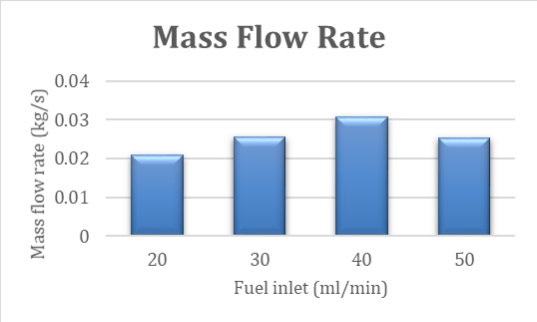

Figure 2: Mass flow rate of internal gas exhaust recirculation for different fuel inlet.

REFERENCES

[1] Wünning, J. A., & Wünning, J. G. (1997). Flameless oxidation to reduce thermal NO-formation. *Progress in energy and combustion science*, *23*(1), 81-94.

BARIATRIC WHEELCHAIR FOR DISABLE PERSON

Mohamad Hafiz Ahmad and Md Afendi M Yusof
School of Mechanical Engineering, Faculty of Engineering,
Universiti Teknologi Malaysia, 81310 UTM Skudai, Johor, Malaysia

INTRODUCTION

Wheelchair purpose is to assist people to become more mobile and independent. Different purpose will lead to different wheelchair design and it is important to know limitation for wheelchair selection [3]. Nowadays, physical disable person does not have proper support equipment [1] that can support their daily activities. Patient that have total physical disabilities need a caretaker to take care their daily routine activities such as bath and wear a cloth. A wheelchair with anthropometric measurement [2] need to be developed with extra function like standing or reclined to ease patient movement and activities.

METHODOLOGY

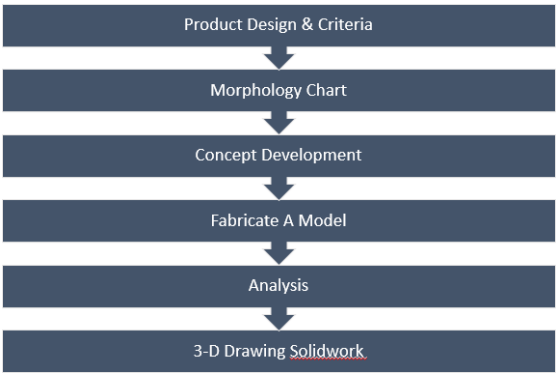

Figure 1 : Planning

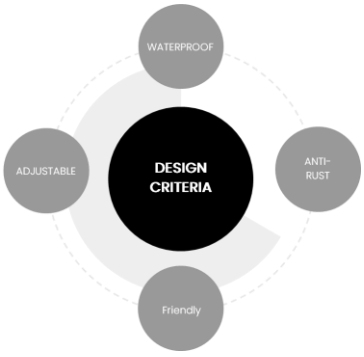

Figure 2 : Design Criteria

In this design, I have set a few criteria as a feature for my design and it must be included in this design. It need to be waterproof and anti-rust since this wheelchair mostly use and involved with water activity. Wheelchair should also be adjustable which mean can recline and standing to ease patient movement. An ergonomic feature should also be considered in this wheelchair to let patient be comfortable while using the wheelchair and operator feel ease while operate the wheelchair.

CONCEPT

Figure 3 : 3-Dimension Concept

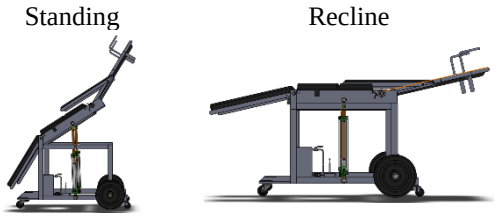

Figure 4 : Adjustable Position

Final concept has been developed based on design criteria. When its recline or standing, backrest and legrest will move simultaneously so no need to adjust backrest and legrest separately. Hence, that will ease caretaker job to handle the patient. An empty space left at below seat is to let the wheelchair fit a toilet bowl below it that later ease the patient to pass motion. Material used for the foam is vinyl acetate propylene which its properties is waterproof, elastic, and tougher than rubber.

CONCLUSION

From concept developed, there are still few improvements that can be work on even though main design criteria had been achieved. A further development still need to be done to design a better wheelchair for humankind.

REFERENCES

[1] Carol Burns. (2006, March). Common wheelchair design, selection and failures. A study into wheelchair options for Aboriginal people with disabilities in rural and remote communities, 6-7.

[2] Nursyahirah, A., & Siti, Z. M. (2018). Applied Anthropometric for Wheelchair User in Malaysia. Measurement.

[3] Seldon, P. T. (1992). Choosing A Wheelchair System. Journal of Rehabilitation Research and Development.

NUMERICAL SIMULATION OF SIX WRAPAROUND FINS ROCKET AERODYNAMIC CHARACTERISTICS

Mohamad Syafiq Abd Hamid and Md Nizam Dahalan
School of Mechanical Engineering, Faculty of Engineering,
Universiti Teknologi Malaysia, 81310 UTM Skudai, Johor, Malaysia

INTRODUCTION

Rocket invention have brought our technologies a step ahead where we can now sent our satellites and humans to outer space to do specific tasks such as space exploration, telecommunication signal, weather forecast and many more. Studies of the aerodynamic characteristics for the wraparound fin rockets have been undertaken by many of the previous researchers. This studies always include the use of analytical analysis, computational fluid dynamics (CFD) and also wind tunnel testing. Accordingly, in this study, USAF, DATCOM, and CFD approach were all used to calculate lift, drag, and pitching moment coefficient. The air flow pattern around the rocket was also studied, using the computational fluid dynamic approach [1]. The results obtained were then compared with wind tunnel testing data.

METHODOLOGY

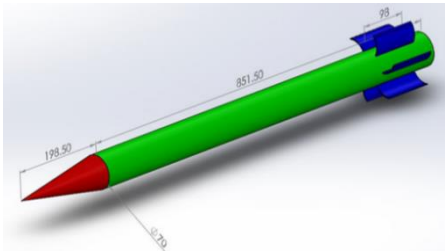

Figure 1: Drawing of the wrapped around fins rocket.

Figure 1 shows the drawing of the wrapped around fins rocket. For USAF DATCOM method, the analysis was divided into three parts, which is fin alone, body alone, and fin-body combination. The speed used for this method were 20, 40 and 60 m/s. The analysis was undertaken at angles of 0° to 25° with an increment of 5°.

The CFD simulations were conducted using ANSYS Fluent in order to study the aerodynamic characteristics and airflow pattern of the wraparound fins rocket. The simulation was done in subsonic and also high subsonic speed. The speed is 20, 40 and 60 m/s for subsonic and Mach number 0.6 and 0.8 for high subsonic. The angle of attack varies from 0° to 20° with an increment of 5°. The air flow pattern was also studied.

RESULTS AND DISCUSSION

From Figure 2, USAF DATCOM method and CFD follows the trend of wind tunnel testing for lift, drag and pitching moment coefficient.

The lift coefficient increase as the angle of attack increase. At zero angle of attack, the lift coefficient is zero. This is due to the shape of the rocket which is cylinder that creates symmetry to the rocket configuration. For drag coefficient, the trend of graph is the same as lift coefficient but at zero angle of attack, the value of drag coefficient is positive. The pitching moment coefficient decrease as the angle of attack increased. This shows that increasing angle of attack have the rocket to be statically stable.

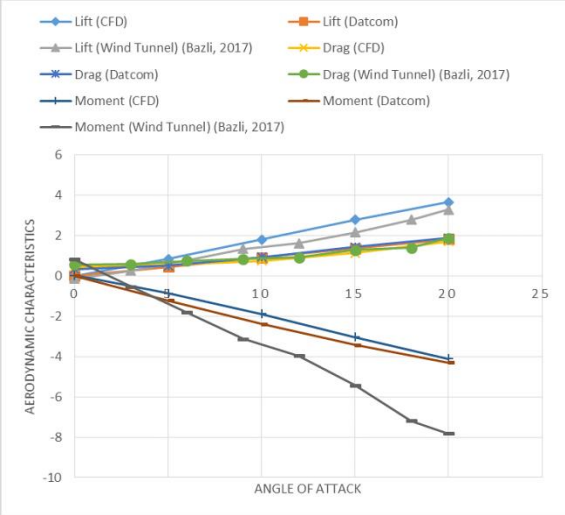

Figure 2: Aerodynamic coefficient at various angle of attack at 60m/s.

CONCLUSION

The trend of graph for USAF DATCOM method and CFD is the same as wind tunnel testing but only different in magnitude. USAF DATCOM method proved that it can give the early prediction for the aerodynamic characteristics. Through CFD, aerodynamic characteristics can be obtained and the results is almost the same as wind tunnel testing. On top of that, CFD can also simulate the flow pattern around the wraparound fins rocket. This shows that CFD can be the best substitute for wind tunnel testing which is expensive and time consuming.

REFERENCES

[1] Li, M., L.K. Abbas, and X. Rui. (2015). The Simulation of Wraparound Fins' Aerodynamic Characteristics. *Nanjing University of Science and Technology*, 10.

SIMULATION OF THE FLOW SEPARATION CONTROL OVER AN AIRFOIL USING A SYNTHETIC JET ACTUATOR

Ahmad Danial Hisyam Ahmad Badri and Md Nizam Dahalan
School of Mechanical Engineering, Faculty of Engineering,
Universiti Teknologi Malaysia, 81310 UTM Skudai, Johor, Malaysia

INTRODUCTION

Over recent years, there has been an explosive growth of interest in Synthetic Jet Actuator (SJA) on airfoil. A synthetic jet actuator (SJA) is a jet generator that produces non-zero momentum output while requires zero mass input. This is due to the fact that the SJA on airfoil increase the performance on an aircraft. Previous studies have successfully demonstrated the possibility in increasing in lift and drag reduction [1].

SIMULATION SETUP

Using a software called ANSYS FLUENT, a 2-D airfoil is setup inside a C-mesh domain to accommodate various angle of attack. The slot of synthetic jet actuator is 1mm and placed at 50% of the chord from the leading edge. The synthetic jet blows 50m/s at 1000Hz frequency. Mesh dependence study was done to increase the accuracy of the data received. The smallest element is set at 0.002 m. The present study target on cases at angles of attack from 0◦ to 20◦. The Reynolds number Re of 500 000 is come to at a free stream speed of U = 35m/s

RESULTS AND DISCUSSION

Figure 1 shows an SJA control effect on the NACA0015‘s lift coefficient. The flow control does not seem to bring any positive effect until 6° AOA. For the higher AOA, the control flow enhances the lift coefficient dramatically by energising the boundary layer and therefore delaying the separation occurrence. The lift coefficient experiences an extraordinary jump about 18% from 1.18 to 1.44. The stall onset is also postponed from 14° to 18. Once reaching the Cl_{max}, The two cases present different slide slope. The controlled airfoil experiences a different behaviour. It abruptly stalls and loses his lift similarly to the leading-edge stalls usually encountered for the medium aerofoils. When the angle of attack is increased, the separation point moves upstream smoothly to half chord and then faster toward the leading edge when stall occurs. These stalls are characterised by forming a bubble just after the leading edge. The size this latter does not vary too much with the AOA increase until it bursts under the action of the high adverse pressure leading to a more aggressive stall. The SJA control does not provide a significant effect on the lift enhancement for the AOA greater than 18 deg.

In Figure 2, the drag coefficient is plotted against the lift one for both controlled and not cases. For the lower AOA, the drag force is mainly composed of a parasitic drag. The SJA makes the boundary layer more turbulent. It, therefore, procures a higher drag level without any consistent lift gain. For higher AOA leading to a Cl > 1.18, the induced drag amount increases significantly for both airfoils. The flow separation leads to an additive drag clearly noticed for the uncontrolled airfoil. This extra drag supposed to result from the wake blockage and the vortex cores shedding can be largely reduced by delaying the flow separation onset, and therefore the SJA succeeds to reduce the drag coefficient dramatically.

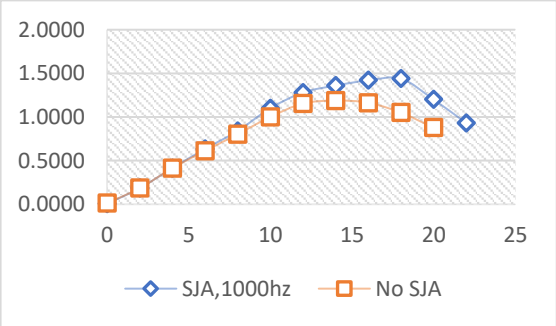

Figure 1: Lift coefficient versus angle of attack.

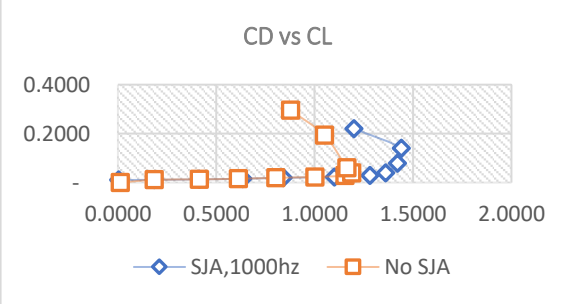

Figure 2: Drag coefficient vs lift coefficient

CONCLUSION

The SJA control was able to expand marvellously the flight domain, where it shifted the critical stall angle from 14° to 18° with a lift gain exceeding 18% accompanied by a huge drag reduction.

REFERENCES

[1] Gilarranz J, Traub L, Rediniotis O. A new class of synthetic jet actuators—part II: application to flow separation control. Journal of fluids engineering. 2005; 127(2):377-87.

DESIGN A WING SPECIMEN FOR THE WING STRUCTURE TEST RIG

Abdul Aziz Abdul Razak and Md Nizam Dahalan
School of Mechanical Engineering, Faculty of Engineering,
Universiti Teknologi Malaysia, 81310 UTM Skudai, Johor, Malaysia

INTRODUCTION

Structure of the wing plays an important role in an aircraft and it is the most feared case if there is a failure on the wing structure. By using test rig, engineers can know the detail of the wing such as, can the wing bending force exceeds more than its safety limit, how many years that it takes for the wing to be without any failure and at what place will the wing of the aircraft fail first. Also, a proper wing structure with good internal supports and preliminary analysis on the wing structure are vital to prevent fatal damage. This will help in designing a good wing's strength and structural rigidity.

METHODOLOGY

There is a great deal of theoretical approaches being applied during the analytical calculation of wing component, including Theory of Elasticity, Energy Method, Schrenk's Method [1], Engineer's Theory of Bending, Failure Analysis [2] and Airforce Method for designing lug attachment of wing specimen [3]. The design involves a multi-cell wing with attachment based on the specification and configuration of the rig. Determination of reference aircraft used for the wing specimen configuration was selected and Schrenk method was used to analyse the wing loading for determining the diagram of shear force, bending moment and torsion. The designed wing specimen's structural components was analysed using Failure Analysis to obtain its margin of safety in order to ensure that there are no failure in the component.

RESULTS AND DISCUSSION

Load that acted on the main wing was calculated from Schrenk's Method [1]. The ultimate loads acting on the wing were obtained by multiplying the maximum load with the design safety factor by 1.5 that resulted in ultimate shear force, bending moment and torsion of 9800.48kN, 9427.24Nm, and 125.07Nm respectively.

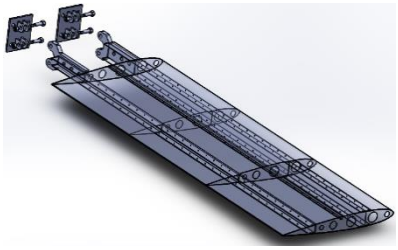

Figure 1: Final full wing modelling with lug attachment

Table 1 : Design Critical Loadings and Safety Margin

Components	Critical Strength	Applied Load	Margin of Safety
Front Spar, I beam	35.00 kg/mm^2	32.35 kg/mm^2	0.08192
Rear Spar, C beam	35.00 kg/mm^2	34.79 kg/mm^2	0.006036
Wing Skin	38.04 MPa (compression) 15.05 MPa (Shear)	20.62 MPa (compression) 5.65 (Shear)	0.2665
Stiffener	123.90 MPa	20.62 MPa	6.01
Rivet	55.60 Mpa	38.04 Mpa	0.46
Wing Attachment, Lug	102.10 kN	9.8 kN	9.42
Pin	101.86	9.8 kN	9.39

From Table 1 above, the margin of safety for the design of the wing attachment to the wing structure test rig are high due to it is design not only to withstand my wing specimen only. The final design of the wing specimen had an optimum positive margin of safety with a minimum of 0.006036 and maximum of 0.46. The margin of safety obtained for the wing components designed approached 0 and does not exceed 0.5 which shows that the structure was safe and were not overdesigned.

CONCLUSION

Full detailed drawing of the wing components and the lug attachment of wing was designed using SolidWorks and are expected to meet the manufacturer's criteria and needs for fabrication. The wing specimen strength was determined and it is adequate for the purpose of teaching and learning process.

REFERENCES

[1] Schrenk, O., a Simple Approximation Method for Obtaining the Spanwise Lift Distribution, Luftwissen, Vol. 7, No 4, USA, 1940.
[2] E.F. Bruhn (1973). Analysis and Design of Flight Vehicle Structures. Second Edition. Indianapolis: Jacos Publishing.
[3] "Stress Analysis Manual," Air Force Flight Dynamics Laboratory, October 1986

APPLICATION OF MODULAR CONSTRUCTION AT MALAYSIA SHIPYARDS

Yahya Samian and Mohamad Ali Hanafi Mohd Yunus

School of Mechanical Engineering, Faculty of Engineering,
Universiti Teknologi Malaysia, 81310 UTM Skudai, Johor, Malaysia

INTRODUCTION

Nowadays, the local shipbuilding and ship repair industry moving towards Industry 4.0[1]. The shipbuilding industry become larger and implement the latest technology. Modular construction is a process of breakdown structure into blocks, sections and units [2]. Modular construction involves the transition of technology from 2D to 3D drawing. The concept of Product Work Breakdown Structure(PWBS) enables the shipyard in planning and control of the production. This method allows parallel working and allows complex structure to be manageable [3]. This concept had introduced a long time ago but the implementation of this concept only 15 percent in Malaysia shipyard [1].

This thesis intends to propose the framework of the modular construction method that is suitable for small vessels construction in local shipyard. Landing Craft 48m were proposed as example.

PROJECT OBJECTIVES

The aims of this project is to propose modular construction framework that is suitable for small vessel construction in Malaysia Shipyards

RESULTS AND DISCUSSION

At the end this research, some modular construction framework was proposing as the guideline to local shipyard to implement modular construction concept. Firstly, the modular were breakdown depend on the type and size of the vessels. Each vessel has different number of block division. The breakdown of modules located at the bulkhead.

Table 1 shows the number of modules produced based on the type of vessels. Next, the breakdown of modules was depending on the weight. It is recommended the weight one block is 30 tonnes and above. On this case, the engine module is the heaviest module compare to another module. The sequence of the production starts with the complex module which engine module. The other modules based on the building strategy of shipyard.

The implementation of the SFI (Senter for Forskningsdrevet Innovation) enables the local shipyard to control of production and distribute the work according to group system. The implementation of the 3D software which ShipConstructor provides building strategy to the local shipyard and produce SFI code. Besides, this software produces accurate 3D stimulation of pipe and electrical system. The accuracy of engineering analysis of the 3D software had minimised the repairs, rework and modification. The shipyard recommended to have lifting capacity 100 tonnes and implement three designer in one project. One designer for the hull and another two designers for piping and the electrical designer.

Table 1 : The number of modules produced based on the type of vessels.

Type of Small Vessels	The number of modules
1. Tugboat 30m	5
2. Landing Craft 48m	7
3. Landing Craft 78m	10
4. Supply Vessels 48m	7
5. Supply Vessels 78m	10
6. Offshore Supply Vessels 48m	7
7. Offshore Supply Vessels 78m	10

CONCLUSION

Framework for small vessel had been proposed by using Landing Craft as example. The number of modules were breakdown based on type of vessels and weight. The production starts with engine modules due to most complex among other module. The production starts with engine modules due to most complex among other module. SFI code be used to determine the breakdown structure

REFERENCES

[1] Ismail, A. R. (2018). 3D Design in Industry4.0. *The Future of SBSR Industry in Malaysia Journal. MyForesight. 22th Edition*, 12-16.

[2] Mokhtar, A. A. (2016). A Review of Modular Construction Shipbuilding in Malaysian. *Proceeding of Ocean, Mechanical and Aerospace Journal, Vol 3*, 135-143.

[3] Pal, M. (2015). Ship Work Breakdown Structures Through Different Ship Lifecycle Stages. *Journal of The Royal Institution of Naval Architects*, 1-15.

MIXTURE OF PALM OIL FIBER (FRUIT BUNCHES) AND GYPSUM TO ENHANCE THE FIRE RESISTANT OF A FIRE DOOR (EXPERIMENTAL)

Noor Idayu Mohamad Sapuan and Mohamad Nor Musa
School of Mechanical Engineering, Faculty of Engineering,
Universiti Teknologi Malaysia, 81310 UTM Skudai, Johor, Malaysia

INTRODUCTION

There are many cases involving fire in big type of building such as factory, hotel, shopping complex, store and hospital. According to the Fire Rescue Department of Malaysia [2], the fire incident of building happens because of the short circuit of electric. The number of the fire breakouts for the building has been increased from 2011 to 2013. Common causes of fatal fires in this kind of buildings is that the escape routes are inadequate in number, size or design. Next, the occupants unaware of alternative escape routes and also delayed awareness of fire incidents.

EXPERIMENTAL SETUP

The sample of this experiment needs to maintain its integrity for a period ranging up from 30 minutes. Firstly, the sample need to be prepared according to the composite ratio for each thickness. Before the experiment been done, the weight of dried sample was measured. The initial Tmean of the sample and the ambient temperature are recorded. The furnace is pre-heat at 650°C -750°C and keeps the temperature constant for 10 minutes. After 10 minutes, the sample is placed inside the furnace with the surface of attached thermocouples is position opposite to the fire source.

The temperature readings of each thermocouple for unexposed surface and the temperature of the furnace at every 3 minutes' interval were recorded. The reading is taken until the failure occur. The time of failure to occur is known as R, the fire resistance rating. The failure occurs when the are cracks and propagation of gaps on the sample, the temperature of the thermocouple that fixed in the sample excess of 180°C from its initial Tmean unexposed face temperature and when the temperature of temperature means of the unexposed surface is increased more than 140 ˚C of its initial value and the required to maintain its integrity for a period ranging up from 30 minutes.

RESULTS AND DISCUSSION

Figure 1: Burnt and Cracked

Table 1: Fire Resistant Rating

Composition		thickness(mm)	Rating,t (Minute)	Maximum Mean Temperature (°C)	Density, ρ (kg/m3)
Gypsum(g)	Palm oil fiber(g)				
500	0	6.4	45	180.9	1148.44
		9.5	51	108.96	1342.11
		12.7	60	197.06	1259.84
490	10	6.4	48	156.7	1523.44
		9.5	54	139.36	1263.16
		12.7	57	166.02	1023.62
480	20	6.4	33	119.36	1113.28
		9.5	45	184.3	1000
		12.7	51	180.17	881.89
470	30	6.4	30	118.34	1179.69
		9.5	42	180.76	1057.89
		12.7	51	179.78	1019.69

CONCLUSION

A total of 12 samples was fabricated according to the three different level of thickness and four different ratios of composition mixture. The samples were fabricated in the form of solid compound. The highest fire rating obtained in the experiment was 60 minutes for the composition of 500g Gypsum: 0g Palm Oil Fiber (Fruit Bunches) with the thickness of 12.7mm. The lowest fire-resistant rating was 30 minutes for the composition of 470g Gypsum :30g Palm Oil Fiber (Fruit Bunches) with thickness of 6.4mm. This clearly shows that the thickness of the sample plays important role in a fire-resistant rating determination. As the thickness decreases, the fire rating also decreases in linear form. Overall, the Gypsum and the Palm Oil Fiber mixture can be used in manufacturing of fire-resistant materials and fabricated on construction materials such as wall panels, ceilings and many more.

REFERENCES

[1] MS1073: PART 2 (1996). Methods for Determination of the Fire Resistance-General Principl. SIRIM, Malaysia.
[2] ASTM E 119-12. Standard Test Methods for Fire Tests of Building Construction and Materials, United States of America

AERODYNAMIC ANALYSIS OF PERODUA MYVI THIRD GENERATION BY EXPERIMENTAL

Muhammad Nabil Azmer Bin Mohd Napi and Mohamad Nor Bin Musa
School of Mechanical Engineering, Faculty of Engineering,
Universiti Teknologi Malaysia, 81310 UTM Skudai, Johor, Malaysia

INTRODUCTION

Aerodynamics basically about the way air flow moves around the object. Through the rule of aerodynamics, it explains how the airplane can fly. Since all the object exist are surrounded by air, it can be said that all object move through air is affected by aerodynamics. Fluid also have their own resistance. When there is body move through it, fluid will resist the motion of the moving object. The aerodynamics force that act on the object which resist it motion is called drag. The drag force will decrease if the body of the object have aerodynamics shape [1].

There are many factors that can affect aerodynamic forces on the car which are the object, movement of the object through medium and the properties of fluid that the object pass through [2].

EXPERIMENTAL SETUP

Adjust the angle of six component balance to 0° so that the model also at the same level. Attach the supporting rod to the balance. Then, mount the scaled model car at the end of the supporting rod. The experimental starts by adjusting the motor speed so that the desired wind velocity is achieved. The velocity is achieved by comparing the theoretical dynamic pressure at the corresponding speed by using the pressure gauge. The nearest experimental dynamic pressure at 10 m/s, 15 m/s, 20 m/s, 25 m/s, and 28m/s were measured and being recorded. The drag force at 5 m/s, 10 m/s, 15 m/s, 20 m/s 25 m/s, and 28m/s will be recorded in the data acquisition software. Lastly, the drag coefficient can be calculated.

RESULTS AND DISCUSSION

From the result obtained from the experiment, there two graph that can be plotted and observed. First graph is Drag Force versus Speed^2 while the other graph is Drag Coefficient versus Reynold number. The figure 1 visualize the trend for Drag Force versus Speed^2 graph. It can be seen that the trend line for the graph is increase linearly and the drag force basically depending on the speed of the car. So, when the speed increase, the drag force will also increase.

Figure 2 show the graph of Drag Coefficient, CD versus Reynolds Number. From the plotted graph, it can be seen that the Drag coefficient value is approaching constant value between 20 m/s and 28 m/s. The drag coefficient value at 20 m/s, 25 m/s and 28m/s is 0.34, 0.34 and 0.33. Due to this phenomena, the value of CD is deplete because of the boundary layer transition, thus cause the wake region to become shorter and form drag magnitude is reduced.

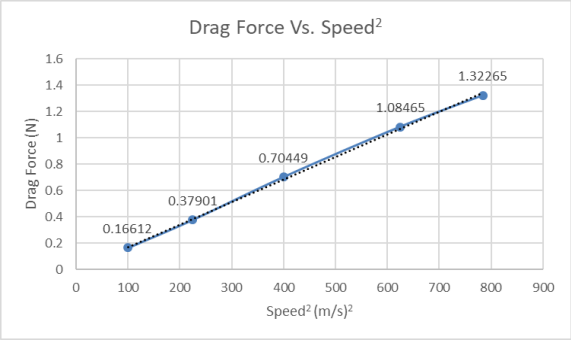

Figure 1: Drag Force vs. Speed^2

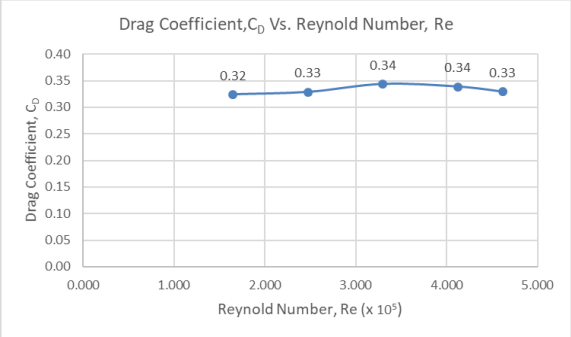

Figure 2: Drag Coefficient, C_D vs. Reynold Number, Re

CONCLUSION

Based on the experiment conducted, the drag coefficient, CD value for Perodua Myvi Third generation is 0.33 and the flow that exist around the car is laminar type because it has stable flow type and smooth.

REFERENCES

[1] Barnard, R. H. (2001). *Road vehicle aerodynamic design-an introduction*.

[2} Hucho, W.-H. (1986). Aerodynamics of road vehicles. *SAE International*.

HYDRODYNAMIC ANALYSIS OF A MODEL PATROL BOAT

Sugaan Balasubramaniam and Mohamad Nor bin Musa
School of Mechanical Engineering, Faculty of Engineering,
Universiti Teknologi Malaysia, 81310 UTM Skudai, Johor, Malaysia.

INTRODUCTION

Hydrodynamics of a boat is the study of the hydrodynamic resistance force on a boat [1]. If an object, such as a boat is immersed in a stream of fluid, the object will be subjected to friction and turbulence. The hydrodynamic study on a boat is very crucial as it gives us understanding on the wide range of complicated phenomena involving fluids. Understanding these phenomenon allow us to make predictions for practical ocean engineering applications such as in boat building [2]. The efficiency of a boat can be analyzed by obtaining its value of drag coefficient value which is denoted as Cd. Drag coefficient is a dimensionless number which indicates how well a boat can move through water. The lower the value of drag coefficient of the boat, the more efficient the boat is. Thus this means it can move more easily through the water.

PROJECT OBJECTIVES

The objective of this project is to find the drag coefficient of a model patrol boat via simulation, to visualize and analyze the fluid flow through the model patrol boat and to compare the value of drag coefficient of simulation and validated data from experiment.

EXPERIMENTAL SETUP

This section presents the experimental setup for the system. We used single EEG signals of 10- 20 international standard location (F8). The reference potential position was placed at the right ear lobe. An EEG paste was used to increase the electrode conductivity. The channel was directly connected into BMA-400 EEG-amplifier which provides specific gain constant for bio signal amplification.

The EEG signal was digitized using National Instruments (NI)-PCI-6229 Data Acquisition Card (DAQ) which was connected into Peripheral Component Interconnect (PCI) slot of a personal computer's (PC) motherboard.

RESULTS AND DISCUSSION

Table 1 shows the coefficient of drag respective to each speed tested from simulation. While Figure 2 shows the visualization of fluid flow around the boat hull.

Table 1: cd respective to each speeds

Speed Vs (knot)	V (m/s)	Vm (m/s)	Rtm (N)	Cd
16	8.23	1.84	12.384	0.01109
18	9.03	2.07	12.553	0.008883
20	10.29	2.3	14.393	0.008255
22	11.32	2.53	16.221	0.007689

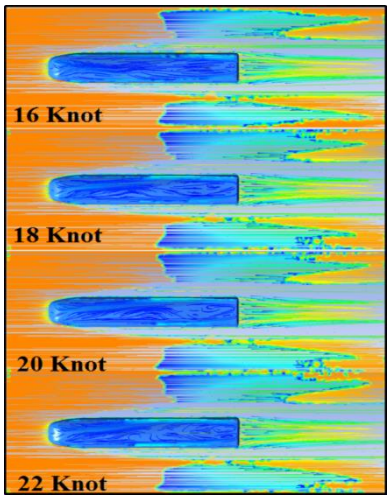

Figure 2 Velocity streamline of the vehicle respective to each case.

REFERENCE

[1] Rana, S. (2012). Introduction of Hydrodynamics and it's Application.
[2] O.C. Zienkiewicz, R.L. Taylor and P. Nithiarasu. (2014). Free Surface and Buoyancy Driven Flows, The Finite Element Method for Fluid Dynamics.

THE EFFECTIVENESS OF JET IMPINGEMENT COOLING SYSTEM ON VARIOUS FLAT PLATE SURFACE

Mohammad Firdaus Mohammad Khalil and Mohamad Nor Musa
School of Mechanical Engineering, Faculty of Engineering,
Universiti Teknologi Malaysia, 81310 UTM Skudai, Johor, Malaysia.

9. Introduction

The purpose of this study is to investigate the effectiveness of jet impingement cooling system on flat plate surface [1]. This type of cooling system is very useful as it may be used in a lot of machine and instruments such as piston, supercomputer, microchip, food technology and hybrid car electronic circuit. [2]

10.

11. Objective

Firstly, this project can determine the best distance from nozzle to plate surface and eventually determine the dimensionless ratio between distance from nozzle to plate surface and the diameter of circular nozzle. Next is this project can observe the best mass blow rate, ranging from laminar flow to turbulent flow. Lastly, by choosing three type of materials that have different surface roughness is to study the effect of surface roughness and cooling effect.

12. methodologies

The air was supplied by the large capacity tank pressurized by automatic shutoff air compressor. Air blow rate can be controlled using pressure regulator attached with nozzle. The jet is impinged at stagnation point with different distance from nozzle to plate surface. Manipulating variables for the projects are air blow rate, dimensionless s/d that is where s is distance from nozzle to surface; d is nozzle diameter and lastly the materials that consist of zinc, aluminium and mild steel.

13. CONCLUSION

Aluminium has the lowest average temperature among the materials which lead to early hypothesis that is has the highest Nusselt number and heat transfer coefficient. However, when calculating the heat transfer coefficient, the difference between plate surface temperature and surrounding are being considered. First, nozzle distance to heat ratio that lead to the dimensionless s/d is at S = 6 and s/d = 10. Next, best mass blowing rate for cooling can be achieve at 8.4 m/s and lastly the best materials among three chosen material is zinc based on overall Nusselt number.

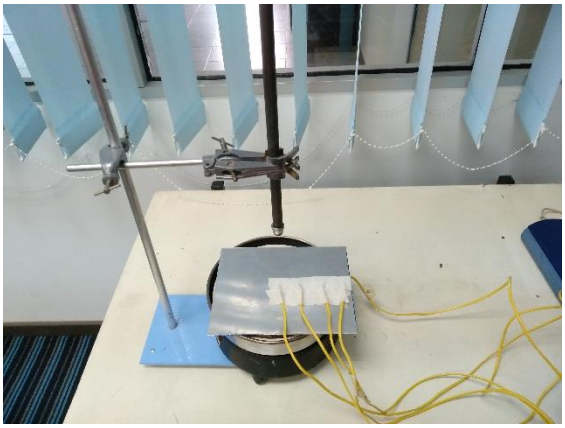

Figure 18: Experimental Setup

14.

15. References

[1] H. Wang, W. Yu and Q. Cai. (2012). Experimental Study of Heat Transfer Coefficient on Hot Steel Plate During Water Jet Impingement Cooling. *Journal of Materials Processing Technology*.

[2] Nasif. G., Barron. R.M. and Balachandar. R. (2016). The Application Of Jet Impingement For Piston Cooling.

FLOW ANALYSIS AND EFFECT OF ROTATION VANE BLADE ANGLE THROUGH 90° PIPE BEND

Siti Mariam binti Sudin and Mohamad Nor bin Musa
School of Mechanical Engineering, Faculty of Engineering,
Universiti Teknologi Malaysia, 81310 UTM Skudai, Johor, Malaysia

INTRODUCTION

When changing direction especially at fitting—90° pipe bend, velocity and pressure of fluid flow will also change. This situation leads to occurence of secondary flow which then pressure drop will exist. High pressure drop will form an erosion at the 90° pipe bend. In order to overcome this situation, rotation vane blade is used within the pipe and installed before the elbow to decrease the pressure drop occurrence.

EXPERIMENTAL SETUP

The basic equipment to run this project are U-tube manometer, anemometer, blower, AC voltage regulator, pipe and rotation vane of 18° and 33° angle blade. The rotation vane blade will be attached before the 90° pipe bend. There are two sections of measurement where located before (A-A) and after (B-B) the elbow with seven points needed to be measured across the cross section of the pipe for each section. The inlet velocity of the fluid flow is 1.20, 1.30, 1.40, 1.45 and 1.50 m/s.

RESULTS AND DISCUSSION

When the rotation vane is installed, the velocity will be lower (compared to A-A), the pressure will be higher (compared to A-A) and 18° produced lower pressure drops between section A-A and B-B than 33° of rotation vane. Then, when Reynolds number increase, velocity will increase, and when velocity increase, pressure will decrease. Figure 1 shows the comparison of pressure drop between 18° and 33° rotation vanes. The relation between Reynolds number and velocity can be explained by Reynolds number equation while Bernoulli equation can proof the relation between pressure and velocity.

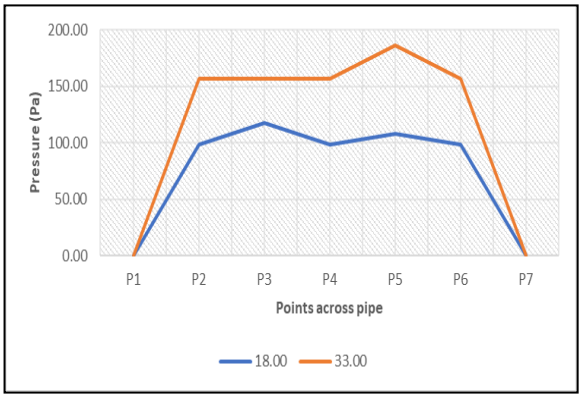

Figure 1 Comparison of pressure drop between 18° and 33° rotation vane angles.

CONCLUSION

The overall result of this experiment has achieved the requirements outline of the objective. In conclusion, the velocity is directly proportional with the Reynold number. When the Reynolds number increase, the velocity will be increase. Next, the pressure can be related with the velocity by using Bernoulli equation as the proof. The pressure decreases when the velocity increase. Then, the pressure drop is corresponded with the Reynold number. the higher the Reynold number, the higher the velocity, thus the pressure drop also will be high. However, when comparison of pressure drops between section A-A and B-B when using both angle of rotation vane blade—18° and 33°, the pressure drops when using 18° rotation vane blade is lower than 33° rotation vane blade.

REFERENCES

[1] J. Lloyd Jones, L. A. (1992). Eliminating Elbow Exit Flow Distortion and its Effect on Downstream Check Valves. Sunnyvale, California: Cheng Fluid Systems Inc.

COMBUSTION PERFORMANCE OF SUNFLOWER OIL-BASED BIODIESEL IN LIQUID FUEL BURNER

Nareenthiran Mavalavan and Mohammad Nazri Mohd Ja'afar
School of Mechanical Engineering, Faculty of Engineering,
Universiti Teknologi Malaysia, 81310 UTM Skudai, Johor, Malaysia

INTRODUCTION

The exponential development of world population would eventually lead to an increase in the energy demand in the world. Majority of the world's energy needs are supplied through petrochemicals sources, which implies that the resources of this sort of non-renewable energy source are limited and would be run out upon non-stop use. The high energy demand in the industrialized world as well as the pollution problems caused due to the use of fossil fuels make it increasingly necessary to develop an alternative renewable energy source.[1]

EXPERIMENTAL SETUP

The set-up incorporates Light oil burner with a standard spray nozzle, a K-type thermocouple, a combustion chamber, and a gas analyser. The burner was fixed at the front part of the combustion chamber to blow air and flame. Eight thermocouples were put along the mass of the top surface of the combustion chamber; each isolated at an equidistance of 100 mm. The thermocouples were associated with a temperature information logger. For the spray nozzle, an angle of 45° was utilized. An outflow chamber was associated with the fumes of the burning chamber to channel the discharge from the ignition to the emission sensors. The shows NOx, SO2, and CO emissions.

RESULTS AND DISCUSSION

The wall temperature reduces when the volume rate of sunflower based biodiesel rises. Diesel has a high calorific value and the energy content of diesel is a lot higher than that of the sunflower based biodiesel blends. The varieties of wall temperature profile for biodiesel blends (B10, B15, B25 and B50) are exceptionally low however their temperature is close to diesel's temperature because their properties have insignificant contrasts with diesel fuel. B50 has the most reduced wall temperature profile on the grounds.

NOx, SO_2, and CO, had been investigated from the burning of Diesel fuel and Sunflower biodiesel blends. NOx emissions rise as the equivalence ratio, Ø increase however it starts to reduce after the stoichiometric point in the burning procedure. The emissions of CO decline as the equivalence ratio, Ø increase yet start to increase after the stoichiometric point in the burning procedure. The SO_2 demonstrates an extremely little to no distinction as the equivalence ratio, Ø increments however start to have a little rise after stoichiometric point in the burning procedure.

Figure 2 shows the length of the flame produced by diesel and different percentage of sunflower oil-based biodiesel blends from combustion. As observed, flame length increase from lean mixture to rich mixture. The length of flame released in rich mixtures of Ø= 1.1 and 1.2 is always higher compared to the lean mixtures Ø= 0.8 and 0.9 because more fuel is burned at rich mixture, and more heat released during combustion

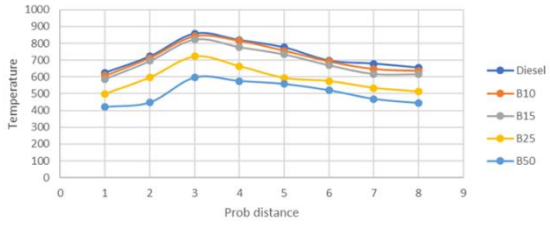

Figure 1: The wall temperature profiles at different prob distance for equivalent ratio, Ø = 1.0

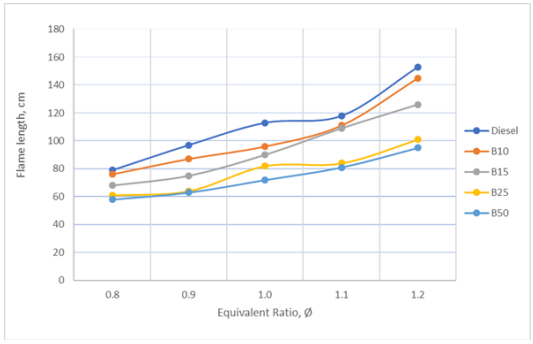

Figure 2: Flame length at various equivalent ratio, Ø

CONCLUSION

Biodiesel is the most appropriate elective fuel for diesel motors, since its properties are extremely near those diesel fuels. Subsequently, biodiesel can be utilized in diesel motors with few or no changes. Diesel-fuel mixes with biodiesel have predominant lubricity, which decreases wear and tear on the diesel motor and makes the motor parts last longer. Biodiesel blends well with diesel fuel and remains mixed.

REFERENCES

[1] 1. Coyne D. (2016) The Energy Transition. Retrieved from https://seekingalpha.com/article/3993718-energy-transition

OPTIMIZATION ON THE PRODUCTION OF NON EDIBLE OIL TO BIODIESEL VIA TRANSESTERIFICATION PROCESS

Nik Nur Fatin Amiera Nik Aziz and Mohammad Nazri Mohd Ja'afar
School of Mechanical Engineering, Faculty of Engineering,
Universiti Teknologi Malaysia, 81310 UTM Skudai, Johor, Malaysia

INTRODUCTION

It is estimated that usage of oil sources might be depleted by the year 2050 from the previous research that has been done on the usage of oil and about 75% of the human caused emissions are from consuming of petroleum derivatives in the course of recent years [1]. The price of WCO is 2-3 times cheaper than virgin vegetable oils and it is readily available at any restaurant or café locally and is considered as one of the options for economical sources of fatty acid methyl ester production.

EXPERIMENTAL SETUP

The waste cooking oils used in the transterification process were obtained from a food stall outside of UTM. There are three stages in the transesterification process; the pre-treatment process, the transesterification process and the post-treatment process. In the pre-treatment process, WCO was heated 100°C and is stirred for 1 hour to remove any moisture. Then the WCO was mixed with different values of condition obtained from Design Expert to produce WCO biodiesel and glycerol. In the post-treatment process, the glycerol formed at the bottom layer was removed and the WCO biodiesel underwent the washing process using distilled water at 50°C at various intervals to remove any impurities and remaining glycerol. Finally, the WCO biodiesel was reheated for 30 minutes and is stirred to remove any remaining water. The final product is a refined WCO biodiesel.

.

RESULTS AND DISCUSSION

The amount of yield for each set of parameters that is generated from Design Expert is shown is Table 1.

Table 1: Biodiesel yield

KOH % (w/w)	Methanol (25 % v/v)	Temperature (°C)	Biodiesel Yield (ml)
2	12	40	87.6
2	4	40	76.5
0.8	12	40	88.1
0.8	4	40	88.6
2	12	65	78.4
0.8	12	65	87.2
2	4	65	50.0
0.8	4	65	69.3

Using Design Expert software, the result of the optimization of biodiesel in term of weight of catalyst, volume of reactant and reaction temperature for the highest yield production of biodiesel can be validated. The linear and combined effects of the parameters were considered to find their impact on the biodiesel yield. The p-value for model is stated as significant, hence proving that this experiment is valid for first order optimization. At 95% confidence level, the p-values less than 0.05 indicate significant effects of those parameters. Based on the coded parameters, the linear model with determined coefficients was given as follows:

$$y = 136.59500 - 4.12500x_1 - 4.51896x_2 - 0.91133x_3 + 1.15104x_1x_2 - 0.25833x_1x_3 + 0.089250x_2x_3$$

Where;

y = Yield (ml)
x_1 = Mass of KOH (% w/w)
x_2 = Volume of Methanol (25% v/v)
x_3 = Temperature (°C)

The volume of methanol has the lowest p-value (0.0123) and the highest F value (2675.71) among the other variables. These results revealed that the volume of reactant is most important variable in biodiesel production from WCO [2]. It has been observed that biodiesel yield will increase when the molar ratio increase but will start to drop after achieving peak [3]. Coefficient of determination was 99.99% and it indicates the accuracy of the model. Optimum condition that will produce the highest yield of biodiesel, 88.4625ml is 0.8(%w/w) of KOH, 4(25%v/v) of methanol and 40°C.

CONCLUSION

In conclusion, the model and equation generated is appropriate for experimental relationship between the variables and the response.

REFERENCES

[1] R. Suresh, "Optimizing Bio-diesel Production by Transesterification for Internal Combustion Engines," 2017.

[2] M. Rahimi, B. Aghel, M. Alitabar, A. Sepahvand, and H. R. Ghasempour, "Optimization of biodiesel production from soybean oil in a microreactor," *Energy Conversion and Management*, vol. 79, pp. 599-605, 2014.

[3] P. Verma and M. Sharma, "Review of process parameters for biodiesel production from different feedstocks," *Renewable and Sustainable Energy Reviews*, vol. 62, pp. 1063-1071, 2016.

PERFORMANCE EVALUATION OF COOLANT CONCENTRATION WHEN END MILLING HIGH STRENGTH STAINLESS STEEL USING UNCOATED CARBIDE TOOL

Siti Munira Binti Kadir, Mohd Azlan Suhaimi and Safian Sharif
School of Mechanical Engineering, Faculty of Engineering,
Universiti Teknologi Malaysia, 81310 UTM Skudai, Johor, Malaysia

INTRODUCTION

In machining, the key essential to any manufacturing operation is always related to quality. Some study also stated that with the correct machining parameter like cutting speed can also affect the performance of various coolant concentration on tool wear and surface roughness [1]. AISI 420 is a martensitic stainless steel that has high mechanical strength and often uses in structural applications. The problem with AISI 420 is that the material itself has high hardness and gummy texture so it will be hard to cut.

EXPERIMENTAL SETUP

Uncoated carbide tool is used as a cutting tool to cut AISI 420 under three different coolant concentration (3%, 6% and 9%) at three different cutting speed (50m/min, 75m/min and 100m/min) using milling machine. All these different range of cutting parameter conducted under constant depth of cut (4mm for axial and 1mm for radial) and feed rate (0.05mm/tooth).

RESULTS AND DISCUSSION

Based on the graph in Figure 1, the lowest cutting speed at 50m/min and highest coolant concentration at 9%, uncoated carbide tool exhibits the longest tool life. This may occur due to the fact when cutting at lowest speed; less vibration occurred. Other than that, highest coolant concentration prolongs the tool life by reducing heat temperature that arise. Based on the graph in Figure 2, at the lowest cutting speed of 50m/min and at the middle range of coolant concentration at 6%, the surface roughness of AISI 420 was better. This may due to the fact is that the difference in composition of AISI 420 with other material. AISI 420 has a gummy texture and high hardness of 50HRC. Thus, the most suitable viscosity for better surface roughness of AISI 420 is moderate which precisely at 6% of coolant concentration. This is because, at the lowest coolant concentration of 3%, lighter viscosity of oil has higher coefficient friction. On the other hand, increasing coolant concentration will generate higher compressive stress on AISI 420 [2]. Overall, dominant tool failure mode was chipping at all conditions. This is due to mechanical shock and thermal fatigue that has occurred where lead to a result of interrupted cutting and the effect of strong vibration during machining process [2].

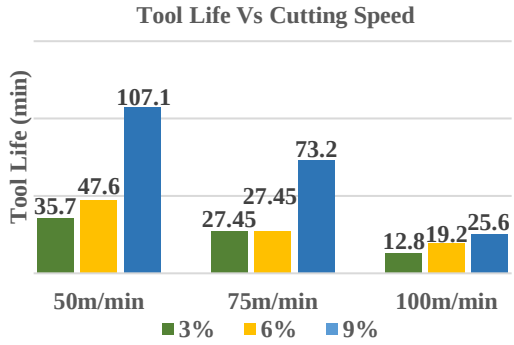

Figure 1: Tool Life vs Cutting Speed under three different coolant concentrations.

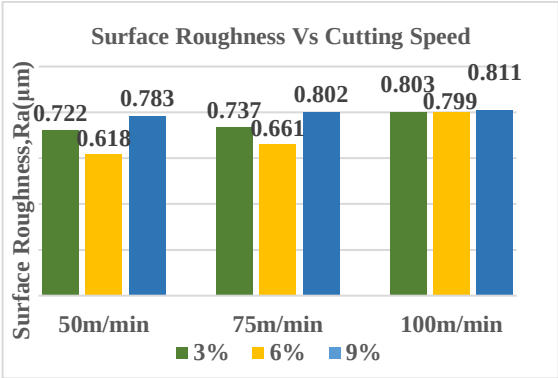

Figure 2: Surface Roughness Vs Cutting Speed under three different coolant concentrations.

CONCLUSION

As a conclusion, the tool life of uncoated carbide tool is longest at the lowest cutting speed under highest coolant concentration. AISI 420 maintained a better surface roughness at the lowest cutting speed under moderate coolant concentration.

REFERENCES

[1] W.Y.H. Liew *and* X. Ding (2008), 'Wear progression of carbide tool in low-speed end milling of stainless steel', *Science Direct Journal W.Y.H. Liew, X. Ding / Wear, 265 155–166.*

[2] Nurfarahin Binti Zainuddin, (2018). *Performance Evaluation of Coolant Concentration When End Milling Hardened Steel Coated Carbide Tool*, Bachelor of Engineering (Mechanical-Manufacturing), School of Mechanical Engineering, Faculty of Engineering, University of Technology Malaysia.

SIMULATING THE MALAYSIAN ACTUAL DRIVING CONDITION AS A REFLECTION TO REAL-DRIVING EMISSION TEST

Fauzi Abdul Noor and Mohd Azman Abas
School of Mechanical Engineering, Faculty of Engineering,
Universiti Teknologi Malaysia, 81310 UTM Skudai, Johor, Malaysia

INTRODUCTION

Nowadays, electric powered electric becoming large in term of popularity and useable form of transport particularly for short distance such daily commutes like going work. There a such factors that driving this growth which is due to development of technology used in electric vehicles, as example battery and motor that make the electric vehicle became an attractive option for production [1]. Advantages of using electric motor over conventional internal combustion engine is low running cost, achieve near to silent operation and no emission. But electric motor got such limitation like needed large and expensive battery pack to get same range as internal combustion engine and time taken to recharge battery longer than time to re-fuel a petrol/ tank.

METHODOLOGY

Use MATLAB to develop the Simulink mathematical model that based on powertrain traction force and power that needed by the electric motor to counter the resisting force (Aerodynamic Drag, Tire rolling resistance, Inertia resistance and gradient resistance) that resist the skateboard to motion VBOX RACELOGIC are used for measuring the speed and position of moving vehicle.

It was based on a range of high performance GPS receiver. Besides, VBOX data loggers can record high accuracy GPS speed measurements, distance, acceleration and position (also height above mean sea level) that needed for determine the skateboard powertrain parameter. By using the VBOX TOOL BOX software, velocity and gradient profile of the route would be obtain. It Purposely to simulate the real driving profile as the are changing of gradient and changing for the speed as the need to slow for bump and turn at junction.

RESULTS AND DISCUSSION

Wheel side motor drive are chosen for drive mode due characteristic that transmit power (torque) to corresponding wheel and shortening transmission. Meanwhile, engine/transmission layout are rear wheel drive for better traction than front wheel drive. Then, to get Lower rolling resistance, less wear out, flexible sidewall and more tractive radial ply tyre type are chosen.

Brushless DC motor chosen as it is more typically to drive the electric skateboard that need for long lifespan and low maintenance.

Each battery are ranked for its characteristic which is include life & cost, affecting thermal design and specific energy and energy density.

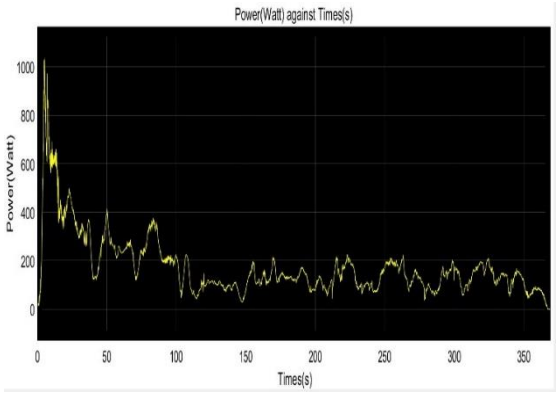

Figure 19: Power required by skateboard

CONCLUSION

But as for this research, the specification that suitable for the electric skateboard in-campus(UTM) usage is Maximum speed at 30 km/h and incline degree of 1.5˚ with rider weight of 66.64 kg. Use Radial ply tyre type with rear wheel drive (wheel side motor drive). Driven by 1 Brushless motor drive at side of wheel using belting with reduction ratio of 2.2:1 and powered by by1550 watt HGLRC0_Flipsky 5065 motor that supply power by 6 Battery LiPo, 5200mAH connected in series (1S6P). Lastly , this electric skateboard weight is 7.95 kg with 4.5 kg battery and 0.45 motor.

REFERENCES

[1] Viswabharathy, P., Boobalan, P., & Wingston, M.A. (2017). Design and fabrication of electric skateboard for off road Application. International Journal of Emerging Technologies in Engineering Research (IJETER), 5(3),1.

DESIGN AND SIMULATION OF SIX DEGREE OF FREEDOM DRIVING SIMULATOR RIG

Khasnor Iskandar Khairul Anwar and Mohd Azman Abbas
School of Mechanical Engineering, Faculty of Engineering,
Universiti Teknologi Malaysia, 81310 UTM Skudai, Johor, Malaysia.

INTRODUCTION

A motion simulator has many applications with its usage growing into various purposes. Among these usages includes flight simulator and driving simulator. With the motion simulator becoming more complex and its usage more significant, the cost to build one depending on its area of usage. Currently a complete motion simulator is not available in Malaysia. Therefore, the cost to buy one of it is very expensive. In addition, the motion simulator is huge and heavy that limit the mobility of it. Plus, it comes with many parts that make it complex. The simulator can be either fixed-base or can create motion feeling by using systems which simulate the normal vibration experienced while driving [1]. The aim of this project is to design a 6-DOF rig model that suitable for driving simulator.

METHODOLOGY

Development of 6-DOF driving simulator rig begins with brainstorming by accumulate all the knowledge about 6-DOF driving simulator. The knowledge will be interpreted into the conceptual design draw by hand sketching. All the conceptual design had been summarized and evaluation in morphology chart. The morphology chart enables the designer to integrate components from distinct design concepts into single final design based on preference. The component of the following conceptual designs was incorporated into a single final design and CAD drawing is develop by using Solid Works 2018. The final design will be analysing on structural analysis so, we know when this product will be failed under certain condition. MATLAB/ Simulink is use to simulate the workability of the final product.

RESULTS AND DISCUSSION

The motion platform model is simulated on different movement which are the normal or idle state, forward 10° and 20° tilt and left-side 10° and 0°. The force will act on top of the upper platform as all the cabin components and the motion platform user will be there. The force acting is set to be 255kg which is about 2501.55kN. Figure 1 and Figure 2 shows the testing result.

Figure 1: Result simulation on stress of motion platform when tilt left-side 10°

The inverse kinematic analysis simulation is done by using MATLAB/ Simulink. This analysis is to see whether the motion platform can move properly or not.

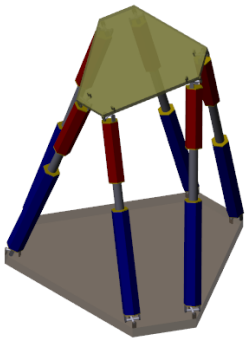

Figure 2 : Simulated Platform at Y angle 20 degree ($\beta = 20°$)

The simulated platform also shows that when the rear actuators pulled the upper platform down and the rest pushed the upper platform upwards, pitching movement was produced

REFERENCE

[1] Blana, E. (1996). Driving simulator validation studies : A literature review. White Rose Research Online. ITS Working Papers, 69

SIMULATING THE MALAYSIAN ACTUAL DRIVING CONDITION AS A REFLECTION TO REAL-DRIVING EMISSION TEST

Muhammad Nazmi Bin Md Shariff and Mohd Azman Bin Abas
School of Mechanical Engineering, Faculty of Engineering,
Universiti Teknologi Malaysia, 81310 UTM Skudai, Johor, Malaysia

INTRODUCTION

RDE test measures the pollutants emitted by cars while driven on the road. RDE does not replace the Worldwide harmonized Light vehicles Test Cycles (WLTC) laboratory test, but complements it. RDE ensures that cars deliver low emissions over on-road conditions. Since the RDE test is conducted on public roads open to traffic, there are requirements set by the EU to make sure that the test trips cover a wide range of driving conditions typically encountered by European drivers, in this study case, Malaysian drivers. RDE trips cover three types of operation which are urban, rural and motorway. These classifications are based purely on speed [1].

METHODOLOGY

Before any route selection is done, it is important to identify the area of urban, rural or motorway. Then road route selection is crucial to identify and categorize the level of traffic flow condition from a congested zone to a free flow zone. Pre-route selection was carried out by referring to the Goggle Map's live traffic where to determine the congested route and its peak hour helps in comparing the condition of the routes from time to time

The speed-time data was collected using onboard measurement technique. Onboard measurement is a method where the driver will drive a spark ignition car along the selected route to collect the data. To construct a precise RDE test, this technique should be repeated to obtain a huge number of data [2].

RESULTS AND DISCUSSION

The data was collected continuously starting from highway and then rural and end in urban area. Figures 1 gives an overview of the speed characteristics of the overall trip RDE test. From table 4, the overall trip took around 3965 seconds or 66 minutes with average speed of 48.8 km/h and total distance of 53.74 km. Comparisons of various drive characteristics was performed between the JB RDE and RDE test from other cities or countries. Average value was taken in each test mode (highway, rural and urban).

During peak hours, almost all highway in JB are congested because they link up directly to JB city center and points of entry or exit to the city. Even though the selected highway route is not congested but the traffic volume is quite high resulting in the average velocity (86.611 km/h) lower than the desired RDE requirements (above 90 km/h).

For urban are, the traffic volume is not high as expected. All the stops are mainly from traffic lights and only a few from stopping traffic. This leads to stable traffic flowing. Resulting in high average speed (28.627 km/h, RDE average speed between 15 and 30 km/h) and the stop periods for at least 10% of urban driving time is not achieved (5.62%).

JB rural trip is the only trip where the data collected meet the RDE requirements for rural trip. This can further be proven based on the rural comparison between Johor Bahru rural trip and ARTEMIS rural trip. This shows that only the traffic condition in Johor Bahru rural area suitable for RDE test.

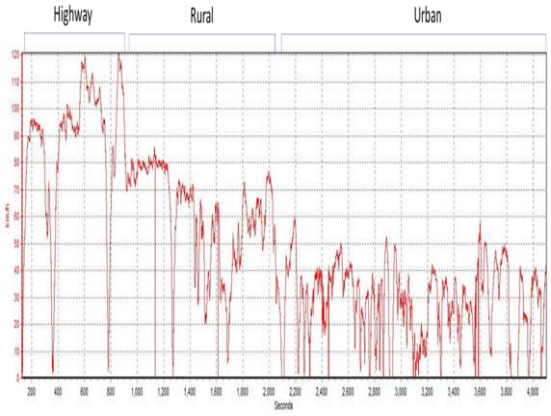

Figure 1: Overall trip speed vs time graph

CONCLUSION

Due to data variations in constructing the RDE test, the selected ideal routes in Johor Bahru to perform RDE data collection does not meet with the established standards and requirements by the Europe Union's RDE.

REFERENCES

[1] Commission Regulation (EU) 2016/427 (2016) 'Amending Regulation (EC) No 692/2008 As Regards Emissions From Light Passenger And Commercial Vehicles (Euro 6)', *Official Journal of the European Union.*

[2] Gamalath I, Fernando C, Galgamuwa U, Perera L and Bandara S. (2014) 'Methodology to develop a driving cycle for a given mode and traffic corridor', *case study for Galle Road, Colombo, Sri Lanka.*

3 DIMENSIONAL SIMULATION INTAKE FLOW PORT ON MOTORCYLE CYLINDER HEAD TO INCREASE ENGINE PERFORMANCE

Luqman Othman and Mohd Azman Abas
School of Mechanical Engineering, Faculty of Engineering,
Universiti Teknologi Malaysia, 81310 UTM Skudai, Johor, Malaysia

INTRODUCTION

Cylinder head intake port modification is one of the part in motorcycle engine that can produce a big impact once it is done. But also depending on the variables changes such as throat diameter, wall surface and air flow intake flow port is basically a passage for the fresh air from the outside entering the cylinder head towards the combustion chamber. By this way CFD simulation provides the fluid velocity and pressure throughout the solution domain with complex geometries and boundary conditions. [1. 2].

SIMULATION SETUP

For this research we will convert from CAD drawing into the Ansys software to detect is as a model drawing. But Ansys only detect the model if it is a solid shape thus the software will automatically change it to the flow model

The base model and data is calculated based on the formula above and we can get the overall information for the modification steps. Modification include the change of throat diameter, surface polishing and straight layer modification.

RESULTS AND DISCUSSION

The 3 dimensional intake port cylinder head is finally achieved and the data obtained from the simulation is approved. Even the motorcycle engine is categorizing as a small engine but it produces higher output as it carries a small load. The aims of this research were to gain an improved understanding of the flow through a restricted intake manifold. Overall, air is a very critical to control on all over the place. Their characteristic is very minimal but affecting huge amount on the engine performance. Increasing the air velocity will produce a high value of mass and volume flow rate but instead of that we also need to ensure that the intake port can support the air flow movement.

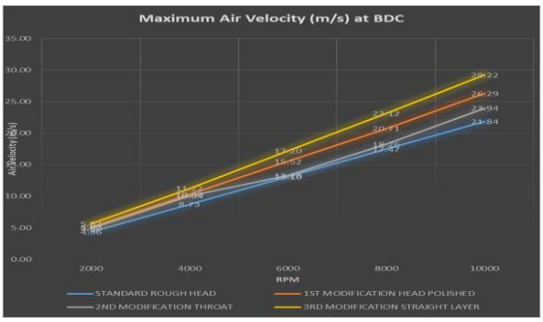

Figure 1: The air flow velocity in graph comparison

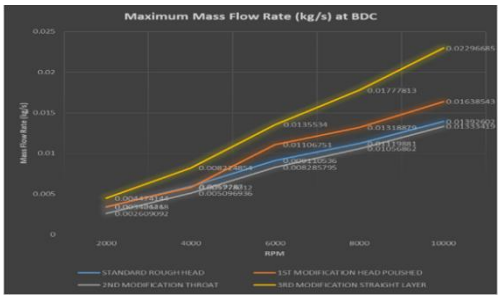

Figure 2: The mass flow rate in graph comparison

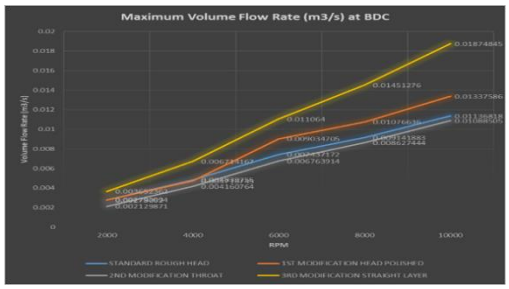

Figure 3: The volume flow rate in graph comparison

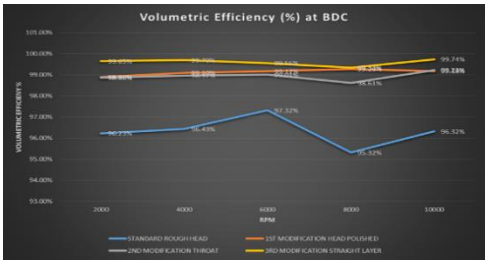

Figure 4: The volumetric efficiency rate in graph comparison

CONCLUSION

Their characteristic is very minimal but affecting huge amount on the engine performance. Increasing the air velocity will produce a high value of mass and volume flow rate but instead of that we also need to ensure that the intake port can support the air flow movement.

REFERENCES

[1] Kadir, M. T. B. A. (2008). Intake Port Flow Study on Various Cylinder Head Using. Intake Port Flow Study on Various Cylinder Head Using Flowbench.

[2] Khan, M. M., & Salim, S. M. (2013). Evaluation of CFD Sub-Models for the Intake Manifold Port Flow Analysis. 93–94.

CARBONIZATION OF PADDY STRAW FOR ELECTRICAL CONDUCTIVITY IN SUPERCAPACITOR

Muhammad Syukri Ramli and Mohd Faizal Hasan
School of Mechanical Engineering, Faculty of Engineering,
Universiti Teknologi Malaysia, 81310 UTM Sekudai, Johor, Malaysia

INTRODUCTION

The accelerating consumption of fossil fuel and the induced global warming put forward higher demand to the development of sustainable energy storage techniques. Energy storage is a critical component of the infrastructure for sustainable energy. Supercapacitors are one of the most vital developments in the field of energy storage and conversion with high power density, fast charge and discharge rate, and long service life. The performance of supercapacitors mainly depends on the electrode material and its structure. As electrodes, carbon materials have the following advantages: high specific surface area, tunable pore size and structure, high electric conductivity, strong mechanical property, and easy to get. However, high-quality carbon materials are hard to synthesize and too expensive for massive production. Therefore, it is crucial to explore high-efficient and environmental-friendly methods to prepare high performance carbon materials with sustainable and low-cost precursors.

RESEARCH METHODOLOGY

In this project, pretreated paddy straw with distilled water (H^2O) or sodium chloride (NaCl) have been used. The carbonization temperature are being varied from 400^{O}C to 800^{O}C with constant heating rate (8^{O}C/min) and continuous flow of nitrogen gas (2ml/min). The heating period also being varied between 3 hours and without any.

There are three types of analysis being tested on the carbonized paddy straw, which are SEM images analysis, CHNS Test analysis and Mass Loss analysis.

RESULTS AND DISCUSSION

CHNS Test to discover the percentage of Carbon, Hydrogen, Nitrogen and Sulphur element in paddy straw. Based on the result shown in Fig. 1, it is proven that carbon are major mass percentage in paddy straw.

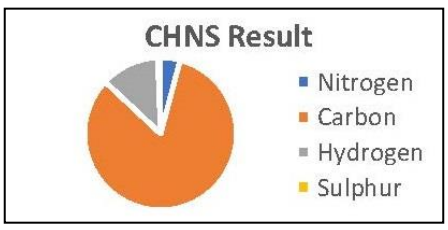

Figure 1: CHNS Result (mass percentage)

Next, mass loss are determined after carbonization of bed furnace process. The significant of this mass loss are to determine the impurities and other element are burned and left the samples with total carbon content left. The result shown in Fig. 2 shown an interesting data that, pretreatment of Sodium Chloride (NaCl) helped in discharge of impurities because high mass loss compared to others.

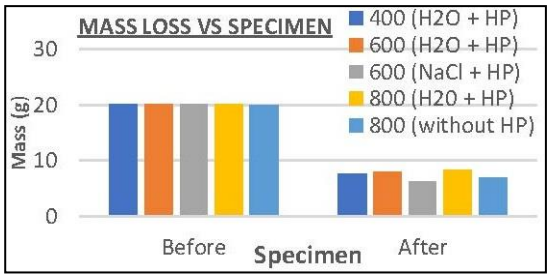

Figure 2: Mass loss against Sample

Lastly, are SEM images analysis to determine the key factor of energy storage such as pore distribution, pore size and specific surface area containing pore. 800oC carbonized paddy straw with NaCl pretreatment and heating period achieve the best condition for all key factor mentioned.

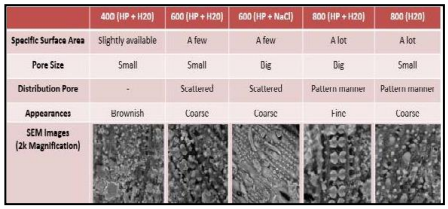

Figure 3: Summary of SEM Images analysis

CONCLUSION

It is shown that the objective is achieved as the feasibility of paddy straw to conduct electricity and store energy in supercapacitor are determined. Paddy straw have the high potential being used as raw materials of supercapacitor electrode based on the result achieved.

REFERENCES

[1] Simon P, Gogotsi Y: Materials for electrochemical capacitors. Nat mater 7 (2008)
[2] Chen M. et. all: Preparation of activated carbon from cotton stalk and its application in supercapacitor, J. Solid State Electrochemical 17 (2013)

TORREFACTION OF PALM KERNEL SHELL BRIQUETTES WITH NATURAL BINDER FOR VARIOUS TEMPERATURES

Zaitul Nadiah and Mohd Faizal Hasan
School of Mechanical Engineering, Faculty of Engineering,
Universiti Teknologi Malaysia, 81310 UTM Skudai, Johor, Malaysia

INTRODUCTION

Densification process can be defined as a compression process of pulverized biomass waste to produce a briquette biomass of uniform shape and sizes, while torrefaction is a thermal process to improve biomass characteristic by converting into a coal-like material. Due to abundant of biomass waste produced year-by-year, it will waste a shortage of places to store the waste. Therefore, a pretreatment needs to be done to improve the propertied of the biomass specifically palm kernel shell (PKS). Besides, previous study have conducted both process, however the torrefied briquettes at 275°C and 300°C cannot be accepted due to the significant physical destruction [1].

EXPERIMENTAL SETUP

This section presents the experimental setup for the experiment. The raw PKS were ground into a small particle and size and sieved to get homogenous size of below 500µm size. The pulverized PKS were mixed with starch and water mixture as binding agent. The ratio of the binding agent was 20:80 while the ratio of the mixture PKS and binder was 60:40. Then, the mixture of PKS and binder were continuously compressed under 7MPa for 30 minutes. After leaving the briquettes for 10 days under ambient temperature, torrefaction process continued. The briquette was place in the torrefaction reactor and the type-K thermocouple sensor is set between 1 cm to 2 cm from the briquette. The temperatures used in this study were 225°C, 250°C, and 275°C and the residence time was 30 minutes. The nitrogen flow rate was set to 1000 ml/min.

RESULTS AND DISCUSSION

Before undergoing torrefaction process, a preliminary test for raw pulverized PKS was done. During this test, calorific value and proximate analysis were determined. From the experiment, the calorific value obtained is 17.88 MJ/kg, which fulfil the minimum requirement stated by DIN51731 (>17.5MJ/kg). For proximate analysis, the value for moisture content and ash content were 6.75% and 4.36% respectively. As stated by the international standard, the required percentage for moisture content and ash content of solid bio-fuels were <10% (EN 14774-3) and <5% (ISO 18122) respectively. Therefore, the values obtained from the experiment meets the standard requirement.

In term of physical properties, the torrefied briquettes could maintain its shape and the color become darker with an increase in torrefaction temperature. The density for briquettes before undergoing torrefaction was higher than torrefied briquettes. After torrefaction, the density and mass yield increases while the compressive strength of the briquettes decrease with an increase in temperature.

In term of combustion properties, the calorific value for torrefied briquettes was higher than raw PKS. Based on figure 1, after torrefaction, the moisture content and volatile matter were lower than raw PKS while ash content and fixed carbon content were higher than raw PKS. Furthermore, when the torrefaction temperature was increased, the moisture content, ash content and fixed carbon content were increased while the volatile matter was decreased. In addition, all the values obtained were fulfil the minimum requirement as stated by international standard.

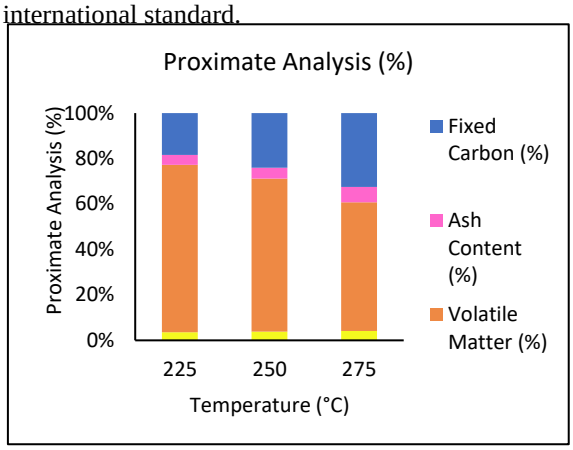

Figure 1: Proximate analysis

CONCLUSION

The combination of palm kernel shell and natural binder increase the compressive strength of densified PKS and the calorific value for torrefied briquette is increase with an increase in temperature. Hence, the densified PKS after undergoing torrefaction have potential to develop as a solid fuel due to competitive performance after comparing with international benchmark.

REFERENCES

[1] Faizal, H. M., Hielfarith, S. S., Hairee, H. M., AriffHanaffi, F. M., Rosdzimin, A. M., Mizanur, R. M., & Latiff, Z. A. (2018). Torrefactionof ensifiedMesocarpFibre and Palm Kernel Shell.Renewable Energy,122, 419-428.

TORREFACTION OF PALM KERNEL SHELL BRIQUETTES WITH NATURAL BINDER FOR VARIOUS FEED FLOW RATES

Mohamad Muslihuddin Razali and Mohd Faizal Hasan
School of Mechanical Engineering, Faculty of Engineering,
Universiti Teknologi Malaysia, 81310 UTM Skudai, Johor, Malaysia

INTRODUCTION

Over recent years, torrefaction had been used to enhance the physical and combustion properties of a solid biofuel. Torrefaction is a form of mild pyrolysis that heat up the solid biofuels in the range of 200 to 320℃ to increase its energy content [1]. The combination of densification and torrefaction can a solution to the energy demands in these days [2]. Besides temperature, gas feed flow rate is also important to make sure the samples are torrefied at the best operating condition. In this research, nitrogen flow rate was varied from 1000 mL/min to and 3000 mL/min

EXPERIMENTAL SETUP

This section presents the experimental setup for the system. We used Palm Kernel Shell as the raw material. Raw PKS is dried, pulverized, and mix with a mixture of water and starch with a ratio of 60:40. The mixture then compressed under 7MPa for 30 minutes. The briquettes were then being torrefied under 275℃ and the nitrogen flow rate was varied from 1000 mL/min to 3000 mL/min.

RESULTS AND DISCUSSION

After the torrefaction, physical properties and combustion properties of the PKS were analysed. Based on the physical properties, all briquettes became darker after torrefaction and the density were reduced. However, various nitrogen flow rate does not affect the density significantly. The briquettes were loss in weight due to the release of vapor-gas during torrefaction. At 1000 mL/min, the loss in weight was at the highest (14.814g). From the proximate analysis shown in figure 1, the moisture content after torrefaction was reduced especially at 1000 mL/min (from 6.21% to 4.28%). The moisture content decrease as the nitrogen flow rate decrease. Volatile matter does not have any correlation with the various nitrogen flow rate. However, the volatile matter reduced for all operating conditions after torrefaction. The fix carbon in the samples were increased dramatically as the lower nitrogen flow rate were used. 1000 mL/min had the highest calorific value which was 34.20%. The calorific value of the samples increased to maximum of 24% at 1000 mL/min when compared with raw PKS. The compression strength data showed that the various nitrogen flow rate do not effect its durability. However, overall the compressive strength of densified PKS increased after torrefaction. The properties of torrefaction of densified PKS had been compared with international standard. Compared with DIN 51731, all samples fulfil all the requirements except for the ash content where the minimum is 0.7%. All samples have relatively high of ash content when compared to the IS0 18122. This is because of mineral components that do not change whereas the mass yield reduces causing the ash content percentage to increase.

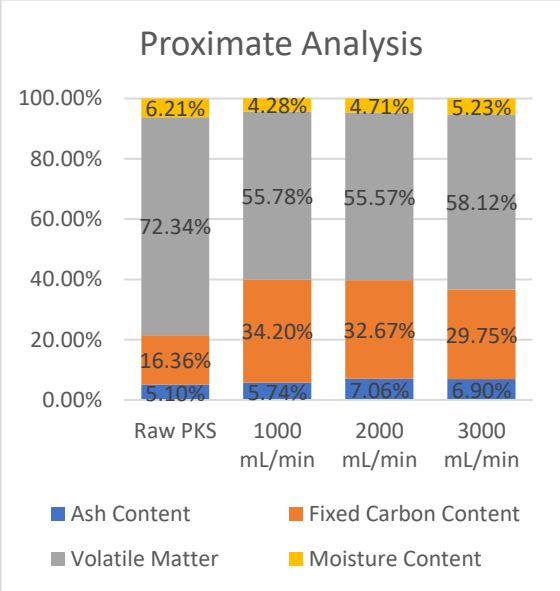

Figure 20 : Proximate analysis

CONCLUSION

We have shown that overall torrefaction can enhances the physical and combustion properties of palm kernel shell. However, the various nitrogen flow rate do not significantly changes it characteristics and can be assume negligible.

16. REFERENCES

[1] A. M. A. N. S. N. H. M. I. S. A. A. Mohammad Asadullah, "Optimization of palm kernel shell torrefaction to produce energy densified bio-coal," *Energy Conversion and Management*, pp. 1086-1093, 17 May 2014.

[2] A. A. A. J. T. A. O. O. B.B. Nyakuma, Torrefaction of pelletized of oil palm empty fruit bunches, Gwangju, Korea: 21st International Symposium on Alcohol Fuels, March 2014.

CONSTRUCTION OF JOHOR DRIVING CYCLE FOR DETERMINATION OF VEHICLE FUEL CONSUMPTION

Nur Shaziera Zaharri and Mohd Farid Muhamad Said
School of Mechanical Engineering, Faculty of Engineering,
Universiti Teknologi Malaysia, 81310 UTM Skudai, Johor, Malaysia

INTRODUCTION

Driving cycle is a series of data collection to produce a graph of speed against time which developed by collecting a result from test driving where additional instructions and conditions may be applied [1]. Driving cycle can leads to analysis of vehicle performance which are vehicle fuel consumption and pollutant emissions. Generally, driving cycle is different at each region because the road categories, time conditions, driving characteristics, type of vehicle and speed phases [2]. There are two part of driving cycle which are legislative cycle and non-legislative cycle. Non-legislative cycle mostly used in research while legislative cycle is the approval test for vehicle emission certification.

OBJECTIVE

The purposes of this project are to develop a MATLAB code for data analysis of on-road vehicle speed data collection, to construct Johor Driving Cycle using developed MATLAB code and to compare vehicle fuel consumption performance at different driving cycle. In addition, the construction of JDC is the continuity of Malaysia Driving Cycle to support government initiatives that have been conducted by collaboration of MARii and Proton on fuel economy development.

EXPERIMENTAL SETUP

The data used for this construction of JDC is taken from monthly progress report for Malaysia Driving Cycle. Data analysis is based on WLTC methodology which involves smoothing, re-sampling and segregation. It is performed by using a suitable code that running the data in MATLAB software. A code is produced into a semi-automatic data analysis that consist of coding for filtering, re-sampling and thinning as the procedure to generate test cycle. Chisquare analysis is performed using Excel to find the least chi-square for the combination of MT. Micro-trip is a vehicle speed that begins and ends with zero speed [3]. Combination of MT must within their speed phases duration which is 492 s for each group and MT below 10 s are eliminated. Small chi-square means that the observed data is fit well with expected data. For construction of JDC, the analysis is compared up to 10 combination of MT for low, medium and high because time limitation. GT-Suite is used to determine vehicle fuel consumption and then it is compared at different driving cycle which is NEDC, WLTC and JDC-V1.

RESULTS AND DISCUSSION

Coding that have been produced for construction of JDC is semi-automatic coding which means that the coding only runs data process for each file at one time but data smoothing and re-sampling can be done both. MATLAB code includes process of data smoothing, data resampling, data segregation and elimination of data. A final JDC is successfully being develop from MATLAB code and chi-square analysis using Excel as shown in Figure 1.

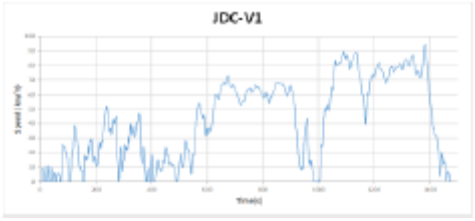

Figure 1: Speed Profile of final JDC-V1

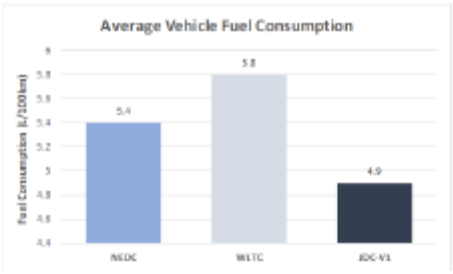

Figure 2: Comparison of average fuel consumption

Figure 2 shows that each driving cycle will produce different fuel consumption depending on many factors such as driving behavior, topography, road categories and time conditions. Therefore, it is important for each country to have their own driving cycle that will represent their own standard driving behaviour which is more effective and accurate.

REFERENCES

[1] Grüner, J. and S. Marker, A Tool for Generating Individual Driving Cycles - IDCB. SAE International Journal of Commercial Vehicles, 2016. 9(2).
[2] Chugh, S., et al., Development of Delhi Driving Cycle: A Tool for Realistic Assessment of Exhaust Emissions from Passenger Cars in Delhi, in SAE Technical Paper Series. 2012.
[5] Mayakuntla, S.K. and A. Verma, A novel methodology for construction of driving cycles for Indian cities. Transportation Research Part D: Transport and Environment, 2018. 65: p. 725-735.

DEVELOPMENT OF WATER SAMPLING DEVICE FOR UNDERWATER REMOTELY OPERATED VEHICLE (UROV) APPLICATION

Nur Syahirah Basri and Mohd Farid Muhamad Said
School of Mechanical Engineering, Faculty of Engineering,
Universiti Teknologi Malaysia, 81310 UTM Skudai, Johor, Malaysia

INTRODUCTION

Simplistically, an UROV is a camera mounted in a waterproof enclosure, with thrusters for manoeuvring, attached to a cable to the surface over which a video signal is transmitted [1]. Due to the chemical content, pressure of water, and oxygen level at underwater, the UROV help to overcome these human limitations that can bring danger to the divers. Sometimes, the UROV are also equipped with water sampler device and manipulator arm in order to perform biological and engineering works. Throughout the years many divers, including Canadian Forces (CF) divers, have gotten sick as a result of exposure to contaminated water [2]. In order to detect and avoid pollutant of water, the attached water sampling device act as a searching tool which identify as a biological sampling.

METHODOLOGY

This section presents the process method in the project. This project is involving design and control of system. Some ideas are sketch based on the requirements and being evaluated using quantitative selection matrices method. The selected design is analysed by using SolidWorks in term of structural and flow analysis. Next, fabrication process is done and the Arduino UNO is used to control the water sampler which is coded using Arduino software. The water sampler is integrated to the UROV and then the ability and functionality of the water sampler device is tested at 5m depth at underwater in a swimming pool.

RESULTS AND DISCUSSION

At the end of fabrication and installation process, the water sampler device is given several tasks to test its ability and functionality. The device consists of a water pump, a valve controlled by servo motor and two separate water sample bottles. From the structural analysis on the copolymer water bottle, the bottle can withstand underwater pressure up to 40m depth which the von Mises stress is 10360kPa which is lower than the material yield strength which is 27600 kPa. The completed device is tested for its capability to take water sample. The real mass flow rate of the water pump is 0.0087 kg/s as obtained from first testing. From the second testing, the average time taken to fill up 200ml of bottle is 30.29s. Figure 1 shows the water sampling device is tested in a basin and Table 1 shows the result from the testing. At within 5m depth, the water pump is able to take water sample. However, some leakage occurred due to the different pressure at underwater.

Figure 1: The water sampler being tested in a basin at vertical position

Table 1: The Time Taken to Fill up 200ml bottle

Observation	Duration (sec)		Total Duration (sec)
	Sample 1	Sample 2	
1	31.23	31.62	62.85
2	30.47	29.13	59.60
3	29.13	22.49	51.62
4	33.99	34.20	68.19
Average	**31.21**	**29.36**	**60.57 For 200ml: 30.29**

CONCLUSION

In conclusion, the water sampler device is able to operate at underwater to take water samples and the structure will not fail within 20m. The device is able to design and build to be integrated to the UROV for underwater application.

REFERENCES

[1] Christ, R.D.a.W., R.L., Underwater Vehicle, in Maritime engineering reference book. 2017, Butterworth- Heinemann: Oxford, UK. p. 731.
[2] Quémerais, L.N.B., Diving in Contaminated Water: Health Risk Matrix October 2006, Defence R&D Canada – Toronto: Canada.

DEVELOPMENT OF AERATOR FOR WATER SAVING

Muhammed Zakariya Bin Hasnol and Mohd Faridh Bin Ahmad Zaharuddin
School of Mechanical Engineering, Faculty of Engineering,
Universiti Teknologi Malaysia, 81310 UTM Skudai, Johor, Malaysia

INTRODUCTION

According to Mc Kinsey,2009 said that there is a report estimating that global water production will increase from 4500 billion m3/ year to this day 6900 m3/ year by 2030 [1]. Nozzle have been used in many applications due to control the size of distribution of droplets, increased possibilities for energy and wide spread in size and form [2]. The operation of development is based on existing aerator in market where it requires nozzle such design transform into aerator water saving. Water discharge present a consistent with the solid-cone nature of the spray with the large droplets [3]. This report describes the development of the spray aerator, the water saving design.

EXPERIMENTAL SETUP

There are three stages starting with first development, improvement the product and final product. By comparison of water discharge, usage percentage and reduction percentage we plot the graph. accordance the recommended chart: bar chart and line chart. For development from stage 1, will be used to get the reference reading.

The stage 3 that will be used as final product for this development This study analyzed using simulation that relative to pressure and velocity. There are numbers of consumer in order to test the water flow, perform ablution and data collection using questionnaire. For questionnaire purpose which is to receive the measuring satisfaction data from consumer.

RESULTS AND DISCUSSION

Figure 1 shows the performance on usage and reduction percentage where it from stage 3 and this is final product that serves as the devices for water spray saving aerator while Figure 2 shows line graph of water discharge of the performance aforementioned above. Generally, even though these aerators had same size but different in value, yet get better result to show.

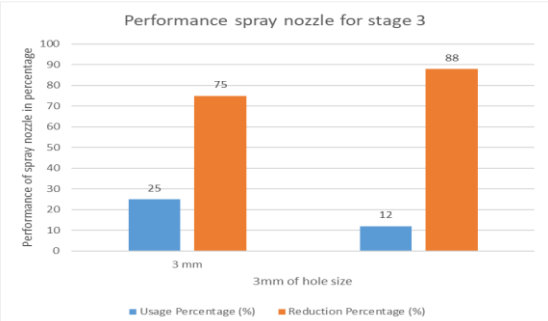

Figure 1: The bar chart of comparison of the performance result with different 3 mm hole size.

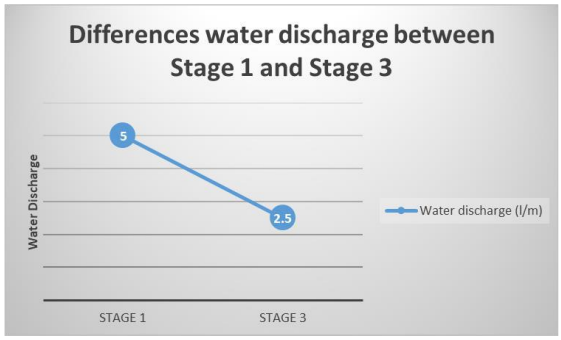

Figure 2: The differences of water discharge

CONCLUSION

In conclusion, an aerator does help improving and provides optimal water flow, and could reduce water consumption. Based on experimental findings, it can be said that the best design adjustment and configuration on the scope given for aerator to be most efficient is at 3mm hole of aerator with set of 1-2 bars

REFERENCES

[1] Hoekstra, E.E (2013). Water footprint scenarios for 2050: A global analysis Environment International, 71-82.
[2] Van Deventer, H., Houben, R., & Koldeweij, R. (2013). New Atomization Nozzle for Spray Drying. Drying Technology, 31(8), 891–897.
[3] A.H Lefebvre, (1989) Atomization and SprayHemisphere, Washington, DC, USA

ERGONOMICS DESIGN OF AN ASSISTIVE BED FOR PEOPLE WITH DISABILITIES

Mohammad Safwan Hasnan and Mohd Firdaus Mohd Taib
School of Mechanical Engineering, Faculty of Engineering,
Universiti Teknologi Malaysia, 81310 UTM Skudai, Johor, Malaysia

INTRODUCTION

Hospitals in Malaysia have started to utilize the benefits of a high technology advanced bed. These hospital beds often imported from the technological nations including United States and the Japan for an expensive prices. This will increase in bed cost and then will affect the hospital fee for quality healthcare. This research analyse the existing models of hospital beds that have in Malaysian hospital and to reduce the cost and improve the functional mechanism for ergonomic purpose. We will also survey an old folk homes manager in Malaysia to determine additional features that could be useful in a modern hospital bed and then begin the design process. The objective of this research is to study the suitable mechanism of hospital bed for paralyzed elderly and to design an ergonomic hospital bed for paralyzed elderly.

METHODOLOGY

In order to get the quality design some site visit has been conduct before starting the assistive bed design. The location of the site visit is at Nur Ehsan Homes in Johor Baharu. All interview, observation and data collection have been done by the site visit. After data was collected, all the data is present in table and chart. This will make more easily to read the data. All the table and chart was separate by types of elderly and aged. In order to brain storm the objective of this design, the cause and effect diagram was illustrate in order to generate more ideas. Other than that, quality function deployment also has been conduct in order to find out the needed of the caregiver and identify the existing products.

Result from the brainstorm has come out of product design specification. Basically the product design specification has three criteria which are performance, maintenance and ergonomics. Some of the emphasis from the performance is the ability of the bed can assistive the caregiver in handle paralyzed elderly. For ergonomics, the consideration is the comfortable for both paralyzed elderly and caregivers while using the assistive bed.

RESULTS AND DISCUSSION

17. From Figure 1 show the design with the human model beside bed in isometric view. The height of the human model is suitable with the height of the bed and can easily for the elderly to use the bed. The length and the width of the bed are huge and ergonomic for the elderly while in the bed.

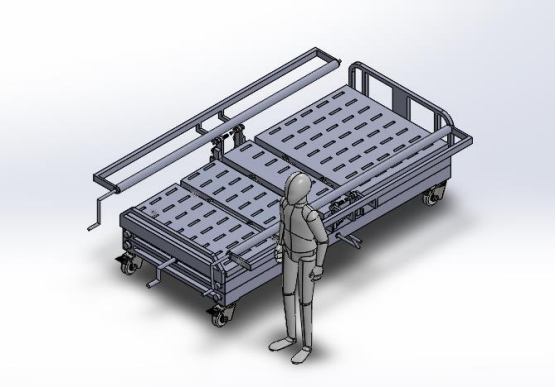

Figure 1: Ergonomics View

CONCLUSION

Through the completion of this design project we have conclude that there is a way to improve the hospital bed for the paralyzed elderly. However in designing the mechanism of the features, we also need to consider the comfortable for caregiver too. Other than that this beds is hopefully can comfort for both caregivers and elderly in daily life.

REFERENCES

[1] Mohammed, M. N. (2012). A New Design of Multifunctional Portable Patient Bed demanding from Patient and Caregivers.
[2] Resnick, M. L. and Chaffin, D. B. 1995. An ergonomic evaluation of handle height and load in maximal and submaximal cart pushing.
[3] Rogers, A. E., Hwang, W. T. Scott, L. D., Aiken, L. H. and Dinges D. F. (2004). The working ours of hospital staff nurses and patient safety.

QUALITY IMPROVEMENT IN SHIP TO STORE (STS) PARTS IN BUCHER EMHART GLASS SDN BHD

Nur Aliyah Dzulkarnain and Mohd Firdaus Mohd Taib
School of Mechanical Engineering, Faculty of Engineering,
Universiti Teknologi Malaysia, 81310 UTM Skudai, Johor, Malaysia

INTRODUCTION

The case study is done at Bucher Emhart Glass Sdn Bhd. This company is located at Ulu Tiram, Johor. The main activity of this company is assembly and supplying forming machine which produce glass bottles or jars to the manufacturing company throughout the world. They are manufacturing Individual Section (IS), Advanced Individual Section (AIS) and AAP forming machine. Most of the parts which will be assemble are made by their suppliers. The incoming parts will undergo inspection by sampling. The quality inspectors are responsible to inspect the parts within 4 days. In order to improve the quality of the movement parts from store to production line. They have categorised the parts into two label which are regular parts and ship to stock parts. The main focus of this case study is ship to stock parts. Element of Quality Functional Deployment (QFD) fourth phase is use because it can control the product characteristics and the associated process variables to ensure capability and stability of the product over time [1].

EXPERIMENTAL SETUP

Data gathered are using observation and discussion. Basically, the data collection was the monthly report composition of deviations in Bucher Emhart Glass, number of deviations by every supplier for regular and Ship to store (STS) parts, number of deviations for every supplier and amount of cases by every supplier.

RESULTS AND DISCUSSION

This project is completed by using DMAIC analysis which are define, measure, analyse, improve and control. Firstly, the problem identification is being identified through the define phase. In the define phase, the problem statement of the project is higher composition percentage of deviations reports from internal (66%) which production floor for ship to store (STS) parts compared with regular parts. Therefore, the project will be focus on the ship to store (STS) parts. Then, the SIPOC diagram is used to identify all relevant elements of a process improvement project before work begins [2]. It also helps define a complex project that may not be well scoped, and is typically employed at the measure phase of the Six Sigma. Next, the analyse phase which by using graphical analysis. There some breakdown of data had been done. Based on the analysis, it shows 3 critical suppliers are Gain Mirage, Gah Hong and CFM shows the highest deviation for both parts which is regular and ship to store (STS) parts. The consideration of more on ship to store (STS) parts.

Next, the improvement plan has divided into two parties which are Bucher Emhart Glass and three critical suppliers. In the improvement phase, the action plan had been developed by using theoretical of Quality Functional Deployments (QFD) fourth phase. The action plan develops by Bucher Emhart Glass and suppliers. Next, the control phase. This is the part where the monitoring data will be shown after the improvement had been done. The data will be comparing from the first phase which are on October 2018 until December 2018 and second phase which are January 2019 until March 2019. The data will be comparing the performance of the supplier on first phase of 2018 and second phase of 2019. The theoretical believe when the performance of the supplier improves thus the quality of the part will be improved.

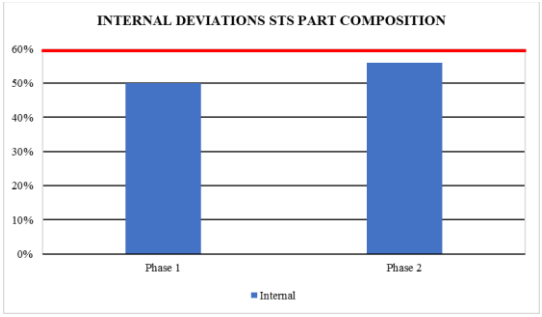

Figure 1 : Percentage of internal deviations for STS parts found on production floor

CONCLUSION

The objectives of the project achieve the reduction percentage of 40% deviations found on the production floor on first and second phase of the project.

REFERENCES

[1] Akao, Y. (1990) Quality Function Deployment: Integrating Customer Requirements into product design, G.H Mazur (trans) Cambridge, M.A: Productivity Press.

[2] Juran, J.M. (1986) The quality trilogy: a universal approach to managing for quality, Quality Progress, 19, pp. 19- 24.

AN APPLICATION OF DESIGN OF EXPERIMENT FOR OPTIMISATION OF LOW FREQUENCY CARD YIELD

Nicholas Soo Xin Ming and Mohd Firdaus bin Mohd Taib
School of Mechanical Engineering, Faculty of Engineering,
Universiti Teknologi Malaysia, 81310 UTM Skudai, Johor, Malaysia

INTRODUCTION

In this fast-paced world, the competition between manufacturing firms has been ever growing more intense and vigorous. Nowadays, most firms optimise their processes to obtain better efficiency in production and improvement in quality. Quality improvement can be achieved through a systematic approach called design of experiment. DOE is a powerful data collection and analysis tool that can be used in a variety of experimental situations. It allows for multiple input factors to be manipulated, determining their effect on a desired output (response). By manipulating multiple inputs at the same time, DOE can identify important interactions that may be missed when experimenting with one factor at a time. All possible combinations can be investigated by using full factorial design.

EXPERIMENTAL SETUP

This section presents the experimental setup for DOE. Cause & effect analysis is conducted to identify the root cause of yield loss in low frequency (LF) cards. The lamination process of LF cards is studied and analysed. The design used for the experiment is 2^3 full factorial design. 3 parameters are tested at 2 levels. After identifying the factors and design, the response of the experiment count of cards without flakes is chosen. Heating temperature, heating pressure and heating time are the main factors in this study.

RESULTS AND DISCUSSION

Analysis of variance is carried out and the significance of the main factors are identified. None of the factors have significant effect on the response, count of cards without flakes. However, there is still effect from the main factors on the response but insufficiently significant. The highest effect from the main factors is heating temperature.

The main effects and two-way interaction effect of the factors are analysed and plotted in graph. From the plot, the optimum setting that result in highest yield is identified. The heating temperature is 175°C, heating pressure is 230N/cm^2 and heating time is 10 mins at optimum setting. A validation run is carried out to confirm the accuracy and validity of the setting and is found out that the setting is optimal with deviation in comparison of only 2.92%.

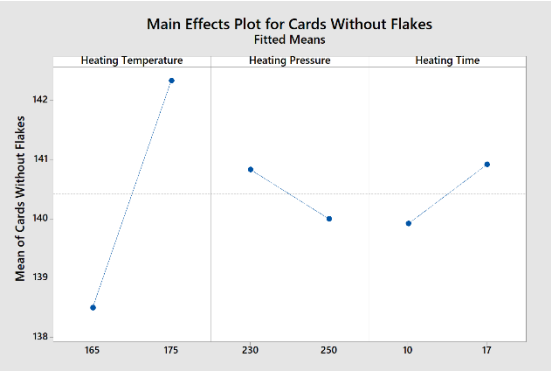

Figure 1: Main Effects Plot for Cards Without Flakes

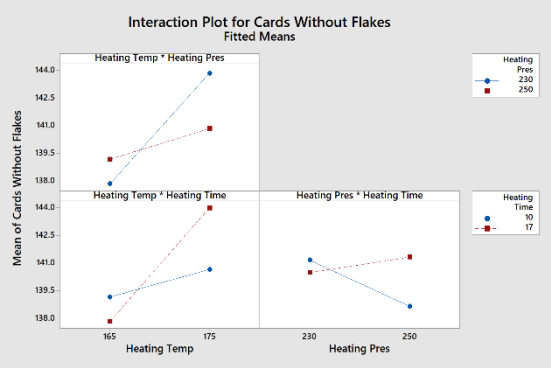

Figure 2: Interaction Plot for Cards Without Flakes

CONCLUSION

The yield of low frequency card is successfully improved with the suggest optimum setting. However, the main factors chosen is has no significant effect on the response variable. Future study is required to identify the significant factors affecting the yield.

REFERENCES

[1] Antony, J. (2001). Improving the manufacturing process quality using design of experiments: a case study. Emerald Insight, 1-14.

[2] Dowlatshahi, S. (2004). An application of design of experiments for optimization of plastic injection moulding processes. Journal of Manufacturing Technology Management.

[3] Jiju Antony, M. H. (1999). Reducing manufacturing process variability using experimental design technique: a case study. Emerald Insight, 1-10.

ERGONOMICS IMPROVEMENT IN FOOD INDUSTRI

Mohamad Afiq Roslan and Mohd Firdaus Mohd Taib
School of Mechanical Engineering, Faculty of Engineering,
Universiti Teknologi Malaysia, 81310 UTM Skudai, Johor, Malaysia

INTRODUCTION

Ergonomic assessment is a guideline for manual handling. It also referred to as workstation assessments, ensure that a worker's workstation is ergonomically designed to minimise the risk of injury and maximize productivity. This study took a tile manufacturing company as a case study. This company is located at Renggit, Johor. There are 4 stations for this company. This study focuses on the departments have more red colour of risk in HIRARC analysis that to be selected and to be suggested for control measure. The improvement is based on conceptual design assisted with functional model without real implementation.[1, 2].

METHODOLOGY

Went the case study company is selected and approve, the background of company such as the total of station and activities each station, organization chat will identified. After that HIRARC analysis every station will conducted and the station that have critical activities more red colour of risk will selected as the improvement station. The company advise also will consider. The selected critical activities in the selection station will do the ergonomic analysis that is REBA analysis. After that the control design is proposed. . Design engineering is preferred to overcome the ergonomics problem. SolidWork will be used for engineering analysis and interview will be done to Safety and Health Officer (SHO) in the company.

RESULTS AND DISCUSSION

The problem scope of work at this case study is to use manually energy. The worker needs to need to lifting the back of cassava by manually and also the peeling process will doing by manually. For the weighted process the worker need to use high required energy to lift up the basket to weight scale.

Improvement is done by create the semiauto system that combine all the activities in station A in a single system. For the problem one the loading bay will design to make the worker easy to unloading the bag of cassava from the lorry. The worker doesn't need to use more energy in loading bay. After that for the peeling process the improvement will design the peeling machine. The worker just stays on that platform to throw away the cassava inside the peeling machine. The mechanism for peel this design is use of the rotation of roller with gross brush. The cassava will fill in the machine is generated by using electric motor. The motor will drive the roller using suitable power and rotation per minutes.

The brush that wrapping the roller will remove the skin of cassava. The water will rain down in the machine is function to drop and clean the cassava skin in the machine. After the cassava finish for peel, the cassava with out with the door located beside the machine and it will fall down into the basket that located already on weight scale. This mean for the weighted process the worker did not need manually put up the basket of cassava because the backed is already on the weighted scale and ready to transfer to next station.

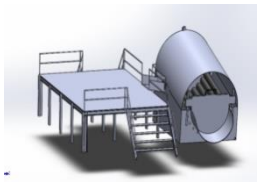

Figure 1: Isometric of Detail Full Design Using Solidwork..

CONCLUSION

The ergonomics hazards have been identified is station A of production in Azharfood manufacturing. This hazard is determined by using the HIRARC analysis and the problem will also analysis by REBA analysis ergonomic tool. A new system of station A have been proposed that is platform for unloading the cassava, peeling machine for peeling process and rearrange the location of the weight scale beside the machine. SolidWork software was used to validate the engineering design. The new design has successfully reduced the ergonomics issues of unloading and lifting the cassava is 62.5%, for the peeling process reduce 62.22% and weighted process reduce about 57.14%.

REFERENCES

[2] Ajibola, B. (2016). Design and Fabrication of a Cassava PeelingMachine. International Journal of Engineering Trends and Technology (IJETT), 42(2), 60-64.

[3] Ali, H.,Azimah Chew Abdullah, N.,&Subramaniam, C. (2009).Management practice in safety culture and its influence on workplace injury: An industrial study in Malaysia. Disaster Prevention and Management: An International Journal, 18(5), 470-477.

ERGONOMICS DESIGN OF AN ASSISTIVE DEVICE FOR DOWN SYNDROME CHILDREN

Syahirah Kamsani and Mohd Firdaus Mohd Taib
School of Mechanical Engineering, Faculty of Engineering,
Universiti Teknologi Malaysia, 81310 UTM Skudai, Johor, Malaysia

INTRODUCTION

Down Syndrome is one of the most common chromosomal disorders affected among babies. Statistically, the average rate of having Down syndrome children is around 1 in every 700 babies pregnancies [1]. As in Malaysia, there is no recent research about statistic of Down Syndrome baby born, however there is previous research state that one in 950 have been reported among the three largest ethnic groups which are Malay by 1:981, Chinese by 1:940 and Indians by 1:860 [2]. Moreover, people that have Down Syndrome typically associated with physical growth delays, characteristic facial features and also developmental delays that causes disabilities. Writing skills is one of the learning disabilities faced among Down Syndrome children.

EXPERIMENTAL SETUP

Several examples of handwriting and hand grasp of Down Syndrome children were taken. Then, implementation of Quality Function Deployment was done based on the interview then next continues with the Product Design Specifications. Morphology Chart was used to lists all the options available for every sub-functions that were required for designing a writing aid tool for Down Syndrome children. Next, evaluation process on three designs with one of the existing products was done in evaluation matrix that results in choosing Sketching B as the final design. Hand abnormalities and 8 children with Down Syndrome hand anthropometric measurements become guidance in determine the dimensions of the final design. Lastly, manufacturing process of the final design was take place in the manufacturing laboratory.

RESULTS AND DISCUSSION

Based on the anthropometric data results in Table 1, the dimensions of the final design was determined. First of all, the typical outer diameter and length of a pencil is 6 mm and 190 mm respectively. Then, the design of triangular pencil holder as a triangular pencil shaped is better and suitable as the pencil grip of Down Syndrome children. Therefore, the inner hole in the triangular pencil holder was made in 8 mm diameter so that any wooden pencil can be used. Next, the size of the triangular pencil holder was made based on the average diameter and length of the fingers and also the typical size of pencil. For the design of the tool supporter, the hole was made based on the mean of the middle finger. Then, the height of the front side of tool supporter was based on the ring finger mean and width of the pencil holder based on the thumb thickness and index finger breadth. The thumb and index finger will positioned at the pencil holder in order to hold it by using tripod grasp. The little finger positioned below the tool supporter as there is issues in hand abnormalities where there are some that faced with the curvature at the little finger towards the index finger. Materials used for pencil holder and tool supporter are Polytetrafluoroethylene or Teflon while wrist supporter used memory foam fitted braces with mild steel inside it in order to provide support to the wrist of Down Syndrome children.

Table 3: ***Anthropometric Measurement Results***

MEASUREMENTS	MEAN	STD. DEVIATION
Hand Length	15.4	0.6
Little Finger Length	4.7	0.3
Ring Finger Length	5.6	0.4
Middle Finger Length	5.8	0.6
Index Finger Length	5.7	0.5
Thumb Length	5.1	0.3
Thumb Thickness	2.0	0.1
Index Finger Breadth	1.7	0.2
Middle Finger Breadth	1.7	0.1
Ring Finger Breadth	1.6	0.1
Little Finger Breadth	1.3	0.1

CONCLUSION

Overall, the writing aid tool able to help and improve only some of the children with Down Syndrome as some of them still not familiar and uncomfortable to use it. Besides, the writing aid tool still has the advantages and disadvantages that need to be improved. Therefore, the recommended improvements are:

i. The design can be improve by try to implement new technology so it can be function automatically.
ii. The materials can also be improved by used different materials.
iii. Divide into several group according to range of ages and collect more data about the measurement and size of the hand of Down Syndrome children so there will be various measurement.

REFERENCES

[1] Crosta, P. (2017, December 6). What to Know about Down Syndrome. *Medical News Today*.
[2] Boo, N.-Y., Hoe, T. S., & Clyde, M. M. (2014). Incidence of Down 's syndrome in a large Malaysian maternity hospital over an 18 month period, (July 1989).

THERMAL ANALYSIS OF A LITHIUM-ION BATTERY MODULE BY USING THERMAL NETWORK

Amirul Rafiq Zulmahari and Mohd Ibthisham Ardani
School of Mechanical Engineering, Faculty of Engineering,
Universiti Teknologi Malaysia, 81310 UTM Skudai, Johor, Malaysia

INTRODUCTION

Lithium-ion batteries are commonly used as the power components of portable electronic devices. In Tesla's Battery pack technology, cylindrical lithium-ion cells are inserted into a battery module before being inserted into the battery pack. The electrochemical reactions inside the individual cells can develop various heat generation inside the battery pack that would cause thermal runaway when heat generated is too high, and it could not be cooled down even with cooler. The simulating method is needed to analysing each of the batteries using the thermal network and by calculating each of the cells by Matlab.

EXPERIMENTAL SETUP

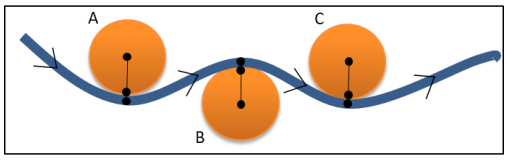

Figure 1: Nodes for Staggered Cells

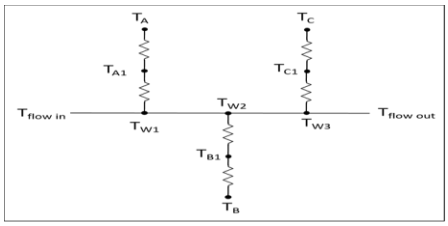

Figure 2: Thermal Network based on Figure 1

According to Noboru Sato [1], the heat generation of battery is made up from 3 components, reaction heat value Q_r, polarization heat value Q_p, and Joule heat value Q_J as the total generated heat, Q_t. For coupling the model, temperature dependent physicochemical properties, ionic conductivity of an electrolyte (k) are needed and dependence can be generally described by Arrhenius Equation. Then the heat generation model can be done by having the two as the heat generation equation, q.

$$Q_t = Q_r + Q_p + Q_J$$

$$k_e = k_{ref} \cdot e^{\left[\frac{-E}{R\left(\frac{1}{T}-\frac{1}{T_{ref}}\right)}\right]}$$

$$q = Q_t \cdot k$$

From this cooling system arrangement, we need to take a small part of it as the arrangement is similar throughout the module. The thermal nodes considering 3 cells of it and the thermal network for each of the nodes as shown in Figure 1 and Figure 2.

RESULTS AND DISCUSSION

The temperature rapidly increases due to the high heat generation. Then the temperature slowly increases almost in a constant temperature due to low heat generation and heat transfer to the liquid coolant. After a while, the temperature suddenly started to increase rapidly again.

Figure 3 also shows that cell C has a higher temperature than cell B and cell B has a higher temperature than cell A, due to the liquid coolant as temperature of the coolant increases as it passed through the cell by cell region.

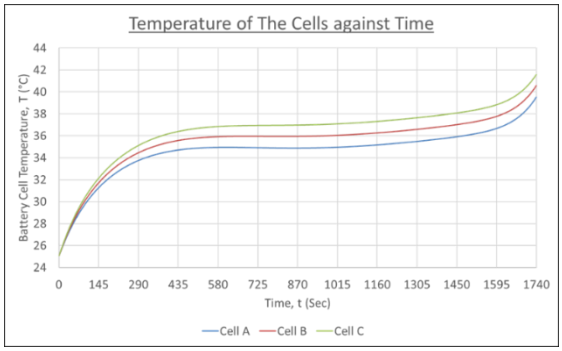

Figure 3: Graph of Cell Temperature against Time

CONCLUSION

As conclusion, the thermal analysis of lithium-ion cells in a battery module was successfully modelled. The temperature trend of the battery cells comparatively similar to the trend of the experimental result conducted by Yuqi Huang [2]. Designing the thermal network which thermally represents the thermal condition in the battery module has achieved and the thermal condition inside the battery module can be predicted.

REFERENCES

[1] N. Sato, Thermal behavior analysis of lithium-ion batteries for electric and hybrid vehicles, Journal of Power Sources

[2] Yuqi Huang, Yiji Lu, Rui Huang, Junxuan Chen, Fenfang Chen, Zhentao Liu, Xiaoli Yu, and Anthony Paul Roskilly (2017), Study on the Thermal Interaction and Heat Dissipation of Cylindrical Lithium-ion Battery Cells, 9th International Conference on Applied Energy, ICAE2017, 21-24 August 2017, Cardiff, UK.

ENERGY CONSUMPTION OF THERMOELECTRIC MODULE (TEM)

Amirul Wafiy Majeed and Ibthisham Ardani
School of Mechanical Engineering, Faculty of Engineering,
Universiti Teknologi Malaysia, 81310 UTM Johor Bahru, Johor, Malaysia

INTRODUCTION

Thermoelectric cooling works by the direct conversion from electrical energy into heat energy. However, the efficiency of thermoelectric system is very low. One of the methods to increase its efficiency is by improving the cooling mechanism at the hot side surface of the TEM [1]. Hence, the main concern of this project is to investigate the effect of different cooling mechanisms on the energy consumption of the TEM.

EXPERIMENTAL SETUP

Two types of hot side cooling mechanisms are tested which are heat pipe cooling and fan-enhanced heat pipe cooling. In the effort to study the energy consumption of the TEM, 5 power inputs are supplied to the module (TEC1-12703) which are 0.6, 4.3, 11.2, 21.2, 34.0 Watts respectively.

The experimental setup consists of an insulated compartment, cold side heat sink, TEM, and hot side heat sink. A temperature data logger is used in conjunction with K-type thermocouples to measure the temperature at six different locations.

In order to compare the effectiveness of both cooling mechanisms, five comparison are made, which are temperature at hot and cold side surfaces of the module, temperature of air inside the compartment, the amount of heat absorbed and the coefficient of performance (COP).

RESULTS AND DISCUSSION

Due to the thermoelectric cooling ability, a heat flux is induced from the air inside the compartment down towards the module, which will effectively transfer the heat energy away from the air, or form another perspective, heat energy is absorbed by the TEM. The amount of heat energy absorbed is influenced by the temperature at the cold side surface of the TEM, which is directly affected by the effectiveness of the cooling mechanism at the hot side surface of the TEM.

The graph in Figure 1 shows that across all power inputs, the cold side surface of the TEM with fan-enhanced heat pipe cooling is able to absorb more heat energy form the air inside the compartment as compared with regular heat pipe cooling. This information indicates that with fan-enhanced heat pipe cooling, the energy consumed is more efficient in the sense that it is converted to obtain a much higher heat absorption, whereas for regular heat pipe cooling, a bigger part of the energy consumed by the module is converted into waste heat at the hot side surface of the module due to its inability to dissipate heat fast enough via the cooling mechanism.

Figure 2 shows the variation of COP across the spectrum of input power. One interesting observation is that at low input power, the COP for regular heat pipe cooling is higher than fan-enhanced heat pipe cooling, but as the power input increases, the opposite happens.

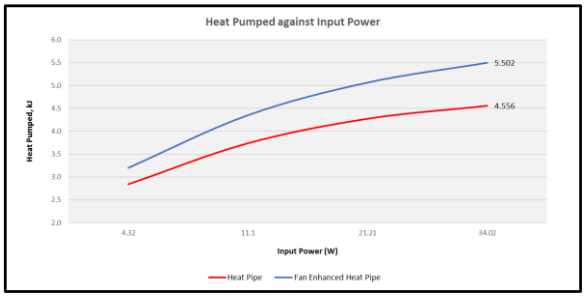

Figure 1: Graph of amount of heat absorbed against input power

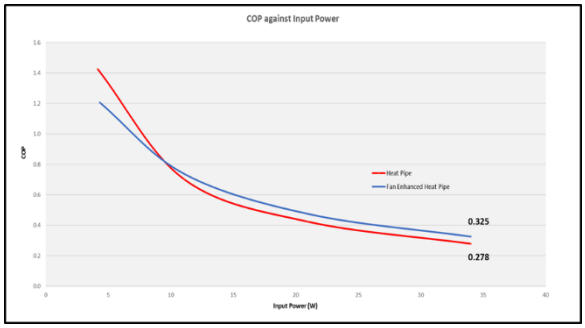

Figure 2: Graph of COP against input power

CONCLUSION

It is found that fan-enhanced heat pipe cooling has better COP at higher input power (11.2, 21.2, and 34.0 Watts), whereas at lower input power (0.6 and 4.3 Watts), heat pipe cooling has higher COP. The crossover point for the COP value is determined to be at around 9 Watts.

REFERENCES

[1] Astrain, D., Aranguren, P., Martinez, A., Rodriguez, A., & Perez, M.G. (2016). A comparative study of different heat exchange systems in a thermoelectric refrigerator and their influence on the efficiency. Applied Thermal Engineering, 103(2016), 1289-1298.

PERFORMANCE OF A THERMOELECTRIC GENERATOR AT VARIOUS TEMPERATURE GRADIENTS

Syahmi Zamri and Ibthisham Ardani
School of Mechanical Engineering, Faculty of Engineering,
Universiti Teknologi Malaysia, 81310 UTM Skudai, Johor, Malaysia

INTRODUCTION

Nowadays, our earth has been subjected through several alarms of global warming alerts. One of the reason of these occurrence is the heat released from the industry is kept unchecked based on Miro at el [1]. Several past studies have been conducted to harness the industrial excess heat by converting the heat energy into electrical energy, by using a thermoelectric generator (TEG). But, the technology of TEG is not widely used in the industry due to the low efficiency of power generated said. Therefore, this study is conducted in order to investigate the performance of a thermoelectric module (TEM) in producing electrical energy when subjected to several temperature differences of its two surfaces.

EXPERIMENTAL SETUP

Two different type of TEM, or commonly known as Peltier element, TEC1-12710 and TEC1-12706, are used in the experiment which one of them is used to generated the electrical power, from temperature difference and the other one is used as the heating element of the generating TEM, when supplied with electrical current

The two TEM is attached with each other, at both the hot side's surface and an aluminium sheet is placed in between as a method to measure the current. Each contacted surfaces is glued with thermal paste to ensure total conduction of heat occurs. All of the involved surfaces are attached with thermocouples in order to record and observe the change in temperature as it will affect the value of the generated electrical power.

The experiment is conducted with the increasing of supplied current value, 0.5, 1.0, 1.5, 2.0, 2.5, and 3.0*A*, into the heating element TEM. Then, the role of the two TEM, TEC1-12710 and TEC1-12706, are switched with one another. The experiment is then repeated with the same range of current supplied.

RESULTS AND DISCUSSION

After all of the experiments regarding to the TEG performance have been conducted, the data obtained from the experiments are tabulated and recorded.. Thus, in order to investigate the performance of the TEM in producing electrical power, a graph of generated power against the temperature difference of the two surfaces of the generating TEM as shown in Figure 1.

Figure 1 shows the two trend lines of the performance of each TEM in generating power from its surfaces' temperature difference. Both of the modules show a polynomial trend which is; as the temperature difference increase, the amount of power generated increased too. In comparison of the two modules, the performance can be differentiate by using a certain value of temperature difference and correspond generated power could be found. In this case, at the 35°C temperature difference, the TEC1-12710 generates up to 1.4334W of power while TEC1-12706 generates only 0.1253W. It shows that the TEC1-12710 perform better in term of generating power compared to TEC1-12706.

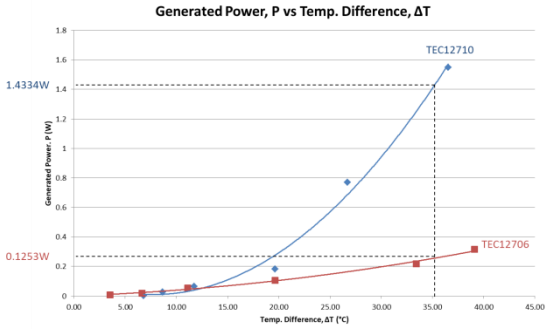

Figure 1: Graph of Generated Power against Temperature Difference

CONCLUSION

In conclusion, the performance of the thermoelectric generator highly depends on its maximum current value it can handle. The higher the maximum current a Peltier module can manage, the better the performance of the Peltier module in generating electrical power.

REFERENCES

[1] Miro, L., Bruckner, S., & Cabeza, L. F. (2015). Mapping and discussing Industrial Waste Heat (IWH) potentials for different countries. Renewable and Sustainable Energy Reviews, 51, 847-855.

[2] Chen, L., Gong, J., Sun, F., & Wu, C. (2002). Effect of heat transfer on the performance of thermoelectric generators. International Journal of Thermal Sciences, 41, 95-99.

[3] Champier, D. (2017). Thermoelectric generators: A review of applications. Energy Conversion and Management, 140, 167-181.

PALM KERNEL OIL (PKO) AS ALTERNATIVE FLUID FOR AUTOMOTIVE SHOCK ABSORBER APPLICATION

Helmi Hariri Arif and Mohd Kameil Abdul Hamid
School of Mechanical Engineering, Faculty of Engineering,
Universiti Teknologi Malaysia, 81310 UTM Skudai, Johor, Malaysia.

INTRODUCTION

The use of vegetable oils as alternative for lubricants in automotive applications has been introduced as they have the potential to replace mineral and synthetic oils due to their beneficial characteristics of non-toxic and biodegradable. However, there are some drawbacks in the use of vegetable oils as lubricants as they exhibit oxidation instability, poor low-temperature attributes, poor response to additives, and sensitivity to tribological properties of lubricant mechanism. In this research, palm kernel oil (PKO) was used as a bio-lubricant by blending it with different weight percentage of Zinc Dialkyldithiophosphate (ZDDP) and Molybdenum dithiocarbamate (MoDTC) as additives. This project is conducted to investigate the performance of the blended PKO with additives and the effect of the additives on the PKO when it is blended with different percentage of ZDDP (0.1%wt, 0.5%wt) and MoDTC (0.1%wt, 0.5%wt).

METHODOLOGY

The main machine used in this experiment was the four-ball tribotester machine. Two main characteristics were tested using this machine are the friction and wear properties of each of the lubricant samples. The experiment conducted was according to ASTM D4172. Seven samples of blended lubricants were prepared and and tested with the four ball tribotest machine with heavy duty shock oil and pure PKO as benchmark oils. The four ball tribotest was conducted each for 60 minutes under the load of 40kg and speed of 1200rpm.

While for wear scar diameter (WSD) and worn surface characteristics observation, the sample of ball bearings tested under the four ball machine was placed under the high power microscope. The worn surface characteristics was observed under lens of 10X of the high power microscope.

RESULTS AND DISCUSSION

From Figure 1, we can observe that the sample of PKO+0.5%wt ZDDP (in yellow) gives the lowest reading of frictional torque, which is the most desired. Figure 2 displays the average COF for each samples lubricant tested.

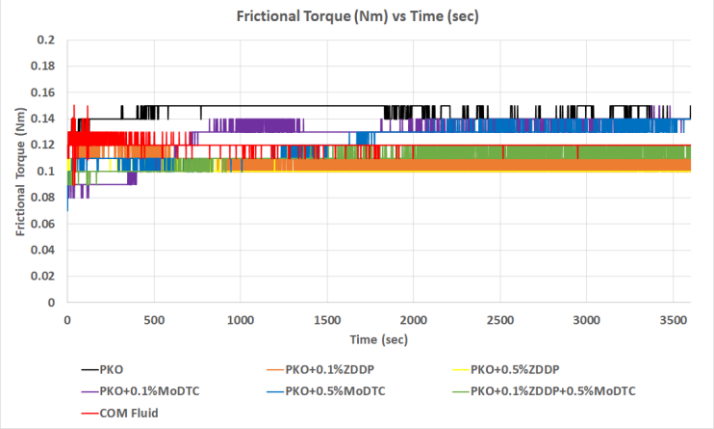

Figure 1: Frictional Torque of sample lubricants against time at 392 N

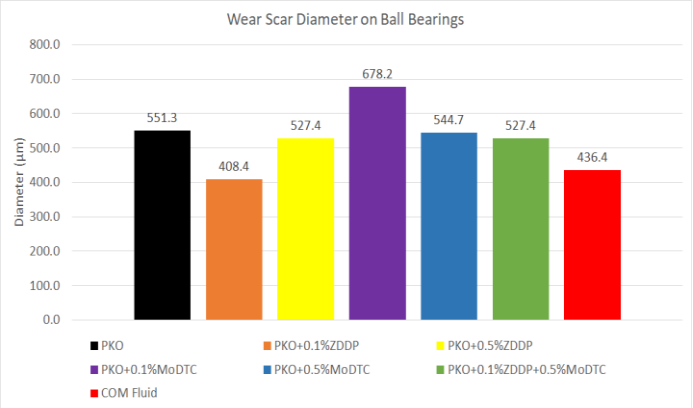

Figure 2: Average COF for each sample lubricants

REFERENCES

[1] Bingfa, B., Syahrullail, S., Abdul Hamid, M., & Samin, P. (2016). Suitable additives for vegetable oil-based automotive shock absorber fluid: an overview. Lubrication Science, 28(6), 381-404.

[2] Jahanmir, S. (1987). Wear Reduction and Surface Layer Formation by a ZDDP Additive. Journal of Tribology, 109(4), 577-586

[3] Kosarieh et al, S. (2012). The effect of MoDTC-type friction modifier on the wear performance of a hydrogenated DLC coating. Wear, 302 (1-2), 890-899

PALM FATTY ACID DISTILLATE (PFAD) FRICTION & WEAR PERFORMANCE ON PISTON RING APPLICATION

: Norhamizah Hithayathullah Khan and Mohd Kameil Abdul Hamid
School of Mechanical Engineering, Faculty of Engineering,
Universiti Teknologi Malaysia, 81310 UTM Skudai, Johor, Malaysia

INTRODUCTION

Lessening of Earth resources is alarming nowadays. Apart from that, all the price is getting higher as a result of this. Vegetable oils are favorable as an alternative because of its availability and safe for the environment. Besides, vegetable oils such as PFAD provide better tribological performance. This study is about PFAD as an alternative for engine oil with analysis done on piston ring-cylinder liner mechanism by evaluating the friction and wear performance with addition of additives.

PROJECT OBJECTIVES

This project is conducted to investigate the performance of PFAD with additives and the effect of the additives on the PFAD when it is mixed with different percentage of additives which are 0.5% (wt) MoDTC, 0.1% (wt) ZDDP and combination of both.

METHODOLOGY

The main machine used in this experiment was the pin on disc tribo-tester machine. Tribological analysis been made through this machine with evaluation of coefficient of friction, wear and fluid film thickness. The experiment conducted was according to ASTM G99. Four samples oils were tested with repetition of three times for each test. Pure PFAD and engine oil (SN 0W-20) also used in testing for comparison. Segmented Proton piston compression ring and a cast iron disc simulate the piston ring-cylinder liner mechanism.

To obtain wear scar diameter (WSD) and worn surface characteristics, the sample of segmented piston ring was placed under the low power microscope. For surface roughness data, the surface roughness tester was used.

RESULTS AND DISCUSSION

Figure 1 shows the coefficient of friction obtained from different type of lubricants. The additional of additives shows a significant decreases in coefficient of friction especially with 0.5% of MoDTC lubricant. 0.5% of MoDTC and 0.1% ZZDDP shows a rise in coefficient of friction. This is because of the chemical reaction occur between the two additives.

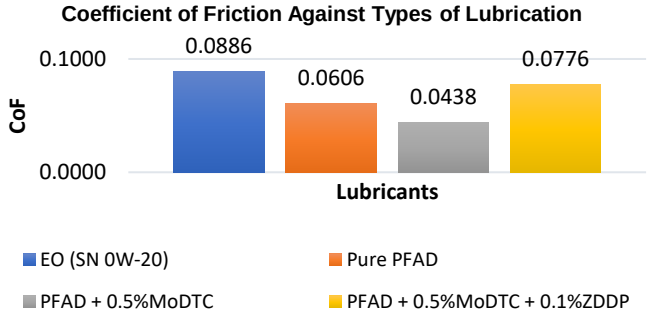

Figure 1: Coefficient of Friction against Type of Lubricants.

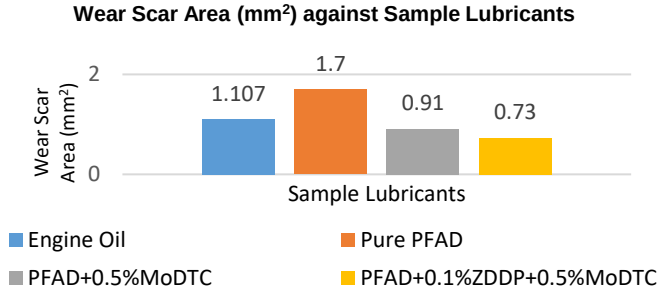

Figure 2: Wear against Sample Lubricant

Figure 2 shows the analysis of wear. PFAD with mixture of two additive provide better performance compared to all lubricants. MoDTC acts as friction modifier and ZDDP provide a tribo-film to reduce wear.

REFERENCES

[1] Campanella, A., Rustoy, E., Baldessari, A., & Baltanás, M. A. (2010). Lubricants from chemically modified vegetable oils. Bioresource Technology, 101(1), 245–254.

[2] Zabala, B., Igartua, A., Fernández, X., Priestner, C., Ofner, H., Knaus, O., & Abramczuk, M. (2017). Friction and wear of a piston ring/cyli study and modelling. Tribiology International, 106(October 2016), 23–33.

IMPACT OF SHOCK ABSORBER OIL BLEND WITH PALM KERNEL OIL (PKO) ON TRIBOLOGY PERFORMANCES

Bonnyface Rengkin Anak Peter Gon and Mohd Kameil Abdul Hamid
School of Mechanical Engineering, Faculty of Engineering,
Universiti Teknologi Malaysia, 81310 UTM Skudai, Johor, Malaysia.

INTRODUCTION

Palm kernel oil is an edible plant oil derived from the kernel of the oil palm and saturated oil same with palm oil. Palm Kernel Oil as adaptive on shock absorber and was blend with in term of weight such as 5%, 10%, 15% and 20%. In this project, the comparison of friction and wear of those lubricant were investigated and find the effect of Palm Kernel weight on the shock absorber oil on tribology performances [1].

RESEARCH OBJECTIVES

The aim of this project is to find friction performance of 5%, 10%, 15% and 20% of Palm Kernel Oil blend with Shock Absorber Oil and analyse wear surface of those lubricant sample

METHODOLOGIES

Four ball machines been used for friction performance analysis of each lubricant that has been prepared which is 5%, 10%, 15% and 20% of PKO blend with shock absorber oil in term of weight. The condition of this experiment is followed this machine standard condition that is ASTM D4172 (Table 1) for each lubricant sample.

Table 1: Condition for ASTM D4172

Parameter	Value
Temperature (˚C)	75
Load (N)	392
Speed (rpm)	1200
Duration (min)	60

RESULT AND DISCUSSION

The value for friction torque is increasing with time for each lubricant until it reaches it limit value of friction torque. The 5% PKO lubricant gave the highest value of friction torque which is 0.168 Nm while 20% PKO has the lowest value of friction torque, 0.1199 Nm by using friction formula (F=μN). Where: μ=friction coefficient and N= normal load.

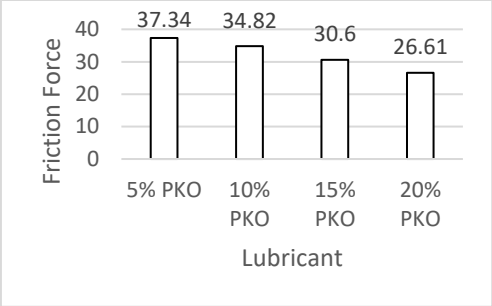

Figure 1: Friction value for each lubricant sample

For the wear surface analysis by using microscope, the 20% PKO gave the lowest amount of wear scar on the surface contact and 5% PKO has the highest amount of wear scar. This due to it friction where the highest value of friction the amount of wear scar that been produced also increase.

CONCLUSION

Through this study, the amount of Palm Kernel Oil on the shock absorber oil is affect the friction performance as a lubricant in term of friction and wear. The 20% of PKO blend with shock oil has the better tribology performances.

REFERENCES

[1] P. Zulhanafi, Syahrullail, S., M. M. Faridzuan, 2017. Tribological Performance of Palm Kernel Oil Added with Nanoparticle Copper Oxidising Fourball Tribometer.

AN EXPERIMENTAL STUDY OF ACOUSTIC EMISSION TESTING ON GLASS FIBRE REINFORCED POLYMER COMPOSITES UNDER QUASI-STATIC TEST

Hafizie Mohd Zakaria and Mohd Yazid Yahya
School of Mechanical Engineering, Faculty of Engineering,
Universiti Teknologi Malaysia, 81310 UTM Skudai, Johor, Malaysia

INTRODUCTION

Non-destructive testing is the technique used to examine the flaws occurred on a material without destroying the material and will be used again. Composites that has been using as an outer part of a structure have being under stress for a period of time. The composites continue will its service as long as its physical characteristic is in a good shape. However, the internal damage is unknown, and it might shorten the life span of the composites. Therefore, Acoustic Emission (AE) technique is used to detect, identify and classified all the internal damage occurred during the load is applied [1].

EXPERIMENTAL SETUP

This section presents the experimental setup for sample preparing, quasi-static indentation and AE monitoring. Chopped strand mat glass fibre and epoxy is chosen to fabricate via vacuum infusion method to create the sample (110x100x4).

Quasi-static indentation testing is conducted referring a standard, ASTM D6264. The indenter size is 12.7 mm is used to indent the sample with three different loading rate (1 mm/min, 10 mm/min, 100 mm/min) AE sensor embedded to the sample to detect all the elastic waves and will amplified by the 34-dB pre-amplifier. For AE data analysis, LabVIEW is used to collect and process all the data produced by the sensor. The experiment is carried out simultaneously.

RESULTS AND DISCUSSION

Based on the result obtained from both experiment, Figure 1 shown the defect is already occurred just after a few second after the loading applied. The AE technique detected the first crack by capturing the energy released form the inside of the sample. All sample in three loading rates experienced the event. The higher the amplitude level the worst the defect happened inside the sample.

The crack identification could be classified by analysing the acoustic activity pattern. Figure 2 shown amplitude level <100 dB characterized as matrix cracking relatively long duration low amplitude and relatively low energy. Figure 3 shown amplitude level >100 dB characterized as fibre/matrix debonding and fibre breaking because it has high amplitude and higher energy.

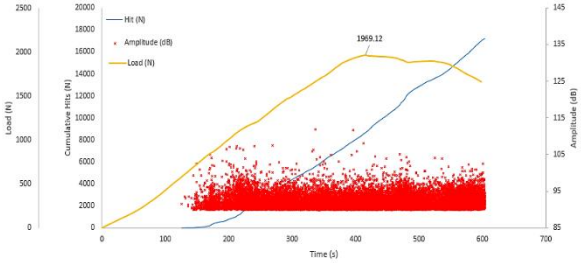

Figure 1: Graph of load, cumulative hits, amplitude versus time (1 mm/min)

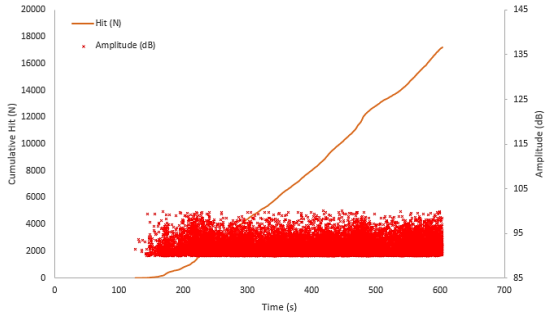

Figure 2: Acoustic activity for first phase (1 mm/min)

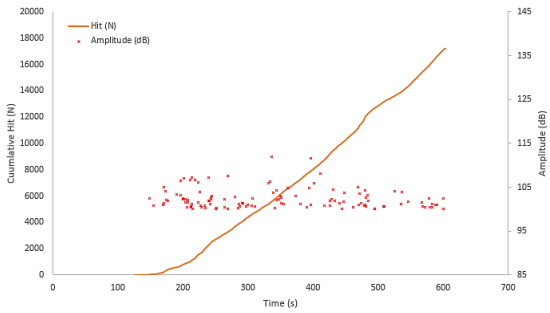

Figure 3: Acoustic activity for second phase (1 mm/min)

CONCLUSION

It appears that the samples experience multiple of defect right after the load is applied. It will continue until the sample could no longer withstand the stress and fail. With AE monitoring the failure could be prevent early to preserve the composite to long life span.

REFERENCES

[1] Shiotani, T., Aggelis, D. G. & Makishima, O. (2009) Global monitoring of large concrete structures using acoustic emission and ultrasonic techniques: Case Study. J. Bridg. Eng. 14(3). 188–192.

PHYSICAL AND MECHANICAL BEHAVIOUR OF CERAMIC FOAM

Mohd Alif Aizat Azman and Mohd Yazid Yahya
School of Mechanical Engineering, Faculty of Engineering,
Universiti Teknologi Malaysia, 81310 UTM Skudai, Johor, Malaysia.

INTRODUCTION

Generally, ceramic membrane functions on filtering. It is being used in certain industries such as biotechnological, dairy, food and beverages and also petrochemical. Ceramic membrane filters liquid in cross-filtration mode. Ceramics foam were implemented to application of tubular membrane in this project.

PROJECT OBJECTIVES

The aim of this study are to determine and compare physical behaviour of kaolin calcined foam and ball clay foam such as density and porosity, investigate and compare the compression and flexural strength of kaolin calcined and ball clay foam and investigate the failure of ceramic foam.

METHODOLOGIES

The materials used in this study were Kaolin clay, Ball clay, distilled water, sponge and Precipitated Calcium carbonate. Slurries are being produced and sponge is immersed in slurry before being dried and sintered. Test involved in this study were Archimedes' test, compressive, flexure test and morphology by microscope.

RESULT AND DISCUSSION

From Figure 1, Figure 2, Figure 3 and Figure 4, factor of Percentage of precipitate Calcium Carbonate has three levels, number 1 represents 5wt% of precipitate Calcium Carbonate while number 2 and number 3 represents 10wt% and 15wt% respectively.

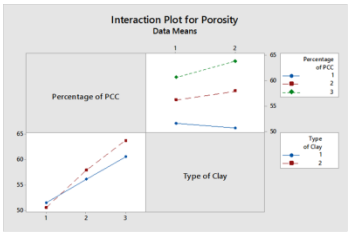

Figure 1: Interaction plot between parameters of factor in this experiment for porosity.

From Figure 1, the porosity seems to be increased within increment of percentage of precipitated calcium carbonate. From From Figure 2, we can also see that type of clay plays role in affecting the ceramic foam density. From Figure 3 and Figure 4, it could be seen that by changing type of clay from kaolin ceramic foam to ball clay ceramic foam, the flexure and compressive strength will be decreased.

From the crack that was happened, the failure was caused by shear stress at degree 45□ from horizontal line of Figure 6.

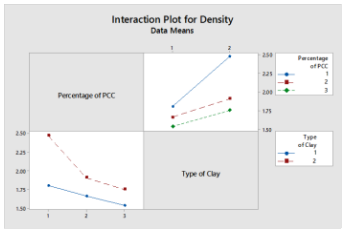

Figure 2: Interaction plot between parameters of factor in this experiment for density.

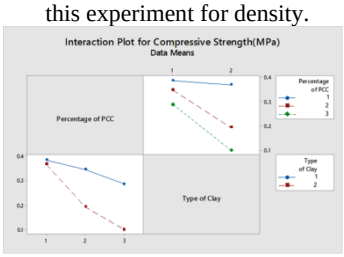

Figure 3: Interaction plot between parameters of factor in this experiment for compressive strength.

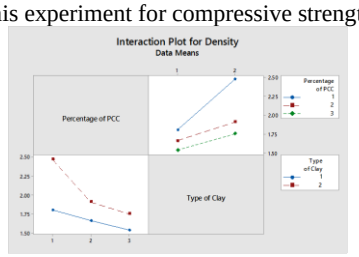

Figure 4: Interaction plot between parameters of factor in this experiment for flexure strength.

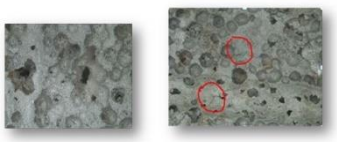

Figure 5: The image of ceramic foam before (left) and after (right) being compressed.

REFERENCES

[6] Deng, M, Chen, R & Liu, S. (2018). Ceramic sciences and Engineering. *Research and Development of Ceramic Filtration Membrane*, 1, 43-53.

[7] Sharif, S.M, Ahmad, Z.A and Othman, M. R. (2012). Science of Sintering, Preparation and Characterization of Tubular Ceramic Support for Use in Transesterification Process. 44, 187-195.

[8] Nor, M, Lee, C.H, Ahmad, Z.A and Akil, H. (2008). Preparation and characterization of ceramic foam produced via polymeric foam replication method. *Journal of Processing Technology*, 207, 235-239.

[9] Olupot, P. W, Jonsson, S. and Byaruhanga, J. K. (2006). Electroporcelains from Raw Materials in Uganda: A Review. *International Conference on Advances in Engineering and Technology*, 454-464

DRILLING ON FIBRE METAL LAMINATES (FML) COMPOSITE MATERIALS

Nur Ilyana Sahira Murizan, Mohd Yazid Yahya and Mohamed Ruslan Abdullah
School of Mechanical Engineering, Faculty of Engineering,
Universiti Teknologi Malaysia, 81310 UTM Skudai, Johor, Malaysia

INTRODUCTION

Fibre metal Laminates (FML) is an outstanding composite materials that have been used widely in aerospace owing to their excellent strength to weight ratio performance, low density and excellent corrosion resistance. However, the application FML in marine industry such as for small boat is still new and need a lot of research. Drilling is the most common machining process applied for joining these materials which not only reduces the structural integrity of the materials, but as well has the potential for a long-term performance deterioration [1].

EXPERIMENTAL SETUP

This section presents the experimental setup for the research. The specimens were fabricated using vacuum infusion process which is one-time process. Then, drilling process was done using Universal Milling Machine DECKEL MAHO DMU 50 at different levels of spindle speed and feed rate. The drilled specimen underwent static loading at constant of 2mm/min loading rate. From tensile test, the machining residual stress was obtained.

Design of experiment was run using Design Expert software with full factorial methods.

RESULTS AND DISCUSSION

From figure 1, it observed that the machining residual stress reduced with increased in spindle speed at feed rate for both 3A4F and 3A2F sample. The highest machining residual stress value was obtained at the lowest range value of spindle speed and feed. In comparison, the 3A4F residual stress value were bigger than in 3A2F. This is because, 3A4F is thicker than 3A2F. It contained much more fibre than in 3A2F. Hence, more load needed to break the sample [2]. Plus, the load is distributed to bigger surface area. In additional, the reduction of machining residual stress due to increase in spindle speed and feed rate was because the stress cannot be transferred from outer plies to inner plies due to delamination. Delamination around the drilled hole fails to transfer stress from plies to plies causing major lost in overall stiffness. Hence, the stress concentration is more severe in outer plies and lead to an early damage to the structure [3].

From figure 2, we observed that residual stress was most affected by feed rate and it decreased with the increased in feed rate, also decreased with the increased in spindle speed. The optimized parameter for 3A2F was 1050 rpm and 0.05 mm/rev, while for 3A4F were 1090 rpm and 0.05 mm/rev. A verification test was conducted to observe the difference obtained between the optimal reading and the experimental reading.

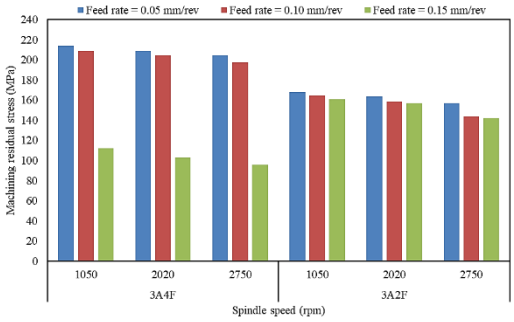

Figure 1: Machining residual stress at different drilling parameters.

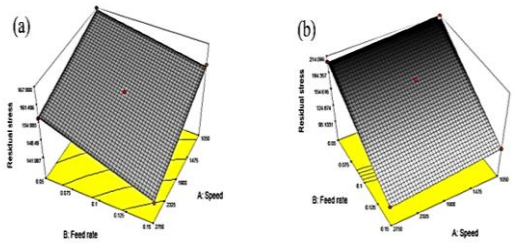

Figure 2: 3D surface plot for (a) 3A2F and (b) 3A4F

CONCLUSION

In conclusion, it was observed that as the spindle speed and feed rate were increased, the machining residual stress were reduced. The thickest FML obtained bigger value of the residual stress.

18. REFERENCES

[1] U. A. Khashaba, "Delamination in drilling GFR-thermoset composites," *Composite Structures*, vol. 63, pp. 313-327, 2004.

[2] M. Santosh Kumar, S. G. Gopala Krishna and S. Rajanna, "Study on Effect of Thickness and Fibre Orientation on a Tensile and Flexural Properties of a Hybrid Composite," *Journal of Engineering Research and Application*, vol. 4, no. 8, pp. 56-66, 2014.

[3] E. Kilickap, B. Yenigun and Y. Hisman Celik, "The effect of drilling parameters on strength of glass fibre-epoxy laminates by produced hand lay-up," *e-Journal of New World Sciences Academy*, vol. 12, pp. 246-254, 2017.

INVESTIGATION ON SHAPE MEMORY ALLOY PERFORMANCE OF FIBRE REINFORCED BASALT/ EPOXY COMPOSITE LAMINATE

Adee Yahya Zaini and Mohd Yazid Yahya
School of Mechanical Engineering, Faculty of Engineering,
Universiti Teknologi Malaysia, 81310 UTM Skudai, Johor, Malaysia

INTRODUCTION

Composite materials have found increasing applications in construction, aerospace and automotive industries due to their good characteristics of light weight, improved strength, corrosion resistance, controlled anisotropic properties, and reduced manufacturing cost[1]. However, there is a growing demand to improve on composite materials to have adaptive capabilities that can sense, actuate and respond to surrounding environment. Therefore, the in-depth investigation on the interfacial behaviour and mechanical properties of SMA composite is remarkably valued.

EXPERIMENTAL SETUP

The experiment consists of a pull-out test and a three-point bending test. The pull-out test was conducted by using Universal Testing Machine Instron 5982 with a constant pulling speed of 3mm/min. Three parameter of surface condition of SMA which are untreated, acetone-coated and roughened surface were embedded into epoxy thermosetting polymer of 20 x 12 x 25 mm. The test was run by pulling the SMA wire uniaxially from the epoxy sample until debonding occurs.

The three-point bending test was conducted according to the standard ASTM D790. The parameters are dictated by the number of SMA wires embedded into the composite and also the effect of activation of SMA wires through Joule heating. The failure modes of the specimens were analysed through Scanning Electron Microscopy (SEM).

RESULTS AND DISCUSSION

Based on Figure 1 which illustrates the result of pull-out test, the roughened SMA wire, exhibits the highest pull-out load resistance with the improvement of up to 62.14% compared to untreated SMA wire because the roughened SMA wire induces interlocking mechanism with the surrounding matrix due to friction, causing it to have a higher grip to surrounding matrix. Thus, enable it to resist more load [2].Figure 2 shows the overall result of the three-point bending test. the SMA embedded BFRP shows relentless increment while the virgin BFRP continues to decrease in the bending force, indicating that the only part that gets affected is the basalt fibre whereas the SMA wire does not fail yet. The effect of embedding more SMA wires into BFRP greatly enhances the stiffness of the composite beams to 55.74%, 81.36% and 87.36%. The effect of activation of 1,2 and 3-SMA composite improved the stiffness by 10.5%, 3.08% and 1.46% respectively.

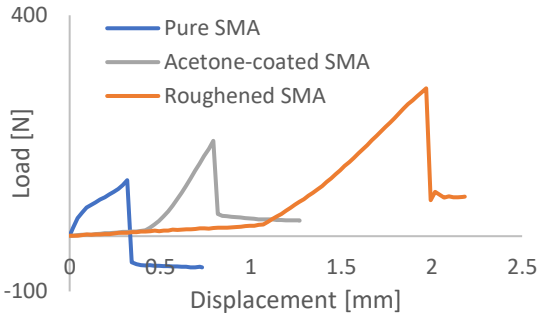

Figure 1: Comparative load versus displacement graph of pull-out test

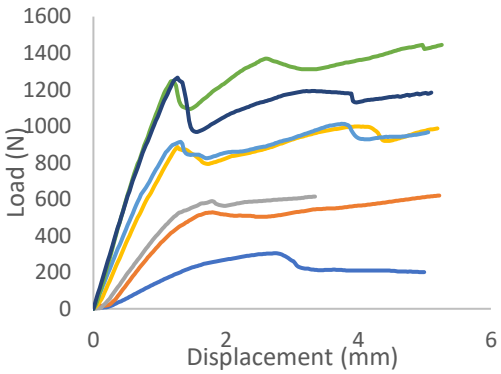

Figure 2: Comparative load-displacement graph of three-point bending test

CONCLUSION

It is concluded that the roughened SMA surface wire embedded into BFRP achieved the highest interfacial bonding strength and resistance to pull-out loading while the effect of activation and embedding more SMA wires enhances the stiffness and flexural modulus of the SMA-based composites.

REFERENCES

[1] O. L. Ayodele, "Investigation of the mechanical properties and behaviour of hybrid polymer composites embedded with shape memory alloys," *M.sc. thesis*, no. The Cape Peninsula University of Technology, 2008.

[2] B. Yang, Y. Zhang, F. Z. Xuan, B. Xiao, L. He, and Y. Gao, "Improved adhesion between nickel–titanium SMA and polymer matrix via acid treatment and nano-silica particles coating," *Adv. Compos. Mater.*, vol. 27, no. 3, pp. 331–348, 2018.

BEHAVIOUR OF SHEAR THICKENING FLUID IMPREGNATED BASALT FIBRE REINFORCED COMPOSITE UNDER LOW VELOCITY IMPACT

Amirul Syafiq Hasrin and Mohd Yazid Yahya
School of Mechanical Engineering, Faculty of Engineering,
Universiti Teknologi Malaysia, 81310 UTM Skudai, Johor, Malaysia

INTRODUCTION

Over recent years, there has been an explosive growth of interest in shear thickening fluid (STF) impregnated in fibre. The shear thickening fluid has a great characteristics under shear load, that the Silica particle accumulate thus jam the flow, or so called hydrocluster forming theory [1]. Many research has been done on study the effect of addition of shear thickening fluid into the fibre and the results is promising. However, not many research currently on STF-fabric with resin composite. Selver et al (2019), studies about the effect of STF-carbon and STF-glass fabric under impact loading [2]. Thus, the purposes of this study is to investigate the effect of addition of STF in composite. In the research scope, the application of basalt is used due to its environmental friendly fibre.

EXPERIMENTAL SETUP

This section presents the experimental setup to achieve the objective of the study. The test that conducted were, quasi static indentation test, drop weight test and flexural test. The test specimen was fabricated by using vacuum infusion method. The size of the sample was based on ASTM D7136, ASTM D6264 and ASTM D790. The tests conducted at Mechanics of Materials lab and Composite Centre UTM. The sample were named based on the composition of silica in STF, where STF-15 referred to 15 % silica content and STF-30 referred to 30 % of silica content.

RESULTS AND DISCUSSION

This section presents the results obtained from the test and its analysis. Figure 1 – 3 shows results obtained from the three tests. The results obtained from quasi static indentation test showed that, addition of STF into fibre do not enhance the impact properties of the material, where the drop in performance about 50 % and 37 % for STF-15 and STF-30 sample. The drop weight test showed a consistent results with the quasi static indentation test, where STF-composite sample showed 49 % decrement in maximum load value. STF-15 and STF-30 sample do not exhibits significant differences in maximum load value. The addition of 15 % of STF into fibre increased the flexural stress of the specimen by 37 %, while the addition of 30 % STF into fibre exhibits decrement in flexural stress.

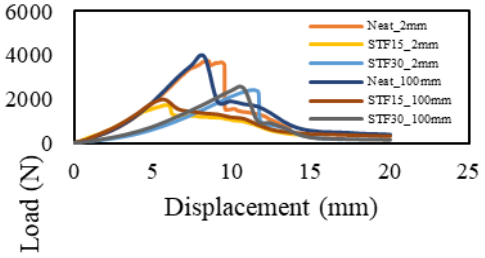

Figure 21: Results of QSI test

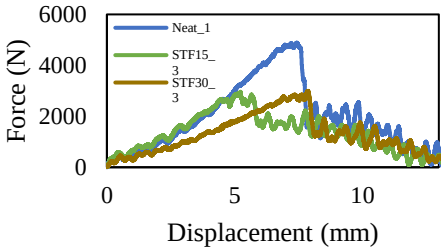

Figure 22: Results of drop weight test

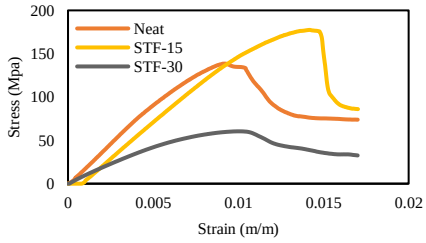

Figure 23: Result of flexural stress

CONCLUSION

The studies showed that addition of STF do not enhance the impact properties of the sample, however the results obtained did not consistent due flexural stress for 15 % STF sample showed an increment. The objective of the studies is achieved.

REFERENCES

[1] J. Ding, P. J. Tracey, W. Li, G. Peng, and P. G. Whitten, “Review on shear thickening fluids and applications,” *Text. Light Ind. Sci. Technol.*, vol. 2, no. 4, pp. 161–173, 2013.

[2] E. Selver, “Impact and damage tolerance of shear thickening fluids-impregnated carbon and glass fabric composites,” 2019.

EFFECTS OF GRAPHENE OXIDE FILLER ON THE MECHANICAL PROPERTIES OF BASALT/EPOXY COMPOSITE

Muhammad Haziq Khalid and Mohd Yazid Yahya
School of Mechanical Engineering, Faculty of Engineering,
Universiti Teknologi Malaysia, 81310 UTM Skudai, Johor, Malaysia

INTRODUCTION

The addition of filler in the composite can affect the strength and mechanical properties of the material. Incorporation of filler by matrix modification is used as it is one of the cheapest method available. Graphene Oxide has a great characteristic to become filler as it has a great amount of surface area and a high strength properties. This study is done to investigate the effect of Graphene Oxide filler on the mechanical strength of basalt/epoxy composite.

EXPERIMENTAL SETUP

Hand lay-up process followed by curing under compressed mould was chosen as a method to fabricate the composite. The nominal thickness for the sample was measured at 1.9 mm $\pm$ 0.2 mm. The dispersion of GO in epoxy was performed by using solution mixing technique. The amount of GO from 0.1% to 0.5% of epoxy resin weight were added to the composite.

Three type of tests were conducted in this study. Tensile test was performed according to ASTM D3039. Flexural and impact test were done according to ASTM D790 and ISO 179-1 respectively.

RESULTS AND DISCUSSION

Figure 1 shows the tensile strength of the material is increasing with the addition of GO until it reaches the amount of 0.2%. Basalt/epoxy added with 0.2% of GO shows the highest improvement, increased by 13% from 398 MPa to 450 MPa. Basalt/epoxy added with 0.2% of GO also has the highest value of Young's modulus, which is 16.25 GPa, improving the strength by 24% from 13.14 GPa, The trend of the Young's modulus shows a rising pattern until it stop at the addition of 0.2% of GO.

The incorporation of GO at 0.2% decreased the flexural strength by 4% to from 109 MPa to 104 MPa. However, the flexural strength and modulus obtained from the experiment shows both the improvement and deterioration with the addition of GO. The inconsistency of the data makes it impossible to conclude the trend with the increasing amount of GO filler. In Charpy impact test, the addition of 0.2% of GO decreases the strength by 17% from 284.5 kJ/m^2 to 237.43 5 kJ/m^2. Based on Figure 2, it is clear that the incorporation of GO decreased the impact properties of basalt/epoxy. The agglomeration of GO particle might contributing to the strength deterioration in the composite [1].

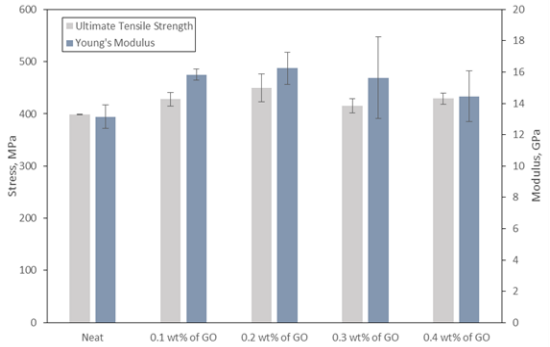

Figure 1: Tensile strength and modulus comparison.

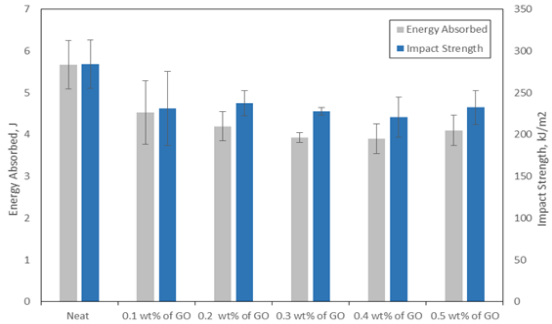

Figure 2: Comparison of impact properties.

CONCLUSION

This study has found the incorporation of GO affects the mechanical properties of basalt/epoxy composite. The addition of 0.2% of GO increased the tensile strength by 13%. Further incorporation of GO reduce the strength by causing low interfacial bonding between the fibers. The improvement in tensile strength is resulting from high interfacial bonding in the composite thus reducing the delamination and fibre pullout during fracture. However, the flexural and impact strength are deteriorated with the incorporation of GO at 0.2%. GO filler has the possibilities to increase composite tensile strength but also can deteriorate its performance in flexural and impact properties by lowering the compressive strength of the material.

REFERENCES

[1] M. Bulut, "Mechanical characterization of Basalt/epoxy composite laminates containing graphene nanopellets," *Journal Composite Part B: Engineering*, vol. 122, pp. 71- 78, 2017

EFFECTS OF GRAPHENE COMPOSITE IN ZINC RICH EPOXY COATING ON CORROSION RESISTANCE OF MILD CARBON STEEL PIPE IN OIL AND GAS APPLICATION

Wilver Philip, Izman Sudin and Mohd Zamri Yusop
School of Mechanical Engineering, Faculty of Engineering,
Universiti Teknologi Malaysia, 81310 UTM Skudai, Johor, Malaysia

INTRODUCTION

Carbon steel pipeline are major used in oil and gas industries due to it low cost and ease of fabrication. Transferring crude sweet or sour oil via pipeline on topside structure posed corrosion risks due to severe exposers in marine environment. The combined effect of the heat, oxygen, moisture and salty humidity aggravate the corrosion rate of carbon steel pipeline (Ameh, Ikpeseni, & Lawal, 2018). Inappropriate selection of coating materials causes catastrophic and expensive failure due to corrosion. The right choice of coating material on the pipeline may reduce the frequency of painting maintenance and extend the pipe life.

In recent years, graphene composite is increasingly being used in many industries (Ding et al., 2018). However, its application is not well applied and reported especially in pipeline as a filler in zinc-rich epoxy coating. Hence, its performance on painted carbon steel pipes is remain unknown. The aim of this study is to compare the effectiveness of zinc-rich epoxy coating with and without graphene composite as a filler on corrosion resistance of carbon steel pipe in oil and gas application.

MATERIAL AND EXPERIMENT SETUP

Zinc-Rich epoxy was mixed with graphene composite at 1%wt, 3%wt and 5%wt ratio and the coating thickness were varied at 80µm, 160µm and 240µm. The substrate material was a low carbon steel with 0.3% C. The corrosion performances on the coated pipe were evaluated using Open Circuit Potential (OCP), potentiodynamic polarization curves (Tafel Plot) and Electrochemical Impedance Spectroscopy (EIS). Salt solution used in potentiodynamic test was 3.5%wt NaCl solution.

RESULTS AND DISCUSSION

Compared the coating with and without graphene content, the 1%wt of graphene composite in 240µm coating thickness has lowest corrosion rate of 0.0087204mmpy and is in optimum value compare to 100% zinc rich epoxy with corrosion rate of 0.0241656mmpy. Although the coating with 5%wt graphene composite in 240µm was slightly better, the lifting space was relatively limited due to the cost of graphene and coating layer.

The result indicated that the passivation capacity of the passive film on the base metal surface was stronger than that of the anodic passivation reaction.In a word, the addition of graphene could effectively improve the corrosion resistance of base metal and as a good filler in zinc rich epoxy coating..

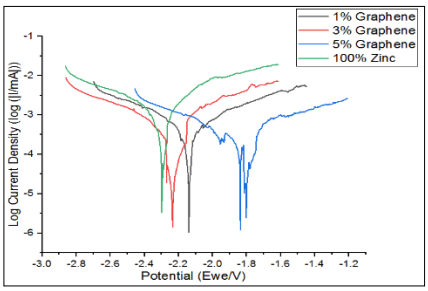

Figure 1 Potentiodynamic curves of coated pipes with and without graphene filler in 3.5%wtNaCl solution.

According to the EIS fitting results in Figure 2, it was seen that the impermeability of the composite coating increased with the addition of graphene. Using characteristic frequency method to evaluate the coating properties, it was found that the incorporation of graphene effectively reduced the corrosion porosity and improved the corrosion resistance of the coating.

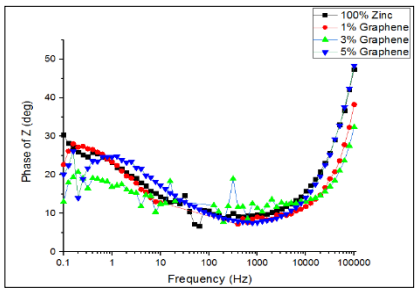

Figure 2 Impedance Bode diagram of EIS Test

CONCLUSION

The EIS and Tafel Polarization data shown in this study have proved the fact that graphene composite as a filler in zinc-rich epoxy coating possessed high effectiveness on corrosion resistance of carbon steel pipe in oil and gas application.

REFERENCES

[1] Ameh, E. S., Ikpeseni, S. C., & Lawal, L. S. (2018). A Review of Field Corrosion Control Upstream Oil and Gas Pipelines. Nigerian Journal of Technological Development, 14, pp.45-67.

[2] Ding, R., Li, W., Wang, X., Gui, T., Li, B., Han, P., Song, L. (2018). A brief review of corrosion protective films and coatings based on graphene Journal of Alloys and Compounds, 764, pp. 1039–1055.

RUBBER TAPPING ROBOT

Lai Cong Yan and Mohd Zarhamdy M. D. Zain
School of Mechanical Engineering, Faculty of Engineering,
Universiti Teknologi Malaysia, 81310 UTM Skudai, Johor, Malaysia.

INTRODUCTION

Malaysia natural rubber production decreased since 2006. There are a few problems that lead to the downfall of Malaysia natural rubber industry. Firstly, the lack of interest from the local community. Most of the rubber estate owner has to hire foreign labour. Besides, rubber tree tapping is considered to be a skill-oriented job and the availability of such labours are getting rare. The second problem is the tiring process of natural tapping. The optimum time is short, which is only from 3 am to 7 am. After the optimum time, the yield will drop. Therefore, rubber tappers have to rush through all the trees besides having to wake up early. This will also increase the risk of harming the trees. The objective of this project is to design a new rubber tapping robot with a stable and consistent tapping.

METHODOLOGY

Product Design Specification (PDS) is done to clarify all the requirement for this product before proceed further into robot design. The robot has to be fully automated and able to perform consistent and precise tapping. Morphology Chart is set up to generate ideas in each critical functions. Evaluation matrix then is done to distinguish the pros and cons of each designs. From the evaluation matrix, the best design can be determined. Analysis is done to calculate the torque for the clamping and power needed for engraving. The design is then embodied in CAD software. The robot prototype is then fabricated. The robot is tested on a wood trunk and the tapping result is determined.

RESULT AND ACHIEVEMENT

Figure 1: Rubber Tapping Robot CAD design

Figure 1 shows the CAD design of the rubber tapping robot. The robot structure consists of clamping mechanism, x-y-z motion and rubber tapping mechanism. Electronic components are implemented to the robot such as: microcontroller board, micro-switches and motor drivers.

Figure 2: Tapping Result

The outcome of the tapping by the robot is consistent. However, the depth of the cut is inconsistent and a pattern on the cut from the tapping can be seen. This problem can be solve by using proximity sensor with higher accuracy and implementation of external encoder.

CONCLUSION

In this work, a new rubber tapping robot has been designed. A stable and consistent tapping has been demonstrated from this newly design rubber tapping robot.

REFERENCES

[1] Ahmad., N., Malek, A. B. K., Mohamed H. M., Muhammad A. A. G., Jiang, J. L., Shamsul. K., & Zulkifli, H. (2012). An automatic tapping machine. Patent WO 2012/121586 Al

DEVELOPMENT OF MOBILE ROBOT FOR EXPLORATION ACTIVITY

Mohd Irwan Rosli and Mohd Zarhamdy Zain
School of Mechanical Engineering, Faculty of Engineering,
Universiti Teknologi Malaysia, 81310 UTM Skudai, Johor, Malaysia.

INTRODUCTION

Mobile robot exploration is the robot that has capabilities to move into the environment which has various surface terrain without a problem and builds body with specification strong enough hold impact while it is operating in a cave. The mobile robot also can move in the small cave which human are not capable to reach there. So the mobile robot is a good invention to help human on monitoring what inside the cave. This thesis focus on survey mobile robot mapping that can be applied on a small and extreme surface such as a cave.

PROJECT OBJECTIVES

The objectives of this study are to design and develop mobile robot exploration that can travel in different surface condition and can support the mapping scanner device.

METHODOLOGIES

As this a design and development project. First, the objectives and scopes need to be clarified. From that, we can start to come out the idea that follows the objectives and scopes. Understanding the developed and design mobile robot by carrying out a literature review to study the existing designs [1]. From this, it helps to establish the design requirement and design creations of the mobile robot.

Figure 1 exploration mobile robot

Hence, a few initial conceptual design ideas or designs were generated and needs to finalize one by choosing the best concept that fulfil the requirement. After that, the finalize design needs to be dimensioning and list all component part. Next, engineering analysis needs to study on final concept design. Proceed to develop the model final design and then ready for testing.

COMPONENT OF EXPLORATION MOBILE ROBOT

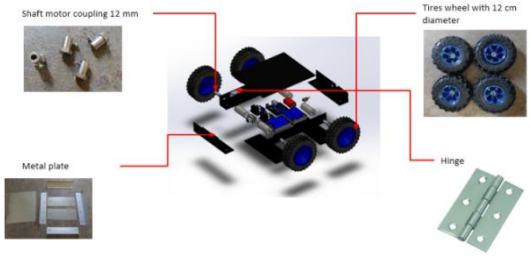

Figure 2 Body part final selection

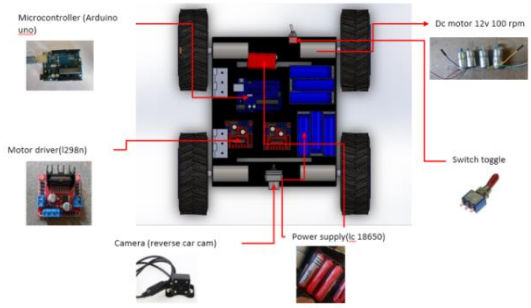

Figure 3 Electronic component final selection

RESULT AND ACHIEVEMENT

The project had achieved the objective which is to design and develop a mobile robot for exploration activity. The exploration mobile robot is able to support mapping scanner device. From exploration mobile robot performances test, the mobile robot is able to travel in a various surface condition which is grass-field, small puddles and etc. Furthermore, the camera shows fully functions in the daylight and able to display image capture in real-time. Moreover, the support light camera able to enhance camera performance in a dark environment.

REFERENCES

[1] Neumann, T., Ferrein, A., Kallweit, S., & Scholl, I. (2014). Towards a Mobile Mapping Robot for Underground Mines.

A SIMULATION OF A SPOON COVER ON HAND ARM TREMOR

Nurul Nadila Saipol Bahari and Mohd Zarhamdy Md Zin
School of Mechanical Engineering, Faculty of Engineering,
Universiti Teknologi Malaysia, 81310 UTM Skudai, Johor, Malaysia

INTRODUCTION

In the last decade, Tissue Engineering (TE) has been beneficiary for new artificial tissue substitute and increasing demand for organ transplantation. The porous scaffold that able to mimic the various of bone properties such as mechanical properties and nutrient transport is been proposed. Permeability studies of cancellous bone has been carried out by many researchers which address the relationship between permeability, mechanical properties and anatomical site [1]. Therefore, TE has emerged rapidly with approach that lead to the development of biomaterial to prepare the porous 3D scaffold as biological substitute to restore, maintain and improve defective tissue. Thus, this paper explains the permeability and wall shear stress of magnesium (Mg) porous scaffold which mimic with human cancellous bone.

METHODOLOGY

The basic principle of permeability fluid flow test is to design model scaffold that mimic with natural cancellous bone parameter using SolidWorks. Therefore, this study proposed a new design of porous scaffold which has biocompatibility and match with bone properties.
The methodologies of the study are as follow:

1. 3D CAD drawing of bone models and check the porosity and surface area
2. Meshing generation and set boundary condition with a variation of flow rates (0.025, 0.4, 0.8 ml/min)
3. Calculate permeability using Darcy's law

RESULTS AND DISCUSSION

At the end of CFD analysis, pressure drop is obtained to be used as referenced to calculate the permeability in each specimen. Figure 1 shows the good correlation between average permeability and pore size within specimens. The permeability of scaffold can be affected by the porosity of structure [2]. However, for the structure with same porosity will have the different permeability due to different pore size and bone surface area. In addition, the variation of flow rates has affected the performance of bone scaffold. Both permeability and WSS illustrate the contrast result as it passes through the type of specimen as in Figure 2. The value of WSS and permeability were compared with cancellous bone. Therefore, the linear correlation has been found between permeability and WSS with bone surface area and pore size.

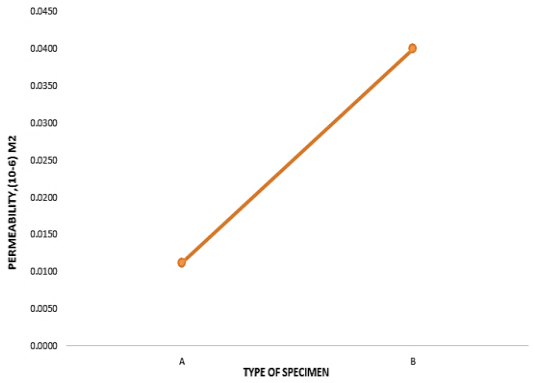

Figure 1: Graph of permeability within the specimens.

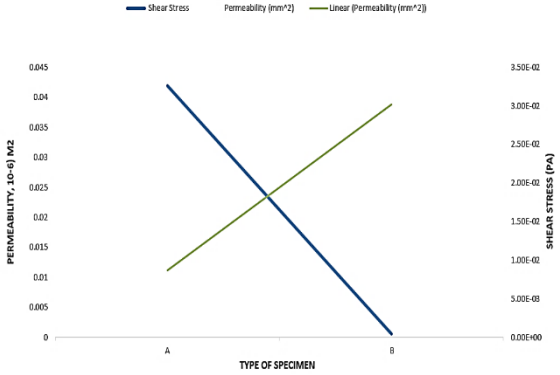

Figure 2: Graph of WSS and permeability within specimen.

CONCLUSION

With the consideration for the induced wall shear stress and permeability requirement for cancellous bone, the models portray the effectively mimic the properties of the human bone. Both results show the linear correlation with pore size and surface area. The results showed that plate-like specimens are in range of permeability as the cancellous bones.

REFERENCES

[1] Syahrom, A. et al. (2015). Medical Engineering & Physics Permeability study of cancellous bone and its idealised structures. Medical Engineering and Physics. Institute of Physics and Engineering in Medicine, 37(1), pp. 77–86. doi: 10.1016/j.medengphy.2014.11.001.

[2] Md Saad, A. P. et al. (2017). The influence of flow rates on the dynamic degradation behaviour of porous magnesium under a simulated environment of human cancellous bone. Materials and Design, 122, pp. 268–279. doi: 10.1016/j.matdes.2017.03.029.

A STUDY ON THE PERFORMANCE OF SEAWATER BATTERY DESIGN

Nor Aswari Ayu Napiah and Mohd Zarhamdy Md Zain
School of Mechanical Engineering, Faculty of Engineering,
Universiti Teknologi Malaysia, 81310 UTM Skudai, Johor, Malaysia

INTRODUCTION

Batteries are capable in storing large amounts of energy per unit weight. According to Geoffrey J. May [1] compact, easy to deploy, economical and provides instant response both to input from the battery and output from the network to the battery that makes the electrochemical energy storage in battery attractive. In addition, the use of seawater as an electrolyte in a battery also is not something new in the energy storage technology. A lot of researches have been done for decades. According to research conducted by Nai-Guang Wang [2], a seawater activated battery system normally includes two indispensable parts which are, active metal anode (e.g. magnesium) and metal chloride cathode. This type of battery is developed to meet the requirement of military application in 1940s. One of the type of seawater battery used is Mg/AgCl battery. The battery is developed as the power source for electric torpedoes.

METHODOLOGY

This section presents the methodology applied to this study. There are several phases and steps involved. The main objective of this study is to select the most reasonable materials to be used as the electrodes in the seawater battery cell. A performance tests is carried out to find the amount of voltage output obtained by each type of electrodes.

The performance test is carried out and recorded by connecting the Arduino to the battery cell with load connected to it. The amount of voltage output is recorded for eight hours period and graphs are plotted. Hence, the selected pair of electrodes will undergo a few series of tests afterwards.

RESULTS AND DISCUSSION

From the experiment conducted, C-Zn and C-Mg pair of electrodes were shortlisted as the potential electrodes to be used in the seawater battery cell since they recorded the highest voltage output compared to other pairs.

The voltage produced by C-Zn battery is slightly lower with 3.35V compared to C-Mg battery with 5.25V before connected to load. After connected to a load, the average voltage drop recorded for C-Zn and C-Mg battery are 0.83V and 2.74V respectively.

Figure 1 and 2 shows the results of the voltage output for both C-Zn and C-Mg electrodes pair. Battery with C-Mg electrodes shows a better performance compared to C-Zn battery. This is because the voltage output for C-Mg after connected to a load is higher compared to C-Zn battery. Furthermore, battery with C-Mg electrodes is able to light up the load (torchlight), where the amount of voltage output produced is enough to light up the load.

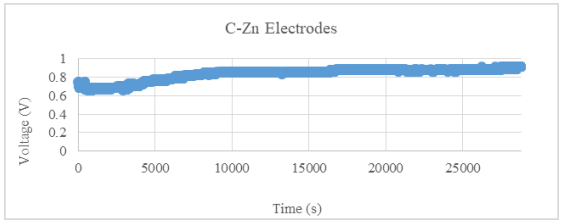

Figure 1: Performance of C-Zn battery with load applied

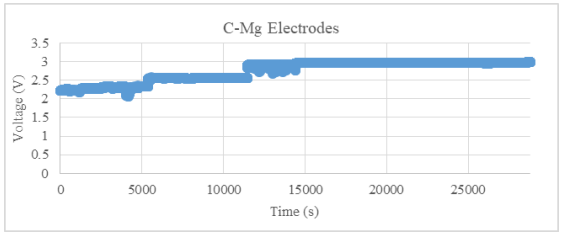

Figure 2: Performance of C-Mg battery with load applied

CONCLUSION

The design of the seawater battery consists of 12 pairs of electrodes connected in a series circuit. The voltage output achieved was not the same as in theory due to some errors and disturbances. To choose a suitable pair of electrode to be used in the seawater battery, a few types of electrode pairs are tested for their voltage output. The results shows that C-Zn and C-Mg pair produced the highest voltage output. Both pairs with the highest voltage output are then tested for their voltage performance in eight hours period.

REFERENCES

[1] Geoffrey, J. M., Alistair, D. and Boris, M. (2018). Lead Batteries for Utility Energy Storage: A Review. Journal of Energy storage, 15(2018), 145-157. doi: 10.1016/j.est.2017.11.008

[2] Nai-Guang, W., Ri-Chu, W., Chao-Qun, P., Cheng-Wang, H., Yan, F. and Bing, P. (2014). Research Progress of Magnesium Anodes and Their Application in Chemical Power Sources. Trans. Nonferrous Met. Soc. China, 24(2014), 2427-2439. doi: 10.1016/S1003-6326(14)63367-7

A SIMULATION OF A SPOON COVER ON HAND ARM TREMOR

Nurul Nadila Saipol Bahari and Mohd Zarhamdy Md Zin
School of Mechanical Engineering, Faculty of Engineering,
Universiti Teknologi Malaysia, 81310 UTM Skudai, Johor, Malaysia

INTRODUCTION

Tremor is one type of disabilities that may happened either to a healthy people or Parkinson Disease (PD) patient. This study will focus on uncontrolled hand vibration happened to Tremor patient during eating activity based on PD patient. Even though the vibration are impossible to be 100% isolated, but the tools or device that can reduce a vibration will really help them to have a better life. So, a simulation of this spoon cover are meant to confirm that the vibration can be reduce by having a passive system for vibration reducer. This passive system attached to the spoon cover and it may absorbed the vibration when PD patient use that device attached to their spoon during eating.

METHODOLOGY

Based on this study, a mathematic model that will take into account is the equation of improved spoon cover for hand arm tremor. The validation of the mathematical modelling have been done by using MATLAB-Simulink software by considering many aspects including materials, boundary condition and also based on their type of vibration absorber. Models of the spoon cover are based on the conceptual design of the spoon. An experimental setup as shown in Figure 1 has been arrange to compare the result between the spoon cover prototype and the simulation analysis result. The accelerometer has been calibrating and connected to Arduino system and the data transferred to PLQ-DLX to plot the data reading by the vibration sensor.

Figure 1: Experimental setup for spoon cover prototype

RESULTS AND DISCUSSION

Result tabulated as in Table 1 and Table 2, confirmed that the passive vibration reducer system can be used to dissipated the uncontrolled motion due to Tremor. There is a reduction by using the existing spoon cover, but by having a new design of spoon cover, we can reduce more vibration.

Table 1: Simulation Analysis Summary Result

Variable	Existing Cover	New Cover	Frequency (Hz)	Magnitude Different
Magnitude reduction from hand tremor vibration	0.8256	0.5689	7.05	0.2567

Table 2: Experiment Summary Result

Variable	Tremor patient	Existing Cover	New Cover	Reduction
Acceleration mm/s2	1023	719	625	YES

REFERENCES

[1] Mathematical Model of Spoon Cover on Hand Arm Tremor Behavior, June2 2018 Liyana Amanina

DEVELOPMENT OF STAIR CLIMBING ROBOT

Muhammad Syahmi Afzal bin Abdul Rahim and Mohd Zarhamdy Md. Zain
School of Mechanical Engineering, Faculty of Engineering,
Universiti Teknologi Malaysia, 81310 UTM Skudai, Johor, Malaysia

INTRODUCTION

Stairs represent a serious challenge to certain type of vehicles and robots during the occurrence of hazard. Each classification of mobile robot possesses their unique advantage and suffers from certain disadvantages. Previous studies have shown that wheeled type have better performance than walking and track. Hence, wheeled type was chosen to continue this study on stair climbing due to its simplicity, light weight and less energy consumption compared to the walking and track type (Mohammed & Mahmoud, 2017).

PROPOSED DESIGN

The robot is based on Tri-Wheel design (Smith, 2015), it consist of different sets of gearing system each for driving and tumbling. The robot can be controlled using two modes which is manual maneuver operation and stair climbing operation. Manual maneuver requires user input while stair climbing is automated.

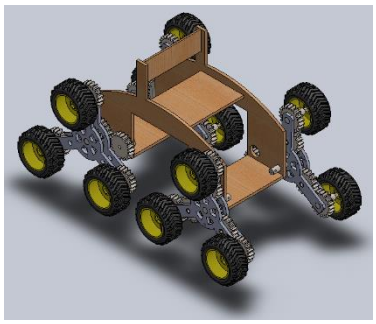

Figure 1: Final design of the robot

RESULTS AND DISCUSSION

Simulation was done using two DC Motor turning at 20 RPM and two servos turning at 15 RPM using SolidWorks Motion Analysis.

Figure 1 indicate that the torque of servo motor is higher compare to DC motor as the servo require a large amount of torque to rotate the whole Tri-Wheel system. The fluctuation of the torque for both of motor was due to the friction on the floor and the collision between each step during the stair climbing motion.

For the servo, the torque rise and fall due to the rotation of the Tri-Wheel, as the Tri-Wheel start to rotate it will require a large amount of torque and as the Tri-Wheel start to land on the next step, the torque on the motor will fall down until the Tri-Wheel successfully land on the step.

The maximum value of torque is 2.1 Nm for DC motor, approximately at 2.3 seconds during the climbing of the first step while the highest value of torque for servo is 15.8 Nm at 8 seconds after successfully climbing the last step.

Figure 2 indicate that both servo and DC motor have the same trend for its power consumption where it fluctuates. For each rotation of the Tri-Wheel system the power consumption will spike up at the early rotation and fall down after completing the rotation. Both motor has the maximum power consumed at 6 Watt and 25 Watt for DC motor and servo respectively.

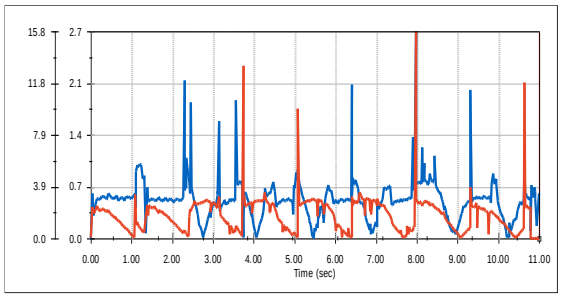

Figure 2: Torque-time graph of DC Motor (Blue) and Servo Motor (Red)

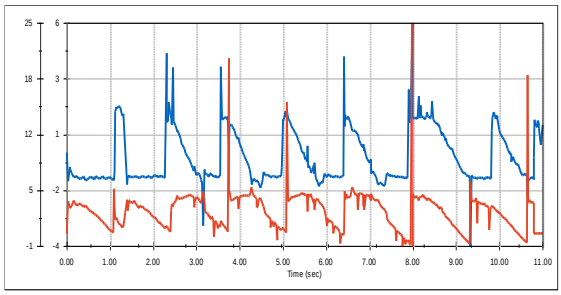

Figure 3: Power consumption-time graph of DC Motor (Blue) and Servo Motor (Red)

CONCLUSION

It shown that wheeled type robot has low power consumption for stair climbing operation and it is vital for the motor and servo to have high torque for better performance.

REFERENCES

[1] Mohammed, D. A., & Mahmoud, K. (2017). *Design of Tri-Star Wheel Robot*. (October).

[2] Smith, L. M. (2015). *The Tri-Wheel: A Novel Robot Locomotion Concept Meeting the Need for Increased Speed and Climbing Capability*.

COLOR DETECTION DEVICE FOR BLIND PEOPLE

Muhammad Afif As-Siddiq Ishak, Mohd Zarhamdy Md Zain
School of Mechanical Engineering, Faculty of Engineering,
Universiti Teknologi Malaysia, 81310 UTM Skudai, Johor, Malaysia

INTRODUCTION

In the world today, the number of people living with visual disabilities or visual impairment are increasing day by day. Not having the abilities to perceive the light in the surrounding, most of them struggled in doing normal daily activities such as identifying colour of object in their surroundings. The process of identifying colour is necessary in many kinds of activities such as buying groceries, buying clothing or even deciding the value of money. Being able to identify colours of object would be a great help to people with visual disabilities and it might boost up their confident to live more independently. Hence, these are basically the reasoning on why this project is being develop which is to develop a colour detection device that could be use to identify the colour of different material such as paper, clothing or even plastic material.

FUCTIONAL ANALYSIS

The working mechanism of the colour detection device relies only on four basic components in order the device to be able to identify colours and to be able to voice out the object colours. The main components are TCS320 colour sensor, microcontroller, sound module and lastly the speaker.

The device firstly works when the colour which is connected to LED light detect the amount of red, green and blue data from the reflected light receive from the surface of the material. These data are then sent to our microcontroller which the Arduino Nano. Th microcontroller will then identify the actual colour of the of the object based the ranges of red, green and blue data that have been programmed inside the Arduino.

The Arduino will then send the right signal to the serial mp3 player to play the sound output. The serial MP3 player which works by playing the track in the SD card. From the signal receive form the microcontroller, the serial mp3 player will then play the track through the speaker connected to it to alert the user the colour of the object.

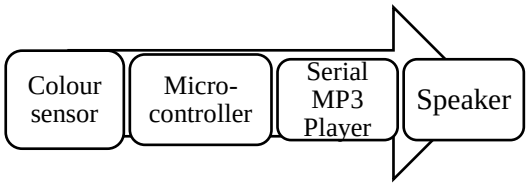

Figure1: The Device Functional Analysis

RESULTS AND DISCUSSION

The identification of colours is made based on the values of red, green and blue data that we have received from the colour sensor itself. Hence, in order to ensure that the device is capable to identify many variation colours, trial is the done on different colours to identify the red, green and blue for each colour. For each colour, a total of 10 trial to is collected to ensure that the red, green and blue data taken is precise. These values are then programmed into the microcontroller Arduino Nano.

	Red			Green			Blue		
Trial	R	G	B	R	G	B	R	G	B
1	8	20	17	18	13	18	27	19	11
2	8	20	17	17	12	19	27	19	11
3	9	20	17	18	13	18	27	19	11
4	9	20	18	18	13	18	27	19	11
5	8	21	17	18	13	18	27	19	11
6	8	20	17	18	13	18	28	19	11
7	8	20	18	18	13	18	27	19	11
8	8	20	17	18	13	18	27	19	11
9	9	20	17	18	13	18	27	19	11
10	8	20	17	18	13	18	27	19	11

Table 1: The RGB data for different colour

So basically as we stated earlier, when this value have been programmed into the Arduino, whenever the colour sensor detected the ranges of value for red, green and blue data that satisfies any of above ranges, the microcontroller will quickly send a signal to the serial MP3 player to play the right sound track to alert the user the colour of the object.

CONCLUSION

In the conclusion, the main objective of the project which is to make a colour detection device for blind people is achieved. Being able to identify the colour of the object in the surrounding would be a great advantage to people with visual impairment, as it would make them more independent and also being more confident in the life.

REFERENCES

[1]. *How Blind People Identify Colours Malaysia*.https://www.evenground.com/blog/how-blind-people-identify-colors, [Accessed: 28 March 20189].

[2]. *Visual Impairment and blindness (n.d.),* http://who.int/mediacentre/factsheet/fs282/en/ [Accessed 15 April 2019]

DEVELOPMENT AND CONCEPT TESTING FOR 4-WING FLAPPING DRONE

Srinivas Balakrishnan and Mohd Zarhamdy Md Zain
School of Mechanical Engineering, Faculty of Engineering,
Universiti Teknologi Malaysia, 81310 UTM Skudai, Johor, Malaysia

INTRODUCTION

Drone is very useful device which is mostly used for airborne monitoring and aerial photography/video. This device can be used to monitor places on earth where can't be reached by human easily. In this project I am using flapping design by using four wings with separate motors connecting where it is mainly used for flight. The purpose of this project is to analyse and design concept for the four-wing flapping drone inspired by insect. Furthermore, this project focuses on the method to fabricate a prototype that follows a drone design that is able to hover using flapping mechanism.

METHODOLOGY

This section presents the analysis of the body of the drone and the wing dynamics that is essential to fabricate the flapping drone. The equations for this study is validated by using [1] as the reference to make sure the wingbeat frequency, the power of motor and the dynamics of the drone is calculated accordingly.

Table 1 Design specification

Parameters	Design Specification
Motor (kV)	HD-Propeller-85-T(motor)
Wing span(cm)	15
Body dimension (cm)	10 X 10
Battery Capacity	9V
Number of wings	4
Body weight (without payload) (g)	190
Material used	Wooden stick, wrap paper, 3D printing (ABS)

The dynamics and analysis of the body of the drone is done and the mechanism and concept is finalised by simulation and animation in Soliworks.

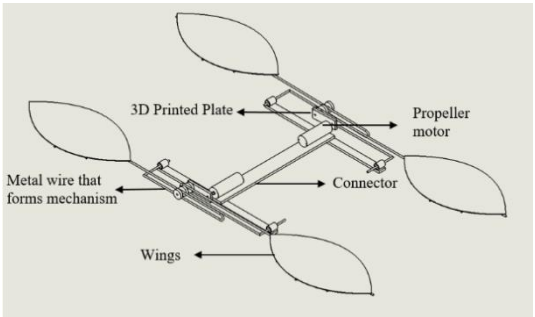

Figure 1 Design drone

Figure 1 shows the body of the drone was designed. This was designed by layer where the two edges will be the propeller motor, followed by the connector, then the body mechanism and lastly the 9V battery and followed by the wing wire that connects the body to the wing.

RESULTS AND DISCUSSION

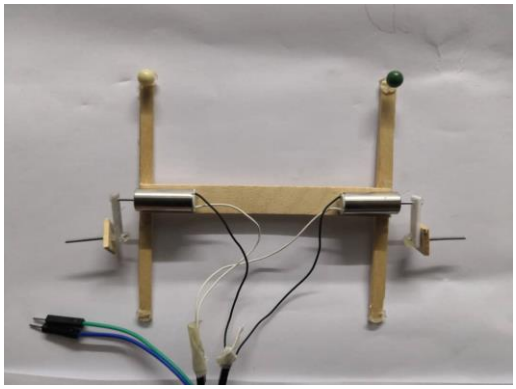

Figure 2 Fabricated drone

Figure 2 shows the body of the drone. There was a need to use lightweight material to fabricate the body structure and joined using hot glue gun.

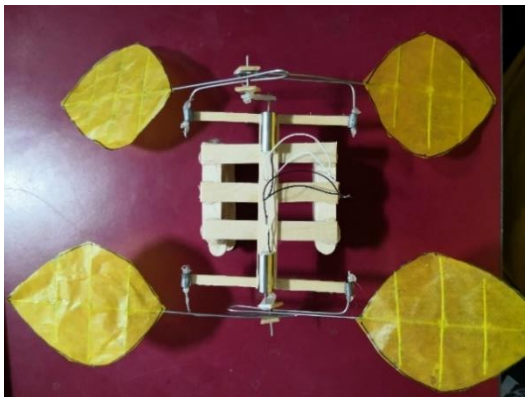

Figure 3 Fabricated drone flapping mechanism

Figure 2 shows the overall assembly of the flapping mechanism. A field test was conducted to check whether the design can fly.

CONCLUSION

We can conclude that the insect-like design theory has been proven to work due to the lightweight body and the high wingbeat frequency.

REFERENCES

[1] C. J. Pennycuick. 1990. "Predicting wingbeat frequency and wavelength of birds". Available: Journal of Experimental Biology 1990 150: 171-185;

DEVELOPMENT OF 3D MAPPING DEVICE USING ULTRASONIC SENSOR

Wan Jamil and Mohd Zarhamdy Md. Zain
School of Mechanical Engineering, Faculty of Engineering,
Universiti Teknologi Malaysia, 81310 UTM Skudai, Johor, Malaysia.

INTRODUCTION

This project is based on difficulty faces by the current method used by the researcher in mapping the structure of the cave. Most of the method used by the researcher in mapping the structure of the cave is still by using the manual ways where most of them still required to manually bring the heavy mapping device into the cave. Some of them are still manual inspection by using a camera where based on the image capture the structure of the cave will be remodelled back by using the software in the lab later.

EXPERIMENTAL SETUP

The flow of methodology starts by listing the specification of the device. The listed specifications then set as a guideline in designing and develop the device. The important specification of the device is it must be able to scan out the structure of the prototypes caves in the dark environment. As the Specification set, two concepts had been made based on it. The best concept had been selected and improvises as the final concept to achieve the objective. Then the 3D model of the device had been made by using Solidworks as in Figure 1.

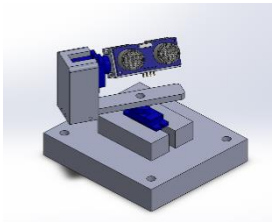

Figure 1: Design of the device

This section presents the experimental setup and servos had been made by following to [1] and [2] respectively to increase the accuracy of the device. After that, Coding and planning process starts. During the coding process, 3 sets of coding had been made which are for Method 1, Method 2 and Method 3 scanning. PLX-DAQ and Solidworks had been selected to act as interface transferring data from the Arduino directly into Excel and visualize the data into 3D point image. Then the device is ready to be tested

RESULTS AND DISCUSSION

The device able to function follows to flow chart as in Figure 2.

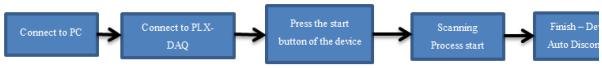

Figure 2: Device Functional Flow Chart

CONCLUSION

As a conclusion, the project had achieved the objective. The device was able to scan out the prototype caves in a dark environment as already set in the specification of the device during the designing process. Based on the image produce, the most reliable result is by using Method 3 as the result produce on only able to produce image resemble to shape of the prototype by also not produce a wavy image. Lastly, all of the scanning methods used in this project unable to detect sharp edges with an angle of 90 degrees and below.

REFERENCES

[1] Wikim0nst3r Productions. (2014). HC-SR04 Ultrasonic Range Finder Calibration.
[2] The Playful Machine: Theoretical Foundation and Practical Realization of Self-Organizing Robots. (2012). Springer Science & Business Media, ISBN 978-3-642-20253-7, 302.

SMART LUGGAGE TROLLEY FOLLOWER

Mohamad Izam Mohd Fuzi and Mohd Zarhamdy Md. Zain
School of Mechanical Engineering, Faculty of Engineering,
Universiti Teknologi Malaysia, 81310 UTM Skudai, Johor, Malaysia

INTRODUCTION

Nowadays, most of the items in this world use the technology for more productive life. The individuals always find something to assist them doing a work rather doing it themselves thanks to their busy life. In manual trolley, human labor remains required to utilize trolley. They still ought to push the trolley or bring the basket to bring the stuff. So, if there's a trolley that may be run automatically, then bring the things are going to be easier and economical.

METHODOLOGY

The system design for both hardware and software for the development of the automatic human guided shopping trolley had been carefully planned. The hardware components comprise ultrasonic sensors, Bluetooth module and motor driver, which are connected to the Arduino Mega 2560. Software implementation is the main software's that are used in completing the project. Arduino and MIT App Inventor is the software used in this project. The Arduino Integrated Development Environment (IDE) is the main text editing program used for Arduino programming.

RESULTS AND DISCUSSION

The trolley moves according to the command given through the Arduino.

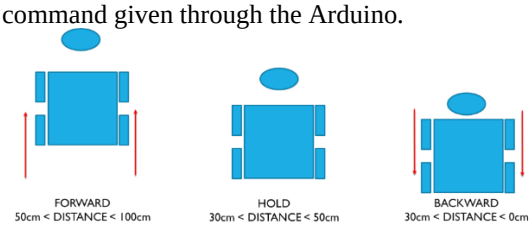

Figure 1: Forward and backward movement of the trolley

Figure 1 shows the movement of forward and backward of the trolley. When the distance is between 100cm and 50cm the trolley will moves forward. At distance 30cm and lower the trolley will back itself to avoid colliding with the user. Between 50cm and 30cm is the safe distance between the user and the trolley.

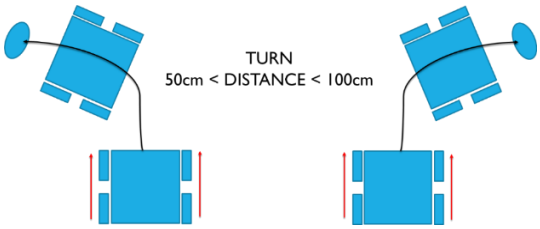

Figure 2: Turning movement at the distance of 100cm and 50cm

Figure 2 shows the turning movement of the trolley at the user distance of 100cmn and 50cm. It have a small arc for the trolley to turns at the given distances.

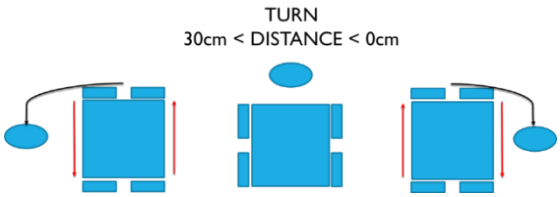

Figure 3: Turning movement at the distance of 30cm and below

Figure 3 shows the turning movement for the trolley at 30cm and below. The motor moves in opposite direction to make the trolley moves in the direction needed by rotating at the same place.

CONCLUSION

The purpose of this project is to develop a functional human following trolley that can also be control by using a smartphone. Using a smartphone as the interface to control the various functions in the trolley is cost saving as smartphone is already in everyone possession. The objective for this research had been achieved as the trolley had been successfully design and fabricated with the implementation of the following system. The following system is achieved by using the ultrasonic sensor.

REFERENCES

[1] Adnan Aqeel (2018). A complete step by step tutorial on the Introduction to Arduino Mega 2560. Retrieved from https://www.theengineeringprojects.com/2018/06/introduction-to-arduino-mega-2560.html

[2] Melanie Pinola (2019). Bluetooth Basics What Bluetooth is, what it does, and how it works. Retrieved from https://www.lifewire.com/what-is-bluetooth-2377412

[3] DC MOTOR – Basics, Types & Application. Retrieved from https://www.elprocus.com/dc-motor-basics-types-application/

BRASS COATING ON STEEL SUBSTRATE FOR STEEL CORD TIRE APPLICATION VIA ELECTROPLATING METHOD

Carmen Wong and Muhamad Azizi Mat Yajid
School of Mechanical Engineering, Faculty of Engineering,
Universiti Teknologi Malaysia, 81310 UTM Skudai, Johor, Malaysia

INTRODUCTION

In industrial sector, brass layer coated around the high carbon steel wire cord is being produced through the method of electroplating of brass in pyrophosphate electrolyte. Recently, the brass coated around the steel cord by 3 working steps follow as: Copper plating, zinc plating and diffusion treatment process. This conventional method has high tendency to produce thick zinc oxide coating which detrimental for subsequent mechanical drawing process to further reduce the diameter of steel wire as it is brittle oxide. Thus, a study has been carried out to investigate the plating parameters towards the brass chemical composition and adhesion strength coated on the ste**el substrate.**

EXPERIMENTAL SETUP

Brass plating had been done on steel substrates (wire and plate) with various plating parameters such as effect of current density, pyrophosphate concentration and copper concentration. Whereas, steel cord acts as substrate. All the samples will be characterized by using X-Ray Diffraction (XRD), Scanning Electron Microscope (SEM) and Field Emission Scanning Electron Microscope with Energy Dispersive X-Ray (FESEM). The effect of each parameter towards the brass alloy composition and its changing of colour had been study. On the other hand, wire samples will be studied further by Surface Roughness Test and Rubber Adhesion Pull Out Test.

RESULTS AND DISCUSSION

The effect of different current densities on the composition of Cu-Zn alloy was determined from Energy Dispersive X-Ray (EDX) analysis. From the results, the composition of zinc in the coating increases as the current density also increases. Figure 1 show the percentage of copper and zinc in the coating with respect to **current density.**

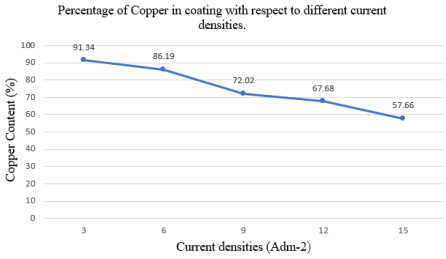

Figure 1: Percentage of Copper in coating versus current densities.

The greater the current density, it will promote the formation of less noble metal which is zinc to be plated on the substrate. This result matches the statement claimed by Ramírez [1] where increasing current density tends to make the partial current of copper move away from the total current density, while the partial current of zinc approaches it. Figure 2 shows the increased of pyrophosphate molarity lead to the increasing of the zinc content in the brass coating. As the pyrophosphate increased, the zinc content in coating increased. This might due to more zinc had reacted with the pyrophosphate which was the complexing agent to form copper complexes thus saturation of zinc complex form.

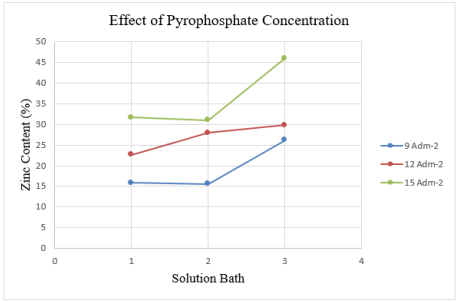

Figure 2: Effect of pyrophosphate concentration in solution baths against zinc content in 9 Adm^{-2}, 12 Adm^{-2} and 15 Adm^{-2}

CONCLUSION

The effect of the plating variables on the composition of the brass coating was investigated. The zinc content in the deposit increases as the increasing of current density and pyrophosphate content [1]. The increasing of copper content made the copper content also increased. Golden-like α-brass coating was deposited at the current density of 9Adm^{-2}. The grain size decreases and more compact with the increases of current densities [2]. Surface roughness will affect the rubber adhesion, due to stress interlocking on the brass coating.

REFERENCES

[1] Ramírez, C. (3 June 2015). *"Study of the Effect of Triethanolamine As A Chelating Agent in the Simultaneous Electrodeposition of Copper and Zinc from Non-Cyanide Electrolytes."* Journal of Electroanalytical Chemistry (Universidad de Antioquia – UdeA, Calle 70 No. 52-21, Medellín, Colombia).

[2] Rashwan, S. M. (2007). *"Electrodeposition of Zn–Cu Coatings from Alkaline Sulphate Bath Containing Glycine."* (Institute of Metal Finishing).

DRAG MEASUREMENT ON HELICOPTER FUSELAGE

Muhammad Izzudin Hazim and Muhamad Azizi Mat Yajid
School of Mechanical Engineering, Faculty of Engineering,
Universiti Teknologi Malaysia, 81310 UTM Skudai, Johor, Malaysia

.

INTRODUCTION

Currently, conventional silica aerogel is often produced using expensive and toxic silicon alkoxides such as tetramethoxysilane Si(OCH3)4 or TMOS, and tetraethoxysilane Si(OC2H5)4 or TEOS [1]. However, recent findings on the uses of rice husk ash as a silica source offers an economical solution as cheap raw material [2]. Rice husk is an abundant agricultural waste in most agriculture based countries such as Malaysia and contains about 80-90% amorphous silica. Reusing the rice husk will also help to reduce the environmental pollution.

In this research study, silica aerogel beads with size ranging between 1-2 mm were synthesized using the ball drop method via ambient pressure drying method. The effect of post curing temperature on the morphological properties and the physiochemical properties of the silica aerogel beads were also investigated. Above all, it was conclude that our current research efforts work will be helpful to provide a general reference on how to synthesis silica aerogel prepared from RHA with desirable structure and properties at high temperature conditions.

EXPERIMENTAL

This section presents the experimental setup for the system. For the synthesis of aerogel, preparation of sodium silicate solution, silica hydrogel beads via ambient dry condition is done. After the silica aerogel beads are made and prepared, further post curing process had been carried out. The silica aerogel beads is then dried on the hot plate at temperature ranging at 200°C, 300°C and 400°C.

The synthesis and post-cured aerogels were characterized by FTIR, SEM and EDX spectroscopies. The properties and behaviour of silica aerogel have been determined by the density and wettability test

RESULTS AND DISCUSSION

Based on the spectrum of Figure 1, the reaction has been analysed with three days gap of ethanol exchange, respectively. For nine days of ethanol exchange of synthesis aerogel, it show a promising result. The strong and sharp absorption peak of Si─O─Si bond at 1092 cm-1 and Si─CH3 bond at 1638 cm-1 corresponds to the silica surface structure. The strong peak shows the interaction between Si─O─Si bond [3], indicating a more pure and complete reaction of synthesis aerogel obtained.

As shown in Figure 2, the results revealed that synthesis and post-cured aerogels all exhibit a globular-aggregated structure, in which silica particles interconnect with each other to form a porous network. The images visualized the aerogel surface with the darker regions are interpreted as the openings to the three dimensional porous structure. Above all, the aerogels keep a similar topography spongy meshwork with magnifying from 5,000 times. Based on the topography, the aerogels sustained its structure after the post curing process at 400°C.

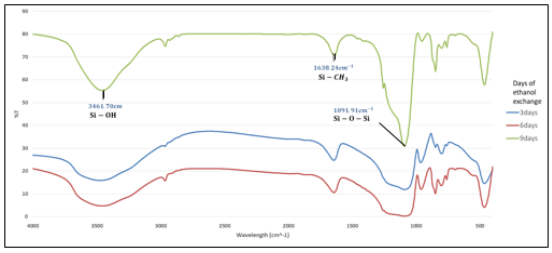

Figure 1: FTIR Spectrum of synthesis aerogel

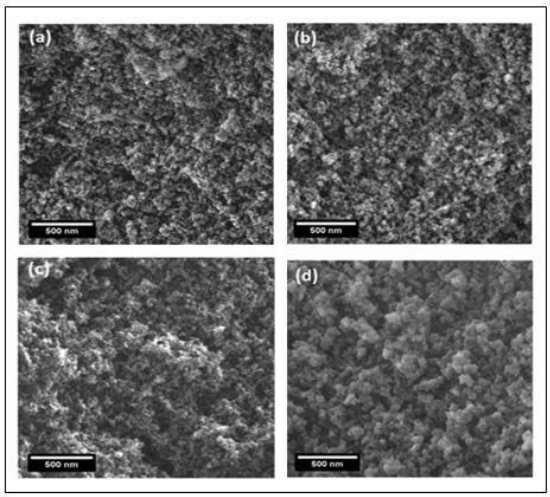

Figure 2: SEM images of synthesis aerogel at (a) 100°C, (b) 200°C, (c) 300°C and (d) 400°C

CONCLUSION

The structure of silica aerogel is preserved and maintained up to its thermal degradation temperature which is 400°C. The aerogels characterized also exhibit a low density at 0.0389 g/cm3, high porosity percentage at 97.22% and high contact angle at 105°. The silica aerogel sustained its property and behaviour at high temperature.

REFERENCES

[1] E.L. Foletto, E. Gratieri, L.H.D. Oliveira, S.L. Jahn, Conversion of rice hull ash into soluble sodium silicate, Mater. Res. 9 (2006) 335-338.

[2] H. Halimaton, U.S. Patent 7,897,648 B2. (2011) [3] S.B. Jung, H.H. Park, Control of surface residual –OH polar bonds in SiO2 aerogel film by silylation, Thin Solid Films 420-421 (2002) 503-507

ENHANCED COOLING PERFORMANCE OF CENTRAL PROCESSING UNIT USING ALUMINA THERMAL PASTE

Muhammad Izzat Bin Mustafa, and Muhammad Noor Afiq Witri bin Muhammad Yazid
School of Mechanical Engineering, Faculty of Engineering,
Universiti Teknologi Malaysia, 81310 UTM Skudai, Johor, Malaysia

INTRODUCTION

Over recent years, there has been an explosive growth of interest in nanofluid technology. More researcher focused on the enhancement of heat transfer on cooling system as LED and heat sink. This is due to the fact that the people want used high performance of computer nowadays to complete their daily task. Performance and power levels of CPU is a growing challenge as device future sizes become decrease. Ensuring effective heat transfer from CPU to surrounding is a vital step in counter this challenge. Thermal interface material (TIM) also call as thermal paste is used between CPU and heat sink. Good thermal paste have high thermal conductivity because more heat can be transfer out from CPU. In order to have high thermal conductivity, nanoparticle is used in the base fluid of thermal paste. Therefore, objective of my study is to examine the thermal conductivity with the effect of nanoparticle concentration.

EXPERIMENTAL SETUP

Alumina thermal paste was prepared by using two-step method. For two-step method, nanoparticle are first produce by companies as dry powders. Then, nano powder will disperse into base fluid with the help of mechanical stirrer. Aluminium Oxide nano powder will be used as nanoparticle while Sodium Dodecyl Benzene Sulphonate (SDBS) as a surfactant. SDBS is used in this experiment in order to enhance the stability of alumina thermal paste.

Thermal conductivity of alumina thermal paste was measured by using thermal conductivity meter (kd2pro). Then, alumina thermal paste was applied on the CPU by using middle dot method. Finally, checking the stability of alumina thermal paste by using consistency test.

RESULTS AND DISCUSSION

Thermal conductivity of alumina thermal paste with and without SDBS was measured at three different temperature which are 30°C, 40°C and 60°C. This study was conducted to check the effect of SDBS on thermal conductivity of alumina thermal paste. The thermal conductivity for both condition were closed each other. Therefore, it can be conclude that SDBS is not a substance that can affect the thermal conductivity of alumina thermal paste. SDBS is used in alumina thermal paste to enhance the stability of nanofluids that might be used in long term period in CPU. [1]

Figure 1 represent the thermal conductivity of alumina thermal paste again volume concentration at different temperature. Thermal conductivity increase with the increasing of volume concentration and temperature. 4.0% volume concentration at 60°C have highest percentage enhancement of thermal conductivity compare to other concentration. The percentage at this volume concentration is 8.2%. Brownian motion is a key mechanism in controlling thermal conductivity of alumina thermal paste. [2] The particle in thermal paste increase when the volume concentration increase. When the temperature increase, the kinetic energy increase, the particle have greater speed and collide each other. The motion of particle increase and the heat diffusion or transfer also increase from CPU to surrounding.

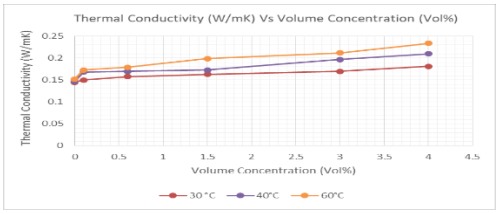

Figure 1: Thermal conductivity (W/mK) vs volume concentration (Vol %)

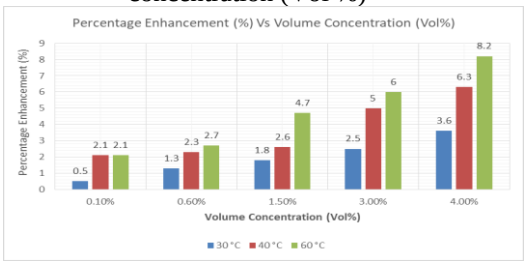

Figure 2: Percentage enhancement of thermal conductivity (%) according to volume concentration (Vol %) and temperature.

CONCLUSION

We have shown the thermal conductivity of alumina thermal paste increase when the volume concentration increase. 4.0% volume concentration have higher percentage enhancement of alumina thermal paste at 60°C. Further study can used higher volume concentration and compare with theoretical value.

REFERENCES

[1] Yu, W. and Xie, H. (2012). A Review on Nanofluids: Preparation, Stability Mechanisms, and Applications. Journal of Nanomaterials, 2012, pp.1-17.

[2] Gupta, M., Singh, V., Kumar, R. and Said, Z. (2017). A review on thermophysical properties of nanofluids and heat transfer applications. Renewable and Sustainable Energy Reviews, 74, pp.638-670.

BORON THERMAL PASTE FOR ENHANCING COOLING PERFORMANCE OF CENTRAL PROCESSING UNIT

Mohamad Shahril Muslim and Muhammad Noor Afiq Witri
School of Mechanical Engineering, Faculty of Engineering,
Universiti Teknologi Malaysia, 81310 UTM Skudai, Johor, Malaysia

INTRODUCTION

According to Yunus et.al, 2007, the number of transistors packed in a single chip has been increasing steadily over a period of time [2]. The innovation of the component or devices is producing a major problem to the product which is high heat generation of the components that may destroy or damage the components unless the heat is transferred away from them. Previous studies have successfully demonstrated the feasibility of various application to overcome this problem. Thermal grease with Hexagonal Boron Nitride (hBN) has been used to enhance the heat dissipation from the electronic devices.

EXPERIMENTAL SETUP

This section presents the experimental setup for the system. Five volume concentrations were used to obtain the optimum value of hBN powder that can be used. The two-step method is selected to mix the compound which consist of thermal grease, hBN nanoparticles and Sodium dodecylbenzene sulphonate (SDBS) with 400 rpm for 15 minutes. The thermal conductivity of the nanogreases was measured by using KD2 Pro device with Ks-1 probe. The nanogreases was applied on the CPU system to verify its CPU temperature and fan speed. CPU-Z software is used to monitor the computer to run at 100% of CPU usage. SpeedFan 4.52 also used to record the temperature of the CPU and record it in notepad.

RESULTS AND DISCUSSION

Figure 1 shows the thermal conductivity of nanogreases increases linearly as the percentage of volume concentration increase. Based on Zhou et.al, 2012, the low thermal conductivity of the nanogreases is at low fillers loading, it is because of the heat conductive of the nanoparticles surrounded by matrix cannot be touch each other [3].

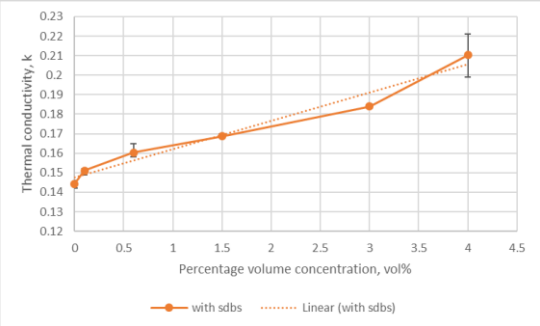

Figure 24 : Thermal conductivity, k versus percentage volume concentration

Figure 2 shows the CPU temperature is moderately decrease as the percentage of volume concentration increase. By observing the data obtained, the maximum temperature is 90◦C by using 4.0 vol% while the minimum temperature is 79 ◦C by using 3.0 vol% of HBN nanoparticles. According to Razeeb et.al, 2018, the bond line thickness (BLT) represent the contact resistance of the TIM with the two-bonding surface, where the thickness BLT must be small as possible to reduce thermal resistance at the junction area [1].

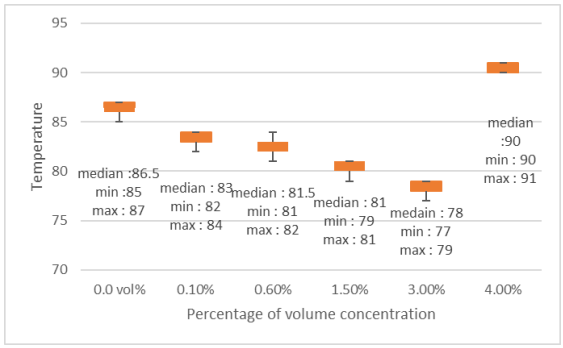

Figure 25 : Boxplot of Temperature

CONCLUSION

As a conclusion, all the objectives of the studies were achieved successfully. The thermal conductivity of the nanogreases is increased as the filler loading increased. The optimum value pf volume concentration of hBN is about 3.0 vol% which reduced the CPU temperature up to 23.33% compared the base thermal grease. SDBS is function as a stabilizer agent, however, it not affects the thermal conductivity of the thermal grease.

REFERENCES

[1] Razeeb, K. M., Dalton, E., Cross, G. L. W., & Robinson, A. J. (2018). Present and future thermal interface materials for electronic devices. International Materials Reviews, 63(1), 1-21.

[2] V. Yunus A.Cengel and Afshin J.Ghajar (2007) Cooling of Electronic Equipment, Heat Transfer, 24(4), pp. 15-2

[3] Zhou, Y., Wang, H., Wang, L., Yu, K., Lin, Z., He, L., & Bai, Y. (2012). Fabrication and characterization of aluminum nitride polymer matrix composites with high thermal conductivity. Materials Science and Engineering: B, 177(11), 892-896

DESIGNING MULTIPURPOSE PRAYER MAT

Nur Dina Balqis Rosmadi and Muhummad Zameri Mat Saman
School of Mechanical Engineering, Faculty of Engineering,
Universiti Teknologi Malaysia, 81310 UTM Skudai, Johor, Malaysia

INTRODUCTION

The prayer rug as a medium of cleanliness because it will be placed between the worshiper and the ground. As been said by [1], these mats' structure and design are in such that way because they contribute to comfort, safety efficiency and ease of use. These multipurpose prayer rug can provide support and great help in case of spinal or back pain, stated by both [2] and [1]. Usually, for older adults and senior citizens which have poor condition of health it was hard for them to do worship. Therefore, they tend to bring their own tripod cane-seat or use the provided chair by the mosque.

The foldable chair was invented to provide a satisfactory feeling of comfort for the user when using it [3]. Therefore, when the user sits upon the upper surface, the pressure of the fluid in the sealed cavity is increased [4]. The problems that occur are the second feature of the multipurpose prayer mat only can used after the prayer, not during the prayer. After that, the older adult need supports during the prayer. The objective of this project was to design a praying mat that can be used not only for religious worship but also for other purpose and produce the prototype.

METHODOLOGY

In methodology, product design specification was used to make sure the dimension and material for of the base structure. After that, some additional features were added to satisfy the customers need. Then, the idea generation is accomplished by creating single systems from different mechanisms illustrated in the morphological chart. It is advised to generate several feasible designs using different mechanisms for each function for each concept. From morphology chat, an evaluation table is form. In this process, the elements that need to be evaluated are point out to get the best design. An evaluation matrix has been made. Figure 1 shows the proposed fabricated multipurpose prayer mat.

RESULT AND DISCUSSION

Two load were used for stress analysis which are 57.7kg and 80kg. When the 566.03N load is applied, each of the components will shows their maximum stress. All the maximum stress for each component are lower than the aluminium yield stress which is 95MPa which are 33.77MPa, 2.55MPa, 28.63MPa and 4.73MPa. Therefore, the components are safe to be used to support the load. When the 784.8N load is applied, each component will show it maximum stress which are 47.74MPa, 3.54MPa, 39.7MPa and 6.55MPa.

Therefore, all the components have lower maximum stress than aluminium yield stress. Hence, the components are safe to be used as the structure.

Figure 1: Fabricated multipurpose prayer mat

CONCLUSION

The objectives of designing multipurpose prayer mat was achieved. The final design satisfied the customers needed. The new feature which is the multipurpose prayer mat can be used during the prayer as a chair was successfully implemented. Due to stress analysis results, all the main components which are front and back leg structures and front and back seat base structures were able to support the maximum targeted weight, 80kg. To be portable and light, the used of aluminium material was installed as the structure and the total mass for this multipurpose prayer mat is 1.376kg. Thus, the result of this project shows that the multipurpose prayer mat design is developed successfully.

REFERENCES

[1] Wallinside, "The Reality about Muslim Prayer Mat," 11 August 2015. [Online]. Available: https://wallinside.com/post-543899-the-reality-about-muslim-prayer-mat-.html.

[2] Arham, "Apt Features Regarding Janamaz Prayer Mat," 20 August 2015. [Online]. Available: https://www.slideshare.net/Prayermat/apt-features-regarding-janamaz-prayer-mat.

[3] P. M. Cuomo and R. B. White, "Fordable Chair," *United States Patent*, 1999.

[4] G. L. Huff, R. Archer and J. P. Haynes, "Stool Seat," *United States Patent*, 1989.

VIBRATION CONTROL OF FLEXIBLE BUILDING STRUCTURE BY USING ACTIVE FORCE CONTROL

Tan Wei Keong and Musa Mailah
School of Mechanical Engineering, Faculty of Engineering,
Universiti Teknologi Malaysia, 81310 UTM Skudai, Johor, Malaysia

INTRODUCTION

Generally, active and passive control system are commonly used to mitigate the vibration of the building structures. For instance, tuned mass damper (TMD) and active mass damper (AMD) are examples of technique used in both control systems. However, passive vibration control (PVC) does not guarantee a satisfying performance in term of stability and solidity [5]. Meanwhile, active vibration control (AVC) may cause stability issue when extra energy is generated within the system, even though AVC system can alleviate vibration response of the building. Hence, Active Force with Iterative Learning Control (AFILC) can be a strategic approach to optimize the PID controller in AVC of the building structure. This project is aimed to develop a robust and adaptive control method to suppress undesired structural motion of a flexible 2-storey building. The proposed control method involves the integration of Active Force Control (AFC) and Iterative Learning Control (ILC) with a conventional Proportional Integral Derivative (PID) controller.

METHODOLOGIES

A simple building structure can be modelled into general dynamic equation by using Newton's Second Law of Motion,

To linearize a 2-storey building model, the floor is assumed as rigid beam and lumped mass at each floor of the structure. Besides, the wall of each floor can be considered by spring constant. In addition, the supporting vertical wall can be also idealized by a damping coefficient. In a meantime, axial deformation in beam and column is negligible. Finally, dynamic equation of the building model can be described in the following equation.

$$\begin{bmatrix} m_1 & 0 \\ 0 & m_2 \end{bmatrix} \begin{Bmatrix} \ddot{x}_1 \\ \ddot{x}_2 \end{Bmatrix} + \begin{bmatrix} c_1 + c_2 & -c_2 \\ -c_2 & c_2 \end{bmatrix} \begin{Bmatrix} \dot{x}_1 \\ \dot{x}_2 \end{Bmatrix} + \begin{bmatrix} k_1 + k_2 & -k_2 \\ -k_2 & k_2 \end{bmatrix} \begin{Bmatrix} x_1 \\ x_2 \end{Bmatrix} = \begin{Bmatrix} P_1 \\ 0 \end{Bmatrix}$$

Next, the mathematical model is converted into block diagram by MATLAB/Simulink. Lastly, heuristic method is used to tune the controller main parameters in the proposed control system.

RESULTS AND DISCUSSION

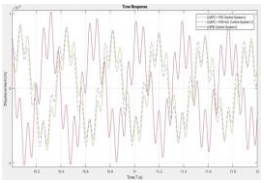

Figure 1: The average score in each question

Simulation has shown that the proposed AFILC method gives the most satisfying performance and robustness during the suppression of undesired vibration at each floor. Although the solely PID control system can give considerable attenuation of vibration, but AFILC approach significantly improve the performance of control system in term of amplitude of vibration and steady state error. AFC managed to provide appropriate estimation of disturbance force to the actuator. Meanwhile, ILC algorithm further enhance the estimated disturbance force in AFC. This combination has managed to reduce the undesired floor's vibration by 32.77% and 30.96% when subjected to harmonic disturbance.

CONCLUSION

The prototype of AR-based instruction manual is successfully developed. The demonstrated functionality of the AR application has great potential to experienced workers as well as new workers to use it as training kits. Besides, it also increases the understanding level of the work procedures of an assembly process.

REFERENCES

[1] Nazir, S., & Manca, D. (2015). How a plant simulator can improve industrial safety. Process Safety Progress, 34(3), 237-243. [2] Neumann, N., & Kubler, A. (2003). Training locked-in patients: a challenge for the use of brain-computer interfaces. IEEE Transactions on Neural Systems and Rehabilitation Engineering, 11(2), 169-172.

[2] Ong, S., & Wang, Z. (2011). Augmented assembly technologies based on 3D bare-hand interaction. CIRP Annals-Manufacturing Technology, 60(1), 1-4

[3] Syberfeldt, A., Danielsson, O., Holm, M., & Wang, L. (2015). Visual assembling guidance using augmented reality. Procedia Manufacturing, 1, 98-109.

INTELLIGENT ACTIVE FORCE CONTROL OF A TWIN ROTOR SYSTEM

Tay Yin Shen and Musa Mailah
School of Mechanical Engineering, Faculty of Engineering,
Universiti Teknologi Malaysia, 81310 UTM Skudai, Johor, Malaysia

INTRODUCTION

Helicopters have been widely used in many applications due to its high versatility. A great deal of research has been done in the modelling control system of helicopters over the past decades to improve its robustness. A twin rotor multi-input multi-output system (TRMS) is commonly used in the research lab to test the effectiveness of a control strategy which is designed for a real helicopter system. The TRMS resembles two main features of the helicopter, which are nonlinearity and cross coupling effect. Therefore, it is important to have a deep understanding of the properties and behaviours of the modelled system in order to design a robust control system. The objective of this project is to implement a robust intelligent Active Force Control (AFC) using iterative learning algorithm to a twin rotor system. The adaptive AFC and Iterative Learning Control (ILC) are proposed to be integrated with a conventional Proportional-Integral-Derivative (PID) control method to improve its robustness and ability of disturbance compensation.

METHODOLOGY

In this paper, a derived TRMS mathematical modelling has been selected as the TRMS dynamic model [1]. The dynamic model is derived by using the standard Euler- Lagrange approach. There are four coordinates to be controlled and lead to the desired output angles, which are pitch angle, ψ, yaw angle, Φ, angles of main rotor, ρm and tail rotor, ρt. The control system has been developed using MATLAB/Simulink via the proposed control techniques which are the PID control, AFC and ILC. Impulse and simple harmonic are the disturbances applied to the TRMS in multiple directions at the pitch, yaw, axis of main rotor and tail rotor which imply the impulse forces and vibration that the TRMS may face in the real experiment. For the actuator and sensor, perfect modelling is assumed, implying that the signal is directly extracted within the system and all the noises are ignored. In addition, saturation block is also included to limit the input signal of each DC motor used to the saturation rated current (1.10 A).

RESULTS AND DISCUSSION

PID is found that generate a poor response where possesses an infinity settling time, high overshoot and large steady state error whenever disturbance is applied. In contrast, the proposed hybrid PIDAFC and PIDAFCIL produce an acceptable response with significant improvement. Besides, observed that the hybrid PIDAFCIL encompasses the ability to compensate the disturbances introduced to the TRMS with a faster settling time and smaller steady state error than PIDAFC. In short, the proposed PIDAFCIL illustrates the robust control design method with the feasibility and effectiveness and suitable to be applied in the TRMS.

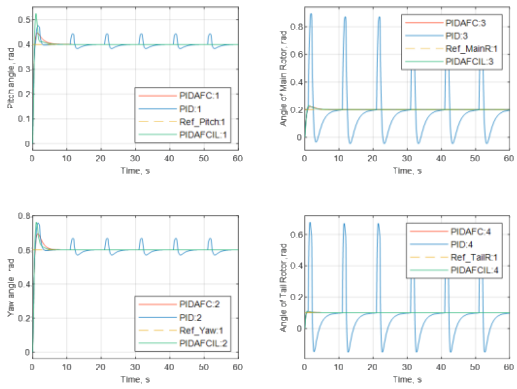

Figure 1: Comparative study of control methods

REFERENCES

[1] Tastemirov, A., Lecchini-Visintini, A., & Morales-Viviescas, R. M. (2017). Complete dynamic model of the twin rotor MIMO System (TRMS) with experimental validation. Control Engineering Practice, 66, 89-98.

FRONTAL IMPACT OF BUS SUPERSTRUCTURE

Mohd Aan Hafeezal Fahmeey Md Sahar and Mustafa Yusof
School of Mechanical Engineering, Faculty of Engineering,
Universiti Teknologi Malaysia, 81310 UTM Skudai, Johor, Malaysia

INTRODUCTION

Road traffic accidents are always a huge issue in developing countries such as Malaysia. For bus, the cases of road traffic accidents increase significantly by 48% between the year 2006 to 2008 [1]. Regulation of UNECE R29 and FMVSS is used to investigate the performance of bus superstructure. Validation of finite element analysis tool (6.10) has been conducted by experimental and simulation.

EXPERIMENTAL SETUP

For validation, rig specimen would be undergoing drop impact by using Drop Tower Machine and the deformation of the structure will be observed. Meanwhile, the assessment technique used in the frontal impact study is ECE R29 and FMVSS, which covered on frontal crash of the vehicle for Bus A and B. The main difference between these two regulations are the type of loading which for ECE R29, the pendulum is used with particular angular velocity, while for FMVSS, the vehicle is moving towards a rigid wall with assigned velocity.

RESULTS AND DISCUSSION

Figure 1 shows the comparison of deformation pattern between experimental and simulation of the rig structure.

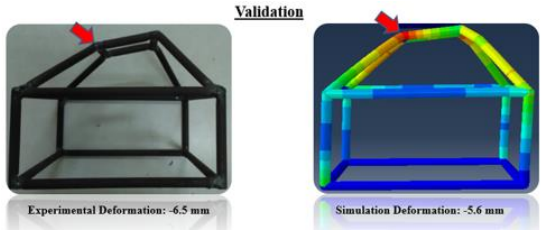

Figure 1: Deformation pattern comparison

The difference of deformation pattern is 13.8%. Similarity of reaction force of indenter is 82.96% while displacement of indenter is 100% similarity.

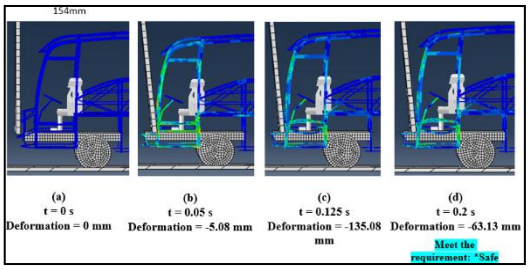

Figure 2: Deformation Response of Bus A based on R29

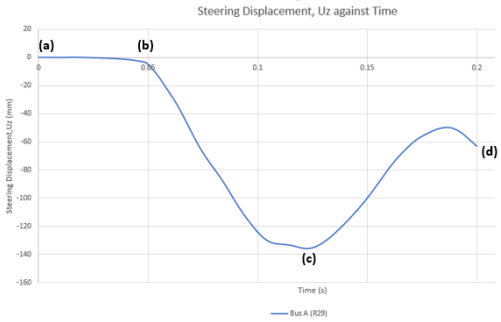

Figure 3: Graph of Steering displacement, z-direction of Bus A(R29) against time

Figure 3 (a) and (b) shows the structure during initial condition and first impact respectively. It can be observed that in Figure 3 (c), the steering wheel is approaching manikin body. However, the maximum deformation is still in elastic region and the steering is displayed in Figure 3. The maximum displacement of -135 mm is recorded at 0.125 s. Bus A superstructure are meeting the requirement of ECE R29. The bus driver is safe from the impact situation.

CONCLUSION

Impact test on rig specimen based on experiment and simulation can be verified as accurate as shown in results and discussion section in term of deformation pattern, reaction force of indenter of impactor, and the displacement of indenter against time between both experimental and simulation. The frontal impact simulation of the bus superstructure by following UNECE R29 and FMVSS have been demonstrated. Results show that both buses are meeting the requirement of regulations.

REFERENCES

[1] Solah MS, Ariffin AH, Isa M, Wong SV. In-depth crash investigation on bus accidents in Malaysia. Journal of Society for Transportation and Traffic Studies. 2013;3(1):22-31.

[2] Mirzaamiri R, Esfahanian M, Ziaei-Rad S. Crash test simulation and structure improvement of IKCO 2624 truck according to ECE-R29 regulation. International Journal of Automotive Engineering. 2012;2(3):180-92.

EVALUATION OF THE PREDICTION OF WAVE PATTERN AND HULL PERFORMANCE OF MTC 092 AND MTC 098 HULL FORM USING COMMERCIAL SOFTWARE

Leow Jing Shuo, Nasrudin Haji Ismail and Arifah Ali
School of Mechanical Engineering, Faculty of Engineering,
Universiti Teknologi Malaysia, 81310 UTM Skudai, Johor, Malaysia

INTRODUCTION

The ship hull models being studies in this thesis are two different type of hulls, which are MTC 092, a planning hull, operate with Froude number (Fn) larger than 0.4, and MTC 098, a displacement hull, operate with Fn smaller than 0.4. This paper is a further study on evaluating the hull form resistance and wave pattern predictions results that was previous done on opensource software OpenFoam with Commercial software, Ansys. The possible reasons regarding the results accuracy difference between the two software would also be discussed in this paper.

METHODOLOGY

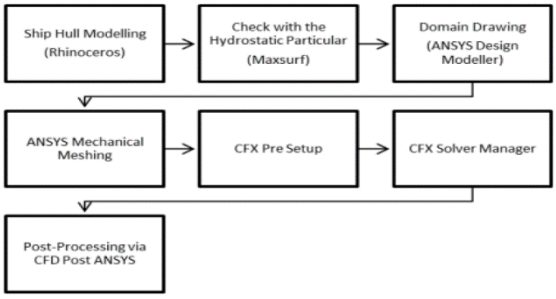

Figure 1: Simulation Work Flow

RESULTS AND DISCUSSION

The simulation setup by the previous student is on even keel condition, but in actual case, it trimmed. Since the model is a planning hull, its trimming angle would affect a lot on the resistance result. Based on Figure 1, we could notice that the trendline for the simulation result at even keel from Ansys is similar with that of OpenFoam. However, at trimmed condition, the Ansys resulted in higher accuracy with percentage error lower than 10 %. Hence, the possible problem for high percentage error for OpenFoam result is caused by the ship condition. Based on Figure 2, we can notice that the trendline for the Ansys result is more near to the experiment result than the OpenFoam result. The shape of the trendline for OpenFoam result also not similar to the experiment result, however, Ansys is capable to result in similar graph shape with experiment. The possible reason for high percentage error of OpenFoam result is due to the wrong setup done by previous student. The type of simulation run by her is rigid body solution, but she does not provide the mass moment of inertia of the ship to the solver. Besides, the CAD model from her is also not complete, it does not have the stern appendage part design on the CAD model.

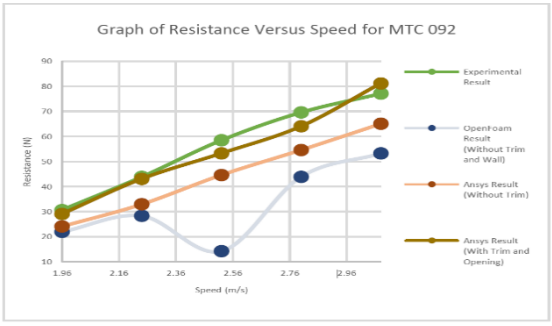

Figure 2: *Graph of Resistance Versus Speed for MTC 092 at Different Condition*

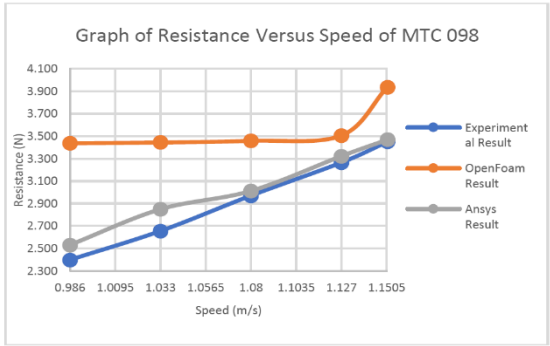

generated form Ansys for the two ship have more than 90% accuracy. The possible cause for low accuracy result from OpenFoam was also identified. A rerun would be need for OpenFoam as to compare the competitiveness of the two software.

REFERENCES

[1] Hasegawa, T., Masaki, S., and Hiroshi, W. (1997). Anomaly of excess pressure drop of the flow through very small orifices. Physics of Fluids, 1-3.

[2] Jitschin, W. (2004). Gas flow measurement by the thin plate orfice and the classical Venturi tube. Vacuum, 2.

PREDICTIONS OF WAVE PATTERN AND HULL PERFORMANCE OF MTC101 HULL FORM BY USING OPENFOAM

Muhammad Faiz Izzuddin Mohd Junaidi and Nasrudin Ismail
School of Mechanical Engineering, Faculty of Engineering,
Universiti Teknologi Malaysia, 81310 UTM Skudai, Johor, Malaysia

INTRODUCTION

Since early 1990, Computational Fluid Dynamic (CFD) has been used in the development of ship hull forms by using the first panel methods which are still widely used today to compute the flow field and wave system around a ship advancing at speed [1],[2]. At first CFD method uses the Navier-Stokes equations to solve the potential flow theory but it was difficult. Then the idea of modifying the Navier-Stokes equations which came up with Reynold-Average Navier-Stokes (RANS) equation to compute the simulation for ship resistance. At the beginning of the design process, hull resistance and needed engine power are estimated by analytical equations, after that, towing tank tests should be performed but they are very expensive. Therefore, CFD is one method uses for doing simulation on the ship resistance performance. Therefore, Open-source CFD software such as OpenFOAM is one of the solutions in the engineering problems for CFD problems.

EXPERIMENTAL SETUP

MTC101 Hull Form Model was chosen as the ship model that will be studied for its hull performance and wave pattern. First of all, the hull resistance and ship hydrostatic particular of MTC101 hull form were obtained from the MTC. The MTC101 CAD model was modelled by using FREE!ship Plus and then the ship hydrostatic particular was compared with the experimental result as validation. In pre-processor, GMSH was being used to analyse the CAD model meshing error and used to optimize the CAD model mesh. As for solver used in CFD, OpenFOAM used to calculate and solve for engineering problems by using a numerical method. Finally, ParaView was used as a post-processor to simulate the simulated result to obtain the graphical of wave pattern. Last but not least, the simulated results were being analysed and tabulated in the form of table and graph for comparison.

RESULTS AND DISCUSSION

Table 1 shows the comparison hull resistance between experimental results with CFD result. As the Froude no., Fn increase then the hull resistance generated by hull form also increases too. Finally, the overall percentage error is below 10% which is quite good obtained from CFD result.

Table 1: Comparison total resistance between experimental result with CFD result

Model Speed, m/s	Froude No.	Total Resistance, Rt		Percentage error, %e
		Simulation	Experiment	
1.61	0.383	7.93	7.27	9.11
1.84	0.437	9.89	10.91	9.31
2.07	0.492	12.08	12.71	4.90
2.30	0.547	14.64	14.78	0.95
2.53	0.601	17.05	16.46	3.56

Figure 1 shows the wave pattern generated at the speed of 2.07m/s. From the figure, its show that the wavelength generated is 602.48mm while the Kelvin Wake angle is 17°. Therefore, the wave pattern angle obeyed the Kelvin Wave angle theory that stated the wave angle generated must below 19.5° for half measured.

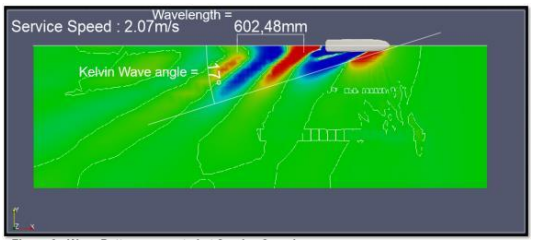

Figure 1: Wave pattern generated at speed of 2.07m/s

CONCLUSION

In a nutshell, all of the objectives in this study were achieved. Firstly, the main objectives of this study are to determine the free-surface wave pattern and hull resistance by analysis of the computed flow field was successfully done by using the OpenFOAM as CFD solver. Next, to assess the hull resistance obtained from the analysis with the model testing results also successfully being compared.

REFERENCES

[1] Delhommeau, G., & Maisonneuve, J. (1986). Calculation of Flow around several Ship Hulls by a Rankine Source Method. Proceedings of the 2th International Conference Hydrosoft. Southampton.

[2] Raven, H. (1998). Inviscid calculations of ship wavemaking capabilities, limitations and prospects. 22nd Symp. on Naval Hydrodynamics, Washington DC.

PREDICTION OF WAVE PATTERN AND HULL PERFORMANCE OF MODEL MTC102 HULL FORM USING OPENFOAM

Nurul Atiqah Zakaria and Nasrudin Ismail
School of Mechanical Engineering, Faculty of Engineering,
Universiti Teknologi Malaysia, 81310 UTM Skudai, Johor, Malaysia

INTRODUCTION

In the advanced marine field in Asia, OpenFOAM software has also been widely used by major companies like Hyundai Heavy Industries except Malaysia [1]. Open source software is also free software to access any software. Commercial CFD software is preferred not only because of its ability to perform powerful calculations, but users are friendly and easy to navigate. So through this research will discuss how to solve the complications using the OpenFOAM software to predict the ship's resistance and produce the MTC102 wave pattern. Based on the above problem, the problem resulted to get the comparison of the accuracy of the analysis results obtained by using OpenFOAM with experimental results.

EXPERIMENTAL SETUP

Vacuum forming is performed by using Formech 300XQ to fabricate a designed plastic packaging for medical device. Polyvinyl chloride (PVC) and High Impact Polystyrene (HIPS) plastic sheets were used to study and make comparison on the effects of materials in manufacturability. A Computer Aided Design (CAD) SolidWorks was fully utilized in the design activity as an additive 3D machine FLASHFORGE was used to print out the mould of the illustrated. The prototypes were tested the functionality and performance by carried out packaging testing methods-visual inspection and drop test.

METHODOLOGY

Set the simulation to run for 6 different speed. There three process in CFD progress which is Pre-processing Process, Solver and Post- Processing Process. Pre-Processing Process divided into two part. Firstly construct the model by using FREE!ship Plus Software and secondly check the mesh part by using GMESH as meshing process. In this study the model hull that has been used is MTC102. The numerical equation for ship resistance analysis is solved by using OpenFOAM as a solver software. Next, the description of the analysis is illustrated by using the ParaView. ParaView is a software for Post- Processing process because it can be simulated wave pattern flow and hydrodynamic analysis simulation.

RESULT AND DISCUSSION Based on Figure 1, shows the relationship between the Total resistance and Froude number. The relationship between total resistance with Froude number is if speed and Froude number increasing, the resistance also increase. The result show that the simulation by using OpenFOAM result is underestimate. The value of total resistance of simulation is less than experiment data. This is because, for this simulation model is using SST k-omega model.

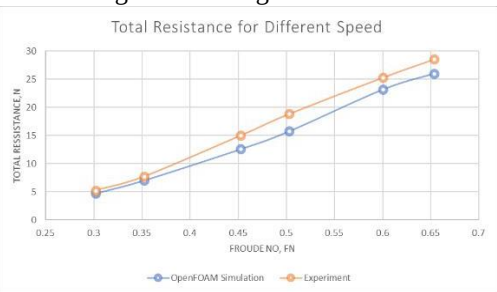

Figure 1: Graph Total Resistance at Different Speed

Based on the objective, to determine the wave pattern at free-surface by analysis of the simulation result. Figure 2 (a) and (b) will show the capture of wave pattern during run the simulation for different speed.

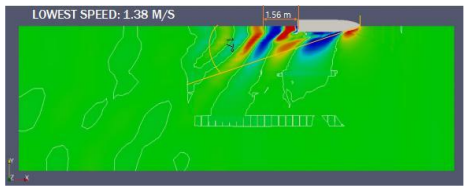

Figure 2 (a): Wave Pattern for Lowest Speed, 1.38 m/s

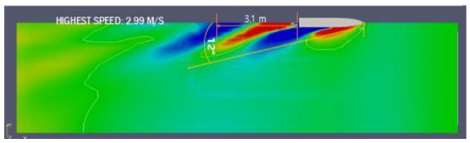

Figure 2 (b): Wave Pattern for Highest Speed, 2.99 m/s

CONCLUSION

In conclusion, OpenFOAM has a potential as a solver for CFD analysis. Beside, OpenFOAM can observed and can calculate the wave pattern result. Hence by using ParaView can visualise wave pattern flow.

REFERENCES

[1] Hong, K. G. (2016, September 30). 현대중공업선박연구소의 OpenFOAM® 을 이용한 선박 성능 해석 'Ship Performance Analysis using OpenFOAM in HHI-Present and Future'. In H. H. Industries (Ed.), 5th OpenFOAM Korea Users' Community Conference, 5th OKUCC (p. 5). Korea: Hyundai Heavy Industries Co., Ltd.

FURTHER TECHNICAL AND ECONOMIC EVALUATION ON DUAL FUEL DIESEL-ELECTRIC PROPULSION PLANT OF A LARGE CONTAINER VESSEL

Mohamad Iskandar Abd Kadir and Nasrudin Ismail
School of Mechanical Engineering, Faculty of Engineering,
Universiti Teknologi Malaysia, 81310 UTM Skudai, Johor, Malaysia

INTRODUCTION

To comply with the new IMO regulation [2], EEDI and EEOI, new approach needed to be made for ship's propulsion plant. DFDE propulsion plant gives a new option for ship owner to reduce the emission level of their ships. The usages of cleaner LNG fuel significantly reduce the emission level of the vessel. However, the propulsion plant is not widely used by marine vessel except for LNG carrier itself due to its convenience. Therefore, a study needs to be done for the conversion since many aspects may be affected due to the conversion.

METHODOLOGY

Technical parameters that have been identified affected due to the conversion will be assessed. Parameters and requirements need to be determined. The components selection will be based on the availability on the market. After all the technical parameter analysis determined, the economic analysis needs to be conducted to determine the value of the investment.

RESULTS AND DISCUSSION

The power determination of the plant needs to consider both propulsion power and auxiliary power requirement of the original vessel to ensure that the operation of the ship is not affected after the conversion. To determine the power required, the efficiency of the equipment need to be taken into account. The total power required is 88,473 kW [1].

Table 4: Machinery selected for the propulsion plant

Engine	WinGD W7X72DF	2 unit
	WinGD W6X72DF	2 unit
Alternator	Siemens SIGENTECS M	4 unit
LNG Tank	Wartsila LNGPac	15 unit
LNG Pump	Venzetti VT-100 62 T	2 unit
Vaporizer	Alternate Energy System WB-7005	2 unit
Heat Exchanger	Alpha Laval MX-25	79 unit
Fresh Water Pump	Azcue CA Close Couple Self Priming Centrifugal Pump	4 unit
Sea Water Pump	Azcue MN VP/EP Close Couple Self Priming Centrifugal Pump	2 unit
Motor	ABB AMZ 1600	2 unit
Gearbox	Flender Multiple Input/Single Output Marine Gearbox	1 unit

The capital cost for the machineries is USD 43.56 million while the annual operating cost is USD 22.66 million.

Table 5: Cost saving after 10 year

	Cost Saving after 10 years (USD)	
Saving type	Original Plant HFO	Original Plant LSHFO
Fuel cost	24,025,697	40,185,370
Penalty	2,295,725	1,465,725
Total	26,321,422	41,651,095

Based on the calculation, the operational cost saving in the long run can offset the capital cost.

CONCLUSION

The objective of this study is to produce detailed design of the DFDE propulsion plant and establish economic performance on a large container vessel is achieved. The design and machinery selection are determined based on the technical parameter calculated. The changes on the system are based on the results of the analysis.

REFERENCES

[1] Adnan, C. K. (2017). Technical and Economic Evaluation on Dual Fuel Diesel-Electric Propulsion Plant of a Large Container Vessel. Johor Bahru.

[2] International Maritime Organization. (n.d.). Greenhouse Gas Emissions. Retrieved 12 8, 2018, from International Maritime Organization: http://www.imo.org/en/OurWork/Environment/PollutionPrevention/AirPollution/Pages/GHG-Emissions.aspx

ENERGY AND EXERGY ANALYSIS OF THERMAL POWER PLANT

Muhammad Fazrul Hisham Nordin and Natrah Kamaruzaman
School of Mechanical Engineering, Faculty of Engineering,
Universiti Teknologi Malaysia, 81310 UTM Sekudai, Johor, Malaysia

INTRODUCTION

Economic power generation with lowest fuel consumption is the main challenge for all engineers working in power generation industry. In order to increase the efficiency of the power plant, a proper analysis need to be made. Any method to increase the power plant efficiency would always cost the company greatly . Usually, the performance and efficiency of thermal power plants is evaluated through energy analysis which is based on the first law of thermodynamics. But, studies found that, the exergy performance analysis which is based on the second law of thermodynamics has found a useful method in the design, evaluation, optimization and improvement of thermal power plants [1].

DATA COLLECTION

The data collection is made by considering all the major components in the power plant such as turbines, condenser, boiler, and pump. The limitation is this experiment is that the data collection can be made only at the devices that have the set up equipment to read the data. The data collection is made based on the 100% load and 60% load to be able to compare the result. There are totally 33 point of data collected throughout the power plant mainly at the inlet and outlet of every major device. The first part of the analysis is to determine the specific enthalpy, specific entropy, specific exergy and exergy destruction rate of each point throughout the power plant.

RESULTS AND DISCUSSION

Similar to energy losses on 100% load, on 60% load, the boiler seems to has the highest energy losses compared to other component with 137813.1 kj/kg losses on 60% load and 232,014.12 kJ/kg of losses for 100% load. Boiler contributed 43.15% of energy losses of the total energy losses in the power plant. Other components did not appear to have the much effect on the energy losses except for condenser. Despite having lower energy losses than boiler, each condenser contributes 27.02% of the overall energy losses. The first law efficiency shows that the condenser has the lowest efficiency among all other components for both load with the efficiency of 75.35%.and 66.52% for 100% load and 60% load respectively. The energy loss associated with the condenser are significant because it represents most of the energy input in the power plant.

From table 3, it was found that the exergy destruction rate of the boiler is dominant for both load condition over all other irreversibilities in the cycle with the destruction rate of 63.30% for 100% load and 86.31% for 60% load. The boiler which the main source of heat in the power plant has the lowest exergy recovered from its process. Apart from that, condenser actually contribute only 10.87% from the total exergy lost in overall power plant despite having the lowest efficiency on the first law. For the second law efficiency, the boiler is having the worst percentage of efficiency for both load with only 40.23% and 40.98% efficiency for 100% and 60% load respectively.

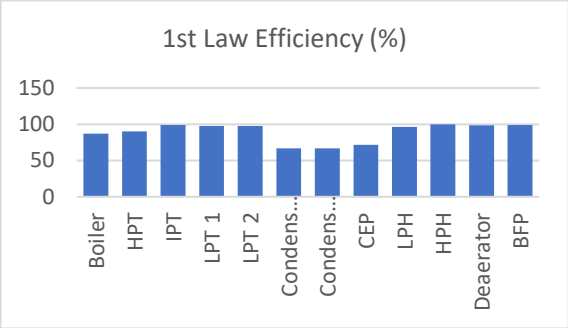

Figure 1: Normalized power for each task correspond to specific direction.

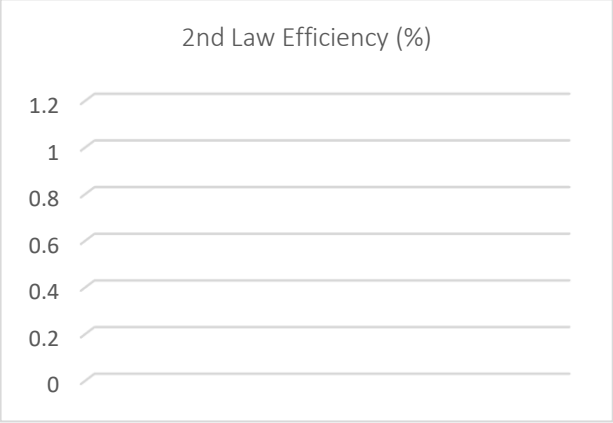

Figure 2: models between control condition

CONCLUSION

it was found that the exergy destruction rate of the boiler is dominant for both load condition over all other irreversibilities in the cycle with the destruction rate of 63.30% for 100% load and 86.31% for 60% load. The boiler which the main source of heat in the power plant has the lowest exergy recovered from its process.

REFERENCES

[1] Aljundi, I. H. (2007). Energy and Exergy Analysis of a Steam Power Plant in Jordan. *Applied Thermal Engineering*, 15-21

ENHANCEMENT OF AIRFLOW VELOCITY AT THE OUTLETS OF AN AUTOMOTIVE HVAC DUCT

Norfatinah binti Olleh, Haslinda Mohamed Kamar and Nazri Kamsah
School of Mechanical Engineering, Faculty of Engineering,
Universiti Teknologi Malaysia, 81310 UTM Skudai, Johor, Malaysia

INTRODUCTION

This study will use CFD method and ANSYS Fluent as a tool. CFD is the most popular method in thermodynamic-fluid application. The parametric analysis is conducted by modifying the elbow angle and shape geometry at the outlets of the automotive HVAC duct. Improvement parameter such as higher velocity and uniformity at the outlets of the duct is adopted to measure performance of the modified ducting geometry. Velocity and uniformity for each parametric cases need to be observed in this study

METHODOLOGY

Simplified geometry model of an automotive HVAC duct is created using CAD software. All dimensions are based on the actual ducting of Proton Persona car. Tetrahedral is selected as element type in meshing set-up. Then, grid Independence test was performed to obtain the suitable number of element while reducing the effect of mesh on the result. Parameters such as condition, type of solver, turbulence model, near wall treatment number of iteration and boundary condition need to be considered in CFD set-up. After that, validation process is conducted by using different turbulence model includes standard k-ε, Realizable k-ε, k-ε RNG, standard k-ω and k-ω SST. Parametric analysis is performed by varying the outlet shape geometry and elbow angle of the duct.

RESULTS AND DISCUSSION

Parametric study was carried out for six different cases. Analysis is done by observing and comparing the velocity at the outlets for each cases. . Uniformity at the outlets are also been observed by comparing the airflow velocity at different position. ANSYS FLUENT is used to obtain air flow and pressure distributions. Then, the comparison for all cases were examined in order to decide the best geometry configuration with uniform airflow and higher airflow velocity at the outlets of the duct.

As refer to Figure 1, Case 1, 3, 4 and 5 indicate the higher velocity difference between outlets. It is shows that the outlet velocity are not equally distributed. Both analysis parameter need to be consider in order to improve the performance of the duct. Case 5 shows the highest airflow velocity at the outlet. But, these case has unsatisfactory uniformity at every outlet. Whereas, case 2 and Case 6 indicate smaller velocity difference between outlets. However, outlet velocity for case 2 is slower compare to case 6. Hence, air flow velocity for both cases are equally distributed. Case 2 shows the smaller pressure difference. Nevertheless, pressure difference is not performance parameter in this study. Therefore, case 6 is the best geometry configuration to improve airflow velocity. Figure 2 shows the geometry configuration for case 6.

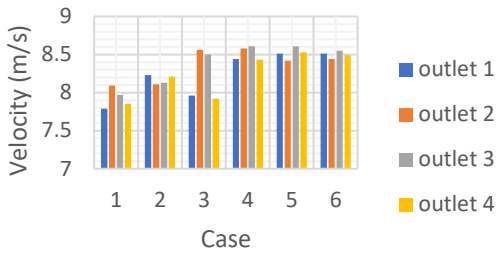

Figure 1: Airflow velocity comparison for all cases

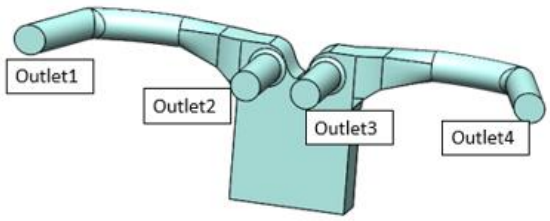

Figure 2: Geometry configuration for case 6

CONCLUSION

Combination of circular outlet with 65˚ elbow angle is offers higher airflow velocity and excellent outlets' uniformity. Airflow velocity at the outlets are increased significantly with range between 4 to 9 percent compare to the baseline case. While the uniformity at the outlet 1, 2, 3 and 4 shows slightly difference which are 0.47 %, 1.29%, 0 % and 0.70 % respectively. Lower percentage difference indicates a good uniformity between outlets.

REFERENCES

[1] Shivanand, D. and Narendra, D. (2015). Numerical Simulation and Analysis of HVAC Duct. International Engineering Research Journal (IERJ), (2), 4878-4880.

NUMERICAL MODELING OF CAVITY FLOW AT LOW REYNOLD NUMBER CONDITION

Hussaini Mohd Marsidi and Nik Ahmad Ridhwan Nik Mohd
School of Mechanical Engineering, Faculty of Engineering,
Universiti Teknologi Malaysia, 81310 UTM Skudai, Johor, Malaysia

INTRODUCTION

Cavities occur in a large number of flight vehicles. High speed flows inside cavities are encountered in many aerospace application including weapons bays of combat aircraft as well as landing gears [1]. The vortex shedding propagates downstream will induce high-intensity oscillation at predominant frequencies. With the increase of emphasis on stealth operation of unmanned combat air vehicles and noise concern near airports, cavity flow attracted the interest of experimentations and computational fluid dynamics analysis to understand the behaviour of the flow inside a cavity [1,2].

METHODOLOGY

This section presents the numerical setup for the simulation. We will be using K Omega SST and DES for this project. The first part of the project is the study on lid driven cavity. A two dimensional domain being tested as a benchmark study for flow in cavity. Reynold number of 100, 400, 1000 and 3200 involved for this study. The contour, velocity and vortex of the lid driven cavity will be compared to Ghia et al [3] and Shankar [4] as validation study. The second part of the project is to simulate the result of experiment flow inside cavity of length to depth 2. The testing carried out in four different flow speed of 10 m/s, 15 m/s, 20 m/s and 25 m/s. The results such as pressure at the floor of cavity, pressure fluctuation, frequency and Spectral Density will be compared and analyse.

RESULTS AND DISCUSSION

Lid driven cavity produce different flow structure at very low Reynold number between Re 100 to 1000. As the Re increase over 1000, another eddy is formed near the entrance of the cavity. The formation of eddies inside lid driven cavity become more consistent and the flow become near static formation with intensity variation. Thus provide us the insight that at the flow inside cavity does not the same between Re number. The higher intensity flow can induce another secondary flow that will produce eddies. Figure 1 shows the fourth eddies inside lid driven cavity that only formed in Reynold number higher than 1000. The flow inside cavity shows huge difference to the experimental results. K Omega SST cannot be used to study unsteady flow inside cavity as the model cannot capture the fluctuation of pressure inside cavity. DES in the other hand can capture pressure fluctuation inside unstead flow as the model has combined functionality of URANS and LES. DES result produce closer approximation to the experimental result. Figure 2 shown that K Omega SST cannot be used to analyse pressure fluctuation and bound to be not accurate.

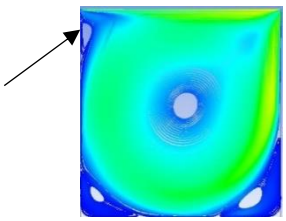

Figure 1: Lid driven cavity contour; the eddy at the top left of the cavity only be verified at Re 1000 and above

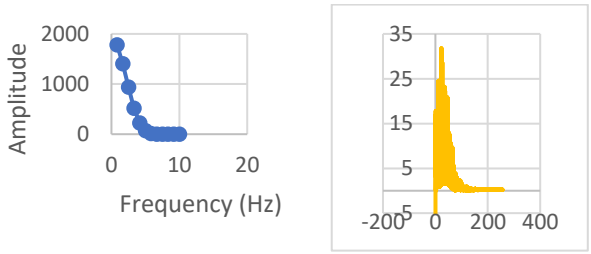

(a) (b)

Figure 2: Comparison amplitude vs. frequency simulation between (a) DES and (b) K Omega SST

CONCLUSION

Lid driven cavity will produce different flow formation inside cavity based on Re. DES should be used instead of K Omega SST because it can capture the fluctuation of pressure inside cavity which is the most critical part of the study. The simulation should be done in three dimensional domain so it can be comparable to the experiment results as two dimensional domain is geometrically too limited to produce similar flow physics in cavity.

REFERENCES

[1] Kung-Ming, C., Kuan-Huang, L., Keh-Chin, C. (2017) Self-sustained oscillation for compressible cylindrical cavity flows. Chinese Journal of Aeronautics 30(4)

[2] Lawson, S., & Barakos, G. (2011). Review of numerical simulations for high-speed, turbulent cavity flows. Progress in Aerospace Sciences, 47(3), 186-216

[3] Ghia, U., Ghia, K. N., & Shin, C. (1982). High-Re solutions for incompressible flow using the Navier-Stokes equations and a multigrid method. Journal of computational physics, 48(3), 387-411.

[4] Shankar, P., & Deshpande, M. (2000). Fluid mechanics in the driven cavity. Annual review of fluid mechanics, 32(1), 93-13.

Numerical Modeling of Hyperbolic Lifting Surface in Harmonic Oscillations

Muhamad Hidayatullah Minhad and Nik Ahmad Ridhwan Nik Mohd
School of Mechanical Engineering, Faculty of Engineering,
Universiti Teknologi Malaysia, 81310 UTM Skudai, Johor, Malaysia

INTRODUCTION

Wing shape is one of the main parts of the aerodynamic performance, so most of the aerodynamic shape optimization effort have been focused mainly on the wing [1]. In modelling a problem that involves the optimization of geometry and meshes, there is a few pre-processors that needs to be considered. Computational Fluid Dynamic, CFD in industry motivate the development of a design or product and also reduce the engineering cost with the desired accuracy and solution cost. After the creation of grid, a solver is able to solve governing equations of the problem. Generation of hyperbolic shape can be done through numerical method by construct an equation.

EXPERIMENTAL SETUP

The method used for validation studies on NACA4412 Airfoil and Hyperbolic wing are different. The studies on 2D is just to get the general idea of CFD meanwhile the main objective is to get CFD data on hyperbolic wing.

For NACA4412 98000 Mesh Elements has been introduced with Spalart-Allmaras turbulence setup has been introduced meanwhile for Hyperbolic Wing, 2Million of Elements with LES turbulence setup has been introduced.

RESULTS AND DISCUSSION

At the end of the method used, a set of results are captured. The main data on hyperbolic wing shape with reduced frequency, k parameters is introduced. The data taken is from -5° to 5° angle of attack. Harmonic motion for full 1 cycle has been selected to study the trend on the change of Cl in Figure 1 and Cd on Figure 2.

The data shows that the increment in the reduced frequency condition leads to more unsteady state. However, as the reduced frequency increased, the value of lift and drag also increased. Therefore, if the harmonic motion is introduced with more parameters introduced, high lift with less drag wing can be performed. For instance, introduced flap on wing and type of materials of the wing.

The data also proved that at less reduced frequency, the results may be almost constant with the static point results where the aircraft is in steady state. The forces needed also decreased in order to control the aircraft at low reduced frequency.

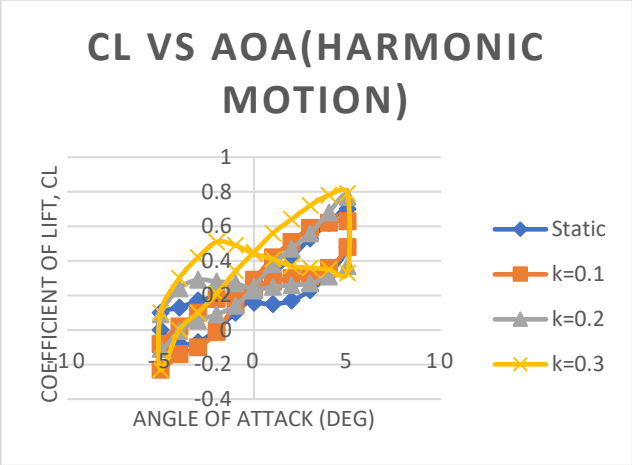

Figure 1: Graph of CL vs AOA in Harmonic Motion

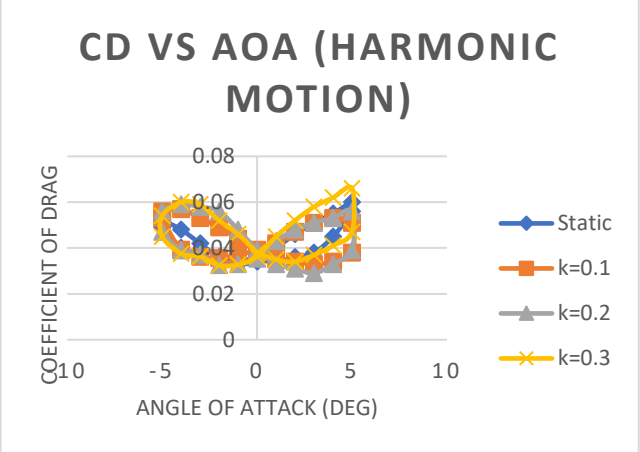

Figure 2: Graph of CD vs AOA in Harmonic Motion

CONCLUSION

I have extracted from this simulation on how the new hyperbolic design from CRM model can be enhanced the limitation of the wing with more aerodynamically shape.

REFERENCES

[1] Chen, S., Lyu, Z., Kenway, G. K. W., & Martins, J. R. R. A. (2015). Aerodynamic Shape Optimization of the Common Research Model Wing-Body-Tail Configuration.

NUMERICAL MODELLING OF UTM CAMAR UAV WITH THE INFLUENCE OF VERTICAL GUST OSCILLATION

Faidzrul Adzari Fakhrul Radzi and Nik Ahmad Ridhwan Nik Mohd.
School of Mechanical Engineering, Faculty of Engineering,
Universiti Teknologi Malaysia, 81310 UTM Skudai, Johor, Malaysia

INTRODUCTION

The study of gust effect on aircraft have been an important subject in the aeronautic industry. This is due to the fact that the sudden fluctuation of wind speed affects the performance of aircraft. Past studies conducted on 2D airfoil shows the effect on the lift and drag when subjected in gust. The study is conducted to evaluate the performance of UTM CAMAR UAV when subjected in a vertical gust oscillation at various reduced frequency.

EXPERIMENTAL SETUP

This section presents the settings for the simulation. Gust is generated by using the relative motion of UAV oscillating in vertical axis in a free stream velocity. The vertical oscillation creates the same effect of gust attack as the velocity attacks the UAV in one complete sinusoidal shape. The boundary conditions were taken from [1]. The oscillation is controlled using a UDF which is governed by angular speed and angular frequency.

RESULTS AND DISCUSSION

`To evaluate the performance of UTM CAMAR UAV, graphs of lift and drag coefficient is plotted against angle of attack. The angle of attack represents the amplitude of gust when in contact with the UAV. Figure 1 shows that at the maximum amplitude or angle of attack, the lift is the highest while the drag is the lowest. However, the study conducted in [1] shows that the drag should also increase with the angle of attack. The inaccuracy of the data might be due to the absence of grid independence study. According to [2], the grid independency test is done to precisely determine the grid size to produce an accurate result.

Figure 2 and 3 shows a comparison of performance of UAV when subjected in different reduced frequency. According to the graphs, higher values of reduced frequency will affect the performance of UAV at faster rate. This is because the frequency also increases with the increase of reduced frequency

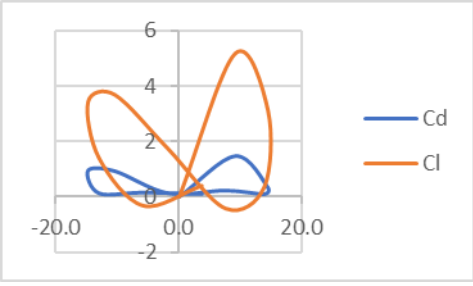

Figure 1: Graph of coefficients vs angle of attack.

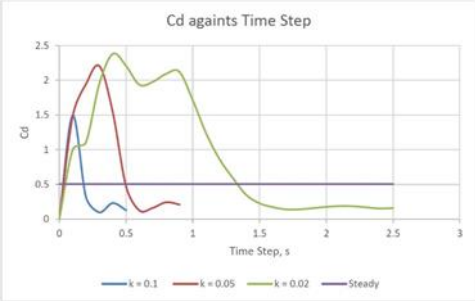

Figure 2: Graph of drag coefficient vs time step at different reduced frequency

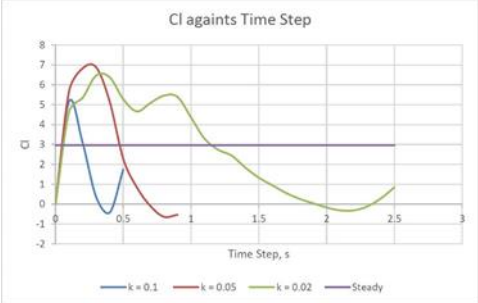

Figure 3: Graph of lift coefficient vs time step at different reduced frequency

CONCLUSION

The performance of UTM CAMAR UAV is determined using the data on lift and drag coefficient. Gust affect the aircraft by increasing its lift and decreasing its drag at maximum gust amplitude. Gust affect last longer at lower reduced frequency because the frequency is lower.

REFERENCES

[1] Rahman, A. H. A., Mohd, N. A. R. N., Lazim, T. M., & Mansor, S. Aerodynamics of Harmonically Oscillating Aerofoil at Low Reynolds Number.

[2] Asyikin, M. T. (2012). CFD simulation of vortex induced vibration of a cylindrical structure (Master's thesis, Institutt for bygg, anlegg og transport).

NUMERICAL INVESTIGATION OF AIRFLOW SIMILARITY AROUND A SURFACE MOUNTED CUBE AT MODEL SCALE AND FULL SCALE

Ameer Syafiq Badlissah and Muhammad Noor Afiq Witri Muhammad Yazid
School of Mechanical Engineering, Faculty of Engineering,
Universiti Teknologi Malaysia, 81310 UTM Skudai, Johor, Malaysia

INTRODUCTION

Computational fluid dynamics (CFD) is very useful tool to predict the flow of air pattern of a building in urban area. The goal of this study is to find out the air flow similarity around a cube by changing into 3 scale: small, medium and full scale. A model scale, 1:150 ratios, from Agricultural Institute of Japan will be our subject and will be validate using the CFD simulation. From there we scale up into 1:60 and 1:1. We going to use the velocity profile, Turbulent Kinetic Energy and Dissipation Rate from AIJ for scale up cases, but manipulate it to fit with urban environment.

EXPERIMENTAL SETUP

- Validate Architectural Institute of Japan case 1:1:2 result with Computational Fluid Dynamic simulation result
- Analyse airflow pattern between 3 different scale
- To study the similarity in kinematic flow of the 3 cases

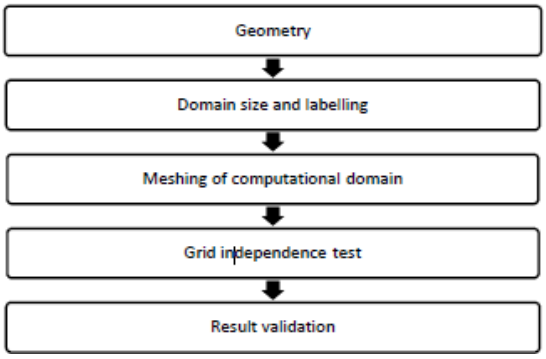

Figure 1: Flow chart of validation

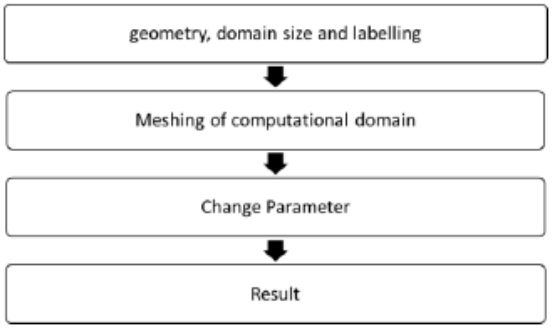

Figure 2: Flow chart of analysis

Table 1: Geometry

Cases	Geometry (w x l x h)
1:150	0.08 x 0.08 x 0.16
1:60	4.8 x 4.8 x 9.6
1:1	12 x 12 x 24

RESULTS AND DISCUSSION

Point	Experiment	558920	error	%error
0.01	0.208	0.330753	12.275300	12.275300
0.04	1.267	1.12747	-13.953000	13.953000
0.08	1.409	1.21866	-19.034000	19.034000
0.12	1.701	1.49463	-20.637000	20.637000
0.14	2.067	1.91677	-15.023000	15.023000
0.16	3.044	3.04268	-0.132000	0.132000
0.17	3.654	3.60693	-4.707000	4.707000
0.19	4.539	4.40269	-13.631000	13.631000
0.22	4.962	4.8797	-8.230000	8.230000
0.28	5.351	5.36748	1.648000	1.648000
			average	10.927030

Figure 3: Validation at x/b = -0.75

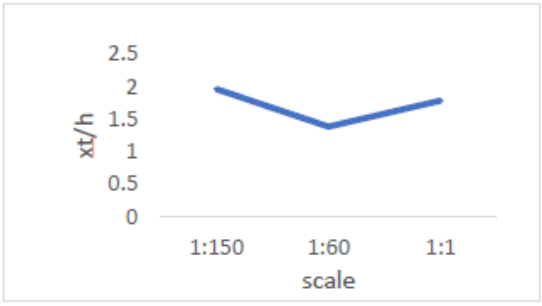

Figure 4: Chart of length for each scale from front region of building

CONCLUSION

- 11% error
- Same pattern between scales
- Similarity followed, can have similar airflow different scale

REFERENCES

[1] Architectural Institute of Japan. (2016). AJJ benchmarks for validation institute of Japan, 1-117.
[2] Burj Khalifa - Wind Tunnel Testing. (n.d.). Retrieved from https://issuu.com/rwdi/docs/burj_khalifa
[3] Blocken, B. (2014). 50 years of computational wind engineering: past, present and future. Journal of Wind Engineering and Industrial Aerodynamics, 129, 69-102.

RELIABILITY TEST FOR METALLIC UNDERLAYER DEPOSITED BETWEEN SILICON WAFER AND COPPER INTERCONNECTION FILLER FOR TSV APPLICATION.

Nazila najwa Iskak and Nor Akmal Fadil
School of Mechanical Engineering, Faculty of Engineering,
Universiti Teknologi Malaysia, 81310 UTM Skudai, Johor, Malaysia

INTRODUCTION

Through Silicon Via (TSV) is a vertical electrical connection that passes completely through a silicon wafer or die. It becomes one of the mainstreams of the packaging industry because it has many advantages such as high density, better electrical performance and lower power consumption[1]. Unfortunately, the CTE value of copper and silicon is very big and causes thermo-mechanical stress happens and cause several issues concerning yield loss and decreased reliability[2]. Nickel and palladium have introduced to become the underlayer and thermal aging test is done to investigate the effect on thermal aging to the sample.

EXPERIMENTAL SETUP

The experiment starts with pre-treatment the silicon wafer. After that, coat the silicon wafer with palladium and copper to become Pd-Cu layer and then nickel and copper to become Ni-Cu layer. The coating method that use is electroless deposition method and the deposition time is 60 minutes. Next, the sample is undergo thermal aging process under temperature 150ºC with vary aging time (0, 1, 3, 5, 100 hours) according to JESD22-A108C standard. Lastly, after the thermal aging test is done, characterization (surface and cross sectional analysis) and performance test(four point probe test) are done on the sample.

RESULTS AND DISCUSSION

The result obtained from this study is the longer the aging time, the higher the amount of oxide presence on the surface of the sample. This is due to oxidation process happened when the thermal aging is done on the sample. From cross-sectional analysis it is observe that the thickness of Ni-Cu coating is increasing until 5 hours and decrease at 100 hours. While for Pd-Cu coating, the average thickness is decreasing as the aging time increasing. The increasing and the decreasing of coating thickness demonstrate that intermetallic diffusion was taking place on nickel-copper layer towards other layers.

Figure 26 shows, the diffusion thickness before thermal aging test for Pd-Cu layer and Ni-Cu layer is same, 1.5µm and as the aging time increase, the diffusion thickness also increases. The diffusion thickness of Ni-Cu layer is increasing gradually from 1.5µm before thermal aging to 4µm after 1 hours and 3 hours. While the diffusion thickness of Pd-Cu is only slightly increase from 1.5µm to 2µm. This is because, the palladium coating is too thin to resist the diffusion between silicon and copper.

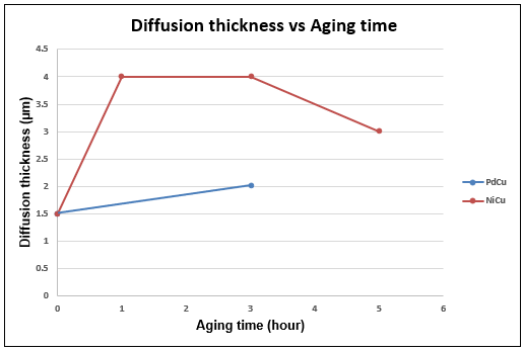

Figure 26: Graph of diffusion thickness vs aging time.

While for four point probe test, it is observe that the resistivity of Pd-Cu layer and Ni-Cu layer before thermal aging is almost the same but after the thermal aging test is done, the resistivity of Pd-Cu layer gradually increase compare to Ni-Cu layer that just slightly increase. The resistivity increases as the aging time increase. this is because, the presence of oxide layer that act as insulator and make the resistivity become high.

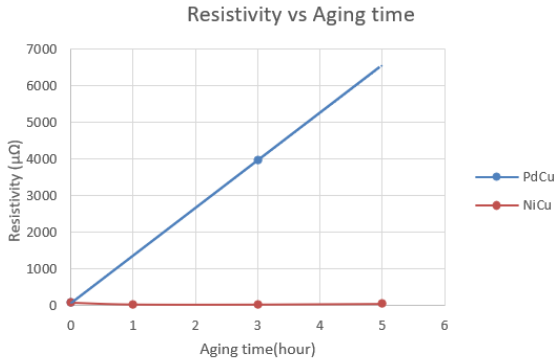

Figure 27: Graph of resistivity vs aging time.

CONCLUSION

19. As a conclusion, as the aging time increase, the diffusion thickness of Ni-Cu layer is thicker than Pd-Cu layer and the thickness of the coating will decrease as the aging time increase.

REFERENCES

1.Ben-Je Lwo, C.-Y.N., *reliability analyses on a TSV structure for CMOS image sensor* 2012, Research Gate

2. Seung ho seo, j.s.H., Jun Mo Yang, Wook-Jung Hwang, Jun Yeob Song, Won Jun Lee, *Failure mechanism of copper through-silicon vias under biased thermal stress.* ELSEVIER, 20013. **546**: p. 14-17.

SEAWATER AS NEW RENEWABLE ENERGY RESOURCE: MATERIAL CHARACTERIZATION AND TESTING FOR THE CELL ELECTRODES

Mohamad Azizi Shadan and Nor Akmal Fadil
School of Mechanical Engineering, Faculty of Engineering,
Universiti Teknologi Malaysia, 81310 UTM Skudai, Johor, Malaysia

INTRODUCTION

Over recent years, the demand on renewable energy shows an explosive growth of interest in the world. In the past few decades the development of new battery technologies and system has been a strong issue to meet the demands of high safety, low cost, sustainable and green energy[1]. The usage of seawater as main resource in seawater battery become most applicable sources because its contain sodium and chlorine ions[2].Basically, a battery must have two different metals connected together in electrolyte solution and produced current flow by redox reaction.

EXPERIMENTAL SETUP

This section presents the experimental setup for the system. Three electrode was used which are magnesium, zinc and carbon. Two set of battery was developed from combination of Mg-C and Zn-C electrodes consist of 12 cell each.

The cell electrodes is connected in series arrangement then wire from anode and cathode terminal is connected to torchlight to determine the ability of battery to light up the torchlight. Another wire then connected to resistor and Arduino to measure the battery voltage at 0, 4 and 8 hour.

MATERIALS CHARACTERIZATION

Microstructure of electrodes has been characterized by Scanning Electron Microscope (SEM), Energy Dispersive X-ray (EDX) and X-ray powder diffraction (XRD) while inductively coupled plasma-mass-spectrometry (ICP-MS) is used to trace element in seawater.

RESULTS AND DISCUSSION

At 0 hour, microstructure of magnesium shows net-like shape of pure magnesium. The microstructure of zinc shows a bunch of strip line across the sample with containing zinc, iron and carbon. Carbon for both battery set has small amount of white precipitate and black area represent carbon, silicon and oxygen.

After 4 hour, magnesium surface are partially covered with white precipitate where new element existed which are chlorine and oxygen. The microstructure of zinc still shows bunch of strip line with new element found on which are sodium and oxygen while carbon for both set shows existences of new element which are chlorine, zinc and oxygen.

At 8 hour, magnesium surface are almost fully covered by precipitate layer compose of chlorine, oxygen and calcium. There are a lot of white spherical dot on zinc surface shows the increment of sodium and oxygen composition. The white precipitate dominates on carbon of both battery set shows the incremental of oxygen and chlorine.

XRD results shows no much different in phase for all electrodes where XRD pattern match to pure magnesium, pure zinc and pure carbon graphite phase from 0 to 8 hour

Figure 1 shows the comparison of voltage reading between two battery set.

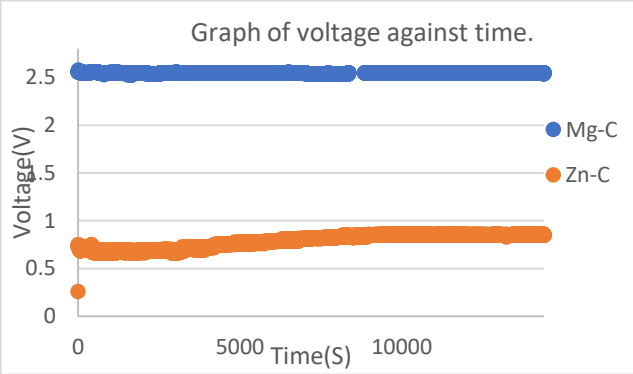

Figure 1: Voltage reading between Mg-C and Zn-C cell.

CONCLUSION

The microstructure of electrodes from 2 set of battery does not shows much changes across 8 hour with no changes in materials phase crystalline structure. Carbon and magnesium electrodes shows better performance with 2.53V and contains safe level of concentration of metals particles in the electrolyte.

REFERENCES

[1] Zhang, Y., et al., A novel rechargeable hybrid Na-seawater flow battery using bifunctional electrocatalytic carbon sponge as cathode current collector. Journal of Power Sources, 2018. 400: p. 478-484.

[2] Kim, J.-K., et al., Rechargeable seawater battery and its electrochemical mechanism. ChemElectroChem, 2015. **2**(3): p. 328-33

EFFECT OF BATH COMPOSITION ON ELECTROLESS DEPOSITION OF Ni-P UNDERLAYER FOR THROUGH SILICON VIA (TSV) APPLICATION

Abang Akmal Azriq Izzat Abang Marzuki and Nor Akmal Fadil
School of Mechanical Engineering, Faculty of Engineering,
Universiti Teknologi Malaysia, 81310 UTM Skudai, Johor, Malaysia

INTRODUCTION

Through Silicon via (TSV) is a high performance interconnect techniques used as an alternative to the traditional way of wire bond and flip chips. This TSV create a 3D packages and 3D integrated circuits. The advantages of using TSV is the device density is substantially higher, and the length of the connection become shorter [1]. Mechanical stress developed coefficient thermal expansion (CTE) mismatch between copper (Cu) and dielectric material such as silicon (Si) substrate with the value of CTE 17 ppm/˚C and 2.8 ppm/˚C respectively. Because of the mismatch it can cause it to be weak and physical damage in the substrate. The induced stress can also affect the performance of transistors that are within its range of influence [2]. This research was conducted to study the effect of concentration on Ni (13 ppm/˚C) deposited as an underlayer between Cu filler and Si substrate.

EXPERIMENTAL SETUP

Initially, the first batch only deposited with Ni. Then the next batch are made by deposits with Ni and followed up with Cu. At the end of the electroless Ni and Cu deposition process, characterizations is done and test were conducted. The sample will be analyse under Scanning Electron Microscope (SEM), optical microscope and Electron Diffraction X-ray (EDX) for microstructural analysis such as cross-sectional analysis, surface analysis and chemical composition analysis. Both samples of Si wafer deposited with Ni and the sample of Si wafer deposited with Ni then Cu will be go through the four-point probe test to check for resistivity of the deposited material. Sample of Si wafer that have been deposited with Ni will undergo adhesion test. This test was carried out to investigate and label the adhesive strength of the Ni layer that have been deposited on the Si wafer.

RESULTS AND DISCUSSION

Figure 1, it shows that as the duration of electroless Ni deposition process carried out increase, the thickness of Ni plated on the Si wafer also will be increases. For the parameter of concentration, at the range concentration of plating bath between 4g until 8g, the thickness of Ni plated seems to be increase over the time steadily and constant. At the concentration of 12g for plating bath, the thickness shows less in value compare to the other. The increment is very small as it reaches the 60 minutes' mark. The highest value for thickness of the Ni plated is recorded at concentration of 4g for 60-minute duration of electroless Ni deposition process carried out which is 8.3µm. At 4g it displays that the rate of electroless Ni deposition process is very high compare to concentration at 8g and 12g. During the concentration of 12g, it shows the lowest value in the thickness of Ni plated over the time. This also indicate that the rate of electroless Ni deposition was very low at high concentration. During the experiment of electroless Ni deposition was conducted at 8g and 12g, the condition of beaker was different compare to the other. The condition of the beaker during 4g shows a very good condition after plating. It is different condition happen for 8g and 12g, after electroless deposition for 40 minutes and 60 minutes, the nickel bath inside the beaker starts to produce muddy bath and some of the nickel is deposited on the beaker.

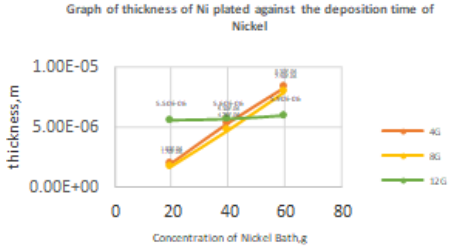

Figure 1: graph of thickness of Ni plated against the duration of electroless deposition process.

CONCLUSION

Nickel has successfully deposited on the Si wafer using various concentration of Nickel bath. The effect of concentration of plating bath on Ni deposited can be seen as the concentration increases, the Thickness of Ni deposited will also increase. Unfortunately as it is for 12g, the deposition rate of Ni decrease due to fact that the Ni will have tendency to deposit on the beaker instead of the sample and produce muddy bath.

REFERENCES

[1] Motoyoshi, M. (2009). "Through-Silicon Via (TSV)." Proceedings of the IEEE 97(1): 43-48.Technologies, Research – Development – Application, 615-640, Pro Literatur Verlag, Germany.

[2] Wang, P. J., et al. (2008). A new bonding technology dealing with large CTE mismatch between large Si chips and Cu substrates. 2008 58th Electronic Components and Technology Conference.

[3] Miao, N., et al. (2018). "Influences of Bath Chemistry and Plating Variables on Characteristics of Electroless Nickel 2013;P Films on Si Wafers from Alkaline Citrate Solutions." Journal of Nanomaterials 2018: 11.hjgil

EFFECT OF PIPE SIGNAL, OFF POTENTIAL AND ON POTENTIAL ON DCVG FOR CORROSION MONITORING OF UNDERGROUND PIPELINE PROTECTED BY ICCP.

M. Hafizi Dzaid and Nor Akmal Fadil
School of Mechanical Engineering, Faculty of Engineering,
Universiti Teknologi Malaysia, 81310 UTM Skudai, Johor, Malaysia

INTRODUCTION

Corrosion is the interaction between a material and environment to which it is exposed [1]. DCVG device is used to detect corrosion in underground pipeline protected by ICCP system by measuring the potential shift between two electrodes in contact with the soil [2]. By measuring the pipe-to-soil potential (potential shift) %IR can be calculated and then the size of coating defect can be predicted from the %IR drop value. However, there is no standard document prepared by DCVG manufacturer to correlate the %IR drop to the defect size. The only information that they have from manufacturer is '5% IR drop equal to$10cm^2$' of defect size. In this project we will focus on pipe signal, OFF potential and ON potential which is main parameters in pipe-to-soil potential.

EXPERIMENTAL SETUP

This experiment was conducted in two pipeline buried in different type of soil with different soil resistivity. The pipelines is prepared with$16cm^2$ of defect size. For each pipeline data taking process was conducted twice which is with and without variable resistor in the connection.

After DCVG survey conducted, OFF potential and ON potential is recorded automatically. While, pipe signal can be calculated manually.

RESULTS AND DISCUSSION

For the relation between %IR drop and pipe signal, pipeline 1 measure without resistor %IR drop reduced exponentially and eventually become constant.

$$y = 3.6803 + 6.3535exp\left[\frac{-(x-40}{28.857}\right]$$

For the pipeline 1 with resistor connected to the circuit, the %IR drop is always constant .

For the second pipeline buried in fine sand, the relation for without resistor it follows:

$$y = 0.90993 + 0.8463exp\left[\frac{-(x-172)}{624.7}\right]$$

For pipeline 2 with resistor it give constant value of %IR drop.

OFF potential is important for assessment of CP system as it depends on polarization value [3]. The relation between %IR drop and OFF potential for pipeline 1 without resistor is:

$$y = 3.7801 + \left\{74.287 \Big/ \left(1 + exp\left[\frac{(-0.93006 - x}{0.012876}\right]\right)\right\}$$

For pipeline 2 without and without resistor it changes polynomially.

Without resistor:

$$y = 29.367x^2 + 75.427x + 49.247$$

With resistor:

$$y = 8.6907x^2 + 21.851x + 14.343$$

ON potential is a potential value that depends on the voltage input of DCVG. From the results of this experiment, for pipeline 1 without resistor the %IR drop reduced exponentially.

$$y = 3.545 + \left\{112.16 \Big/ \left(1 + exp\left[\frac{(-0.76549 - x)}{0.06164}\right]\right)\right\}$$

For with resistor, the %IR drop remain constant as OFF potential changes.

For pipeline 2, without resistor the %IR drop reduced exponentially:

$$y = 091833 + \left\{0.88491 \Big/ \left(1 + exp\left[\frac{-0.751 - x}{0.080459}\right]\right)\right\}$$

While with resistor in connection, the %IR remain constant as OFF potential changes.

For all the relation y represents %IR drop, x represents pipe signal or OFF or ON potential.

CONCLUSION

In conclusion, all these three parameters will affect the %IR drop. However for different parameters it effect the %IR drop differently with one another.

REFERENCES

[1] Ramesh, S. (2014). Corrosion control for offshore structure: cathodic protection and high efficiency coating. Gulf Professional Publishing, Oxford, UK.
[2] Roberge, P. R. (2008). Corrosion engineering principles and practice. McGraw-Hill, New York, USA.
[3] Mujezinovic, A, (2014). Impact of the soil resistivity on IR drop of CP system.

ELECTROLESS DEPOSITION OF DIFFERENT METALLIC UNDERLAYER BETWEEN Si WAFER AND Cu INTERCONNECTION FILLER FOR TSV APPLICATION

Ika Irdina Izham and Nor Akmal Fadil
School of Mechanical Engineering, Faculty of Engineering,
Universiti Teknologi Malaysia, 81310 UTM Skudai, Johor, Malaysia

INTRODUCTION

Nowadays, the modern technology are getting advanced from time to time throughout this globalization era especially in the engineering field. Through Silicon Vias (TSV's) are holes created polymer in a silicon wafer that undergoes an etching process. It is a type of via (vertical interconnect access) connection that used in microchip and manufacturing engineering that passes completely through a silicon wafer [1]. Mismatch will occur over the time due to the development of internal stress between the layer of Cu filler and Si, when the Cu with CTE value of 16.7x 10^{-6}/K were directly deposited to Si which has 3.0x 10^{-6}/K value of CTE Ni is the suitable material to be deposited as an underlayer between Cu and Si in order to avoid the bad results to happen Palladium also can be used as a soldering preservative and as a barrier inner layer in applications where it is plated directly onto copper circuitry [2].

EXPERIMENTAL SETUP

Pre-treatment process of the Si-substrate been carried before undergoes the electroless deposition process of Ni, Pd and Cu deposited ith Ni and Pd.

The surface morphological analysis (SEM & EDX), the cross sectional analysis (SEM & EDX), adhesion test (ASTM D3359) and the electrical resistivity test (Four point probe test) been carried out to test the performance and behaviour of the coating.

RESULTS AND DISCUSSION

The research was conducted to study and compare the characteristic of both (Ni and Pd) underlayers. The electroless Ni process has been established and the optimum plating parameter was used in this study. For electroless Pd, various plating bath temperature (55° C, 40° C, 35° C) and the deposition time (30, 45, and 60 mins) were studied.

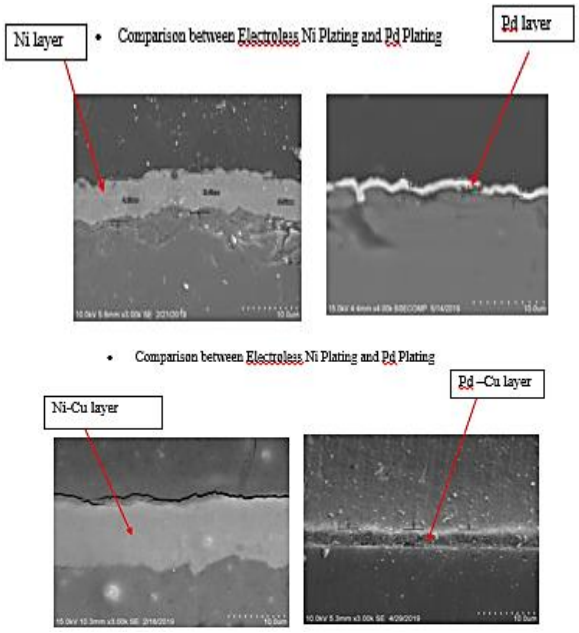

Figure 1: The thickness of the metallic underlayers deposited on the Si substrate.

Figure 2: The average resistivity of the deposited under layers

CONCLUSION

In conclusion, electroless is not suitable process to deposit sufficient thickness of uniform Pd underlayer.

REFERENCES

[1] Cheng et al. (2016) Heat dissipation assessment of through Silicon Via (TSV) – based 3D IC package for CMOS Image Sensing 59, 84-94.

[2] Azmah Hanim M. A. (2017) From electroless plating as surface finishing in electronic packaging

THE EFFECT OF SOIL RESISTIVITY OF %IR DROP OF DCVG SURVEY FOR ICCP SYSTEM

Mohamad Shukri Jamaluddin and Nor Akmal Fadil
School of Mechanical Engineering, Faculty of Engineering,
Universiti Teknologi Malaysia, 81310 UTM Skudai, Johor, Malaysia

INTRODUCTION

An impressed current system uses a power source to force current from inert anodes to the structure to be protected [1]. Direct Current Voltage Gradient (DCVG) is the most effective method to monitor the defect of underground pipeline protected by ICCP system. The defect can be detected by the value of %IR drop. The only information provided by the manufacturer of DCVG is 5% of %IR drop equals to 10cm^2. Calculated %IR drop cannot give accurate of defect size. There are several parameter in DCVG survey such as %IR drop, pipeline-to-soil potential and soil resistivity [2]. The main purposes are to measure coating defect size of the underground pipeline protected by ICCP system and to correlate between soil resistivity and pipe to soil potential with %IR drop.

EXPERIMENTAL SETUP

Direct Current Voltage Gradient (DCVG) survey are used to measure the pipeline to soil potential and the location of the defect coating on the buried pipeline. The Impressed Current Cathodic Protection (ICCP) system used to protect the buried pipeline from corrosion. This project is an extension of the project conducted by the previous student [4]. She provided the site and buried both pipelines with installed ICCP.

RESULTS AND DISCUSSION

Figure 1 shows the value of %IR drop of pipeline 1 decreases sharply as the pipe signal increase before it turns to constant. This decreases in range between 40 mV to 800 mV. Pipeline 2 also shows the slightly decreases in range between 172 mV to 1681 mV. So, this can be conclude that the %IR drop at the pipe signal below than 800 mV of both pipelines are having decreases of pipe signal then after 800 mV, %IR drop will having a constant value.

Figure 2 for OFF potential graph, both of trend line pipeline 1 and pipeline 2 could be said constant with increases of negative value of OFF potential. However, it is only acceptable when the pipeline 1 is above -1.11V and pipeline 2 is above -1.17V because at this value the pipe signal value has reach 800 mV and above.

Figure 3 for ON potential graph, both pattern line shows constant with increases of negative value of ON potential. However, it is only be acceptable when pipeline 1 is above -4.32V and pipeline 2 is above -2.84V because at this value the pipe signal value has reach 800 mV and above. Basically, case of %IR drop with ON potential almost same with %IR drop with pipe signal. Based on the graph of %IR drop vs pipe signal, the graph can be say that ON potential be main data for pipe signal

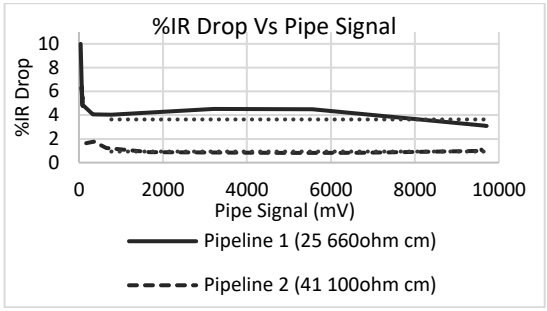

Figure 1: Effect of %IR drop with pipe signal.

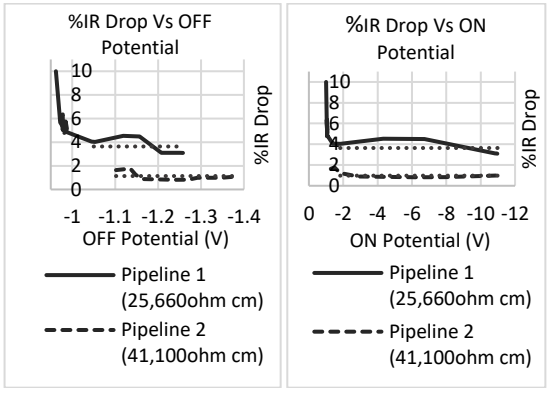

Figure 2: Effect of %IR drop with OFF and ON potential

CONCLUSION

%IR drop value is high when the soil resistivity is low as the Pipeline 1 which is 25 660 ohm cm compare to Pipeline 2 that is 41 100 ohm cm. The %IR drop will be varies depending on the soil resistivity and pipe to soil potential data at the defect location. Larger than 800mV of pipeline to soil potential gives more reliable information based on constant value of %IR drop. The value obtained gives more information to the standard set by DCVG where %IR drop of 5% is equivalent with 10 cm2 of defect size.

REFERENCES

[1] Nurul Faziera. (2017). Correlation of Soil Resistivity and Pipeline to Soil Potential with %IR Drop.
[2] Mc Miller. *DCVG Training Manual – Gx Version.*

EFFECT OF TEMPERATURE ON ELECTROLESS DEPOSITION OF BLACK NICKEL-PHOSPHORUS SOLAR ABSORBER COATING ON CARBON STEEL

Abdullah Azzam Muhammad and Nor Akmal Fadil
School of Mechanical Engineering, Faculty of Engineering,
Universiti Teknologi Malaysia, 81310 UTM Skudai, Johor, Malaysia

INTRODUCTION

Solar heating system is one of the applications for solar energy. In the solar collector has a component that absorber plate that use for absorbing solar radiation. The efficiency of the solar absorber is cruel to make solar heating system working effectively[1]. The efficiency of conversion solar radiation into heat energy can be characterized by the capacity of the solar device to absorb solar radiation and minimize thermal back radiation.

EXPERIMENTAL SETUP

This section presents the experimental setup for the research. The substrate for this experiment is carbon steel. The dimension for the sample is 2×4cm. Samples will be going pre-treatment before conducting electroless nickel plating. Bath solution consists of nickel sulfate as source of nickel ion, sodium hypophosphite as reducing agent, sodium citrate and sodium acetate. Operation condition is constant pH at 4.5. deposition temperatures are 75^0C, 85^0C and 95^0C. At each temperature consist of three deposition times that are one, two and three hours. After that, sample will be etch using 9mol L^{-1} nitric acid at room temperature and without stirring for 40s.

Samples will be characterized by scanning electron microscope (SEM), energy dispersive X-ray (EDX), powder X-ray diffraction analysis (XRD) and optical microscope. The performance of the sample is tested by visible-near infrared to study the reflectance and absorptance of spectrum.

RESULTS AND DISCUSSION

The surface morphology analysis was conducted by scaning electron microscope (SEM) to study the surface morphology of nickel deposit layer.

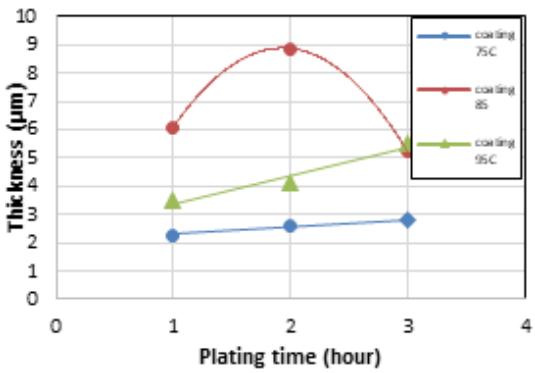

Figure 1: Graph of deposition time versus coating thickness

According to surface morphology by SEM, all sample at three temperature show a successful coating. Unsuccessful coating is measure by visual observation when the surface of coating is not show silver surface. Phosphorus content from EDX is 7% which is medium phosphorus[2]. Figure 1 shows that the coating at 75^0C is a slow deposition rate compare to others temperature. 85^0C show the fastest deposition rate until two hours because unstable bath was occurred at three hours deposition time. 95^0C show the medium deposition rate and unstable bath was occur at early two hours deposition time. The thickness of coating affecting the etching for blackening process. The thinner the coating, the severe the acidic attack on the coating. Active acidic attack is good for blackening process.

Figure 2 show the performance of the samples based on fixed deposition time at three hours. All samples show a good absorption by having below 10% reflectance.

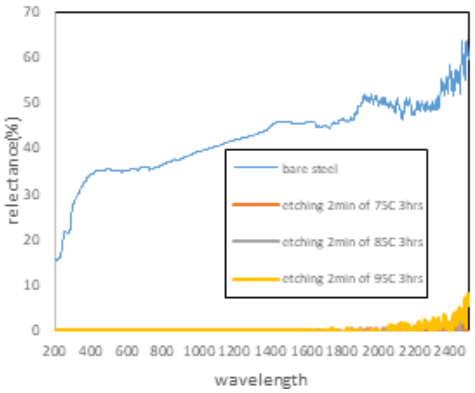

Figure 2: Graph of %reflectance against wavelength

CONCLUSION

The study shows a positive result for coating process. Temperature at 85^0C is the fastest deposition rate of electroless nickel plating. However, for blackening process, etching at 40s is fail to produce black surface but the sample start to change into black surface at 2 minutes etching time.

REFERENCES

[1] Lira-Cantu, M., et al., *Electrochemical deposition of black nickel solar absorber coatings on stainless steel AISI316L for thermal solar cells.* Solar energy materials and solar cells, 2005. **87**(1-4): p. 685-694.

[2] Domínguez, A.S., et al., *Characterization and corrosion resistance of electroless black Ni-P coatings of double black layer on carbon steel.* Surface and Coatings Technology, 2017. **326**: p.192-199

EFFECT OF ETCHIG PARAMETER ON BLACKEN ELECTROLES NI-P SOLAR ABSORBER

Wesley Sudiah and Nor Akmal Fadil
School of Mechanical Engineering, Faculty of Engineering,
Universiti Teknologi Malaysia, 81310 UTM Skudai, Johor, Malaysia

INTRODUCTION

Solar collector is the major and most important part in solar thermal technology [1]. Solar collector plays an important role in ensuring the functionality of the solar thermal technology used. Basically, the function of this component is to absorb solar radiation and converts it to thermal energy and transfer it to the working fluid in the system [2]. From previous study that conducted, it is found that electroless deposited Ni-P coatings can be blackened and have the potential to be as a selective surface. Electroless nickel-plating is a plating method that do not required electrical power. he benefits of using EN-P are improve in corrosion resistance, wear and abrasion resistance, microcrystalline deposit and high hardness [3]. In EN-P, black surface can be obtained by performing surface treatment on the substrate. The surface treatment for surface blackening is called the black treatment [4]. According to Takadou et al., the black treatment can be done by etching the electroless plating nickel in oxidizing acid solution [4]. By performing black treatment on the electroless deposited nickel, the optical properties of the substrate when it is to be used for solar application will increase [4].

EXPERIMENTAL SETUP

The experiment was carried out by first performing electroless nickel plating (EN-P) on the substrate (carbon steel). Pre-treatment was conducted prior to the plating process. This is to ensure uniform coating can be obtained on the substrate. After pre-treatment, some sample will be kept uncoated while some will be coated by using EN-P at constant parameter.

The plated sample are then taken for blackening process. Finally, all the prepared sample will be analysed in term of characterization and performance.

RESULTS AND DISCUSSION

For characterization test, the surface morphology was observed by using SEM with 15.0kv and 2.00k magnification. From this test, t is found that severe chemical attack occurred when higher concentration of acid is used. For EDX analysis, it is found that the element composition on the coating will be differ as the concentration varied. On the other hand, from cross sectional analysis, it is observed that. the coating thickness will be decreasing as the acid concentration and immersion time increase. This analysis was performed using optical microscope and SEM.

To study the effect of the etching parameter towards the performance of the samples, the percentage of reflectance of the sample are tested using UV-Vis. From this test, it is found that, all sample except raw sample (bare steel) give reflectance below 10%. The graph showing this result is shown in Figure 1.

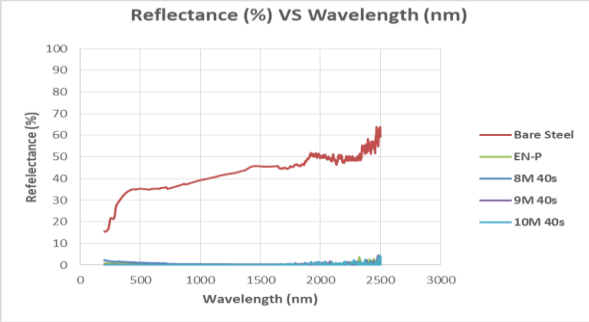

Figure 1: UV-Vis result on reflectance

CONCLUSION

The effect of varying the acid etching concentration and immersion time during blackening process of EN-P sample are studied in term of characterization and performance. However, to obtain more accurate and precise result, a thorough experiment on this topic should be conducted.

REFERENCES

[1] Mekhilef, S., R. Saidur, and A. Safari, A review on solar energy use in industries. Renewable and Sustainable Energy Reviews, 2011. **15**(4): p. 1777-1790.
[2] Kalogirou, S.A., Solar thermal collectors and applications. Progress inenergy and combustion science, 2004. **30**(3): p. 231-295.
[3] Agarwala, R. and V. Agarwala, Electroless alloy/composite coatings: A review. Sadhana, 2003. **28**(3-4): p. 475-493.
[4] Takadoum, J., Black coatings: a review. The European Physical JournalApplied Physics, 2010. **52**(3).

OPTIMIZATION ON ENGINE PARAMETERS TOWARDS HIGHER PERFORMANCES OF TURBOCHARGED ENGINE

Nur Arisa Mohd Azhari, Nor Hasrul Akhmal Ngadiman and Mohd Azman Abas
School of Mechanical Engineering, Faculty of Engineering,
Universiti Teknologi Malaysia, 81310 UTM Skudai, Johor, Malaysia

INTRODUCTION

Recently, researchers studied on development of engines with good fuel consumptions which is low consumption [1]. The main reason of the study is because resources of fuel especially petrol decrease ultimately [2]. Hence, an action needs to be taken to produce an engine with low fuel consumption but high performance. However, by having engine with low fuel consumption, it will decrease the performance of engine [3]. Optimization process need to be done in order to find the optimum setting of engine which can satisfy both conditions where it consume low fuel but enhance engine performance [4]. The problem is number of studies done in optimizing the engine parameter setting to optimize fuel consumption and engine performance simultaneously is low. Hence, this study is to find the significant figure which affect turbocharged engine performance and fuel efficiency, also to optimize the turbocharged engine setting to enhance both engine performance and fuel efficiency, simultaneously, in the studied region.

METHODOLOGY

The determination of significant parameters was done through literature review, and measurement of standard range of the parameters was collected. Design of experiment was developed. Data of responses were collected via engine calibration process experiment. The optimization was then done by using Design Expert software. The technique that had been used Central Composite design. After the result had been obtained, confirmation run was done in order to verify the model produced.

RESULTS AND DISCUSSION

From the previous researches, the most significant parameters of turbocharged engine that influenced the engine performance and fuel efficiency were determined which are ignition timing, variable valve timing and wastegate solenoid DC. In the optimization processes, three different results were produced which are optimized parameters for maximum engine performance, optimized parameters for minimum fuel consumption, and optimized parameters for both maximum engine performance and minimum fuel consumption. Central Composite Design analysis has yielded the optimized parameters for maximum engine performance, minimum fuel consumption, and maximum engine performance and minimum fuel consumption, simultaneously. The result of the optimized parameters is shown in the Table 1.

Table 6: Optimized Parameters

		Max. EP	Min. FC	Max EP & Min FC
Optimized Parameter	Ignition Timing (°bTDC)	20.016	25.394	26.000
	VVT (°bTDC)	13.686	25.973	10.000
	Wastegate DC (%)	16.221	29.651	25.944
Optimized Result	EP (Nm)	126.107	-	123.938
	FC (kg/hr)	-	7.891	7.923

CONCLUSION

As a conclusion, the significant parameters had been identified. We also had optimized the significant parameters of the turbocharged engine so that it can enhance the engine performance and fuel efficiency of the automobile.

REFERENCES

[1] P. Sawant and S. Bari, "Effects of Variable Intake Valve Timings and Valve Lift on the Performance and Fuel Efficiency of an Internal Combustion Engine," *SAE International,* pp. 1-2, 2018.

[2] P. A. Owusu and S. A. Sarkodie, "A review of renewable energy sources, sustainability issues and climate change mitigation," *Cogent Engineering,* vol. 3, no. 1, 2016.

[3] H. Zhou, Advanced Direct Injection Combustion Engine Technologies and Development, Gasoline and Gas Engines, North America: Woodhead Publishing Limited and CRC Press LLC, 2010.

[4] A. Yao, X. Shi, H. Li, P. Zeng and T. Li, "Heat loss from a turbo-charged spark ignition off-road engine operated on gaseous fuels," *Scopus* , 2017.

INCORPORATING DESIGN AND OPTIMIZATION PROCESSES ON AIR INTAKE SYSTEM FOR A NATURALLY ASPIRATED ENGINE

Nur Syahirah Mustafa, Nor Hasrul Akhmal Ngadiman and Mohd Azman Abas
School of Mechanical Engineering, Faculty of Engineering,
Universiti Teknologi Malaysia, 81310 UTM Skudai, Johor, Malaysia

INTRODUCTION

Air intake system plays an important role in ensuring the engine performance and fuel efficiency of an automobile due to its function to provide sufficient amount of air to perform a complete combustion[1]. One of the most important components of air intake system is an airbox which helps to suck in sufficient amount of a good quality air. The performance of airbox can be influenced by the location of filter and the geometry of airbox [2]. The higher the volumetric efficiency of an airbox, the higher the engine performance which will eventually increases the fuel consumption [3]. However, up to this date and our knowledge, there no researches done on optimizing an airbox design that will contribute to improvement of engine performance and fuel efficiency. Therefore, the optimized parameters in designing an airbox should be studied in order to satisfy both condition.

METHODOLOGY

We designed a flow simulation of engine by using AVL Boost software. The determination of significant parameters was done through literature review, and measurement of standard range of the parameters was collected. Design of experiment was developed. Data of responses were collected via simulation by using AVL Boost software. The optimization was then done by using Design Expert software which adopted response surface methodology. The techniques that had been used are Box-Behnken analysis and Central Composite design. After the result had been obtained, confirmation run was simulated in order to verify the model produced.

RESULTS AND DISCUSSION

From the previous researches, we found out the most significant parameters that influenced the performance of airbox are diameter of inlet or snorkel, volume of airbox, diameter of throttle body and length of intake runner. In the optimization processes, we came out with three different results which are optimized parameters for maximum engine performance, optimized parameters for minimum fuel consumption and optimized parameters for both maximum engine performance and minimum fuel consumption. Box-Behnken analysis had yielded the optimized parameters for maximum engine performance and maximum engine performance and minimum fuel consumption, simultaneously. In order to find optimized parameters for minimum fuel consumption, Central Composite design had been adopted with two significant factors which were diameter of throttle body and volume of airbox. The lowest possible value used for the diameter of throttle body is 32mm [4]. The result of the optimized parameters is shown in the Table 1.

Table 7: Optimized Parameters of an Airbox

	Optimized Parameter				Optimized Result	
	Diameter of Inlet / Snorkel (mm)	Volume of Airbox (litre)	Diameter of Throttle Body (mm)	Length of Intake Runner (mm)	Engine Performance (Nm)	Fuel Consumption (10^{-4} kg/s)9
Maximum Engine Performance	90.49	1.13	58.86	1.04	95.9887	-
Minimum Fuel Consumption	70.24	0.298	32	800	-	18.0377
Maximum Engine Performance & Minimum Fuel Consumption	81.07	1.04	44.63	425	93.3732	21.3695

CONCLUSION

As a conclusion, the significant parameters had been identified which are diameter of inlet or snorkel, volume of airbox, diameter of throttle body and length of intake runner. We also had optimized the significant parameters of the airbox geometry in order to enable us to enhance the engine performance and promote low fuel consumption. The successful of this study can contribute to a new design of airbox geometry that will improve the engine performance and fuel efficiency of an automobile.

REFERENCES

[1] W. M. I. . Harun, “Optimization of Air Intake System For In-Line Diesel Engine,” no. June, 2012.

[2] A. B. Shahriman *et al.*, “Computational studies of an intake manifold for restricted engine application,” *J. Phys. Conf. Ser.*, vol. 908, no. 1, pp. 1685–1693, 2018.

[3] A. De Vita and L. Di Angelo, “CFD-Aided Design of an Airbox for Race Cars CFD-Aided Design of an Airbox for Race Cars,” no. July, 2002.

[4] J. Suresh Kumar, V. Ganesan, J. M. Mallikarjuna, and S. Govindarajan, “Design and optimization of a throttle body assembly by CFD analysis,” vol. 20, no. October, pp. 350–360, 2013.

OPTIMIZATION DESIGN PARAMETERS OF INTAKE MANIFOLD FOR NATURAL ASPIRATED ENGINE

Amirul Aliff Mohd Hisham, Nor Hasrul Akhmal Ngadiman and Azman Abas
School of Mechanical Engineering, Faculty of Engineering,
Universiti Teknologi Malaysia, 81310 UTM Skudai, Johor, Malaysia

INTRODUCTION

The automotive industry is currently experiencing pressures due to the fluctuation of gas price. This is going to be a year unlike many, where you're going to see gas prices fall and rise [1]. Nowadays, people are demanding on having a good fuel economy car that can give a better performance. In Malaysia, it is critical for drivers in a town area where people have to faced traffic`s condition. Design of engine components, measuring and control methodology of the parameters are very important to improve the engine capabilities [2]. Up to this date, there is no study on design of intake manifold for NA engine that consider two responses which are engine performance and fuel consumption for the optimization process. As we know that, both of the responses are having inversely proportional relationship, so we need to find a condition which satisfy for both responses.

EXPERIMENTAL SETUP

This section presents the methodologies of this study. The parameter involved were determined by finding the factors that affects both engine performance and fuel consumption through previous case study and brainstorming with related officer. The selected parameters were Runner Length (A), Runner Diameter (B), Plenum Volume (C), and Surface Roughness (D). Necessary steps have been taken involving Design of Experiment (DOE) to find the optimum result for all the factors that have been selected. Box-Behnken Design (BBD) is used. The data of torque and fuel consumption are obtained from the 1Dimensional Computational Fluid Dynamic (CFD) on AVL Boost software. Then the collected data were analysed using Design Expert software.

RESULTS AND DISCUSSION

This section presents the results of this study. Within the range studied, the optimized parameters value for maximum engine performance and minimum fuel consumption was runner length; 200.00mm, runner diameter; 33.56mm, plenum volume; 0.5L, and surface roughness; 0.15µm. The value for maximum engine performance and minimum fuel consumption was 99.541Nm/rpm and 8.8652×10^{-4}kg/s respectively. Confirmation run was conducted and the percentage error were less than 10% shows that the data is valid to be used. Then, new model of intake manifold with optimum parameters was developed using NX8.0. Apart from that, selection of materials and manufacturing process also had been done in this study. Polyamide and injection molding had been identifying as the best material and manufacturing process for the development intake manifold. Figure 1 visualize the model of optimized intake manifold.

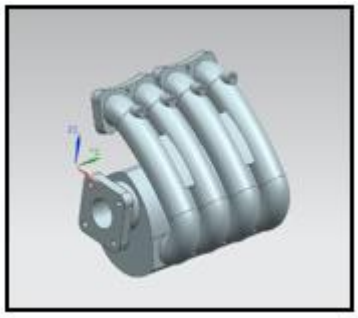

Figure 1 : Model of optimized intake manifold

CONCLUSION

As a conclusion, the significant parameters had been identified. We also had optimized the parameters of the intake manifold geometry so that it can enhance the engine performance and at the same time has a good fuel economy.

REFERENCES

[1] D. Potenteau, "Gas prices likely to rise in 'wild, bumpy' 2019," 2018. [Online]. Available: http://centurypiano.com.sg/this-is-going-to-be-a-year-unlike-many/.

[2] M. A. Ceviz and M. Akın, "Design of a new SI engine intake manifold with variable length plenum," Energy Convers. Manag., vol. 51, no. 11, pp. 2239–2244, 2010.

OPTIMIZATION OF WASTE COOKING OIL USING RESPONSE SURFACE METHODOLOGY FOR BIODIESEL PRODUCTION

Hafiz Tarmizi Noor Azizi and Norazila Othman
School of Mechanical Engineering, Faculty of Engineering,
Universiti Teknologi Malaysia, 81310 UTM Johor Bahru, Johor, Malaysia

INTRODUCTION

The world is getting bigger day by day as the world energy demand is predicted to increase The society starts to realize that the fossil fuels are declining due to the overly usage and demand around the globe. Thus, the potential alternative of fossil fuels such as biodiesel production is explored to meet the necessary of domestic and industrial economies. Biodiesel can be produced edible and non-edible feedstocks such as waste cooking oil (WCO). Edible feedstocks such as edible oils like palm oil, canola oil and more will be great for making biodiesel but continuous and large-scale production of biodiesel from edible oil will disturb the food supply chain and cause in balance as it has high demand from food industry as well as biodiesel industry. In order to overcome this problem, switching from edible feedstocks to non-edible feedstocks such will be a great solution to this problem [1] and concurrently the analysis of optimum condition based on parameter effect to produce the biodiesel. The response surface methodology (RSM) will be used for the optimization process by using appropriate procedures [2] from yield of fatty acid produce from non-edible feedstocks.

METHODOLOGY AND EXPERIMENTAL SETUP

The method of biodiesel production used is transesterification process of experiment. This process will convert waste cooking oil into biodiesel, and it involves three variables such as potassium hydroxide, methanol and temperature.

The optimization methodology of biodiesel is made using response surface methodology (RSM) approach. The design of experiment (DOE) used is central composite design rotatable type with the use of first order model and second order model.

RESULTS AND DISCUSSION

Based on the experimental data conducted, the analysis of variance (ANOVA) was obtained by using second order model generation as shown in Table 1. From Table 1, the model is significant, and confirms the second order model can be applied in this result and the lack of fit is not significant, that means data is accurate each running order. Thus, the solution for this model response will be as Eq. (1). In addition, the yield of FAME for response surface can be illustrated in Figure 1. Therefore, the maximum yield of FAME was effecting from the following variables shown in Table 2. From optimum condition based on response surface, the repetition experiment was done. The actual yield of FAME obtained by experiment is 95.04 ml. There was 4.77 % error and since it is less than 5 % it is acceptable.

Table 1: ANOVA with 2nd order model of RSM

Source	F-value	p-value	
Model	9.34	0.0008	**significant**
A-KOH	6.83	0.0227	
B-Methanol	10.02	0.0081	
C-Temperature	9.79	0.0087	
BC	4.08	0.0662	
B^2	16.00	0.0018	
Lack of Fit	8.07	0.0564	**not significant**

$$y = 108.2285 - 8.6488x_1 + 8.7437x_2 - 1.2080x_3 - 0.7405x_2^2 + 0.08925x_2x_3 \quad (1)$$

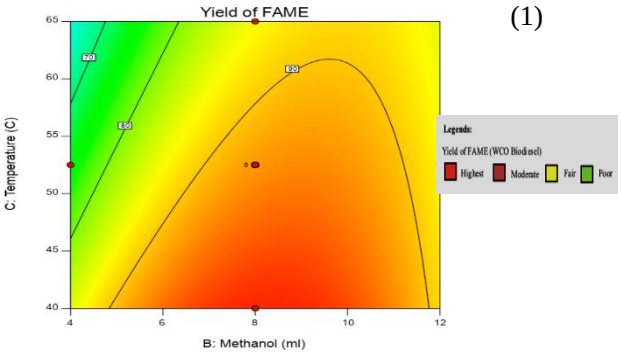

Figure 1: Yield of FAME (biodiesel) with respect to methanol and temperature.

Table 2: The variables for maximum yield of FAME based on response surface methodology.

Variables	Values
KOH (%)	1.21
Methanol (ml)	8.40
Temperature (℃)	41.70
Yield of FAME (ml)	99.80

CONCLUSION

The transesterification method was confirmed to obtained biodiesel from waste cooking oil (WCO). The response surface methodology (RSM) approach was confirmed to find the optimization of waste cooking oil with the following variables 1.21% KOH, 8.40 ml methanol and 41.7℃ temperature in order for maximum yield of FAME (biodiesel).

REFERENCES

[1] Lee, H.V., Yunus, R., Juan, J. C. and Taufiq-Yap, Y. H. (2011). Process optimization design for jatropha-based biodiesel production using response surface methodology. Fuel Process. Technol. 92(12), 2420-2428

[2] Hamza, H., Akia, M., and Yazdani F. (2015). Optimization of biodiesel production from the waste cooking oil using response surface methodology. Process Saf. Environ. Proc. 94, 1-10

STUDY OF COLD PLASMA PEN FOR THE TREATMENT OF MUSHROOM SUBSTRATE

Nor Azyan Syahirah Idris and Norhayati Ahmad
School of Mechanical Engineering, Faculty of Engineering,
Universiti Teknologi Malaysia, 81310 UTM Skudai, Johor, Malaysia

INTRODUCTION

Plasma is the fourth state of matter besides solid, liquid and gas which is an ionized gas containing an array of active species such as electrons, ions, photon.

In food industry, cold plasma is used as food decontamination, food quality improvement, toxin degradation and surface modification of packaging material [1]. It uses charged, highly reactive gaseous molecules and species to inactivate contaminating microorganisms on foods and packaging materials [2]. In agricultural industry, cold plasma is used to enhance the seed germination and growth

EXPERIMENTAL SETUP

To analyse the effectiveness and efficiency of cold plasma treatment on mushroom soil, a few testing are conducted such as bacteria colony, moisture and pH. Plate count method was used to measure the reduction of bacteria concentration in soil and oven-dry weight method was used to measure the water content of soil after plasma treatment. Both mushroom soil treated by conventional steam and plasma are inoculated in Petri dish to observe the mushroom growth..

RESULTS AND DISCUSSION

Figure 1 shows the effect of plasma treatment on the bacteria concentration in the mushroom soil with different treatment time Results show that the bacteria reduced where without treatment (untreated) soil has highest bacteria concentration compared to the treated soil. For treatment time, the best one is 10 min treatment where the bacteria concentration decreases significantly. While for voltage and flowrate, the best in reduction of bacteria are 8 kV and 4 SLM respectively.

The treatment time, voltage and air flowrate does affect the water content of soil. As treatment time increase, the heat exposures of sample from plasma also increase, thus reducing the water content. However, the water content of soil after treatment is still suitable for mushroom growth which the range of water content for mushroom growth is 55% to 70%.

From the result, pH values of samples after cold plasma treatment were higher than without treatment sample. Reactive species produced react with moist or water to produce acidic nature, thus responsible in reducing the pH. Reduced in water content is the factor for 25 min treatment to have high pH value. At 5 min, the pH reading is the lowest for treatment time parameter as at that time the water content is still high and the reactive species react with the high water content of sample. However, the pH values of all samples are still in range which 6.4 to 7.8 where rapid mycelial growth takes place.

Parameter of 1 SLM and 2 SLM flowrates with 20 minutes of treatment show the fastest growth where the pin heads of mushroom started to form on day 14. Air flowrate of 2 SLM produces 19 of mushrooms with 0.7 cm of height and 0.6 cm of diameter. Meanwhile, 1 SLM has produced 16 of mushrooms with 0.9 cm of height and 0.5 cm of diameter. 2 SLM produced more mushrooms compared to 1 SLM. Thus, the different of flowrates does effect the growth of mushroom.

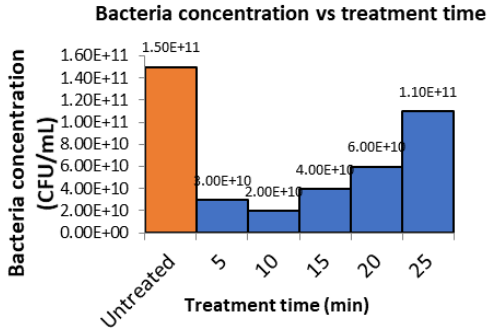

Figure 1: Bacteria concentration of sample against treatment time

CONCLUSION

It has shown that the cold plasma treatment can be used to sterilize the mushroom soil replacing the conventional method. Besides, cold plasma treatment can reduce the period of mushroom growth.

REFERENCES

[1] Pankaj, S. K., & Keener, K. M. (2017). Cold plasma: background, applications and current trends. Current Opinion in Food Science, 16, 49–52.

[2] Mandal, R., Singh, A., Singh, A.P. (2018). A review on recent developments in cold plasma decontamination technology in the food industry. Trends in Food Science & Technology, 80, 93–103.Transactions on Neural Systems and Rehabilitation Engineering, 11(2), 169-172.

CHARACTERIZATION AND MICROSTRUCTURE ANALYSIS OF CERAMIC COATING BY GAS TUNNEL TYPE PLASMA SPRAY

Shuhada Shelly and Norhayati Ahmad
School of Mechanical Engineering, Faculty of Engineering,
Universiti Teknologi Malaysia, 81310 UTM Skudai, Johor, Malaysia

INTRODUCTION

Gas tunnel plasma type system is a new development of conventional plasma spray with high energy and high efficiency [1]. Strong vortex flow in the gas tunnel that stabilize the plasma jet makes gas tunnel type plasma spray a versatile process and allow to sintering powder at high melting point as well as to perform good surface coating. This study was aimed to investigate the correlation of platting distance (distance between the plasma torch and substrate) with the microstructure of alumina coating on stainless steel together with thickness of coating that produce good adherence on the surface.

EXPERIMENTAL SETUP

The substrates (stainless steel) was horizontally set on the substrate holder and the central area was placed perpendicular to the centre of plasma torch. Argon gas acted as a carrier gas was set to 15 L/min and deposition time of 30s was set to each of the samples in atmospheric condition. The alumina powder feedstock with flowrate of 5 L/min was spray at angle of 90° to the plasma discharge and the plating distance is varies from 4mm to 14mm. The coated sample were then allowed to cool down in atmospheric surrounding. Surface morphology of the coating were characterised by Scanning Electron Microscope (SEM) with energy dispersive X-ray spectroscopy (EDX) as well as performed a Pull-off adhesion testing.

RESULTS AND DISCUSSION

Figure 1 shows the SEM-EDX line scan of the alumina coating started at point A and end at point B cutting across the coating layer and the substrate. The presence of high intensity alumina (Al-KA) was observed at the region A Thermal insulation properties on the stainless steel can be improve with nu forming the single layer alumina at the coated layer. The presence of oxygen was observed due to the ceramic coating process was conducted in air atmospheric condition where it contribute to the existence of oxygen at the coating layer while in region B, high intensity of iron was observed. When the spray was increased from 4 mm to 8 mm, 10 mm, 12 mm, and 14 mm, the agglomerated alumina particles were gradually reduced on the surface of stainless steel. Figure 2 (A) shows that at platting distance 4mm alumina grain was overheated on the stainless steel while figure 2(B) an equaixed alumina grains was obtained at platting distance 12mm that show without any discontinuity in interface between the coating and stainless steel substrate. Conduct coating process at optimum distance to enhance the deposition efficiency of ceramic coating. The weight percentage of Alumina coating thickness correlated to the effect of spray distance as the near the distance the dense the alumina coating will be [2]. Lastly, thick coating will form low adhesion performance.

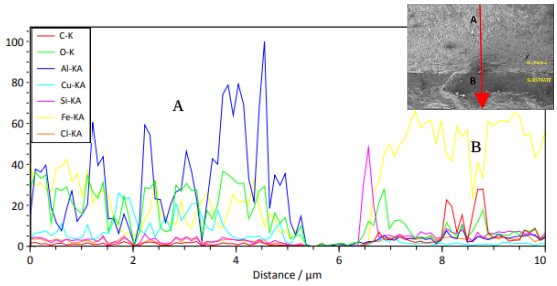

Figure 1: SEM- EDX line scan of alumina coating

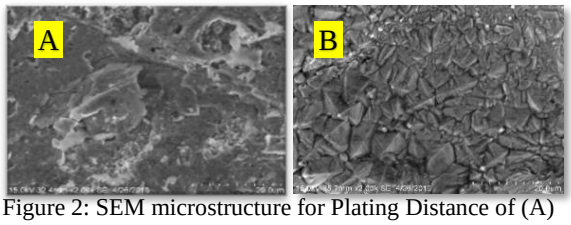

Figure 2: SEM microstructure for Plating Distance of (A) 4mm (B) 12 mm.

CONCLUSION

The results have indicated the sustainability of plasma spray technique with regards to the production of a good quality alumina coating at distance of 12 mm and having good adherence to the stainless steel.

REFERENCES

[1] A.Kobayashi. (2008). Smart coating technology by Gas Tunnel Plasma Spray. 24th Summer School and International Symposium on the Physics of Ionized Gases (p. 133). Japan: IOP Publishing.

[2] Djendel, M., Allaoui, O., & Bouzid, A. (2016). Effect of air plasma spraying parameters on the quality of coating. International Journal of Computational and Experimental Science and Engineering, 1-5.

DEVELOPMENT OF INTEGRATED SUBSTRATE MIXER AND HIGH-POWER COLD PLASMA TREATMENT FOR MUSHROOM CULTIVATION

Mohd Raffaei Rabbi and Norizah Hj. Redzuan
School of Mechanical Engineering, Faculty of Engineering,
Universiti Teknologi Malaysia, 81310 UTM Skudai, Johor, Malaysia

INTRODUCTION

Cold Atmospheric Plasma (CAP) is one alternative way that used for treatment especially in agricultural food. Since (CAP) operated at non-equlibrium energy and low gas temperature, it is called as non-thermal treatment Previous study have successfully demonstrated about the treatment of agricultural soil which is mushroom substrate give positive impact to the quality of mushroom substrate. Regardless of what the applications are, a small design of the mixer mushroom substrate needs to exist even though it can only occupy in small quantity of substrate that integrated with CAP system. The purpose of this study is to design a substrate mixer for mushroom cultivation and also to study the effect of Cold Atmospheric Plasma (CAP) [1, 2]

EXPERIMENTAL SETUP

This section presents the experimental setup for the system. Firstly, the preparation of (CAP) need to be done in order to integrated with substrate mixer for treatment purpose. The experimental parameter was varies with time treatment such as 0min, 5min, 10min and 15min.

Next, Colony Forming Unit (CFU) testing is used to observe the amount of bacteria in the sample from first the experiment by using one dilution which is $20x10^{-5}$ µL Generally, the objectives of this experiment is to compared the amount of bacteria on non-treated and treated of mushroom substrate.

RESULTS AND DISCUSSION

After have some modification, the function ability had been tested. As a result, the mechanism flow of the substrate on the spiral stirrer in positive result. The mechanism is work properly but not too efficient. Seems that there is no previous study about mixing process by using spiral stirrer type, but it already improved that the mechanism flow of substrate is work properly. Thus, The integration of substrate mixer with the Cold Atmospheric Plasma (CAP) system have been done.

Figure 1 shows that the bacteria colony of plate A is the highest and the number of bacteria colony reduced following the trend plate B is lower than A but higher than C while plate D have the least number of bacteria colony. The reduction of bacteria colony increases with the increase of Cold Atmospheric Plasma (CAP) treatment time for plate A, B, C, and D which have treatment time of 0min, 5min, 10min, and 15min respectively. Therefore, it can be observed that CAP with higher time treatment can reduce the number of bacteria colony.

Table 2 shows the colony forming unit for each sample of substrate according to its treatment time and dilution. The bacteria considered too numerous to count (TNTC) if the number of colony exceeded 300 colonies. This is because the amount of bacteria in mushroom substrate is higher compared to other product. As a result, the amount of bacteria cannot be counted with serial dilution 10^{-5} at temperature of 37˚C

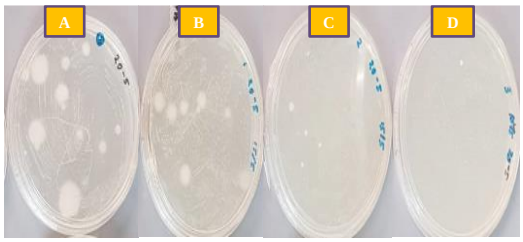

Figure 1: Growth of bacteria according to treatment time for dilution 10^{-5}

Table 2: CFU/ml according to treatment time and dilution (1day)

Time(min) / Dilution (µL)	Non treated	5 minutes treatment	10 minutes treatment	15 minutes treatment
$20x10^{-5}$	TNTC	TNTC	TNTC	TNTC

CONCLUSION

In this study, a design of cold plasma treatment for mushroom substrate has been proposed. As a result, the Cold Atmospheric Plasma (CAP) can be used for the decontamination of mushroom substrate as the result obtained shows a positive result. Even just by observing the number of bacteria colony for non-treated and treated, the result shows that the reduction of the bacteria colony can be observed with increasing of time treatment.

REFERENCES

[1] Fridman A, Chirokov A, Gutsol A. (2005). Non-thermal atmospheric pressure discharges. *J Phys D: Appl Phys*, 38, 11(2), 169-172.

[2] Anwar, Q. A., & Norizah, R. (2017). *Cold Atmospheric Plasma treatment for Bio Decontamination*. Universiti Teknologi Malaysia.

DESIGN AND DEVELOPMENT OF MECHANISM FOR COLD PLASMA TREATMENT ON GRAINS OF FOODS

Muhamad Azwandi Mohd Sakri and Norizah Hj Redzuan
School of Mechanical Engineering, Faculty of Engineering,
Universiti Teknologi Malaysia, 81310 UTM Skudai, Johor, Malaysia.

INTRODUCTION

The study is about design and development of mechanism for cold plasma treatment on grains of foods, which has utilized to treat the rice in continuously production. Rice has highly possibility to be attacked by the rice weevil at the interval of time after being harvested and before being processed. Previous study has proven that the rice weevil can be killed using atmospheric pressure cold plasma jet (APPJ) [1]. Cold plasma is a chemical free treatment and has been proven their efficient in degradation of many pesticides in various food products [2]. Further improvement of mechanism will be design and fabricate for increasing the treatment quality of rice grains.

PROJECT OBJECTIVES

The aim of this project is to design and develop the mechanism for cold plasma rice treatment machine.

METHODOLOGIES

Pugh method is one of the approaches that have being used in this study in order to determine the most suitable concept. Factors considered for evaluating are safety, functionality, weight, ease of manufacturing, mechanism, and cost.

Rice is being treated using atmospheric pressure cold plasma jet (APPJ) that made of glass tube having thickness 2mm, height 100mm and internal diameter 8mm. The control variable of this project is treatment duration, which is set for 10seconds, 20seconds, 30seconds, and 40seconds.

To determine the effectiveness of cold plasma treatment, CFU experiment has been done to analyse the reduction of the microbial after being treated with cold plasma.

RESULT AND ACHIEVEMENT

Figure 1(a) shows the development of selected concept design integrated with cold plasma reactor Result for mechanism analysis shown the reaction forces exerted on conveyor belt are 352.797N and 458.98N. The system also capable in treat rice 3.68kg in one hour with speed rate of 0.0103m/s.

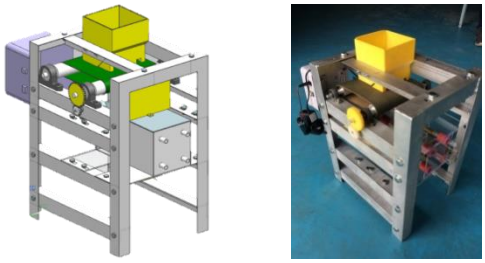

Figure 1: Development of mechanism

Sample	Dilution (μl)							
	10×10^{-2}	10×10^{-3}	10×10^{-4}	10×10^{-5}	Increased dilution	10×10^{-7}	10×10^{-8}	10×10^{-9}
Non-treat	TNTC	TNTC	TNTC	TNTC		TNTC	6	3
10sec	TNTC	TNTC	TNTC	TNTC		TNTC	1	1
20sec	TNTC	TNTC	TNTC	TNTC		1	TNTC	1
30sec	8	4	TNTC	TNTC		0	0	0
40sec	5	4	2	TNTC		0	0	0

Number of microorganism is reduced

Figure 2: CFU result

The forming of microbial colonies on agar plate for all samples has been observed and recorded. Based on Table 1 the sample of dilution 10×10^ (-9), microbial colonies does not form for sample 30s and 40s as compared to non-treated which is 3 microbial colonies is observed. Since the number of colonies forming unit is reduced as the treatment duration is increased. Therefore, cold plasma treatment is effective in decontaminate the present of microbial on rice.

REFERENCES

[1] Izzuddin Roslan, M. *Design and development of cold plasma discharge for rice treatment*. B.Eng Thesis. Universiti Teknologi Malaysia, Malaysia; 2018.

[2] Bai Y, Chen J, Mu H, Zhang C, Li B. (2009). Reduction of dichlorvos and omethoate residues by O2 plasma treatment. *J Agric Food Chem*, 57:6238-6245

DEVELOPMENT OF COLD PLASMA FOR VOLATILE ORGANIC COMPOUNDS TREATMENT

Muhammad Hakim Samsudin, Norizah Redzuan and Raja Kamarulzaman Raja Ibrahim
School of Mechanical Engineering, Faculty of Engineering,
Universiti Teknologi Malaysia, 81310 UTM Sekudai, Johor, Malaysia

INTRODUCTION

Most of the time volatile organic compounds (VOCs) are released from waste treatment facilities are harmful to human health as it spread in the air (Mustafa et al., 2018). Current issue such as Kim Kim river pollution that causes catastrophic to people of Pasir Gudang in term of breathing difficulty and headaches is a good example of how VOCs affects people. Thus, non-thermal plasma is one of the alternatives of decomposing VOCs that is considered to be green and potentially effective in air pollutant remediation (Nozaki & Okazaki, 2013). Therefore, we believe that we have designed a miniaturized plasma reactor to treat and decompose harmful VOCs by using cold plasma treatment that can be fit inside electrical appliances such as air conditioner and vacuum cleaner and also can be scaled up or down according to suitability.

PROJECT OBJECTIVES

The aim of this project is to design and fabricate miniaturize non-thermal plasma (NTP) reactors. The plasma reactors operate to analyze the parameters effects of discharge voltage, air flow rate and treatment time on treatment of dilute ethanol act as VOC. Optimize conditions for treatment also being studied to find best settings that produce higher removal efficiency.

METHODOLOGIES

The design of miniaturized plasma reactor consists of three main components of copper electrode, pyrex glass tubes and graphene as discharge electrode. Plasma reactor tested in an experimental setup that consists of helium as carrier gas, beaker filled up with dilute ethanol with bubbling vaporised process, plasma generator as power supply for plasma generation, white cell for enclosed treated or untreated gas and FT-IR for enclosed gas analysis. Full factorial 2^k design of experiment was used in planning of experiment with three factors of discharge voltage, flow rate of air and treatment time. Total of eight experiments with three additional experiment for centre point. Response collected was removal efficiency from the concentration reduced after treatment of plasma over untreated concentration of VOC. Performance analysis and optimization carried out using Design Expert 11.0.

RESULT AND ACHIEVEMENT

Figure 1(a) and (b) show untreated and treated gas spectrum analysis by FT-IR. CH concentration been reduced after the treatment showing plasma could treat VOC.

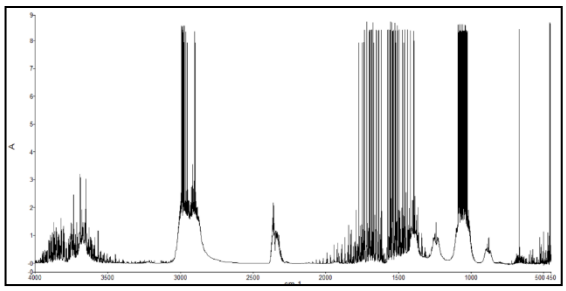

FIGURE 1 (a): Untreated gas spectrum.

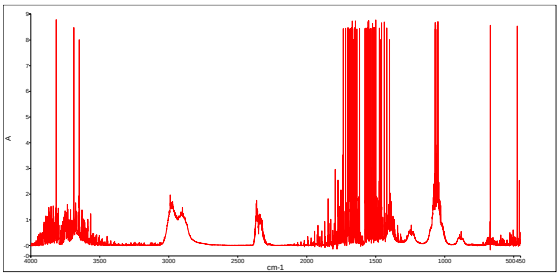

FIGURE 1 (b): Treated gas spectrum.

Reference

[1] Kim, E. H., & Chun, Y. N. (2016). VOC decomposition by a plasma-cavity combustor. Chemical Engineering and Processing: Process Intensification, 104, 51–57.

[2] Mustafa, M. F., Fu, X., Liu, Y., Abbas, Y., Wang, H., & Lu, W. (2018). Volatile organic compounds (VOCs) removal in non-thermal plasma double dielectric barrier discharge reactor. Journal of Hazardous Materials, 347(December 2017), 317–324.

DEVELOPMENT OF COLD PLASMA TREATMENT MACHINE FOR PROCESSED FOOD

Muhammad Amir Arif Mohd Yusoff and Norizah Redzuan
School of Mechanical Engineering, Faculty of Engineering,
Universiti Teknologi Malaysia, 81310 UTM Sekudai, Johor, Malaysia

INTRODUCTION

Until today, the utilization of Cold Atmospheric Plasma CAP isn't simply just concentrated on one kind of treatment. It been utilized in different field of concentrates studies had demonstrated that the cool plasma medicines are influencing significantly positive the subject tested. Existing decontamination procedures, chemical treatment, ethylene oxide sanitization more often than not endure a disadvantage of hints of the dynamic compound stays on the sample [2]. autoclave cleansing procedure are commonly inapplicable because of the item poor protection from heat, [1] has tried to develop a system to make surface treatment that decontaminate the '*keropok lekor*'

There are many uses of plasma technology in various field such as electrical, medical, mechanical and automotive. This shown that the technology has been used widely and have been used throughout the whole world. CAP technology can be applied in numerous fields whether for mechanical, electrical and even medical field If this technology been developed in food industry that provide immense benefits to the industry

PROJECT OBJECTIVES

To design and develop a machine compatible with cold atmospheric plasma treatment using semi-automatic function for treatment purpose

METHODOLOGIES

First phase of design, in order to make a concept design, a few limitations are set on the design to make sure that the concept designs are applicable for this project This project carried out with a proper engineering design process. The design had satisfied CAP system and bio-product constraint throughout design and material selection using morphological chart and for concept selection Pugh method are used. Several test are done to ensure the effectiveness experiment the setup following Figure 1. Distend between *keropok lekor* and plasma discharge are 5mm, Electrode for high voltage are graphite, Electrode for ground are stainless steel, 5kv are supply at high voltage electrode, Helium gas are used to help indicate plasma as it glows pink when discharge, Gas flow are 1.5 ℓpm. Sample from single source which is from danga *keropok lekor* manufacturer, treated on machine individually with constant voltage (5kv), gap discharge sample between discharge plasma (5mm) and gas flow rate (1.5 ℓpm), The variable is treatment time which is 30s,40s,50s and 60s.

RESULT AND ACHIEVEMENT

Figure 1 shows a setup used for *keropok lekor* plasma treatment this actual setup are been use to run the CFU experiment

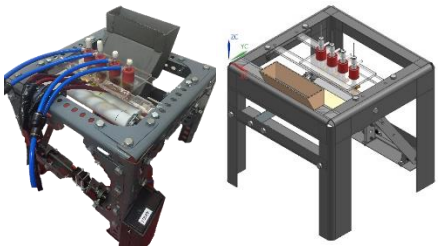

Figure 1: comparison of actual prototype and concept

Table1: microbial colonies count

	DILUTION				
SPECIMEN	10^{-4}	10^{-5}	10^{-7}	10^{-8}	10^{-9}
Non treat	Tntc	Tntc	Tntc	Tntc	93
30s	Tntc	Tntc	Tntc	Tntc	6
40s	Tntc	570	59	36	3
50s	Tntc	429	31	13	0
60s	Tntc	271	1	1	0

CONCLUSION

Prototype was completely function well with the plasma discharge system. to complete this prototype, speed analysis had been done as stated in the objectives in term before the fabrication process. The *keropok lekor* undergo plasma treatment with rotation of 31 rad/s for each treatment time of 30 s, 40 s, 50 s and 60 s.

Cold plasma processing has been shown to affect the quality attributes of the food products during treatment as well as in Optimization studies are also required to avoid the negative impacts on quality, the CFU test shows that 60s treatment time have most effect on *keropok lekor*.

REFERENCES

[1] Aminuddin (2018). Design and development of cold plasma treatment feeder mechanism, Bachelor Degree, Universiti Teknologi Malaysia, Johor Bahru

[2] Smeu, I. & Nicolau, A. (2014). Enhancement of Food Safety – Antimicrobial Effectiveness of Cold Plasma Treatments. Food Technology, 3(1), 9-20.

MAXIMIZATION OF THE TEMPERATURE DIFFERENCE ACROSS THE STACK UNIT IN A THERMOACOUSTIC REFRIGERATOR USING PARTICLE SWARM OPTIMIZATION

Chan It Sing, Normah Mohd Ghazali, and Maziah Mohamad
School of Mechanical Engineering, Faculty of Engineering,
Universiti Teknologi Malaysia, 81310 UTM Skudai, Johor, Malaysia.

INTRODUCTION

Recently, evolutionary algorithm such as genetic algorithm has become popular among the researchers in optimizing the performance of the thermoacoustic refrigerator due to its capability to provide a solution with a global maximum or minimum through simultaneous optimization of several objectives. The results from the past studies by using MOGA has proved the potential of evolutionary algorithms in improving the performance of thermoacoustic refrigerator Zolpakar et al. [1]. Hence, this study maximize the temperature difference across the stack unit using the Multi-objective Particle Swarm Optimization (MOPSO), an evolutionary optimization tool that has not been tried in this field before.

METHODOLOGY

The controlling parameters that affects the temperature difference across the stack are first identified, which are the stack length, stack centre position, blockage ratio, and drive ratio.

Then, a MOPSPO programing code is developed using MATLAB. By using the equations and system settings designed by Tijani et al. [2] together with the parameters range set by Zolpakar et al. [1], simultaneous optimization of multiple inter-dependent parameters are performed to solve for the two conflicting objectives; the maximum cooling power and minimum acoustic power required. Two, three, and four parameters simultaneously optimization are performed. Lastly, the optimized parameters are analysed and compared with the results of past studies [1].

RESULTS AND DISCUSSION

Figure 1 shows the Pareto front obtained from the MOPSO which can provide more solutions to the problem. Figure 2 compares the cooling power and *COP* achieved when the number of inter-dependent variables to be optimized increases. The figure shows that four parameters optimization achieved the highest *COP* and cooling power compared to two and three variables optimization.

Comparison between MOGA and MOPSO for two parameters optimization L_{sn} and x_n shows that for the same arrangement of other parameters, placing the stack at a position of x_n = 0.20 instead of 0.22 can increase the cooling power generated by 2 % Then, the four parameters optimization involving the drive ratio, *D* shows a significant difference between MOGA and MOPSO. MOPSO provides a better overall result by having a higher *COP* of 1.39 compared to the MOGA with a COP of 1.35. The cooling power achieved is also double that of the MOGA with Q_c = 10.8 W compared to that of MOGA with Q_c = 5.22 W. The cooling power generated is the highest among past studies with a considerable improvement in COP.

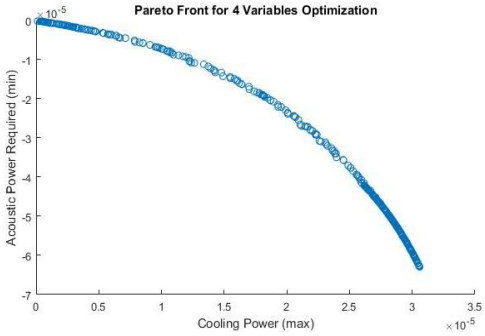

Figure 1: Pareto Front obtained from MOPSO

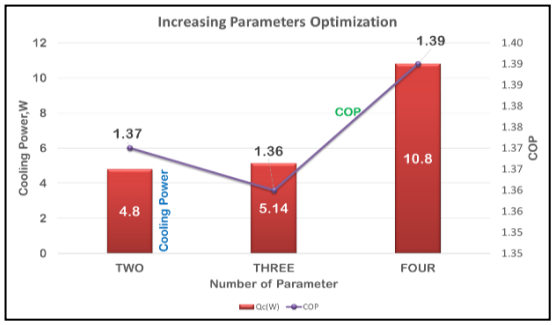

Figure 2: Effect of increasing parameters to be optimized simultaneously

CONCLUSION

Thus, this study has highlighted the potential of MOPSO in providing optimized conditions for conflicting objectives desired for a thermoacoustic system.

REFERENCES

[1] Zolpakar, N. A., Mohd-Ghazali, N., Ahmad, R. (2014a). Analysis of increasing the optimized parameters in improving the performance of a thermoacoustic refrigerator. *Energy Procedia*, *61*, 33–36.

[2] Tijani, M.E.H., Zeegers, J.C.H., De Waele, A.T.A.M. (2002). Design of thermoacoustic Refrigerators. *Cryogenics*, *42*, 49–57.

THERMAL PERFORMANCE OF A MICROCHANNEL HEAT SINK OF VARIOUS GEOMETRY

Sithamparam Sivaraman and Normah Mohd Ghazali
School of Mechanical Engineering, Faculty of Engineering,
Universiti Teknologi Malaysia, 81310 UTM Skudai, Johor, Malaysia

INTRODUCTION

Electronic Chips tends to produce more heat when it is subjected to high performance with high efficiency. This confrontation will affect the performance and life span of the microelectronic device that leads to frequent replacement of the device. The most suitable way to cool the microelectronic device is by introducing microchannel heat sinks, which provide efficient cooling of high performance applications.

METHODOLOGY

This section presents the values being used to calculate the total thermal resistance of rectangular, circular and trapezoidal microchannel heat sink. The equations for this study is validated by using [1] as the reference to make sure the equations are correct. Therefore, the values from [1] is used with current equations and compared to the current value.

Table 1: Parameters involved in thermal resistance calculation.

Parameter	Values
Length of MCHS (m)	0.01
Width of MCHS (m)	0.000056
Width of MCHS wall (m)	0.000044
Height of MCHS (m)	0.00032
Water(Coolant) Pressure (bar)	1
Flow rate of Water (cm^3/s)	4.7
Total Thermal Resistance (°C/W)	0.110

RESULTS AND DISCUSSION

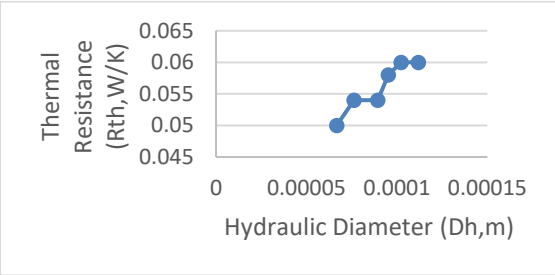

Figure 1: Trend of total thermal resistance against hydraulic diameter (rectangular shaped)

Figure 1 shows the trend of total thermal resistance against hydraulic diameter for rectangular microchannel without R_{cons} (Constriction resistance). The thermal resistance tend to increase as hydraulic diameter increases.

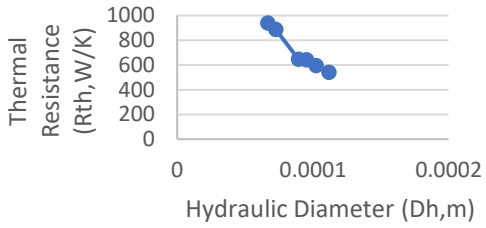

Figure 2: trend of total thermal resistance against hydraulic diameter (circular shaped)

Figure 2 shows the trend of total thermal resistance against hydraulic diameter for circular microchannel. The trend shows that the thermal resistance decreases as the hydraulic diameter increases.

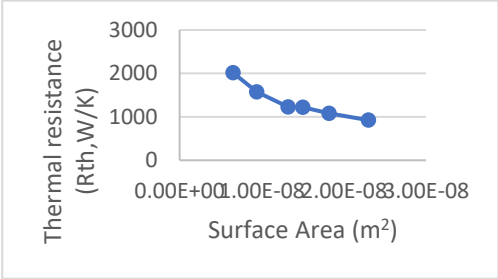

Figure 3: Trend of total thermal resistance against surface area (trapezoidal shaped)

Figure 3 shows the trend of total thermal resistance against surface area of trapezoidal microchannel. The trend shows that the thermal resistance tend to decrease when the surface area increased.

CONCLUSION

We can conclude that the suitable geometry to be classified as good microchannel in terms of heat transfer per unit area is rectangular microchannel without constrictive resistance (R_{cons}) when compared to other two geometries.

REFERENCES

[1] Tuckerman, D. B., & Pease, R. F. W. (1981). High-performance heat sinking for VLSI. IEEE Electron device letters, 2(5), 126-129.

[2] 20. Normah, G. M., Oh, J. T., Chien, N. B., Choi, K. I., & Robiah, A. (2015). Comparison of the optimized thermal performance of square and circular ammonia-cooled microchannel heat sink with genetic algorithm. Energy conversion and management, 102, 59-65

ANALYSIS OF WIND FLOW AROUND A LOW COST APARTMENT BUILDING

Lai Zi Ying, Normah Mohd Ghazali and Shabudin Mat
School of Mechanical Engineering, Faculty of Engineering,
Universiti Teknologi Malaysia, 81310 UTM Skudai, Johor, Malaysia

INTRODUCTION

For low-cost buildings in Malaysia, developers tend to maximize the usage of land for buildings without consideration to orientation to wind flow and consequently natural ventilation [1]. The analysis of wind flow needs to be carried out in order to study the effects of building orientation and height ratio in this case low-cost buildings, for a better ventilation outside of the buildings and consequently lower demand on the air conditioning system.

EXPERIMENTAL SETUP

The proposed case studies to be tested using wind tunnel testing involves a minimum of two buildings and it can be separated into two major categories which are height ratio and orientation. The pressure model is an acrylic model whereas the dummy model is made from wood. The models are tested in wind tunnel with a wind speed of 20m/s.

RESULTS AND DISCUSSION

Figure 1 shows the side view arrangement of height ratio case study whereas Figure 2 states the comparison of results for both case studies.

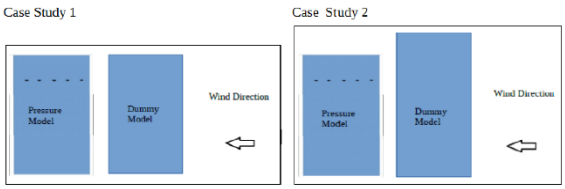

Figure 1: Side View arrangement of height ratio case study

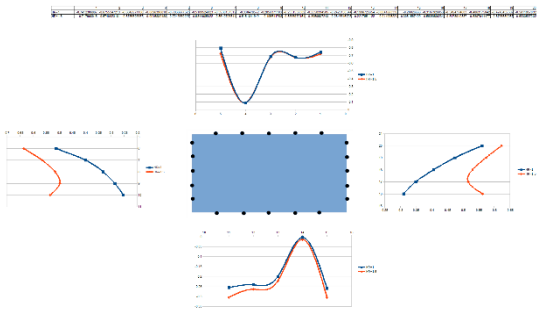

Figure 2: Results on height ratio case study

Figure 3 shows the arrangement of case study on building orientation and the compared results are shown in Figure 4.

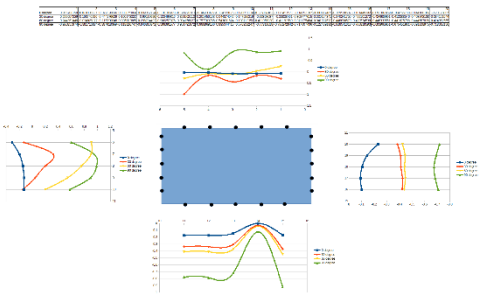

Figure 3: Side View arrangement of building orientation case study

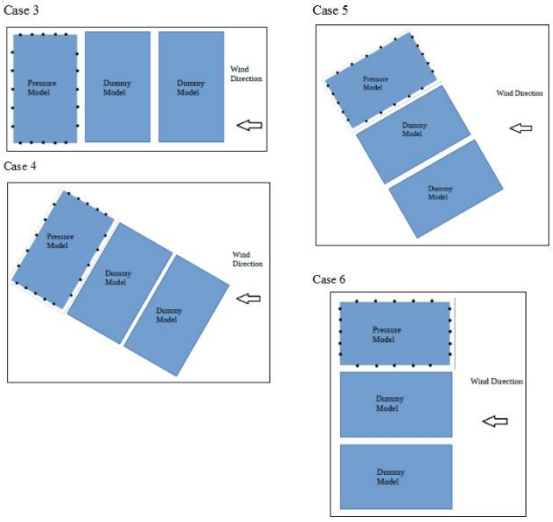

Figure 4: Results on building orientation case study

CONCLUSION

Results show that the height ratio affect less towards the wind flow around the buildings and it has nearly the same stagnation point (dead zone are) in case study 1 and case study 2. Results also shows that the effect of building orientation towards the surrounding wind flow pattern through the wind tunnel testing with different building orientation. Building orientation with an angle between 30° to 60° gives a better ventilation since the wind does not move directly to either only windward area or leeward area.

REFERENCES

[1] Lau, K. Y.. *Heat Transfer Analysis For A Double Storey Housing Unit.* PSM Thesis. Fakulti Kejuruteraan Mekanikal, Universiti Teknologi Malaysia. 2006.

SIMULATION OF SOLID-FLUID INTERACTION AROUND THE THERMOACOUSTIC STACK

Tarit Das and Normah Mohd Ghazali
School of Mechanical Engineering, Faculty of Engineering,
Universiti Teknologi Malaysia, 81310 UTM Skudai, Johor, Malaysia

INTRODUCTION

Thermoacoustic devices has become a perfect alternative to existing refrigeration system, due to its low cost, low power consumption and sustainable ability. Over past few decades, many have contributed to this system, still the performance is not as high as expected comparing with the existing system. Solid-fluid interaction around the stack is one of the most important phenomena in this system, because the viscous losses occur near the stack and oscillations caused back flow which reduces the expected cooling at one end of the stack [2]. That's why to model the fluid flow in the full resonator is important to increase the system performance.

THEORETICAL FORMULATION

The main three governing equations used here are:

$$\frac{D\rho}{Dt} + \rho\left(\nabla.\vec{V}\right) = 0$$

$$\rho\left(\frac{D\vec{V}}{Dt}\right) = -\nabla.p + \mu\nabla^2\mu + \frac{\mu}{3}\nabla(\nabla.\vec{V})$$

$$\rho c_p \frac{DT}{Dt} = \nabla.(k\nabla T) + \frac{Dp}{Dt} + \Phi$$

Using the assumptions, dimensionless parameter and various manipulation, the partial differential equation to be solved are:

$$\frac{\partial^2 u}{\partial t^2} = \frac{1}{M^2\gamma}\left(\frac{\partial^2 u}{\partial x^2} + \frac{\partial^2 v}{\partial x \partial y} - \frac{\partial^2 T}{\partial x \partial t}\right) + \frac{1}{Re}\frac{\partial}{\partial t}(\nabla^2 u) + \frac{1}{3Re}\frac{\partial}{\partial t}\left(\frac{\partial^2 u}{\partial x^2} + \frac{\partial^2 v}{\partial x \partial y}\right)$$

$$\frac{\partial^2 v}{\partial t^2} = \frac{1}{M^2\gamma}\left(\frac{\partial^2 v}{\partial y^2} + \frac{\partial^2 u}{\partial x \partial y} - \frac{\partial^2 T}{\partial x \partial t}\right) + \frac{1}{Re}\frac{\partial}{\partial t}(\nabla^2 v) + \frac{1}{3Re}\frac{\partial}{\partial t}\left(\frac{\partial^2 v}{\partial y^2} + \frac{\partial^2 u}{\partial x \partial y}\right)$$

NUMERICAL FORMULATION

Here explicit finite difference method is used to model and simulation the flow [1]. The computational domain was calculated to stabilize the simulation using $c(\Delta t/\Delta x)<1$, this equation.

RESULTS AND DISCUSSION

First the MATLAB code and numerical method was validated with 1d wave equation and comparing with earlier results. Then fluid flow is modelled and simulated in full resonator with single, double and multiple (11) plates.

In all three cases, flow is visualized in different times and compared with each other. As there are not enough model done with multiple plates, the fluid flow with multiple plates are different than as expected and those of single and double plate. The vortex generation increased in numbers and in different sizes. The flow is not perfectly linear. The forward flow around the plates are effected by the back flow in the system. The boundary layers are mostly back flow [3]. The fluid works as bulk motion with multiple plates and it effects the nearby plate flow.

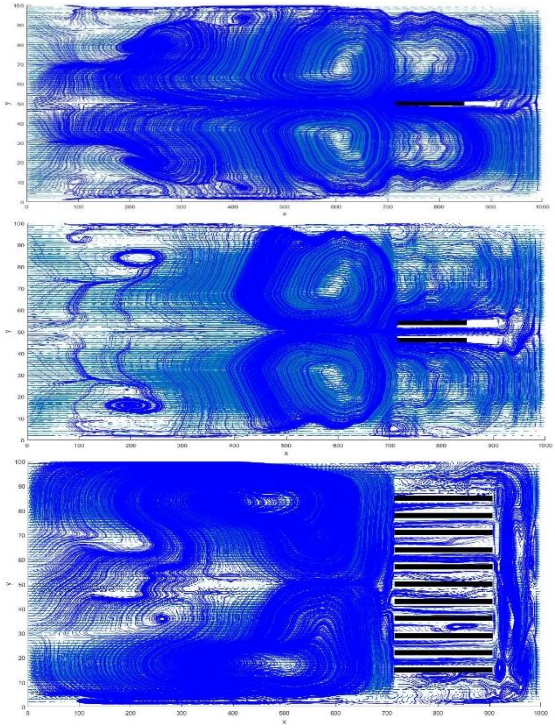

Figure 1: Vector plot and streamline at 3.1 second for a single, double and multiple plates respectively.

CONCLUSION

The flow is mostly symmetric, but with the increase of the plate number, the flow tends to be asymmetric at certain times. The fluid flow between the plates are different with multiple plates. More vortices occur with multiple plates.

REFERENCES

[1] Kim Fa, liew. (2013). *Simulation of the Fluid Flow Around the Stack Unit in a Thermoacoustic Resonator*. Univerisiti Teknologi Malaysia.

[2] Mohd.Ghazali, N. (2001). *Numerical simulation of acoustic waves in a rectangular chamber*.

[3] Swift, G. W. (2017). *thermoacoustics*.

COMPARISON OF CORRELATIONS USED TO PREDICT THE HEAT TRANSFER COEFFICIENTS IN SMALL CHANNELS

Jeevamunissen Ramachandran and Normah Mohd Ghazali
School of Mechanical Engineering, Faculty of Engineering,
Universiti Teknologi Malaysia, 81310 UTM Skudai, Johor, Malaysia.

INTRODUCTION

As new refrigerants are being used in the smaller channels, more research need to be done to study the flow in a small channel especially the complex two phase flow. Many correlations have been introduced to calculate the heat transfer coefficient but they were tested using refrigerants like R11, R12, R112 and R22. The accuracy of the data obtained from the correlations will vary as refrigerants change. Many modifications and improvement has been done to Chen [1] flow boiling heat transfer coefficient yet the heat transfer coefficient in small channel could not be accurately predicted over a wide range of parameters (Thome) [2]. Each developed or modified correlations since Chen [1] introduced his correlation showed reduced error from the previous correlations in predicting the heat transfer coefficient when compared to experimental results. However, discrepancies still exist when the correlations are compared with later experimental data generating interest in improving the correlations. The aim of this project is to look at the difference between two correlations that have been modified or developed for small channels to analyse their trend and patterns as the vapour quality changes. The outcome of this study would help us towards a better approach in future development of the heat transfer coefficient correlation for a small channel.

METHODOLOGY

The two selected correlations for this study are Bertsch et al. [3] and Fang et al. [4]. R134a is the chosen refrigerant for this study as it has a wider range of applications compared to other refrigerants but due to its high Global Warming Potential, this is only a short term solution. Natural refrigerants, R717 and R744 were chosen to be compared with results of R134a as both these refrigerants can be used as a replacement for the hazardous refrigerants which are being phased out. This study was first completed parametrically then with Genetic Algorithm (GA) to obtain the results at various vapour quality. Parametric studies allows the user to examine the way a model behaves as the input parameters are varied in a defined range. The value of chosen parameter for assessment are 0.21mm, 100kW/m^2 and 300kg/m^{2}s for hydraulic diameter, heat flux and mass flux respectively with refrigerant properties obtained at temperature of 283K. At a value of vapour quality, x, data for both correlations is recorded simultaneously on the same graph. The process is repeated at different x values to find the effect of vapour quality on the prediction of the heat transfer coefficient using the two selected correlations. GA imitates a biological evolution with five phases which are initial population, fitness function, selection function, crossover function and mutation function. After trying multiple times, the overall best functions were chosen where fitness scaling function is rank, selection function is stochastic uniform, mutation function is adaptive feasible and crossover function is two point.

RESULTS AND DISCUSSION

From the results of R134a and R717, the effect pre-dryout and post dryout is significant for Bertsch et al. [3] correlation. However this effect does not appear in R744 due to significance of nucleate and convective boiling contribution towards heat transfer coefficient as surface tension is low for R744. Results obtained for Fang et al. [4] gave different trends for all refrigerants compared to Bertsch et al. [3] due to the use of different parameters in the correlation. Fang number used by Fang et al. [4] correlation includes effect of bubble flow extensively compared to Bertsch et al. [3] through Eötvös number, Eo and Weber number, We. Heat transfer coefficient obtained for three refrigerants are different due to the properties of refrigerants. Heat transfer coefficient obtained for R717 is twice the value of R134a due to favourable thermal conductivity of R717.

REFERENCES

[1] Chen, J. C. (1966). A correlation for boiling heat transfer to saturated fluids in convective flow. Industrial and Engineering Chemistry. 5, 2755-2771.
[2] Thome, J. R. (2003). Recent advances in modelling of two-phase flow and heat transfer. Heat Transfer Engineering. 24(6), 46-59.
[3] Bertsch, S. S., Groll, E. A. & Garimella, S. V. (2009). A composite heat transfer correlation for saturated flow boiling in small channels. International Journal of Mass and Heat Transfer. 52(7-8), 2110-2118.
[4] Fang, X., Zhou, Z., & Wang, H. (2015). Heat transfer correlation for saturated flow boiling of water. Applied Thermal Engineering. 76, 147-156.

THERMAL AND HYDRODYANAMIC PERFORMANCE OF A MICROCHANNEL HEAT SINK COOLED WITH CARBON NANOTUBE (CNT) NANOFLUID

Lee Wei Tong and Normah Mohd Ghazali
School of Mechanical Engineering, Faculty of Engineering,
Universiti Teknologi Malaysia, 81310 UTM Skudai, Johor, Malaysia

INTRODUCTION

The size of the modern technology electronic chips has become smaller while the power density has increased. The coolant used in a rectangular microchannel heat sink (MCHS) used to cool the chips is a major concern to improve the heat removal capacity due to decreasing sizes of these heat exchanging devices. CNT nanofluid N2 and N3 with surfactant Lignin and Sodium polycarboxylate are promoted to increase the rate of heat transfer.

MATHEMATICAL MODEL

To determine the thermal performance of a nanofluid-cooled MCHS, the model system is evaluated optimized using the total thermal resistance equation referenced from Adham et al. [1]. The total thermal resistance consists conductive, convective, and capacitive thermal resistance described as:

$$R_{total} = \frac{t}{k_{hs}} + \frac{1}{h_{av}} \frac{1+\beta}{1+2\alpha n} + \frac{L}{Cp_{nf}\mu_{nf}} \frac{2}{Re} \frac{1+\beta}{1+\alpha} \quad (1)$$

The hydrodynamic performance is evaluated using the pressure drop, Δp, across the heat sink and pumping power, Pp, equation as:

$$P_p = \Delta p \times G \quad (2)$$

In the optimization process, the channel aspect ratio and wall width ratio are the controlling variables used to determine the maximum optimized thermal performance. Mathematical model validation of current model has been carried out against the experimental result of Turkerman and Peace [2]. Optimization validation using Multi objective particle swarm optimization (MOPSO) algorithm was developed to minimize the thermal resistance and pumping power simultaneously by optimizing the controlling parameters.

RESULTS AND DISCUSSION

Figure 1 presents the relationship between thermal resistance and pumping power for water and CNT nanofluids at 20°C. The graph showed that the lowest total thermal resistance is accompanied with the highest pumping power for all working fluids. The optimized results show that the total thermal resistance of both CNT nanofluid N2 and N3 are lower than water at 20°C. The total reduction of thermal resistance between water and CNT nanofluid is 26.53 %. CNT nanofluids contain nanoparticles which increases the thermal conductivity. The increase in the thermal conductivity enhances the heat transfer coefficient.

The increment of heat transfer coefficient leads to a decrease in the convective thermal resistance, a major contributor towards the total resistance to heat transfer.

CNT Nanofluid with surfactant Sodium polycarboxylate obtained the highest pumping power followed by CNT nanofluid N2 and water. CNT nanofluids N2 and N3 have the same thermophysical properties except the viscosity. In 0.1% volume concentration, the viscosity of CNT nanofluid N3 is higher than the CNT nanofluid N2. The decrease in the viscosity plays a role in reducing the Reynolds number. The lower the Reynolds number, the higher the friction factor. This increases the pressure drop and pumping power.

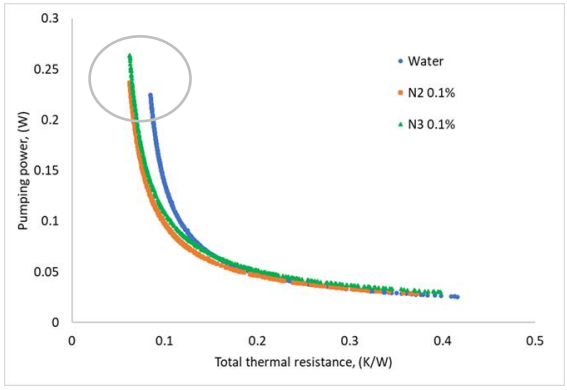

Figure 1: Optimized pumping power against total thermal resistance for water and CNT nanofluids at 20°C.

CONCLUSION

The total thermal resistance of both CNT nanofluids and water are 0.0623°C/W and 0.0848°C/W at 20°C, respectively. The optimized pumping power of CNT nanofluid N3 with is higher than CNT nanofluid N2 and water at 20°C.

REFERENCES

[1] Adham A. M., Mohd-Ghazali N., & Ahmad R. (2012). Optimization of an ammonia-cooled rectangular microchannel heat sink using multi-objective non-dominated sorting genetic algorithm (NSGA2). Heat Mass Transfer, 48, 1723-1733.

[2] Tuckerman D. B., & Pease R. F. W. (1981). High-performance heat sinking for VLSI. IEEE Electron Device Letters, 5:126-129.

PERFORMANCE OF OPTIMIZED 3D PRINTED STACK IN A THERMOACOUSTIC REFRIGERATOR

Muhammad Nazmi Hadi Bin Roslan and Normah Mohd Ghazali
School of Mechanical Engineering, Faculty of Engineering,
Universiti Teknologi Malaysia, 81310 UTM Skudai, Johor, Malaysia

INTRODUCTION

A thermoacoustic refrigerator (TAR) system is an alternative environmentally friendly cooling system. The TAR system use inert gases as the working fluid. The system operates based on the compression and expansion of gas parcels in a closed tube that creates a temperature difference at both ends of a stack, a porous medium. Unfortunately, the low coefficient of performance (COP) limits the practical application of the technology to date [1]. Being the core of the system, the stack final product has been dependent on the fabrication mechanism. To date, an optimized stack fabricated from a 3D printer shows promising results [2-3].

EXPERIMENTAL SETUP

The stacks tested is an optimized stack with optimized parameters (Case 1) [2], non-optimized stacks each with different plate spacing of 0.5 mm and 0.7 mm (Case 2 and 3) and non-optimized stacks each with different plate thickness of 0.7 mm and 1.0 mm (Case 4 and 5). The resonator is a quarter-wavelength resonator from an Acrylic material having its fundamental resonance frequency at 400 Hz with inner diameter of 21 mm. At the end of the tube is a rigid end (aluminium reflector) and the other end was connected to a mid-range loudspeaker. The measurement of the temperatures is taken with thermistors. The duration of each experiment is 240 s to achieve steady state.

RESULTS AND DISCUSSION

Figure 1 illustrated the temperature difference obtained for Case 1, 2 and 3. The results obtained is unexpected. Case 1 should have the highest temperature difference because it is the stack with the optimized parameters. However, the results obtained show that Case 3 has the highest temperature difference. When the stack plate spacing is too far apart, the heat transfer between gas bundles and stack wall cannot occur successfully. This results was probably because of the size of the stack. In Zolpakar *et al.* [3] study, the stack size was 36 mm while this experiment used a 21 mm stack. Since the stack used in this experiment was smaller, the optimized stack parameter may be different.

Figure 2 illustrated the temperature difference obtained for Case 1, 4 and 5. When the plate thickness is bigger, the harder for gas molecules to passed through it. In other words, with thinner plates, the blockage ratio is lower and it is produces a higher thermal performance. Thinner plates could provide more area for heat transfer relative to the given resonator ensuring a faster cooling rate. Due to the limitation of the current 3D printer available, the minimum thickness achieved was 0.5 mm.

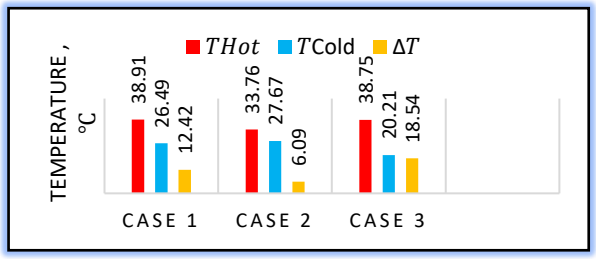

Figure 1: Temperatures for the stack with different plate spacing.

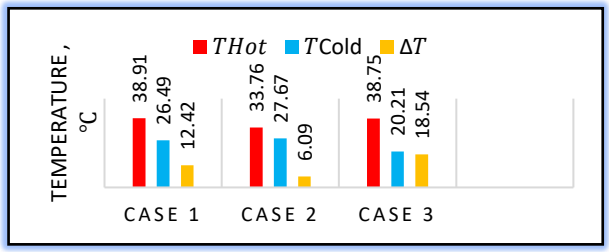

Figure 2: Temperatures for the stack with different plate thickness

CONCLUSION

The results have shown the importance of choosing the stack parameters. It is expected that the performance of the thermoacoustic refrigerator can be further improved if the fabrication technology can keep up with the optimization theory.

REFERENCES

[1] Girgin I, Turker M., 2012. Thermoacoustic system as an alternative to conventional coolers. *Journal of Naval Science and Engineering*, **8**:14-32.

[2] Zolpakar NA, Mohd-Ghazali N, Ahmad R., 2016. Experimental investigations of the performance of a standing wave thermoacoustic refrigerator based on multi-objective genetic algorithm optimized parameters, *Applied Thermal Engineering*, **100**: 296-303.

[3] Zolpakar NA, Mohd-Ghazali N, Ahmad R., Mare T., 2017. Performance of a 3D-printed stack in a standing wave thermoacoustic refrigerator, *The 8th International Conference on Applied Energy*, Beijing, China.

ENHANCEMENT OF CONVECTIVE BOILING HEAT TRANSFER COEFFICIENT IN A SMALL CHANNEL

Wan Mohd Faiz and Normah Mohd Ghazali
School of Mechanical Engineering, Faculty of Engineering,
Universiti Teknologi Malaysia, 81310 UTM Skudai, Johor, Malaysia.

INTRODUCTION

In recent years, small channels had been used in many applications such as electronic cooling, mobile air conditioning, biomedical instrumentation and compact heat exchanger. It is because they provide significant advantages like low cost, optimized compactness, and high thermal efficiency. To enhance the heat transfer coefficient in such systems, a study on phase-change phenomenon in the boiling process has to be made. An environmentally friendly refrigerant, R290 was used due to the strict regulation that required to reduce ozone depletion and global warming in the future. It also requires low cost, widely available, has very low global warming potential and no ozone depletion potential.[1].

PROJECT OBJECTIVES

The main objective of this study is to determine the optimized conditions of two-phase flow boiling heat transfer due to convective boiling in a small channel. Although two phase flow boiling involves both nucleate boiling and convective heat transfer, this study only looks at the convective boiling contribution

EXPERIMENTAL SETUP

The main objective of this study is to determine the optimized conditions of two-phase flow boiling heat transfer due to convective boiling in a small channel. Although two phase flow boiling involves both nucleate boiling and convective heat transfer, this study only looks at the convective boiling contribution

RESULTS AND DISCUSSION

The first case, the effect of mass flux toward heat transfer coefficient through varies vapor quality was studied and the result was depicted in Figure 1. Generally observed, the heat transfer coefficient of convective boiling, hcv was increasing throughout vapor quality. Only for [2] correlation, the heat transfer coefficient was peak at vapor quality 0.5 and continuously dropped at high quality region. The value of hcv for [3] and [4] along the vapor quality agrees well with the statement of both authors in literature review.

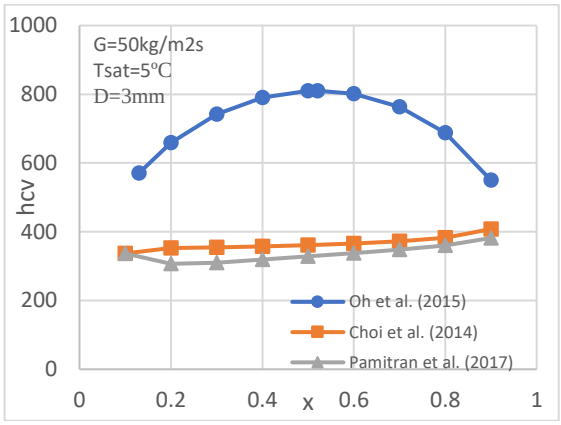

Figure 1: Control system of PMBLDC

REFERENCES

[1] Powade R.S, Rane A.A, Rane A.D, Sutar O.S, Bagade V.S, (2018). Performance Investigation of Refrigerants R290 and R134a as an Alternative to R22. 4668-4675.

[2] Oh J.T, Choi K.I and Chien N.B. (2015). Pressure Drop and Heat Transfer during a Two-phase Flow Vaporization of Propane in Horizontal Smooth Minichannels. 105-127.

[3] Choi K.I, Oh J.T, Saito K, Jeong J.S, (2014). Comparison of heat transfer coefficient during evaporation of natural refrigerants and R-1234yf in horizontal small tube, International Journal of Refrigeration 41 210-218.

[4] Pamitran A.S., Novianto S, Normah M.G., Yushazaziah M.Y. (2017). Analysis of the Two-Phase Heat Transfer Coefficient of Propane in a Small Channel. 4635-4640.

DESIGN AND DEVELOPMENT OF WATER TANK CONTROL SYSTEM

Mohamed Asyraf Mohamed Aidil and Nur Safwati Mohd Nor
School of Mechanical Engineering, Faculty of Engineering,
Universiti Teknologi Malaysia, 81310 UTM Skudai, Johor, Malaysia

INTRODUCTION

Malaysia is a country that has a potential to be as success as another first world country such as Sweden, Germany and our own neighbour Singapore. Thus, in aiming for those objectives the people must have a first-class thinker. However, many of us overlooked the system of the water tank either in our home or factory. The traditional tank only use ballcock to control water level and the flow cannot be control which will cause the water to depleted very fast. Thus, the objective of this paper is to fabricate a fully working control system for water tank using microcontroller. In order to do this, the parameters such as water level and output flow must be clearly stated. The type of material uses to make tanks are polyethylene tanks, meatal tanks, fiberglass tanks, PVC tanks and concrete tanks. Most of the tanks use are for above ground usage except for concrete tanks which is usually for underground purposes [1]

EXPERIMENTAL SETUP

For this paper, the apparatus is set-up using microcontroller which is Arduino and sensor to detect the parameter. Ultrasonic sensor is used for detecting the water level sensor. The G ½ water flowrate sensor is as its name which is to detect the flowrate. The motor is being fitted into the ball valve's head to control the opening of the valve which in this case control the flowrate. The sensor and valve were fitted to the fibreglass tank

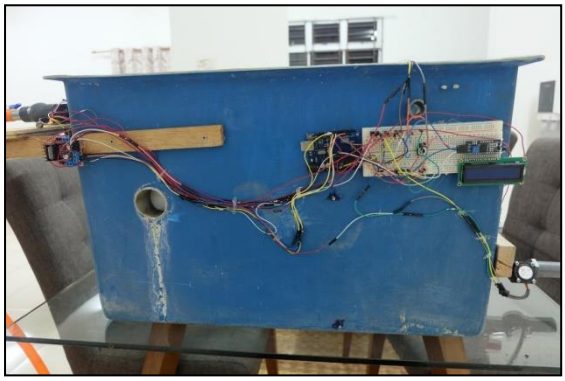

Figure 1: Normalized power for each task correspond to specific direction

The water tank was tested under 3 specific conditions which is 10cm,1L/min, 15cm,1L/min and 15cm,3L/min. the experiment was run until a steady state was reached for at least 3 minutes

RESULTS AND DISCUSSION

In figure 2 we can see that the flowrate out increase linearly as the water height are still not sufficient to provide the desired flowrate. And the water input is around 5L/min. when the water level is enough to provide the desired flowrate, the graph is constant from that point forward and when the water level reach 10cm the flowrate for input dropped to 0L/min. once the water level are lower than desired than it will turn the valve again and let the water to fill the tanks

From figure 3 we can see that the water level rises slowly and linearly until it reached 10cm and it will maintain from 10cm to 7cm. it is flat from that point forward with a little up and down in the water level and will not go lower than 7cm. this proves that it is able to control the water level by using motor and valve as turn on and off

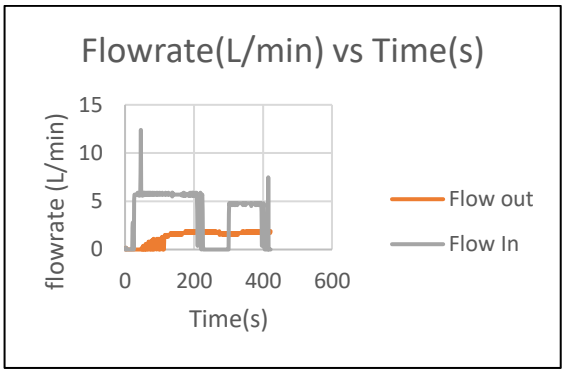

Figure 2: output flowrate vs time

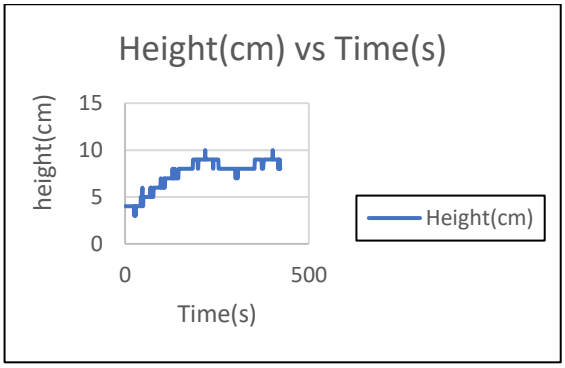

Figure 3: water in water tank level vs time

CONCLUSION

The paper has proved that the using of microcontroller to control and monitor the flowrate and water level is a success. Both of the parameters are able to be control

REFERENCES

[1] Khan, S. Sanitation and wastewater technologies in Harappa/Indus valley civilization.

ARDUINO-BASED DATA LOGGER FOR DRVING CAR ANALYSIS

Timothy Wong Xiu Wen and Nur Safwati Mohd Nor
School of Mechanical Engineering, Faculty of Engineering,
Universiti Teknologi Malaysia, 81310 UTM Skudai, Johor, Malaysia

\

INTRODUCTION

Ride comfort is defined as the overall comfort and well-being of the vehicle's occupants during vehicle travel. The main sources of discomfort are oscillations which reach the vehicle's passenger compartment and cause noise, vibration, or both. Some of the suspension system is still not fully categorized as ride comfort. It is very important to comfort the vehicle passengers. The vibration sensed by the passenger is depending upon the vibration frequency. Such vibration might cause many types of health disorders depending on its magnitude and location. The peak acceleration value of the human body is affected by the suspension system. [1]

EXPERIMENTAL SETUP

There are five different road profiles chosen for the comfort analysis which are smooth road surface, rough road surface, cobbled road surface, yellow lines road surface and road bump surface. A simple and easy-to-get data logger is developed to collect and record the data in smartphone memory. The system is the combination of Arduino and 1Sheeld. The data is collected at different speed which are 30km/h and 50km/h.

RESULTS AND DISCUSSION

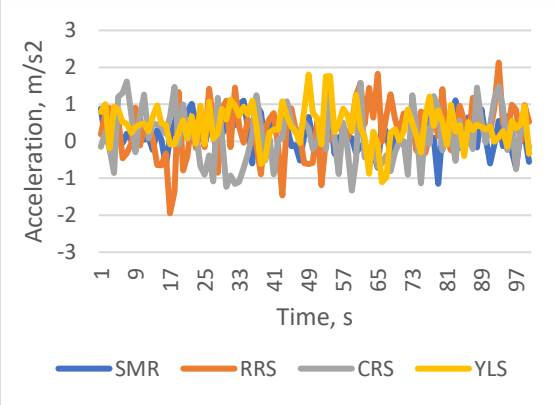

Figure1: Different road surfaces with speed 30km/h and 50km/h

Figure 1 shows the acceleration data collected when a driving car on different road surfaces. As seen in the figure, rough road surfaces have the highest peak acceleration value due to the small potholes and small stones on its surfaces. Since there are potholes, noise are created during collecting the data, this may cause discomfort to passenger too.

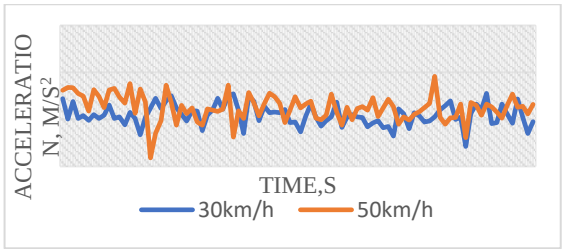

Figure 2: Smooth Road surface

Figure 2 shows that acceleration data collected on smooth road surface with speed 30km/h and 50km/h. Smooth road surface act as a based-line for others road surfaces. The passenger only feel fairly uncomfortable on smooth surface at certain time. However, the passenger feel not uncomfortable during the whole journey.

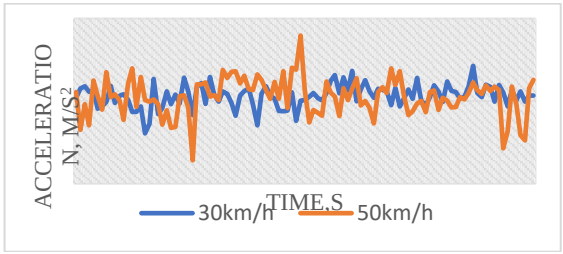

Figure 3: Rough road surface

Figure 3 shows the acceleration data form rough road surface with speed 30km/h and 50km/h. The acceleration data is varied with time. Big different in the values. The passenger is very uncomfortable when driving fast on a rough road surfaces. The administrators should always repair the rough road for the comfortability to all road users.

CONCLUSION

Design and development of low cost mobile data logger has been successfully carried out. The outdoor testing results have shown that the developed data logger could satisfactory perform the observation and data logging. The Arduino microcontroller and the 1Sheeld work properly with smartphone application.

REFERENCES

[1] Bernd, H. and Metin, E. (2011). Chassis Handbook: Fundamentals, Driving Dynamics, Components, Mechatronics, Perspectives. 1st Edition. Germany: Springer.

THE INFLUENCE OF ARRAY PARAMETERS ON PERFORMANCE OF OCEAN TIDAL TURBINE

Nurul Najihah Hussain and Omar Yaakob
School of Mechanical Engineering, Faculty of Engineering,
Universiti Teknologi Malaysia, 81310 UTM Skudai, Johor, Malaysia

INTRODUCTION

Ocean energy produces several types of energy such as tidal energy, tidal range, wave energy, ocean thermal energy and salinity gradient energy [1]. Tidal currents have many favourable characteristics that lend themselves to electricity generation. The installation of marine current turbine farm required large surface area. This cause by the fluid passing through a marine current turbine experiences a reduction in velocity across the rotor plane. Hence, the study on array spacing between the turbines is essential to make sure the turbine can generate maximum power output.

EXPERIMENTAL SETUP

Two vertical axis ocean tidal turbines are used to generate power output. The turbines are arranged in one row. The turbines in a rectangle channel and will be stimulated with the aim of evaluating the velocity inlet of the turbines. The simulation will be conducted at a fixed inlet speed of 0.56 m/s. The array arrangement of two turbines is simulated, where the lateral (Y) spacing with a diameter of the turbine. The number from one and two is the number of each turbine. This type of array spacing been used for two turbines. Six different simulations are made with six different lateral spacing. The spacing is expressed in multiples of turbine diameter. During the simulation, the turbines will rotate in clockwise direction.

RESULTS AND DISCUSSION

The array spacing is designed for two turbines only. It to observe the effect of both turbines. The described turbine spacing is modelled by using double stage Savonius turbine. The array spacing is made to investigate the power produced from tidal current of Malaysia Sea through the turbines. The different spacing between each turbine are taken into consideration to determine the best power output efficiency. The spacing been used in simulation are 0.336 meter, 0.672 meter, 0.84 meter, 1.008 meter, 1.344 meter and 1.68 meter.

Table 1 show the power efficiency for each turbine spacing. Spacing 3 has the highest power output efficiency which is 96.31%. Followed by spacing 2 and spacing 1 which are 92.43% and 76.28% respectively. Spacing 5 has 44.52% of power efficiency. The least power output efficiency is spacing 6, 20.76%.

The higher efficiency means the velocity entered the turbines is also high. Velocity that enter the turbine will determine the power output that generate by the turbine.

The result of the simulation that obtained may due to the interaction between the turbines. There are two types of interaction, positive and negative. The positive interaction will make the velocity of flow increased. High velocity make the turbines generate more power output. Meanwhile, the negative interaction will make the velocity flow decreased. The lower velocity that enter the turbine will make the turbine generate lower power output.

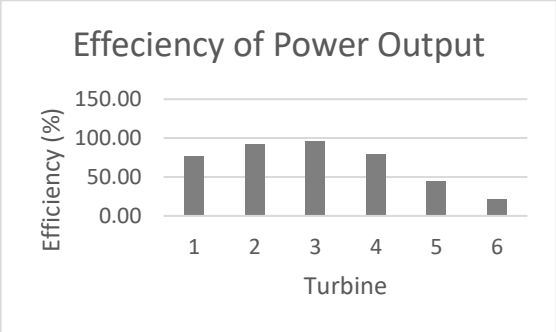

Figure 1: Efficiency of Power Output of the turbine spacing

Table 1: Value of efficiency of Power Output of the turbine spacing

Array	Efficiency of Power Output (%)
1	76.28
2	92.43
3	96.31
4	78.61
5	44.52
6	20.76

CONCLUSION

The results show the power output generated from six different spacing between two turbines. The highest power output comes from spacing 3. This may due to positive interaction that makes the velocity faster before entering the turbines.

REFERENCES

[1] Pelc R. and Fujita R. M. (2002) 'Renewable Energy from Ocean'. Journal of Marine Policy, 26(6), pp 471-479.

IMPROVEMENT OF UTM CANOE SPEED PERFORMANCE

Ratisafikaputri Zulkifli and Omar Yaakob
School of Mechanical Engineering, Faculty of Engineering,
Universiti Teknologi Malaysia, 81310 UTM Skudai, Johor, Malaysia

INTRODUCTION

From previous thesis [1], he had identified the best hull form design. Results show that the changing on prismatic coefficient plays a more important role in influence on resistance than changing length centre of buoyancy. After thesis completed, Mohd et al. [2] followed up by constructing the selected hull form from previous thesis and tested in towing tank. However, resistance result shows that the selected hull form does not reduce resistance of the basis hull. There is a need to improve hull resistance and its speed performance. Eric [3] and Koh [4] shared same method by reducing block coefficient to avoid excessive wave resistance. Another method by Eric [3] and Marsh [5], they stated fast ship requires longer length to beam ratio compared to slow ship to reduce wave resistance. Thus, more efficient speed performance.

EXPERIMENTAL SETUP

There are five stages of reverse ship hull modelling methodologies. First, basis hull form design is needed as a reference to compare with improved hull form design. Next, a parameter space of systematic series was created before do the hull modifications. The modification process has varied the block coefficient and length of waterline of the basis hull. Thirdly, all the modified hulls were analysed using Maxsurf Resistance. In fourth stage, the best modified hull will be selected. Several requirements needed to be verified for the selected hull form. After the selected hull was finalized, it had been analysed using Computational Fluid Dynamics (CFD) simulation. The purpose of resistance analysis using CFD is to determine the total resistance of a designed hull form at its designed speed.

RESULTS AND DISCUSSION

Figure 1 shows the power required for paddler at varying speeds. At the men category, paddler required 159.64 Watt of power to obtain speed 6.244 knots using actual canoe. By using the Hull G71, paddler only requires 140.12 Watt of power to maintain the same speed. It means the paddler required 12.23% less power to propel the canoe. On speed performance, to obtain speed at 6.224 knots, paddler required 159.64 Watt of power using actual canoe, meanwhile by using hull G71 with the same energy, paddler will propel the canoe at 6.44 knots.

In women category, paddler required 63.91 Watt of power to obtain speed 4.663 knots. By using Hull G71, paddler requires 60.14 Watt of power to maintain the same speed. It means the paddler required 5.9% less power to propel the canoe. On speed performance, to obtain speed at 4.66 knots, paddler required 63.21 Watt of power using actual canoe, meanwhile by using hull G71 with the same energy, paddler will propel the canoe at 4.80 knots. Hull G71 give advantages to the paddler in improving speed performance.

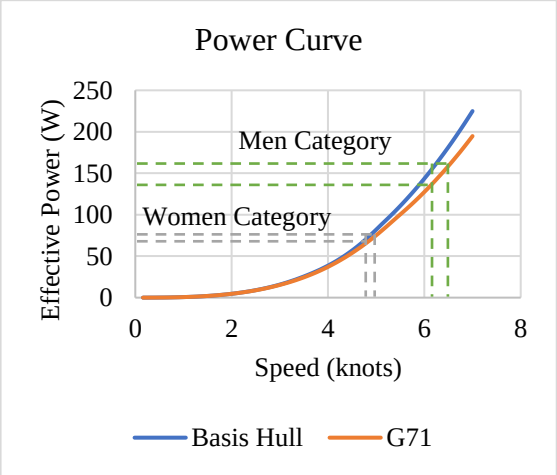

Figure 1: Power Curve for Basis Hull and Hull Form G71

CONCLUSION

The main objective to improve the speed performance of K1 category UTM canoe while maintaining within competition rules was achieved. Hull form G71 has improved the speed performance 3.5% for men category and 3% for women category.

REFERENCES

[1] Othman, M. R., (2007), Hydrodynamics Design of One Person Canoe, B. Sc. Thesis, Universiti Teknologi Malaysia, Johor Bahru, Malaysia
[2] Mohd, H. A., Nadzri, M., (2014), Canoe Resistance Comparison for 2008 versions and Maxsurf for F51 model, Report, Universiti Teknologi Malaysia, Johor Bahru, Malaysia
[3] Eric C., (2013), Resistance, Introduction to Naval Architecture, 131-160
[4] Koh K. K., (2013), Lecture Notes Ship Design I, Universiti Teknologi Malaysia, Johor Bahru, Malaysia
[5] Marsh M. B., (2013), Length-Beam Ratio, Retrieved from http://marine.marsh-design.com/content/length-beam-ratio, 4/2/2019, 11.15 pm

TECHNOECONOMICS ASSESMENT OF TIDAL ENERGY BARRAGE IN PENINSULAR MALAYSIA

Nurul Shafiqa Norsham and Omar Yaakob
School of Mechanical Engineering, Faculty of Engineering,
Universiti Teknologi Malaysia, 81310 UTM Skudai, Johor, Malaysia

INTRODUCTION

The vast area of Malaysia's coastline is a huge advantage making tidal range energy a reliable alternative energy source for the country. Hence, Malaysia has the potential to develop an ocean energy program such as tidal energy barrage.

From the previous research, the potential location to implement a tidal barrage is at Pulau Langkawi. The proposed design consists of a single basin, sluice gates and embankment. The tidal barrage also generates energy from a two-way generation method. By using the two-way generation method, an estimated Annual Output Power of 0.46Gwh was produced from the concept design.

EXPERIMENTAL SETUP

First and foremost, a new estimation was made on the annual power output of the tidal barrage. The calculation was made using the highest tidal rang in the year of 2017 from the previous study to produce the maximum annual power output. The annual power output is calculated theoretically with an average efficiency of 33%. Next, the selection of the turbine was done using a turbine selection graph by calculating the turbine discharge at first and the parameters of turbine is calculated also using such as the throat area of the turbine and the turbine diameter. The development of preliminary design of tidal energy plant is established on the basis of Saemangeum tidal power plant at Korea [1]. The dimensions of the powerhouse are achieved in conjunction with the specific site conditions and turbine parameters. Lastly, the technoeconomics assessment is done using Net Present Value (NPV) method. Based on the basis of Saemangeum tidal power plant at Korea, the investment cost is simplified to the construction cost of the tidal barrage. The NPV is calculated with a 40 years' lifetime expectancy, 10% discount rate and two turbine installation.

RESULTS AND DISCUSSION

The energy potential of the tide cycle calculated is a total of 192759.14 J with duration of 12 hours and 50 minutes. Annual energy output calculated using Equation 2.2 and Equation 2.3 at low efficiency is a total of 1.48 GWh/year. There is an increment in the value from the previous study which is an estimated amount of 0.46 GWh/year. This is due the highest tidal range is taken into consideration for the maximum estimated value.

The calculations in determining the dimensions and particulars are with the reference of the turbine discharge. Thus, an iteration of step height is used accordingly. The calculated diameter of the bulb-type turbine is 0.72 m with the rated power of 0.0051MW/turbine. The turbine discharge flow rate is 2.41 m^3/s. As for the sluice gate, it is designed with the width of 1.66 m, height of 1.80 m and discharge of 17.70 m/s

The powerhouse's dimensions are calculated with the combination of specification site realities and the dimensions of the selected bulb type. The total length of the barrage follows the width of the basin which is 310 m. The powerhouse's dimensions are shown in Figure 1.

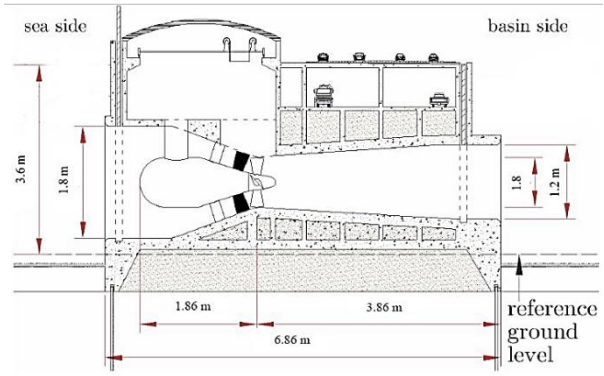

Figure 1 Dimension of Design Powerhouse

From an economical perspective, the project is feasible and profitable as the Net Present Value (NPV) is positive after the first three years.

CONCLUSION

The development of tidal energy barrage at Pulau Langkawi has the potential to be established to harness tidal energy and it is also profitable. Tidal energy barrage is a suitable alternative for generating electricity in selected sites in Malaysia.

REFERENCES

[1] Swane, H. (2007). Tidal power plant in Saemangeum (Master thesis, Delft University of Technology, Netherlands).uuid:2895d44d-aa15-40cf-a4b1-89d21478c51f.

SEMI-ACTIVE SUSPENSION SYSTEM FOR PASSENGER CAR

Muhammad Asyraf Mohamed Shaari and Pakharuddin Mohd Samin
School of Mechanical Engineering, Faculty of Engineering,
Universiti Teknologi Malaysia, 81310 UTM Sekudai, Johor, Malaysia

INTRODUCTION

Suspension system is a system between tires and car body in which to support the body weight, absorbs and dampens shock and helps maintain tire contact. The suspension system allow the relative motion between the tires and the car body (Ankita R. Bhise, 2016). Nowadays, the demand in better ride comfort and stability be a crucial required in every passenger car user and semi-active suspension is the solution. Half car model is used to analyse and evaluate the performance of suspension system by using MATLAB Simulink (S Abramov, 2009). This evaluation can be made analytically and the result is expected same with the real condition.

SIMULATION WORK

First of all, the passive suspension system will be developed by using MATLAB Simulink. Then, the results of the passive suspension system will be analysed and verified to confirm the car model. After that, the semi-active suspension will be developed by developing the controller for the ideal case. Next, the Magneto-rheological damper will be developed by using MATLAB Simulink. Semi-active suspension system can be developed by combining the car model, controller, voltage generator and magneto-rheological damper model. Finally, the results of the semi-active suspension system will analyse and compared with the passive suspension system to see which suspension system is better in order to serve a better ride comfort and stability. For the input, three road profile are used which are rolling effect, pitching effect and combination effect.

RESULTS AND DISCUSSION

The results that will be discussed are Passive Suspension System, Ideal Semi-active Skyhook, Magneto-rheological Damper and also Semi-active Suspension System with MR Damper. The results of the simulation are shown by using scope. Then, the results are exported to the MATLAB Workspace to plot a proper graph results. The passive suspension system model is successfully built by using MATLAB Simulink. The passive suspension model is differ from the semi-active suspension model because the passive suspension model only have a fix characteristic of damping coefficient. Due to that, the settling time for the suspension spring is longer than the semi-active suspension system. Based on the figure 1 the semi-active suspension is better than the passive suspension system. The body displacement is lower than the passive and the settling time is faster than the passive suspension system. This show that the semi-active suspension system is better than the passive suspension system. For the rolling angle, the first road profile result do not involve the rolling rate, therefore the rolling angle is not available for this road condition.

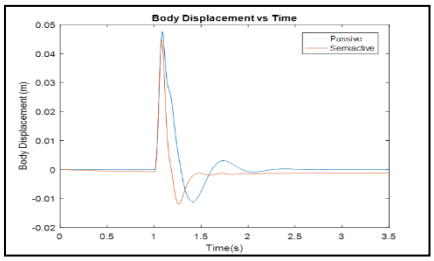

Figure 1: Body Displacement vs Time Passive and Semi-active.

Table 8 The RMS value for improvement.

	Passive	Semiactive	Improvement%
Body Displacement	0.007879	0.006116	22.38
Roll Angle	0	0	0
Body Acceleration	4.753	5.259	-10.65
Tire Displacement	0.01126	0.01122	0.355

CONCLUSION

The semi-active suspension system offer a better ride comfort, road handling and stability than the passive suspension system based on the results of passive suspension model and semi-active suspension model that have developed by using MATLAB Simulink. Body displacement, settling time, body acceleration and roll angle improved.

THE INVESTIGATION OF SHRINKAGE, WELD LINE AND SINK MARK OF INJECTION MOULDING PRODUCT AND PREVENTION

Siti Nur Aisyah Chik and Rozaimi Mohd Saad
School of Mechanical Engineering, Faculty of Engineering,
Universiti Teknologi Malaysia, 81310 UTM Skudai, Johor, Malaysia

INTRODUCTION

Injection Moulding is a manufacturing process where the molten will be injected into different type of mould. In manufacturing the simulation is use to indicate the defects exist and this software will helps to eliminate or minimize the effect before real production start to produce the product. This will help in saving waste of the material and become more efficient [1].

METHODOLOGY

This project is being conduct in steps that involve variety software. For the design, software use is the Unigraphics NX8.0. While for the analysis the software involve is MoldFlow to run the simulation and Minitab is use for the data interpretation. The method use is DOE approach. The selected plastic product is the speaker cover. The material use will be Acrylonitrile-butadiene-styrene, (ABS) and 10% Recycle-Acrylonitrile-butadiene-styrene,
(R-ABS)

RESULTS AND DISCUSSION

The results of the simulation test were taken from MoldFlow software. The results of each response then are combining together as overall evaluation criteria (OEC). There will be two (2) OEC data which is from ABS and also 10% R-ABS.

To observe the defect of shrinkage, sink mark and weld line when using different type of materials between ABS and R-ABS. From figure 1 and 2 shows the significant parameter, the significant parameter is the bar that past through the t-limit. The t-limit from the graph ABS is 0.1160 and 10% R-ABS is 0.1238. The significant parameter for both material was A, melt temperature.

From the ANOVA table, the p –value of each response that less than 0.05 shows that the response is significant. But the interaction parameter also need be analyze carefully because the slightly change of value will interact the other parameter. Because each of the parameter is mostly have interaction between each other [2].

The individual analysis is to find out the effect of the parameter to each parameter respectively. For individual analysis, the steps to analyze them are similar with OEC analysis. The only different is the quality characteristic which is depends on the response itself which mean the smaller is better for this analysis. The percentage of error for this analysis must be less than 5%.

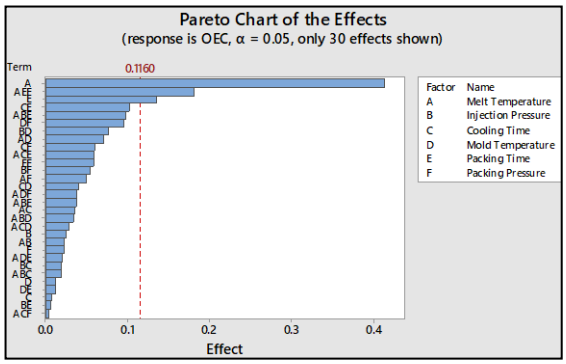

Figure 1: The Pareto chart for ABS

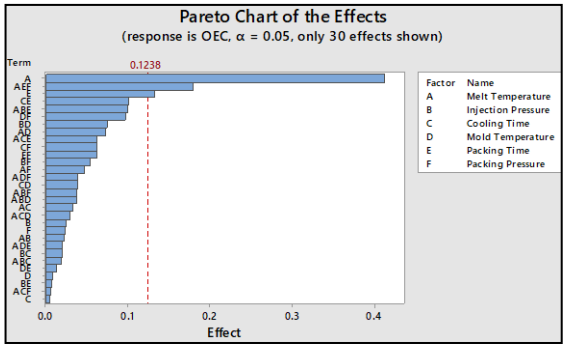

Figure 2: The Pareto chart for 10% R-ABS

CONCLUSION

In this project, the injection moulding characteristics for optimal speaker cover were successfully being simulated using MoldFlow software. The defects investigate which is shrinkage, sink marks and also weld line are improve using the parameter selected which are melt temperature, injection pressure, cooling time, mould temperature, packing time and packing pressure. The optimum parameters for both materials are also determined using DOE approach.

REFERENCES

[1] The Cycles of the Injection Moulding Process. (2015, February 17). Retrieved from http://www.automaticplastics.com/the-cycles-of-the-injection-moulding-process/

[2] Masthead. (1963). The Journal of Organic Chemistry, 28(3). doi:10.1021/jo01038a700

INTERVENTION PROGRAM OF SAFETY AND HEALTH IN A KINDERGARTEN

Izzaidah Amin@Muhali and Rozlina Md Sirat
School of Mechanical Engineering, Faculty of Engineering,
Universiti Teknologi Malaysia, 81310 UTM Skudai, Johor, Malaysia.

INTRODUCTION

Keeping children of 4years to 6years ages safe and healthy is one of the most important tasks of child care providers. Whether children are in center- or home-based care, providers are responsible for ensuring safety both inside and outside their child care setting. Health and safety are major concerns for child care providers when transporting children. They should be prepared to prevent injuries and illnesses to handle emergencies. As a child care provider, you know that unintentional injuries will happen from time to time. The best way to handle an unintentional injury is to be prepared before it happens. When you know how to respond in an emergency, and have the supplies you need, you are confident and can respond in a timely manner. The objective of this undergraduate project is to identify safety and health issues (macro and micro) in a kindergarten and to develop an intervention program for safety and health in a kindergarten.

EXPERIMENTAL SETUP

The study starts with literature review. Some analysis tool that has been used for the work study was identified. Interview has been done with teachers, students and parents to get the specific information and identify the safety and health management problems. Direct observations and discussions with teachers and students were made on complete process flow to identify the lack of safety issues here. Data was analysed using layout flow chart, and process flow chart and previous study. The safety and health problems were analysed using Pareto and HIRARC. Suggestion on improvement of management on safety issues with engineering analysis has been done.

RESULTS AND DISCUSSION

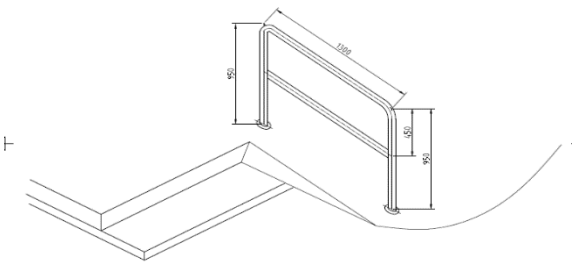

Figure 1: Engineering Control: To suggest a handrail to fix at uneven stairs

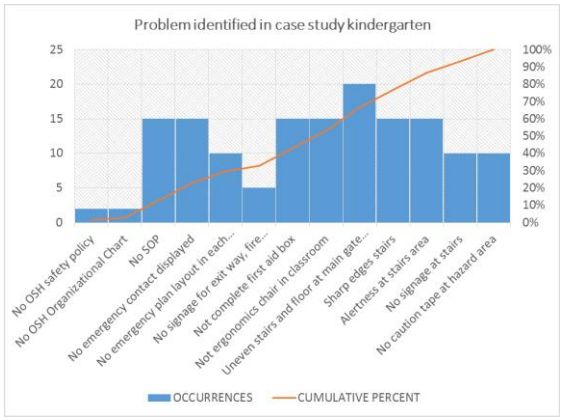

Figure 2: Pareto chart problem identification in case study kindergarden

CONCLUSION

All the objectives have been achieved:

- Hazards have been identified in macro and micro ergonomics.
- Control measures have been suggested from engineering design and administrative control.

REFERENCES

[1] (DOSH), D. O. O. S. A. H. M. (2008) Guidelines for hazard identification, risk assessment and risk control (HIRARC). In: MALAYSIA, D. O. O. S. A. H. (ed.). Kuala Lumpur: Department of Occupational Safety and Health, Ministry of Human Resources, Malaysia.

WORK STATION DESIGN FOR TYRE LINER SANDING DEPARTMENT: ERGONOMIC SOLUTION

Mohd Farezuan Muhamad Fadli and Rozlina Md. Sirat
School of Mechanical Engineering, Faculty of Engineering,
Universiti Teknologi Malaysia, 81310 UTM Skudai, Johor, Malaysia.

INTRODUCTION

The purpose for this project is to identify the ergonomic hazard at the rubber company and suggest an improvement in order to reduce the ergonomic hazard. HIRARC and Pareto chart were used to determine the process in the production that has high risk. There are 5 departments in the production line such as mixing, extruded, molding, splicing and sanding. 3 processes were selected from the HIRARC results that have high score for the risk level. The initial ergonomic risk assessment (ERA) was used to determine the ergonomic hazard in the 3 process that selected from the HIRARC analysis. Process of transferring the liner from the pallets to the table conveyor has high risk with high score. Next the advance ERA used to determine the suitable method for the selected hazard. An assessment repetitive task (ART) was used to determine the risk level in the repetitive motion factor while Manual Handling Assessment Chart (MAC) was used to determine the risk level in the forceful exertion factor. Both methods show the high level of risk. The morphological chart was constructed in order to get some idea to create some design that help to reduce the ergonomic hazard at the selected process.3 conceptual design was sketched and have been evaluate using concept matrix selection. Adjustable platform was selected as a final design. Existing conveyor assisted with the proposed adjustable platform were suggested. The solid work was used to design and make the simulation on the final design. The engineering analysis was conducted on the adjustable platform in order to identify the safety condition when applied the force. The result of the initial ERA, ART and MAC after using the adjustable platforms shows the improvement compare to the result on the existing activity. This show the adjustable platform was helped to reduce the ergonomic hazard.

PROJECT OBJECTIVES

The aim of study are to identify the ergonomic hazard and suggest some engineering control based on the problem identified.

METHODOLOGIES

The data collected by interview with the SHO and oberservation in the production line in order to identify the ergonomic hazard and come out with the design improvement. Solidwork was used to perform the engineering analysis and validate the design

RESULT AND ACHIEVEMENT

Proses of the transferring the liner from the pallet to the conveyor table was identified as a high risk process based on the HIRARC, initial ERA, MAC and ART. The adjustable design was purpose in order to reduce the risk of ergonomic.

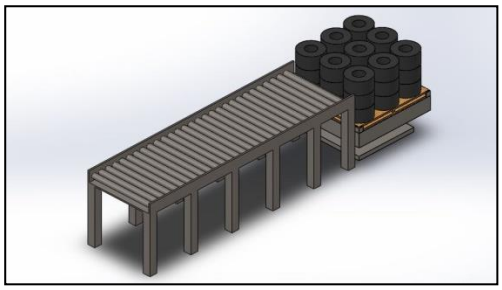

Figure 1: adjustable platform with existing conveyor

Figure 1 show the adjustable platform that abended with the exisitng conveyor. The workers only need to adjust the suitable level of the platfrom and transfer the liner to the convayer

Table 1: the result of the Advance ERA after improvement

METHOD	SCORE	DISCRIPTION	PERCENTAGE OF IMPROVEMENT
ASSESSMENT REPETITIVE TASKS			
• LEFT HAND	9	LOW RISK	62.5%
• RIGHT HAND	9	LOW RISK	62.5%
MANUAL HANDLING ASSESSMENT			
• LIFTING OPERATION	3	GREEN COLOUR(LOW RISK)	84.21%
• CARRYING OPERATION	3	GREEN COLOUR(LOW RISK)	81.25%

Besed on the table 1, assessment repetetive task (ART) and Manual Handling Assesmet Chart (MAC) were used to identify the risk level for forceful exertion and repetetive motion factor respectively. Both method show the result more that 50 percent of improvement when using the adjustable platform.

REFERENCES

[1] DOSH. (2017). Guideline for Ergonomic Risk Assessment (ERA).

[2] Boenzi, F, Digiesi, S, Fachini, F and Mummolo, G. (2016). Ergonomic Improvement Through Job Rotation in Repetitive Manual Task in Case of Limited Specification and Differentiate Ergonomic Requirement. *IFAC Paper Online*, 49-12.

WORK STATION DESIGN FOR BOX ARRANGEMENT ON PALLET IN PACKAGING DEPARTMENT: ERGONOMICS SOLUTION

Mohamad Mustaqim Rusdi and Rozlina Md Sirat

School of Mechanical Engineering, Faculty of Engineering,
Universiti Teknologi Malaysia, 81310 UTM Skudai, Johor, Malaysia

INTRODUCTION

Ergonomics is defined as a science of interactions between man and technologies which has the aim to make compatible tasks, equipment, environments and systems with the needs, abilities and limitations of people. Therefore, the optimizing of this interaction can create the best working conditions and increasing work efficiency [1][2]. The ergonomics study is done at a tile manufacturing company. This company is located at Pasir Gudang, Johor. It focuses on the departments of QA inspection, Warehouse and Packaging. However, Firing department that have critical issues been selected to be suggested for control measure. The improvement is based on conceptual design assisted with functional model without real implementation.

CASE STUDY AND PROBLEM ANALYSIS

Three departments were chosen which QA inspection, Warehouse and Firing. The problem were analysed by using initial ERA from the Guidelines on Ergonomic risk assessment at Work Place (DOSH, 2017). After going through all the elements in the factors of ergonomic, the summary score of initial ERA were obtained as shown in the Table 1.

Table 9: Summary score of initial ERA from 3 department

Risk factor	Number of checklists	Limitation	QA inspection	Firing	Warehouse
Awkward posture	13	≥ 6	0	6	5
Static and sustained work posture	3	≥ 1	1	2	0
Forceful exertion	7	1	2	4	4
Repetitive motion	5	≥ 1	0	3	2
Vibration	4	≥ 1	0	0	0
Lighting	1	1	0	0	0
Temperature	1	1	0	0	0
Ventilation	1	1	0	0	0
Noise	2	1	0	0	0
Total Factors exceed limits			2	4	2

According to Table 1, firing department shows the highest number of factors that exceed the maximum value. This department were exposed with awkward posture, static and sustained work posture, forceful exertion and repetitive motion. Then, advanced ERA is conducted in this department for further investigation. Table 2 shows the advanced ERA using REBA, NIOSH lifting and ART tool. The score proved that the firing workstation has high risk for awkward posture, forceful exertion and repetitive motion.

Table 2: Advanced ERA tools

No.	Risk factors	Advanced tools	Result	Benchmark
1	Awkward posture	Rapid Entire Body Assessment (REBA)	11	Very high risk
2	Forceful exertion	NIOSH Lifting	3.00	Intervention should be done
3	Repetitive motion	Assessment of Repetitive Tasks (ART)	31	High risk

As a control measure, the engineering design should be done in this department.

PROPOSED DESIGN AND DISCUSSION

Current job is the worker need to lifting the boxes from existing conveyor to the pallet. Improvement is done by redesigning the workstation. Pallet will be located just beside the conveyor. Then it will be assisted by a new machine called Box Arrangement Machine. The machine consists of ball table conveyor (to assist in arranging the box easily with the pattern required), hydraulic lift table (to higher and lower the level of box layer according to level on the pallet) and fixed bar (to assist in holding the boxes and control the arrangement on the pallet).Figure 1 show the full layout of the proposed design.

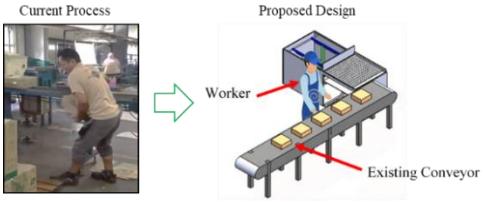

Figure 1: Layout of proposed design

CONCLUSION

The ergonomics hazards have been identified in a tile manufacturing company. Initial ERA from the Guideline provided by DOSH have been used. Advanced ERA such as REBA, NIOSH lifting and ART were used to further detail the ergonomics problem. A new arrangement of workstation assisted by a Box Arrangement Machine have been proposed. Based on the assumption using advanced ERA tools, the new workstation has successfully reduced the ergonomics issues of awkward posture 90%, forceful exertion for 98% and repetitive motion 71%.

REFERENCES

[1] J.R. Wilson. (2000). Fundamentals of ergonomics in theory and practice. Applied Ergonomics. United Kingdom

[2] Sirat, R. M., Rohani, J. M., Ahmad, N., Shaharoun, A. M and Haroun, H. (2018). 'Education level, working experience and training effect on ergonomic awareness and practices in Malaysia',International Journal Of Engineering And Technology(UAE), 7(3), pp.12-17

WORK STATION DESIGN FOR MANUAL HANDLING AT A BALL MILLING PROCESS: ERGONOMIC SOLUTION

Solehuddin Salam and Rozlina Md. Sirat
School of Mechanical Engineering, Faculty of Engineering,
Universiti Teknologi Malaysia, 81310 UTM Skudai, Johor, Malaysia.

INTRODUCTION

Over recent years, there has been an explosive case study is done at a ball milling department at a tile manufacturing company. Ergonomic hazards are identified and engineering design was proposed. Pareto Analysis is used to identify the critical process. Ball milling department was selected and Ergonomic Risk Assessment (ERA) including REBA, ART and Lifting NIOSH were used to analyse existing activities. Engineering analysis was done to the proposed design. It was going through evaluation matrix of conceptual design. A system that integrating conveyor, cutter and chute were proposed. Improvements based on engineering analysis such as static analysis was done using SolidWorks. Validation of final design was done by the Safety and Health Officer from the company. REBA analysis shows that the score before improvement was 12 while after improvement was suggested, the score was 5. For ART, before improvement, the penalty score was 21.75 while after the suggestion, the score was 8.25. For Lifting NIOSH analysis, before improvement, the origin and end lifting index were 3.91 and 2.19. After suggestion, the lifting index were 3.06 and 1.89

PROJECT OBJECTIVES

The aim of study are to identify ergonomic hazards in a ball milling production at a tile manufacturing company and to suggest a work station design that reducing ergonomics hazards at least 10%.

METHODOLOGIES

Study starts with literature review. Some analysis tool that has been used for the work study was identified. Interview has been done with Safety and Health of the company and the workers to get the specific information and identify the ergonomic problems. Direct observations and discussions with workers were made on complete process flow to identify the critical hazard. Data was analyzed using layout flow chart, and process flow chart and previous study. The ergonomic problems were analyzed using Pareto, Ergonomic Risk Assessment, REBA, ART and Lifting Niosh. Improvement of workstation design with engineering analysis has been done including functional analysis, design concept, and morphological chart. The final design has been selected by evaluation matrix and is validated by SolidWork and discuss with SHO. From the final design, ergonomic analysis has been done by using REBA, ART and NIOSH Lifting analysis.

RESULT AND ACHIEVEMENT

After all the analysis and problem identification, the major problem is at ball milling production. There is no design of the workstation, which leads to ergonomic problem. Worker need to lift manually 15 bags of 25 kg of raw materials from the pallete to the manhole one by one (distance 3m) and he need to bend down his body in order to cut the bag and pour them into the manhole. Worker has to repeat this activity for about 15 times for one ball milling station. Study on the existing method shown opportunities for improvement.

Figure 1 Ball milling workstation

Figure 1 shows the new workstation design that will used to move the bag from the pallet to the manhole by using slat conveyor and roller. It also equipped with a cutter system to open up the bag in order to reduce bending posture. The worker just need to pull the bags from the pallet to the salet conveyor and it will move automatically to the roller.

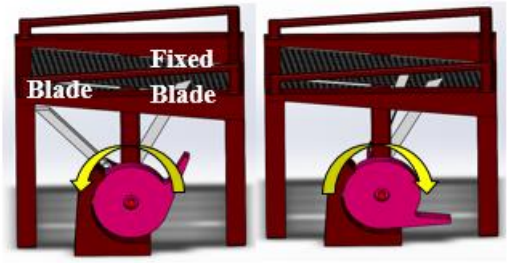

Figure 1 Sanding Tool

Figure 2 shows the cutter system equipped in the workstation design. The paddle at the cutter is used to move the blade. The spring at the paddle allows the balde to back to the original position. Other than that, it would be easier for the worker to cut the bag compared to existing method used.

REFERENCE

[1] Baba Md Deros, Dian Darina Indah Daruis, Ishak Mohamed Basir. (2015). A Study on Ergonomic Awareness among Workers Performing Manual Material Handling Activities. Procedia Social and Behavioral Science, 1666-1673

DEVELOPMENT OF AN ONBOARD AND WIRELESS DATA TELEMETRY SYSTEMS FOR ELECTRIC VEHICLE

Kamalraj Sundralingam and Saiful Anuar Abu Bakar
School of Mechanical Engineering, Faculty of Engineering,
Universiti Teknologi Malaysia, 81310 UTM Skudai, Johor, Malaysia.

INTRODUCTION

Electric vehicle (EV) is a vehicle that uses electric motor(s) to provide rotating forces to the wheels to move the vehicle. It mainly uses battery to power up and does not produce tailpipe emissions. A data telemetry system is a data monitoring and acquisition system that records and transmits data from one location to another through wire, wireless or combination of both methods. As the usage of remote control (RC) cars becomes more prominent in various fields, it is important for these cars to have a telemetry system for monitoring purposes. This research focuses on a telemetry system for an RC car that can record and transmit data for real time data monitoring and acquisition. The objective of this research is to design and develop an onboard data monitoring & acquisition system for electric vehicle and to design and develop a wireless data telemetry system for electric vehicle.

METHODOLOGY

The data telemetry system is made up of two subsystems; onboard and wireless systems. The development of both subsystems starts with hardware selection followed by hardware integration and RC car integration. The hardware used are Arduino Uno, MPU6050 IMU Sensor, MAX471 Voltage Sensor, HC-12 Serial Communication Module (RF 433Mhz), LCD Display Shield and Memory Card Shield. All of the hardware are integrated together using Arduino IDE software. The onboard system is fitted to the RC car and is powered by a 9V battery. As the RC car is driven around the area of study, it will record data and transmit it to the wireless system stationed at a fixed location. The wireless system is connected to a laptop for real-time data monitoring.

RESULTS AND DISCUSSION

Figure 1 shows the circuit diagram of the onboard system and the arrangement of hardware on the RC which will collect data, save it in an SD card and transmit it to the wireless system. Figure 2 shows the circuit diagram of the wireless system and the hardware of the wireless system which will receive data from the onboard system. Table 1 shows comparison of the CRMS values of the data collected from both the systems. The CRMS values are calculated using MATLAB-Simulink. The percentage of error indicates the difference between the data from both the systems. A zero percent error means that there is no difference in the data. This shows that there is no data loss between the systems during data transmission.

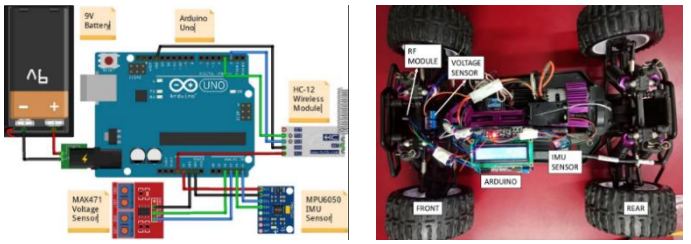

Figure 1: System layout and hardware of onboard system

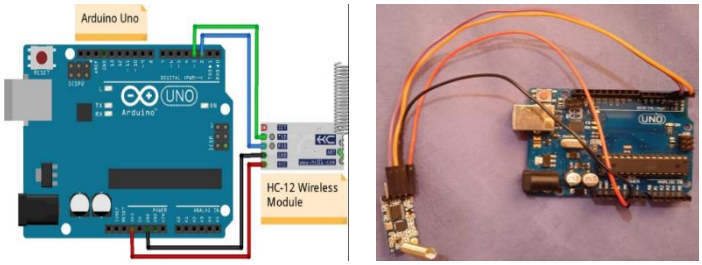

Figure 2: System layout and hardware of wireless system

Table 1: Comparison of CRMS Values of Both Systems

Parameters Recorded	Onboard	Wireless	Error (%)
Longitudinal Acceleration (A_x)	0.7802	0.7802	0
Lateral Acceleration (A_y)	0.8333	0.8333	0
Voltage	7.831	7.831	0

REFERENCES

[1] Hay, M. & Nebel, S. (2012). The Use of Biotelemetry in the Study of Animal Migration. Nature Education Knowledge 3(12):5

[2] Onler, E., Celen, S., Moralar, A., & Celen, I. (2016). Development of telemetry system for electric powered vehicle. International Journal of Current Research 8(09) 38715-38719

LONGITUDINAL STATIC STABILITY OF SME-MD3 LIGHT AIRCRAFT UNDER DUAL EXTERNAL STORES

Mohd Aniq Akmal Maludin and Shabudin Mat
School of Mechanical Engineering, Faculty of Engineering,
Universiti Teknologi Malaysia, 81310 UTM Skudai, Johor, Malaysia

INTRODUCTION

Due to its light, quiet, small, cheap characteristics, many light aircraft converted into light attack aircraft for Close-Air Support (CAS) mission in war. Such aircraft usually designed to have external stores mounted below its wing. Previous study by Mithcam [1], Yeakly [2], and Lazim [3] was done on fighter aircraft discovered that the installation of external stores increased drag coefficient, reduced lift coefficient, aircraft static stability in longitudinal and directional mode. Manaf [4] did a study to the same light aircraft model used in this paper and found the same results. Hence, this paper interested to study the effect of installing dual external store in series to SME-MD3 aerodynamic characteristics.

EXPERIMENTAL SETUP

SME-MD3 aircraft model is a 15% scaled down model which was fabricated based on MD3-160 AeroTiga. Three sets of experiment were done in UTM-LST at 30 m/s, namely clean wing, single store, and dual stores configuration. Two measurement techniques were utilised namely using steady external balance to obtain six components of forces and moments and surface pressure distribution along wing airfoil.

RESULTS AND DISCUSSION

According to Figure 1(a), lift curve, and maximum lift coefficient decreased with dual stores installed. It is due to pressure increased on the upper surface of the wing which generates significantly low lift force compared to clean wing and single store configuration.

Drag coefficient shown in Figure 1(b), increased at low angle of attack because of parasite drag also increased corresponding to addition of aircraft planform and surface area. As it pitches even higher drag coefficient was reduced. This is due to the flow is still attached due to Coanda effect occurred in between of external store and wing leading edge.

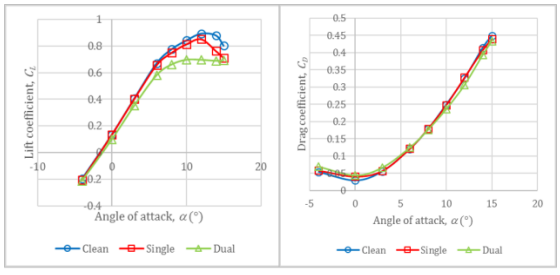

(a) (b)

Figure 2: (a) Lift coefficient against angle of attack, (b) Drag coefficient against angle of attack

Graph depicted in Figure 2 shows that the longitudinal static stability of the aircraft reduced due to the magnitude of pitching moment coefficient for dual external stores configuration is greater compared to the other configurations.

Figure 3: Pitching moment coefficient against angle of attack

CONCLUSON

Installation of dual external stores reduced lift coefficient while increases drag coefficient at low angle of attack. At higher angle of attack, with dual stores installed, drag decreased and flow separation was delayed. Furthermore, the longitudinal static stability of the aircraft decreased, and trim angle of attack shifted up.

REFERENCES

[1] Mitcham, G. L., Blanchard, W. S., Jr., & Hastings, E. C., Jr. (1952). Summary of Low-Lift Drag and Directional Stability Data from Rocket Models of the Douglas XF4D-1 Airplane with and without External Stores and Rocket Packets at Mach Numbers from 0.8 to 1.38. *NACA Research Memorandum*. Langley Field, VA: Langley Aeronautical Laboratory.

[2] Yeakley, P. L. (1979). Evaluation of Aerodynamic Characteristics of a 1/20-Scale A-10 Model at Mach Numbers from 0.30 to 0.75. Coffee, TN: Arnold Engineering Development Center, Arnold Air Force Station.

[3] Lazim, T. M., Mat, S., & Saint, H. Y. (2003). Computational Fluid Dynamic Simulation (CFD) and Experimental Study on Wing-external Store Aerodynamic Interference of a Subsonic Fighter Aircraft. *Acta Polytechnica*, 43(5), 60-65.

[4] Manaf, M. Z. A., Mat, S., Mansor, S., Nasir, M. N. M., Lazim, T. M., Ali, W. K. W. and Othman, N. (2018). Wind Tunnel Experiment of UTM-LST Generic Light Aircraft Model with External Store. *International Review of Mechanical Engineering (I.RE.M.E.)*, 12(3), 263-271.

EXPERIMENTAL INVESTIGATION OF SME MD3-160 LIGHT AIRCRAFT MODEL WITH DUAL EXTERNAL STORES

Soh Khai Yuet and Shabudin Mat
School of Mechanical Engineering, Faculty of Engineering,
Universiti Teknologi Malaysia, 81310 UTM Skudai, Johor, Malaysia

INTRODUCTION

Light aircraft is defined as aircraft with maximum take-off less than 12500lbs or 5670kg whereas external stores are comprised of fuel tank, missiles, bombs and camera that installed externally on the aircraft [1]. Due to the lightweight characteristic of the aircraft and high performance in combat mission results to high interest in converting the light aircraft to combat aircraft. However, when the external stores are mounted underneath the wing, it may affect the performance of the aircraft such as changes in the aerodynamic characteristics and promote flow separation [2].

EXPERIMENTAL SETUP

The experiment is conducted in UTM Low Speed Wind Tunnel (UTM-LST) with model tested of SME MD3-160 light aircraft model. The objective of the project is to investigate the effect of dual external stores installed in the light aircraft model. Thus, the model is tested with three configurations of clean wing, single external store and dual external stores. Two methods are applied to obtain the aerodynamic characteristics and the pressure distribution which are UTM-LST external force balance measurement and surface pressure measurement.

The aircraft model is tested at 30m/s corresponds to Reynolds Number 0.463×10^6, angle of attack, α ranges from -4° to 15° and yaw angle from -10°to 10°

RESULTS AND DISCUSSION

In the calculation of aerodynamic characteristics and pressure coefficient, the equations used are based on Anderson [3] and the blockage correction such as solid and wake blockage are considered to increase the accuracy of the results based on Rae [4]. Figures show below indicate the result to compare the effect of store at different yaw angles and three configurations as stated above.

The installation of external stores has reduced the lift at 13% and increased the drag of the aircraft at 1.2% as shown in Figure 1. This may due to the increase of frontal area on the aircraft model and the addition of wake generates by the external stores to initial wake of wing to create bigger wake behind the aircraft.

The longitudinal stability of aircraft shows reduction and increased in trim angle when external stores are installed as shown in Figure 2. However, the configurations of single external store and dual external stores are considerably small at a percentage of 0.5% compare to clean wing configuration of 6%. It can be said that the effect in adding another external store on the model does not affect much in stability of the aircraft. Overall, the aircraft is said to be longitudinally stable as negative slope is obtained

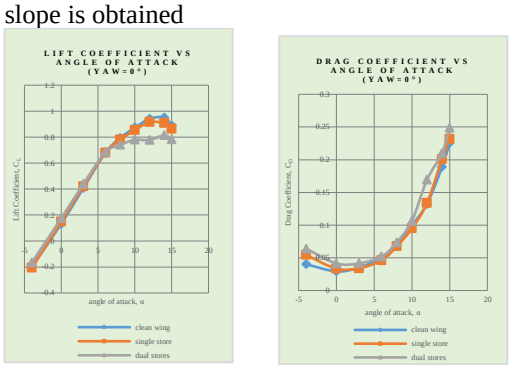

Figure 1: C_L vs α and C_D vs α

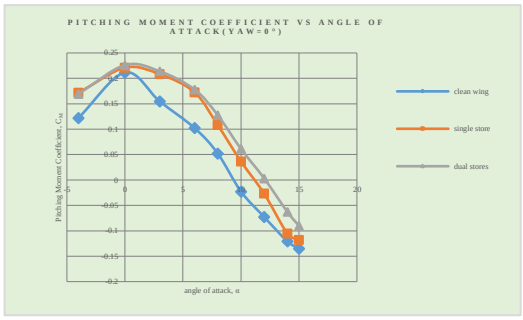

Figure 2: C_M vs α.

CONCLUSION

The experiment shows that installation of dual external stores has reduced lift increased in drag. Longitudinal stability is also reduced with an increased of trim angle. But it is said to be stable as negative slope is obtained.

REFERENCES

[1]. Turner, C., *Effect of store aerodynamics on wing/store flutter*. Journal of Aircraft, 1982. **19**(7): p. 574-580.

[2] Marsden, P. and A. Haines, *Aerodynamic loads on external stores: A review of experimental data and method of prediction*. 1967: Citeseer.

[3] Anderson Jr, J.D., *Fundamentals of aerodynamics*. 2010: Tata McGraw-Hill Education.

[4] Rae, W.H. and A. Pope, *Low-speed wind tunnel testing*. 1984: John Wiley.

EXPERIMENTAL FLOW VISUALIZATION STUDIES ON UTM BLENDED WING BODY

Farrith Firdaus Izzamil Adnan and Shabudin Mat
School of Mechanical Engineering, Faculty of Engineering,
Universiti Teknologi Malaysia, 81310 UTM Skudai, Johor, Malaysia

INTRODUCTION

The Blended Wing Body (BWB) configuration is a new design concept in aircraft design in which provide greater volume, aerodynamic and structural efficiency and significantly improved on travel cost-per-seat [1]. The approach design of BWB is to maximize the overall performance and efficiency by integrating fuselage and wing into single lifting body. BWB is a unique tailless single entity where the fuselages merged with wing and tail. Salazar [2] studies that BWB has flattened and airfoil-shape body which contributes higher lift than conventional ones. This paper will focus on experimental flow visualization studies on UTM-BWB model. The aerodynamic characteristic such lift coefficient, drag coefficient, pitching and yawing moment coefficient are obtained and compared. In addition, tuft visualization on the surface of BWB is performed in the wind tunnel to observe the flow pattern at various angle of attack and sideslips angle.

EXPERIMENTAL SETUP

The test was run at single airspeed of 25 m/s and the corresponding to the Reynold number of 0.666×10^6 based on mean aerodynamic chord length of 423.4 mm. The angles of attack, α varied from, α = -3° to 15° with the orientation of sideslip angle, β =-8°, -4°, 0°, 4°and 8° for steady balance measurement and tuft visualization. The main objective of the experiment was to analyze the flow properties on the model surface through aerodynamic characteristic obtained from steady balance and tuft data. Steady balance measurement[3] is used to obtained six-degree of freedom, forces and moments which then be convert to obtained aerodynamic properties. The data will be plotted and observed the flow characteristic. Flow tuft visualization technique[4] used to show the instantaneous flow pattern formed by the tufts stuck on to the BWB model surface.

RESULTS AND DISCUSSION

Figure 1: flow visualization at high region

In Fig. 1, at high angle of Attack, α = 15°, it can be seen that the vortex breakdown occurs on the upper surface of the BWB. Vortex breakdown is a phenomenon due to abruption and the drastic change of vortex generation in at the high angle of attack region. The flow fully separated on the outer wing. The vortex breakdown in this case occur on the merging side of fuselage and outer wing which is shown in Figure 4.8. The thread on a particular area seem to tangled and tie up due to roll-up vortex that suddenly happen after changing to high angle of attack. The major factor that contributing the vortex breakdown are the shape of BWB model itself and high angle of attack when conducting the experiment. The vortex development and breakdown pattern for both left and right side are symmetrical. [5]

CONCLUSION

The results presented in this paper showed that the steady streamline flow does not separate at low region. As the angle of attack increase, the flow started to separate. The size of spiral- vortex expand in chordwise as well as spanwise direction to the downstream on the model surface. Approaching high angle of attack region, the vortex phenomenon occurs before it reached maximum angle of attack of 15°. The vortex generation affect the aerodynamic properties.

REFERENCES

[1] P. Mahamuni, A. Kulkarni, and Y. Parikh. Aerodynamic Study of Blended Wing Body. Vol. 9, pp. 29247-29255, 2014.

[2] O. V. Salazar, J. Weiss, and F. Morency. Development Of Blended Wing Body Aircraft Design. 2015.

[3] S. Mansor. Low Speed Wind Tunnel Universit Teknologi Malaysia. [Online].

[4] W. Shen and A. Pang. Tuft Flow Visualization. ed. University of California, Santa Cruz, 2001.

[5] L. Z. Yong and Z. L. Guo. Study on Forms of Vortex Breakdown over Delta Wing. Chinese Journal of Aeronautics, vol. 17, 2004.

ARCHITECTURE IMPROVEMENT OF ELECTRONIC BRAILLE AL-QURAN BASED ON SINGLE-BOARD COMPUTER

Ahmad Syahrin bin Shahriman and Shaharil Mad Saad
School of Mechanical Engineering, Faculty of Engineering,
Universiti Teknologi Malaysia, 81310 UTM Skudai, Johor, Malaysia

INTRODUCTION

eBraille Al-Quran is a project aimed to aid the visually impaired and blind Muslims in their journey of reading the Al-Quran. Although the eBraille Al-Quran provides ease of access for the blind people to recite the Holy Quran [1], it can be further improved with Single-Board Computer (SBC). SBC is a complete functioning computer built on a single circuit board excellent for simple computing purposes. Raspberry Pi 3B+ is the chosen SBC for this project that aims to propose an improved architecture that can implement the same functionalities with added features and benefits.

EXPERIMENTAL SETUP

The methodology of the project comes out as a step by step process. First, the main issue of the eBraille Al-Quran is identified. Constructing a new architecture of the eBraille Al-Quran does not mean a complete overhaul of the existing one hence the existing features of eBraille Al-Quran is identified. Next comes the designing phase of the new architecture using Raspberry Pi 3B+ based on the existing functionalities identified. A prototype circuit is then designed and fabricated for testing of functionalities, start-up time, OS corruption and battery consumption.

RESULTS AND DISCUSSION

A program made out from Python language is developed which tested out the functionalities proposed. Input keys which serves as navigational keys were tested and they function as intended. Execution of the program allows for reading and selection of *surah*, *ayah*, and verses of the Holy Quran using the navigational keys. Output of braille cells can be read, and audio cue is heard for each verse. An additional feature of Virtual Network Computing (VNC) allows for ease of access and updating, which the eBraille Al-Quran needs. The startup-time and OS corruption are also tested which concludes that the proposed architecture starts 1 second slower but is acceptable while OS condition is fine throughout. Result of battery consumption test shows an improvement by 1.2% as shown in table below.

Table 1: Battery consumption test

Test	eBraille	Raspberry
1	8.11%	6.04%
2	5.45%	4.19%
3	5.80%	5.50%
AVG	**6.45%**	**5.25%**

CONCLUSION

It can be concluded that the proposed architecture using Raspberry Pi 3B+ can carry out all the functionalities proposed while having slightly longer start-up time and no corruption to OS. The battery consumption is also lower by 1.2%

REFERENCES

[1] UTM. (2014). eBraille Al-Quran. Retrieved from http://ebraille.weebly.com/
[2] R Sarkar, S. D. (2012). Analysis of Different Braille Devices for Implementing a Cost-effective and Portable Braille System for the Visually Impaired People. International Journal of Computer Applications,60(9), 1-5.
[3] RaspberryPi. (2018). Raspberry Pi 3 Model B on sale now at $35. Retrieved from https://www.raspberrypi.org/blog/raspberry-pi-3-model-bplus-sale-now-35/
[4] J Levine, T. R. (2011). The Remote Framebuffer Protocol. Internet Engineering Task Force (IETF).

IMPROVING GRAPHICAL USER INTERFACE FOR INDOOR POSITIONING SYSTEM

F.H. Gita, S.M. Saad and M. Hussein
School of Mechanical Engineering, Faculty of Engineering,
Universiti Teknologi Malaysia, 81310 UTM Skudai, Johor, Malaysia.

INTRODUCTION

In an era that is very advanced in technology as today, the Graphical User Interface (GUI) is very necessary in all applications such as navigation application. It is a tool that has been used to navigate people in public places such as airports, shopping centers, hospitals and so forth [1-2]. However, the development of GUI for Local Positioning System (LPS) especially in indoor navigation is still lacking and inaccurate in term of no shortest routes and audio guidance presented. This project was undertaken to improve this development – which aims to help people to get clear navigation and direction to their navigation inside a building or local area. This project not only provide the navigation by visual but also with audio, where blind people also can use the functions of GUI. The development of GUI and all algorithms are completed by using LABVIEW while the LPS is based on Ultra Wide Band (UWB) technology which can give the accuracy less than 30cm [3]. At meanwhile, the user positioning is calculated through trilateration method.

EXPERIMENTAL SETUP

An experiment setup is conducted in order to measure the accuracy of UWB. In this experiment, firstly was set the position of tags in a 4x4 layout and then followed by 3m x4m. Each layout uses 3 tags to place on 3 points, and 1 tag is held by the user. When the user is at a certain point, then the 3 tags placed on the layout will try to give information to the user where the real user is located. But usually the results of the information that the user gets will not be exactly the same as real value. Therefore, this test was conducted to find out how accurate this tag is to achieve real value.

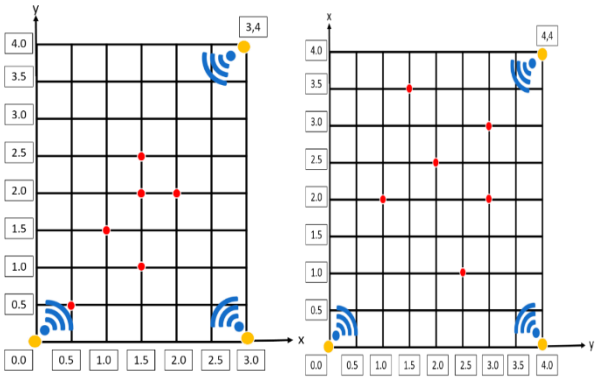

(a) (b)

Figure 1: (a) Layout of 3m x 4m; (b) Layout of 4m x 4m

RESULT AND DISCUSSION

Figure 2 shows the results of the functionality of route marker, shortest route, distance, audio guidance, static routes and boundary (1-meter acceptable) of the route are in accordance with expectations. To test the performance of GUI in lab environment, reliability test is conducted. The result in Figure 3 shows that the maximum accuracy is 0.34 pixel (0.68m) while the minimum is 1 pixel (0.02m).

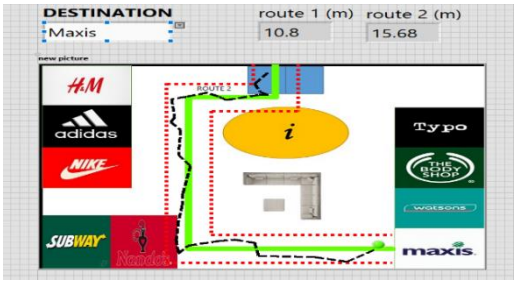

Figure 2: Results of Functionality Test

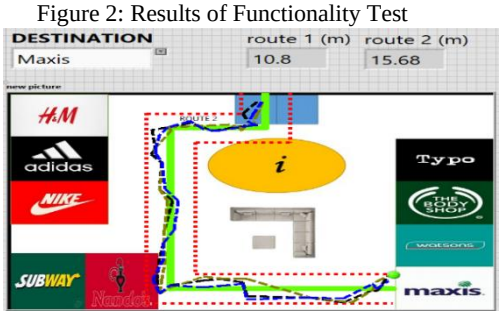

Figure 3: Results of Reliability Test

CONCLUSION

The result shows that the GUI of the system is function properly, where it able to show the shortest routes, distances in meter, and also audio guidance successfully. Several experiments are conducted in a test bed environment which has layout 9m x 12m in order to test the reliability of the system. The result shows that the data obtained is still in one-meter walking boundary (1m acceptable limit) and meaning that the system is reliable.

REFERENCES

[1] M. Shchekotov, "Indoor Localization Method Based on Wi-Fi," in *Proceeding of The 16th Conference of Fruct Association* , Russia, 2014.

[2] H. S. Hasan, M. Hussein, S. M. Saad and M. A. M. Dzahir, "Graphical User Interface (GUI) for Local Positioning," vol. 9, 2019.

[3] B. Cook, G. Buckberry, I. Scowcroft, J. Mitchell and T. Allen, "Indoor Location Using Trilateration Characteristics," 2005.

LONGITUDINAL STATIC STABILITY AND PERFORMANCE OF CAMAR-3 UTM UAV

Asyraf Izham Rosli and Shuhaimi Mansor
School of Mechanical Engineering, Faculty of Engineering,
Universiti Teknologi Malaysia, 81310 UTM Skudai, Johor, Malaysia

INTRODUCTION

UTM researchers have collaborate in the development of local Unmanned Aerial Vehicle (UAV) to provide design methods and solutions to support the advancement of local UAV industries. The prototype UAV has also potential to be commercial because of its technical. Camar-3 is the latest version of UTM UAV. Since Camar-3 is being developed through Computational Fluid Dynamics (CFD). Camar-3 is blended wing body. The airfoil for Camar-3 wing is SD 7062 and for the tail is NACA 0009.

EXPERIMENTAL SETUP

Most widely used approach is calculation method by using USAF-DATCOM method, Roskam or Raymer method. Each of the methods has their own accuracy and approximation dependent on requirement. However, most widely used method is USAF-DATCOM and the method is being implemented throughout this study. Other method are Raymers and Roskam method. Both methods are very helpful in this study and they are also being implemented throughout the project[1]. In order to make work easier and faster, all the formulations were done using Mathcad[2]. Mathcad is very helpful when dealing with many equations.

RESULTS AND DISCUSSION

Power required defined as the power we need to be providing in order for the aircraft to maintain a constant airspeed and constant altitude. Power available is the maximum power that we can produce with the electric motor. From Figure 1, we can observe there is a gap between the power required and power available. The gap in the Figure 1, shows that there is extra thrust for the aircraft to climb. The bigger the gap, the higher the extra thrust that the aircraft can be used to climb at certain altitude. There is intersection between the power required and power available curve. The intersection point indicates that the power required and power available for the maximum speed of the aircraft. The speed at the intersection point is at 33.475 m/s which is the aircraft maximum speed, the power required is 185.437 W, and the power available is at 190 W. When the aircraft achieved its maximum speed, there is no extra thrust for the aircraft to climb, therefore the aircraft cannot climb when it achieved its maximum speed.

.

Figure 1: Power required and power available against speed

CONCLUSION

Based on the results, the aircraft should be flying at around 17 to 20 m/s. At that speed there is minimum drag acting on the aircraft. The aircraft can be trimmed at that speed. While flying at the speed, the aircraft can save a lot of power from battery the aircraft also can climb to the higher when it has more thrust. When we can save a lot of power, the aircraft can travel a longer distance and time. The distance and time of aircraft travel is depending on the power of the battery and electric motor of the aircraft that can provide. The higher the power, the longer the distance and time travel by the aircraft. Therefore, the study is a success as all of the objectives of the study has been successfully achieve which are to study the longitudinal static stability and the aircraft performance. The trim speed is at around 17 to 20 m/s.

REFERENCES

[1] Finck, R. D., *USAF STABILITY AND CONTROL DATCOM*, 1978.

[2] Cook, M. V., *Flight Dynamics Principles*, 3rd ed., 2013.

AIRCRAFT GUST LOAD EFFECT DURING TURBULENCE

Syamil Rosli and Shuhaimi Mansor
School of Mechanical Engineering, Faculty of Engineering,
Universiti Teknologi Malaysia, 81310 UTM Skudai, Johor, Malaysia

INTRODUCTION

The aircraft nowadays are getting longer in dimension and travels farther than previous days. Every time an aircraft is on a flight cycle, the center of gravity (CG) will never be the same; even on a cruising flight, the CG of an aircraft will be shifted due to the movement activities on-board as well as the reduction of fuel throughout the flight. An aircraft with excellent stability control design will maintain the aircraft within the safe flying envelope.

However, the air above is never going to be smooth all way long. An unpleasant occurrence called clear air turbulence (CAT) can pose threat to flying aircraft. CAT is air movement created by atmospheric pressure, jet streams, air around mountains, cold or warm weather fronts or thunderstorms. It can be unexpected and can happen when the sky appears to be clear [(Door & Adams, 2018)1]. For a very long aircraft, a turbulence can cause chaos to passengers, especially when the passenger is at the last row of seat due to see-saw effect.

EXPERIMENTAL SETUP

Aircraft Boeing 747-100 is used as aircraft selection for this simulation. The position of CG changes is created, and mathematical model is created to find moment of inertia in pitch, I_y due to changes in CG. Aircraft state-space equation is developed to incorporate the effect of wind gust input.

The gust model is simulated using one minus cosine idealization and three different gust frequencies are used as gust input towards aircraft; aircraft short-period frequency, 1 Hz and 10 Hz. Using MATLAB programme, the simulation code is written using “m-file”.

RESULTS AND DISCUSSION

The aircraft response violently when the gust hit at 1 Hz frequency when all cases show the high magnitude response of the aircraft at that frequency. However, the aircraft does not shift much when frequency of gust reaches 10 Hz, although it will be a very uneasy feeling in flight. The CG changes affects the aircraft when the frequency of gust is same as the frequency of aircraft or more, as shown in Figure 1.

If the gust of same frequency with aircraft hits the aircraft, the magnitude of response is same for every CG changes, but the time response will be longer when CG is moved further backwards. Logically, the aircraft is heavier at the front when CG is moved to the rear, thus, more time is needed to “push” the aircraft vertically upwards.

As for the gust hitting at 1 Hz, the aircraft acts vigorously as the magnitude of response show a staggering almost 1000 fps. Ironically the response magnitude is higher when the CG moves backwards of the aircraft. We believe that most of the severe turbulence effect are due to this range of frequency hitting the aircraft. It is similar as an aircraft being tumbled up and down like a washing machine.

If the frequency of gust is increased further, 10 Hz for instance, it seems like the aircraft does not shifted in vertical direction due to very small magnitude response. CG changes is believed not making any significant different in the response. It can consider as a noise to the aircraft.

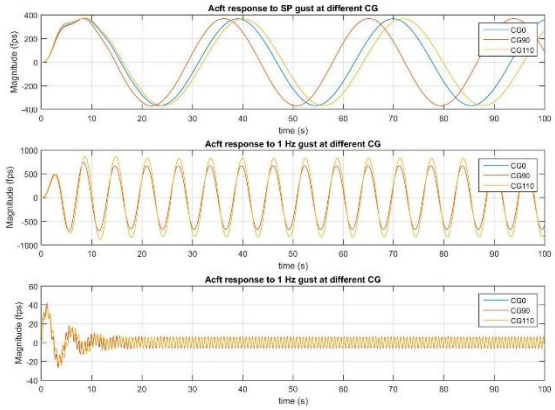

Figure 4 Aircraft response to various gust load frequencies at different CG. CG0 is CG optimum at 104.1667 from nose

CONCLUSION

CG changes only affects the aircraft when the turbulence of same frequency of aircraft or higher hits the cruising plane. If the frequency of gust is same as aircraft frequency, the response magnitude is same for all CG change, but the responsive time is slower if the CG is shifted backwards. But if frequency of gust is at 1 Hz, the aircraft will have higher magnitude response when the CG is shifted backwards. We can conclude that backward CG will have more devastative effect towards the aircraft if hit by turbulence

REFERENCES

[1] Door, L. and Adams, M., "Fact Sheet - Turbulence," ed. US: Federal Aviation Administration, 2018.

LONGITUDINAL STABILITY OF TAILLESS UAV

Tanzia Rashid and Shuhaimi Bin Mansor
School of Mechanical Engineering, Faculty of Engineering,
Universiti Teknologi Malaysia, 81310 UTM Skudai, Johor, Malaysia

INTRODUCTION

To determine the aerodynamic coefficients for pitching of an aircraft with tail and without tail wind tunnel test has been conducted. A modified version with tail and without tail of an unmanned aerial vehicle (UAV) named CAMAR have been used to conduct the wind tunnel test. At the same time for an initial estimation, the coefficients have been calculated following the semi empirical method. How an aircraft without tail behaves with the longitudinal stability has been observed in this project with the value for pitching coefficients. And thus this project investigates the comparison between two methods to find aerodynamic derivatives for pitching. The objective is to investigate the longitudinal stability of an unmanned aerial vehicle(UAV) with tail and without tail following wind tunnel testing method and semi empirical method and come out with the value of pitching coefficients for both models.

METHODOLOGY

- Modified 3D version for both models have been printed to conduct the wind tunnel test.
- Wind tunnel test has been done at different air velocities.
- Using the software 'TRACKER' the oscillation graphs have been found for the pitching of the models.
- From the graphs 〖W_n〗^2 and ζW_n have been found which later derived the value for 〖C_m〗_α for both model with tail and without tail

RESULTS AND DISCUSSION

Figure 1 shows the procedure of wind tunnel testing where the testing has been done at two different conditions and for wind on condition it has been three different wind velocities.

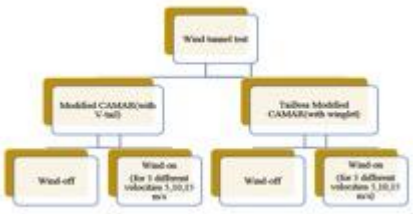

Figure 1: Chart of the procedure of wind tunnel test.

	Aerodynamic coefficients	Estimated value by semi-empirical method (rad^{-1})	Measured value by wind tunnel test (rad^{-1})
CAMAR(V-tail)	C_{M_α}	-15.76	-14.24
CAMAR(winglet)	C_{M_α}	0.3484	0.2927

Figure 2: value of 〖C_m〗_α from two different methods

Figure 2 shows the comparison between two methods with the results of the calculation and the results from wind tunnel test. The two methods have around 10% to 15% difference with the values for CAMAR with V-tail and CAMAR with winglet. However, the value from wind tunnel test is believed to be more realistic and accurate.

REFERENCES

[1] D. I. Greenwell. Frequency Effects on Dynamic Stability Derivatives Obtained from Small-Amplitude Oscillatory Testing. Journal of Aircraft, Vol. 35, No. 5, pp. 776–783, 1998

NUMERICAL COMPARISON ON THE MOTION CHARACTERISTIC OF CYLINDRICAL FLOATING STRUCTUREIN IN REGULAR WAVE AND IRREGULAR WAVE

Muhammad Haziq Zubir and Siow Chee Loon

School of Mechanical Engineering, Faculty of Engineering,
Universiti Teknologi Malaysia, 81310 UTM Skudai, Johor, Malaysia

INTRODUCTION

In this research a cylindrical floating structure is used as a FPSO to study the numerical comparison on the motion characteristic of the cylindrical floating structure in regular wave and irregular wave. Basically, regular wave is wave that has same wavelength, same amplitude, *a* and same period, *T* while the irregular wave can be viewed as the superposition of number of regular waves with different frequencies or wavelength and amplitudes. The realistic ocean waves on an ocean do not look like this but the ocean waves are almost always irregular or random.

EXPERIMENTAL SETUP

The first thing that need to concern to find the dimension and then design a cylindrical floating structure with AutoCAD. The catenary mooring system of 4x3 configuration is attached to the floating FPSO. The design and length are calculated depends on the depth of water. After that all the input to be key is determined based on scope of study for numerical simulation such as the depth of water, wave period, wave height and et-cetera. The wave type of Pierson-Moskowitz (PM) is decided to use during numerical simulation due to PM is the simplest spectrum that known as a fully developed sea. The motion of structure is focus at the heave and peak. Finally, the simulation of Ansys AQWA is running to obtained certain data.

RESULTS AND DISCUSSION

For the results, the data and graph that need to analyse is the comparison of the RAO of the motion structure frequency domain simulation and irregular wave time domain simulation. Also, the graph of the irregular short crest wave when the power of spreading function is remains constant while increase the number of sub-spectra.

Based on Figure 1 and Figure 2, line of the graph should be reach to the zero line and remain zero, but the graph obtained is not behave like that. Therefore, it may be due to the cutting or the point perhaps is not occurred at the maximum position during simulation. Also, maybe that the position of the occurrence of natural frequency in not enough or maybe the frequency domain simulation not closely enough.

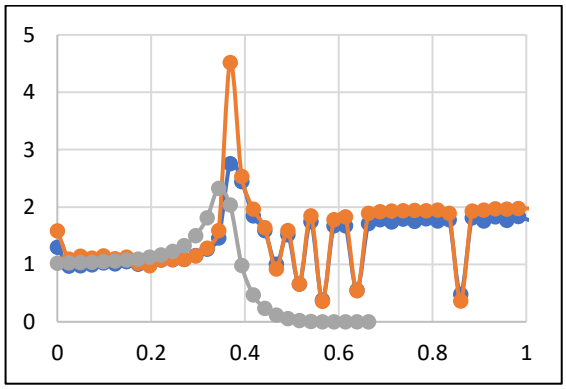

Figure 1: The comparison of RAO at heave

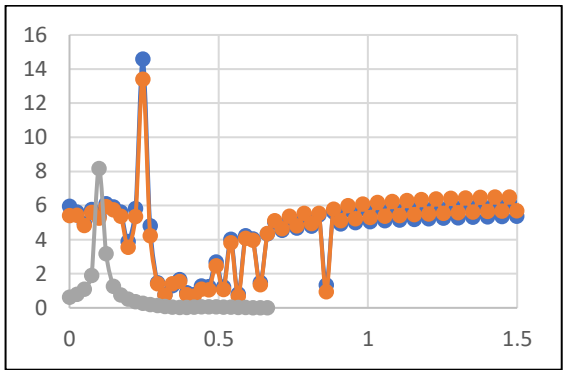

Figure 2: The comparison of RAO at pitch

CONCLUSION

Based on the results, the frequency domain shows the lowest value of the RAO compare to long crest and short crest for both at heave and pitch. Also, at heave short crest has the highest RAO and at pitch long crest has the highest. In conclusion, in this project, Ansys AQWA package is used to run and to complete the research. Based on the results, the difference and comparison of the RAO of cylindrical floating structure estimate by frequency domain simulation and irregular wave time domain simulation is obtained. Thus, the main objective of the research is achieved.

REFERENCES

[1]. Chee, l. S. (2016). Numerical modelling for hydrodynamic behavior of round shape flng interacting with lng carrier. Johor Bahru. Universiti Teknologi Malaysia

NUMERICAL STUDY ON COLUMNS ARRANGEMENT EFFECT TO THE MULTIPLE COLUMNS FLOATING STRUCTURE

Mohamad Farid Rahim and Siow Chee Loon
School of Mechanical Engineering, Faculty of Engineering,
Universiti Teknologi Malaysia, 81310 UTM Skudai, Johor, Malaysia

INTRODUCTION

Columns are used to provide structural strength and extra buoyancy force for any floating structure. The semi-submersible is one of the most reliable and cost effective structures for offshore oil and gas exploration in deep water [1].

The involving of columns in semi-submersible's structure design, provide good stability and seakeeping characteristic due to weather conditions (wave, current, and wind) requires high-safety standards for structures designed to operate in them. Compared with the traditional fixed/rigid structures, the floating/flexible state of the submersibles tends to attract much less forces [2].

SIMULATION SETUP

The simulation setup is based on the variable of multiple column arrangement for semi-submersible case. The other manipulated variable are the draft of each column arrangements model, number of columns and the columns diameter and its arrangement for each model and the waterplane area of each arrangements. The simulation also focuses of Tawau Sea region. The simulation software used is Ansys AQWA. The wave propagation condition is in head sea flow.

RESULTS AND DISCUSSION

For frequency domain analysis, the RAO from the simulation result is achieved. The analysis only focuses at heave and pitch case. Figure 1 illustrates the RAO for heave condition where the 8 column same diameter arrangement show the highest peak of response.

For figure 2, the pitch RAO is plotted for all multiple column arrangement which are 4 column, 6 column different mid diameter, 6 column same diameter, 8 column different mid diameter and 8 column same diameter. The highest unstable arrangement for pitch is 8 column different mid diameter.

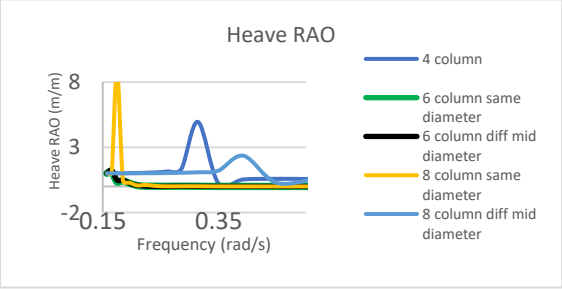

Figure 1: Heave RAO predicted by Ansys AQWA for comparison.

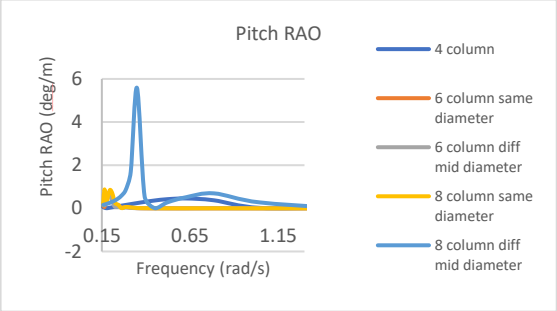

Figure 2: Pitch RAO predicted by Ansys AQWA for comparison.

The finalize selection of which column arrangement has the most stable capability by undergoes minimal motion of heaving and pitching movement is for the time domain analysis.

The significant motion value can be calculated and the result show the analysis from the RAO data is the same. The most stable multiple column arrangement for the multiple column floating structure is the 6 column with different mid diameter.

CONCLUSION

The RAO characteristic is valid from the frequency domain simulation the multiple column arrangement. The different of the frequency domain simulation compared to time domain simulation is the wave period involve in frequency domain is various compared to time series which is only one wave period is involved.

REFERENCES

[1] Liu, M., Xiao, L., Liang, Y., & Tao, L. (2017). Experimental and Numerical Studies of the Pontoon Effect on Vortex-Induced Motions of Deep-Draft Semi-Submersibles. Journal of Fluids and Structures.

[2] Odijie, A. C., Wang, F., & Ye, J. (2017). A review of floating semisubmersible hull systems: Column stabilized unit. Ocean Engineering.

NUMERICAL STUDY ON THE SAFETY GAP DISTANCE BETWEEN TANDEM ARRANGEMENTS OF FLOATING STRUCTURE IN WAVE

Mohd Syamim Shah and Siow Chee Loon
School of Mechanical Engineering, Faculty of Engineering,
Universiti Teknologi Malaysia, 81310 UTM Skudai, Johor, Malaysia.

INTRODUCTION

The use of the oil and gas as a reliable energy are increasing due to numerous used in the industrial, therefore the number of the offshore structure is increasing due to the offshore exploration activity to get the natural source. In the recent development in offshore industry floating structure are placed close to each other to help the system in offloading, bunkering and accommodation. Therefore, the safe gap distance and relative motion need to be study in order to have an optimum system.

EXPERIMENTAL SETUP

First and foremost, the semi-submersible and TLP model are modelled in AutoCAD using the actual scale. The modelled then import into the Ansys AQWA to determine the hydrodynamic diffraction which is response amplitude operator, RAO and the actual response of the models in hydrodynamic response.

A different distance is used to study the relative motion of the semi-submersible and TLP structure and to find the minimum gap between them. The simulation is simulated in irregular wave. The wave data that were used are from 10-year period data with 3s-5s period and 1m-4m wave height. The minimum gap distance was calculated from actual response data.

RESULTS AND DISCUSSION

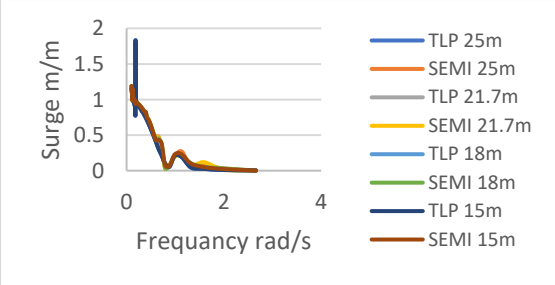

Figure 1: shows Semi and TLP Surge RAO comparison

From the surge graph comparison, it shows the highest surge motion for a different distance are by TLP 15m with 1.8 m/m, while lowest surge motion for a different distance are by Semi 15m with 0.02 m/m. The line graph for Semi and line graph for TLP of surge motion shows about the same pattern with steadily decrease and became constant with 15m distance have the highest and lowest peak.

From the figure 2, the graph show decreasing minimum distance with decreasing distance of the initial distance however at 15 meters initial distance, the minimum distance grew up a little. It shows the minimum distance occur at 18 meters with 3.16 meter. From figure 3, 18 meters' initial distance had the most movement percentage between the structure with 82% from initial distance. The lowest movement is by 25 meters initial with 59%. It also shows the pattern of maximum percentage movement of the both structures toward the surge motion increase with the decreasing initial distance however on the 15 meters initial distance, the percentage decrease about the same with 21.7 meters

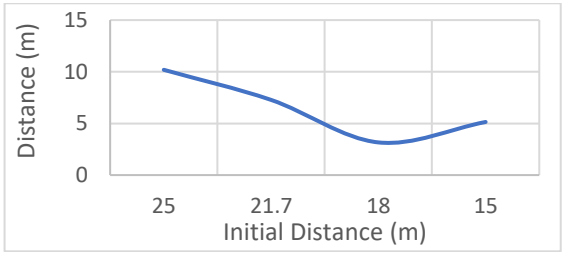

Figure 2: Minimum distance of initial distance

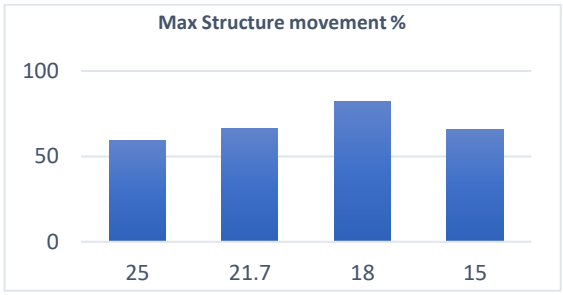

Figure 3: Percentage movement of the structure from initial distance

CONCLUSION

The strong relationship between the minimum distance with the structures motion shows that the floating structures motion could be minimized by shorter distance. However, optimum is still needed especially in multiple floating structures system when both structures are place close to each other such as during the TAD system operation.

REFERENCES

[10] Abyn, H. *Hydrodynamic Interactions And Relative Motions of Floating Bodies in Waves*. Ph.D. Thesis. Universiti Teknologi Malaysia; 2014.

[11] Koto, J., and Siow, C. L. (2014). Experimental Study of Gap Distance between Floating. *Journal of Ocean, Mechanical and Aerospace-Science and Engineering-*. 9.

THE EVALUATION OF DRAG FORCE OF GROOVE FLAT PLATE IN WIND TUNNEL

Muhammad Haziq Mohamad and Syahrrullail Samion
School of Mechanical Engineering, Faculty of Engineering,
Universiti Teknologi Malaysia, 81310 UTM Sekudai, Johor, Malaysia

INTRODUCTION

Aerodynamics is the study of the motion of air when it flows around a solid object. This research focus on the effect of groove on a flat plate. Groove acts as a vortex generator Vortex generator acts in the flow around the airfoil, by modifying the flow pattern through generation of small vortex so that the circulation around the airfoil changes. This experiment focus on evaluation of drag and lift force and pressure distribution on groove flat plate

EXPERIMENTAL SETUP

The experiment was conducted by using wind tunnel test. There is 4 different type of surfaces tested which are smooth, front, back and full groove. The drag and lift coefficient were obtained using 3 component balance and data are recorded by data acquisition software. The pressure distribution was conducted by using manometer

RESULTS AND DISCUSSION

Figure 1 shows the results for smooth and grooved surface flat plate, There is a significant drop in C_D value at the velocity of 5.2 m/s of the experiment between smooth and grooved flat plate. The drag coefficient between all groove surface flat plates are much lower to the smooth surface. The presence of groove on the surface of flat plate resulting in decrease in drag coefficient compared to the smooth flat plate. The addition of grooves on flat plates can reduce the drag coefficient up to 3.54% [1].

Based on the result obtained from Figure 2, it shows the inversely proportional trend smooth, front and back groove flat plate while for full groove flat plate it shows the mirror trends of those three surfaces. However, the comparison between smooth groove with front and back groove shows a different values in lift force where the smooth surface have a higher lift coefficient than front and back grooves.

Figure 3 shows that the pressure distribution against distance from leading edge for smooth surface is lower compared to the grooved surface and for front and back groove, the pressure distribution is almost similar to smooth flat plate characteristics where there is no significant changes in this condition compared to the full groove

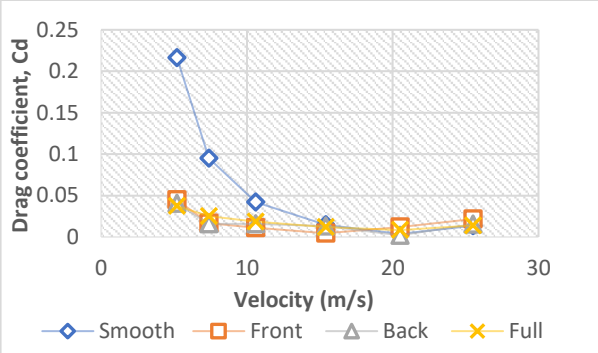

Figure 1: Drag coefficient vs velocity

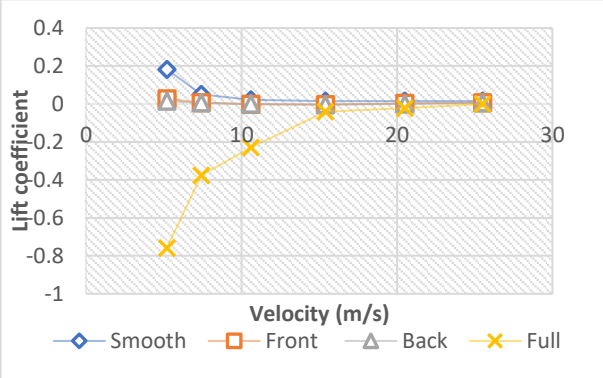

Figure 2: Lift coefficient vs velocity

Figure 3: Pressure coefficient vs distance from leading edge

CONCLUSION

In conclusion, the addition of groove causes reduction in drag of flat plate. It generate lift for smooth front and back groove while downfall for full groove. Pressure distribution of full groove is lower compared to other.

REFERENCES

[1] Ranjan, P., Ranjan, A. R., & Singh, A. P. (2011). Computational analysis of frictional drag over transverse grooved flat plates. *International Journal of Engineering, Science and Technology*, *3*(2)

THE EVALUATION OF DRAG AND LIFT FORCE OF GROOVE CYLINDER IN WIND TUNNEL

Naim Aiman and Syahrullail Samion
School of Mechanical Engineering, Faculty of Engineering,
Universiti Teknologi Malaysia, 81310 UTM Skudai, Johor, Malaysia

INTRODUCTION

Cylindrical structures are submitted to wide applications in offshore and marine engineering field and structural applications. Circular cylinder produces large drag due to pressure difference between upstream and downstream direction of the flow [1]. But, with a passive control method applied, the drag can be reduced. Therefore, drag reduction towards cylinders has been the main objective in various investigations. Groove is a surface modification that could control flow. This research focuses on the drag reduction of groove cylinders.

EXPERIMENTAL SETUP

This section presents the experimental setup for the project. Three test models consists of a smooth cylinder, half groove cylinder and full groove cylinder were tested in the low speed open end wind tunnel set at desired speed. The speed ranged from 5.2m/s to 35.5m/s. the drag and lift coefficient values are measured using a three component balance and the readings are recorded through the data acquisition software. For the flow visualization test, a smoke visualization technique was employed. A 1500W fog machine was used to produce the smoke. Streamlines are created with the help of honey comb. The flow behaviour on the test models was recorded using a DSLR camera.

RESULTS AND DISCUSSION

The drag and lift coefficient test was conducted on every types of cylinder which are smooth surface, full groove surface, groove on front half surface (Front), groove on rear half surface (Rear) cylinders. The trend of the drag coefficient results can be seen clearly in Figure 1. The smooth and half groove surface (Rear) produces highest drag coefficient while the other two cylinders showed a lower drag coefficient value. It can be seen that graph trend of all the cylinders indicates that drag coefficient decreases as the speed increases. This shows that the presence of grooves are effective in reducing the drag coefficient of cylinders.

To relate the results of the drag coefficient, the flow visualization test have been conducted. Figure 2 shows the flow separation point with the aid of the red arrow as the flow separation point start. It can be seen clearly that the effects of the grooves in delaying the separation point are effective. Besides that, the recirculation length of smooth cylinder is much longer compared to other cylinders. Full groove cylinder showed the shortest recirculation length.

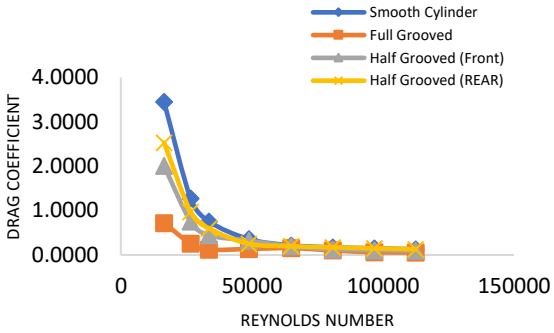

Figure 1: Drag Coefficient against Reynolds number.

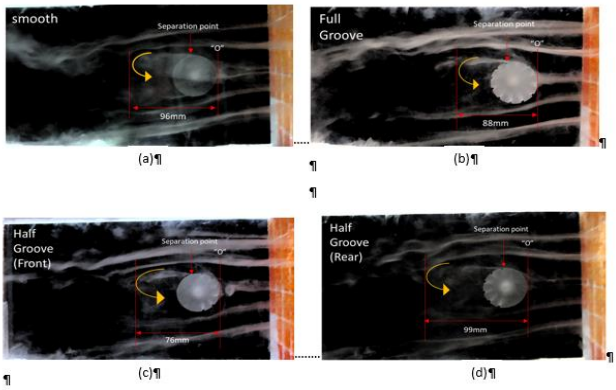

Figure 2: Flow Visualization test results.

CONCLUSION

The result indicates that groove surfaced cylinder are effective in reducing drag and lift coefficient on the cylinder especially in the higher Reynolds number branch. The drag and lift coefficient test is consistent with results of smoke visualization test. The smoke visualization test showed that groove surface roughness reduces the recirculation length.

REFERENCES

[1] U. Butt and C. Egbers, “Aerodynamic Characteristics of Flow over Circular Cylinders with Patterned Surface,” vol. 1, no. 2, 2013.

[2] B. Zhou, X. Wang, W. Guo, W. M. Gho, and S. K. Tan, “Experimental study on fl ow past a circular cylinder with rough surface,” *Ocean Eng.*, vol. 109, pp. 7–13, 2015.

[3] X. Song, Y. Qi, M. Zhang, G. Zhang, and W. Zhan, “Application and optimization of drag reduction characteristics on the flow around a partial grooved cylinder by using the response surface method,” vol. 2060, 2019.

IMPLEMENTATION OF LEAN MANUFACTURING IN AN ELECTRONIC ASSEMBLY COMPANY

Celine Koh Xian Lin and Syed Ahmad Helmi Syed Hassan
School of Mechanical Engineering, Faculty of Engineering,
Universiti Teknologi Malaysia, 81310 UTM Skudai, Johor, Malaysia

INTRODUCTION

Lean manufacturing is one of the most effective ways that many industries have applied to sustain competitiveness in the international market. Over recent years, most of the leading manufacturing companies have significant rise in profit because of implementation of lean manufacturing. This research is related to implementation of lean manufacturing to reduce the waste for an assembly process in an electronic assembly company. Ohno had identified seven categories of MUDA as: overproduction, waiting, transporatation, inventory, motion, and over-processing [1]. This case study focuses on reducing lead time of the process to improve the performance of the manufacturing system. Suitable lean tools were applied to eliminate the main wastes in the assembly line to increase the productivity of the process.

METHODOLOGY

Relevant data are gathered through observation, interview, document and record and data collection. Pareto diagram are built based on the process flow matrix rated to determine the major waste in the production system through interviewing the expert workers. Current value stream mapping (VSM) is constructed to evaluate the current manufacturing system. The most suitable lean tools are proposed to improve the system after reviewing the journals, articles and previous case study. Future VSM is built according to the proposed solutions and analyzing by calculating the value-added ratio (VAR). Lastly, simulation model is built to show the performance of the production system.

PROBLEM IDENFICATION

Waiting, transportation and inventory had contributed 77.6% to the overall waste. Therefore, they classified as major waste. The waiting waste is due to the long oven curing time. The long distance travelled for movement of parts between the station causes transportation waste. Besides, stagnation of inventory in certain station due to long processing time in previous station and overproduction.

RESULT AND EVALUATION

From the current VSM, VAR for current process is 6.46%. The proposed solutions to reduce the major wastes are eliminate of oven curing, layout rearrangement and Kanban card System. Based on the proposed method, future VSM is built and the analysis is done. The VAR for future state had increased to 17.56%. The simulation for both states had proved that the number of outputs increases by 40.90%.

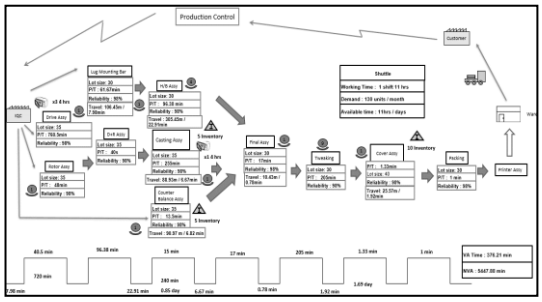

Figure 1: Current VSM

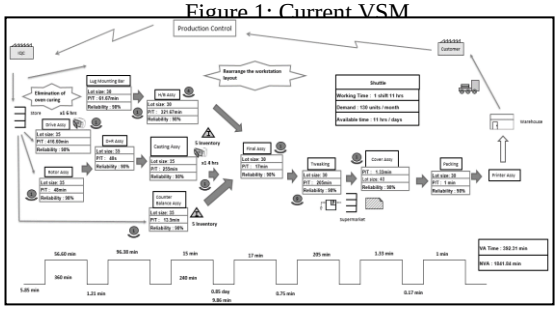

Figure 2: Future VSM

CONCLUSION

The implementation of lean shows that the production lead time and work-in-progress had decreased. Besides, the simulation models also prove that the output had increased by practicing the lean production system. Hence, it can be concluded that implementation of lean manufacturing can improve the efficiency of the production system.

REFERENCES

[1] Ohno, T. (1998). *Toyota Production System: Beyond Large Scale Production.* CRC Press.

[2] Jasti, N., & Sharma, A. (2014). Lean Manufacturing Implementation using Value Stream Mapping as a Tool: A case study from auto component industry. *International Journal of Lean Six Sigma Vol 5 Issue 1*, 89-116.

IMPROVEMENT OF FACILITY LAYOUT IN A MANUFACTURING INDUSTRY

Teeneshkumar Guru Balan and Syed Ahmad Helmi Syed Hassan
School of Mechanical Engineering, Faculty of Engineering,
Universiti Teknologi Malaysia, 81310 UTM Skudai, Johor, Malaysia

INTRODUCTION

This project is about the improvement of the current existing layout of a manufacturing company by suggesting a much better layout alternatives for this company. In this thesis, IE tools will be implemented in order to assist the company in solving the current existing problem. The existing plant layout of the manufacturing company is not properly designed and organized. The workers need to go through a long distance travel. Therefore, much time is consumed for distance travelling between departments. Besides that, backtracking and cross-traffic cause the ineffectiveness of current layout to be prolong. As a result, proper evaluation and improvement to the existing layout is done to overcome this problem [1-4].

EXPERIMENTAL SETUP

To complete this project successfully, methodologies are determined. The project is initiated by searching for a company to conduct the case study. Several visits to the company has been made to understand more about the operation of the company, process flow of product, department layout and others. Next to justify the existing problem in the company, data collection and analysis are carried out using the IE Tools. The first step for the improvement, is by applying the Group Technology techniques for the existing layout. From there, two alternatives can be generated via SLP and MULTIPLE. Both of this alternatives will be compared together with the existing layout through manual calculation and also simulation model.

.

RESULTS AND DISCUSSION

There are two main problem found via IE tools which are the material flow smoothness and the total distance travelled for each department. From the Pareto chart shown in Figure 1, we can observe that this both problem accumulates almost 86% of the overall problem criteria.

Simulation models were developed to make the comparison between the current and the layout alternatives. All three models built are evaluated by using WITNESS simulation through interpreting the results obtained from the model.

Based on table 1, the alternative generated by using MULTIPLE method has the much lower value of total distance travelled between departments, 2422.56 metre per week as compared with the alternative developed by using SLP method, 2454.62 metre per week. From the comparison of alternative (MULTIPLE) with the existing layout, the reduction of total distance travelled between departments is 47.91%. At the aspect of reduction of total distance travelled between departments, alternative layout (MULTIPLE) is better than alternative layout (SLP).

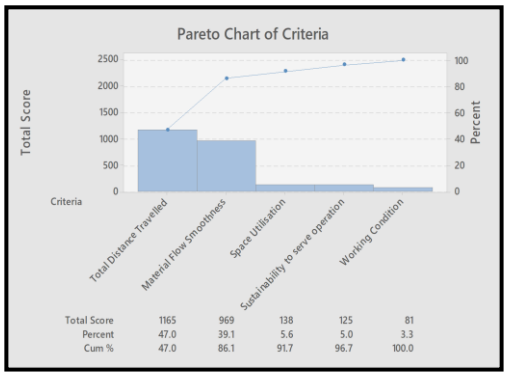

Figure 1: Pareto chart of Problem Identification

Table 1: Comparison between models

Model	Manual Calculation	Results	
	Total Distance Travelled	Average Total Outputs	Average Work in Progress (AWIP)
Existing Layout	4650.84	2861	53.787
Alternative (MULTIPLE)	2422.56	3124	35.609
Alternative (SLP)	2454.62	3115	39.201

CONCLUSION

This study discusses the existing floor layout of the company and then propose a better alternative layout for the production floor. From this proposed alternative layout, the material flow and total distance travelled between each departments can be optimized. Two layout techniques has been used which are the Systematic Layout Planning (SLP) and MULTIPLE.

REFERENCES

[1] Bozer, Y., Meller, R., & Erlebacher, S. (1994). An Improvement-type layout algorithm for Single and Multiple-Floor Facilities. 950-962.

[2] Burbidge, J. (1991). Production Flow Analysis for planning group technology. *Journal of Operations Management*, 5-30.

[3] Muther R., & Hales L. (2015). Sytematic Layout Planning, 4th ed. *Management & Industrial Research Publications*.

[4] Tompkins, J. A., John, A., Bozer, Y., & Tanchoco, J. (2010). Facilities Planning, 4th Edition. 3-13.

REDUCTION OF NON-VALUE-ADDED ACTIVITY AND SPACE REQUIREMENTS OF AN ELECTRONIC INDUSTRY

Anuar Muhamad and Syed Ahmad Helmi Syed Hassan
School of Mechanical Engineering, Faculty of Engineering,
Universiti Teknologi Malaysia, 81310 UTM Skudai, Johor, Malaysia

INTRODUCTION

Basically, this case study is related to Industrial Engineering (IE) tools. Industrial Engineering (IE) is a subject about designing, improving and setting up the integrated system of personnel, materials, equipment, energy and information. It verifies, calculates and evaluates the outcomes of the integrated system by systematically using the knowledge of math, physics and social science and the principle of engineering analysis [1]. For this case study, it was conducted in E-Gov/CID production department of HID Global (M) Sdn. Bhd. It is an electronic manufacturing industry which produce Radio Frequency Identification (RFID) products.

PROBLEM IDENTIFICATION

From the observation, interview and data collection, high non-value-added activity in term of high waiting time of operators is the major problem for CID/E-Gov production department. This problem is identify based on the production line of the highest product demands which is SOM21 production line. This problem causes the operators are not fully utilized and high usage of operators in the production line. The critical workstation has been identified which is Hacker machine workstation and Zund machine workstation.

RESULTS AND DISCUSSION

The process for Hacker machine is bonding of wire to a module and wire transfer to a sheet of material of SOM21. There are four machines in the production line of SOM21. The operator of the Hacker machine wasting his/her time waiting for the process to be done for about an average time of 147.6 seconds or 2.5 minutes. There is one Zund machine for production line of SOM21, the process involved is trimming process of SOM21. The operator of Zund machine wasting his/her time waiting for about 46.2 seconds for the trimming process to be done.

The operator takes an average of 93 seconds or 1.55 minutes to collate one sheet of SOM21. This shows that, it is capable for Hacker machine operator to do collating while Hacker machine is in process as shown in Figure 1(a).

For Visual Inspection workstation, there is one workstation. The operator inspects two sheets of SOM21 where the average time is 39.44 seconds. By assigning the operator to do visual inspection while the Zund machine is in process as shown in Figure 1(b), it reduces the percentage loss of operator due to waiting time from 55.00 % to 8.05%

Referring to Figure 2, by combining the Zund machine and Visual Inspection, the operator does not need to travel because the distance between both workstations have been eliminated. From this proposed layout, it also reduces the space requirements and defect of trimming process can be detected earlier.

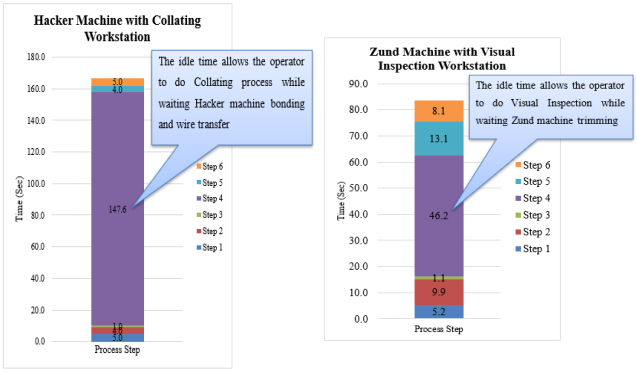

(a) (b)

Figure 1: Graph of Proposed Steps for (a) Hacker machine and Collating Workstation and (b) Zund machine and Visual Inspection Workstation.

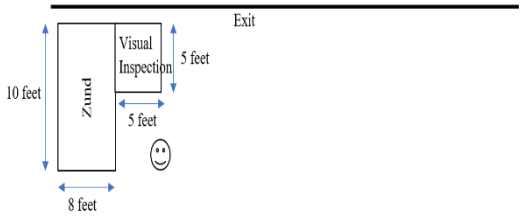

Figure 2: Proposed Layout for Zund Machine and Visual Inspection

CONCLUSION

The results for this case study show that, for Hacker machine operator the percentage of loss due to waiting time reduce from 57.83 % to 21.39% and for Zund machine operator 55.00% to 8.05%. Total of 5 existing operators for Collating and Visual Inspection workstation also being eliminated from 24 operators to 19 operators per shift for the production department. Proposed layout of combining the Zund machine and Visual Inspection workstation, it reduces space requirements from 290 ft^2 to 130 ft^2, eliminate the distance travelled by the operator between both stations and earlier detection of trimming defects.

REFERENCES

[1] Bo WANG, Y.-s. Z. (n.d.). *An Analysis of The Function of Industrial Engineering in Equipment Manufacturing Industry Based on DEA.* China: College of Management and Economics, Tianjin University, Tianjin, China and Taiyuan Heavy Machinery Group Co., Ltd.

ERGONOMIC IMPROVEMENT IN MANUFACTURING COMPANY

Tuan Ahmad Farhan Hakimi Tuan Isa and Syed Ahmad Helmi Syed Hassan
School of Mechanical Engineering, Faculty of Engineering,
Universiti Teknologi Malaysia, 81310 UTM Skudai, Johor, Malaysia

INTRODUCTION

Nowadays, factor such as heavy loads, static posture repetitiveness of work expose workers to risk of musculoskeletal disorder. Especially in manufacturing sector according to (Malaysia Industrial Development Authority [MIDA], 2010). Based on the previous studies we have found that workers' major concerns regarding OSH are in fact related to the lack of attention given to the implementation of ergonomics ((Mohd nasir selamat, n.d.) Shaliza, Sharul, Zalinda, & Mohzani, 2009; Shikdar & Sawaqed, 2003).

METHODOLOGY

This section presents the method used to achieve the objective of studies. Body Discomfort Survey and Rapid Upper Limb Assessment were used in this study to collect and analysis data. Body Discomfort Survey used to identify musculoskeletal disorder among the workers in different kind department in manufacturing company. After musculoskeletal have been identified RULA will be used to evaluate the posture of worker whether worker experienced musculoskeletal disorder or not.

RESULTS AND DISCUSSION

Based on the result obtain from the BDS it show that grinding department has highest score (OFTEN) on musculoskeletal disorder involving Shoulder(3), Upper Back(3), Lower Back(3),and Wrist(4) as shown in Figure 1. Therefore studies have been focus on grinding department to make an ergonomic improvement and RULA assessment is used to measure the posture of workers in grinding department. The score based on RULA show that there need implement immediate change (7) to avoid or prevent workers getting Musculoskeletal Disorder during working.

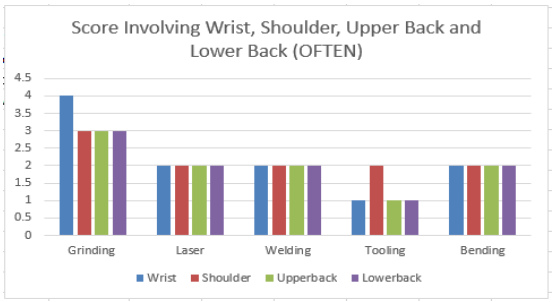

Figure 1: Score of Musculoskeletal Disorder involving 4 main part of body

Figure 2 shows final design solution generated by using Solidwork after evaluation of matrix have been done. Before final design is generate there are few process such as conceptual function analysis, morphology and evaluation matrix. After final design solution have been proposed RULA is used to evaluate the new proposed design solution and comparison between current and new design show that change in term score which is 7 to 2. Therefore, musculoskeletal disorder can be avoid and prevent on workers while working.

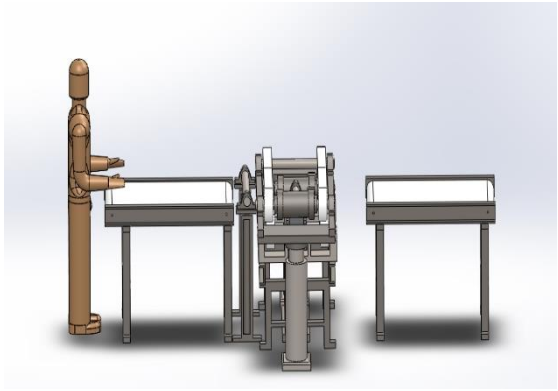

Figure 2: Final Design solution

CONCLUSION

Objective of studies have been achieve which to identified musculoskeletal disorder experience by particular workers and reduce the level of musculoskeletal risk in workplace. The implementation of final design solution shows that RULA score have been reduce from 7 to 2.

REFERENCES

[1] Mohd nasir selamat. (n.d.). Ergonomic Work System And Occupational Safety And Health Performance: Mediating Effects Of Psychosocial Work Factors. Universiti Sains Malaysia, 62(1), 27–40.

[2] Mustafa, Shaliza Azreen, K. S. (2009). The Effect of Ergonomics Applications in Work System on Mental Health of Visual Display Terminal Workers. European Journal of Scientific Research, 31(3), 341–354.

SHIP ROLL MOTION COMPENSATION THROUGH SCISSOR-PAIRED GYROSTABILIZER

Muhammad Zahir Bin Ahmad and Tang Howe Hing
School of Mechanical Engineering, Faculty of Engineering,
Universiti Teknologi Malaysia, 81310 UTM Skudai, Johor, Malaysia

INTRODUCTION

Marine vessel is exposed to the rough sea condition of which it is exposed to yaw, pitch and rolling motion. These motions were induced by the sea wave due to it propagation to vessel hull structure. The safety and productivity of machineries and sailor onboard are not in optimum condition. The application of Gyrostabilizer onboard of marine vessel will counterbalance this rolling motion. This research comprises of simulation studies part and hardware experimentation part. The integration of PID controller is important to ensure control system stability. Experiment involves Data Acquisition System (DAQ), Micro-Controller (Arduino) and Gyrostabilizer hardware.

EXPERIMENTAL SETUP

The experiment setup was done with the integration of National Instrument DAQ (NI)-USB-6343, Arduino Mega and Gyrostabilizer. The integration of DAQ and Micro-controller is important as to reduce the control load on the Micro-controller, while NI-DAQ prevalent for its reliability and the acquired data accuracy.

NI-DAQ was not able to read the Pulse Width Modulation (PWM) signal, hence the interaction between NI-DAQ and Micro-controller is important as Arduino provides signal conversion for DAQ to be able to read signal to acquire data.

RESULTS AND DISCUSSION

At 45*o*precession angle, the flywheel rotational speed is 1000rpm, 1500rpm and 2000rpm. The variation of rotational speed yields a different torque of which the torque is 2Nm, 1.5Nm and 1Nm for 1000rpm, 1500 rpm and 2000rpm respectively. The sample time taken for Figure 1 system response is t= 10s and Figure 2 is t=120s.

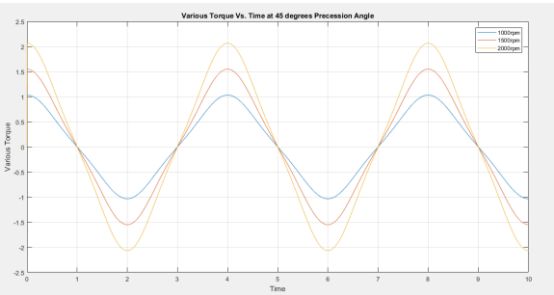

Figure 1: Simulink torque at 45*o*precession angle

The hardware experiment has the same 45*o*precession angle and rotational speed of 1000rpm, 1500 rpm and 2000rpm. And the torque output is the highest for 2000rpm, and lowest for 1000rpm flywheel rotational speed.

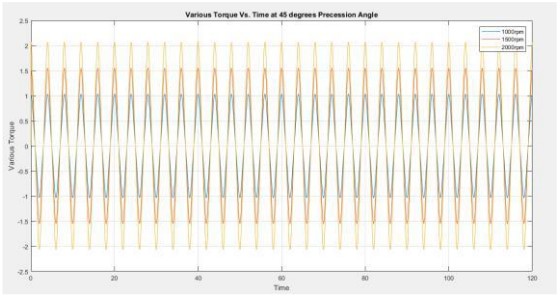

Figure 2: Gyrostabilizer torque at 45*o*precession angle

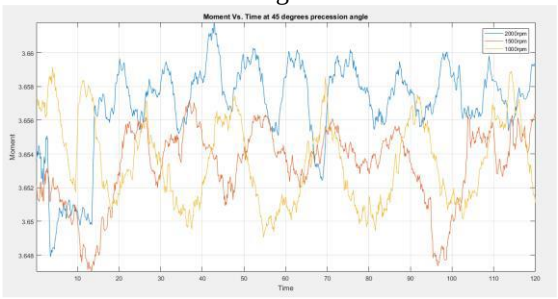

Figure 3: Gyrostabilizer torque at 45*o*precession angle

CONCLUSION

Increasing flywheel speed and precession speed could increase the magnitude of rolling moment. In this experiment, the increase of precession speed is achieved by increasing the sinusoid amplitude of the precession motor displacement input. Varying the sinusoid frequency, the precession speed could be increased, and hence the generated rolling moment.

REFERENCES

[1] Steinmann, T. P. (2009). Analysis of Ship Roll Gyrostabiliser Control. *Proceedings of the 8th IFAC International Conference on Manoeuvring and Control of Marine Craft* (pp. 1-6). Guarujá, Brazil: International Federation of Automatic Control.

[2] Shenoi, N. C. (2014). Control Strategiesfor Marine Gyrostabilizers. *Oceanic Engineering*, 1-13.

[3] Perez, A.D. (2013). Energy-based Nonlinear Control of Ship Roll Gyro-stabiliser with Precession Angle Constraints. *9th IFAC Conference on Control Applications in Marine Systems* (pp. 1-6). Osaka, Japan: The International Federation of Automatic Control.

INTEGRATION OF EGGSHELL IN POLYMER COATING FOR FERROUS ALLOY CORROSION PROTECTION

Khairul Kasyidi Mazlan and Tuty Asma Abu Bakar
School of Mechanical Engineering, Faculty of Engineering,
Universiti Teknologi Malaysia, 81310 UTM Skudai, Johor, Malaysia

INTRODUCTION

About 94 to 94% of eggshell is made up of calcium carbonate in the form of calcite [1]. It is known that eggshell waste can be utilized into commercial products and create new values from waste materials. By formulating and applying different concentration of calcium carbonate in the form of eggshell powder in polymer coating, the performance and the corrosion protection properties are investigated. The possibility of using eggshell as a substitute pigment material for the conventional precipitated calcium carbonate from limestone is analysed.

EXPERIMENTAL SETUP

The paint was formulated using a high speed stirrer at 800 RPM. Four sample of different eggshell weight percentage (0, 2.5, 5.0,7.5) was formulated and applied on the substrate. The paint is let to fixate before being characterized and tested. The coated specimen thickness was measured under an optical microscope at X200 magnification to analyse the uniformity of the coating. The hardness was then measured using Vickers hardness tester to measure the effect of eggshell on the coating hardness. Substrate were then subjected to an immersion test for 7 days before being analysed visually and also using XRF analysis. The rate of corrosion of the sample was tested using a Linear Polarization Resistance test.

RESULTS AND DISCUSSION

The XRD analysis of the eggshell powder indicates that the crystalline mineral phase of eggshell is similar in comparison to the mineral phase of calcium carbonate in the form of calcite. The average thickness of coating applied was found to be 93.02µm with a maximum deviation of 4.5µm. The hardness test showed decreasing hardness with increasing weight percentage of eggshell. However, this is only an estimation to the actual hardness value of the coating as it was impossible to measure the hardness perpendicularly to the coating as it is too thin.

As Figure 1 suggest, the rate of corrosion decline when the weight percentage of eggshell is increased from 0 to 2.5%. It can be seen that the effect of eggshell is still not clearly visible as the decline is only by a small margin. Only when the weight percentage is increased to 5% does the rate of corrosion exhibit rapid decline. This suggest that the weight percentage of eggshell used is almost at its pigment volume concentration.

The second evaluation done was XRF element analysis. This was done to analyse the element content on the surface of the specimen after immersion. The result of the analysis shows that the increment of eggshell weight percentage resulted in the presence of less oxygen and more iron on the surface. Reduction of iron and a rise in oxygen relates to rust and organic structures [2] hence the increase in iron percentage and the decrease of oxygen percentage could be related to the decrease in corrosion rate of the specimen.

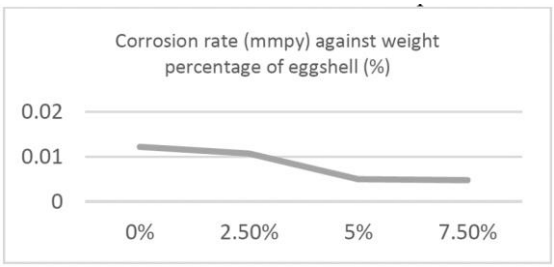

Figure 1: Figure 1: Graph of corrosion rate (mmpy) against weight percentage of eggshell.

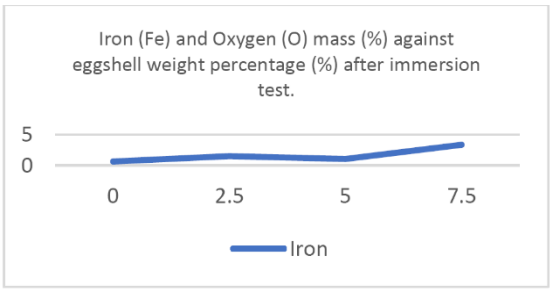

Figure 2: Graph of iron and oxygen percentage against weight percentage of eggshell.

CONCLUSION

The corrosion protection properties of polymer coating with the addition of eggshell was studied. The weight percentage of eggshell used in each coating sample was varied between 0 to 7.5 % and it was found that the specimen with the largest percentage of eggshell exhibit the best corrosion protection properties.

REFERENCES

[1] Hunton, P. (2005). Research on Eggshell Structure and Quality: An historical overview. Brazilian Journal of Poultry Science, 1-5.

[2] N.M Ahmed, M.G Mohamed, and W.M.A El-Gawad. (2019) 'The assessment of anticorrosive behaviour of calcium carbonate from different sources in alkyd-based paints', Progress in Organic Coatings, 128, 168-180

MEASUREMENT OF WEAR PROPERTIES OF ALUMINIUM METAL MATRIX COMPOSITES

Mohd Islahuddin Abdul Aziz and Tuty Asma Abu Bakar
School of Mechanical Engineering, Faculty of Engineering,
Universiti Teknologi Malaysia, 81310 UTM Skudai, Johor, Malaysia.

INTRODUCTION

Nowadays, Aluminium Metal Matrix composites had being widely used thorough out various application in industries. Aluminium MMC is a strong composite that has high strength to density ratio. However, this Aluminium alone is lack of wear resistance. Therefore, this study was done to measure the effect of Praseodymium addition on the wear resistance and their microstructure.

EXPERIMENTAL SETUP

Aluminium MMC of AL-15Mg2Si was casted with different percentage Praseodymium addition by using in-situ method. Percentage of Pr addition that was used in this project are 0.3%, 0.5%, 1%, 2%, and Base. Then this composite will undergoes microstructure analysis, Wear Characterisation and Hardness Test.

Optical microscope with up to 500 time magnification was used to analyse microstructure. Dry sliding wear tests were conducted to ASTM: G99-06 in a pin on disc wear testing apparatus (Ducom TR20-LE) using 20N and 40N to vary the result [2]. Then, the same wear sample was used on SEM/EDX machine to study the wear severity and pattern.

RESULTS AND DISCUSSION

From microstructure analysis, we can see the difference of abundance and density of primary Mg2SI phase represented by black clump area. The density of this phase was different between the sample and 0.5% has highest amount of it. . A possible explanation for the modification of primary Mg2Si by addition of Pr might be associated with the nucleation and/or growth of Mg2S. [2]

Wear rate of the sample was measure and calculated by using Archard's Law and presented as show in figure 1. The value of wear rate when 20N load being applied did not have a significance variation. However, when 40N load was used, the wear rate show a significance change. As show in the graph, the increase in Pr addition %wt will decrease the wear rate until the point of 0.5%wt, then the wear rate will start to increase as Pr addition increase. It shows that, the optimum value of Pr to produce the best Wear resistance is 0.5%wt.

Figure 2 shows the hardness value for different quantity of Pr addition. From the result it can be said that there are no significance effect of Pr addition to Hardness value even though Hardness should be related to wear rate according the Archard's Law. [1]

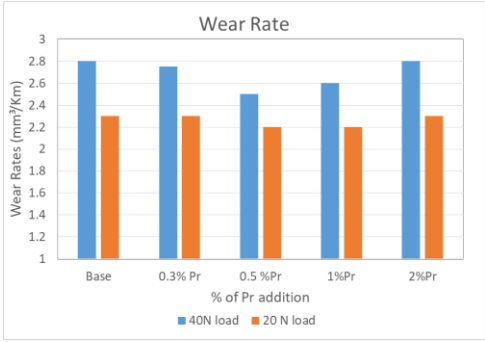

Figure 1: Wear rate of sample for 20N and 40N load

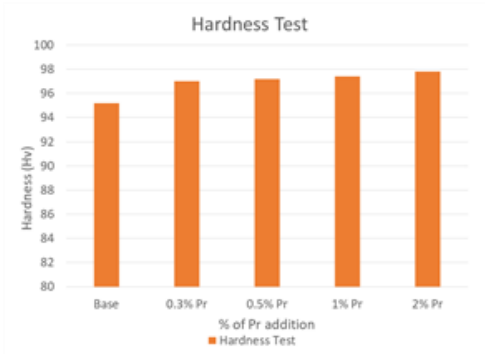

Figure 2: Hardness Value

CONCLUSION

From the microstructure analysis and wear characterisation, it can be conclude optimum Pr addition on Al-15Mg2Si is 0.5%wt. However, the hardness test show an almost a same hardness value with only a slight increase as the Pr addition increase. In nut shell, it can be said that Pr addition can really improve the wear properties of Aluminium composite if a right casting process is used.

REFERENCES

[1] Stankovic, M. *Determination of Archard's wear coefficient and wear simulation of sliding bearings.* Belgrade, Serbia: Emerald Publishing Limited. 2018.

[2] Saeed, F., Hamidreza, G., Nur Azmah, N., and Ali, O. (2016). Effect of Primary and Eutectic Mg2Si Crystal Modifications on the Mechanical Properties and Sliding Wear Behaviour of an Al–20Mg2Si–2Cu–xBi Composite. *Journal of Materials Science & Technology*, 1084-1088.

DEVELOPMENT OF HIGH PERFORMANCE ALUMINIUM MATRIX COMPOSITE USING YTTRIA STABILIZED ZIRCONIA

Nadirah Binti Othman and Tuty Asma Binti Abu Bakar
School of Mechanical Engineering, Faculty of Engineering,
Universiti Teknologi Malaysia, 81310 UTM Skudai, Johor, Malaysia

INTRODUCTION

Composite materials have been used hundreds years ago before Christ in construction even though human civilization during the time were not really understood how it works [1]. The improvements and innovations of composite materials have been done as time passes by until now. Composite material is made up of two or more distinct constituents which results in better properties than alloys. The two constituents act as a reinforcement and a matrix. The reinforcement is embedded to the matrix and in most cases it provides the strength and stiffness to the material. Development of aluminium metal matrix composite (Al MMC) reinforced with yttria stabilized zirconia (YSZ) had been conducted to see its properties.

EXPERIMENTAL SETUP

The methodology of this research started with the preparation of aluminium matrix composite reinforced with 3, 6, 9wt. % YSZ by using stir casting technique. Then, the samples were tested with various testing procedures and then were analysed. The samples were prepared for characterization, tensile test and impact test.

Characterization of the specimens was conducted using optical microscope (OM) and scanning electron microscope (SEM) and microstructural analysis and elemental analysis were done. To analyse the mechanical properties of the samples, hardness test, tensile test and impact test were done.

RESULTS AND DISCUSSION

Characterization of the composite using OM shows that the particle of YSZ were circular in shape and grey in colour while using SEM, YSZ particles were shown as the brighter particles as shown in figure 1. The distribution of the particles were not uniform since YSZ particles can be seen only at certain area and not at the other area.

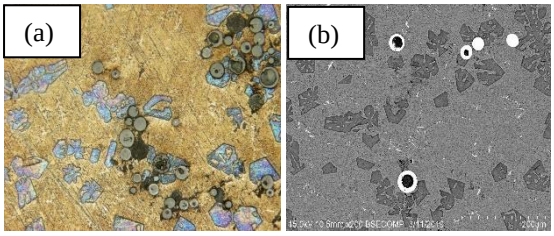

Figure 1: Al MMC reinforced with 3wt. % YSZ under (a) OM using 20x magnification and (b) SEM using 200 magnification.

For the mechanical properties of the composite, the hardness increasing with respect to the increasing of YSZ particles content as shown in figure 2. Figure 3 shows the ultimate tensile strength (UTS) for Al MMC with 3wt. % YSZ exhibit the highest value. This condition happened due to the porosities and agglomeration of the composites for 6 and 9wt. % YSZ that affect their UTS [2].

Figure 2: The value of average hardness of specimens containing 0, 3, 6 and 9wt. % YSZ.

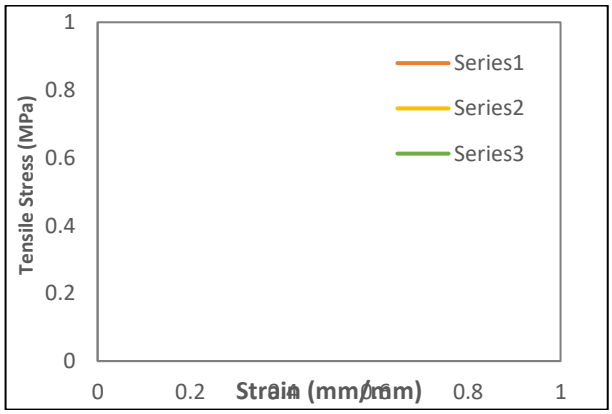

Figure 3: The stress-strain graph of Al MMC with 3, 6 and 9wt. % YSZ content.

CONCLUSION

The addition of reinforcement particles which are YSZ particles into the aluminium matrix can enhance the hardness properties of the composite. The hardness of the composite can be improved by increasing the content of YSZ particles.

REFERENCES

[1] Sharma, S. (2000). Composite Materials. Delhi: Narosa Publishing House.
[2] Sukiman, N. A. (2018). Microstructure Characterization and Mechanical Properties of Al-Mg2Si-xYSZ Hybrid Composite. Universiti Teknologi Malaysia.

FABRICATION AND CHARACTERIZATION OFYSZ/NICKEL CERMET USING AS THERMAL BARRIER COATING FOR AUTOMOTIVE TURBOCHARGER APPLICATIONS

Mohammad Zahir Zambri and Uday M.Basheer Al-Naib
School of Mechanical Engineering, Faculty of Engineering,
Universiti Teknologi Malaysia, 81310 UTM Skudai, Johor, Malaysia

INTRODUCTION

Turbocharging is common technique use to increase power density in internal combustion engine. Turbocharging reduce fuel consumption and pollutant emissions. Thermal barrier coating(TBCs) was used to increase. This research was conducted to select the best methods using process using various composition. The aim of this project is to investigate on the integrity and reliability of coating using film applicator, brushing, and dipping methods and also various composition of formula. The coating will be evaluate using SEM and adhesion test.

METHODOLOGIES

The experiments conducted using 30wt%YSZ: 70wt%Ni and deposited sing film applicator, brushing and dipping.

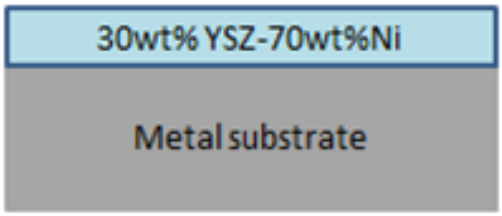

Figure 1: Illustration of single ceramic layer of coating

All 12 samples will be evaluate using SEM and adhesion test.

RESULT AND ACHIEVEMENT

For 30wt%YSZ:70wt%Ni using 3 different methods the thickness of coating are as 43.6,88.7 and 35.1μm for film applicator, brushing and dipping respectively. For experiment using film applicator using (30wt%YSZ: 70wt%Ni, 40wt%YSZ: 50wt%Ni: 10wt%Cr and 50wt%YSZ: 30wt%Ni: 20wt%Cr) the thickness of coating are as 43.6,45.1 and 53.8 μm respectively.

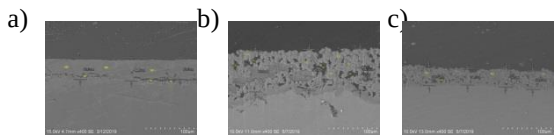

Figure 2: SEM images of the coating which has the same formula (30wt%YSZ:70wt%Ni) with different methods.

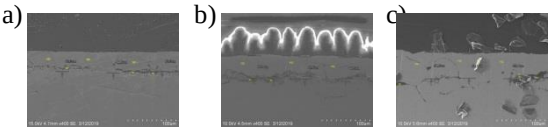

Figure 3:SEM Images of 3 different methods coat using film applicator

For adhesion test, for 30wt%YSZ:70wt%Ni using 3 different methods the results are as 5.21,7.09 and 4.77Mpa for applicator, brushing and dipping. Next, for the film applicator with 3 different composition the results as 5.21, 4.88and 4.66Mpa for (30wt%YSZ: 70wt%Ni, 40wt%YSZ: 50wt%Ni: 10wt%Cr and 50wt%YSZ: 30wt%Ni: 20wt%Cr) respectively.

REFERENCES

[1] Bozza, F. and Bellis, V. D. (2014). Steady modeling of a Turbocharger turbine for automotive engines. *ASME J. Eng. Gas Turbines Power*, 136 (011701) 1–13.

[2] Hellstrom, F. (2010). Numerical computations of the unsteady flow in turbochargers. *Technical Reports of Royal Institute of Technology*, Sweden.

[3] Holger, M., Mathias, V., Roland, B. and Andreas, K. (2014). Impact of measurement uncertainty in the characteristic maps of a turbocharger on engine performance. *ASME J. Eng. Gas. Turbines Power,* 136 (021201) 1–12.

[4] Cao, X. Q., Vassen, R. and Stoever, D. (2004). Ceramic materials for thermal barrier coatings. *J. Eur. Ceram.Soc.* 24 (1) 1–10.

EFFECT OF FLY ASH ADDITION REINFORCEMENT ON THE MICROSTRUCTURE AND MECHANICAL PROPERTIES OF ALUMINIUM CASTING ALLOY AA6061

Mainuranis Meor Shamsool and Uday M.Basheer Al-Naib
School of Mechanical Engineering, Faculty of Engineering,
Universiti Teknologi Malaysia, 81310 UTM Skudai, Johor, Malaysia

INTRODUCTION

FLY ash (FA) has a higher demand as reinforcement due to its potential for metal matrix composites (MMCs) to enhance the properties and reduce the cost of production. Fly ash is the most cheapest and lower density reinforcement available in large quantities as solid waste by-product. Aluminium alloys is the highest demand in the industries due to its mechanical properties and low density compare to steel. However, due to certain weakness at the aluminium alloy it needs reinforcement in order to improve the performance of the aluminium alloy. The addition of reinforcement will help to extend the usage of aluminium alloy in many applications such as under wider service conditions. In this paper, stir casting technique is be used in order to fabricate the A6061-Fa composite. During the stir casting process, the different percentage of fly ash will be added into the AA6061 matrix. The percentage that been used in this project was 3%, 5% and 7%. This study will investigate the effect of fly ash addition on the mechanical properties and microstructure of AA6061-Fa composites.

EXPERIMENTAL SETUP

This section presents the experimental setup for the system. We used fly ash that been provided by Tanjung Bin Company and AA6061 alloy as raw material. Stir casting technique is used to fabricate the AA6061-Fa composite. During the casting process, three differences percentage of fly ash is added into molten matrix. After finish the casting process, molten matrix will be poured into steel mould for solidification process. Ingot will produce after the solidification process and it will be cut into tensile specimen. The mechanical properties and microstructure of AA6061-Fa composite will be studied in this project.

.

RESULTS AND DISCUSSION

1. The tensile strength of AA6061 alloy increased as increases of percentage of fly ash (figure 1).
2. The microhardness and the strength significantly increased with increase of fly ash content (figure 2).
3. The microstructural results showed good distribution of FA particles in the AA6061 matrix with interfacial bonding as the percentage of fly ash in increasing (figure 3).

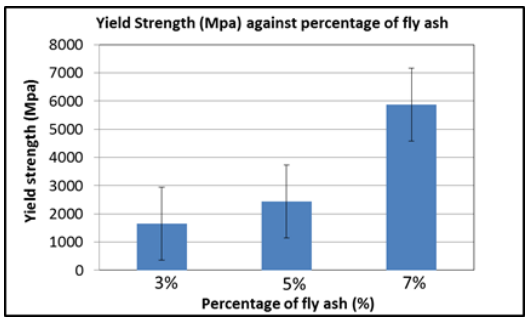

Figure 1: Increase of yield strength as the percentage of fly ash increase

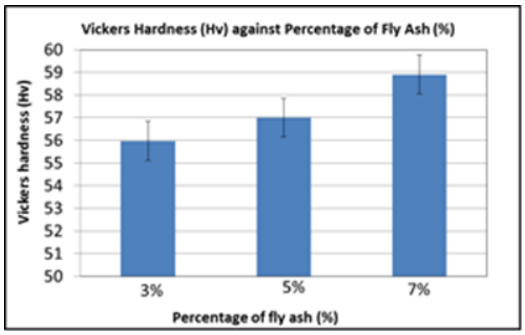

Figure 2: Increase of hardness as the percentage of fly ash is increase

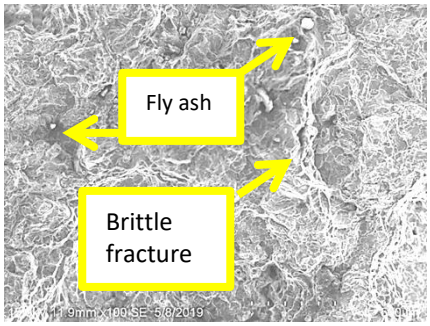

Figure 3: FESEM images of AA6061-Fa composite at 7% of fly ash fracture surface

CONCLUSION

As conclusion, it shows by increase the percentage of fly ash, it will improve the mechanical properties of the matrix. As the percentage of fly ash is increase, the good distribution of fly ash will be.

REFERENCES

[1] Mohammed Razzaq, A., et al., Effect of fly ash addition on the physical and mechanical properties of AA6063 alloy reinforcement. Metals, 2017. **7**(11): p. 477.

MAGNETIC MICROBEADS TRAPPING USING PERMANENT MAGNET

Nurul Zafirah Zaini and Ummikalsom Abidin
School of Mechanical Engineering, Faculty of Engineering,
Universiti Teknologi Malaysia, 81310 UTM Skudai, Johor, Malaysia

INTRODUCTION

Over recent years, there has been an explosive growth of interest microfluidic studies especially on the separation technique of permanent magnet. It is commonly used for manipulation and analysis of fluid flow because the system requires small amount of sample and due to the reduction of fabrication cost and it offers multivariable functions [1]. Permanent magnet provides simple setup and higher biocompatibility [2] that utilize microbeads that are used as a carrier in medical application such as resonance imaging, hyperthermia and medicine delivery [3]. The trapping efficiency of the system were investigated using different flow rates and configurations of magnets.

EXPERIMENTAL SETUP

This section presents the experimental setup for the system. A dual syringe pump with model of NE 4000 (KdScientific) was used to manipulate the flow rate at 5, 10, 15, and 20 µl/min. A 10 ml B-D syringe was attached to the pump and the syringe tip was connected to the 2 mm tube at the inlet of microchannel. An end of 2mm tube was linked to the outlet and the other end was placed into 10 ml bottle were collected the samples for each flow rates.

Microscopic images of all the samples were analysed by using ImageJ software to calculate the amount of microbeads at the outlet.

RESULTS AND DISCUSSION

The percentage of trapping efficiency at each flow rates were obtained as shown in Figure 1. At lower flow rate of 5 µl/min, the trapping efficiency were 92.06% and 95.24% for single and double magnet respectively. In contrast, as flow rate increases at 20 µl/min, the trapping efficiency dropped significantly at 15.87 % for single magnet and 20.63% for double magnet.

The permanent magnet was not capable to trap more microbeads at higher magnets because higher drag forces were generated with higher flow rates. Trapping action was highly effective when magnetic force bigger than drag force. In this experiment, the value of magnetic force was fixed as same magnet was used while the experiment was conducted. The permanent magnet loses the ability to capture microbeads in the trapping chamber when the drag force was higher than the magnetic force as the microbeads followed the dynamic flow in the fluid chamber and experienced less attraction from the permanent magnet due to minimum effect of magnetic properties.

The comparison between both configurations of magnet shows that there is no significant difference of trapping efficiency throughout all the flow rates. The factors that contribute to the differences between the trapping efficiency of single and double magnet were the intrinsic properties, extrinsic properties and the structures of the magnetic beads.

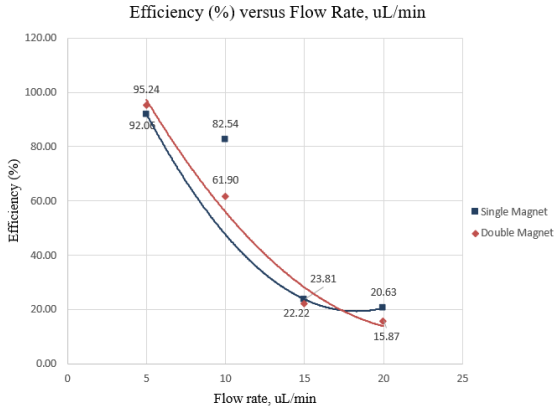

Figure 1: Graph of efficiency versus flow rates

CONCLUSION

The trend shown in this study is at lower flow rate, the trapping efficiency is higher. As flow rates increases, the trapping efficiency decreases. The relationship of trapping efficiency and configuration of magnet is insignificant.

REFERENCES

[1] Yılmaz, B., & Yılmaz, F. (2018). Lab-on-a-Chip Technology and Its Applications. Omics Technologies and Bio-Engineering, 145–153. https://doi.org/10.1016/B978-0-12-804659-3.00008-7

[2] Sackmann, E. K., Fulton, A. L., & Beebe, D. J. (2014). The present and future role of microfluidics in biomedical research. Nature, 507, 181..

[3] Shoshi, A., Schotter, J., Schroeder, P., Milnera, M., Ertl, P., Charwat, V., … Brueckl, H. (2012). Magnetoresistive-based real-time cell phagocytosis monitoring. Biosensors and Bioelectronics, 36(1), 116–122. https://doi.org/10.1016/J.BIOS.2012.04.002

OUTDOOR ATMOSPHERIC WATER GENERATION USING THERMOELECTRIC COOLER

Ahmad Izzat Hussain and Ummikalsom Abidin
School of Mechanical Engineering, Faculty of Engineering,
Universiti Teknologi Malaysia, 81310 UTM Skudai, Johor, Malaysia

INTRODUCTION

Water has been an essential element for human survival. With all these issues on water supply and basic sanitization, an alternative for water supply must be researched to help resolve these issues. With the device known as atmospheric water generator (AWG), we can convert water vapour into liquid water. This device takes advantage of Peltier effect by using a device called thermoelectric cooler (TEC). Peltier-based concept works by using an electric current to produce a temperature gradient, thus cooling surrounding air until dew point temperature, where condensation occurs.

EXPERIMENTAL SETUP

Sensor DHT22 was used for measuring humidity and temperature. A source code was developed for Arduino and the result is printed on serial monitor. The sensor was calibrated by using a hygrometer, and the correction was placed into the Arduino code. For this experiment dehumidifier chosen is XROW-600A. The TEC component inside this dehumidifier is called TEC1-12706. Other components and instrument included are laptop fan, anemometer and measuring cylinder

RESULTS AND DISCUSSION

At the end of experiment, it was found that as the value of RH increases, the water generated by dehumidifier will increase. The average water generated during the day is 11.83 ml/hr while during the night is 12.75 ml/hr. During the day, total amount of water generated is 118 ml while during night is 156 ml. Figure 1 shows the difference between day and night water generation. The study on airflow velocity effect on water generation shows that the higher airflow velocity will have a negative impact to the amount of water generation by dehumidifier. Where there was no airflow, the water produced was 6.33 ml/hr while when there is airflow, the maximum water generated was 5.5 ml/hr. Figure 2 shows the effect of airflow on water generation.

Looking at the bar chart plotted in Figure 3, the AWG that uses higher amount of power for its system generally will increase the water generation rate. However, for Amir's AWG, even though it uses a lower power consumption than Suryaningsih's AWG, the amount of water generated is relatively higher. Even when compared to current study and Kiara's AWG, the amount of water generated by Amir's AWG is really high. This may happen because all studies did not put an emphasis on the design of fin at the cold side of TEC, except for Amir. Amir's studies also included the design of fin extended surface

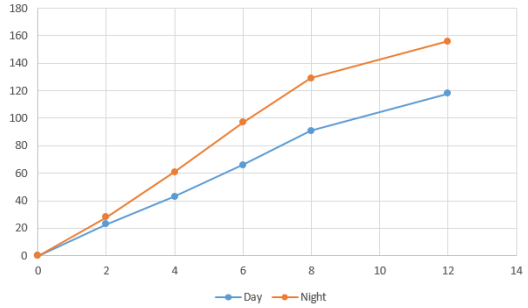

Figure 1: Time vs water generated

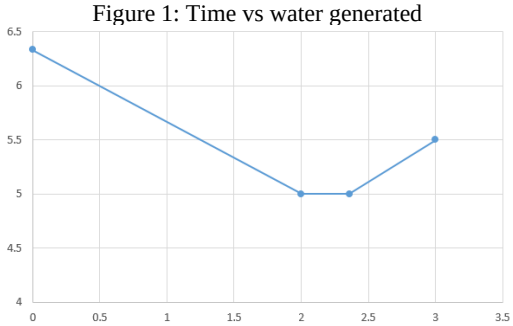

Figure 2: Airflow velocity vs water generated

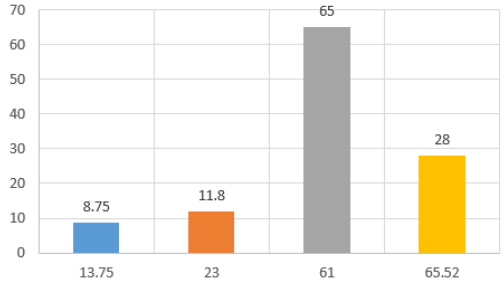

Figure 3: Power vs water generated

CONCLUSION

This experiment shows that the AWG will behave differently at different conditions. Generally, higher RH will produce higher water generation, higher airflow velocity will produce lower water if time is short and higher power will produce higher water generation.

REFERENCES

[1] Suryaningsih, S. and Nurhilal, O. (2016) 'Optimal design of an atmospheric water generator (AWG) based on thermo-electric cooler (TEC) for drought in rural area', in *AIP Conference Proceedings*, p. 030009.

[2] Liu, S., He, W., Hu, D., Lv, S., Chen, D., Wu, X., Xu, F. and Li, S. (2017) 'Experimental analysis of a portable atmospheric water generator by thermoelectric cooling method', in *Energy Procedia*, pp. 1609–1614.

EVALUATION OF THERMOELECTRIC BASED ATMOSPHERIC WATER GENERATOR FOR INDOOR CONDITIONS

Nabilah Mohd Sham and Ummikalsom Zainal Abidin
School of Mechanical Engineering, Faculty of Engineering,
Universiti Teknologi Malaysia, 81310 UTM Skudai, Johor, Malaysia

INTRODUCTION

Water is very important for the life continuity of living being, The number of fresh water source that is being polluted is increasing by day. A thermoelectric (TEC) based Atmospheric Water Generator (AWG) is an alternative way to generate water as it extracts water vapour from air for drinking or for general use. The TEC/Peltier module is an electrical component that acts as a heat pump that has a cold and a hot side. The cold side temperature will drop below the dew point temperature of the air in order to condense the water vapour.

EXPERIMENTAL SETUP

This section presents the experimental setup for the system. Two TEC dehumidifiers were used as AWG as they have the same function and used the same components. The Peltier module used was TEC-12706. The experiment was divided into two, firstly the baseline study o understand how the water production would differ during day and night. Next, one of the AWG was used as a control while the other was modified where a fan was added to the set up to see whether it would affect the water production. Finally the fan was used together with an air channel to investigate the effectiveness of an air channel in producing more water. The water sample collected was then sent for water quality testing.The AWG was used together with an Arduino based sensor, the DHT22 sensor to monitor the ambient temperature and RH of the room.

RESULTS AND DISCUSSION

While the experiment was running the data from the sensor could be plotted to observe the temperature ad relative humidity (RH) variation during day and night. It was found that the temperature rises as the day progresses and declines during night time. This is because during the day, the sun acts as a major source of heat that is absent at night.

It was also found that as temperature rises, the RH decreases. This is because higher temperature can hold more moisture. Therefore for a fixed amount of moisture, when the capacity to hold moisture increases, the RH will decrease. This explains the declining RH during the day and rising RH at night.

Next, the variation of the indoor RH was not significant as the RH of the room is relatively stable. The range of RH recorded in the room was between 85%-89%. Therefore the amount of water collected per hour was also relatively constant. The average volume of water collected were 12 ml/hour.

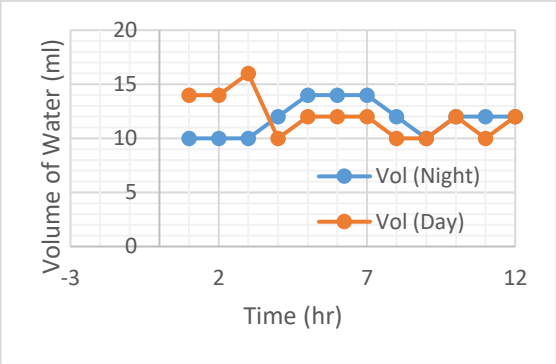

Figure 1: Shows the variation of water collected during the night and day session.

When the only the fan was attached to the AWG, the volume of water collected decreased after 3 hours compared to controlled AWG. However, when it was used together with an air channel, the amount of water collected had increased. This is because the channel had guided the air to flow through the cooling surface more effectively [1].

The water collected showed higher pH and ammoniacal nitrogen than the standard set by the Ministry of Health (MOH), Malaysia. Therefore, in order to consume the water, it needs to go through distillation or neutralisation in order to comply with MOH standard.

CONCLUSION

RH increases with decreasing temperature. As RH increases, more water can be collected from the surrounding. The water collected are relatively constant as the change in RH is insignificant enough. Experiment needs to be run in rooms of different sizes to study the variation of RH in the room that'll will affect the water production.

REFERENCES

[1] Yao, Y., Sun, Y., Sun, D., Sang, C., Sun, M., Shen, L., & Chen, H. (2017). Optimization design and experimental study of thermoelectric dehumidifier. Applied Thermal Engineering, 123, 820–829.

MAGNETIC MICROBEADS TRAPPING USING MAGNET WIRE

Badrul Amin Hanafi and Ummikalsom Abidin
School of Mechanical Engineering, Faculty of Engineering,
Universiti Teknologi Malaysia, 81310 UTM Skudai, Johor, Malaysia

INTRODUCTION

Cell separation is a key for lab-on-chip (LOC). One of the technique for the cell separation is by using magnetic separation through the microchannel [1]. One of the method that can be used for the cell separation is by using magnet wire. The effectiveness of the separation is the main key for the application of the cell separation. Polydimethylsiloxane (PDMS) is being used for replica molding to create the microchannel from SU-8 mold. This paper will explain about the trapping efficiency of microbeads that pass through the SU-8 microchannel with the different flowrate and different current supply.

EXPERIMENTAL SETUP

The preparation of the experiment had been done, PDMS replica molding had been carry out by using SU-8 mold to get the PDMS microchannel. Then, the fabrication of the of spiral planar coil using 0.3 mm copper enamel wire had been carry out. Measurement of magnet wire is compulsory to check the functionality.

For the experiment, the PDMS microchannel and magnet wire were set up. The trapping efficiency of the magnetic microbeads is being study by varying the value of flowrate and current.

The ImageJ software had been used to analysed all the capture image to calculate the amount of microbeads at the outlet

.

RESULTS AND DISCUSSION

The measurement of the magnet wire show that the coil as figure below:

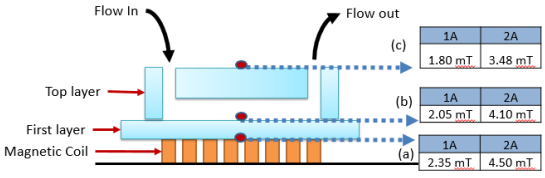

Figure 1: Magnetic Strength measured

Trapping of microbeads will happen if it attracts to the magnetic field produce at the first layer if the value of the magnetic field is higher than the drag force of the microbeads. The reading for 2 A has the higher magnetic strength compare to 1A. For 1A, the range of the 1.8 mT to 2.05 mT while for 2A is 3.48 mT to 4.5 mT.

The trapping efficiency of the microbeads can be calculated by the formula

$$\text{Trapping Rate} = \frac{(input\ -\ outlet)of\ microbeads}{input\ of\ microbeads} \times 100$$

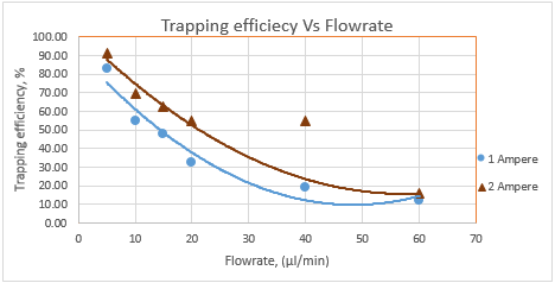

Figure 2: Graph Trapping efficiency vs Flowrate

The higher the current, the higher the trapping efficiency but across the increasing value of flowrate the efficiency will be reduce for both of the current value. As the drag force of the microbeads increase, the magnetic force cannot overcome the drag value and pass through the magnetic field. The trapping efficiency will be drop The result shows a huge reduction as the flow rate for both 1A and 2A passes 15 µl / min. The trapping that is higher than 50% efficiency can be seen from 15 µl/min or 20 µl/min only. Lastly, the graph shows the polynomial curve to indicate the trapping drop significantly after 20 µl/min

CONCLUSION

The PDMS microchannel and magnet wire fabrication was carried out and tested successfully. The microbeads trapping efficiency was performed, calculated and recorded. For 1A, the highest efficiency is at 82.86% at 5 µl/min and the lowest is 12.14%. at 60 µl/min. For 2A, the highest efficiency 91.43% at 5 µl/min and the lowest is 15.71%. at 60 µl/min.

Thus, two things that can be justified by microbeads trapping efficiency. As the current increase, the efficiency will be higher, but at the low flow rate. As the flow rate increases, the efficiency percentage drops both parameters. Overall, all the experiment's goal was achieved

REFERENCES

[1] Cao, Q., Han, X., & Li, L. (2014). Configurations and control of magnetic fields for manipulating magnetic particles in microfluidic applications: Magnet systems and manipulation mechanisms. Lab on a Chip, 14(15), 2762–2777.

DESIGN AND CHARACTERIZATION OF SORBENT BED BASED ATMOSPHERE WATER (AWG)

Muhamad Hafizul Ariff and Ummikalsom Abidin
School of Mechanical Engineering, Faculty of Engineering
Universiti Teknologi Malaysia, 81310 UTM Skudai, Johor, Malaysia

INTRODUCTION

Atmosphere water generator is a device that using dehumidification concept to extract moisture from the humidity in the air and turn it into a water. The air will condense to become a liquid and for the atmosphere water generator that using a filtration system, the liquid produced must passed through the system before being stored in the tank [1]. Sorbent bed-based method is the method that using material to absorb or adsorb liquids or gases. In this case, the material will adsorb water vapor from atmosphere and release them as water droplet. The purpose of having the Atmosphere water generator placed in Malaysia is a benefits because of humid climate and high in relative humidity value. Malaysia has clear sky in the day for the whole year with the range of 3.7 to
8.7 hours per day while the amount of sunshine received is about six hours per day. The relative humidity value ranges from 74% to 86% throughout the years [2].

EXPERIMENTAL SETUP

The experiment begin with the selection of the location of the experiment. Selected location must be measured the value of relative humidity and temperature using DHT-22 sensor and Arduino controller that had been calibrated. Calcium chloride had been used as a solid adsorbent to adsorb moisture from air. The measurement parameter of the adsorbent is 200g, 300g and 400g. The adsorbent had been placed inside the water container and leave in the time range of adsorption process at selected location.

Desorption process using the same parameter is conducted after adsorption process end within it range of time. Water production at the end of desorption process will be measured before water quality test were conducted.

RESULTS AND DISCUSSION

At the end of the experiment, the water production results were tabulated in Table 1. The amount of water produced from different mass of calcium chloride is presented and discussed. The average humidity and temperature value when doing the experiment is recorded and the relationship between them with amount of water generated is shown in Figure 1. Calcium Chloride dissolves into a liquid brine partially due to the fact that it is able to attract several times its own weight in water [3] Furthermore, the different characteristic between silica gel and calcium chloride has been analyzed and the adsorption weight after adsorption phase is measured. The average diameter between the adsorbents also being conducted and compared with the weight after adsorption phase. Nevertheless, the water sample from the experiment has been compared to the drinking water standard provide by MOH

Table 1: Volume of water produced for different mass of CaCl.

Mass Cacl (g)	Water produced	Avg RH during adsorpti	Avg temp during adsorpti
200	100	96.73	28.2
300	156	97.06	28.73
400	200	97.09	28.4

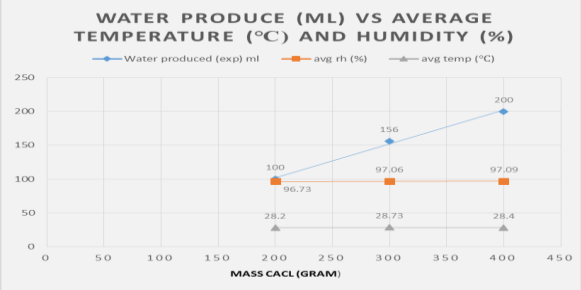

Figure 1: Relationship between water produced and average Rh and T value.

CONCLUSION

The objectives of this experiment is achieved. The water sample has been analysed and compared to the drinking water standard provide by MOH and the results show that the water sample is not suitable for drinking.

REFERENCES

[1] A. Tripathi, S. Tushar, S. Pal, S. Lodh, Tiwari, and P. R. S. Desai, “Atmospheric Water Generator,” vol. 5, no. 4, pp. 69–72, 2016.

[2] N. Jamaludin and N. Izma, “Thermal Comfort of Residential Building in Malaysia at Different Micro-Climates,” *Procedia - Soc. Behav. Sci.*, vol. 170, pp.613–623, 2015.

[3] C. Badrakia, “Performance Review of Aqueous Calcium Chloride Liquid Desiccant Based Air Dehumidifier for HVAC Applications : A Review,” vol. 2, no. 12, 2015.

QUALITY IMPROVEMENT AT DRAWING PROCESS IN WIRE MANUFACTURING COMPANY

Nurul Khairin Nisa' Anddrye and Wan Nazdah Wan Hussin
School of Mechanical Engineering, Faculty of Engineering,
Universiti Teknologi Malaysia, 81310 UTM Skudai, Johor, Malaysia

INTRODUCTION

In this study, the drawing process at the Small Wire rope Factory (SWF) of Kiswire Company is looked into with the aim in mind to improve the quality of the process. As such, quality of the product should and must be ensured at all times. This means that the rate of defects must be minimized where applicable. The defects of wire were observed by using Six Sigma. Six Sigma is a structural and systematic method for development of processes and the Improvement of new techniques, with the purpose of reducing defects defined by customer (1). In order to obtain lower rate of defects, the main causes of defects needed to be identified to propose improvement.

METHODOLOGY

A Six Sigma approach was taken which is the DMAIC steps. Defining the problem, measuring them, analyzing for root causes, propose improvement and controlling them. The main problem identified is wire break. Through analysis, the factors contributing to wire break are found which are lumpy, tangle and welding. Further analysis is done to find the root causes of these three factors. Then, countermeasures are proposed and controlled.

RESULTS AND DISCUSSION

From analysis, the most significant parameters that influences the lumpy are found which are size of diameter, temperature of zinc and dipping length. Design of Experiment (DoE) was conducted to know the optimum settings to minimize the diameter of wire after coating that causes lumpy. For tangle problem, a No-Go Gauge was designed to avoid worn out or deformed bobbins. Another countermeasure is the traverser pitch was set up to make sure different pitch for left and right coiling. Lastly for welding, monthly evaluation is scheduled to ensure the improvement of operators. The implementations were done early March and the frequency of defects are as shown in table below.

Table 1: Frequency of defects

Factory		Unit	Result	Target	Result 2019			
			2018	2019	Jan	Feb	Mar	Apr
Wire Break		no.	1,056	482	45	51	**27**	**28**
1.	Lumpy (>2.04mm)	no	49	~	3	2	**1**	**1**
1.	Lumpy (<2.04mm)	no	480	~	6	6	**4**	**3**
2.	Welding	no	31	~	2	1	**2**	**1**
3.	Tangle	no	141	~	15	13	**4**	**5**

CONCLUSION

We were able to find the root causes of wire break which are lumpy, tangle and welding. Afterwards, countermeasures for each of them were proposed and implemented to reduce their frequency. From the results, we can see that the frequency of the root causes of wire break has been reduced.

REFERENCES

[1] Douglas C. Montgomery, W. H. (2008). An Overview of Six Sigma. International Statistical Review, 329-346.

ERGONOMIC STUDY IN MANUFACTURING COMPANY

Abdul Aziz Mohd Khairuddin, and Wan Nazdah Wan Hussin
School of Mechanical Engineering, Faculty of Engineering,
Universiti Teknologi Malaysia, 81310 UTM Skudai, Johor, Malaysia

INTRODUCTION

Ergonomics is the science of fitting workplace conditions and job demands to the capabilities of the working population by Occupational Safety and Health Administration, Ergonomics (2010). There are kind of hazards occurs in many ways and involves most of the field of works, types of tasks as well as working area. Hazard can be characterized as the working environment or worker movement that have inclination to cause in damage, property misfortune, sickness or the misfortunes in process(DOSH,2008). Ergonomic hazards also can be define as physical conditions that may be pose to risk of getting Musculoskeletal Disorder (MSD). They result from one or more of these tissues being more difficult to work than they are intended to (DOSH, 2018).

METHODOLOGY

Ergonomic hazard can be achieve by conducting the discomfort survey and questionnaire. The ergonomic risk factor was then being clarify on the working activity using an ergonomic assessment which was Rapid Entire Body Assessment (REBA). (McAtemney, 1999) stated that the analyses used to indicate the body part ranges into group A and group B based on the body part diagram from REBA. The part of group A that is trunk position, neck position and leg position. For group B body part is upper arm, lower arm and wrist. Next, a good solution was generated in order to reduce the worker's movement and reduce MSD.

RESULTS AND DISCUSSION

Total of respondent 100% from the respondent is man. This show the worker for this industry fully manipulated by man. There were 5% workers age below 20 years old. 35% workers at the age of 20 to 29 years. 40% worker are from 30 to 40 years and the 20% workers were more than 40 years. By looking at the position the table show that there are all the respondent came from operator.

The highest reported in muscle pain was stranding process with 8 out of 10 respondents meanwhile packaging process reported about 6 having muscle pain. Meanwhile, for drawing and inline process both reported about 6 and 2 respondents respectively in having muscle pain.

Data has been recorded due to the amount of respondents from stranding process claim that they suffer from muscle pain. Result from the survey has proved that workers from stranding process suffer muscle pain at their waist where about 0.8 from total respondent suffer this pain. This statistic show that further study is needed on stranding process in order to reduce the risk of getting muscle pain.

Design has been proposed to achieve the study objective. Design technically depend on safety, ergonomic, cost, user friendly and maintenance cost. The design has been defined using Solidworks. The design also reduce the risk of getting the MSD and reduce the worker movement.

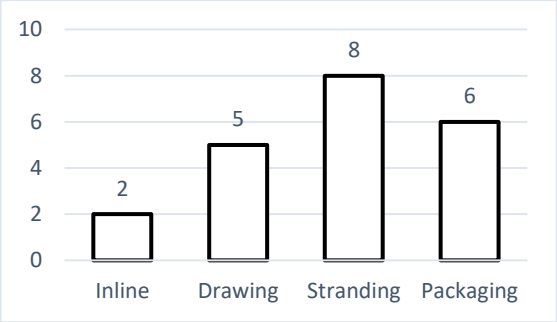

Figure 1: Data recorded on muscle pain report from each process line.

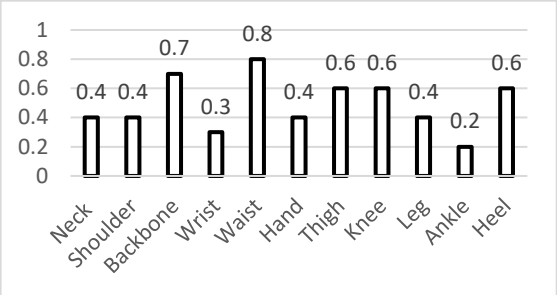

Figure 2: Mean Average of Pain in Stranding Process Operators

CONCLUSION

The issue on ergonomic and health is one of the important things in any industry. This project is about improving ergonomic at manufacturing industry. The main case study in this project is ergonomic problem in selected workplaces. In this thesis, the problem identified and the solution for improvement was advanced.

REFERENCES

[1] Department safety and health Malaysia (2016).Occupational Accidents.
[2] 4. Sue Hignett, Lynn McAtamney. 'Rapid Entire Body Assessment (REBA). Applied Ergonomics'.1999.31(2000):201-205
[3] 7. M. L. Wang 1, H. F. Lin, (2011), 'The Analysis of Musculoskeletal Disorder in Workers in the Food and Baking Industry'

SAFETY IMPROVEMENT AT MANUFACTURING COMPANY

Muhammad Syukri bin Subahir and Wan Nazdah binti Wan Hussin
School of Mechanical Engineering, Faculty of Engineering,
Universiti Teknologi Malaysia, 81310 UTM Skudai, Johor, Malaysia

INTRODUCTION

Until 2018, the highest recorded accident is manufacturing sector with total of 1303 cases recorded [1]. This including industry of wire rope manufacturing. Safety always been a concerned of any individual or organization. Safe workplace is one of the key for workers to have enjoyment in health, security and opportunity to achieve or get what we want [2]. Hazard Identification, Risk Assessment and Risk Control (HIRARC) method was planned and implemented to manage risk. HIRARC was used to identify possible hazards by studying operation involved in drawing process and stranding process. Survey and interview from both employers and safety officer to have expert evaluation regarding to the studies.

RESULTS AND DISCUSSION

As the HIRARC completed, two hazard from two different process of drawing and stranding is identified. Identification is strengthen by the record of previous cases, scenarios example and regulation and laws according to Factory and Machinery act (FMA) 1967, Occupational safety and Health Act (OSHA) 1994.

First hazard identified to give the highest risk is hazard from uncover moving part at drawing machine, due to unsafe act of not placing the safety cover at the right place. The second hazard is hazard of uncover roller due to machine have no cover or safety guarding facilities.

Cause effect diagram is developed regarding to effect of both hazard. The causes that included are from man, machine, environment, and material/equipment.

PROPOSED SOLUTION AND DESIGN

Hazard on uncover moving parts (wire and cooling block) is proposed with solution of engineering approach (automation), using the concept of Poka-Yoke (mistake proofing). The technical concept on how the automation work are as follow:

i. Safety cover not at right place will trigger limit switch momentarily using physical motion.
ii. Limit switch put the whole machine into open circuit and machine will not operate
iii. As the safety cover put at the right place, limit switch toggle will back to original place
iv. Circuit of machine closed and machine can operate normally.

Workers left with no choice but to follow the system in order to complete their task.

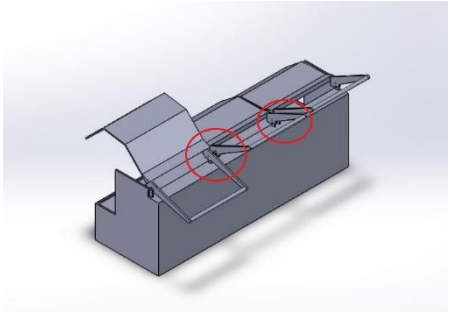

Figure 1: Limit switch placement (red circle)

Hazard on uncover moving roller also proposed with solution of engineering approach. The specified approach is known as barrier. Safety guard proposed are safety cover and sliding fence. Safety cover is chosen due to higher score in selection matrix relative to fulfilment of customer's requirement. Analysis using von mises stress analysis on SolidWork software is used in the need of customer's requirements.

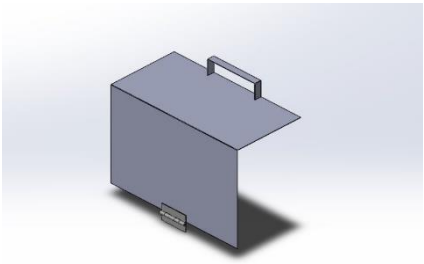

Figure 2: Safety cover design for roller

CONCLUSION

Hazard chosen is based on the highest risk from (HIRARC). Analysis of risk is using qualitative and semi-quantitative approach. HIRARC is developed base on guidelines provided by Department of Safety and Health (DOSH). Both proposed solution is using engineering approach.

REFERENCES

[1] Department of Occupational Safety and Health (DOSH, Guidelines for Hazard Identification, Risk Assessment, and Risk Control, 2008.
[2] Mahalia Soediono, Brian H. Kleiner, (2002) "Developments concerning the Occupational Safety and Health Act", Managerial Law, Vol. 44 Issue: 1/2, pp.37-44

COMPUTATIONAL FLUID DYNAMICS AND EXPERIMENTAL ANALYSIS OF LINEAR TURBINE CASCADE

Mohammad Noor Iman Kamari and Wan Zaidi Wan Omar
School of Mechanical Engineering, Faculty of Engineering,
Universiti Teknologi Malaysia, 81310 UTM Skudai, Johor, Malaysia

INTRODUCTION

The efficiency of the gas turbine engine is based on the performance of the turbine blades inside the engine. Thus, there are several studies regarding on flow analysis through a linear turbine cascade and the purpose of these studies is to understand and investigate the flow behaviour around the turbine cascade. The turbine blades inside a linear cascade were designed to have aerodynamic similarity as in the real machine [1]. The experimental testing was conducted by measuring static pressure distribution around the turbine blade as this is the common parameter measured in many types of flow analysis [2]. For the current work, the investigation of linear turbine cascade will involve of experimental testing and computational simulation.

METHODOLOGY

For this case study, it is emphasized on the experimental and CFD analysis and the validation study will be conducted by comparing the data between the CFD and experimental. For the experimental testing, the pressure taps have been installed around the turbine blade in order to measure the static pressure distribution for several different incidence angles by using multi-manometer transducer system.

For the CFD analysis, the simulations have been conducted for several different incidence angle which is same as the experimental. A suitable method for modelling the flow through a linear turbine cascade have been determined and the effect of different incident angle to the aerodynamic characteristics of the blade will be studied studied as well.

RESULTS AND DISCUSSION

For the mesh independence study, the minimum number of elements require in order to achieve solutions independency were 104224 elements. Meanwhile, the validation study was conducted for three different negative angle and the -40° incidence angle shows a good agreement as the static pressure distribution curve for both experimental and CFD show almost similar pattern. Nevertheless, at the -20° and -30° incidence angles, the static pressure distribution curve at the suction side of the blade show a difference between the CFD and experimental.

For the aerodynamic characteristics, the blade stall region is at the incidence angles between -20° and -40°. The highest drag coefficient of the turbine blade is at -40° incidence angle and this can be observed from the flow visualization figures which show that as the incidence angle changed from the 20° to -40°, the flow separation is getting larger and cause the blade drag to increase.

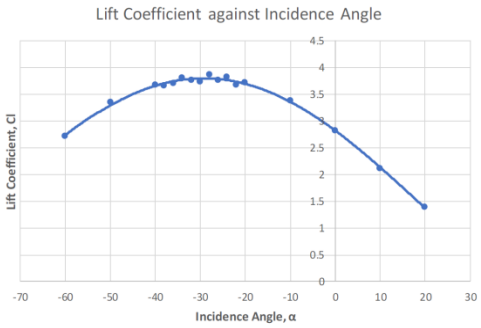

Figure 1: Lift Coefficient Graph

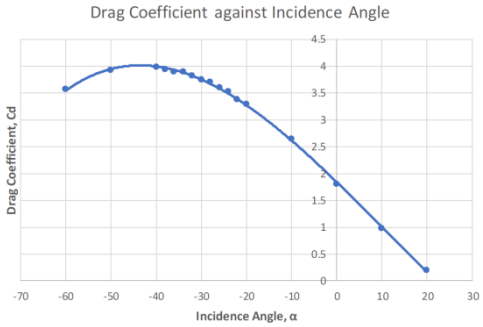

Figure 2: Drag Coefficient Graph

CONCLUSION

From the studies, it can be concluded that the optimum conditions for the turbine blade to achieve high lift coefficient is at the incidence angle between -10° and 10°.

REFERENCES

[1] Ingram G. L. *Endwall Profiling for the Reduction of Secondary Flow in Turbines*. Durham Theses, Durham University; 2003

[3] Treaster, A. L. and Yocum, A. M. (1979). The calibration and application of five-hole probes. *ISA Transactions*, 18(3), 23 – 34.

DESIGN AND TEST A PERMANENT MAGNET GENERATOR SUITABLE FOR LOW ROTATIONAL SPEED INPUT

Nurul Ain Zakaria and Wan Zaidi Wan Omar
School of Mechanical Engineering, Faculty of Engineering,
Universiti Teknologi Malaysia, 81310 UTM Skudai, Johor, Malaysia

INTRODUCTION

Development of permanent magnet generator (PMG) has been receiving an endless amount of attention for application in direct-driven power due to its simple structure, reliable performance and high availability of permanent magnets [1]. PMG is used in vast range of applications and its design varies according to its purpose and area of application.

METHODOLOGY

A design of a PMG for low rotational speed input and small-scale application is made. The selection and acquisition of materials are made prior to fabrication process. Each part of the PMG is measured and fabricated by using machines and tools safely. The final prototype is an axial flux PMG with 16 poles and 12 coils is manufactured. The product is tested by using oscilloscope to study the relationship between variables.

.

RESULTS AND DISCUSSION

The amount of voltage generated at different rotational speed when all coils are connected alternately in series is illustrated in Figure 1.

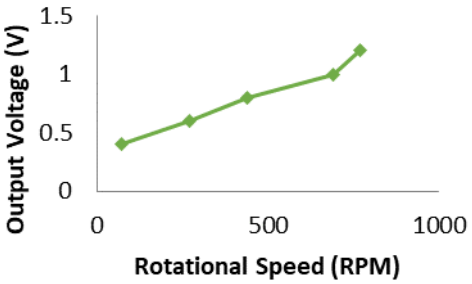

Figure 1: Output voltage at different speed

From the results above, it shows that when speed increases, the induced voltage increases as well. This is due to higher rate magnetic flux passing through the coil [2].

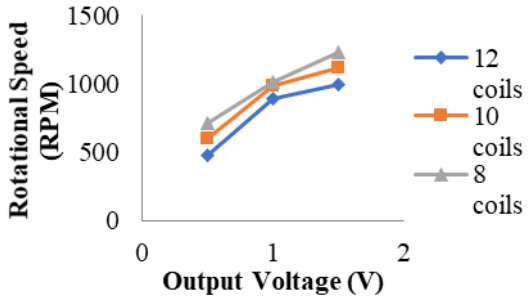

Figure 2: Rotational speed for different number of coil to induce same value of EMF

The variation of rotational speed to induce EMF of 1.0 V, 1.5 V and 0.5 V for three different numbers of coils are shown in Figure 2.The results shown indicate that; the higher the number of coils cuts through magnetic field, the lower the rotational speed it needs to rotate to produce same amount of voltage. This is because higher number of coil will have more flux cutting which will generate more EMF.

The effect of arrangement and direction of coils on induced EMF is illustrated in Figure 3 below.

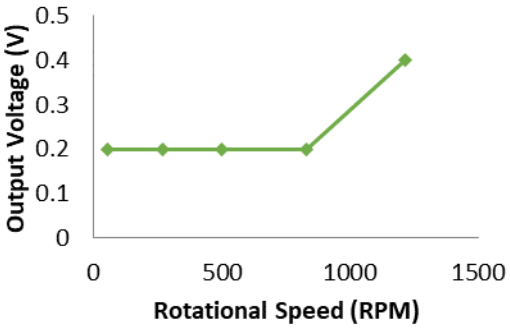

Figure 3: Output voltage at different speed for coils connected in same direction

When all coils are connected in same direction, the direction of changes of magnetic flux will be cancelled out [3].

CONCLUSION

In conclusion, the designed PMG is suitable for low RPM input shaft and it is low cost. The PMG generates AC voltage that varies due to many factors. This study focuses the effect of rotational speed, number of coils, arrangement of magnets and coils on the AC voltage induced. Further development on PMG should be made as it promotes benefits to power application.

REFERENCES

[1] N. Taran and M. Ardebili, "Multiobjective Optimal Design of an Axial Flux Permanent Magnet Generator for Directly Coupled Wind Turbines," 22nd Iranian Conference on Electrical Engineering (ICEE), vol. 5, pp. 298-305, 2014.
[2] R. C. Dorf and J. A. Svoboda, Introduction to Electric Circuits: John Wiley & Sons, 2010.
[3] M. Sibley, Introduction to Electromagnetism: Elsevier Science, 1995.

DESIGN AND TEST OF A BANKI WATER TURBINE (BWT)

Muhammad Amzar Mohd Asri and Wan Zaidi Wan Omar
School of Mechanical Engineering, Faculty of Engineering,
Universiti Teknologi Malaysia, 81310 UTM Sekudai, Johor, Malaysia

INTRODUCTION

Hydropower is known an ancient technology that already been used throughout the world. Hydro plant goanna be used to generate the electricity from water sources, which is from hilly regions or from water-falls [1]. Hydro plant are suitable to generate electricity in Malaysia due to season which provide a continuous flow of running water all year. For Small River which provide low flow rate, Cross-Flow seems the most suitable because of its design and its function [2]. Cross-Flow or Banki turbine operate by extracting the energy from water flow and transfer it to the shaft to produce output power to run the generator to generate the electricity [2].

EXPERIMENTAL SETUP

This design started by determine the parameter of the water source of E07 UTM River, which the flow rate is 0.04814 m^3/s, head of 1 meter and input power of 236.127 Watt. This parameter used as guideline to design the water turbine.

To design the Banki water turbine, the parameter needed such as runner outer and inner diameter, width of runner, width of the nozzle, angle of attack for blade, blade inlet and outlet angle, blade thickness, blade curvature, blade angle and also the shaft radius. All this parameter are determine from previous research and from technical design of SolidWorks

The blade produce by using 6 inch PVC pipe which 3 mm thickness. For runner plate, aluminium plate be used to support 20 blade. Carbon steel be used as the main shaft.

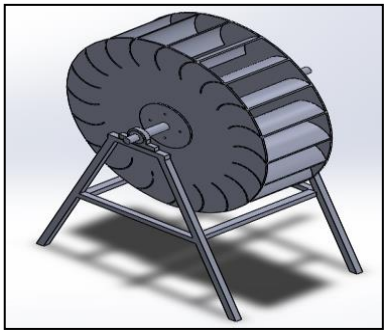

Figure 1: Completely design of BWT

RESULTS AND DISCUSSION

The turbine testing was done at E07 UTM River, which provide flow rate of 0.0043943 m^3/s and input power of 51.7297 Watt at 1 meter head. The load was applied to the shaft starting from 0, 0.75, 1.5, 2.25, 3, 3.75, 4.5, 5.25 and 6 kg of the load. Load applied by using Prony brake to determine the torque produce by the shaft at certain RPM.

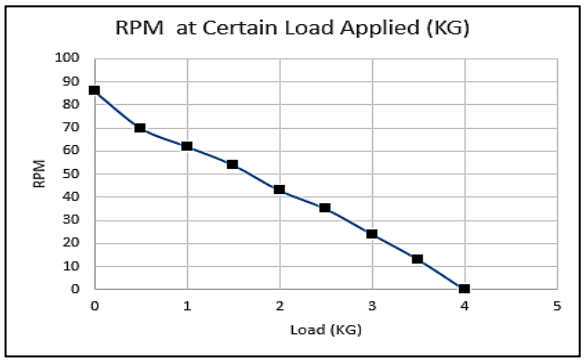

Figure 4: RPM produce at certain load

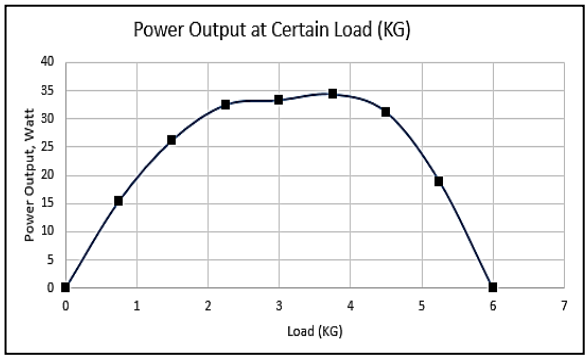

Figure 5: output power produce at certain load applied

From the Figure 4, we can see that the rotation become slower after the load applied increase, and the shaft stop rotating when enough load applied which is 6 kg. So, from the graph the highest output power produce was 34.329 Watt at 3.75 kg load applied. So overall efficiency produce by this Banki Water Turbine was 66% which at 3.75 kg load applied.

CONCLUSION

The Banki turbine is suitable for Small River of low head and flow rate. The output power produce was 34.329 Watt when load 3.75 kg been applied to the shaft. The maximum efficiency produce was 66% and bit lower than current theoretical efficiency which is 75%. This can be improve if certain error during testing can be avoid.

REFERENCES

[1] C. Vincenzo, Armando, Oreste and Tullio, 17 April 2013. Banki-Michell Optimal Design by Computational Fluid Dynamics Testing and Hydrodynamic Analysis.
[2] F. M. Mockmore, February 1949. The Banki Water Turbine.

DESIGN, CONSTRUCT AND TEST A SOLAR POWERED ICE MAKER

Muhammad Hamizan Bin Zaidi and Wan Zaidi Wan Omar
School of Mechanical Engineering, Faculty of Engineering,
Universiti Teknologi Malaysia, 81310 UTM Sekudai, Johor, Malaysia

INTRODUCTION

Refrigeration system is one of the most important systems for food storage and freezing. Conventional vapour refrigeration system needs a lot of electrical power to operate [1]. Solar power has been selected due to high intensity of solar radiation in Malaysia. Furthermore, adsorption system is more choosen because it is simple, requires no additional electricity and quiet in operation [2].

The adsorbent-adsorbate pair used in adsorption refrigeration system is activated carbon-methanol, because it has low desorption and adsorption temperature [3]. Methanol is also often used as refrigerant in ice making system as it able to produce cooling temperature below 0°C [3].

METHODOLOGY

The solar ice maker consists of the solar generator, a condenser, an evaporator ball valves water tank and insulation. The amount of activated carbon and methanol used were 0.7kg and 1.8 kg respectively.

The working principle of this solar powered ice-making machine starts with generator is heated by the solar radiation, which heat up the activated carbon that causes the temperature and the pressure of the methanol to rise. When the activated carbon reaches the desorption temperature, the methanol will desorb and vaporizes from the activated carbon. The desorbed methanol vapour would be condensed into liquid by the condenser and flows into the evaporator.

As the night cycle begins, the temperature and pressure of the generator reduces. This would cause the activated carbon to adsorb back the methanol vapour from the evaporator. The cooling effect is produced when the methanol in the evaporator vaporizes, extracting heat from the water, and ice is formed in the insulated water tank.

RESULTS AND DISCUSSION

From the Figure 1, we can see the temperature of the generator is decreasing from the ambient temperature meanwhile the temperature of the evaporator increases.

The temperature drop of generator and the temperature rise of the evaporator is due to minimal mass and heat transfer of the methanol vapour under vacuum operating conditions. This is due to activated carbon deterioration Therefore, ice could not be produced.

From the Figure 4, we can see at 1800H, a slight increase in pressure as cooling process starts due to methanol in the evaporator starts to evaporates. However, the pressure of the system becomes constant after 30 minutes due to equilibrium pressure reached by the generator and the evaporator which indicates the adsorption process of the methanol vapour come to an end.

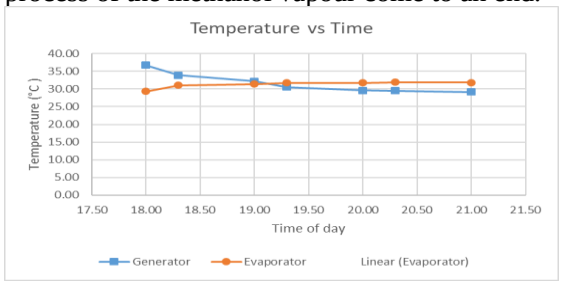

Figure 1: Graph of temperature of the evaporator and generator during cooling process

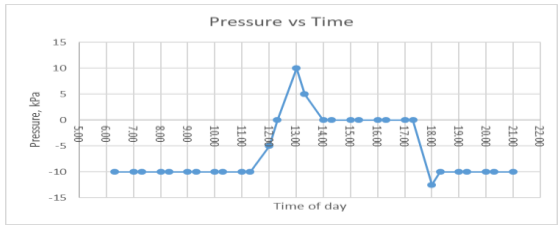

Figure 2: Graph of system pressure

CONCLUSION

The testing of the solar ice maker to produce ice could not be achieved due to the deterioration of activated carbon that unable to adsorb methanol vapour which causes the cooling process to become stall and fail to produce further cooling effect.

REFERENCES

[1] W. A. B. John A. Duffie, Solar Engineering of Thermal Processes, New York: John Wiley and Sons Ltd , 2006.

[2] R. A.O.Dieng, "Literature review on solar adsorption technologies for ice-making and air-conditioning purposes and recent developments in solar technology," *Renewable and Sustainable Energy Reviews*, pp. 313-342, 2001.

[3] R. W. R. O. L.W. Wang, "A review on adsorption working pairs for refrigeration," *Renewable and Sustainable Energy Reviews*, vol. 13, no. 3, pp. 518-534, 2009.

PREDICTING FRICTIONAL LOSSES GENERATED BY PISTON CONNECTING-ROD BIG END JOURNAL BEARING FOR AN INTERNAL COMBUSTION ENGINE

Bryan Chai Yen Book and William Chong Woie Fong
School of Mechanical Engineering, Faculty of Engineering,
Universiti Teknologi Malaysia, 81310 UTM Skudai, Johor, Malaysia.

INTRODUCTION

Friction has long existed as one of the biggest challenges in the automotive industries in producing energy efficient vehicles. The engine system contributed almost one-third of the friction in the overall friction that existed in a vehicle. One of the major frictional losses experienced by an engine system is generated from the piston connecting rod big end journal bearing. Therefore, it is vital to study the tribological performance of the journal bearing in order to mitigate the frictional losses generated along the journal bearing.

RESEARCH OBJECTIVES

The aim of the study is to determine the tribological behaviour and the power loss as a result of friction generated by the connecting-rod big end journal bearing under dynamic loading for a full engine cycle.

METHODOLOGIES

Reynolds equation reflects tremendous insight into fluid behaviour in bearing lubricant films. A simplified version of the 2-D Reynolds equation as shown below is being employed:

$$\frac{\partial}{\partial x}\left(\frac{\rho h^3}{\eta}\cdot\frac{\partial P}{\partial x}\right)+\frac{\partial}{\partial y}\left(\frac{\rho h^3}{\eta}\cdot\frac{\partial P}{\partial y}\right)=12\left\{\frac{\partial(\rho h u)}{\partial x}\right\}$$

Hence, a numerical analysis is used for solving the 2-D Reynolds equation based on Reynolds boundary condition. In addition, the 2-D Reynolds solution was derived by using a combination of approaches, namely finite difference method, Newton-Raphson method, and Taylor expansion series. Nevertheless, the mathematical model for both rigid and deformable journal bearing was also derived.

RESULT AND DISCUSSION

The results simulated from the mathematical model, written in C-language, are compared with the analytical and experimental results from the referred journals [1] and [2], respectively. For low loading conditions, the simulation results from both rigid and deformation models have only shown minor differences, demonstrating correlation with existing analytical and experimental results. However, simulation results from the deformation model assumption is much closer to the experimental results obtained from real engine analysis during high loading condition. Figure 1 shows the minimum oil film thickness between simulation and experimental results.

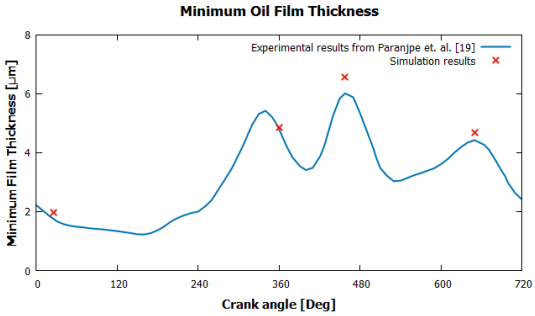

Figure 1: Minimum Oil Film Thickness between Simulation and Experimental results

REFERENCES

[1] Chu, J.H. A Friction Study on Automotive Connecting-Rod Big End Journal Bearing Lubrication System. UGP Thesis. Universiti Teknologi Malaysia; 2017.

[2] Paranjpe RS, Tseregounis SI, Viola MB. Comparison between theoretical calculations and oil film thickness measurements using the total capacitance method for crankshaft bearings in a firing engine. Tribology transactions. 2000 Jan 1;43(3):345-56.

THE EXTENT OF MOISTURE ATTACK TOWARDS MECHANICAL AND TRIBOLOGICAL PROPERTIES OF FIBER REINFORCED EPOXY COMPOSITE MATERIALS

Mohamad Syazwan Azman, William Chong Woei Fong and Wong King Jye
School of Mechanical Engineering, Faculty of Engineering,
Universiti Teknologi Malaysia, 81310 UTM Skudai, Johor, Malaysia.

INTRODUCTION

Epoxy composites are becoming an essential part of today's materials because they offer advantages, such as low weight, corrosion resistance high fatigue strength and ease of component assembly. Its behavior can differ when there is moisture inside the composite [1,2]. This study presents an analysis on two types of composite materials, which are
1) Carbon fiber Reinforced epoxy (CFRE),
2) Flax fiber reinforced epoxy, (FFRE) composite sheet.

RESULT AND ACHIEVEMENT

Table 1 shows the reduction pattern of Young's modulus of CFRE and FFRE composite before and after moisture absorption test. Table 2 and 3 show the coefficient of friction for CFRE and FFRE when rotating against steel and silicon ball respectively. It shows the opposite trend for Young's modulus, which decrease when the moisture content increases in both CFRE and FFRE composite materials. Furthermore, frictional properties are observed to be higher when the composite material is being rotated against the steel ball when compared with the use of silicon nitride ball.

PROJECT OBJECTIVES

The aim of this project is to determine the extent of moisture absorption for both CFRE and FFRE composite.

Table 1: Young's Modulus of CFRE and FFRE before and after moisture test

Type of composite	Young Modulus, E (GPa)		% of Change
	Before	After	
Carbon Fibre Reinforced Epoxy	57.68	54.70	-5.17
Flax Fibre Reinforced Epoxy	3.117	2.106	-32.44

Table 2: Coefficient of friction for CFRE and FFRE when rotated against steel ball before and after moisture test

Type of composite	Coefficient of Friction		% of Change
	Before	After	
Carbon Fibre Reinforced Epoxy	0.146	0.208	42.19
Flax Fibre Reinforced Epoxy	0.137	0.144	4.72

Table 3: Coefficient of friction for CFRE and FFRE when rotated against silicon nitride ball before and after moisture test

Type of composite	Coefficient of Friction		% of Change
	Before	After	
Carbon Fibre Reinforced Epoxy	0.145	0.149	2.98
Flax Fibre Reinforced Epoxy	0.131	0.148	12.81

METHODOLOGIES

Specimens of CFRE and FFRE composite are fabricated using vacuum infusion method. Specimens for moisture absorption test need to be prepared onto six (6) coupon size of 50 mm x 50 mm with 3-ply of every fiber. Specimens for tensile testing need to be prepared in several size in accordance of standard of ASTM D638 and ASTM D3039. Moisture test is conducted using Water bath containing 60° of distilled water. For Tensile test is conducted by using Universal Testing Machine and executed with a rate of 2mm/min to obtain its Young's modulus.
While for friction test, it is conducted based on ASTM G99 by using Pin-on-disk tribo-tester. The applied normal load for the friction test is 20N and for each of the test, the test duration is set to be 60 seconds. The test speed is first set to 500 rpm and the steel and silicon nitride ball's diameter used in this study is 8 mm with a wear track radius of 20 mm. Obtained experimental results for these tests composite materials will then be analysed and correlated.

REFERENCES

[1] Herrera-Franco, E. Pérez-Pacheco :J. I. Cauich-Cupul :A. Valadez-González :P. J. (2013). Effect of moisture absorption on the mechanical behavior of carbon fiber/epoxy matrix composites. Journal of Materials Science, 1873-1882.
[2] Abdul Moudood, Anisur Rahman, Andreas Ochsner, Mainul Islam, Gaston Francucci. (2018). Flax fiber and its composites: An overview of water and moisture absorption impact on their performance. Queensland, Australia: Griffith School of Engineering, Gold Coast Campus, Griffith University.

EFFECTS OF STACKING SEQUENCE ON THE TENSILE BEHAVIOUR OF QUASI-ISOTROPIC COMPOSITE LAMINATES

Wong Tze Thong and Wong King Jye
School of Mechanical Engineering, Faculty of Engineering,
Universiti Teknologi Malaysia, 81310 UTM Skudai, Johor, Malaysia

INTRODUCTION

Conventional laminate theory suggests that a quasi-isotropic composite, fails at the same level with similar tensile strengths regardless of different stacking sequence with constant ply orientations. However, past studies conducted show that even though a quasi-isotropic composite laminate with various stacking sequences have the same stiffness for all, the tensile strengths displayed differently [1,2]. Failure theories of composites were implemented to test the effectiveness and credibility in predicting failures [3].

METHODOLOGY

In this section, MATLAB code was developed to calculate the Classical Laminate Theory against the failure theories (Maximum Stress, Maximum Strain, Tsai-Hill and Tsai-Wu) to determine failure predictive capabilities. A finite element model is then created to perform tensile simulation on four specimens with different stacking sequences ([45/-45/0/90]s, [-45/0/45/90]s, [-45/45/90/0]s and [45/90/-45/0]s) which failure pattern of each lamina was analyzed.

RESULTS AND DISCUSSION

The force per unit length for maximum stress and maximum strain failure theories only satisfy the failure for cross-ply orientation composite which is comprises of only 0 and 90-degree ply orientation. However, both Tsai-Hill and Tsai-Wu failure theories meet the requirements of the ideal ply failure. This is largely due to the nature of the failure theories where Maximum Stress and Maximum Strain do not consider the interaction of strength parameters in direction-1, direction-2 and shear direction whereas Tsai-Hill and Tsai-Wu, both consider. Table 1 shows the ply failure load under different failure theories. The results of a finite element model under tensile simulation of an 8-ply unidirectional laminate also further clarifies that the Tsai-Hill failure theory does have interactive elements and Maximum Stress and Maximum Strain failure theories do not interact well with shear failure at certain ply angles. In ply damage pattern, we can observe that stages and contour of failure is different for 0, ±45 and 90-degree under various stacking sequences. Figure 1 shows the intra-ply stress contour for +45 ply at different stacking sequence. It was found that 0-degree plies in the middle serve as the structure core which will affect the tensile properties of other nearby plies.

Table 1: Force per unit length (N_X) required for each lamina to fail under different failure theories

Ply Orientation	Force per unit length, N_X (N/m)			
	Maximum Stress	Maximum Strain	Tsai-Hill	Tsai-Wu
45	1017000	1017000	720000	770000
90	600000	600000	565000	495000
-45	1017000	1017000	720000	770000
0	900000	900000	900000	900000

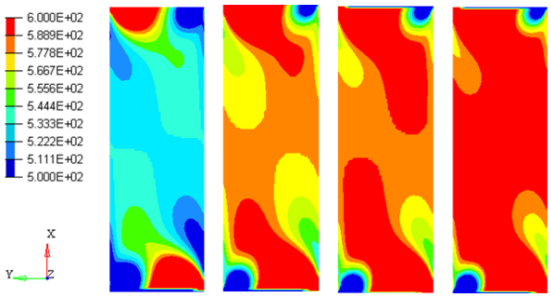

Figure 1: Intra-ply stresses for +45-degree ply orientation of each stacking sequences

CONCLUSION

We have demonstrated the predictive capabilities of the failure theories and effects of stacking sequence towards the tensile properties of a quasi-isotropic composite using finite element simulation. However, more experimental data has to be conducted to further justify the simulation results.

REFERENCES

[1] Grigoriou, K., & Mouritz, A. P. (2017). Influence of ply stacking pattern on the structural properties of quasi-isotropic carbon-epoxy laminates in fire. *Composites Part A: Applied Science and Manufacturing*, *99*, 113-120.

[2] Majidi, B., Hessabi, Z. R., & Aghazadeh, J. (2005). Effect of Stacking Sequence on Fracture Mechanisms in Quasi-isotropic Carbon/Epoxy laminates. *Iranian Polymer*, *14*(6), 531-538.

[3] Hinton, M. J., Kaddour, A. S., & Soden, P. D. (2002). A comparison of the predictive capabilities of current failure theories for composite laminates, judged against experimental evidence. *Composites Science and Technology*, *62*(12), 1725-1797.

QUALITY IMPROVEMENT AND REDESIGN OF A PRINTER COMPONENT

Yeap Rong Kai and Wong Kuan Yew
School of Mechanical Engineering, Faculty of Engineering,
Universiti Teknologi Malaysia, 81310 UTM Skudai, Johor, Malaysia

INTRODUCTION

The use of techniques and activities to achieve and sustain the quality of a product is known as quality control. Whereas, the use of techniques and tools to improve the product or service is known as quality improvement. Statistical quality control (SQC) is a tool for use in quality activities, which is the collection, analysis, and interpretation of data. Quality assurance is the systematic actions or plans to make sure a product or service meets the quality requirements. This includes a continuing evaluation of adequacy and effectiveness with a view to having timely corrective measures and feedback initiated where necessary [1].

METHODOLOGY

Product average usage life and customer reported issue are collected. SPC and AHP analytic tools are used to analyse the collected data. Vibration experiment is then carried out to determine the suitable weight range for the counterbalance. Seven conceptual design are created for redesign counterbalance. The best design has chosen by evaluating through PDS and VOC. Detailed design is created. The design is then undergone simulation analysis. The simulation result is verified by comparing theoretical and actual results. Five samples of counterbalance have added certain weight and tested to validate the results.

RESULTS AND DISCUSSION

At the end of problem identification, bearing failure and vibration have the highest rank after analysis as shown in Figure 5. Whereas, the spoiled bearing sample had inspected by bearing expect. The result of bearing sample had reported bearing specification is in control, and the bearing failure is due to other factors. Thus, component redesign will be focusing on reducing the vibration that cause shuttle jam.

160 gram of additional weight is determined as a suitable additional weight for current counterbalance through vibration experiment as shown in Figure 6. Whereas, instead of 160 gram, 150 gram has been chosen. 10 gram reduction is an anticipation plan for the weight tolerance of counterbalance. The redesign counterbalance as shown in XX. Counterbalance might be produced underweight or overweight. Anticipation plan with underweight is chosen as additional weight on the counterbalance has less cost compare to the cost of weight reduction process. Additional weight plate has lower cost. Weight reduction process for each overweight counterbalance involve direct cost and overhead cost.

	Weightage of Criteria	0.31190	0.49048	0.19762			
No.	Criteria	Severity	Occurrence	Detection	Rank	Score	Pareto	%
6	Bearing Failure	0.09747	0.20518	0.25086	1	0.216151393	1	100%
4	Shuttle operating vibration	0.05076	0.32123	0.02639	2	0.162624316	0.783848607	78%
1	Shuttle operating temperature	0.05076	0.04305	0.25086	3	0.13821098	0.62122429	62%
3	Shuttle operating angle	0.05076	0.04305	0.12041	4	0.07891477	0.48301331	48%
2	Shuttle operating period	0.01721	0.04305	0.12041	5	0.075865303	0.40409854	40%
7	Type of bearing used	0.09747	0.04305	0.04632	6	0.049483397	0.328233237	33%
8	Incorrect counterbalance assembly method	0.09747	0.04305	0.02639	7	0.040428031	0.27874984	28%
9	Incorrect hammerbank assembly method	0.09747	0.04305	0.02639	7	0.040428031	0.23832181	24%
10	Incorrect shuttle frame assembly method	0.09747	0.04305	0.02639	7	0.040428031	0.197893779	20%
11	Incorrect drive assembly method	0.09747	0.04305	0.02639	7	0.040428031	0.157465748	16%
12	Incorrect final assembly method	0.09747	0.04305	0.02639	7	0.040428031	0.117037717	12%
13	Incorrect printer assembly method	0.09747	0.04305	0.02639	7	0.040428031	0.076609687	8%
5	Shuttle operating impulsive force exerted on the component (exp, bearing)	0.05076	0.04305	0.02639	13	0.036181656	0.036181656	4%
	SUM	1	1	1		1		

Figure 5: Overall Score and Rank of Problem Identification.

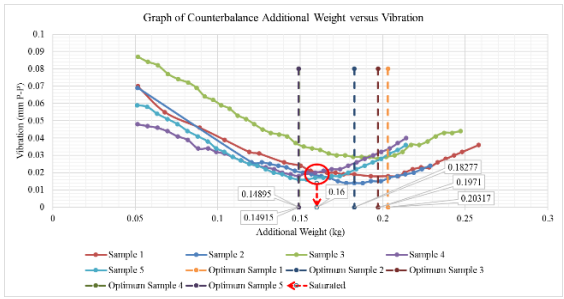

Figure 6: Vibration Experiment Result.

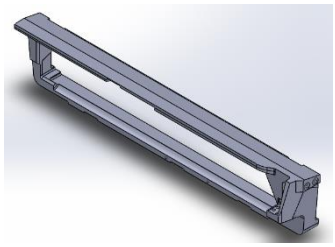

Figure 7: Redesign Counterbalance.

CONCLUSION

Vibration is the main cause to the product quality issue. The vibration experiment has shown that the additional weight on the counterbalance can reduce the vibration. This also show that the product quality and performance can be improved. Thus, it is believed that this can reduce the chance of component breakdown, reduce extra costs, increase product reliability, gain customer satisfaction and promote sustainability.

20. REFERENCES

[1] Besterfield, D. (2014). Quality Improvement. British: Pearson.

LINE BALANCING IMPROVEMENT AND SIMULATION OF A PRINTER CARTRIDGE ASSEMBLY LINE

Lui Wilson and Wong Kuan Yew
School of Mechanical Engineering, Faculty of Engineering,
Universiti Teknologi Malaysia, 81310 UTM Skudai, Johor, Malaysia

INTRODUCTION

This project seeks the line balancing improvement in printer manufacturing company in order to improve the productivity of one of the assemblies in this company, cartridge assembly line. Line balancing has various methods that can be implemented to improve the efficiency of the assembly line. In this project, Largest Candidate Rules (LCR), Moodie Young Method, and Hoffman Method are being used

METHODOLOGY

Line balancing is used to generate the new alternative work schedule for the assembly line. The table of the work element with the standard time of each work element is showed in order to rearrange the work schedule. The theoretical cycle time is determined to avoid the work station cycle time to exceed it. The line efficiency for the new work schedule is calculated by both using MS Excel and manual calculation. The simulation is conducted by using a discrete event simulation software, WITNESS 14

RESULTS AND DISCUSSION

Table 1: ***Comparison between the Line Balancing Algorithms***

	Line Efficiency(%)	**Production Rate/ day**
Actual	50.98	2457
LCR	**80.12**	**2534**
Hoffman	**80.12**	**2534**
KBW	75.7	**2534**
Moodie Young	75.7	**2534**

Table 1 shows the line efficiency and production rate among the five models. These five models are the actual assembly line, Largest Candidate Rules, Hoffman Method, Kilbridge and Wester Method(KBW) and Moodie Young Method. From the table, Hoffman Method and LCR have the highest line efficiency compare to the other line balancing algorithms. The line efficiency of these two-line balancing algorithms reaches to 80.12% and the production rate increase to 2534 units per days. Hence, The LCR is the best in the line balancing algorithms comparison. From Table 2, Hoffman Method and Kilbridge and Wester have the highest production output which is 69255 units per month The average operator utilization of Hoffman Method is 78.08% and is higher than KBW. Due to having a higher percentage of average worker utilization and the results from the line efficiency, Hoffman Method is chosen as the best alternative to solve the poor line balancing problem.

Table2: ***Performance Measurements in Simulation***

System	**Production Output (unit/month)**	**Average Worker Utilization (%)**
LCR	66124	74.55
Hoffman	**69255**	**78.08**
KBW	**69255**	73.99
Moodie Young	66124	70.64

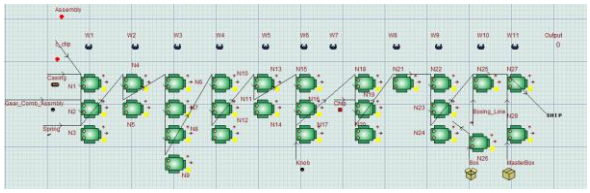

Figure 1: Simulation of actual scenario generated by WITNESS

CONCLUSION

From the results of the simulation, Hoffman Method has the best line efficiency and the production output compared to the alternative solution.

REFERENCES

[1] Stevenson, W. J. (2012). Operation Management 11th edition. New Yorks: McGraw-Hill/Irwin, The McGraw-Hil Companies, Inc.
[2] Lee J. Krajewski, Larry P. Ritzman, Manoj K. Malhotra. (2013). Operations Management Processes and Supply Chains 10th edition. New Jersey: Pearson Education, Inc.

FACILITY LAYOUT IMPROVEMENT AND SIMULATION IN A PRINTER MANUFACTURING COMPANY

Poh Tsu Chauw and Wong Kuan Yew
School of Mechanical Engineering, Faculty of Engineering,
Universiti Teknologi Malaysia, 81310 UTM Skudai, Johor, Malaysia

INTRODUCTION

Layout planning is one of the most vital decisions that determine the long-run efficiency of a company's operations. Layout planning also has its strategic implications because it helps organizations establishes their competitive priorities. A case study has been done on a printer manufacturing company. The existing plant layout of the company is not properly designed and it is ineffective. Problems in the company are identified and solutions are proposed.

PROBLEM IDENTIFICATION

This section presents problems found from the current existing layout. The process flow of the printer assembly process is not smooth and unsystematic. There is unnecessary long distance travelled and crossover along the material flow path. These problems are time consuming which lead to longer production time and lower efficiency of the assembly process.

ALTERNATIVE DEVELOPED AND SIMULATION

Two alternative layouts were developed by using SLP method and CORELAP method after the problems were identified in the existing layout. Figure 1 and Figure 2 shows the alternative layouts developed using SLP method and CORELAP method respectively.

After both alternative layouts developed, total distance travelled are calculated and flow of materials in each layout is drawn. After that, simulation models are built for the existing layout as well as alternative layouts. The number of outputs produced by the existing layout and the alternative layouts are compared. Based on evaluation, alternative layout developed using SLP is the best among the three layouts as the layout has the shortest travelled distance between departments and the highest average total output.

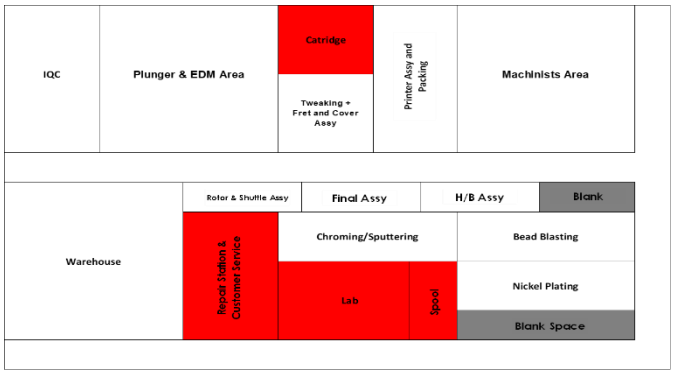

Figure 1: Alternative layout by SLP

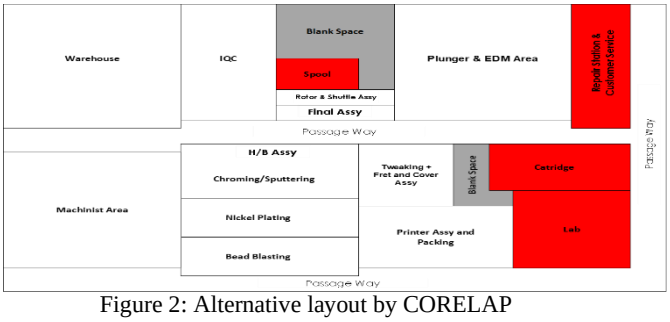

Figure 2: Alternative layout by CORELAP

CONCLUSION

The total distance travelled between departments is calculated and the flow of materials is drawn to determine the problems of the existing layouts. The proposed layouts showed a great improvement to the current existing layout from the aspect of distance travelled and number of outputs.

REFERENCES

[1] J. A. Tompkins, J. A. White, Y. A. Bozer and J. M. A. Tanchoco, (2010), Facilities Planning, John Wiley & Sons, Inc.

[2] R. Muther, (1973), Systematic Layout Planning, Boston: Cahners Books.

[3] J. Heizer, B. Render and C. Munson, (2017) Operations Management, Sustainability and Supply Chain Management, Pearson Education Limited.

SIMPLIFIED FREEBOARD CALCULATION FOR LOCAL SMALL BOAT

Nur Amira Yusri and Yahya Samian
School of Mechanical Engineering, Faculty of Engineering,
Universiti Teknologi Malaysia,81310 UTM Skudai, Johor, Malaysia

INTRODUCTION

Freeboard is one of the terms in maritime terminology. Considering freeboard at any type of vessel will provide a stability and safety of the vessel on certain waterways. Freeboard is defined as the vertical distance measured amidships, from the upper edge of the deck line to the upper edge of the related load lines. Malaysia is using International Convention of Load Lines 1966 (ICLL) to calculate the freeboard of the vessel. However, referring to the Freeboard Table (Regulation 28) provided in the ICLL 1966 where it determined the tabular freeboard, the minimum provided length of ship is 24 meter with 200 mm freeboard. Hence for vessel categorizes below 24 meter, the ICLL is not suitable to calculate freeboard of the vessel. Therefore, this study will be focused to simplified freeboard method and formulation for local small boat.

EXPERIMENTAL SETUP

This section presents the procedure to analyse the developed simplified method. Using drawing collected, built the model. Import the model into MAXSURFStabilityAdvanced64 to analyse the stability. Choose the suitable draft for the vessel and set the VCG. Run the upright hydrostatics analysis and obtain the displacement at design draft. Next, use Large Angle Stability and set the trim and heeling angle of the vessel. Run the analysis and determine either the vessel pass of fail the IMO stability criteria. If failed, change the draft and repeat the step. If passes, continue to calculate the freeboard by depth of vessel minus draft of vessel.

RESULT AND DISCUSSION

At the end of the analysis, the freeboard of the vessel can be determined. The IMO criteria will show a passed result when the chosen draft is suitable with the vessel.

Table 1: The Freeboard at Different Vessel Dimension

Tug boat	Length (m)	Beam (m)	Depth (m)	Draft (m)	Fb (mm)
1	22.354	6.4	3.255	2.60	655
2	23.5	7.32	3	2.25	750
3	23.15	7.3	3	2.3	700
4	23.5	7.315	3.048	2.32	728
5	23.8	6.1	2.7	2.035	665
6	23	7.315	3.048	2.3	748
7	23.26	7	2.9	2.22	680
8	23.9	7.2	3.5	3.645	855
9	20.97	5.486	2.316	1.766	550
10	23	7	3.2	2.6	600

Equation to calculate the freeboard are as follow:

Freeboard (Fb) = Depth (m) - Draft (m)

CONCLUSION

The result of this project show that the simplified method and formulation using MAXSURFStabilityAdvanced64 can be used to determine the freeboard of the vessel with length below 24 meter once the stable draft of the vessel was known.

REFERENCE

[1] Bentley Offshore Analysis. (2016). MAXSURF Stability- Large Angle Stability. Retrieved from: https://www.youtube.com/channel/UCW3O3jM48Ugy7mSB9duUUqw/about. (Accessed on 10th May 2019)

[2] International Maritime Organization. (2005). International Convention on Load Lines 1966. Chevron Texaco.

SIMPLIFIED TONNAGE MEASUREMENT METHOD FOR LOCAL VESSEL LESS THAN 24 METERS

Ryan Spencer Richard Liangson and Yahya Samian
School of Mechanical Engineering, Faculty of Engineering,
Universiti Teknologi Malaysia, 81310 UTM Skudai, Johor, Malaysia

INTRODUCTION

The current international standard for tonnage measurement, the International Conference on Tonnage Measurement of Ship 1969, ITC'69 [1], is not suitable for vessel below 24 meters in length. Simplified tonnage measurement method is a simplified formulation for tonnage measurement where only the basic dimensions are required and the calculation process is simple and fast. It is a simplified version of the ITC'69 method and was invented mainly to calculate tonnage for vessel less than 24 meter in length. There are three simplified tonnage measurement methods that had been developed in Malaysia, but each have its own weaknesses. Hence the reason for this study, to develop a simplified tonnage measurement method for local small vessels accurately and fast.

EXPERIMENTAL SETUP

First and foremost, lines plan and general arrangement plan of nine ships with length less than 24 meter were gathered from reliable sources. Data such as the basic dimension of a ship and the volume calculated using Simpson's Rules and Boxing method were measured and gathered.

A series of measurement methods were formulated to calculate the volume of a ship. This was done by comparing different types of methods to calculate volume against the volume calculated using DigitizeIt and Boxing method. From there, a scatter chart with a best fit line were plotted in order to generate a whole new equation to calculate volume of a ship using only its basic dimension.

Derivation of K_1 was based on ITC'69 method. Hence the developed simplified tonnage measurement methods is as shown in Table 1.

Table 1: The proposed simplified tonnage measurement methods

	Simplified Method 1	Simplified Method 2
Measurements	Drawings	On-board
Volume under deck, Vu	$(0.69 \times LBP \times B \times D) + 39.47$	$(0.56 \times MDL \times B \times D) + 87.15$
Volume above deck, Vh	$(0.36 \times Vu) - 2.5$	$(0.36 \times Vu) - 2.5$
Total Volume, V	$Vu + Vh$	$Vu + Vh$
Coefficient, K1	0.249	0.249
Gross Tonnage, GT	K_1V	K_1V
Net Tonnage, NT	$GT \times 0.3$	$GT \times 0.3$

RESULTS AND DISCUSSION

The tonnage for all nine ships were then calculated using all the existing simplified methods as well as the two proposed simplified methods. The results obtained were then compared with the result obtained from ITC'69 method. The closer the average error percentage to zero, the more accurate it is.

Table 2: Average error percentage for gross tonnage

Gross Tonnage		Average Error, %
ITC'69		Reference
Indonesia	Non-Conventional Vessel Standard	-9.454
United Kingdom	British Simplified Method 1982	63.321
	British Simplified Method 1977	-28.916
Canada	Standard For Small Vessels	-7.722
Malaysia	Simplified Method For Non-Conventional Tug And Crew Boat	7.062
	Simplified Method For Vessel Less Than 24M	-24.387
	Simplified Method Used By Dept. Of Fisheries Malaysia	15.539
USA	Coast Guard Simplified Method	23.573
Proposed	Simplified Method 1	-1.683
	Simplified Method 2	-1.005

Table 3: Average error percentage for net tonnage

Net Tonnage		Average Error, %
ITC'69		Reference
Indonesia	Non-Conventional Vessel Standard	-9.454
United Kingdom	British Simplified Method 1977	136.945
Canada	Standard For Small Vessels	130.695
Malaysia	Simplified Method For Non-Conventional Tug And Crew Boat	7.062
	Simplified Method For Vessel Less Than 24M	-24.387
	Simplified Method Used By Dept. Of Fisheries Malaysia	15.539
USA	Coast Guard Simplified Method	311.911
Proposed	Simplified Method 1	-1.683
	Simplified Method 2	-1.005

CONCLUSION

Based on Table 2 and Table 3, both the proposed simplified methods achieved the closest average error percentage to zero among the rest when compared with ITC'69 method. Hence this shows that both proposed simplified methods are accurate. In addition to that, both methods are very simple to use since it only requires the basic dimension of a ship.

REFERENCES

[1] International Maritime Organization (IMO) (1983). International Conference on Tonnage Measurement of Ships 1969. London: International Maritime Organization.

CONTROL SYSTEM DESIGN OF AN ANIMAL-BASED TREE CLIMBING AND CUTTING ROBOT

Ahmad Hafeez Badlissah and Zainab Asus
School of Mechanical Engineering, Faculty of Engineering,
Universiti Teknologi Malaysia, 81310 UTM Skudai, Johor, Malaysia

INTRODUCTION

Harvesting a coconut tree involves hard work as a worker will have to climb up to 30 meters in height to harvest around 30 to 75 fruits per year. This can be quite a challenge for the coconut harvester as it involves a lot of energy and time to harvest one coconut tree. Thus, to reduce the workload of a coconut harvester and follow today's industrial transition to industry 4.0, a development of tree climbing and cutting robot can be useful and beneficial to them. The use of Arduino and MIT App Inventor 2 can help in the development of the control system. Robot control system is used to implement the sequence of the robot's movement due to the actuation of forces or torques under the influences of disturbances that may contribute to unpredictable error [1].

SYSTEM SETUP AND DEVELOPMENT

The process of designing a control system for robot involves several analysis dan describes the system and several mechanism testing. Some analysis includes functional analysis and mechanism analysis of the robot. Afterwards, we will be designing a control system based on the mechanism which will be tested first to test its functionality.

Several main components are selected based on the requirement needed for the robot to function very well. The requirement needed includes the selection of motor, servo motor, motor driver, microcontroller and the power supply. The components that fulfil these requirements are RS-775 DC motor, MG995 Servo motor, MDD10A motor driver, Arduino Mega and 18650 Rechargeable Battery. Extra components needed includes, HC-05 Bluetooth Module and LM2596 Voltage Regulator.

The final system that has been connected is shown in Figure 1. The software development is done through several programming of Arduino to instruct it to give response to the input given by the application on mobile phones. Figure 2 shows the completed functional application that will give the input instruction to Arduino through Bluetooth module.

SYSTEM ANALYSIS

The calculated power consumption of the robot is 650.27 W. The robot needed at least this much power to functions. For the power efficiency, it is calculated that if the motor produced the desired performance, it will be 56.16%. However, the efficiency based on the measured voltage and current without load is 98.53% This shows that the power supply is still enough to support the robot

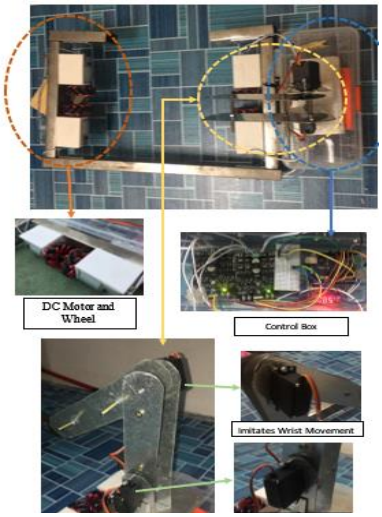

Figure 1: Complete Prototype

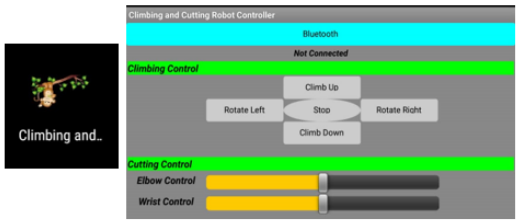

Figure 2: Complete Functional Application

with or without load. The problem faced is that the required climbing torque is miscalculated. From that the component used is insufficient to climb a tree. Thus, the robot cannot be exactly tested to observe is functionality.

CONCLUSION

We have shown the process of designing the control system of the climbing and cutting robot. Even though, the robot is unable to climb, the system it is still functioning, and the components can move based on instructions selected via smart phone application.

REFERENCES

[1] Mailah, M., & Tang, H. H. (2017). Introduction to Robotic Systems and Control. Johor Darul Takzim: PENERBIT UTM PRESS.

DESIGN OF A DEVICE USED FOR CLEANING PURPOSE

Muhammad Syahmi Sulhi Bin Abdullah and Zainab Binti Asus
School of Mechanical Engineering, Faculty of Engineering,
Universiti Teknologi Malaysia, 81310 UTM Skudai, Johor, Malaysia

INTRODUCTION

Floor cleaning is an endless activity consist of repetitive task which is boring and time consuming [1]. Apparently, variety of cleaning products are available in the market, designed to assist human for cleaning purpose. For instance, a vacuum cleaner is used to eliminate dust from floor surface. Basically, these devices capable to reduce cleaning time and improve cleaning depth [2] but they consumed high-power, expensive and had uncertain performance for certain products. Therefore, robotic cleaners took place recently [3]. Undoubtedly, robotic cleaners are more expensive, have low running time and some of them are difficult to troubleshoot. Because of that, the project will design a floor cleaning device specifically for dry cleaning condition to assist human for cleaning purposes.

EXPERIMENTAL SETUP

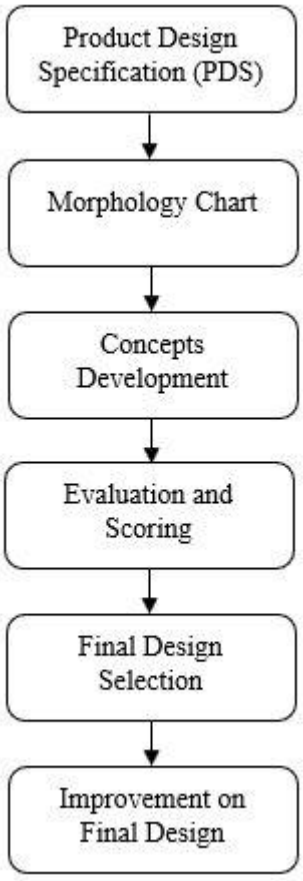

Product design specification (PDS) is the guidance to generate several possible features for morphology chart. There were eight design concepts developed through random selections. Concept Design 2 with the highest score about 71%, was selected as final design. The selected concept has rounded shape chassis and has low tendency getting stuck between obstacles. The design was equipped with two front caster wheels. Therefore, it has good stability during movement. Despite the advantages, the final design has had little improvement. The design used D-shape chassis instead of using rounded shape. The idea is to have more space for components installation.

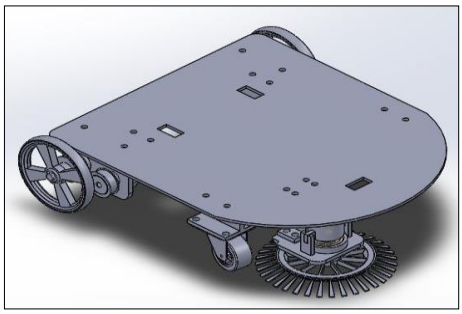

Figure 2: Improved version of final design

CONCLUSION AND RECOMMENDATION

A floor cleaning device for dry cleaning condition has been successfully designed and fabricated, capable to effectively wipe and store dirt using spinning sweeper as cleaning mechanism. However, the cleaning device can be improved in the future. The cleaning mechanism should be replaced with a dry vacuum. Suctioning method is apparently the most efficient for floor cleaning mechanism and compatible with compact size cleaning device.

In addition, the cleaning device should used four-wheel drive, Omni-directional wheel system. The wheel system enabling the device to move diagonally and having precise positioning. Basically, the wheel system will enhance cleaning device mobility.

REFERENCES

[1] Erwin Prassler, A. R. (2000). A Short History of Cleaning Robots. *Autonomous Robots 9*, 211–226.

[2] Jasper Westenbroek, J. D. (2014). *Designing a Robotic Vacuum Cleaner*. Twente: University of Twente.

[3] T.B. Asafa, T. A. (2018). Development of a vacuum cleaner robot. *Alexandria Engineering Journal*, 1-7.

DESIGN AN ANIMAL BASED TREE CLIMBING AND CUTTING ROBOT

Mohamad Rafiq Raihan Zuhar and Zainab Asus
School of Mechanical Engineering, Faculty of Engineering,
Universiti Teknologi Malaysia, 81310 UTM Skudai, Johor, Malaysia

INTRODUCTION

Through billions of years of evolution, many types of animal robots have developed to deal with these challenges. A comprehensive study and analysis of tree-climbing methods have been conducted to the selecting of the most efficient mechanism to climb and cut, motion planning, finding the suitable components need to use, the procedure used to produce the final concept of the robot and many more.

An animal-based tree climbing and cutting robot is design to help the workers from risky and unsafe task which it involves climbing up and down the tree while balancing the body at the dangerous height. By designing this robot, coconut harvesting can be done efficiently and in directly, increase the agriculture's productivity.

METHODOLOGY

This section presents the flow of the procedure needed to follow in order to design and produce the prototype of the robot. Firstly, conduct a comprehensive study and analysis of existing climbing robot and cutting mechanism. Next, propose conceptual designs for this climbing and cutting animal-based robot and improvise the chosen design. Then, analyse and propose the suitable components and materials use for this climbing and cutting robot. After that, develop engineering analysis on the final design where power analysis and finite element analysis is calculated to produce an efficient robot. Lastly, fabricating the final design and come out with a prototype.

RESULTS AND DISCUSSION

At the end of design procedure, an animal-based tree climbing and cutting robot is selected based on the Product Design Specification and Evaluation matrix.

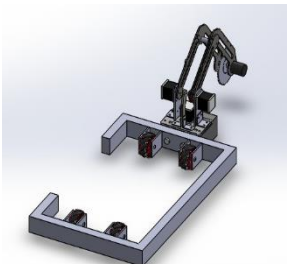

Figure 1: the final design selected.

A limited analysis performed on this robot where power analysis is conducted in order to find maximum torque needed by the robot to climb the tree.

The forces are calculated by determine the force at wheel point based on the free body diagram. Firstly, calculate the moment force at any point with higher unknown. Then, calculate the axial forces at x-axis and y-axis.

Table 1 below shows the forces needed by the robot at several cases,

No.	Cases	F (N)	N (N)
1	Static motion	38.75	25.92
2	Rectilinear motion (up)	48.23	29.53
3	Rectilinear motion (down)	29.27	22.35
4	Curvilinear motion	48.23	1.47
5	Rectilinear motion (θ max)	48.23	16.67

Table 1: Forces required by the robot.

This is to observe the effect of using different motion of the robot to climb at tree, the value of force was varied. This is mainly due to the inconsistency in generated force when the robot is in different condition. Thus, we chose the maximum force to calculate the torque and the power. The torque required to overcome this force is; $T = Fr$, where r = radius of the wheel, $T = 1.45Nm$. Lastly, Calculate the power, $P = T\omega$ and give $P = 580\ W$.

From the power obtained, a motor is with suitable condition is selected. The motor should supply enough power to the system. Otherwise, the system will not function due to insufficient power.

CONCLUSION

The objective of this research has been achieved where to design the robot and produce the prototype. The design procedure is important to be followed. This is because every phase of the procedure will help massively in the development of the prototype. However, the prototype unable to perform its task smoothly where it unable to climb due to several problems like the size of the wheels used, the type of the wheels used, insufficient power supply, too heavy and wrong assumptions at first analysis.

REFERENCES

[1] Meriam, J., & Kraige, L. G. (2013). DYNAMICS. Singapore: John Wiley & Sons Singapore Pte. Ltd.

[2] Tin, L. L., & Yangsheng, X. (2012). Tree Climbing Robot, Design, Kinematics and Motion Planing. Springer Heidelberg New York Dordrecht London: Springer-Verlag Berlin Heidelberg.

CONTROL IMPROVEMENT OF A DEVICE USED FOR CLEANING PURPOSE

Mohamad Izham Shah Hamdan and Zainab Asus
School of Mechanical Engineering, Faculty of Engineering,
Universiti Teknologi Malaysia, 81310 UTM Skudai, Johor, Malaysia

INTRODUCTION

This project will be conducted basically on the function of microcontroller in cleaning device. This project is supposed to be an improvement of previous cleaning device that is conducted by previous students. The suggested improvement is the device can be controlled by smartphone with Bluetooth connection. The device also can be steered to any position before mapping the route. If there is any obstacle or steep, the device can stop immediately and warn the user. The device should be able to do at least 2 methods of cleaning, which is sweeping and mopping.

METHODOLODY

This section presents the planning of development for the system. It is decided to reuse the previous project for component selections in keeping the previous function in cleaning purpose. Afterwards, new subsystem is developed for improvement of the device, such as Bluetooth control, obstacle avoiding and memorizing path. New components selection is done for fulfilling these subsystems.

System build up is done through coding implementation and wiring. Then, the components are patched up onto a body device for modelling test.

RESULTS AND DISCUSSION

The device is successfully built and ready for test modelling. It is shown that Bluetooth control is successful, where every instruction given like moving forward can be run by the device flawlessly. Voltage step down is done beforehand on the Bluetooth module because the signal is not stabilized when Arduino supplies 5 V to Bluetooth module, where the best results is 3.3 V.

For obstacle prevention, the device is capable to avoid the obstacle with the help of ultrasonic sensor. At certain distance when the device is near the obstacle, it will be changing direction for cleaning next area to it.

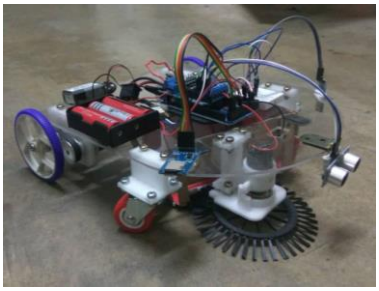

Figure 1: Cleaning device model

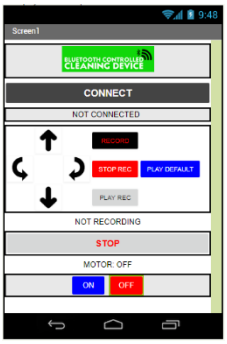

Figure 2: Apps for Bluetooth Control.

Recording path function is not working well due to certain bugs in the coding like retrieving the data from MicroSD which is saved in character data (.txt file). Data is needed to be read in integer for the device to run correctly.

CONCLUSION

It is concluded that improvement has been done on the device, like Bluetooth control and obstacle prevention, except that the memorizing function is suggested for another way of storage instead using MicroSD. The best way to store and read a data directly is by using array in variables. Future development can be done regarding on this issue.

REFERENCES

[1] Comparison between Ultrasonic Sensors and Optical Sensors. (n.d.). Retrieved from Introductary Guide to Sensors: https://www.keyence.com/ss/products/sensor/sensorbasics/ultrasonic/comparison/

[2] Reneker, D. (13 July, 2017). PLC vs. Arduino for industrial control. Retrieved from Control Design: https://www.controldesign.com/articles/2017/arduino-vs-plc-for-industrial-control/

[3] Tech, B. o. (5 March, 2018). Comparing the Arduino UNO, Nano and Pro Mini - arduino-lessons.com. Retrieved from YouTube: https://www.youtube.com/watch?v=e0DJtcXVQa0

[4] Teel, J. (n.d.). Bluetooth or WiFi – Which is Best for Your New Wireless Product? Retrieved from Predictable Designs: https://predictabledesigns.com/what-type-of-wireless-is-right-for-your-product-bluetooth-wifi/

IMPACT CHARACTERISTIC AND ENERGY ABSORPTION OF GUARD RAIL POST UNDER LATERAL LOADING

Muhammad Yusri Bin Aluwi Shakir and Zaini Bin Ahmad
School of Mechanical Engineering, Faculty of Engineering,
Universiti Teknologi Malaysia, 81310 UTM Skudai, Johor, Malaysia

INTRODUCTION

Develop safer roadways and more crashworthy roadside safety features is the most important things for public as it can low the possibility of the serious injuries and fatalities of vehicle occupants. Therefore, median barriers have been developed and used on highways for compulsory safety purpose including concrete barriers, W- beam, Thrie-beam guardrails and cable barriers [1]. So, the purpose of this study is to evaluate the impact characteristic and energy absorption performances of guard rail post under crash loading by relate it with finite element modelling using LS-DYNA as a nonlinear finite element code.

EXPERIMENTAL SETUP

This section presents the experimental setup for the system. Tensile test was conducted by followed ASTM E-8 [2] and quasi static bending test followed ASTM E-9 will loading rate 5 mm/min.

For simulation, there were two components designed using LS-DYNA. Guardrail Post was designed followed quasi static requirement with the impactor assigned as prescribe rigid motion with constants acceleration. Guardrail System designed followed dynamic test with velocity of impactor constants V= 10 m/s.

RESULTS AND DISCUSSION

Figure 1 shows the result of tensile test. This material has yield stress of 433.00 MPa and Maximum tensile stress 507.00 MPa. Young's Modulus is equal to 278.67 GPa.

Figure 2 shows the results of validation compared with experiment and FE. For percentage error peak load has 9.13 %, Mean load has 4.64 %, CFE 4.12 % and EA 9.52 %.

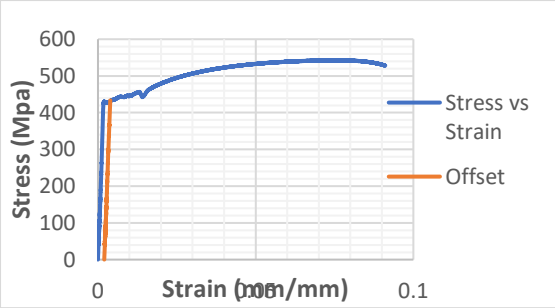

Figure 1: Stress-strain curve for galvanize mild steel material

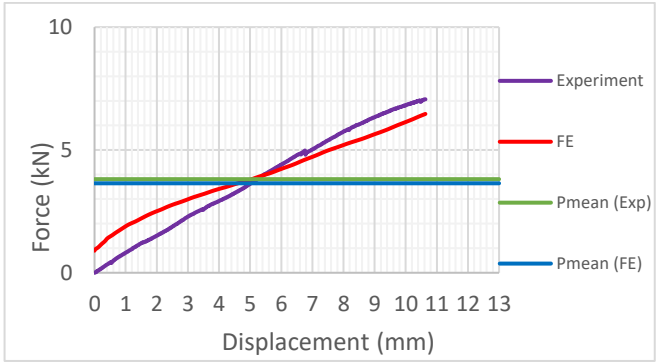

Figure 2: Load-displacement comparison curve for FE model validation

PARAMETRIC STUDY

For parametric study, there were five (5) parameter had been studied, configuration, radius, width, height and velocity.

Table 1: Overall results of parametric study

Design	Height (mm)	Radius (mm)	Width (mm)	Velocity (m/s)	Pmax (kN)	Pmean (kN)	CFE (%)	Internal Energy (kJ)	Energy Absorption (kJ)	Mass (kg)	SEA (kJ/kg)
C1	700	10	65	10	195.0	107.8	55.3	83.0	89.6	110.3	0..812
C2					184.0	113.5	61.7	81.2	94.3	110.3	0.860
C3					140.0	109.0	77.9	72.8	89.8	110.3	0.814
C4					190.0	105.7	55.6	73.3	87.1	110.3	0.790
Radius	700	10	65	10	188.0	97.0	51.6	69.6	80.3	110.3	0.73
		15			196.0	124.8	63.7	85.6	102.2	110.3	0.93
		20			202.0	123.4	61.1	87.5	101.3	110.3	0.92
		25			204.0	124.5	61.0	89.7	102.3	110.3	0.93
		30			227.0	119.6	52.7	95.3	99.3	110.3	0.90
Width	700	10	55	10	175	100.9	57.7	74.1	83.20	110.3	0.76
			65		176	101.0	57.4	71.5	84.70	110.3	0.77
			75		176	119.4	67.8	83.7	97.81	110.3	0.89
			85		176	119.4	67.8	83.5	97.82	110.3	0.89
			95		177	119.5	67.5	80.8	98.14	110.3	0.89
Height	500	10	65	10	188.0	93.9	50.0	67.2	78.6	109.2	0.72
	700				188.0	97.0	51.6	69.6	80.3	110.3	0.73
Velocity	700	15	75	10	196.0	124.5	63.5	85.6	102.0	110.3	0.92
				15	202.0	129.0	63.9	127.0	162.5	110.3	1.47
				20	214.0	121.9	57.0	106.0	132.9	110.3	1.20
				25	208.0	118.6	57.0	121.0	160.1	110.3	1.45
				30	211.0	119.9	56.8	124.0	164.2	110.3	1.49

CONCLUSION

Radius of guardrail post is critical part based on parametric study as the average specific energy absorption more than 0.9 kJ/kg

REFERENCES

[1] Baker, R. M. (2014) Performance Evaluation of W-beam Guardrails on Sloped Medians using Nonlinear Finite Element Simulation,1

[2] AASHTO Standard, A. A (2008) Standard Test Methods for Tension Testing of Metallic Materials ASTM E-8, 3

PROTOTYPECRUSHING RESPONSE OF THIN-WALLED CIRCULAR RING WITH AUXETIC AND HONEYCOMB CELL-STRUCTURE

Amirul Syafiq Baharuddin and Zaini Ahmad
School of Mechanical Engineering, Faculty of Engineering,
Universiti Teknologi Malaysia, 81310 UTM Skudai, Johor, Malaysia

INTRODUCTION

Thin-walled structure widely used as an energy absorber. Energy absorption of circular ring under lateral loading is inefficient due to plastic strains localization around the plastic hinges. Nested tube system proposed by Baroutaji et al. , Olabi et al. and Wang et al. to increase the energy absorption[1-3]. Niknejad et al. and Fan et al proposed foam filled tube.[4, 5]. Auxetic structure as filler structure is expected having good energy absorption due to negative Poisson's ratio.

METHODOLOGY

The auxetic-filled ring is fabricated from aluminium due to high ductility. Tensile test was conducted to determine the mechanical properties. Quasi static compression test is conducted to validate the numerical simulation. Both have a good agreement. Auxetic-filled ring, honeycomb-filled ring and empty ring is analysed numerically to determine the better energy absorber. The better energy absorber will be selected to perform a parametric studies .

RESULTS AND DISCUSSION

Based on the result that have been recorded in, both numerical and experiment have good agreement.

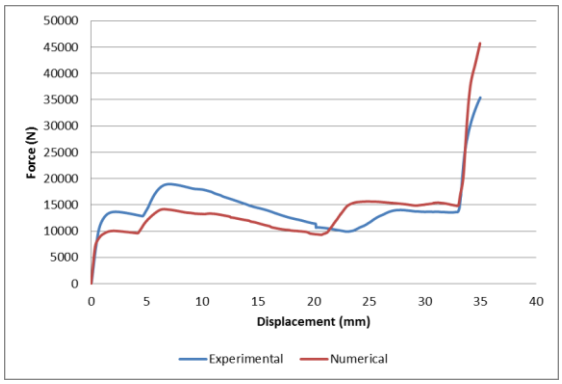

Figure 8: Numerical vs Experimental

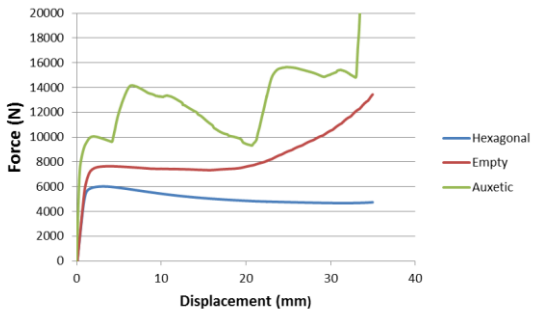

Figure 9: Load-displacement comparison on different filler

Auxetic-filled structure absorb more energy due to the structure deform simultaneously and synchronously. Honeycomb-filled is lower due to the ineffective of the materials deformation. The honeycomb deforms only at the plastic hinges make them inefficient. The parametric study is performed to auxetic filled to investigate the effect of geometry on energy absorption.

CONCLUSION

To conclude that, as the thickness increase, the energy absorption will increase. It will increase the SEA, MCF, and CFE. As the diameter decrease, the energy absorption is increase due o increasing collapse load. The angle increase, the collapse load decrease and energy absorption is slightly decrease.

REFERENCES

[1] Baroutaji, A., M.D. Gilchrist, and A.G. Olabi, *Quasi-static, impact and energy absorption of internally nested tubes subjected to lateral loading.* Thin-Walled Structures, 2016. **98**: p. 337-350.

[2] Olabi, A.G., et al., *Optimised design of nested circular tube energy absorbers under lateral impact loading.* International Journal of Mechanical Sciences, 2008. **50**(1): p. 104-116.

[3] Wang, H., et al., *Internally nested circular tube system subjected to lateral impact loading.* Thin-Walled Structures, 2015. **91**: p. 72-81.

[4] Fan, Z., et al., *Dynamic lateral crushing of empty and sandwich tubes.* International Journal of Impact Engineering, 2013. **53**: p. 3-16.

[5] Niknejad, A., S.A. Elahi, and G.H. Liaghat, *Experimental investigation on the lateral compression in the foam-filled circular tubes.* Materials & Design (1980-2015), 2012. **36**: p. 24-34.

MODELLING AN ELECTRIC VEHICLE WITH RANGE EXTENDER

Nor Shaharizal Yuhani and Zul Hilmi Che Daud
School of Mechanical Engineering, Faculty of Engineering,
Universiti Teknologi Malaysia, 81310 UTM Skudai, Johor, Malaysia

INTRODUCTION

Electric vehicles have several disadvantages compared to conventional vehicles, such as their road ability and vehicle weight. To overcome these problems, range-extended engine technology has been developed. A range extender is a generator set that consists of an internal combustion engine coupled with a generator that operates when it is required.

PROJECT OBJECTIVES

The aim of this project is to develop electric vehicle with range extender model by using MATLAB/Simulink and use developed model to predict fuel consumption and battery performance when completing different driving cycle.

METHODOLOGY

This project is done with a few equations by Guzella [1]. The collected data was used to build a model of electric vehicle in MATLAB/Simulink. The engine model was applied to an electric vehicle model as a range extender, and its performance was simulated while piloting two driving cycles. The result is presented in the form of graph that produced by MATLAB/Simulink.

RESULTS AND DISCUSSION

Based on the results produced, there are three section of conclusion that can be conclude and the conclusion were made based on fuel consumption of the engine used as range extender, state of charge (SOC) and the used of two driving cycle (NEDC & Artemis driving cycle). For the first section, the fuel consumption was compared between model developed in Matlab/Simulink and model existing in market. Its shown that the fuel consumption developed used less fuel when SOC is set to 0.27. The differences are about 0.127L at the same distance and time. Next, battery state of charge (SOC) is compared by different ICE power set in the simulation. EV using high ICE power (3kW) show that the battery usage is longer with more range compared with EV using less ICE power (2kW). The EV can travel about 66km in 2hours. However, the less power EV can travel 54km in 1.68hour before its need to recharge. Last but not least, the comparison between two cycle was make. Artemis driving cycle with average speed (57.49km/h) can travel about 64.95km in 1.14hour meanwhile NEDC driving cycle with average speed 32.22km/h can travel 66.58km in 2.1hour.

REFERENCES

[1] L. Guzzella and A. Sciarretta. Vehicle Propulsion Systems (Introduction to Modelling and Optimization). Springer, New York, second edition, 2007

[2] Chen M., Rincon-Mora A. A. “Accurate Electrical battery Model Capable of Predicting Runtime and I-V Performance”, IEEE Transactions on Energy Conversion, June 2006; 21: 504–511.

[3] Erdinc O., Vural B., Uzunoglu M. “A Dynamic Lithium-ion Battery Model Considering the Effects of Temperature and Capacity Fading”, IEEE Transactions, 2009: 383-386.

EXPERIMENTAL STUDY OF BATTERY TEMPERATURE UNDER CONSTANT DISCHARGE RATE

Akmal Fahruddin and Zul Hilmi Che Daud
School of Mechanical Engineering, Faculty of Engineering,
Universiti Teknologi Malaysia, 81310 UTM Skudai, Johor, Malaysia

INTRODUCTION

In recent years, many car manufacturers leaning towards producing alternative ways apart from internal combustion vehicle. The production of Hybrid Electric Vehicle (HEV) and Electric Vehicle (EV) are growing fast. The main purpose of using these alternative ways is that to reduce the usage of petrol and diesel and also to reduce exhaust emission which instigating greenhouse effect. Almost all HEV and EV available in the market are using NiMH batteries, but LiB batteries are expected to grow fast in HEV and EV markets. The LiB a more preferable power storage medium for HEV and EV since it has high energy density, low self-discharge rate, low maintenance and lightweight [1]. In this experimental study, the Lithium-ion battery module will be placed in the airflow tunnel while Resistor Temperature Detector (RTD) sensors are placed on the battery surface and anemometer is used to measure the air velocity in determining the distribution of temperature of various points on the battery cell surface during the discharging process with different discharging strategy of discharging rates and air velocities.

EXPERIMENTAL SETUP

An air flow tunnel is used in this experiment. Battery module is made up of 3 units of Lithium-ion battery cells connected in series with the voltage of 12V. The battery capacity is 40Ah. Between battery cells has gap of 3mm to let air flow through the battery module to remove heat away from discharging process. Battery module terminal is then connected to copper plate and next connected to cable with the other end connected to the discharger, DC DC Programmable Electronic Loads Series IT8514C+ for discharging process. Axial fan is used to create constant air velocities in the airflow tunnel. Resistance Temperature Detector (RTD) is placed on 3 different positions on battery cell surface. Discharging strategies are varied between constant discharge rates, 1C, 3C and 5C. While air velocities are varied with 1.5m/s and 3.0m/s. All the instruments used are then connected to LabVIEW software as data logger.

RESULTS AND DISCUSSION

Figure 1 shows the temperature behaviour at point 1 with different discharge rates, 1C, 3C and 5C with the same air velocity of 1.5m/s. For the comparison between the discharge rates, the data is taken at the most critical condition which is at point 1, where in all condition of discharge rates, it produced the highest temperature. While data also taken with the least cooling effect, which is with the air velocity of 1.5m/s. It is clear that with discharge rate of 5C, marked the highest temperature at 52.2˚C, while discharge rate of 3C, marked 48.1˚C and discharge rate of 1C, marked the lowest temperature at 32.7˚C. In contrary, the discharging time, 1C discharge rate has the longest time of 2777s, while 3C discharge rate marked 517s and 5C has the shortest time of 197s.

From this data, we can say that the higher the discharge rate, the higher the temperature produced. While in the aspect of discharging time, the higher the discharge rate, the shorter the discharging time. Also, the air velocity does give an impact in the thermal behaviour of the battery. As higher air velocity will result in lower battery temperature. From this study also proved that battery temperature across the battery surface is non-uniform. The point nearest to positive terminal marked the highest temperature, while the point nearest to negative terminal came second and the point on the centre between positive and negative terminal marked the lowest temperature.

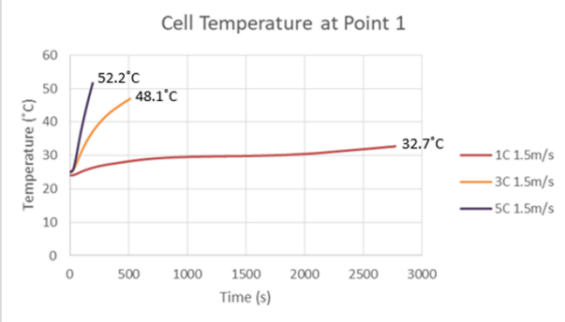

Figure 10 : Cell temperature at point 1

CONCLUSION

It is clear that discharge rate and air velocity affects the thermal behaviour of Lithium-ion battery. Besides, the temperature across the battery cell surface is non-uniform under discharging process.

REFERENCES

[1] Hannan, M.A., et al., *Review of energy storage systems for electric vehicle applications: Issues and challenges*. Vol. 69. 2017. 771-789.

MEASUREMENT OF POWER REQUIRED FOR EMDAP CVT RATIO CHANGE

Muhammad Amirul Mohd Basri and Zul Hilmi Che Daud
School of Mechanical Engineering, Faculty of Engineering,
Universiti Teknologi Malaysia, 81310 UTM Skudai, Johor, Malaysia

21. INTRODUCTION

Regular CVT which generally utilized in the market is electro-hydraulically actuated type. It needs nonstop capacity to supply power to keep up the ideal proportion what's more, avoiding gross belt slip. Along these lines, it can decrease CVT effectiveness [1]. An elective answer for empower financial fuel utilization is to utilize electromechanical CVT type with single acting pulley framework since it just works amid changing the transmission proportion [2]. The single acting pulley mechanism utilized in this framework causes misalignment of metal belt. This belt misalignment may lessen the belt life.

22. EXPERIMENTAL SETUP

This section presents the experimental setup for the system. I used Matlab Simulink as my work platform to conduct the experiment. In order to determined the power require when ratio change, I used existing FKM's EMDAP CVT and LEM 55-P Hall Sensor

The conducted test was intended to find the suitable battery power. The experiment was done to get CVT output speed, EMDAP CVT ratio change and DC motor current input. All the result was calculated by the system or computer itself.

23. RESULTS AND DISCUSSION

Figure 1 show the output speed of EMDAP CVT when we go under drive to over drive then reverses. At first gear, the output speed is ±25 RPM, 2nd gear is ±30 RPM, 3rd gear is ±40 RPM, 4th gear is ±55 RPM and 5th gear is ±75 RPM. For the reverse gear which is from over drive to under drive the output speed almost same but in descending order of output speed. Figure 2 show the ratio change of EMDAP CVT when we go under drive to over drive then reverses. We follow the standard ratio change for Proton Persona car year 2016. The results show from under drive to over drive the ratio change decrease and for over drive to under drive the ratio change increasing.

Figure 3 show the DC motor current input when going under drive to over drive and reverse. The measurement results have shown that the current needed for ratio change was constant and independent of the initial ratio value. However, twice more is needed to operate from underdrive to overdrive than opposite. It is constant around 50 Amp when ratio go from underdrive to overdrive and 25 Amp when goes the opposite direction.

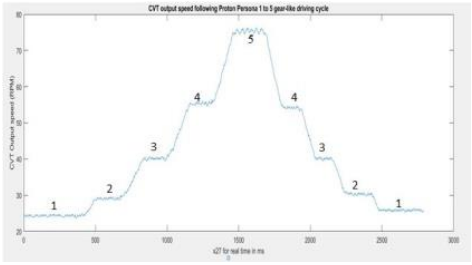

Figure 1: EMDAP CVT Output Speed

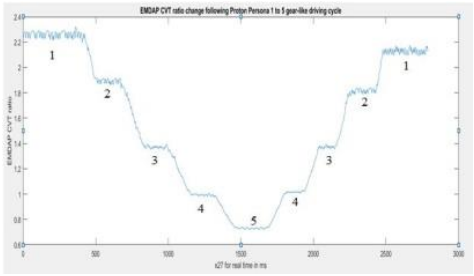

Figure 2: EMDAP CVT Ratio Change

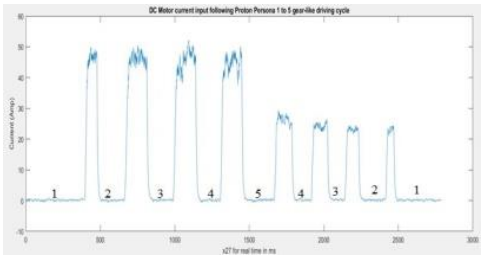

Figure 3: DC Motor Current Input

24. CONCLUSION

The measurement results have shown that the current needed for ratio change was constant and independent of the initial ratio value. However, twice more is needed to operate from underdrive to overdrive than opposite.

25. REFERENCES

[1] Tawi, K. B., Supriyo, B., Ariyono, S., Husain, N. A., Hamid, A. R. A., Mazali, I. I., & Kob, M. S. C. (2015). Design of Electro-Mechanical Dual-Acting Pulley Continuously Variable Transmission. Journal of Mechanical Engineering and Sciences, 8(June), 1332–1342.

[2] Supriyo, B., Tawi, K. B., Jamaluddin, H., Budianto, A., & Mazali, I. I. (2013). Shifting Performance Fuzzy-PID Ratio Controller of Electro-Mechanical Continuously Variable Transmission. WSEAS Automatic Control and Signal Processing, (1), 272–277.

MODELLING AN ELECTRIC VEHICLE WITH RANGE EXTENDER

Mohamad Aidell Fahmy Mohd Akmal and Zulhilmi Che Daud
School of Mechanical Engineering, Faculty of Engineering,
Universiti Teknologi Malaysia, 81310 UTM Skudai, Johor, Malaysia

INTRODUCTION

As fully electric cars are still not capable to compete with internal combustion engine cars, electric vehicle with range extender is the solution to the limited driving range and extremely high cost of electric vehicle. For this configuration of powertrain, only the electric motor drives the powertrain. They operate basically as a normal battery electric vehicle until their battery depletes to a certain point. At that point, the internal combustion engine will work as an auxiliary power unit to power the electric motor or to recharge the batteries and allow the vehicle to continue operating [1].

MODEL DEVELOPMENT

MATLAB/SIMULINK software is utilized for the modelling and simulation of electric vehicle with range extender. The model developed will be based on an existing battery electric vehicle ATV. There are five important component in developing an electric vehicle with range extender model which are vehicle dynamic model, electric motor transmission, battery, internal combustion engine and fuel consumption. New European Driving Cycle (NEDC) and Common Artemis Driving Cycle (CADC) will be repeated for 5 hours to be use as driving cycle for model simulation. Model is develop referring to Erdinc [2] and Guzella [3].

RESULTS AND DISCUSSION

The model is firstly run without the internal combustion engine component. This is to depict the model without the range extender, making it a Battery Electric Vehicle (BEV). The model is then run with the addition of internal combustion engine component. The internal combustion engine will supply 5 kW of power if state of charge is below 90%. Result of simulation will show battery performance, distance covered, and fuel consumption.

Figure 1 shows result of simulation for 5 hours of NEDC driving cycle. The BEV model only covers 75.73 km while PHEV manages to cover 158.2 km. Referring to figure 2, the state of charge of battery for BEV depletes completely at 8484 seconds/141.4 minutes. For PHEV, state of charge of battery does not depletes fully as it is recharged by internal combustion engine. This is possible due to there is many instances in NEDC cycle that the power required to propel the vehicle is below than 5 kW, hence the excess power is used to recharge the battery.

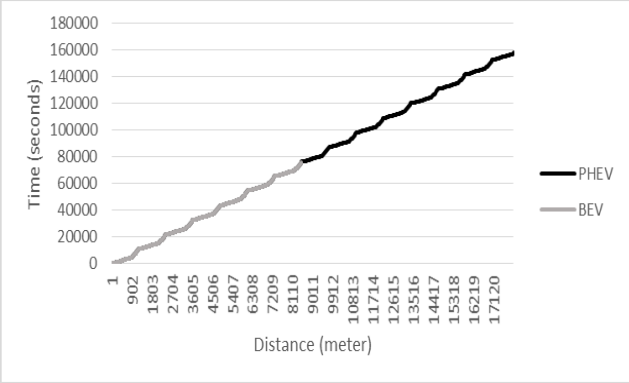

Figure 1: Simulation result for distance covered for 5 hours of NEDC cycle

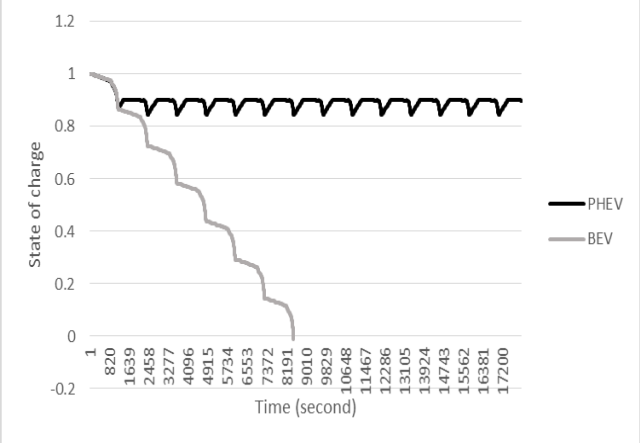

Figure 2: Simulation result for battery performance for 5 hours of NEDC cycle

CONCLUSION

We have shown the ability of a range extender to increase the driving range of an electric vehicle. The benefit of installing a range extender is clearly seen through the model simulation.

REFERENCES

[1] EAI. (2018, December 22). Electric Vehicle Transmission System. Retrieved from EAI India: http://www.eai.in/blog/2018/12/electric-vehicle-transmission-system.html

[2] Erdinc O. V. (2009). A Dynamic Lithium-ion Battery Model Considering the Effects of Temperature and Capacity Fading. IEEE Transactions, 383-386.

[3] Guzella L., S. A. (2007). Vehicle Propulsion Systems/Introduction to Modeling and Optimization, 2nd edition. New York, USA: Springer.

PORTABLE BADMINTON SHUTTLECOCK LAUNCHER

Muhammad Zikri Saifullah and Zul Hilmi Che Daud
School of Mechanical Engineering, Faculty of Engineering,
Universiti Teknologi Malaysia, 81310 UTM Skudai, Johor, Malaysia

INTRODUCTION

Over recent years, there has been an increasing growth of interest in development and research study in badminton field are carried out in order improve the quality of this sport. Nowadays kind of training for professional in the badminton circles. The repeatedly training used is "Multi-Shuttle" training period. Multi shuttlecock involves the coach to distribute the shuttlecock to player at different type of shot during training session. The shot consists of drop shot, middle court, lob shot and smash which allow the player to read all time. A set of this training usually requires hundreds of shuttlecock where the coach repeat the serve for the player.Which shuttlecock launcher, coach can freely concentrate on coaching and analysing their player instead of serve the shuttlecock every time. [1].

DESIGN PROCESS

This section presents the design process for the function of mechanical component and system. Design process consist of eight-step basic process that are usually used in a problem solving (figure 1).

Define the Problem	Analyse and select a solution.
Do Background Research	Do Development Work.
Specify Requirements	Build a Prototype.
Brainstorm Solutions.	Test and Redesign.

Figure 1: Basic steps of design process

The process of selection for the final design mechanism is be done by using the Weight Objective Method table 2 and Eleven Point Scale Method table 3. List of objective and requirement are Functional Ability, Maintenance, Cost, Size and Weight and Safety. [2]

Table 1: Weight objective method.

Objective	Ranking Order	Scale	Weight Percentage	Weight factor
Functional Ability	1	10	33.33%	0.333
Maintenance	3	6	20.00%	0.200
Cost	4	6	20.00%	0.200
Size and Weight	2	8	26.67%	0.267
Total		30	100.00%	1.000

RESULTS AND DISCUSSION

In this result also we can list that the design specification for the shuttlecock after finish fabricating. The detailed for the shuttlecock we obtained is shown in Table 3.

Table 2: Eleven points scale method.

Point	Description
0	Totally useless solution
1	Inadequate solution
2	Very poor solution
3	Poor solution
4	Tolerable solution
5	Adequate solution
6	Satisfactory solution
7	Good solution
8	Very good solution
9	Excellent solution
10	Perfect solution

Table 3: Product Design Specification

Specification	Details	SHUTTLECOCK LAUNCHER
Dimension	Size	200 x700x 300 mm
	Weight	Around 4-5 kg
Power Supply	Power Supply	10 000 mAh power bank + lithium ion battery
	Battery Life	Up to 30 minutes
	Rechargable	Yes
Materials	Frame	Aluminium Profile
	Launcher roller	Plastic 3D Print
	Tripod Stand	Aluminium
	Dispenser	Aluminium Rolled Plate
	Speed	20 km/h to 161km/h
	Frequency	5s/shuttlecock
	Lifting stand	Up to 100cm
Development Cost	Cost	RM 450- RM 600

CONCLUSION

Main focus of this chapter is to conclude overall summary for the study and to propose a recommendation for the shuttlecock launcher. All mechanism of the shuttlecock launcher was design by using available materials such as aluminium profile, L joint, DC motors, stepper motors and etc. The shuttlecock launcher was design using CAD Drawing using SolidWorks 2017 and was analysed by using static analysis Von Mises in order to determine the failure of the design using the material proposed. Using existing material help to reduce the cost of shuttlecock launcher. The main objective of the study is to design the mechanical component and systems that are portable and affordable shuttlecock launcher for badminton users is archived.

REFERENCES

[1] Nur. A. (n.d.). History. Retrieved from http://adilahjester.blogspot.com/p/history.html

[2] D. T. (2016, September 06). Types of Badminton Shots | Badminton Clear, Drop Shots, Net Shots and Smashes. Retrieved fromhttps://www.masterbadminton.com/badminton-shots.html

FLOW MEASUREMENT OF EJECTOR AIR-CONDITIONING SYSTEM

Fikri Zulhaziq Shubandrio and Zulkarnain Abdul Latiff
School of Mechanical Engineering, Faculty of Engineering,
Universiti Teknologi Malaysia, 81310 UTM Skudai, Johor, Malaysia.

INTRODUCTION

Flowmeters are used to measure the flowrate of a flow within a system. For this project, the type of flowmeter used is an orifice flowmeter. It uses constrictions to create pressure difference when a flow is flowing through it. Mass flowrate value can be obtained from the pressure difference that occurred. Previous study also shown that orifice has been used for liquid and vapour state of flow. Hasegawa et al. [1] mentioned that they tested Stoke flow of water through orifice. Jitschin [2] tested gas flow through orifice as it is an interesting approached to measure gas flow by using constriction. For this project, the flowmeters will be used to measure the flow in liquid and vapour state. One flowmeter will be used in each state. Calibration test is done to validate the mass flowrate reading obtained from the flowmeters compared to the actual value.

METHODOLOGY

Fabrication process involved in fabricating the flowmeters are turning, facing and drilling. The raw materials that is used is Aluminium for the tube and metal plate for orifice plate. After the design have been fabricated, calibration test will be done. For vapour state, compressed air will be used as the medium of flow. The mass flowrate obtained from the orifice will be compared to the actual value of mass flowrate obtained from the mass of air contained in a balloon over time. The same concept is used for the liquid state of flow. The medium of flow is water. The mass flowrate value obtained from the orifice will be compared to the actual value of mass flowrate obtained from the mass of air flowing in a bucket over time. The data will be tabulated and plotted to be analyzed.

RESULTS AND DISCUSSION

For Figure 1, the graph is plotted to visualizes the error in value differs between the mass flowrate obtained from the orifice and the actual mass flowrate.

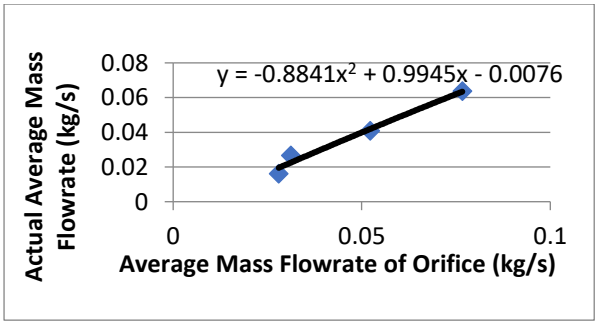

Figure 1: Graph actual mass flowrate against mass flowrate obtained from orifice

For Figure 2, the graph is plotted to visualizes the error in value differs between the mass flowrate obtained from the orifice and the actual mass flowrate.

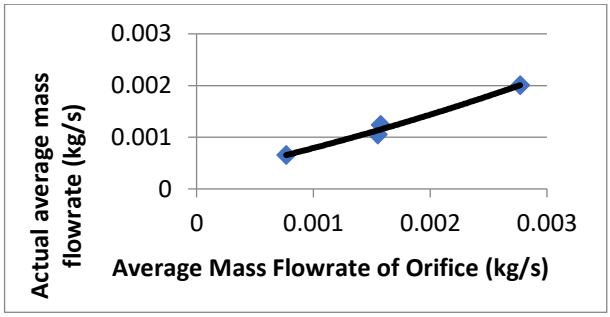

Figure 2: Graph actual mass flowrate against mass flowrate obtained from orifice.

CONCLUSION

In conclusion, it is obvious that the orifice reading does not produced the same value with the actual value. The high percentage in error may be caused by errors during the testing procedure. For liquid test, the unstable reading of u-tube manometer affected the accuracy in obtaining the pressure difference reading to be recorded. For vapour state of flow, the air flow disturbance may have caused the weighing scale reading unstable in producing accurate reading of mass. In the future, a proper test with better equipment need to be done to get more accurate result with minimal errors.

REFERENCES

[1] Hasegawa, T., Masaki, S., and Hiroshi, W. (1997). Anomaly of excess pressure drop of the flow through very small orifices. Physics of Fluids, 1-3.

[2] Jitschin, W. (2004). Gas flow measurement by the thin plate orfice and the classical Venturi tube. Vacuum, 2.

DATA ACQUISITION METHOD AND TECHNIQUE FOR EJECTOR AIR CONDITIONING SYSTEM TEST RIG

Mohd Hisyam Mohd Hanafi and Zulkarnain Abdul Latiff
School of Mechanical Engineering, Faculty of Engineering,
Universiti Teknologi Malaysia, 81310 UTM Skudai, Johor, Malaysia.

INTRODUCTION

In conventional car cooling system, it makes use of compressor to compress refrigerant in order to lower its pressure and temperature. This project promotes the alternatives use of compressor by using air ejector. By doing so, the mechanical energy of the system is significantly reduced. There are three parameters that must be obtained from the experiment which are pressure, temperature. These parameters will be used to determine the enthalpy of the system. Significantly, to achieve reliable result, an efficient data acquisition methods and techniques must be developed.

PROJECT OBJECTIVES

The objective of this project is to complete the ejector air conditioning system test rig with measurements in order to evaluate the system performance. Therefore, correct methods and techniques are very crucial in achieving the desired result.

METHODOLOGIES

The flow of methodology starts by listing the available instruments to be installed in the test rig. The instruments selected fulfilled the purpose of the data acquisition process. The main instruments selected in measuring pressure and temperature are bourdon pressure gauge and thermocouple (type T):

Figure 1: Pressure Gauge (left) and Thermocouple

The location of installation is crucial as it will represent the state of refrigerant right before and after condenser, evaporator, and thermal generator. The pressure gauge can be represented by the blue highlighted colour in Figure 2 and red represents thermocouple. Next up, the data acquired was analysed using dimensionless analysis and simulation.

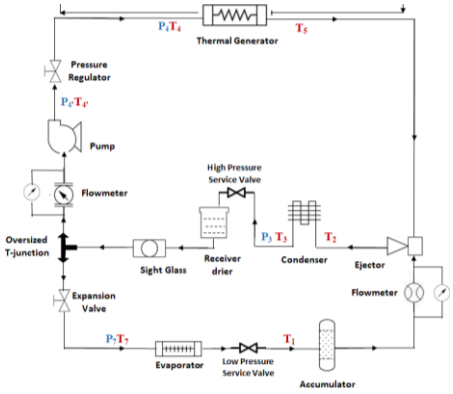

Figure 2: Location of Pressure and Temperature in the Test Rig Schematic

RESULTS

The analyses done using dimensionless analysis or simulation shows small error between surface temperature of tube and internal fluid temperature.

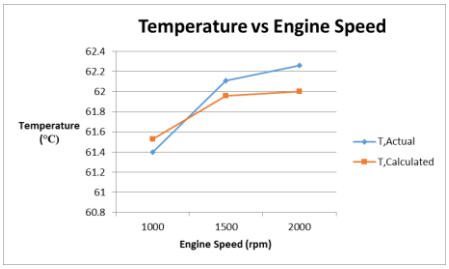

Figure 3: Result of Dimensionless Analysis

CONCLUSION

In conclusion, the internal temperature of the fluid flowing through tube is the same as the surface temperature of the tube with insulation.

REFERENCES

[12] J.M Gorman et al. *Differences between Measured Pipe Wall Surface Temperatures and Internal Fluid Temperatures*. United States: Elsevier Ltd. 2013.

DESIGN AND DEVELOPMENT OF THERMAL GENERATOR SYSTEM FOR EJECTOR AIR CONDITIONING SYSTEM

Mohamad Nassar Mohamad Alias and Zulkarnain Abdul Latiff
School of Mechanical Engineering, Faculty of Engineering,
Universiti Teknologi Malaysia, 81310 UTM Skudai, Johor, Malaysia.

INTRODUCTION

The function of the radiator in the car is used to cool down the temperature of the cooling water produce by the engine. The hot water from the engine flow into the radiator and the fan will automatically switch on when the thermostat detects the temperature of the water is higher than 85°C. So, the fan will blow out the heat to the environment and become waste heat. The waste heat from the radiator can be used to heat up the refrigerant in the ejector refrigeration systems. Thus in this study, the experiment has been constructed to identify the ability of the waste heat energy to heat up the refrigerant (R-134a) in the Ejector Air Conditioning (EAC) system.

METHODOLOGIES

The preliminary testing will used hot water in the water circulation and cold water from utilities as the replace for the refrigerant. The hot water will be adjust by various flow rate refer to real car engine speed while the flow rate of the cold water is fix or constant. The water temperature of the thermal storage is set up to 65°C.

This experiment is conducted to analyse the ability of the electrical heater to heat the volume of water in thermal storage at desired temperature and identify characteristics of the heat exchanger. Based on Figure 1, temperature of T1w, T2w, T3w, T4 and T5 will be measured in the experiment with adjusting the flow rate of the hot water. The data collected will be used to determine the ability of thermal storage and characteristics of the heat exchanger.

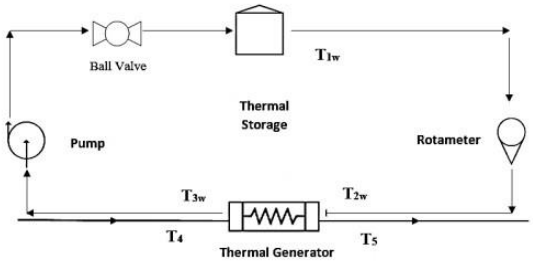

Figure 1: Schematic diagram of thermal generator system.

RESULT AND ACHIEVEMENT

This project is successful in achieving the objective and scopes. The thermal storage and electrical heater with thermostat control is able to maintain the temperature inside thermal storage at desired temperature. From the experiment, the maximum temperature of hot water is 63°C and the maximum cold water is 61°C. The maximum thermal ratio is 0.33 at 10 lpm (1000 rpm) and lowest is 0.18 at 22 lpm (3000 rpm). From this preliminary experiment, based on Figure 2, it shows that when the flow rate of the water pump is increasing, the heat transfer between two fluids will be lower and the thermal ratio will decrease.

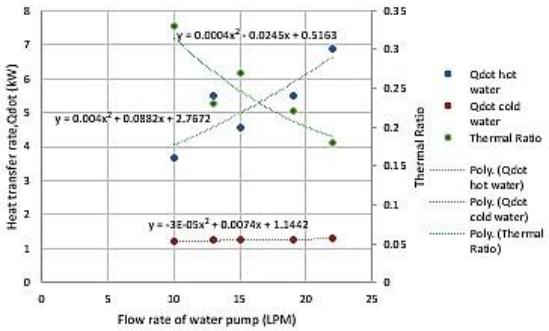

Figure 2: Graph of heat transfer rate and thermal ratio against flow rate of water pump

REFERENCES

[13] Please Crouse, W. *Automotive Fuel, Lubricating and Cooling System*. 4th ed. McGraw-Hill Companies, Inc. 1971.

[14] Yunus A. Cengel and Afshin J. Ghajar. *Heat and Mass Transfer: Fundamentals & Applications*. New York: McGraw-Hill Education. 2015.

DEVELOPMENT AND EVALUATION OF EJECTOR FOR VEHICLE AIR CONDITIONING SYSTEM

Wan Muhammad Nizar, Zulkarnain Abdul Latif, Natrah Kamaruzaman
School of Mechanical Engineering, Faculty of Engineering,
Universiti Teknologi Malaysia, 81310 UTM Skudai, Johor, Malaysia.

INTRODUCTION

Vehicle Ejector Air conditioning system is one of the alternative systems that can replace current vehicle air conditioning system. It can produce refrigeration by using waste heat from car radiator. An ejector is the heart of the system according to Stefan Elbel (1), it produces low pressure region for suction process of evaporator. This system also will reduce the usage of fossil fuel since eliminated compressor from the system. The COP of the system is depending on the ejector performance, by entrainment ratio between secondary flow and primary flow and limited by critical pressure .According to Aphornratana (2) The main interest of this project is to study the performance of the ejector by varies the distance between nozzle and mixing chamber.

EXPERIMENTAL SETUP

For evaluate the ejector, some modifications such as material and component have been done from the previous design to vary the distance between nozzle and mixing chamber for the evaluation purposed. From the final drawing of the ejector, simulation of stress analysis has been done to know the limitation of the pressure that can be apply to the ejector based on the safety factor of the components. An experiment needs to be conducted to evaluate of the ejector. This preliminary evaluation goal is to know the performance of ejector based on entrainment ratio and distance between nozzle and mixing chamber. Air have been chosen as a working fluid for this experiment. Selection of proper instrument also has been done to get data.

RESULTS AND DISCUSSION

An ejector has been fabricated and Electrical Discharge Machining method has been chosen by referring of its capability. The ejector has been divided to 3 majors' component and Aluminium Alloy 6061 has been chosen.

Figure 1 Fabricated Ejector with variable distance.

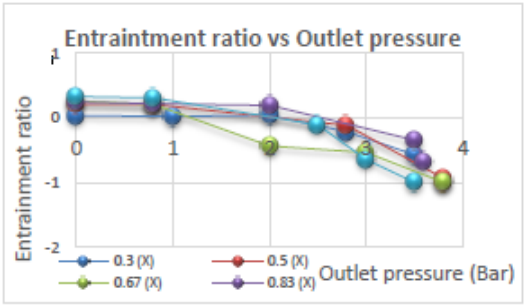

Figure 2 Entrainment ratio vs outlet pressure.

The result form experiment was, the ejector produces higher entrainment ratio with higher spacing to diameter ratio. It limited by critical pressure. The reduction of this spacing to diameter ratio will allow the ejector to operate with higher critical pressure and vice versa with increase of spacing to diameter ratio.

CONCLUSION

As a conclusion, ejector with variable distance of nozzle to mixing chamber is more versatile because it can operate with different working pressure with the highest performance of the system.

REFERENCES

[1] Elbel S, Hrnjak P. Ejector Refrigeration: An overview of historical and present developments with an emphasis on air conditioning applications. Int Refrig Air Cond Conf - Purdue Univ. 2008; 1:1–8.

[2] Aphornratana S, Eames IW. A small capacity steam-ejector refrigerator: Experimental investigation of a system using ejector with movable primary nozzle. Int J Refrig. 1997;20(5):352–8.

DESIGN AND DEVELOPMENT OF WASTE-HET ASSISTED AIR CONDITIONING TEST RIG

Mohamad Nazmi Abdul Ghani and Zulkarnain Abdul Latiff
School of Mechanical Engineering, Faculty of Engineering,
Universiti Teknologi Malaysia, 81310 UTM Skudai, Johor, Malaysia

INTRODUCTION

The use of compressor to operate the conventional air conditioning system to provide cooling effect for the car passengers consumes high amount of energy from car engine. On the other hand, Ejector Air Conditioning (EAC) system uses an ejector which operates mechanically by using low grade thermal energy from the car cooling system to replace the function of the compressor [1]. Despite providing energy saving, one limitation of this system is the difficulty to obtain the high pressure, low flow rate pump which is required to increase the pressure of the liquid refrigerant from the condenser to be transferred to the thermal generator before the heat gained from the thermal generator is converted to kinetic energy and used to operate the ejector by creating suction of the refrigeration flow from the evaporator [2].

METHODOLOGY

The first step in designing the system is to set the parameters of the temperature at generator, condenser and evaporator are set at 80℃, 40℃ and 6℃ respectively. Meanwhile the mass flow rate at the same components are 2.184 kg/min, 3.318 kg/min and 1.134 kg/min respectively. Next, the component selection is done so that they comply to the parameters that had been set. Third stage is design, followed by development of the test rig. The processes involved problem analysis and troubleshooting along each stage.

RESULTS AND DISCUSSION

The schematic diagram in Figure 1 shows the design of the EAC system based on the position and arrangement of each component. The components in red is the main components while those in blue are the auxiliary components.

Among all components, high pressure, low flow pump is the most difficult to obtain. The suitable pump for those requirements is the positive displacement pump. In the market this type of pump is rarely used for this kind of purpose. As a solution, High Pressure Common Rail Fuel Pump that is used for the Diesel engine is recommended due to its capability to supply very high pressure yet still can be regulated by its own pressure regulator at low flow rate suitable to our requirements.

The actual test rig layout is shown in Figure 2 where the size of the components, their interconnections as well as their mechanical properties such as air flow at condenser and evaporator are being considered before all the components are integrated into the system.

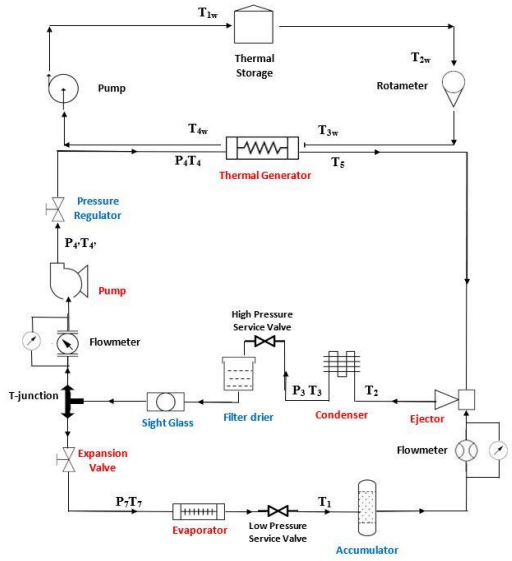

Figure 1: Schematic diagram of EAC system

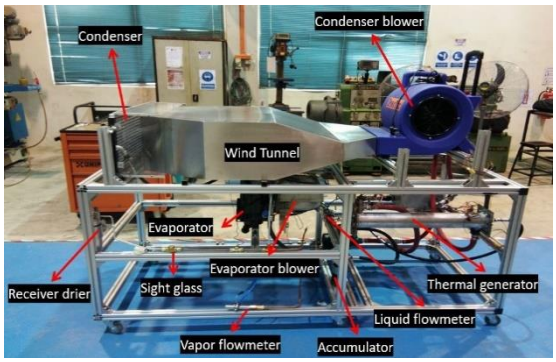

Figure 2: Actual layout of the components in the test rig

CONCLUSION

As a conclusion, the test rig developed serve as a platform for future testing, research and improvement on EAC system. It is also recommended to come out with a project to design and fabricate a specific pump for the system.

REFERENCES

[1] Memet, F., & Preda, A. (2015). An analysis of the performance of an ejector refrigeration cycle working with R134a. In IOP Conference Series: Materials Science and Engineering (Vol. 95).

[2] Saleh, B. (2016). Performance analysis and working fluid selection for ejector refrigeration cycle. Applied Thermal Engineering, 107, 114–124.

ANCHHOVY WASTE PROCESSING

Nur Suhaili Zafirah and Zulkepli Hj Muhamad
School of Mechanical Engineering, Faculty of Engineering,
Universiti Teknologi Malaysia, 81310 UTM Skudai, Johor, Malaysia

INTRODUCTION

Anchovies is one of famous fish that usually used in food making and fish industry. The split anchovies usually come with clean from its heads, guts and bone part. These parts defined as waste where the usage of the fish approximately between 60% to 70% and the amount of waste for about 40% [1]. The part of fish waste can be categorized into several part where each of part contain its nutrient that can be benefits towards living things [2]. In order to add-value of the waste, a few products can be produced from the waste such as anchovy pallet. A few steps of process can be done to making the anchovy pallet which are sieving, grinding, mixing, palletizing and drying.

DETAILED DESIGN ANALYSIS AND FABRICATION

This section presents the analysis of design where the sieving/classifying process required to be fabricated. The slider crank mechanism can be used for sieving/classifying process. This mechanism used convert rotational motion into a reciprocating motion and vice versa [3]. The sieving/classifying can be done if the size of one kind of particles is bigger than the size of holes in the sieve and the size of other kind of particles is smaller than the size of holes in the sieve.

RESULTS AND DISCUSSION

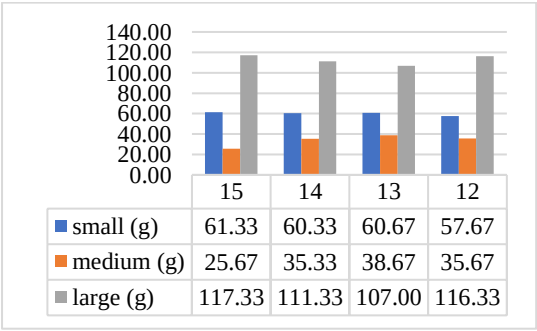

	15	14	13	12
small (g)	61.33	60.33	60.67	57.67
medium (g)	25.67	35.33	38.67	35.67
large (g)	117.33	111.33	107.00	116.33

Figure 11: Results of Sieving/Classifying Process

Figure 1shows the average results of the anchovy retained on the mesh number 6 and 10 where the mesh size used is 2.03mm and 3.13mm respectively. The average weight for large, medium and small size are 113g, 33g, and 60g respectively. This shows that the batch for this waste anchovies have a lot small size retained compared to medium size. As general that separation by sieving sieve only removes particles that are larger than the pores in the sieve.

Adding value is the process of changing or transforming a product from its original state to a more valuable state. Many raw products have intrinsic value in their original state. Value added production is just one of many possible strategies that must be considered before marketing. The palettizing product of waste anchovy is one of the alternatives to be added value where it required further process to obtained product.

Grinding process can produce the waste anchovy into powder where the machine rotated at high speed and crushed the anchovies into fines powder. Then, the mixing of the powder anchovy with water increases the moisture and easy for shaping the product into certain shape such as pallet. The pallet can be made using the mincer where this can be done after the mixing of the anchovy powder with water to reduce the force to rotate the screw conveyor. The fineness of the shape depends on the size of the holes of the plate used is about 5mm with 6cm of the size of plate.

Figure 12: End product of waste anchovy

CONCLUSION

The waste anchovy that can be classifying into 3 size which is small, medium and large can be separated using the sieving process. Mesh size that used for sieving process is between 2mm to 4mm where in this project the size of sieve used is 2.03mm and 3.13mm. Anchovy waste successfully convert into added value product which is anchovy pallet by continue to next process which is grinding and palletizing.

REFERENCES

[1] Forristall, A. (2011). A more profitable use for fish waste. 2018, from https://www.seafoodsource.com/news.supply-trade/a-more-profitable-use-for-fish-waste

[2] Henry, C. J., Bi, X., Lim, J., & Lau, E. (2016). Mineral decline due to modernization of food habits. Food Chemistry, 194-196.

[3] Darina, H., Peter, F., & Gabriel, B. (2016). Kinematical Analysis of Crank Slider Mechanism with Graphical Method and by Computer Simulation. American Journal of Mechanical Engineering, 4, 329-343. doi: 10.12691/ajme-4-7-18

DEVELOPMENT OF A PORTABLE STEAM GENERATOR FOR EVAPORATIVE PATTERN FACILITY (EPC)

Ahmad Hafiz Mohd Rozi and Zulkepli Muhamad
School of Mechanical Engineering, Faculty of Engineering,
Universiti Teknologi Malaysia, 81310 UTM Skudai, Johor, Malaysia

INTRODUCTION

Evaporative pattern casting (EPC) is a metal casting process that uses polystyrene pattern to shape the casting. To produce the polystyrene pattern, it requires continuous steam flow. But the polystyrene pattern production needs only small input of steam. It doesn't require a high temperature of the steam and high pressure of steam. The steam generator in the market today usually large, heavy and required large space to be placed. This demands a new design of steam generator for small production quantity. The previous study on this matter was very well functioning and able to supply the steam to the steam chest. But, this steam generator doesn't equip with a steam separator and proper exhaust heat recovery. From all of this, the system of the steam generator will be improves for further usage.

EXPERIMENTAL SETUP

The steam produced by the steam generator must meet the requirement of expanded polystyrene for the patterning process. Future improvement planning to develop the steam generator was to install an exhaust heat recovery systems to pre-heat the feed water and to install a steam separator to increase the steam quality. After that, the analysis was done to determine the variable such as the safety of the design of the steam separator and the heat energy required to transform water into steam without the pre-heat water and with the pre-heat feed water. During the testing process on the steam generator, the performance of the product is measured and the steam flow rate of the steam generator will be taken. After that, the recomen how to make the design more better in the future.

RESULTS AND DISCUSSION

The objective to develop steam generator is achieved but there are a few recommendations on the system that been suggested to improve the system before been introduced to the market. Because of the lack measuring device to measure the steam flow rates, it is suggested that the next researcher try to develop a steam measuring device using a microcontroller to get a better and accurate reading.

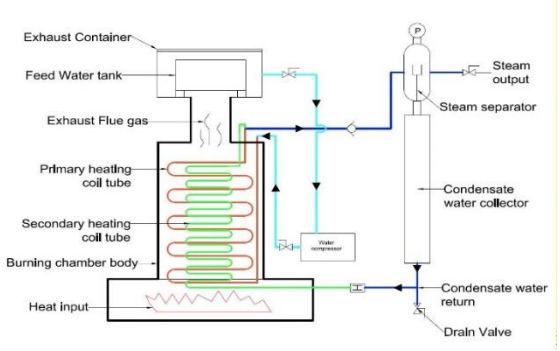

Figure 1: The circuit diagram of the steam generator.

CONCLUSION

The objective of this research is to design and develop a small and portable steam generator for evaporative pattern casting (EPC) facility.

REFERENCES

[1] Mior Faizzuddin Bin Mior Abdul Rahman (2016), Development of Portable steam generator For Evaporative Pattern Casting (EPC) Facility, Universiti Teknologi Malaysia.
[2] Aizzuddin Abdul Rahman (2015), Development of Portable steam generator For Evaporative Pattern Casting (EPC) Facility, Universiti Teknologi Malaysia
[3] Swagelok Energy Advisors (2013), Steam Systems Best Practices, Pennsylvania USA, Swagelok Energy Advisors Inc.

DEVELOPMENT OF FRICTION WELDING CONTROL INTERFACE MODULE

Danial Asyraf Zolkapli and Zulkepli Muhamad
School of Mechanical Engineering, Faculty of Engineering,
Universiti Teknologi Malaysia, 81310 UTM Skudai, Johor, Malaysia.

INTRODUCTION

Friction welding works when materials from two different chucks, rotating and non-rotating are brought together into contact to develop friction. Hence, the welding speed will increase directly proportional to friction force until a certain parameter before it becomes constant through friction heating process. Later, the welding speed will drop at instant while friction force will continue to increase until the second parameter for forge force through welding forging process until a certain time before the operation complete. Along the process, the length of upset will be developed to ensure the joint is succeed. This control interface module developed to give the command to the process as to what user intended. Thus, the machines being controlled could respond as stated by the user. The module will have four parameters that control pressure and process time during friction heating and welding forging.

RESEARCH OBJECTIVES

This development aims to establish quality friction welding through precision controlling welding parameter during the forging stage

METHODOLOGY

There will be three processes including design the welding control system, testing and prototyping, and fabrication of the controller before obtain the final product and others. AISI 1020 or mild steel was used as it has a low hardenability and low tensile carbon steel which suitable for testing the control interface module and machine with secure parameter indeed. Over the succeeding operation, control interface module has been applied to the test run after several modifications and troubleshoots been done to counter the axial alignment problem at the contact surface. It is the outcome that process time has been reduce to less than 250 seconds with lower pressure on process 1 and more well built on upset formed. The data in the control interface module will be transfer to Matlab Simulink for validation and verification on the friction welding process. As a result, the first step up for friction force to achieve 8 bar is about 8 seconds while the second step up for forge force to achieve 50 bar is 20 seconds.

RESULT AND ACHIEVEMENT

Figure 1: Final product after fabrication

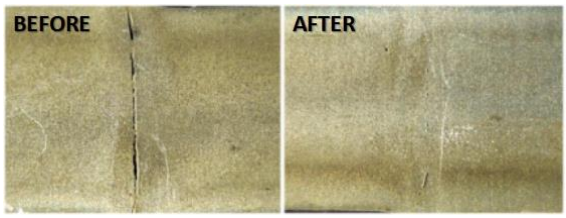

Figure 2: Result on workpieces cross-section after cut using wire EDM

CONCLUSION

This result proves that too many errors can be found on joint quality since the part on both side not completely attached. After the implementation of control interface module, the errors were minimized. This could happen due to the consistent pressure distributed through the friction and forge process. Since the process supported by control interface module, the results are highly repeatable.

REFERENCES

[1] Paulraj Sathiya, S.Aravindan, A.Nooral Haq, “Optimization for friction welding parameters with multiple performance characteristics”, Int.J.Mech Mater Des, 3:309-318K.Y, 2006.

[2] Duffin, F. D., & Bahrani, A. S. (1973). Frictional behaviour of mild steel in friction welding. Wear, 26(1), 53-74.

.